



POLITECHNIKA POZNAŃSKA

Wydział Inżynierii Materiałowej i Fizyki Technicznej

Sandra Witkiewicz-Łukaszek

Kompozytowe scyntylatory na bazie warstw i kryształów granatów: krystalizacja metodą epitaksji z fazy ciekłej oraz badania ich właściwości luminescencyjnych i scyntylacyjnych

Rozprawa doktorska

Promotor
prof. dr hab. Yu. Zorenko

Promotor pomocniczy
dr V. Gorbenko

POZNAŃ 2020

Przedmowa

Niniejsza rozprawa doktorska była realizowana w ramach Studium Doktoranckiego Fizyka Techniczna na Wydziale Fizyki Technicznej Politechniki Poznańskiej.

Badania dotyczące rozprawy doktorskiej były częścią realizacji projektów Narodowego Centrum Nauki pt.:

- Nowe ekrany scyntylacyjne na bazie warstw monokrystalicznych mieszanych perowskitów i tlenków (2016/21/B/ST8/0320);
- Nowoczesne fosfory na bazie ceramiki, warstw i struktur epitaksjalnych mieszanych granatów, jako konwektory dla diod białych wysokiej mocy (2017/25/B/ST8/02932)

oraz projektu

- Nano-ceramiczne fosfory dla diod białych wysokiej mocy na bazie domieszkowanych jonami Ce^{3+} oraz parami jonów $\text{Ce}^{3+}\text{-}\text{Eu}^{2+}$ granatów krzemianowych, NANOLUX 2014 ID 286, ścieżka Era NET RUS Plus S&T w programie Horyzont 2020.

które doktorantka jako wykonawca i stypendystka dokonała na Katedrze Materiałów Optoelektronicznych Instytutu Fizyki Uniwersytetu Kazimierza Wielkiego w Bydgoszczy.



*„Jak przy wielu ludzkich poczynaniach, jak w życiu w ogóle,
badacz porusza się między dwoma biegunami: pożądaniem
i możliwym. Bez tego, co możliwe, pożądania są tylko
marzeniem, a możliwości bez pożądań są tylko nudą.*

*Badanie naukowe polega więc na nieustannym
konfrontowaniu tego, co być może, z tym, co jest.”*

[François Jacob]

Chciałam wyrazić głęboką wdzięczność Panu prof. dr hab. Y. Zorenko, za czuwanie nad tą rozprawą przez cały okres moich studiów doktoranckich aż po etap publikacji. Dziękuję za inspirację do badań, niezastąpioną pomoc w planowaniu doświadczeń oraz kreatywne podejście w poszukiwaniu rozwiązań problemów fizycznych. Pragnę również podziękować za pomoc w redagowaniu pracy oraz motywację do opracowania samodzielnych koncepcji na tle istniejącej literatury naukowej.

Pragnę podziękować Panu dr V. Gorbenko, promotorowi pomocniczemu, który z nieocenioną mądrością i cierpliwością, dzielił się ze mną swoim doświadczeniem i wiedzą w trakcie powstawania tej pracy.

Wyrazy wdzięczności składam pracownikom Instytutu Fizyki, Uniwersytetu Kazmierza Wielkiego w Bydgoszczy za przekazaną wiedzę, pomoc w zakresie technik eksperymentalnych oraz prawdziwie naukową atmosferę w pracy.

W szczególności pragnę podziękować Pani mgr T. Zorenko za pomoc w wykonywaniu pomiarów i okazaną życzliwość.

Dziękuje rodzinie, za nieustanne wsparcie oraz motywację. W szczególności dziękuję moim rodzicom Kamili i Jerzemu Witkiewicz za pomoc w wyborze drogi zawodowej oraz nigdy niegasnącą wiarę we mnie.

Niniejszą pracę pragnę dedykować MAMIE i TACIE.

Spis skrótów i oznaczeń

Oznaczenie	Opis
LPE	(z ang. liquid-phase epitaxy) epitaksja z fazy ciekłej
SCF	(z ang. single crystalline films) warstwy monokrystaliczne
TL	termoluminescencja
Z_{eff}	efektywna liczba atomowa
LuAG	granat lutetowo-aluminiowy ($\text{Lu}_3\text{Al}_5\text{O}_{12}$)
YAG	granat itrowo-glinowy ($\text{Y}_3\text{Al}_5\text{O}_{12}$)
GAGG	granat gadolinowo-aluminiowo-galowy ($\text{Gd}_3\text{Al}_2\text{Ga}_3\text{O}_{12}$)
VB	(z ang. valence band) pasmo walencyjne
CB	(z ang. conduction band) pasmo przewodnictwa
FWHM	FWHM (z ang. full width at half maximum) szerokość połówkowa
ER	(z ang. energy resolution) rozdzielcość energetyczna
LY	(z ang. light yield) wydajność luminescencji
RT	(z ang. room temperature) temperatura pokojowa

Spis treści

STRESZCZENIE	2
ABSTRACT	3
АННОТАЦИЯ	4
1. Wstęp	5
2. Forma pracy doktorskiej oraz wkład doktoranta	9
3. Metody eksperymentalne	13
3.1. Krystalizacja warstw i kompozytowych scyntylatorów metodą LPE	13
3.2. Materiały do produkcji kompozytowych scyntylatorów	15
3.3. Metody badań właściwości optycznych kompozytowych scyntylatorów i termoluminoforów	17
3.4. Wybrane parametry optyczne oraz metody analizy	18
3.4.1 Wydajność świetlna scyntylacji (z ang. Light yield-LY)	18
3.4.2 Amplitudowe widma scyntylacji	18
3.4.3 Rozdzielcość energetyczna (ER-energy resolution)	18
3.4.4 Kinetyka zaniku scyntylacji	19
3.4.5 Prametry t_α/t_γ lub t_γ/t_α	20
3.4.6 Termoluminescencja	21
3.4.7 Parametr ΔT	21
4. Krótki opis badań składających się na rozprawę doktorską	21
5. Podsumowanie rozprawy doktorskiej	36
Literatura	38
Dorobek naukowy doktoranta	40
Oświadczenie współautorów o wkładzie w publikacje naukowe doktoranta	45
Przedruki:	
Publikacja C1.1	
Publikacja C1.2	
Publikacja C2.1	
Publikacja C2.2	
Publikacja C2.3	
Publikacja C2.4	
Publikacja C3.1	
Publikacja C3.2	
Publikacja C4.1	
Publikacja C4.2	

STRESZCZENIE

Niniejsza rozprawa doktorska stanowi cykl artykułów naukowych, w których przedstawiono przegląd osiągnięć w opracowaniu kompozytowych materiałów luminescencyjnych na bazie cienkich warstw monokrystalicznych (z ang. SCF) i monokryształów (z ang. SC) granatów, otrzymanych metodą epitaksji z fazy ciekłej (z ang. LPE). Opracowane kompozytowe materiały mogą znaleźć zastosowanie jako detektory scyntylacyjne do monitorowania składu promieniowania mieszanych wiązek jonizacyjnych oraz jako ekrany scyntylacyjne w mikroobrazowaniu.

Główny temat badań związany jest z opracowaniem kompozytowych scyntylatorów oraz materiałów termoluminescencyjnych opartych na warstwach i kryształach związków granatu do jednoczesnej rejestracji różnego rodzaju promieniowania jonizującego w mieszanych wiązkach jonizacyjnych cząstek i kwantów. Warstwy i podłoża kompozytowych scyntylatorów można z powodzeniem wytwarzać używając metody epitaksji z fazy ciekłej w oparciu o granat $\text{Lu}_3\text{Al}_5\text{O}_{12}$ (LuAG), domieszkowany jonami Ce^{3+} , Pr^{3+} i Sc^{3+} , oraz bazując na domieszkowanych jonomi Ce^{3+} mieszanych granatach $\text{Gd}_{3-x}\text{A}_x\text{Al}_{5-y}\text{Ga}_y\text{O}_{12}$, gdzie A = Lu lub Tb; x = 0-1; y = 2-3 z istotnie różną kinetyką zaniku scyntylacji.

Praca doktorska przedstawia także analizę wyników badań właściwości luminescencyjnych warstw, kryształów oraz struktur epitaksjalnych granatów, prowadzonych metodami spektroskopii optycznej takimi jak absorbcja, katodoluminescencja i fotoluminescencja. Przeprowadzone zostały również pomiary właściwości scyntylacyjnych i termoluminescencyjnych opracowanych materiałów przy wzbudzeniu cząstками α i β oraz kwantami γ .

Warstwy, kryształy i struktury epitaksjalne prostych i mieszanych granatów zostały zbadane i przeanalizowane pod kątem opracowania najbardziej wydajnych składów kompozytowych materiałów scyntylacyjnych i termoluminescencyjnych do zastosowań w detektorach do monitorowania mieszanych wiązek promieniowania jonizującego.

ABSTRACT

The Ph.D. thesis is a review of scientific articles in which achievements in the development of composite luminescent materials based on the single crystalline films and single crystals of simple and mixed garnet compounds using the liquid-phase epitaxy (LPE) method are presented. Such composite materials can be applied as scintillating and thermoluminescent materials for radiation monitoring of the mixed ionization fluxes and screens in the microimaging technique.

The main topic of the research is connected with the development of multilayer composite scintillators and thermoluminescent materials based on SCFs and SCs of garnet compounds for simultaneous registration of different types of ionizing radiations in mixed ionization fluxes of particles and quanta. The film and crystal parts of composite scintillators can be fabricated from effective scintillation materials based on Ce³⁺, Pr³⁺ and Sc³⁺ doped Lu₃Al₅O₁₂ garnets as well as the Ce³⁺ doped Gd_{3-x}A_xAl_{5-y} Ga_yO₁₂ mixed garnets, where A= Lu or Tb; x=0-1; y=2-3 with significantly different scintillation decay kinetics.

The thesis presents also an analysis of the results of investigation of optical properties of films, crystals and epitaxial structures of garnets, using absorption, cathodoluminescence and photoluminescence. The scintillation and thermoluminescent properties of the developed materials under α -and β particles and γ quanta excitations are studied as well.

The properties of films, crystals and epitaxial structures of simple and mixed garnets were measured and analyzed for the selection of the most efficient compositions of the composite scintillation and thermoluminescent materials for application in detectors for monitoring of the content of mixed fluxes of ionizing radiation.

АННОТАЦИЯ

Кандидатская диссертация является серией научных статей, в которых представлен обзор достижений в разработке композиционных люминесцентных материалов на основе монокристаллических пленок (МКП) и монокристаллов (МК) простых и смешанных соединений гранатов, используя метод жидкофазной эпитаксии (LPE). Разработанные композиты могут найти применение в качестве сцинтилляционных и термolumинесцентных материалов для радиационного контроля смешанных ионизирующих потоков и в детекторах для микрообразования.

Главной темой исследования является разработка многослойных композиционных сцинтилляторов и термolumинесцентных материалов на основе МКП и МК соединений гранатов для одновременной регистрации разных типов ионизирующего излучения в смешанных потоках ионизирующих частиц и квантов. Пленки и кристаллические части композитных сцинтилляторов могут быть изготовлены из эффективных сцинтилляционных материалов на основе активированного ионами Ce^{3+} , Pr^{3+} и Sc^{3+} граната $\text{Lu}_3\text{Al}_5\text{O}_{12}$, а также легированных ионами Ce^{3+} смешанных гранатов $\text{Gd}_{3-x}\text{A}_x\text{Al}_{5-y}\text{Ga}_y\text{O}_{12}$, где $A = \text{Lu}$ или Tb ; $x = 0-1$; $y = 2-3$ с существенно различной сцинтилляционной кинетикой затухания.

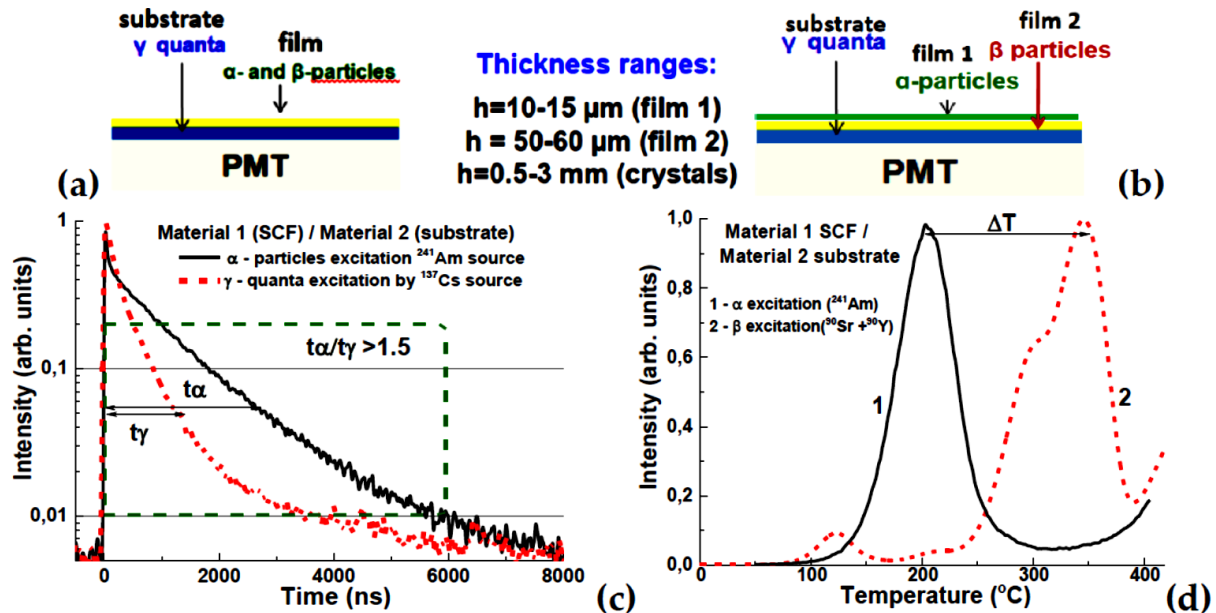
В диссертации представлен анализ результатов измерений люминесцентных свойств пленок, кристаллов и эпитаксиальных структур гранатов с использованием методов оптической спектроскопии, таких как поглощение, катодолюминесценция и фотолюминесценция. Измерения сцинтилляционных и термolumинесцентных свойств разработанных материалов проводились при возбуждении α и β частицами, а также γ квантами.

Свойства пленок, кристаллов и эпитаксиальных структур простых и смешанных гранатов были исследованы и проанализированы с целью разработки наиболее эффективного сочетания композиционных сцинтилляционных и термolumинесцентных материалов для использования в детекторах контроля смешанных потоков ионизирующего излучения.

1. Wstęp

Rozwój technologii epitaksji z fazy ciekłej (LPE) w ciągu ostatnich 30 lat otworzył nowe możliwości do opracowywania innowacyjnych materiałów luminescencyjnych opartych na warstwach monokrystalicznych (SCF) różnych związków tlenkowych, w szczególności granatów. Takie badania przyczyniły się do rozwoju szeregu dziedzin inżynierii materiałowej, optoelektroniki, fizyki jądrowej, a także biologii, medycyny i archeologii. Między innym, nowopowstałe materiały luminescencyjne w postaci SCF znalazły zastosowanie jako podstawowe elementy funkcjonalne w laserach mikro-chipowych, ekranach katodoluminescencyjnych, detektorach scyntylacyjnych do rejestracji cząstek α i β , oraz w detektorach mikrotomograficznych wykorzystujących źródła promieniowania rentgenowskiego lub promieniowania synchrotronowego.

Metoda LPE wykazuje również możliwość tworzenia zaawansowanych typów scyntylatorów kompozytowych typu „phoswich” („kanapka fosforów”) do rejestracji różnych składników promieniowania jonizującego, wykorzystywanych do analizy zawartości mieszanych strumieni cząstek i fotonów o różnych głębokościach penetracji w materiałach scyntylacyjnych [1-4]. Takie kompozytowe scyntylatory lub materiały termoluminescencyjne (TL) stanowią epitaksjalne układy monokrystaliczne przeznaczone do jednoczesnej rejestracji cząstek o niskiej penetracji α - i β - (warstwa) oraz promieniowania o wysokiej penetracji takich jak kwanty X lub γ (podłoże) (Rys.1).



Rys. 1. Schematy dwuwarstwowego (a) i trójwarstwowego (b) kompozytowego scyntylatora oraz materiału TL, (c) – przykład detekcji cząstek α i kwantów γ w sposób rejestracji czasu zaników scyntylacyjnych, pochodzących od warstwy i podłoża kompozytowego scyntylatora, (d) – przykład rejestracji różnicy w temperaturach głównych pików krzywych jarzenia TL od warstwy i podłoża kompozytowego materiału TL, wyrażonej przez parametr ΔT (rozdział 3).

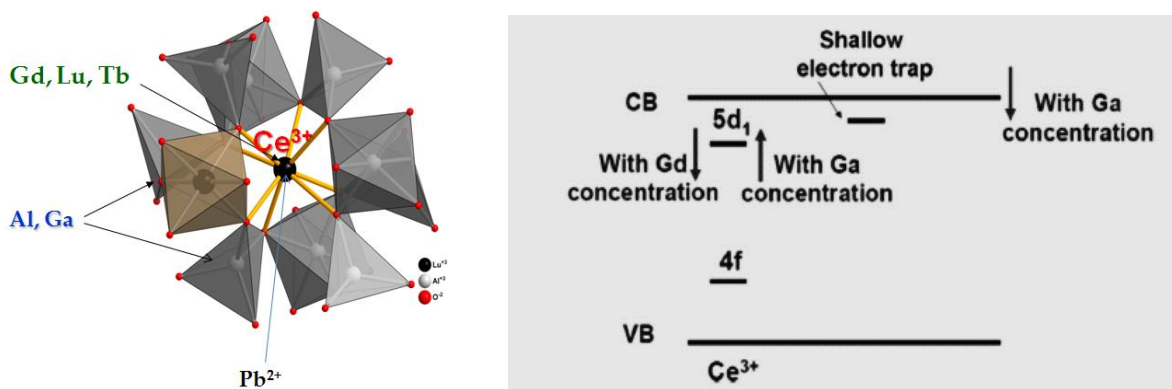
Pierwsze typy scyntylatorów kompozytowych powstały na podstawie epitaksjalnych struktur granatu $\text{Y}_3\text{Al}_5\text{O}_{12}$ (YAG) [1]. Były nimi jednowarstwowe scyntylatory kompozytowe oparte na warstwach YAG:Ce i podłożu YAG:Nd (YAG:Ce SCF / YAG: Nd SC) oraz warstwach YAG: Ce i podłożu YAG: Sc (YAG: Ce SCF / YAG: Sc SC), a także trójwarstwowy scyntylator kompozyty oparty na dwóch warstwach YAG: Ce i YAG: Nd, i podłożu YAG: Sc (YAG: Ce SCF / YAG: Nd SCF / YAG: Sc SC). Te scyntylatory kompozytowe zostały wyhodowane metodą LPE, a następnie badane przy jednoczesnym wzbudzeniu przez cząstki α i kwanty γ [1]. Rozdzielenie sygnałów scyntylacyjnych pochodzących od warstwy i podłoża takich złożonych scyntylatorów przeprowadzono przy użyciu analizy ich kinetyki zaniku scyntylacji.

Należy zauważyć, że ze względu na niską gęstość $\rho = 4,57 \text{ g/cm}^3$ i efektywną liczbę atomową $Z_{\text{eff}}=29$ scyntylatory oparte na podłożach granatu YAG można stosować tylko do rejestracji niskoenergetycznego promieniowania jonizującego [1, 2]. Z tego powodu zaistniała potrzeba wykonania scyntylatorów kompozytowych do rejestracji mieszanych strumieni cząstek i kwantów wysokoenergetycznych przy użyciu innych związków granatów, które charakteryzują się wysokimi wartościami ρ i Z_{eff} [2, 3].

Pierwszym materiałem, na który zwrócono szczególną uwagę jest granat $\text{Lu}_3\text{Al}_5\text{O}_{12}$ (LuAG) [5, 6]. Matryca LuAG ma znacznie wyższą gęstość $\rho = 6,73 \text{ g/cm}^3$ i efektywną liczbę atomową $Z_{\text{eff}}=59$ w porównaniu z granatem YAG. To pozwala zasadniczo zwiększyć efektywność absorpcji promieniowania rentgenowskiego lub γ w porównaniu z podłożami opartymi na YAG. Domieszkowane jonami Ce, Pr oraz Sc kryształy granatu LuAG są dobrze znany scyntylatorami do monitorowania promieniowania rentgenowskiego w tomografii komputerowej [7, 8]. Z tego powodu powstała duża szansa na uzyskanie dobrej jakości podłoże z komercyjnie dostępnych kryształów LuAG:Ce, LuAG:Pr i LuAG:Sc.

Wcześniej przeprowadzone badania [11-14] wykazały, że wydajność scyntylacyjna (LY) domieszkowanych jonami Ce, Pr i Sc kryształów i warstw na bazie LuAG przekracza wydajność odpowiedników opartych na YAG. To stało się kolejnym powodem do produkcji nowej generacji wysokowydajnych kompozytowych scyntylatorów na bazie opracowanych wcześniej scyntylatorów w postaci domieszkowanych warstw i kryształów LuAG.

Ważnym wynikiem badań dotyczących krystalizacji warstw LuAG metodą LPE było uzyskanie możliwości krystalizacji tych warstw nie tylko na stosunkowo drogich podłożach LuAG (homo-epitaksja), a także na zdecydowanie tańszych podłożach YAG (kwasi-homo-epitaksja) w warunkach dużego (do 1%) niedopasowania stałych sieci krystalicznej warstwa/podłoże. Jednak w celu zmniejszenia niedopasowania parametrów sieci między podłożem YAG a warstwą opartą na LuAG można wykorzystać podstawienie jonów Lu^{3+} w pozycjach dodekaedrycznych matrycy granatu na większe kationy Gd lub Tb oraz podstawienie kationów Al^{3+} w pozycjach oktaedrycznych i tetraedrycznych na jony Ga (Rys. 2a) [5].



Rys. 2. (a) Struktura sieci krystalicznej granatu z ukazaniem pozycji krystalograficznych zajmujących przez różne kationy [18]; (b) - zmiany w pozycji pasma 5d jona Ce³⁺ w granacie (Lu_{3-x}Gd_x)₃(Al_{5-y}Ga_y)O₁₂:Ce spowodowane zmianami w koncentracji kationów Gd oraz Ga. CB, VB - pasma energetyczne granatu [17].

Przeprowadzone wcześniej badania nad procesami krystalizacji warstw LuAG za pomocą metody LPE pozwoliły także na rozpoczęcie badań polegających na opracowaniu kompozytowych scyntylatorów opartych na LuAG przy użyciu różnego typu domieszek bez zmiany matrycy. W tym celu, jako aktywatory, zaproponowano jony o różnej i wystarczająco szybkiej kinetyce zaniku scyntylacyjnego, m. in., Ce³⁺, Pr³⁺ i Sc³⁺ [5, 14, 16].

Kolejnym ważnym sukcesem w opracowaniu materiałów luminescencyjnych w postaci warstw monokrystalicznych była hodowla przy użyciu metody LPE warstw granatów R₃Al₅O₁₂ (R = Lu, Tb, Yb, Eu – Y) na podłożach YAG bez dopasowania parametrów sieci krystalicznych tych materiałów, które wynosiło około ±1%. Ten sukces otworzył bogate perspektywy do opracowania nowych warstwowych materiałów scyntylacyjnych do aplikacji w różnych dziedzinach nauki i przemysłu, m. in. ekranów scyntylacyjnych w detektorach mikrotomograficznych do wizualizacji zdjęć rentgenowskich (Rys. 3). W szczególności, opracowane warstwy monokrystaliczne TbAG:Ce, w porównaniu z właściwościami warstw LuAG:Ce wykazują większą o 30% wydajność scyntylacyjną oraz unikatowo niski poziom fosforescencji [C1.1].

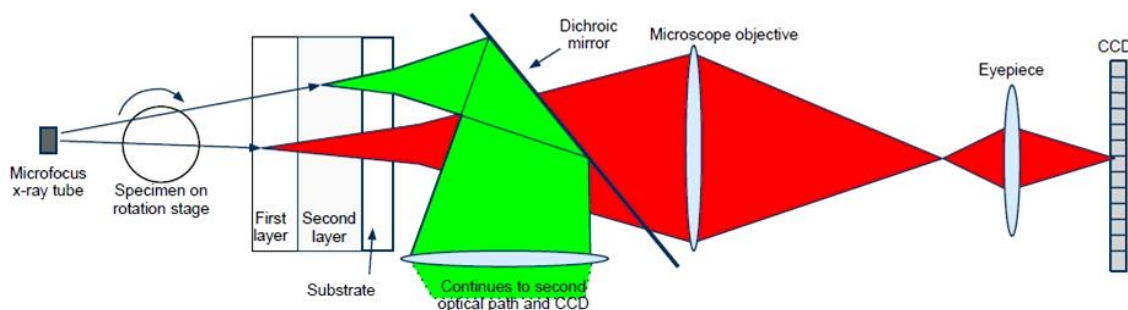
W ciągu ostatnich dziesięciu lat zostało także wdrożone nowatorskie podejście do opracowywania materiałów scyntylacyjnych, które opiera się na inżynierii składu kationu mieszanych granatów i innych złożonych materiałów tlenkowych. Polega ono na korzystnej modyfikacji struktury energetycznej matrycy oraz aktywatora (przeważnie jonów Ce³⁺) w sposób celowej zmiany w składzie kationów (Rys.2b). W taki sposób uzyskuje się optymalne warunki do przekazania energii wzbudzenia od matrycy do centrum luminescencji, co skutkuje znaczącym wzrostem wydajności scyntylacji oraz rozdzielczości energetycznej materiału. W szczególności, kryształy granatu Gd₃Al_{5-x}Ga_xO₁₂ przy x= 2-3 (GAGG:Ce) posiadają bardzo wysoką wydajność scyntylacyjną (LY) do 50 000 Fotonów/MeV przy wzbudzeniu kwantami γ ze źródła ¹³⁷Cs (662 keV) [C1.1] (Tabela1).

Nieco późniejsze badania pokazały ze mieszane granaty o wzorze $\text{Lu}_{3-x}\text{Gd}_x\text{Al}_{5-y}\text{Ga}_y\text{O}_{12}:\text{Ce}$, gdzie $x=1-3$; $y=2-3$ (LGAGG:Ce) są również bardzo obiecującymi materiałami do produkcji scyntylatorów w postaci warstw monokrystalicznych o wysokiej zdolności absorpcji promieni rentgenowskich oraz bardzo wysokiej wydajności przy wzbudzeniu cząstkami α [19–21]. Okazało się, że scyntylatory w postaci warstw LGAGG:Ce z powodu większej stałej sieci również można krystalizować nie tylko na podłożach YAG, ale także na podłożach GAGG. Następna sukcesywna krystalizacja metodą LPE warstw scyntylatorów opartych na TbAG:Ce na niedomieszkowanych podłożach GAGG [C1.1], udowodniła hipotezę o możliwości krystalizacji dobrej jakości warstw monokrystalicznych nawet z dużym (do 2%) niedopasowaniem stałych sieci warstwa/podłoże.

W celu opracowania nowych typów kompozytowych scyntylatorów do monitoringu radiacyjnego środowiska dość sensownym wydaje się połączenie wymienianych kryształów GAGG:Ce oraz warstw LGAGG:Ce lub TbAG:Ce w jeden materiał kompozytowy przy użyciu metody LPE [22,23]. To także pozwoliło rozważyć możliwość opracowania *innego podejścia do konstrukcji kompozytowych scyntylatorów w oparciu o połączenie różnych matryc materiałów scyntylacyjnych domieszkowanych tym samym typem aktywatora (Ce^{3+})*.

Szczegółowe informacje związane z doborem materiałów do opracowania kompozytowych scyntylatorów zostały przedstawione w podrozdziale 3.2 pt. „Materiały” oraz w tabeli 1.

Warto podkreślić, że oba wyżej wymienione podejścia do konstrukcji kompozytowych scyntylatorów w postaci złożonych struktur epitaksjalnych granatów lub innych materiałów scyntylacyjnych mogą być także bardzo korzystne do produkcji nowoczesnych detektorów mikrotomograficznych z wielokanałowym sposobem rejestracji i nałożenia uzyskanych obrazów optycznych (Fig.3).



Rys. 3. Schemat nowoczesnego detektora dla mikroobrazowania zawierającego kompozytowy ekran scyntylacyjny w postaci dwóch warstw monokrystalicznych, otrzymanych metodą LPE na tym samym podłożu [C1.1].

Ostatnią część pracy doktorskiej tworzą artykuły pokazujące możliwość opracowania nowych kompozytowych materiałów termoluminescyjnych (TL) opartych na strukturach epitaksjalnych granatów, zawierających warstwy i kryształy YAG:Ce i LuAG:Ce oraz warstwy $\text{Lu}_{3-x}\text{Gd}_x\text{Al}_{5-y}\text{Ga}_y\text{O}_{12}:\text{Ce}$. W tych kompozytowych

materiałach TL skupiono się na obserwacji różnicy w temperaturach i wydajności głównych pików krzywych jarzenia dla warstw i podłoż przy wzbudzeniu cząstkami α i β . Obserwowana różnica we właściwościach termoluminescencyjnych warstw i kryształów-podłoż pozwoliła rejestrować jednocześnie promieniowanie α i β w mieszanych wiązkach jonizujących. Z tego powodu opracowane struktury epitaksjalne można uważać za prototypy do dalszego rozwoju nowej generacji kompozytowych detektorów TL, opartych na strukturach epitaksjalnych różnych związków tlenkowych.

W oparciu o podany wyżej przegląd osiągnieć w opracowywaniu materiałów luminescencyjnych metodą epitaksji z fazy ciekłej, *celem pracy doktorskiej* była krystalizacja metodą LPE oraz badanie właściwości luminescencyjnych i scyntylacyjnych kompozytowych materiałów opartych na strukturach epitaksjalnych typu „warstwa-kryształ” na bazie prostych i mieszanych granatów.

Osiągnięcie tego celu wymagało rozwiązania następujących zadań naukowych:

1. Krystalizacja hetero-epitaksjalna wysokowydajnych scyntylatorów w postaci warstw monokrystalicznych mieszanych granatów $(\text{Tb},\text{Gd})_3(\text{Al},\text{Ga})_5\text{O}_{12}:\text{Ce}$ metodą LPE w warunkach znacznej różnicy parametrów sieci SCF i podłoż GAGG.
2. Szczegółowe badanie absorpcji, luminescencji oraz właściwości scyntylacyjnych i termoluminescencyjnych warstw mieszanych granatów w celu optymizacji ich właściwości oraz ustalenia możliwości skutecznych modyfikacji składu warstw przy opracowaniu kompozytowych scyntylatorów i materiałów termoluminescencyjnych.
3. Opracowanie z użyciem metody LPE kompozytowych scyntylatorów na bazie warstw i kryształów-podłoż LuAG z domieszkami jonów Ce, Pr i Sc.
4. Opracowanie metodą LPE kompozytowych scyntylatorów na bazie warstw TbAG i LGAGG oraz kryształów-podłoż GAGG, domieszkowanych jonami Ce^{3+} .
5. Pilotowe badania nad opracowaniem prototypów kompozytowych materiałów termoluminescencyjnych na bazie struktur epitaksjalnych granatów.
6. Badania nad optymalizacją składu warstw oraz typów domieszek w celu uzyskania jak najlepszej separacji sygnałów pochodzących od warstw i podłoż kompozytowych materiałów scyntylacyjnych i termoluminescencyjnych.

Wyniki badań przedstawiono w artykułach opublikowanych w czasopismach naukowych z listy JCR.

2. Forma pracy doktorskiej oraz wkład doktoranta

Praca doktorska pt. „Kompozytowe scyntylatory na bazie warstw i kryształów granatów: krystalizacja metodą epitaksji z fazy ciekłej oraz badania ich właściwości luminescencyjnych i scyntylacyjnych” stanowi cykl artykułów opublikowanych w recenzowanych czasopismach naukowych:

Tematycznie praca doktorska składa się z **4 części**.

Część I. Opracowanie scyntylatorów w postaci warstw monokrystalicznych granatów $Tb_{3-x}Gd_xAl_{5-y}Ga_yO_{12}$ metodą LPE

C1.1 Y. Zorenko, P. Douissard, T. Martin, F. Riva, V. Gorbenko, T. Zorenko, K. Paprocki, A. Iskalieva, **S. Witkiewicz**, A. Fedorov, P. Bilski, A. Twardak. Scintillating screens based on the LPE grown $Tb_3Al_5O_{12}:Ce$ single crystalline films. *Optical Materials* 65 (2017) 73-81

C1.2. V. Gorbenko, T. Zorenko, **S. Witkiewicz**, K. Paprocki, O. Sidletskiy, A. Fedorov, P. Bilski, A. Twardak, Y. Zorenko. LPE growth of single crystalline film scintillators based on Ce^{3+} doped $Tb_{3-x}Gd_xAl_{5-y}Ga_yO_{12}$ mixed garnets. *Crystals* 7 (2017) 262.

Część II. Kompozytowe scyntylatory oparte na strukturach epitaksjalnych granatu LuAG z domieszkami jonów Ce, Pr i Sc

C2.1 **S. Witkiewicz-Lukaszek**, V. Gorbenko, T. Zorenko, K. Paprocki, O. Sidletskiy, I. Gerasymov, J.A. Mares, R. Kucerkova, M. Nikl, Yu. Zorenko. Novel all-solid-state composite scintillators based on the epitaxial structures of LuAG garnet doped with Pr, Sc and Ce ions. *IEEE Transactions on Nuclear Science* 65 (2018) 2114 – 2119

C2.2 **S. Witkiewicz-Lukaszek**, V. Gorbenko, T. Zorenko, K. Paprocki, O. Sidletskiy, I. Gerasymov, J.A. Mares, R. Kucerkova, M. Nikl, Yu. Zorenko. Composite scintillators based on the crystals and single crystalline films of LuAG garnet doped with Ce^{3+} , Pr^{3+} and Sc^{3+} ions. *Optical Materials* 84 (2018) 593-599

C2.3 J.A. Mares, **S. Witkiewicz-Lukaszek**, V. Gorbenko, T. Zorenko, R. Kucerkova, A. Beitlerova, C. D'Ambrosio, J. Dlouhy, M. Nikl, Yu. Zorenko. Alpha and gamma spectroscopy of composite scintillators based on the LuAG:Pr crystals and single crystalline films of LuAG:Ce and (Lu,Gd,Tb)AG:Ce garnets. *Optical Materials* 96 (2019) 109268

C2.4 **S. Witkiewicz-Lukaszek**, V. Gorbenko, T. Zorenko, O. Sidletskiy, P. Arhipov, A. Fedorov, J.A. Mares, R. Kucerkova, M. Nikl, Yu. Zorenko, High-performance composite scintillators based on the single crystalline films and crystals of LuAG garnet. *CrystEngComm* (2020) opublikowany on-line 06.04.2020, <https://doi.org/10.1039/D0CE00266F>

Część III. Kompozytowe scyntylatory oparte na warstwach i kryształach mieszanych granatów z domieszką jonów ceru

C3.1 **S. Witkiewicz-Lukaszek**, V. Gorbenko, T. Zorenko, O. Sidletskiy, I. Gerasymov, A. Fedorov, A. Yoshikawa, J. A. Mares, M. Nikl, Yu. Zorenko. Development of Composite Scintillators Based on Single Crystalline Films and Crystals of Ce^{3+} -Doped $(Lu,Gd)_3(Al,Ga)_5O_{12}$ Mixed Garnet Compounds. *Cryst. Growth Des.* 18 (2018) 1834–1842

C3.2 **S. Witkiewicz-Lukaszek**, V. Gorbenko, T. Zorenko, K. Paprocki, O. Sidletskiy, A. Fedorov, R. Kucerkova, J. A. Mares, M. Nikl, Yu. Zorenko. Epitaxial growth of composite scintillators based on $Tb_3Al_5O_{12}:Ce$ single crystalline films and $Gd_3Al_{2.5}Ga_{2.5}O_{12}:Ce$ crystal substrates. *CrystEngComm* 20 (2018) 3994-4002

Część IV. Opracowanie prototypów kompozytowych materiałów termoluminescencyjnych na bazie struktur epitaksjalnych granatów

C4.1 S. Witkiewicz-Lukaszek, V. Gorbenko, T. Zorenko, Y. Zorenko, W. Gieszczyk, A. Mrozik, P. Bilski. Composite thermoluminescent detectors based on the Ce³⁺ doped LuAG/YAG and YAG/LuAG epitaxial structures. *Radiation Measurements* 128 (2019) 106124

C4.2 S. Witkiewicz-Lukaszek, A. Mrozik, V. Gorbenko, T. Zorenko, P. Bilski, Yu. Zorenko, LPE growth of composite thermoluminescent detectors based on the Lu_{3-x}Gd_xAl₅O₁₂:Ce single crystalline films and YAG:Ce crystals. *Crystals* 10 (2020) 189.

Zgodnie z załączonymi oświadczeniami współautorów, wkład doktoranta w powstanie publikacji był następujący:

Część I

C1.1 Scintillating screens based on the LPE grown Tb₃Al₅O₁₂:Ce single crystalline films.

- analiza całości materiału eksperymentalnego;
- przygotowanie materiałów (rysunki, tabele) do publikacji;
- uczestnictwo w pisaniu części manuskrytu, dotyczącej właściwości optycznych warstw oraz korekt manuskrytu po uwagach recenzentów

C1.2 LPE growth of single crystalline film scintillators based on Ce³⁺ Tb_{3-x}Gd_xAl_{5-y}Ga_yO₁₂ mixed garnets.

- analiza wyników badań właściwości strukturalnych i optycznych warstw Tb_{3-x}Gd_xAl_{5-y}Ga_yO₁₂:Ce na podłożach GAGG;
- uczestnictwo i przygotowaniu materiałów do publikacji (rysunki, tabele) oraz w napisaniu części manuskrytu dotyczącej właściwości optycznych warstw, a także korekty manuskrytu po uwagach recenzentów

Część II

C2.1 Novel all-solid-state composite scintillators based on the epitaxial structures of LuAG garnet doped with Pr, Sc and Ce ions.

- udział w powstaniu koncepcji pracy;
- pomiary widm absorbcji warstw i kompozytowych scyntylatorów;
- -opracowanie wyników badań absorbcji, katodoluminescencji i kinetyki zaniku scyntylacji oraz przygotowanie odpowiednich rysunków i tabeli do publikacji;
- opracowanie metody opisu różnic w krzywych zaniku scyntylacji kompozytowych scyntylatorów przy wzbudzeniu cząstками α i kwantami γ , wyrażonych jako stosunek t_α/t_γ lub t_γ/t_α ;
- uczestnictwo w napisaniu manuskrytu pracy, oraz przeprowadzenie korekt pracy po uwagach recenzentów (autor korespondencyjny)

C2.2 Composite scintillators based on the crystals and single crystalline films of LuAG garnet doped with Ce³⁺, Pr³⁺ and Sc³⁺ ions.

udział w powstaniu koncepcji pracy;

- opracowanie wyników badań absorbcji, katodoluminescencji, kinetyki zaniku scyntylacyjnego, widm amplitudowych scyntylacji oraz zależności wydajności i rozdzielczości energetycznej scyntylacji od czasu rejestracji sygnału scyntylacyjnego;
- wykonanie zdjęć próbek przy użyciu mikroskopu elektronowego;

- opracowanie wyników badań różnic w krzywych zaniku scyntylacji od warstwowej i krystalicznej części kompozytowych scyntylatorów przy wzbudzeniu cząstkami α i kwantami γ przez stosunki t_α/t_γ lub t_γ/t_α ;
- uczestnictwo w napisaniu manuskryptu, a także przeprowadzenie korekt po uwagach recenzentów (autor korespondencyjny)

C2.3 Alpha and gamma spectroscopy of composite scintillators based on the LuAG:Pr crystals and single crystalline films of LuAG:Ce and (Lu,Gd,Tb)AG:Ce garnets.

- udział w powstaniu koncepcji pracy;
- analiza krzywych zaniku scyntylacyjnego pochodzących od różnych części scyntylatora kompozytowego;
- ustalenie możliwości skutecznej modyfikacji składu warstwy przy opracowaniu kompozytowych scyntylatorów typu (Lu,Tb)AG:Ce/LuAG:Pr;
- wprowadzenie parametru Δ opisującego różnice krzywych zaniku scyntylacji kompozytu przy wzbudzeniu cząstkami α i kwantami γ na różnych poziomach intensywności zaniku luminescencji;
- uczestnictwo w pisaniu publikacji w części dotyczącej zaników scyntylacyjnych oraz korekty manuskryptu po uwagach recenzentów

C2.4 High-performance composite scintillators based on the single crystalline films and crystals of LuAG garnet.

- udział w powstaniu koncepcji pracy;
- prezentacja materiału pracy na konferencji EURODIM 2018;
- analiza właściwości strukturalnych i optycznych otrzymanych warstw i kompozytowych scyntylatorów;
- analityczne opracowanie widm amplitudowych i krzywych zaniku scyntylacyjnego kompozytowych scyntylatorów przy wzbudzeniu cząstkami α oraz kwantami γ ;
- badanie wpływu grubości warstw na właściwości kompozytowych scyntylatorów;
- uczestnictwo w pisaniu publikacji, a także przeprowadzenie korekt manuskryptu po uwagach recenzentów (autor korespondencyjny)

Część III

C3.1 Development of Composite Scintillators Based on Single Crystalline Films and Crystals of Ce³⁺-Doped (Lu,Gd)₃(Al,Ga)₅O₁₂ Mixed Garnet Compounds.

- udział w powstaniu koncepcji pracy;
- prezentacja materiału pracy na konferencji IWASOM 2018;
- opracowanie wyników badań absorbcji, katodoluminescencji, kinetyki zaniku scyntylacji, widm amplitudowych scyntylacji oraz zależności wydajności i rozdzielczości energetycznej scyntylacji od czasu rejestracji sygnału scyntylacyjnego;
- uczestnictwo w pisaniu publikacji, a także przeprowadzenie korekt manuskryptu po uwagach recenzentów (autor korespondencyjny)

C3.2 Epitaxial growth of composite scintillators based on Tb₃Al₅O₁₂:Ce single crystalline films and Gd₃Al_{2.5}Ga_{2.5}O₁₂:Ce crystal substrates.

- udział w powstaniu koncepcji pracy;
- wykonanie pomiarów absorpcji warstw oraz kompozytowych scyntylatorów;
- przygotowanie materiałów (rysunki, tabele) do publikacji;
- uczestnictwo w pisaniu części manuskryptu, dotyczącej właściwości optycznych warstw oraz korekt manuskryptu po uwagach recenzentów

Część IV

C4.1 Composite thermoluminescent detectors based on the Ce³⁺ doped LuAG/YAG and YAG/LuAG epitaxial structures.

- udział w powstaniu koncepcji pracy;
- prezentacja materiału pracy na konferencji LUMDETR 2018;
- opracowanie wyników badań absorbcji, katodoluminescencji, oraz krzywych jarzenia warstw i kompozytowych struktur epitaksjalnych przy wzbudzeniu częstotliwościami α i β ;
- uczestnictwo w pisaniu publikacji oraz przeprowadzenie korekt manuskryptu po uwagach recenzentów (autor korespondencyjny)

C4.2 LPE growth of composite thermoluminescent detectors based on the Lu_{3-x}Gd_xAl₅O₁₂:Ce single crystalline films and YAG:Ce crystals

- prezentacja materiału pracy na konferencji PGSCC 2019;
- opracowanie wyników badań absorbcji, katodoluminescencji, oraz krzywych jarzenia warstw i kompozytowych struktur epitaksjalnych przy wzbudzeniu częstotliwościami α i β ;
- napisanie tekstu publikacji oraz przeprowadzenie korekt manuskryptu po uwagach recenzentów (autor korespondencyjny)

3. Metody eksperymentalne

3.1. Krystalizacja warstw i kompozytowych scyntylatorów metodą LPE

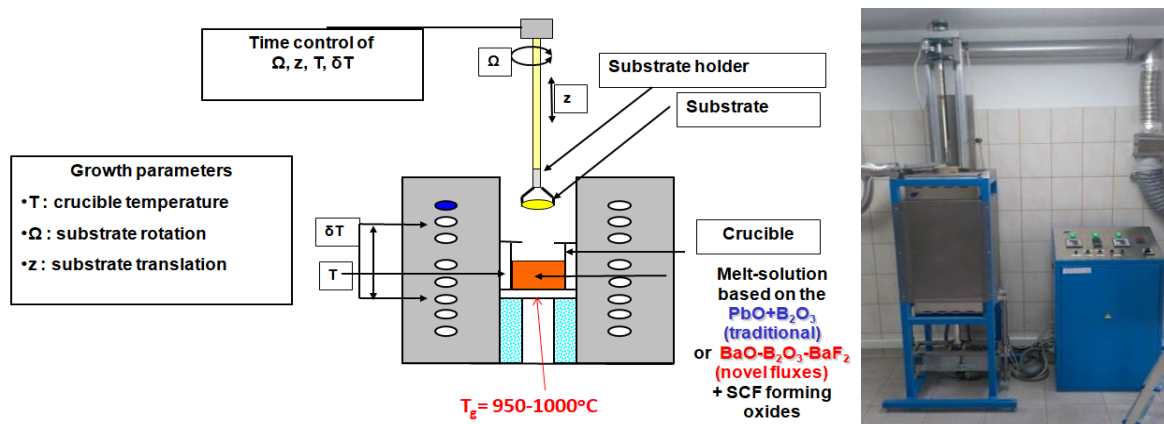
Kompozytowe materiały scyntylacyjne w postaci warstw i kryształów granatów zostały wyhodowane przy użyciu metody LPE w Laboratorium Epitaksji Katedry Materiałów Optoelektronicznych w Instytucie Fizyki Uniwersytetu Kazimierza Wielkiego w Bydgoszczy (Rys. 4). Metoda ta zapewnia możliwość krystalizacji warstw o pożądanej grubości przy uzyskaniu bardzo dobrej jakości strukturalnej i optycznej.

Głównym założeniem metody LPE jest wytworzenie przesycenia w roztworze krystalizowanego w postaci warstw, materiału w ciekłym topniku, co umożliwia wzrost warstwy przy stosunkowo niskich temperaturach (około 1000° C) w porównaniu z warunkami krystalizacji tego materiału ze stopu przy temperaturach ≥ 2000° C. Wsad do krystalizacji warstw przygotowuje się mieszając w odpowiednich proporcjach surowce, zawierające pierwiastki, które wchodzą w skład warstwy. Aby obliczyć ilość poszczególnych pierwiastków, potrzebnych do uzyskania końcowego produktu, potrzebna jest znajomość masy molowej surowca, z której można dobrą ten pierwiastek w odpowiedniej proporcji. Czystość surowców do produkcji warstw monokrystalicznych standardowo powinna wynosić powyżej 99,99 %.

Podczas przygotowywania wsadu do produkcji cieńskich warstw monokrystalicznych granatów metodą LPE oblicza się tzw. współczynniki Blanka-Nielsena i R_1 , R_2 , R_3 i R_4 . Są one odpowiedzialne za stosunki

$$R_1 = \frac{P_{flux_{PbO}}}{P_{flux_{B_2O_3}}} ; R_2 = \frac{\Sigma P_{garnet(dod)}}{\Sigma P_{garnet(oct+tet)}} ; R_3 = \frac{\Sigma P_{garnet}}{\Sigma P_{garnet} + \Sigma P_{flux}} ; R_4 = \frac{\Sigma P_{dopant}}{\Sigma P_{garnet}},$$

gdzie P oznacza masy molowe składników topnika (flux - PbO i B₂O₃), materiału warstwy (garnet) i aktywatora (dopant), które zajmują pozycje dodekaedryczne (dod), octaedyryczne (oct) i tetraedyryczne (tet) sieci granatu.



Rys. 4. Schemat oraz zdjęcie aparatury służącej do krystalizacji warstw monokrystalicznych metodą LPE w Katedrze Materiałów Optoelektronicznych UKW.

Stosunek $R_1=11-12$ określa kinetyczną charakterystykę roztworu i rozpuszczalność tlenków tworzących warstwę. $R_2 = 0.02-0.035$ określa typ fazy granatu jako głównej fazy przy krystalizacji warstw. Natomiast wybór stosunków molowych R_3 i R_4 odpowiednio w zakresach 0.02-0.035 i 0.01-0.15 wiąże się z optymalizacją wydajności scyntylacyjnej warstw.

Aby doprowadzić wsad do postaci ciekłej, jako typowy topnik użyto stopu tlenku ołowiu (PbO) i boru (B_2O_3) w stosunku 90%:10%, który był ustalony doświadczalnie. Stężenie molowe topnika, wyrażone przez współczynnik R_3 , wynosi 95%-97% w stosunku od całego roztworu. Atomy topników, w szczególności jony ołowiów mogą również wchodzić w skład otrzymanych warstw i dawać niepożądane efekty. Ołów jest pierwiastkiem, który jako domieszka wywołuje obniżenie wydajności luminescencji innych domieszek, takich jak Ce^{3+} , Pr^{3+} i Sc^{3+} . Z drugiej strony stopy PbO i BaO charakteryzują się bardzo dobrą rozpuszczającą materiałami, tworzących warstwy, ze stosunkowo niską gęstością oraz dużą płynnością, co jest bardzo ważnym atutem podczas krystalizacji warstw o wysokiej jakości strukturalnej i optycznej.

Przygotowany wsad wybrany według wielkości współczynników R_1-R_4 umieszcza się w platynowych (Pt) tyglach o średnicy $\varnothing = 30-40$ mm. Materiał tygla wybrany został ze względu na wysoką temperaturę topnienia - $1768^{\circ}C$, oraz mały wpływ domieszki Pt na właściwości optyczne warstw.

Podstawowym mechanizmem warunkującym powstawanie monokrystalicznej warstwy na podłożu jest proces przechłodzenia roztworu. W tym celu tygiel umieszcza się w piecu (Rys. 4) rozgrzanym do temperatury $1050-1100^{\circ}C$. W takiej temperaturze materiały po stopieniu tworzą roztwór nienasycony, charakteryzowany przez pewną temperaturę (temperaturę *solidus* lub temperaturę nasycenia T_s), będącą funkcją wielkości współczynnika R_3 . Wraz z obniżeniem temperatury roztworu do temperatury wzrostu T_g w zakresie $950-1050^{\circ}C$ poniżej temperatury solidus T_s , roztwór osiąga stan przechłodzenia, przez co nadmiar substancji rozpuszczonej zaczyna osadzać się na obracającym podłożu wprowadzonym do tygla.

Wymiary podłoża nie powinny przekraczać połowy średnicy tygla, tj. 15-20 mm. Prędkość wzrostu warstwy monokrystalicznej zależy od kilku czynników, głównie

od temperatury wzrostu T_g w stosunku do temperatury nasycenia stopu T_s . W ogólnej postaci grubość warstwy jest proporcjonalna do stopnia przechłodzenia $\Delta T = T_g - T_s$ oraz pierwiastka kwadratowego od prędkości obracania podłoża ω .

3.2. Materiały do produkcji kompozytowych scyntylatorów

W procesie konstrukcji kompozytowych scyntylatorów główną rolę spełnia odpowiednie dopasowanie szeregu właściwości zarówno warstw jak i kryształów. Poniżej w Tabeli 1 przedstawiono wybrane parametry kryształów granatów, używanych jako podłoża do krystalizacji kompozytów metodą LPE, które pozwoliły na wybór najbardziej optymalnych kombinacji do konstrukcji takich scyntylatorów.

Wybrane właściwości warstw granatów, które zostały wymienione w publikacjach autora, podane są w Tabeli 2. Są one niezbędne do oszacowania właściwości różnych typów kompozytowych scyntylatorów, opracowanych w pracy doktorskiej.

Możliwość uzyskania warstw granatu LuAG:Ce na podłożu YAG przy dużym (około -0.8 %) niedopasowaniu sieci warstwa-podłoże jest bardzo ważnym wynikiem opracowania scyntylatorów w postaci warstw monokrystalicznych z dużym współczynnikiem absorbcji kwantów rentgenowskich. Wydajność scyntylacyjna LY warstw LuAG:Ce może być nawet dwa razy większa od wydajności warstwy YAG:Ce.

Inżynieria składu kationów pozwala na otrzymanie warstw z domieszką Tb^{3+} lub Gd^{3+} z znacznie większymi promieniami jonów w porównaniu z promieniami kationów Lu^{3+} . To powoduje zmniejszenie niedopasowania stałych sieci warstwa/położen nawet do zera w wypadku krystalizacji warstw $Lu_{1.5}Gd_{1.5}Al_5O_{12}:Ce$ na podłożach YAG. Wymiana kationów Lu^{3+} na Tb^{3+} i Gd^{3+} powoduje zwiększenie siły pola krystalicznego w pozycjach dodekaedycznych granatu, co daje możliwość przesunięcia emisji jonów Ce^{3+} w LuAG w

Tabela. 1. Wybrane właściwości kryształów, użytych przy konstruowaniu kompozytowych scyntylatorów. Dane pobrane zostały ze stron internetowych producentów od jakich były zakupione podłoża, przygotowane z takich kryształów. *Cieniowanie* - www.crytur.cz (pomarańczowe), www.advatech-uk.co.uk (szare), w nawiasie podano dane literaturowe, które mogą różnić się od danych przedstawionych przez producentów.

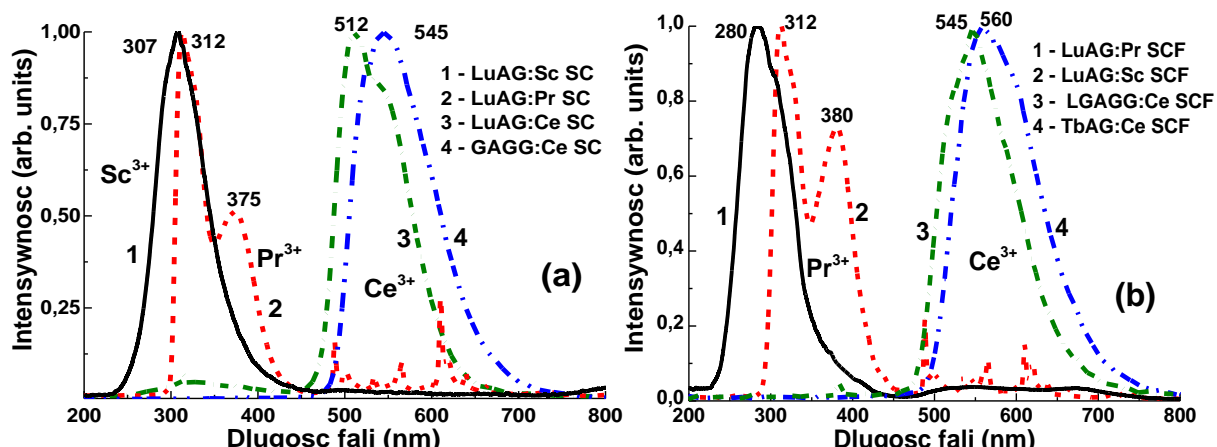
Parametr	YAG:Ce	LuAG:Ce	LuAG:Pr	LuAG:Sc	GAGG:Ce
Gęstość [g/cm ³]	4.57	6.73 ^[12,14]	6.73	6.73 ^[8,13,28,29]	6.63
Efektywna liczba atomowa	74	58.9	62.9	61	54.4
Maksymalna długość fali emisji [nm]	550	535 ^[12,14]	310 ^[12,14,16,27]	280 ^[8,13,28,29]	520
Czas zaniku [ns]	70	70	20(19-28) [12,14,16,27]	245-610 [8,13,28,29]	50-150
Wydajność scyntylacyjna przy wzbudzeniu źródłem γ kwantów ^{137}Cs [ph/MeV]	$30*10^3$	$25*10^3$ ^[12,14]	$15-18*10^3$	$22.5*10^3$ [8,13,28,29]	$40-60*10^3$
LY_α/LY_γ w zakresie 0.5-10 μ s		0.1-145 ^[C2.2]	0.31-0.34 ^[C2.3]	0.38-0.42 ^[C2.4]	0.19-0.2 ^[C3.1]
Rozdzielcość energetyczna [%]	6.7 ^[26]	5.5-7 ^[12,14,26]	<5 ^[12,14,16,27]	7 ^[8,13,28,29]	6.68

Tabela. 2. Wybrane właściwości warstw granatów. m - niedopasowanie stałych sieci warstwy a_{SCF} i podłoża a_{sub} , które wyraża się wzorem $m = (a_{SCF} - a_{sub}/a_{sub}) * 100\%$, λ_{max} - maximum widma emisji, $t_{1/e}$ - czas zaniku scyntylacyjnego do poziomu $1/e$; LY - wydajność scyntylacyjna przy wzbudzeniu α cząstkami źródła ^{239}Pu w porównaniu z wydajnością warstwy wzorcowej YAG:Ce 360 fotoelektronów/MeV (24000 fotonów/MeV) Cieniowanie - własne prace, przypis oznacza numer czasopisma omawianego w rozprawie

Warstwa	Podłoże	$m, \%$	λ_{max}, nm	$t_{1/e}/t_{1/20}, \text{ns}$	LY, %
LuAG:Ce	YAG	-0.82 [11]	509 [11]	53 [11]	205 [11]
LuAG:Pr	YAG	-0.8	305 [12,14]	17 [12,14]	79 [CII]
LuAG:Sc	YAG	-0.8	280 [13]	245; 390 [13]	96 [CII]
Lu _{1.5} Gd _{1.5} Al ₅ O ₁₂ :Ce	YAG	+0.02 [15]	548 [15]	50 [15]	86 [15]
Lu _{1.5} Gd _{1.5} Al _{2.75} Ga _{2.25} O ₁₂ :Ce	GAGG	-0.73 [11]	519 [11]	51/130 [11]	145 [11]
TbAG:Ce	YAG	+0.55[C1.1]	555[C1.1]	242/1645[C1.1]	253-264[C1.1]
	GAGG	-1.29[C1.2]	560[C1.2]	306/1795[C1.2]	195[C1.2]
Tb _{1.5} Gd _{1.5} Al _{2.5} Ga _{2.5} O ₁₂ :Ce (PbO)	GAGG	-0.12[C1.2]	543[C1.2]	333/990[C1.2]	380[C1.2]
Tb _{1.5} Gd _{1.5} Al ₃ Ga ₂ O ₁₂ :Ce (BaO)	GAGG	-1.30[C1.2]	543[C1.2]	228/728[C1.2]	380[C1.2]

zakres długofalowy. Możliwość przekazania energii wzbudzenia do jonów Ce³⁺ przez podsieci kationów Gd³⁺ i Tb³⁺ może także powodować wzrost wydajności scyntylacyjnej (LY) warstw. Znaczący wzrost LY w porównaniu z warstwami LuAG:Ce obserwuje się m. in. w warstwach TbAG:Ce oraz Tb_{1.5}Gd_{1.5}Al_{2.5}Ga_{2.5}O₁₂:Ce (Tabela 2). Jednak wydajność scyntylacyjna warstw Lu_{1.5}Gd_{1.5}Al₅O₁₂:Ce jest stosunkowo niska (Tabela 2).

Na Rys. 5 przedstawiono widma katodoluminescencji, charakteryzujące właściwości luminescencyjne kryształów i warstw granatów, użytych do wytwarzania kompozytowych scyntylatorów. Dominującą emisję jonów Pr³⁺ (przejście promieniste 5d-4f) i Sc³⁺ (domieszka izoelektronowa) w kryształach i warstwach LuAG uzyskuje się w zakresie UV. Luminescencje jonów Ce³⁺ (przejście 5d-4f) w kryształach i warstwach granatów obserwuje się w zakresie widzialnym, przy czym położenie maximum emisji przesuwa się w stronę dłuższych fal z 512 nm w LuAG:Ce do 560 nm w TbAG:Ce w skutek zwiększenia siły pola krystalicznego w pozycjach



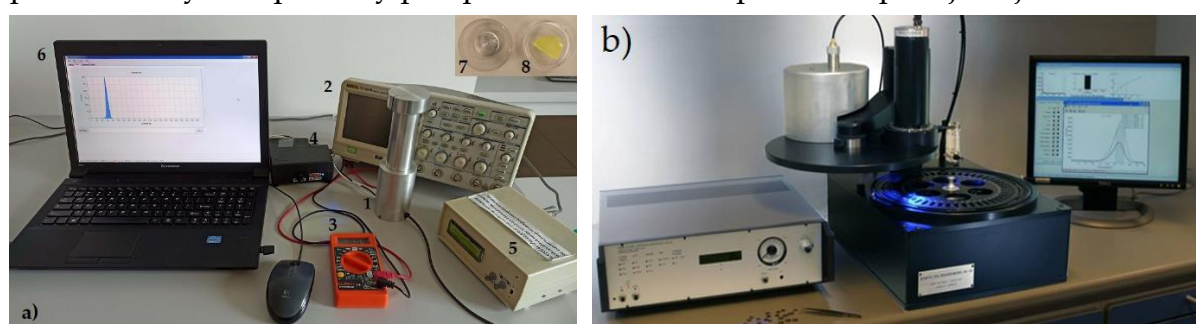
Rys. 5. Znormalizowane widma katodoluminescencji kryształów (SC) (a) i warstw (SCF) (b) granatów LuAG, TbAG, LGAGG i GAGG z domieszkami Ce³⁺, Pr³⁺ i Sc³⁺.

dodekaedrycznych granatu, spowodowanego ze zwiększeniem promieni jonowych odpowiednich kationów ziem rzadkich.

3.3. Metody badan właściwości optycznych kompozytowych scyntylatorów i termoluminoforów

W celu charakteryzacji właściwości optycznych warstw, kryształów oraz kompozytowych scyntylatorów wykorzystano widma absorpcji, widma katodoluminescencji (CL), widma emisji i widma wzbudzenia oraz kinetykę zaniku fotoluminescencji (PL), pomiary wydajności scyntylacyjnej (LY) oraz zaniku scyntylacyjnego przy wzbudzeniu cząstkami α i kwantami γ , a także pomiary krzywych jarzenia (z ang. glow curves) i składu spektralnego termoluminescencji (TL) w zakresie od temperatury pokojowej (z ang. RT) do 600 K. Badania te wykonano na Katedrze Materiałów Optoelektronicznych w Instytucie Fizyki UKW w Bydgoszczy (absorbca, CL, PL, LY oraz zanik scyntylacji przy wzbudzeniu izotopem ^{239}Pu), w Instytucie Fizyki Akademii Nauk w Pradze (LY oraz zanik scyntylacji przy wzbudzeniu źródłem α -cząstek ^{241}Am i kwantów ^{137}Cs) oraz w Instytucie Fizyki Jądrowej w Krakowie (TL).

Widma absorpcyjne badano za pomocą spektrometru Jasco 760 UV-Vis w zakresie 200-1100 nm. Widma KL zmierzono w temperaturze pokojowej (RT) za pomocą mikroskopu elektronowego SEM JEOL JSM-820, dodatkowo wyposażonego w spektrometr Stellar Net pracujący w zakresie 200-925 nm. Wydajność scyntylacyjna i zanik scyntylacji zostało zbadane przy użyciu układu wyposażonego w fotopowielacz Hamamatsu H6521 (PMT), analizator wielokanałowy oraz oscyloskop cyfrowy Tektronix TDS3052 przy wzbudzeniu cząstkami α pochodzącyymi z izotopu ^{239}Pu (5,15 MeV) (Rys. 6). LY warstw porównano ze próbką referencyjną YAG:Ce SCF z wydajnością fotoelektryczną 360 fotoelektronów (phels)/MeV oraz absolutną wydajnością scyntylacyjną 2650 fotonów/MeV, a także z LY odpowiadającym im podłożem. Wszystkie pomiary przeprowadzono w temperaturze pokojowej.



Rys. 6. (a) - układ pomiarowy użyty przy pomiarach wydajności oraz kinetyki zników scyntylacyjnych badanych materiałów przy wzbudzeniu przez α -cząstki ^{239}Pu (5,15 MeV). 1 - tuba z fotopowielaczem i źródłem cząstek α (7), 2 - oscyloskop z możliwością eksportu danych, 3 - multimetr, 4 - zasilacz wysokiego napięcia, 5 - analizator wielokanałowy, 6 - komputer z oprogramowaniem (MCA) służącym do analizy wydajności scyntylacji, 7 - źródło ^{239}Pu , 8 - próbka referencyjna warstwy granatu YAG:Ce, używana do porównawczej analizy wydajności scyntylacyjnej badanych materiałów. (b) - Czytnik Risø TL/OSL-DA-20 w Instytucie Fizyki Jądrowej w Krakowie.

Badania wydajności oraz kinetykę zaników scyntylacyjnych wybranych warstw, kryształów oraz kompozytowych scyntylatorów w szerokim (0.5-10 mikrosekund) zakresie czasu rejestracji sygnału scyntylacyjnego, przeprowadzono przy użyciu zestawu składającego się z hybrydowego fotopowielacza HPMT DEP PP0475B, wzmacniacza ORTEC model 672 oraz analizatora wielokanałowego ORTEC model 972TM w Instytucie Fizyki Czeskiej Akademii Nauk w Pradze. Do pomiaru użyto cząstki α pochodzące z radioizotopu ^{241}Am (energia 5,5 MeV) i kwantów γ z radioizotopu ^{137}Cs (energia 662 keV). Należy tutaj zauważyć, że cząstki α pochodzące z radioizotopów ^{239}Pu i ^{241}Am umożliwiają tylko wzbudzenie warstw o grubości odpowiednio powyżej 12 i 15 mikrometrów, co odpowiada głębokości penetracji tych cząstek w badanych materiałach. Jest to bardzo ważna uwaga ze względu na dobranie odpowiedniej grubości warstwy do konstrukcji kompozytowych scyntylatorów (Rys. 1).

3.4. Wybrane parametry optyczne oraz metody analizy

3.4.1 Wydajność świetlna scyntylacji (z ang. Light yield - LY)

Jednym z parametrów scyntylatora o dobrych właściwościach jest jego wysoka wydajność świetlna scyntylacji (LY). Wyrażona jest w fotonach dzielonych na energię promieniowania photon/MeV i opisuje się wzorem:

$$LY \left(\frac{\text{ph}}{\text{MeV}} \right) = N_{e-h} \cdot S \cdot QE = \left[\frac{10^6}{\beta \cdot E_g} \right] \cdot S \cdot QE \quad (1)$$

gdzie N_{e-h} - jest liczbą wytwarzanych par elektron-dziura na MeV energii wzbudzenia, S - oznacza efektywność przenoszenia par elektron-dziura do jonów aktywatora, β - jest stałą, E_g - jest szerokością pasma wzbronionego (eV), QE - to wydajność kwantowa procesu luminescencji zachodzącego w aktywatorze. Energia potrzebna dotworzenia jednej termalizowanej pary elektron-dziura jest opisana przez β^*E_g , gdzie β - to liczba wskazująca, ile razy energia przerwy pasmowej jest potrzebna do tworzenia jednej pary elektron-dziura. Zostało to szczegółowo omówione przez Bartrama i Lempickiego, którzy wykazali, że β jest bliskie 2.5 dla najlepszych scyntylatorów [24].

3.4.2 Amplitudowe widma scyntylacji

W przypadku badań właściwości scyntylacyjnych warstw, kryształów oraz ich kompozytów warto również zwrócić uwagę na pomiary amplitudowych widm scyntylacji (ang. Pulse Height Spectra). Korzystnym jest to, że, przy wzbudzeniu cząstkami α pozycje głównych pików scyntylacji kompozytowego scyntylatora zasadniczo różnią się od siebie, co oznacza, że, cząstki α wzbudzają tylko część warstwową kompozytu. Natomiast widma otrzymane przy wzbudzeniu kwantami γ pochodząymi od radioizotopu ^{137}Cs pokazują bliskie pozycje głównych pików, co dowodzi, że promienie γ wzbudza głównie podłożę kompozytowego scyntylatora.

3.4.3 Rozdzielcość energetyczna (ER-energy resolution)

Bardzo ważnym jest, aby scyntylator mógł odróżnić fotony γ różniące się energią. Jest to określone przez rozdzielcość energetyczną (ER) układu scyntylator-detektor.

ER określić można wzorem $ER=FWHM/H_o$, gdzie FWHM (z ang. full width at half maximum) oznacza szerokość połówkową piku całkowej absorbcji cząstki lub kwantu o określonej energii, H_o -maksimum wysokości tego piku. Pomiary położenia oraz FWHM pików całkowej absorbcji α cząstek i kwantów γ przeprowadzono za pomocą programu MAESTRO, który wykorzystuje krzywe Gaussa do dopasowań i późniejszych obliczeń FWHM oraz ER.

Rozdzielcość energetyczna, uzyskana dla najnowocześniejszych układów kryształ-scyntylator-detektor na bazie FWHM wynosi zwykle około 5-8%.

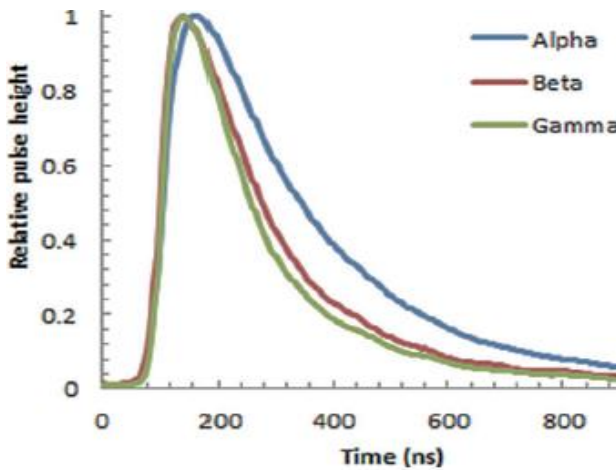
3.4.4 Kinetyka zaniku scyntylacji

Aparatura pomiarowa do badań kinetyki zaniku scyntylacji jest przedstawiona na Rys. 6a.

Podczas badań kinetyki zaniku scyntylacji do wzbudzenia materiałów używa się cząstek α, β- oraz kwantów γ. Każde ze źródeł promieniowania jonizującego w różny sposób oddziaływało ze składnikiem chemicznym warstwy i podłożem, a główna różnica między sygnałami scyntylacyjnymi powstaje na skutek różnic w grubościach i składach chemicznych kompozytu. Grubość warstwy zwykle znajduje się w zakresie 10-80 μm, natomiast grubość podłoża wynosi 0.5–2 mm, m. in., przy wzbudzeniu podłożu LuAG kwantami γ z radioizotopu ^{137}Cs o energii 662 KeV, całkowity współczynnik tłumienia (z ang. *total attenuation coefficient*) wynosi około 0,095 cm²/g (wartość pobrana z danych do kalibracji NIST- www.nist.gov). Taka wartość pozwala na wzbudzenie scyntylacji przeważnie w podłożach tego granatu. Dla cząstek β (elektronów wysokoenergetycznych) ze średnią energią 1.1 MeV, głębokość penetracji w granacie LuAG powinna wynosić około 0.8 mm [25]. Natomiast cząstki α oddziałują z elektronami jonów materialu warstw i ich głębokość penetracji dla granatu LuAG i mieszanych granatów wynosi około 12–15 μm.

Aby obiektywnie porównać różnice pomiędzy krzywymi zaniku scyntylacji niezbędnym narzędziem okazało się obliczenie odpowiednich czasów zaniku intensywności scyntylacji do poziomów 1/e (szybki składnik emisji $t_{1/e}$), oraz 0,1, 0,05 ($t_{1/20}$) lub 0,01 (długotrzymiowe składniki emisji) (Tabela 2), a także stosunku pomiędzy wartościami tych czasów przy wzbudzeniu badanych materiałów cząstками α, β oraz kwantami γ (t_α/t_β , t_α/t_γ lub t_α/t_γ).

Podczas analizy krzywych zaniku scyntylacji materiałów kompozytowych w pierwszej kolejności bardzo ważnym jest przeprowadzenie analizy krzywych zaniku scyntylacji podłoż na bazie kryształów LuAG:Pr, LuAG:Sc LuAG:Ce lub GAGG:Ce przy wzbudzeniu cząstkami α, β i kwantami γ. W literaturze [10] znany jest już przykład takiej analizy dla kryształu scyntylatora $\text{Gd}_3\text{Al}_2\text{Ga}_3\text{O}_{12}:\text{Ce}$ (Rys. 7). Jak wynika z tego rysunku, kinetyka zaniku scyntylacji przy wzbudzeniu cząstkami α oraz cząstkami β i kwantami γ znaczco różni się od siebie. Dzięki temu jest możliwe uzyskanie separacji sygnału dla cząstek alfa, beta oraz kwantów gamma przy użyciu czasu zaniku scyntylacyjnego nawet pojedyńczego kryształu.



Rys. 7. Krzywe zaniku scyntylacyjnego kryształu $\text{Gd}_3\text{Al}_2\text{Ga}_3\text{O}_{12}:\text{Ce}$ przy wzbudzeniu cząstkami alfa, beta i kwantami gamma [10].

Opracowanie kompozytowych scyntylatorów złożonych z dwóch lub więcej materiałów w postaci warstw i kryształów daje szanse na zasadnicze zwiększenie stopnia separacji sygnałów scyntylacyjnych, pochodzących od różnych składników promieniowania jonizacyjnego. Zwiększenie separacji sygnałów od warstw i kryształów, zależy głównie od ich oddziaływanego z kwantami i cząstками oraz różnych właściwości warstw i podłoż użytych przy krystalizacji.

3.4.5 Parametry t_α/t_γ lub t_γ/t_α

Podczas analizy krzywych zaniku scyntylacji przy wzbudzeniu kompozytowego scyntylatora cząstkami α i kwantami γ niezbędnym okazało się określenie parametru t_α/t_γ lub t_γ/t_α . Parametr ten jest wyznaczony na podstawie porównania różnic w czasach zaniku na wybranych poziomach intensywności ($1/e$, 0.1, 0.05 oraz 0.01) dla krzywych zaniku scyntylacji przy wzbudzeniu cząstkami α i kwantami γ (w publikacjach oznaczone jako ratio t_α/t_γ lub t_γ/t_α).

Rys. 1c pokazuje analizę i odczyt wartości t_α i t_γ obu krzywych zaniku dla przykładowej próbki kompozytowego scyntylatora. Wartości t_α i t_γ , odczytane na różnych poziomach rejestracji intensywności scyntylacji, można przedstawić za pomocą wykresu zależności intensywności od stosunku czasu t_α/t_γ lub t_γ/t_α . Uważa się, że stosunek t_α/t_γ lub t_γ/t_α większy od 1.5 jest wystarczający aby zapełnić możliwość czasowej dyskryminacji sygnałów scyntylacyjnych od różnych jego części. Dla tego linią przerywaną na Rys.1c oznacza optymalny przedział czasowy, w którym stosunek t_α/t_γ lub t_γ/t_α jest większy od 1.5.

Podczas analizy krzywych zaniku scyntylacyjnego także wzięto pod uwagę dodatkowy parametr jakim jest przedział czasowy rejestracji scyntylacji. Przy ocenie kompozytowych scyntylatorów oprócz różnicy między sygnałem scyntylacyjnym, pochodzącym z ich warstwowej i krystalicznej części, ważnym jest znalezienie równowagi między wartością stosunku t_γ/t_α oraz wielkością przedziału czasowego. Najbardziej korzystną sytuacją jest dobry rozdział krzywych zaniku (stosunek t_γ/t_α powyżej 1.5) w możliwie jak największym przedziale czasowym (Rys.1c).

3.4.6 Termoluminescencja (TL)

Pomiary TL badanych materiałów w zakresie temperatur 300-600 K wykonano w Zakładzie Dozymetrii Instytutu Fizyki Jądrowej w Krakowie (Rys. 6b). W tym celu wykorzystano automatyczny czytnik Risø TL/OSL-DA20 (Rys.6). Napromieniowanie badanych materiałów dokonano częstotliwościami α (50 Gy) ze źródła ^{241}Am oraz częstotliwościami β (0.97 Gy) ze źródła $^{90}\text{Sr}/^{90}\text{Y}$. W celu rejestracji luminescencji w zakresie widzialnym krzywe TL rejestrowano stosując zielony filtr BG 39).

Podobnie jak w przypadku kinetyki zaniku, warto zauważyc, że krzywe jarzenia przy wzbudzeniu częstotliwościami α odpowiadają wyłącznie części warstwowej kompozytowego materiału ze względu na większą grubość (powyżej 15 μm) w porównaniu z obliczonym przejściem dla częstotliwości α o energii 5.15-5.5 MeV w tych materiałach w zakresie 12-15 μm . Głębokość penetracji częstotliwości β (źródła $^{90}\text{Sr} + ^{90}\text{Y}$) o typowej energii odpowiednio 546 keV i 2280 keV wynosi odpowiednio 0.8 i 1.3 mm, (dla średniej energii 1.1 MeV). Dlatego w przypadku struktur epitakjalnych energia promieniowania β zostanie zaabsorbowana głównie w podłożu. Przykładową analizę krzywych jarzenia TL przedstawia rysunek 1d.

3.4.7. Parametr ΔT

W części IV pracy doktorskiej skupiono się na problemie opracowania kompozytowych detektorów TL do jednoczesnej rejestracji różnych składników mieszanych strumieni jonizacji, z wykorzystaniem różnic między głównymi pikami krzywych jarzenia TL, pochodząymi z części warstwowej oraz podłoża takiego materiału kompozytowego (Rys.1d). Analizując krzywe jarzenia, przy wzbudzeniu kompozytowego materiału TL częstotliwościami alfa oraz beta, należy wyznaczyć położenie pików TL o jak największej intensywności oraz parametr ΔT (Rys.1d).

4. Krótki opis wyników składających rozprawę doktorską

Część I

Początek pracy doktorskiej jest związany z opracowaniem scyntylatorów w postaci warstw monokrystalicznych TbAG:Ce za pomocą metody LPE z wykorzystaniem topnika $\text{PbO}-\text{B}_2\text{O}_3$ nie tylko na „tradycyjnych” podłożach YAG, lecz także na podłożach $\text{Gd}_3\text{Ga}_{2.5}\text{Al}_{2.5}\text{O}_{12}$ (GAGG) ze stałymi sieci odpowiednio 12.01 i 12.232 Å [C1].

W celu scharakteryzowania struktury warstw wykonano pomiary XRD i obliczono niedopasowanie stałych sieci \mathbf{m} warstwy TbAG:Ce i podłoż YAG i GAGG, również odpowiednio + 0.53-0.56 % oraz - 1.29 % (Tabela 2). Te znaczenia wielkości \mathbf{m} podają granice brzegowe w odniesieniu do możliwości krystalizacji warstw TbAG na podłożach granatów. Powodem tego, że warstwa monokrystaliczna TbAG wzrasta na podłożach YAG i GAGG przy takim dużym niedopasowaniu stałych sieci tych granatów jest tworzenie strefy przejściowej w postaci roztworu stałego na granicy rozdziału “warstwa-podłoże”, w celu zmniejszenia tego niedopasowania.

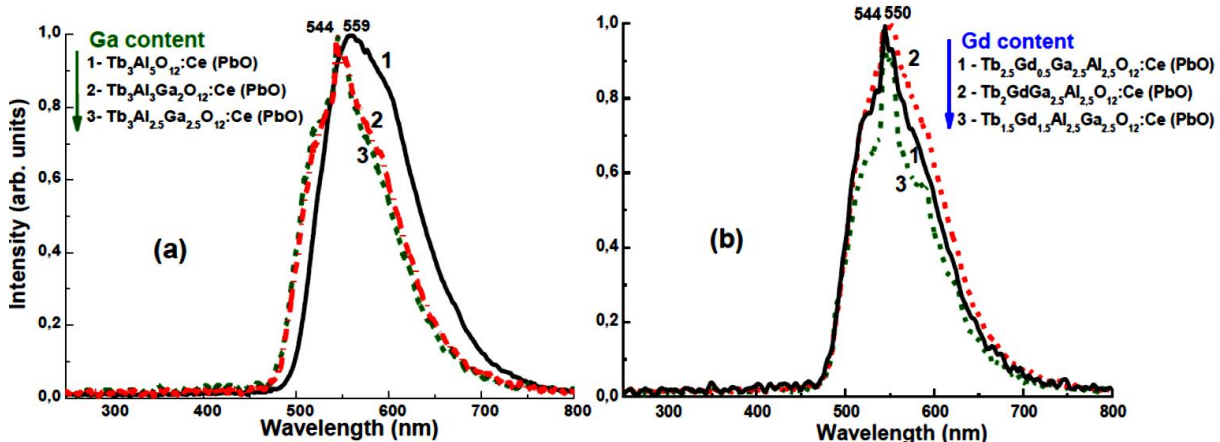
Badania właściwości scyntylacyjnych warstw TbAG:Ce wykazały dobre wyniki. Warstwy TbAG:Ce, krystalizowane na podłożach YAG i GAGG, posiadają do 30%

większą wydajność scyntylacji (Tab. 1) oraz unikatowo niski poziom fosforescencji w porównaniu z warstwami YAG:Ce i LuAG:Ce. Te warstwy także charakteryzują się stosunkowo szybkim zanikiem scyntylacji w zakresie 0-1000 ns (Fig.8a) Z tego powodu warstwy TbAG:Ce są bardzo objęcującym materiałem scyntylacyjnym dla ekranów w detektorach mikrotomograficznych, a także odpowiednim składnikiem do konstruowania kompozytowych scyntylatorów na bazie podłoż GAGG:Ce (Fig.7c).

Inżynieria składu kationów otwiera nowe możliwości w opracowaniu scyntylatorów opartych na warstwach monokrystalicznych mieszanego granatu $Tb_{3-x}Gd_xAl_{5-y}Ga_yO_{12}:Ce$, hodowanych za pomocą metody LPE na podłożach YAG i GAGG z konwencjonalnego topnika $PbO-B_2O_3$, a także z bezolowiowego topnika $BaO-B_2O_3-BaF_2$ (Rys.8 and Tab. 2). Krystalizacja warstw na różnych podłożach z użyciem różnych topników pozwala na optymalizację warunków wzrostu oraz warunków do przekazania energii wzbudzenia od matrycy do aktywatora niezbędnych do uzyskania wysokiej wydajności scyntylacyjnej tych warstw.

W tym celu zastosowano kombinację kationów Gd^{3+} , Tb^{3+} i Ga^{3+} do zmian przerwy energetycznej pomiędzy pasmem przewodnictwa i pasmem walencyjnym granatu oraz poziomów energetycznych 5d jonów Ce^{3+} w prezerwie energetycznej tych materiałów (Rys. 2a). Zmiany te powodują podstawienie kationów Gd^{3+} i Tb^{3+} w pozycjach dodakaedrycznych oraz zastąpienie jonami Ga^{3+} kationów Al^{3+} zarówno w pozycji tetraedrycznej jak i oktaedrycznej granatu (Rys.2a). Wynikiem tych zmian jest przesunięcie widma luminescencji jonów Ce^{3+} w granacie $Tb_{3-x}Gd_xAl_{5-y}Ga_yO_{12}:Ce$ do zakresu niebieskiego lub czerwonego w skutek wzrostu zawartości odpowiednio Ga^{3+} (Rys. 8a) lub Gd^{3+} (Rys. 8b).

W tak skomplikowanym materiale, jakim jest granat $Tb_{3-x}Gd_xAl_{5-y}Ga_yO_{12}:Ce$ o dużej koncentracji kationów Gd^{3+} i Tb^{3+} , obserwuje się złożony kaskadowy transfer energii wzbudzenia $Gd^{3+} \rightarrow Tb^{3+} \rightarrow Ce^{3+} \rightarrow Tb^{3+}$. Powodem takiego transferu jest nakładanie się pasm emisji Gd^{3+} i Tb^{3+} oraz pasm absorpcji jonów Ce^{3+} w zakresie UV, oraz pasm emisji jonów Ce^{3+} i pasm absorpcji Tb^{3+} w zakresie niebieskim. Dla tego



Rys. 8. (a) – znormalizowane widma KL warstw $Tb_3Al_{5-y}Ga_yO_{12}:Ce$ (PbO) przy stężeniu Ga w zakresie $y=0.2.5$ (a) oraz warstw $Tb_{5-x}Gd_xAl_{2.5}Ga_{2.5}O_{12}:Ce$ (PbO) przy stężeniu Gd w zakresie 0,5-1,5 (b).

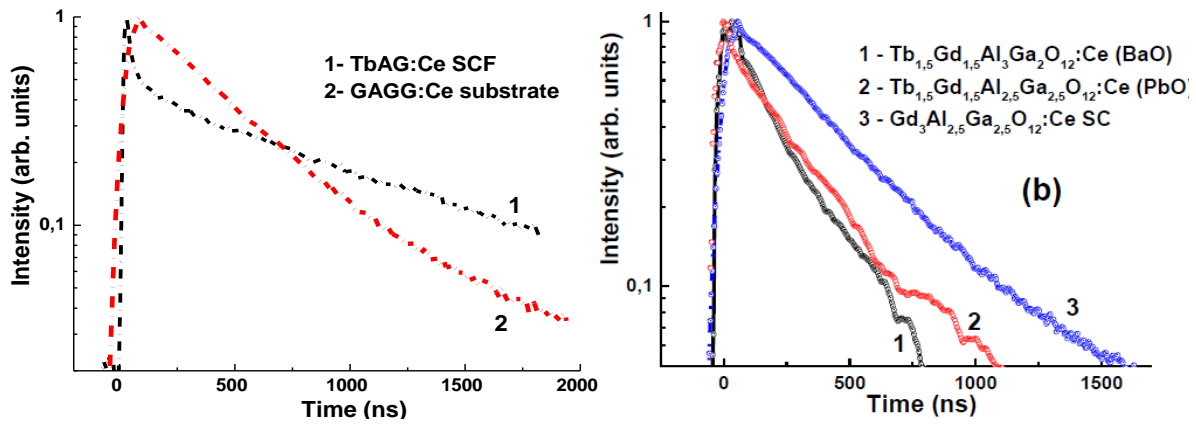


Fig. 9. Znormalizowane krzywe zaników scyntylacyjnych warstw TbAG:Ce (a, 1), Tb_{1.5}Gd_{1.5}Al₂Ga₃O₁₂:Ce (BaO) (1b) i Tb_{1.5}Gd_{1.5}Al_{2.5}Ga_{2.5}O₁₂:Ce (PbO) (2b) w porównaniu z kryształem Gd₃Al_{2.5}Ga_{2.5}O₁₂:Ce (2a; 3b).

optymalizacja zawartości Gd³⁺ i Tb³⁺ oraz Ga³⁺ w granacie Tb_{3-x}Gd_xAl_{5-y}Ga_yO₁₂:Ce, gdzie x=1.5 oraz y=2–2.5, powoduje znaczną poprawę wydajności scyntylacyjnej warstw ze względu na korzystniejsze warunki transferu energii wzbudzenia, spowodowane zmianami wielkości przerwy pasmowej i struktury energetycznej jonów Ce³⁺.

Warstwy Tb_{3-x}Gd_xAl_{5-y}Ga_yO₁₂:Ce (PbO), wyhodowane ze stopu na bazie topnika PbO, wykazują bardzo wysoką jakość strukturalną jednak nieco mniejszą wydajność scyntylacyjną w skutek wpływu jonów ołowiu. Natomiast warstwy, hodowane ze stopu na bazie topnika BaO wykazują doskonałe właściwości scyntylacyjne, jednak nieco mniejszą jakość struktury z powodu dużej gęstości tego topnika. Tym nie mniej, wydajność scyntylacyjna warstw Tb_{1.5}Gd_{1.5}Al_{2.5}Ga_{2.5}O₁₂:Ce (PbO) i Tb_{1.5}Gd_{1.5}Al₃Ga₂O₁₂:Ce (BaO) jest o 10 % większa od wydajności najlepszych warstw LGAG:Ce (BaO) i GAGG:Ce (BaO), opracowanych w [11].

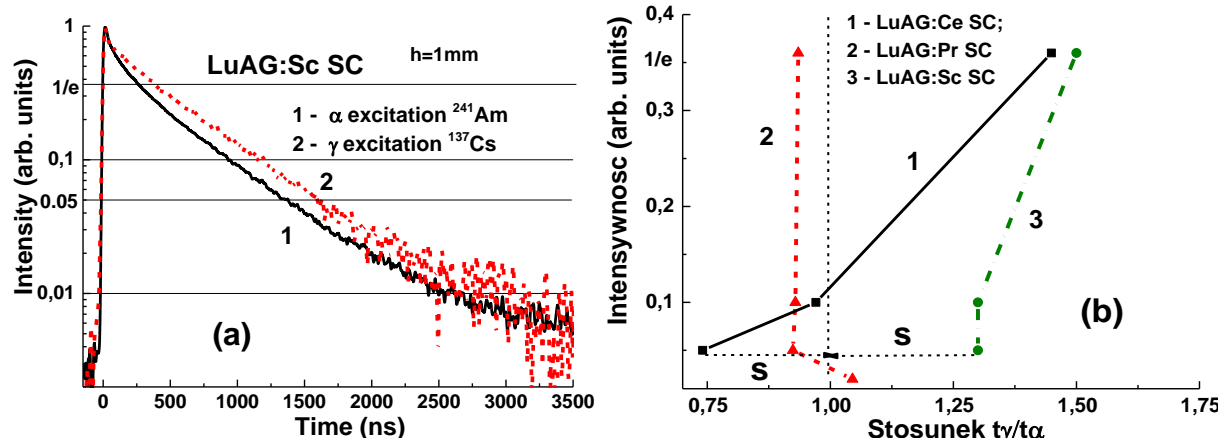
Bardzo ważnym jest fakt, że zanik scyntylacji warstw Tb_{1.5}Gd_{1.5}Al_{2.5}Ga_{2.5}O₁₂:Ce (PbO), a zwłaszcza Tb_{1.5}Gd_{1.5}Al₃Ga₂O₁₂:Ce (BaO) w zakresie 0–2 μs jest szybszy o co najmniej 2 razy w porównaniu z kryształem GAGG:Ce (Rys. 9b). W ten sposób kombinacje warstw Tb_{3-x}Gd_xAl_{5-y}Ga_yO₁₂:Ce i kryształu GAGG:Ce także mogą być stosowane do tworzenia kompozytowych scyntylatorów do jednoczesnej rejestracji różnych składników mieszanych wiązek jonizacyjnych. Koncept pracy takiego typu kompozytowego scyntylatora można opierać się na separacji sygnałów pochodzących od warstwy i podłoża za pomocą różnic w kinetyce zaniku ich scyntylacji (Rys. 1c).

Część II

Pierwszym podejściem, stosowanym w pracy doktorskiej do stworzenia kompozytowych scyntylatorów przy użyciu technologii LPE było wykorzystanie już istniejącej wiedzy o dobrze znanych scyntylatorach w postaci kryształów i warstw monokrystalicznych opartych na domieszkowanych jonami Pr³⁺, Sc³⁺ i Ce³⁺ granat LuAG (Tabele 1 i 2). Przeprowadzone badania różnych typów struktur epitaksjalnych na bazie LuAG z domieszkami jonów Pr³⁺, Sc³⁺ i Ce³⁺ udowodniły możliwość jednoczesnej rejestracji cząstek α i kwantów γ w sposób separacji kinetyki zaniku scyntylacyjnego warstwy i podłoża.

Podłoża na bazie kryształów LuAG [C.2.1-C.2.3]. W pierwszej fazie konstruowania kompozytowych scyntylatorów bardzo ważna jest analiza krzywych zaniku scyntylacji podłów na bazie kryształów LuAG z domieszkami jonów Ce^{3+} , Pr^{3+} i Sc^{3+} przy wzbudzeniu częstotliwościami α i kwantami γ . Ta analiza została przeprowadzona na podłożach LuAG:Ce, LuAG:Pr i LuAG:Sc o grubości 1 mm (Rys.10).

Badania te pokazują stosunkowo małą różnicę w krzywych zaniku scyntylacji dla podłoża LuAG:Pr (Rys.11d). Nieco większą różnicę obserwuje się dla podłów LuAG:Ce i LuAG:Sc, gdzie stosunek t_γ/t_α odpowiednio dochodzi nawet do 1.45 i 1.5 przy spadku intensywności scyntylacji do poziomu $1/e$ (Rys.10a,b). Jest to związane z osobliwością interakcji cząstek α i kwantów γ z wymienionymi materiałami, co powoduje także dużą różnicę w ich wydajności scyntylacyjnej, wyrażonej przez stosunek LY_α/LY_γ (Table 1).

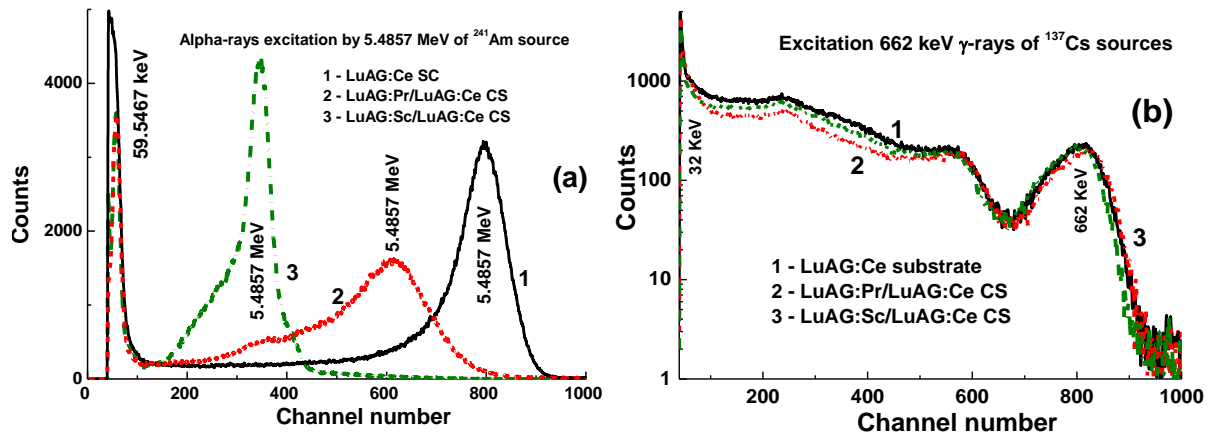


Rys. 10. (a) - kinetyka zaników scyntylacji podłów LuAG:Sc przy wzbudzeniu częstotliwościami α ze źródła ^{241}Am (1) i kwantami γ ze źródła ^{137}Cs (2). (b) – wartość stosunku t_γ/t_α dla różnych poziomów spadku intensywności scyntylacji dla podłów LuAG:Ce (1), LuAG:Pr (2) i LuAG:Sc (3). Parametr S określa odległość od miejsca, gdzie stosunek t_γ/t_α wynosi 1, co oznacza, że nie ma różnic w krzywych zaniku scyntylacyjnego.

Kompozytowe scyntylatory na bazie podłów LuAG:Ce [C2.1, C2.2]. W pierwszej kolejności przy użyciu metody LPE zostały opracowane dwa typy kompozytowych scyntylatorów LuAG:Pr SCF/LuAG:Ce SC i LuAG:Sc SCF/LuAG:Ce SC na bazie podłów LuAG:Ce.

Na Rys. 11 podane są widma amplitudowe kompozytowych scyntylatorów LuAG:Pr SCF/LuAG:Ce SC i LuAG:Sc SCF/LuAG:Ce SC przy rejestracji α -cząstek i γ -kwantów odpowiednio ze źródeł ^{241}Am i ^{137}Cs . Główny pik na Rys. 11a odpowiada całkowitej energii absorpcji α -cząstek o energii 5.5 MeV, natomiast pik w lewej części widma związany z absorpcją γ kwantu źródła ^{137}Cs o energii 59.65 keV. Ważnym na Rys. 11a jest to, że położenie głównych pików w wypadku wzbudzenia α częstotliwościami warstw LuAG:Pr i LuAG:Sc jest różne w wymienionych typach kompozytowych scyntylatorów, w porównaniu z podłożem LuAG:Ce. To znaczy, że α -częstki rejestrują się wyłącznie w warstwowej części kompozytowego scyntylatora i nie wzbudzają podłów.

W wypadku wzbudzenia kompozytowych scyntylatorów LuAG:Pr/LuAG:Ce i LuAG:Sc/LuAG:Ce promieniowaniem γ ze źródła ^{137}Cs , dodatkowy i główny pik w



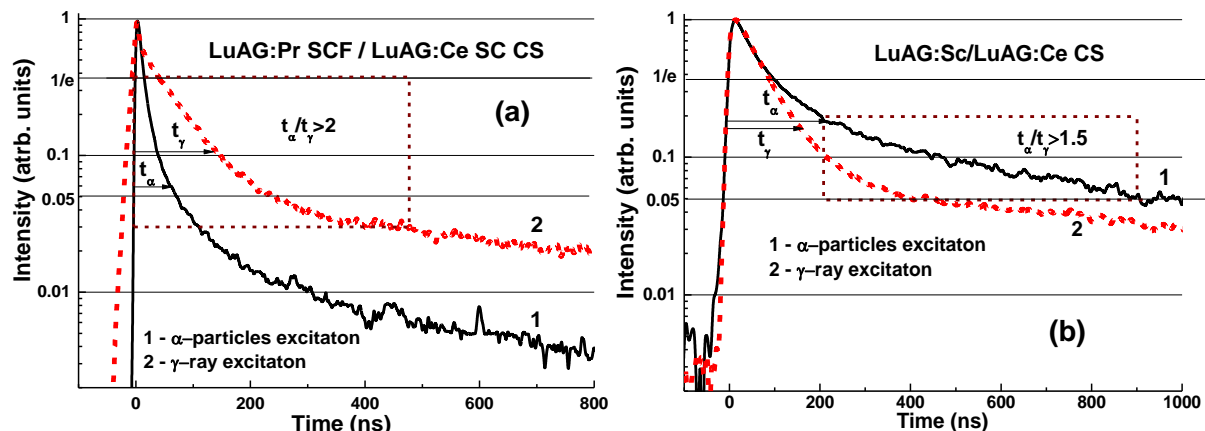
Rys. 11. Widma amplitudowe scyntylacji podłoża LuAG:Ce (1) oraz kompozytowych scyntylatorów LuAG:Pr SCF/LuAG:Ce SC (2) i LuAG:Sc SCF/LuAG:Ce SC (3) przy wzbudzeniu α cząstkami ze źródła ^{241}Am (5.5 MeV) (a) i γ kwantami ze źródła ^{137}Cs (662 keV) (b) [C2.2].

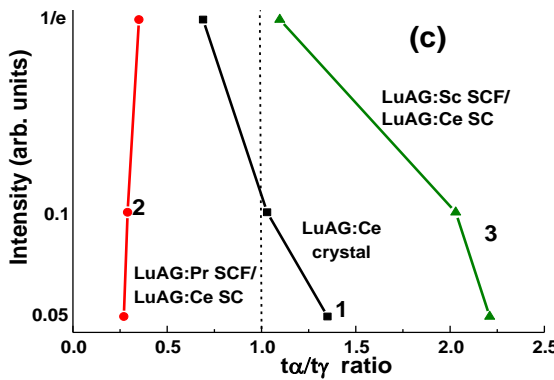
amplitudowych widmach odpowiadają całkowitej absorpcji γ kwantów o energii 32 keV i 662 keV (Rys.11b). Jednak ważnym tutaj jest to, że główne fotopiki na Rys.11b mają podobne położenie zarówno w wypadku wzbudzenia obojęga kompozytowych scyntylatorów, jak i podłoża LuAG:Ce. To znaczy, że γ kwanty przeważnie absorbują się w podłożu kompozytowych scyntylatorów.

Przy wzbudzeniu kompozytowych scyntylatorów LuAG:Pr SCF/LuAG:Ce SC i LuAG:Sc SCF/LuAG:Ce SC cząstками α i kwantami γ , obserwuje się wyraźną różnicę w kinetyce zaniku scyntylacji (Rys.12 a, b). Ta różnica charakteryzuje się stosunkiem odpowiednich czasów zaniku t_α/t_γ , które dla wymienionych scyntylatorów są równe 0.27–0.35 i 1.1–2.2 przy spadku intensywności scyntylacji z poziomu 1/e do poziomu 0.05 (Rys.12 c).

Kompozytowy scyntylator LuAG:Pr SCF/LuAG:Ce SC ma pewną przewagę w stosunku do struktury LuAG:Sc SCF/LuAG:Ce SC w związku z tym, że sygnały scyntylacyjne od warstwy i podłoża pierwszego typu kompozytu mogą być separowane z większym stosunkiem czasów zaniku t_α/t_γ w całym czasowym przedziale z 0 do 700 ns przy spadku intensywności scyntylacji od poziomu 1/e do poziomu 0.05 (Rys.12a).

Jednak dla drugiego typu kompozytowego scyntylatora LuAG:Sc SCF/LuAG:Ce SC sygnały scyntylacyjne od warstwy i podłoża także mogą być separowane nawet



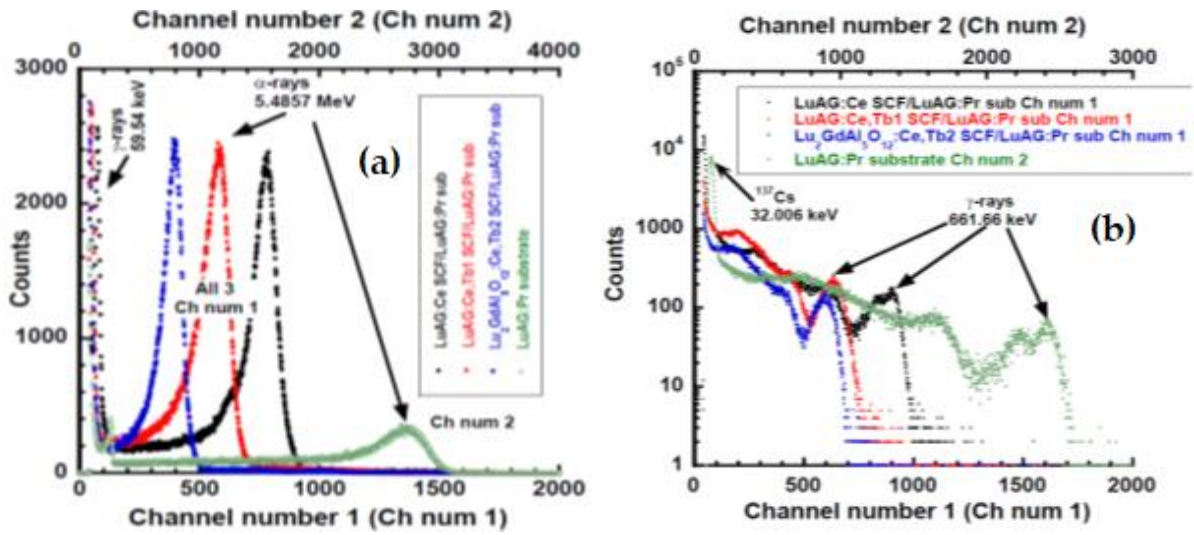


Rys. 12. Kinetyka zaników scyntylacji kompozytowych scyntylatorów LuAG:Pr SCF/LuAG:Ce SC (a) i LuAG:Sc SCF/LuAG:Ce SC (b) przy wzbudzeniu α cząstkami ze źródła ^{241}Am (5.5 MeV) (1) i kwantami γ ze źródła ^{137}Cs (662 keV) (2). (c) – wartość stosunku t_α/t_γ dla różnych poziomów spadku scyntylacji dla wymienionych wyżej typów kompozytowych scyntylatorów (1, 2) w porównaniu z podłożem LuAG:Ce (3) [C2.1,C2.2]. *z większym stosunkiem czasów zaniku t_α/t_γ , lecz w wąskim czasowym interwale z 200 do 900 ns i w mniejszym przedziale spadku intensywności scyntylacji od pomiędzy poziomami 0.2 i 0.05 (Rys.12b). To świadczy o tym, że obydwa typy kompozytowych scyntylatorów mogą być z sukcesem stosowane do rozdzielczej rejestracji α -ciastek i γ -kwantów w mieszanych wiązkach jonizacyjnych.*

Kompozytowe scyntylatory na bazie podłoża LuAG:Pr [C2.3]. W kolejnym etapie badań, z użyciem metody LPE, został opracowany zestaw kompozytowych scyntylatorów opartych na podłożu LuAG:Pr. Na materiał scyntylatora warstwowego zostały wybrane mieszane granaty $\text{Lu}_{2-x}\text{GdTb}_x\text{Al}_5\text{O}_{12}:\text{Ce}$ i $\text{Lu}_{3-x}\text{Tb}_x\text{AG}:\text{Ce}$ o wartości x w zakresie 0.15–2.285. Zmiana stężenia kationów w wymienionych składach granatów powoduje korzystne zmiany ich właściwości scyntylacyjnych, potrzebne do konstrukcji kompozytowych scyntylatorów.

Widma amplitudowe kompozytowych scyntylatorów LuAG:Ce SCF/LuAG:Pr SC, $\text{Lu}_{2.85}\text{Tb}_{0.15}\text{AG}:\text{Ce}$ SCF/LuAG:Pr SC i $\text{Lu}_{1.7}\text{GdTb}_{0.3}\text{AG}:\text{Ce}$ SCF/LuAG:Pr SC przy rejestracji cząstek α i kwantów γ od źródeł ^{241}Am i ^{137}Cs podane są na Rys. 13. Rożne położenie głównych pików w wypadku wzbudzenia α cząstkami warstw LuAG:Ce, $\text{Lu}_{2.85}\text{Tb}_{0.15}\text{AG}:\text{Ce}$ i $\text{Lu}_{1.7}\text{GdTb}_{0.3}\text{AG}:\text{Ce}$ w wymienionych typach kompozytowych scyntylatorów w porównaniu z podłożem LuAG:Pr świadczy o tym, że cząstki α absorbowują się wyłącznie w warstwowej części kompozytowego scyntylatora. Natomiast przy wzbudzeniu wymienionych kompozytów kwantami γ ze źródła ^{137}Cs główne piki tez wykazują różne położenie w stosunku do podłoża LuAG:Pr (Rys.13b); przy czym wielkość tej różnicy zależy od typu, grubości i wydajności warstwowych scyntylatorów (Rys.13a). To świadczy o znaczącym wpływie warstw na bazie LuAG na absorbcje promieniowania γ w badanych typach kompozytowych scyntylatorów, opartych na podłoże LuAG:Pr.

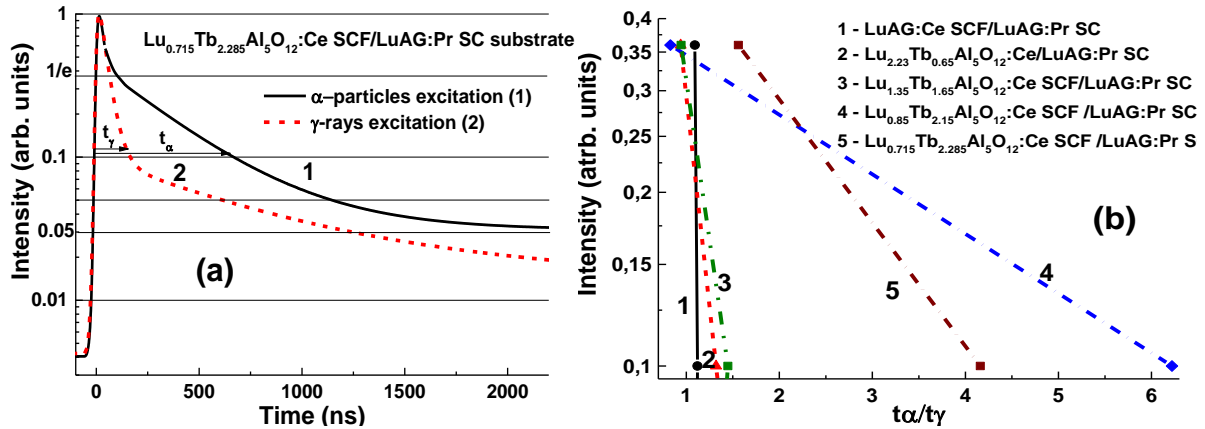
Ze względu na mało satysfakcjonujący wynik separacji krzywych zaników scyntylacyjnych podłoża LuAG:Pr i warstw $\text{Lu}_{3-x}\text{Tb}_x\text{AG}:\text{Ce}$ SCF przy koncentracjach Tb $x=0.15-0.3$, dobrym rozwiązaniem okazała się kryształizacja kompozytowych scyntylatorów na bazie warstw mieszanych granatów Lu_{3-x}Tb_xAG:Ce SCF/LuAG:Pr SC



Rys. 13. Widma amplitudowe scyntylacji podłożą LuAG:Pr oraz kompozytowych scyntylatorów LuAG:Ce SCF/LuAG:Pr SC, Lu_{2.85}Tb_{0.15}AG:Ce SCF/LuAG:Pr SC i Lu_{1.7}Gd Tb_{0.3}AG:Ce SCF/LuAG:Pr SC przy wzbudzeniu α -cząstkkami źródła ²⁴¹Am (5.5 MeV) (a) i γ -kwantami źródła ¹³⁷Cs (662 keV) (b) [C2.3].

przy dużym stężeniu kationów Tb³⁺ ($x=1.65-2.285$). W tym celu także zbadano wpływ domieszki jonów Tb³⁺ na właściwości scyntylacyjne warstw granatów Lu_{3-x}Tb_xAG:Ce ($x=0.65, 1.05$ i 2.15), krystalizowanych na podłożach YAG przy wzbudzeniu cząstkkami α . Na postawie tych badań przypuszczone, że w przypadku udanej krystalizacji warstw Lu_{3-x}Tb_xAG:Ce przy $x>1.5$ na podłożu LuAG:Pr, separacja krzywych zaniku scyntylacji kompozytowego scyntylatora przy wzbudzeniu cząstkkami α i kwantami γ może być znacznie większa. Krystalizacja takich próbek wiązała się jednak z wysokim nieodpasowaniem stałych sieci krystalicznych warstwa-podłoże powyżej 1%.

Natomiast dzięki pomyślnie przeprowadzonej krystalizacji warstw metodą LPE powstały dwa nowe zestawy kompozytowych scyntylatorów na bazie warstw Lu_{3-x}Tb_xAG:Ce SCF z zawartością Tb $x=1.6-1.65$ i $2.275-2.285$ i podłożu LuAG:Pr ze znacząco



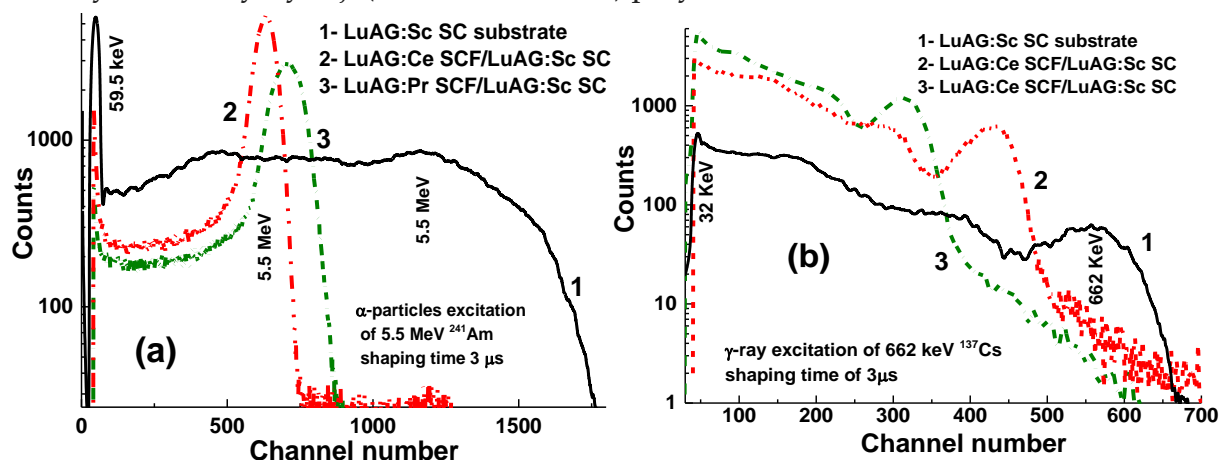
Rys. 14. (a) - kinetyka zaników scyntylacji kompozytowego scyntylatora Lu_{0.715}Tb_{2.285}Al₅O₁₂:Ce SCF/LuAG:Pr SC (b) przy wzbudzeniu α -cząstkkami ze źródła ²⁴¹Am (5.5 MeV) (1) i kwantami γ ze źródła ¹³⁷Cs (662 keV) (2). (b) – wartość stosunku t_γ/t_α dla różnych poziomów spadku intensywności scyntylacji dla kompozytowych scyntylatorów Lu_{3-x}Tb_xAl₅O₁₂:Ce SCF/LuAG:Pr SC przy zawartości Tb x=0 (1), 0,65 (2), 1,65 (3), 2,15 (3) i 2,285 (4) [C2.3].

lepszymi właściwościami scyntylacyjnymi w porównaniu z kompozytami na bazie warstw z niskim stężeniem Tb (Fig.14). m. in, przy wzbudzeniu kompozytowego scyntylatora Lu_{0.715}Tb_{2.285}AG:Ce SCF /LuAG:Pr SC częstotliwościami α i kwantami γ , obserwuje się dużą różnicę w kinetyce zaniku scyntylacji (Rys.14 a), która charakteryzuje się stosunkiem odpowiednich czasów zaniku t_α/t_γ w zakresie 1.56-4.16 przy spadku intensywności scyntylacji z poziomu 1/e do poziomu 0.1 (Rys.14 b).

Kompozytowe scyntylatory na bazie podłoża LuAG:Sc [C2.4]. Ostatnie zestawy kompozytowych scyntylatorów opartych na strukturach epitaksjalnych LuAG to kompozytowe scyntylatory na bazie podłoża LuAG:Sc i warstw LuAG:Ce i LuAG:Pr. W tej serii zbadano po dwie próbki z wyżej wymienionych kompozytowych scyntylatorów o różnych grubościach warstw LuAG:Ce i LuAG:Pr SCF w zakresie 12-30 μm , hodowanych na podłożach LuAG:Sc.

Widma amplitudowe kompozytowych scyntylatorów LuAG:Ce SCF/LuAG:Sc SC, i LuAG:Pr SCF/LuAG:Sc SC oraz podłoże LuAG:Sc przy wzbudzeniu α -częstotliwościami od źródła ^{241}Am (5.5 MeV) i kwantami γ od ^{137}Cs (662 keV) podane są na Rys.15. Warto zauważyć, że przy rejestracji częstek α pozycje głównych pików są położone z pewnymi przesunięciami względem siebie oraz względem podłoża (Rys.15a). Oznacza to, że częstotliwości pobudzają tylko część warstwowych materiałów kompozytowych. Przy rejestracji kwantów γ kompozytowymi scyntylatorami także obserwuje się różne pozycje głównych pików (Rys.15b), co oznacza, że wzbudzenie następuje nie tylko podłoża, ale również części warstwowych. Z tego powodu położenie głównych pików, odpowiadające całkowitej absorpcji kwantów γ o energii 662 keV źródła ^{137}Cs zależy także od typu, grubości i wydajności scyntylacyjnej warstw, co wpływa również na podstawowe właściwości scyntylacyjne opracowanych kompozytów.

Dla kompozytowych scyntylatorów LuAG:Ce SCF/LuAG:Sc SC i LuAG:Pr SCF/ LuAG:Sc SC porównano różnice w czasach zaniku na różnych poziomach spadku intensywności scyntylacji (1/e, 0.1, 0.05 i 0.01) przy wzbudzeniu częstotliwościami α i kwantami

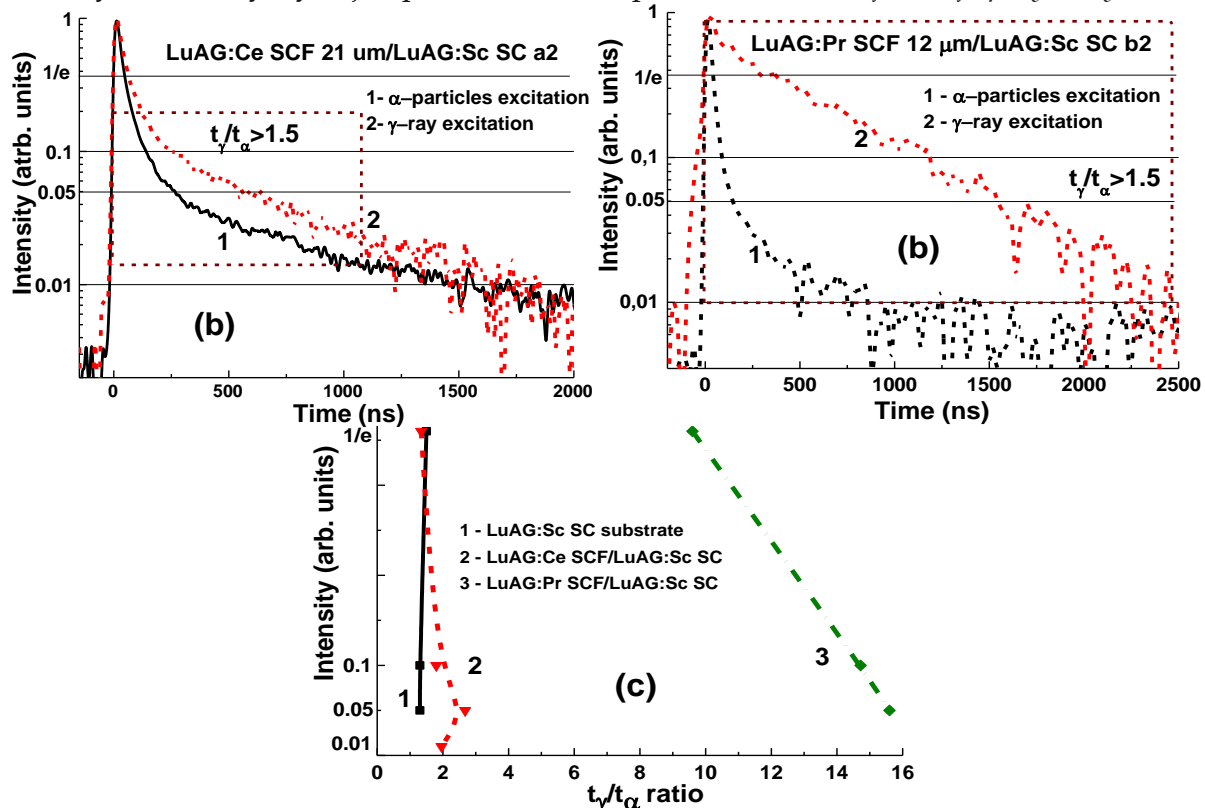


Rys. 15. Amplitudowe widma kompozytowych scyntylatorów LuAG:Ce SCF /LuAG:Sc SC (1) i LuAG:Pr SCF/LuAG:Sc SC (2) oraz substratu LuAG:Sc (3) zmierzone w przedziale czasu 3 μs przy wzbudzeniu częstotliwościami α ze źródła ^{241}Am (5.5 MeV) (a) i przy wzbudzeniu kwantami γ ze źródła ^{137}Cs (662 keV) (b) [C2.4].

γ (Rys.16). Dobór próbek o różnej grubości warstw w zakresie 12-30 μm pozwolił także na analizę wpływu tego czynnika na właściwości scyntylacyjne oraz możliwość poprawy separacji krzywych zaniku przy różnych typach wzburzenia. W przypadku wymienionych kompozytów optymalne oddzielenie sygnału scyntylacyjnego, pochodzącego od warstwy i podłoża, szczególnie dla struktury LuAG:Pr SCF/ LuAG:Sc SC, można uzyskać w całym zakresie czasowym (Rys.16b).

Jak widać z Rys.16, kompozytowy scyntylator LuAG:Ce SCF/LuAG:Sc SC także posiada zdolność do separowanej rejestracji cząstek α i kwantów γ . Przy wzbudzeniu tego typu kompozytowego scyntylatora częstotliwościami $t_\gamma/t_\alpha > 1.5$, obserwuje się dobrą separację krzywych zaniku scyntylacji (Rys.16a), która charakteryzuje się stosunkiem odpowiednich czasów zaniku t_γ/t_α w zakresie 1.34-1.96 przy spadku intensywności scyntylacji z poziomu 1/e do poziomu 0.01, która jednak nie jest zbyt wysoka w porównaniu nawet z samym podłożem LuAG:Sc (Rys.10a i Rys.16c).

Jednak najlepsze właściwości scyntylacyjne zostały uzyskane dla kompozytowego scyntylatora LuAG:Pr SCF/LuAG:Sc SC przy grubości warstwy 12 μm i podłoża 1mm. Ten typ scyntylatora charakteryzuje się unikalną dobrą separacją krzywych zaniku scyntylacji przy rejestracji cząstek α i kwantów γ . Dla tego kompozytu stosunek odpowiednich czasów zaniku t_γ/t_α jest bardzo duży w zakresie 9,6-15,6 przy spadku intensywności scyntylacji z poziomu 1/e do poziomu 0,05, co jest najlepszym wynikiem



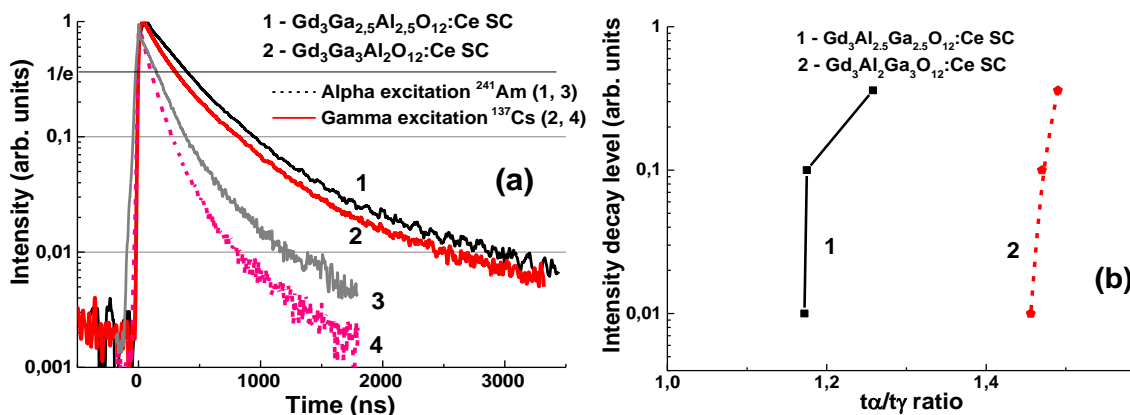
Rys. 16. Kinetyka zaników scyntylacji od kompozytowych scyntylatorów LuAG:Ce SCF/ LuAG:Sc SC (a) i LuAG:Pr SCF/ LuAG:Sc SC (b) przy rejestracji α cząstek ze źródła ^{241}Am (1) i kwantów γ ze źródła ^{137}Cs . (c) – wartość stosunku t_γ/t_α dla różnych poziomów spadku intensywności scyntylacji dla struktur epitaksjalnych LuAG:Ce SCF/LuAG:Sc SC (2) i LuAG:Pr SCF/LuAG:Sc SC (3) w porównaniu z podłożem LuAG:Sc (1) [C2.4].

ze wszystkich opracowanych typów kompozytowych scyntylatorów na bazie struktur epitakjalnych LuAG z domieszkami jonów Ce^{3+} , Pr^{3+} i Sc^{3+} .

Część III

Sukcesy związane z krystalizacją warstw i kryształów mieszanych granatów $(Lu,Gd,Tb)_3(Al,Ga)_5O_{12}:Ce$ otwierają nowe możliwości do konstruowania nowych typów kompozytowych scyntylatorów opartych na warstwach i kryształach tych materiałów. Rozważając proponowane składы scyntylatorów kompozytowych na bazie mieszanych granatów, szczególną uwagę zwrócono na poprawę zdolności absorpcyjnej warstw i kryształów odpowiednio cząstek α i kwantów γ , oraz ich wydajności scyntylacyjnej w porównaniu z opracowanymi składami kompozytów na bazie LuAG. Po pierwsze, w skutek mniejszej gęstości i liczby efektywnej, warstwy mieszanych granatów mają mniejszą zdolność do absorbacji kwantów γ w porównaniu z warstwami na bazie granatu LuAG, co może znaczco zmniejszyć zaburzenie sygnału scyntylacyjnego przez warstwy od podłoż GAGG:Ce przy rejestracji innego typu promieniowania. Po drugie, granaty $Gd_3Al_{5-x}Ga_xO_{12}$ ($x=2-3$), przy zachowaniu dużej gęstości i wysokiej liczby efektywnej, charakteryzujące znacznie większą wydajnością scyntylacyjną przy wzbudzeniu γ kwantami (^{137}Cs , 662 keV) na poziomie do 50 000 foton/MeV w porównaniu z podłożami LuAG:Ce, LuAG:Pr i LuAG:Sc (Tabela 1). Z tych powodów warstwy i kryształy mieszanych granatów są także idealną podstawą do uzyskiwania coraz lepszych typów kompozytowych scyntylatorów.

Podłoża na bazie kryształów GAGG:Ce [C3.1]. Przed rozpoczęciem konstruowania kompozytowych scyntylatorów na bazie warstw i kryształów mieszanych granatów została przeprowadzona analiza krzywych zaniku scyntylacji dwóch typów podłoż na bazie $Gd_3Al_{5-x}Ga_xO_{12}:Ce$ z koncentracją Ga=2.5 i 3 o grubości 1 mm przy wzbudzeniu cząstkami α i kwantami γ (Rys.17). Zaobserwowano, że przy wzbudzeniu kwantami γ kinetyka zaniku scyntylacji tych podłoż jest systematycznie szybsza niż w przypadku wzbudzenia cząstkami α , co jest spowodowane specyficzną interakcją cząstek α i γ



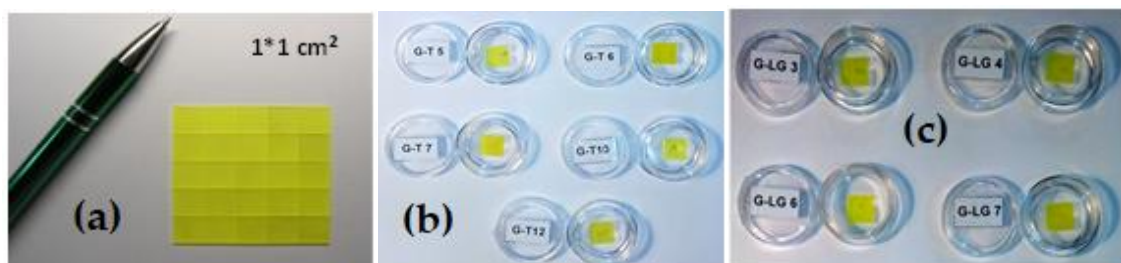
Rys. 17. (a) - kinetyka zaników scyntylacji podłoż $Gd_3Ga_{2.5}Al_{2.5}O_{12}:Ce$ (1, 2) i $Gd_3Ga_3Al_2O_{12}:Ce$ (3, 4) przy wzbudzeniu α cząstkami ze źródła ^{241}Am (5,5 MeV) (1, 3) i kwantami γ ze źródła ^{137}Cs (662 keV) (2, 4) [C3.1]. (b) – wartość stosunku τ_γ/τ_α dla różnych poziomów spadku intensywności scyntylacji dla wymienionych wyżej typów podłoż.

kwantów z materiałem scyntylatora. Różnica w wydajności scyntylacyjnej podłoż GAGG :Ce przy tych typach wzbudzenia, wyrażona przez stosunek LY_α/LY_γ jest rozwa 0.195-0.2.

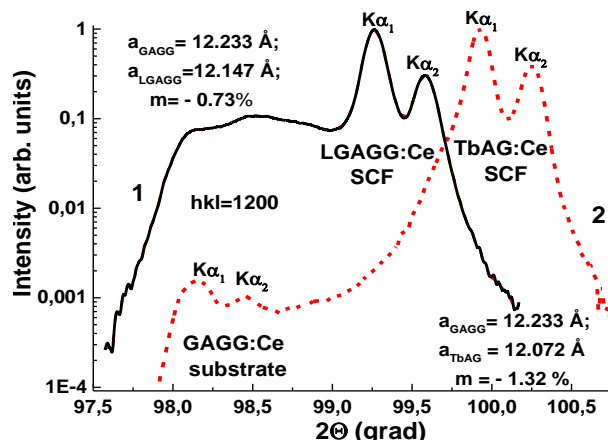
Jak widać na Rys.17a, zwiększenie koncentracji Ga z $x=2.5$ do 3 powoduje znaczące przyspieszenie zaniku scyntylacji dla obuch typów wzbudzenia, a także zwiększenie stopnia separacji kinetyki zaników scyntylacyjnych przy rejestracji cząstek α i kwantów γ (Rys.18b). m. in., znacznie większa różnica krzywych zaniku obserwuje się dla podłoż GAGG:Ce ze stężeniem Ga=3.0, gdzie stosunek t_γ/t_α dochodzi nawet do 1.46-1.49 przy spadku intensywności scyntylacji od poziomu 1/e do 0.01 w porównaniu wielkością tego stosunku 1.17-1.26 dla podłoż GAGG:Ce ze koncentracją Ga=3.0 (Rys.17b).

Kompozytowe scyntylatory na bazie podłoża GAGG:Ce [C3.1, C3.2]. Informacja o możliwości krystalizacji metodą LPE warstw mieszanych granatów na podłożach GAGG [C1.1 i C1.2], były omówione w części II i podane w Tabeli 2. Ta informacja pozwoliła na pomyślnie prowadzenie krystalizacji dwóch typów kompozytowych scyntylatorów na bazie podłoż GAGG:Ce oraz warstw LAGG:Ce i TbAG:Ce (Rys.18).

Pierwszym krokiem było określenie właściwości strukturalnych otrzymanych scyntylatorów LGAGG:Ce SCF/GAGG:Ce oraz TbAG:Ce SCF/GAGG:Ce na podłożach GAGG:Ce. m. in., niedopasowanie stałych sieci warstwa-podłoże wyniosło dla tych kompozytów odpowiednio -0.73% oraz -1.32% (Rys.19), co okazało się wystarczające do otrzymania dobrej jakości optycznej warstw, a także uzyskania ich odpowiednich właściwości scyntylacyjnych, spełniających wymogi do konstruowania



Rys.18. Podłoża GAGG:Ce (a) oraz kompozytowe scyntylatory TbAG:Ce SCF/GAGG:Ce SC (b) i TbAG:Ce SCF/GAGG:Ce SC (c).



Rys. 19. Dyfraktogramy epitaksjalnych struktur LGGAG:Ce SCF/GAAG:Ce SC (1) i TbAG:Ce SCF/GAGG:Ce SC (2).

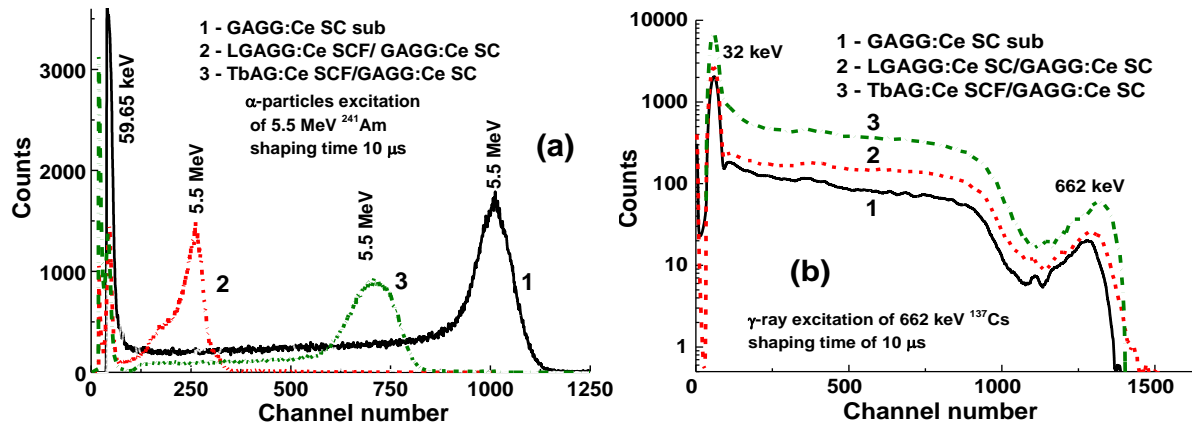
wysokowydajnych kompozytowych scyntylatorów. Ważnym jest także to, że kryształizacja warstw LAGG:Ce i TbAG:Ce na podłożach GAGG:Ce z zawartością Ga $x=3.0$ nie powiodła się w skutek dużego (powyżej 2%) niedopasowania stałych sieci warstwa-podłoże.

Wyniki, podane w części I, odnoszące się do kompozytowych scyntylatorów na bazie podłów granatów LuAG:Pr i LuAG:Sc wyraźnie pokazują, że jednoczesne wzbudzenie kwantami γ warstwy i podłoża znaczco wpływa na ich sumaryczne widma amplitudowe (Rys.13b i 15b) oraz krzywe zaników scyntylacyjnych (Rys.14 i 16). Jednak dla kompozytowych scyntylatorów, opartych na mieszanych granatach LGAGG:Ce SCF/GAGG:Ce SC i TbAG:Ce SCF/GAGG:Ce SC, ta sytuacja jest odmienna w korzystny sposób. Cząstki α wzbudzają tylko warstwy LGAGG:Ce i TbAG:Ce w tych typach kompozytowych scyntylatorów, co pokazuje różnicę w położeniach głównych pików odpowiednich widm amplitudowych w stosunku do podłoża GAGG:Ce (Rys.20a). Przy wzbudzeniu kwantami γ charakterystyczne są bliskie pozycje głównych pików zarówno kompozytowych scyntylatorów, jak i podłoża GAGG:Ce, a to oznacza, że wzbudzone zostaje głównie podłoże w tych kompozytach (Rys.20b).

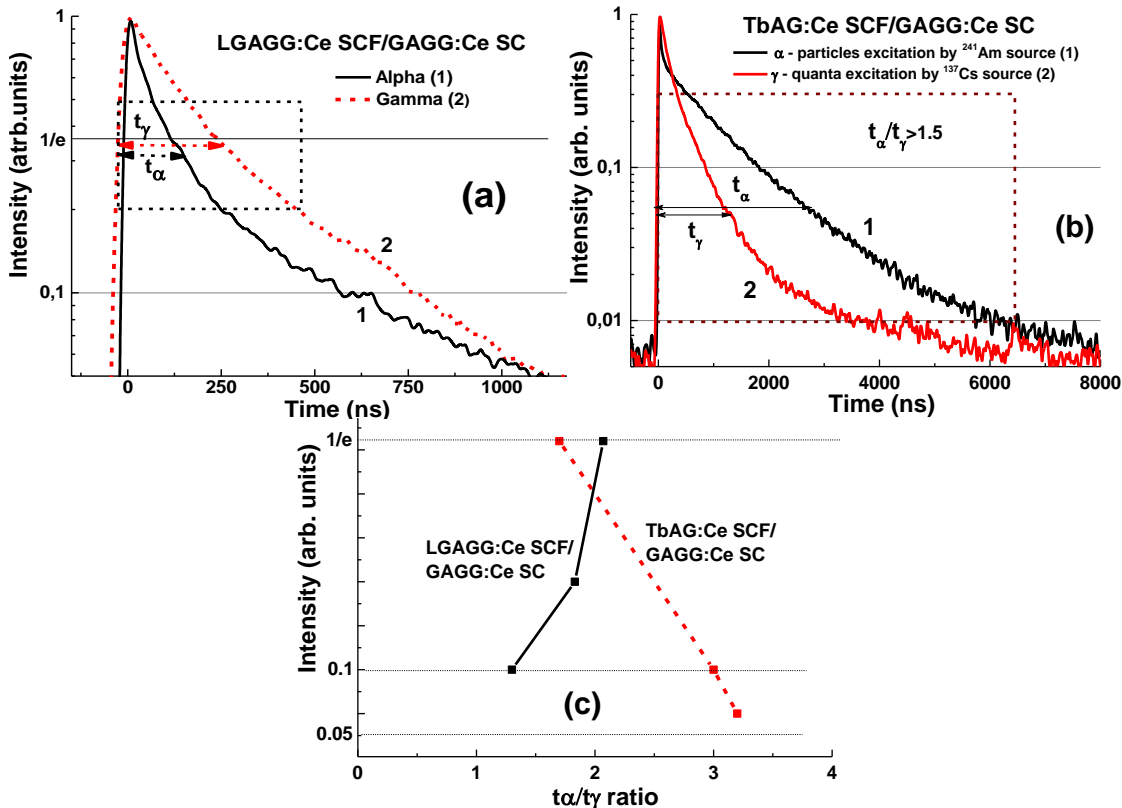
Przy wzbudzeniu kompozytowych scyntylatorów LGAGG:Pr SCF/GAGG:Ce SC i TbAG:Ce SCF/GAGG:Ce SC α cząstками i γ -kwantami, obserwuje się dużą różnicę w krzywych zaniku scyntylacji (Rys.21a, b). Ta różnica charakteryzuje się stosunkiem odpowiednich czasów zaniku t_α/t_γ , które dla wymienionych typów scyntylatorów są równe 1.3–2.07 i 1.7–3.2 przy spadku intensywności scyntylacji z poziomu 1/e do poziomów odpowiednio 0.1 i 0.05 (Rys.21c).

Dla kompozytowego scyntylatora LGAGG:Ce SCF/GAGG:Ce SC sygnały scyntylacyjne od warstwy i podłoża także mogą być separowane z wysokim stosunkiem czasów zaniku t_α/t_γ , w krótkim czasowym interwale z 0 do 500 ns, lecz w nieco węższym przedziale spadku intensywności scyntylacji pomiędzy poziomami 1/e i 0.1 (Rys.21a).

Kompozytowy scyntylator TbAG:Ce SCF/GAGG:Ce SC posiada bardziej korzystne właściwości w stosunku do struktury LGAGG:Ce SCF/GAGG:Ce SC w związku z tym, że sygnały scyntylacyjne od warstwy i podłoża tego typu kompozytu mogą być



Rys. 20. Widma amplitudowe kompozytowych scyntylatorów LGAGG:Ce SCF/GAGG:Ce SC (2) i TbAG:Ce SCF/GAGG:Ce SC (3) oraz podłoża GAGG:Ce (1), zmierzone w przedziale czasu 10 μs przy wzbudzeniu cząstkami α ze źródła ^{241}Am (5,5 MeV) (a) i przy wzbudzeniu kwantami γ ze źródła ^{137}Cs (662 keV) (b).



Rys. 21. Kinetyka czasów zaników scyntylacji od kompozytowych scyntylatorów LGAGG:Ce SCF/GAGG:Ce SC (a) i TbAG:Ce SCF/GAGG:Ce SC (b) przy rejestracji α cząstek ze źródła ^{241}Am (1) i γ kwantów ze źródła ^{137}Cs (2). (c) – wartość stosunku t_γ/t_α dla różnych poziomów zaniku intensywności scyntylacji dla tych dwóch typów kompozytów.

separowane z większym stosunkiem czasów zaniku t_α/t_γ w szerokim czasowym przedziale z 0 do 6000 ns przy spadku intensywności scyntylacji od poziomu $1/e$ do poziomu 0.01 (Rys. 21b).

Te wyniki świadczą o tym, że oba typy kompozytowych scyntylatorów na bazie warstw i kryształów mieszanych granatów mogą być sukcesywnie stosowane do rozdzielczej rejestracji α -ciastek i γ -kwantów w złożonych wiązkach jonizacyjnych.

Część IV

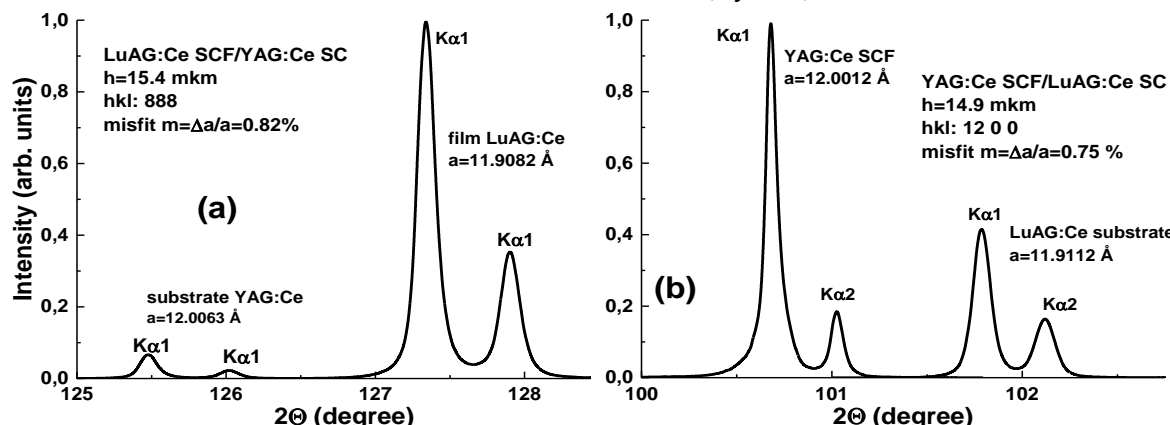
Opracowane w części II i III kompozytowe scyntylatory na bazie wybranych struktur epitaksjalnych granatów, wytworzonych metodą LPE, wykazują zdolności do jednoczesnej rejestracji składników mieszanych wiązek jonizujących w sposób pomiaru kinetyki zaniku sygnałów scyntylacyjnych, pochodzących od warstwy i podłoża kompozytowego scyntylatora przy wzbudzeniu cząstками α i kwantami γ . Natomiast detekcja cząstek β w mieszanych wiązkach jonizujących z energiami w dość szerokim zakresie od keV do MeV nie może być dokonana przy pomocy takiego kompozytowego scyntylatora w sposób rejestracji krzywych zaniku scyntylacji. Użycie kompozytowych scyntylatorów, pracujących w trybie "in situ", jest także utrudnione przy rejestracji niskich dawek promieniowania oraz przy długotrwałej ekspozycji badanych obiektów na promieniowanie jonizujące.

Rozwiążanie tego problemu stało się motywacją do rozważań nad innym podejściem do wytwarzania kompozytowych detektorów do jednoczesnej rejestracji

różnych składników promieniowania jonizującego. Nową możliwością okazało się wykorzystanie różnic między krzywymi termoluminescencji (TL), pochodząymi od warstwy i podłoża kompozytowego materiału, wytwarzanego za pomocą metody LPE.

Celem tej części pracy doktorskiej jest pokazanie możliwości stworzenia kompozytowych detektorów TL, opartych na strukturach epitaksjalnych dobrze znanych materiałów optycznych, którymi są warstwy i kryształy na bazie domieszkowanych jonami Ce^{3+} granatów LuAG i YAG. Takie detektory TL mogą być używane do jednoczesnej detekcji cząstek α i β oraz kwantów X lub γ .

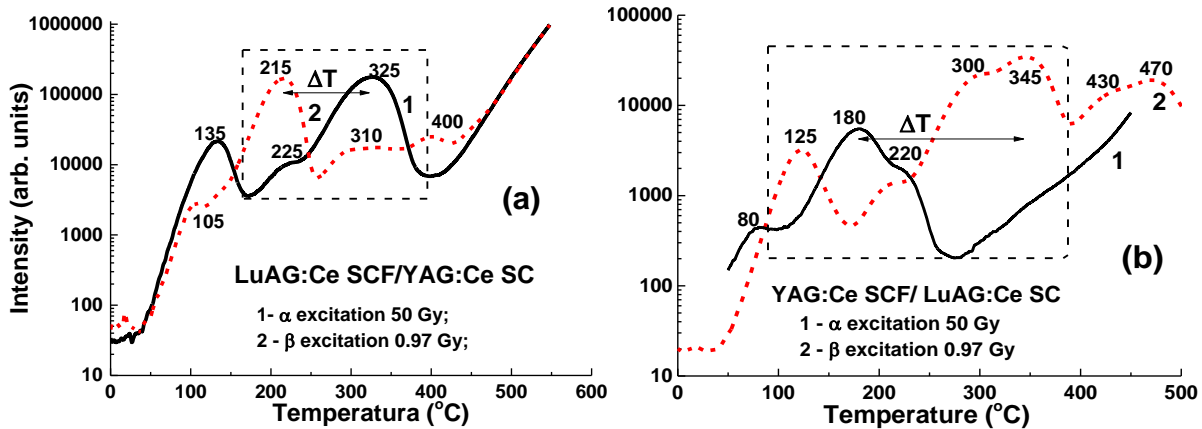
Kompozytowe materiały TL LuAG:Ce SCF/YAG:Ce SC i YAG:Ce SCF/LuAG:Ce SC [C4.1]. Pierwszymi prototypami kompozytowych materiałów TL były struktury epitaksjalne granatów YAG:Ce SCF/LuAG:Ce SC i LuAG:Ce SCF/ YAG:Ce SC. M. in., bardzo dużym sukcesem technologicznym było udowodnienie możliwości krystalizacji takich kompozytów metodą LPE przy dużym niedopasowaniu stałych sieci krystalicznej materiałów warstwy i podłoża, które wyniosiło 0.8 % dla struktur LuAG:Ce SCF/YAG:Ce SC i 0.75 % dla struktur YAG:Ce SCF/LuAG:Ce SC (Rys.22).



Rys. 22. Dyfraktogramy epitaksjalnych struktur LuAG:Ce SCF/YAG:Ce SC (a) i YAG:Ce SCF/LuAG:Ce SC (b).

Konstruowanie tych kompozytów było także oparte na poprzednich badaniach, dotyczących zaobserwowania różnic we właściwościach TL warstw i podłoż tych granatów. Te różnice spowodowane są różnymi warunkami krystalizacji warstw i kryształów, a mianowicie dużą różnicą w temperaturze wzrostu, składzie atmosfery gazowej oraz typach defektów i domieszek. Biorąc pod uwagę, że jony Ce^{3+} typowo są domieszkami do pułapkaowania dziur, za piki TL w warstwach i kryształach odpowiadają centrom pułapkaowania elektronów. Takimi centrami w granatach mogą być luki po tlenie oraz ich agregaty z innymi defektami, w szczególności defektami podstawienia w kryształach lub jonami ołowiu w warstwach tych materiałów [30].

Nadrzędnym zadaniem był odczyt głównych pików TL, pochodzących od warstw i kryształów YAG:Ce i LuAG:Ce w kompozytowych detektorach TL przy ich ekspozycji cząstkami α i β . Korzystając z wiedzy zawartej we wcześniejszych publikacjach dotyczących opracowania kompozytowych scyntylatorów było wiadomo, że cząstki α źródła ^{241}Am (5,5 MeV) są całkowicie zatrzymywane w części warstwowej (SCF) kompozytu, natomiast cząstki β źródła $^{90}\text{Sr} + ^{90}\text{Y}$ o średniej energii 1,1 MeV mogą być absorbowane przez podłoża YAG o grubości 1,3 mm i LuAG 0,8 mm. Dlatego sygnały



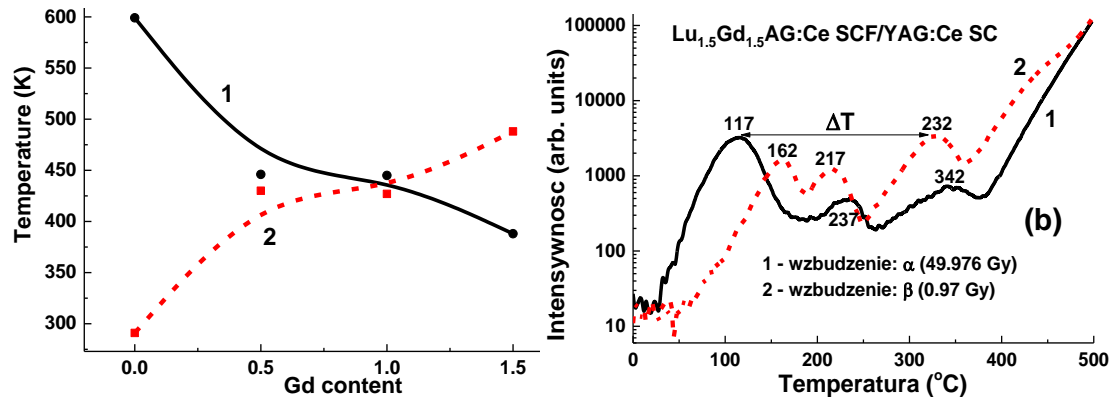
Rys. 23. Krzywe jarzenia TL kompozytowych materiałów TL LuAG:Ce SCF/YAG:Ce SC (a) i YAG:Ce SCF/LuAG:Ce SC (b) po napromieniowaniu cząstkami α (1) i β (2).

TL od warstw i podłoż obu badanych kompozytowych struktur odpowiadają głównie rejestracji cząstek α i odpowiednio cząstek β .

Główne piki dla kompozytów LuAG:Ce SCF/YAG:Ce SC obserwuje się w temperaturach 325°C i 215°C po napromieniowaniu odpowiednio cząstkami α i β (Rys. 23a), natomiast dla struktur YAG:Ce SCF/LuAG:Ce SC odpowiednie piki znajdują się odpowiednio w 180°C i 345°C (Rys. 23b). Dlatego różnica ΔT między głównymi pikami TL, używana jako miara separacji tych dwóch cząstek dla wymienionych typów kompozytów odpowiednio jest równa 110°C i 165°C .

Kompozytowe materiały TL $\text{Lu}_{3-x}\text{Gd}_x\text{Al}_5\text{O}_{12}:\text{Ce}$ SCF/YAG:Ce SC [C4.2]. Zakończone sukcesem opracowanie pierwszych typów kompozytowych materiałów TL pozwoliło na dokonanie modyfikacji składów warstw LuAG:Ce w tym typie kompozytu poprzez dodanie do składu Gd.

W strukturach $\text{Lu}_{3-x}\text{Gd}_x\text{Al}_5\text{O}_{12}:\text{Ce}$ SCF/YAG:Ce SC, gdzie $x=0-1,5$ (Rys. 24), różnica między położeniami głównego piku TL po napromieniowaniu cząstkami α i β stopniowo wzrasta wraz ze wzrostem zawartości Gd w zakresie 0-1,5. W ten sposób



Rys. 24. (a) - zależność położenia głównego piku TL $\text{Lu}_{3-x}\text{Gd}_x\text{Al}_5\text{O}_{12}:\text{Ce}$ SCF/YAG:Ce SC po wzbudzeniu α -cząstkami (1) oraz różnicy między głównymi pikami TL od warstwowej i krystalicznej części struktur $\text{Lu}_{3-x}\text{Gd}_x\text{Al}_5\text{O}_{12}:\text{Ce}$ SCF/YAG:Ce SC po wzbudzeniu α (^{241}Am) i β ($^{90}\text{Sr}+^{90}\text{Y}$) cząstkami (2). (b) - krzywe jarzenia TL kompozytowego materiału po wzbudzeniu cząstkami α (1) i β (2).

uzyskana wartość różnicy (ΔT) w położeniu głównych pików TL jest znacznie większa od tej otrzymanej dla struktury epitaksjalnej LuAG:Ce SCF/YAG:Ce SC. Parametr ΔT wzrósł z poziomu 110 do 215°C.

Prowadzone badania, opisane w części IV, pozwoliły na otrzymanie kompostowych materiałów ze zdolnością do jednoczesnej rejestracji promieniowania alfa i beta w mieszanych wiązkach jonizujących, wykorzystując zjawisko TL.

Opracowane struktury epitaksjalne stały się protopopami do konstruowania nowej generacji kompozytowych detektorów TL, opartych na strukturach epitaksjalnych różnych związków tlenkowych, krystalizowanych przy użyciu metody LPE.

5. Podsumowanie rozprawy doktorskiej

Celem pracy doktorskiej była weryfikacja możliwości realizacji *trzech różnych podejść do konstruowania kompozytowych scyntylatorów i materiałów TL do jednoczesnej detekcji cząstek i kwantów w mieszanych wiązkach jonizujących, z wykorzystaniem metody LPE*. *Pierwsze podejście* polega na zmianie domieszek w warstwach i podłożu tej samej matrycy w postaci granatu LuAG, co powoduje ich różne właściwości scyntylacyjne (część II). *Drugie podejście* oparte jest na wykorzystaniu różnych typów warstw i kryształów mieszanych granatów, domieszkowanych jonami Ce³⁺ z bardzo odmiennymi właściwościami scyntylacyjnymi (części I i III). W tabeli 2 przedstawiono zestawienie kompozytowych scyntylatorów opracowanych w części II i III pracy. Pogrubiona linią zostały rozdzielone poszczególne wyniki z odpowiadających im publikacji.

Tabela 2. Porównanie właściwości scyntylacyjnych różnego typu kompozytów na bazie struktur epitaksjalnych granatów.

Kompozytowy scyntylator	Najlepsza wartość t_α/t_γ	Poziom intensywności dla najlepszego stosunku t_α/t_γ	Optymalna wartość intensywności	Zakres czasowy (ns)
LuAG:Pr SCF /LuAG:Ce SC	3.6	0.1	0.03-0.4	0-700
LuAG:Sc SCF /LuAG:Ce SC	2.2	0.05	0.05-0.2	200-900
LuAG:Ce SCF/LuAG:Pr SC	1.1	0.05	0.05-0.2	60-320
Lu _{2.85} Tb _{0.15} AG:Ce SCF/LuAG:Pr SC	1.2	0.05	0.1-0.02	200-1500
Lu _{1.75} Tb _{0.3} AG:Ce SCF/LuAG:Pr SC	1	-	-	-
Lu _{1.35} Tb _{1.65} AG:Ce SCF/LuAG:Pr SC	1.4	0.1	0.05-0.2	250-1000
Lu _{0.715} Tb _{2.285} AG:Ce SCF/LuAG:PrSC	4.2	0.07	0.05-0.36	100-3000
LuAG:Ce SCF/ LuAG:Sc SC	2.7	0.05	0.02-0.2	250-110
LuAG:Pr SCF/ LuAG:Sc SC	15.6	0.05	0.01-0.5	0-2500
TbAG:Ce SCF/GAGG:Ce SC	3	0.05	0.05-0.2	450-3700
LGAGG:Ce SCF/GAGG:Ce SC	2	1/e	0.2-0.5	50-500

Trzecie podejście polega na wykorzystaniu różnych właściwości termoluminesencyjnych warstw i kryształów prostych i mieszanych granatów, domieszkowanych jonami Ce³⁺ (część IV).

Najważniejsze wnioski rozprawy doktorskiej

1. Używając metody epitaksji z cieczy z roztworów na bazie topników PbO i BaO, pokazano możliwość syntezy na podłożach YAG i GAGG nowych typów efektywnych scyntylatorów w postaci warstw monokrystalicznych mieszanych granatów $(\text{Gd},\text{Tb},\text{Lu})_3(\text{Al},\text{Ga})_5\text{O}_{12}:\text{Ce}$ z bardzo wysoką zdolnością do absorpcji promieniowania rentgenowskiego. Opracowane warstwowe scyntylatory mogą być zastosowane przed wszystkim jako ekrany scyntylacyjne w detektorach mikrotomograficznych. Jednocześnie takie warstwy oraz struktury epitaksjalne na bazie tych warstw można również stosować do detekcji częstek alfa lub beta w monitoringu radiacyjnym.
2. Warstwy TbAG:Ce oraz $(\text{Gd},\text{Tb})(\text{Al},\text{Ga})\text{O}_{12}:\text{Ce}$ posiadają bardzo wysoką wydajność scyntylacyjną, która przekracza wydajność najlepszych znanych odpowiedników scyntylatorów w postaci warstw monokrystalicznych granatów, otrzymanych z topników opartych na PbO, oraz wykazują bardzo niski poziom długotrwałych składników scyntylacji, zbliżony do tego, który uzyskuje się w najlepszych obecnie ekranach scyntylacyjnych.
3. Wśród opracowanych kompozytowych scyntylatorów, opartych na warstwach i kryształach granatów LuAG, domieszkowanych jonami Ce^{3+} , Pr^{3+} i Sc^{3+} , najlepsze właściwości scyntylacyjne posiadają struktury epitaksjalne LuAG:Pr SCF/LuAG:Ce SC oraz LuAG:Pr SCF/ LuAG:Sc SC. Dla kompozytowego scyntylatora LuAG:Pr SCF/LuAG:Ce SC stosunek t_α/t_γ osiągną odpowiednio wartość 3.6 przy zaniku intensywności scyntylacji do poziomu 0.1 w przedziale czasowym 0–750 ns, a dla LuAG:Pr SCF/ LuAG:Sc SC wartość 15.6 przy zaniku intensywności scyntylacji do poziomu 0.05 w przedziale czasowym 0–2500 ns.
4. Nowoopracowane wysokowydajne scyntylatory w postaci warstw monokrystalicznych $\text{Gd}_{1.5}\text{Lu}_{1.5}\text{Al}_{2.25}\text{Ga}_{2.75}\text{O}_{12}:\text{Ce}$ i $\text{Tb}_3\text{Al}_5\text{O}_{12}:\text{Ce}$ można z powodzeniem stosować do produkcji kompozytowych scyntylatorów na bazie podłoż GAGG:Ce, używając metody LPE.
5. Opracowane metodą LPE kompozytowe scyntylatory na bazie warstw i kryształów domieszkowanych jonami Ce^{3+} mieszanych granatów posiadają lepsze właściwości do rozdzielnej detekcji α częstek i γ kwantów oraz większą wydajność scyntylacyjną w porównaniu z odpowiednikami na bazie domieszkowanych warstw i kryształów LuAG.
6. Z opracowanych kompozytowych scyntylatorów, opartych na warstwach i kryształach mieszanych granatów, najlepsze właściwości scyntylacyjne posiada scyntylator kompozytowy $\text{Tb}_3\text{Al}_5\text{O}_{12}:\text{Ce}$ SCF/ $\text{Gd}_3\text{Al}_{2.5}\text{Ga}_{2.5}\text{O}_{12}:\text{Ce}$. Dla tego scyntylatora stosunek t_α/t_γ osiąga wartość 3 przy zaniku intensywności scyntylacji do poziomu 0,05 w przedziale czasowym 450–3700 ns.
7. Wykorzystując metodę LPE, opracowano prototypy kompozytowych materiałów termoluminescyjnych opartych na strukturach epitaksjalnych, zawierające warstwy i kryształy YAG:Ce i LuAG:Ce. Pokazano, że takie kompozyty można stosować do

detekcji α i β częstek, wykorzystując różnice między krzywymi termoluminescencji (TL), pochodząymi od warstw i podłoż tych granatów.

8. Wśród opracowanych kompozytowych materiałów termoluminescyjnych, opartych na warstwach i kryształach granatów, najlepsze właściwości do jednoczesnej rejestracji α i β częstek pozdają struktury epitaksjalne YAG:Ce SCF/LuAG:Ce SC oraz Lu_{1.5}Gd_{1.5}AG:Ce SCF/YAG:Ce SC. Dla tych struktur wielkość różnicy pomiędzy położeniem głównych pików TL, które odpowiadają detekcji częstek α i β wynosi odpowiednio 165 i 215 °C.

Literatura

1. Y. V. Zorenko et al., Epitaxial structures of garnets as scintillation detectors of ionizing radiation. *J. Appl. Spectrosc.*, 52 (1990) 645–649.
2. Y. V. Zorenko et al., Scintillators on the base of single crystalline films of Al₂O₃-Y₂O₃ system oxides. Proc. 5th Int. Conf. Inorganic Scintillators Appl., Moscow, Russia, Sierpień 16-20 (1999) 476–481.
3. M. Globus et al., New type of scintillation detectors for biological, medical, and radiation monitoring applications. *IEEE Transactions on Nuclear Science* 51 (2004) 1297-1303.
4. Y. V. Zorenko et al. Scintillators based on CdWO₄ and CdWO₄:Bi single crystalline films. *IEEE Trans. Nucl. Sci.*, 59 (2012) 2281–2285
5. Y. V. Zorenko, V. Gorbenko, I. Konstankevych, B. Grinev, M. Globus, Scintillation properties of Lu₃Al₅O₁₂: Ce single-crystalline films. *Nucl. Instrum. Methods Phys. Res. A, Accelerators, Spectrome Detectors Assoc. Equip.*, 486 (2002) 309–314.
6. A. Koch, C. Raven, P. Spanne, A. Snigirev, X-ray imaging with submicrometer resolution employing transparent luminescent screens. *J. Opt. Soc. Amer. A, Opt.* 15 (1998) 1940–1951.
7. M. Nikl, Ed., Nanocomposite, Ceramic, and Thin Film Scintillators. Pan Stanford Publishing, 2017.
8. M. Nikl, J. Tous, J.A. Mares, P. Prusa, E. Mihokova, K. Blazek, A. Vedda, Yu. Zorenko, V. Gorbenko, V. Babin, Lu₃Al₅O₁₂-based materials for high 2D-resolution scintillation detectors. Proc. SPIE 7310 (2009) 731008.
9. S. Yamamoto, J. Kataoka, K. Kamada, A. Yoshikawa, An ultrahigh spatial resolution radiation-imaging detector using 0.1 mm × 0.1 mm pixelated GAGG plate combined with 1 mm channel size Si-PM array. *Nuclear Inst. and Methods in Physics Research A*, 919 (2019) 125–133
10. Yu. Zorenko, V. Gorbenko, Growth peculiarities of the R₃Al₅O₁₂ (R=Lu, Yb, Tb, Eu-Y) single crystalline film phosphors by liquid phase epitaxy. *Radiation Measurment* 42 (2007) 907-910
11. Y. Zorenko, V. Grobenko, T. Zorenko, O. Sidletskiy, A. Fedorov, P. Bilski, A. Twardak, High-perfomance Ce-doped multicomponent garnet single crystalline film scinyllators. *Phys. Status Solidi RRL* 9 (2015) 489-493
12. M. Nikl, A. Yoshikawa, K. Kamada, K. Nejezchleb, C.R. Stanek, J.A. Mares, K. Blazek, Development of LuAG-based scintillator crystals – A review. *Progress in Crystal Growth and Characterization of Materials* 59 (2013) 47-72

13. Y. Zorenko, V. Gorbenko, A. Voloshinovskii, G. Stryganyuk, S. Nedliko, V. Degoda, O. Chukova, Luminescence of Sc-related centers in single crystalline films of Lu₃Al₅O₁₂ garnet. *Phys. Stat. Sol.* 1 (2005) 105–108
14. J.M. Ogieglo, A. Zych, T. Justel, A. Meijerink, C. R. Ronda, Luminescence and energy transfer in Lu₃Al₅O₁₂ scintillators co-doped with Ce³⁺ and Pr³⁺. *Optical materials* 35 (2013) 322-331
15. Yu. Zorenko, V. Gorbenko, Ja Vasylkiv, A. Zelenyj, A. Fedorov, R. Kucerkova, J.A. Mares, M. Nikl, P. Bilski, A. Twardak, Growth and luminescent properties of scintillators based on the single crystalline films of Lu_{3-x}Gd_xAl₅O₁₂:Ce garnet. *Material Research Bulletin* 64 (2015) 355-363.
16. Y. Zorenko, V. Gorbenko, T. Voznyak, T. Martin, P.-A. Douissard, J. A. Mares, M. Nikl, LuAG:Pr, LuAG:La, and LuAP:Ce thin film scintillators for visualisation of x-ray images". Proc. SPIE 7310 (2009) Non-Intrusive Inspection Technologies II 731007
17. K. Kamada, T. Endo, K. Tsutumi, Composition Engineering in Cerium-Doped (Lu,Gd)₃(Ga,Al)₅O₁₂ Single-Crystal Scintillators. *Cryst.GrowthDes.* 11 (2011) 4484–4490
18. M. Nikl, A. Yoshikawa, Recent R&D Trends in Inorganic Single-Crystal Scintillator Materials for Radiation Detection. *Advanced Optical Materials* 3 (2015) 463–481
19. Y. Zorenko, V. Gorbenko, Ja. Vasylkiv, T. Strzyżewski, A. Fedorov, R. Kucerkova, J. A. Mares, M. Nikl, P. Bilski, A. Twardak, Growth and luminescent properties of scintillators based on the single crystalline films of (Lu, Gd)₃(Al, Ga)₅O₁₂:Ce garnets. *Journal of Luminescence* 169 (2016) 828-837
20. P. Prusa, M. Kucera, J.A. Mares, M. Hanus, A. Bejtlerova, Z. Onderisinova, M. Nikl, Scintillation properties of the Ce-doped multicomponent garnet epitaxial films. *Optical Materials* 35 (2013) 2444-2448
21. P. Prusa, M. Kucera, J. A. Mares, Z. Onderisinova, M. Hanus, V. Babin, A. Bejtlerova, M. Nikl, Composition Tailoring in Ce-Doped Multicomponent Garnet Epitaxial Film Scintillators. *Cryst. Growth Des.* 15 (2015) 3715-3723
22. Y. Zorenko et al., Scintillating screens based on the single crystalline films of multicomponent garnets: New achievements and possibilities. *IEEE Transactions on Nuclear Science* 63 (2016) 497-502
23. Y. Zorenko, V. Gorbenko, T. Zorenko, K. Paprocki, P. Bilski, A. Twardak, T. Voznyak, O. Sidletskiy, Y. Gerasimov, B. Gryniow, A. Fedorov, Composition engineering of single crystalline films based on the multicomponent garnet compounds. *Optical Materials* 61 (2016) 3-10
24. R. H. Bartram, A. Lempicki, Efficiency of electron-hole pair production in scintillators. *J. Lumin.* 68 (1996) 225-240.
25. F. Glenn, Knoll, *Radiation Detection and Measurements*, third ed., John Wiley & Sons, Inc., New York, 2000.
26. W. Chewpraditkul et al., Scintillation Properties of LuAG:Ce, YAG:Ce and LYSO:Ce Crystals for Gamma-Ray Detection. *IEEE Transactions on Nuclear Science* 56 (2009) 3800-3805
27. V. Gorbenko, A. Krasnikov, M. Nikl, S. Zazubovich, Yu Zorenko, Luminescence characteristic of LuAG:Pr and YAG:Pr single crystalline films. *Opt. Mater.* 31 (2009) 1805.

28. Yu V. Zorenko, Luminescence of La³⁺ and Sc³⁺ Isoelectronic Impurities in Lu₃Al₅O₁₂ Single Crystalline Films. Optic Spectrosc. 100 (2004) 572-580.
29. Yu Zorenko, V. Gorbenko, T. Voznyak, V. Savchyn, S. Nizhankovskiy, A. Dan'ko, V. Puzikov, V. Laguta, J.A. Mares, M. Nikl, K. Nejezchleb, M. Batentschuk, A. Winnacker, Luminescent and scintillation properties of Lu₃Al₅O₁₂ single crystal and single crystalline films. Opt. Mater. 34 (2012) 2080.
30. P. Dorenbos, Relation between Eu²⁺ and Ce³⁺ f↔d-transition energies in inorganic compounds. J. Phys. Condens. Matter 15 (2003) 8417–8434.

Dorobek naukowy

Publikacje ujęte w pracy doktoranckiej

1. Y. Zorenko, P. Douissard, T. Martin, F. Riva, V. Gorbenko, T. Zorenko, K. Paprocki, A. Iskalieva, **S. Witkiewicz**, A. Fedorov, P. Bilski, A. Twardak. Scintillating screens based on the LPE grown Tb₃Al₅O₁₂:Ce single crystalline films. *Optical Materials* 65 (2017) 73-81
2. V. Gorbenko, T. Zorenko, **S. Witkiewicz**, K. Paprocki, O. Sidletskiy, A. Fedorov, P. Bilski, A. Twardak, Y. Zorenko. LPE growth of single crystalline film scintillators based on the Ce³⁺ doped Tb_{3-x}Gd_xAl_{5-y}Ga_yO₁₂ mixed garnets. *Crystals* 7 (2017) 262
3. **S. Witkiewicz-Lukaszek**, V. Gorbenko, T. Zorenko, K. Paprocki, O. Sidletskiy, I. Gerasymov, J.A. Mares, R. Kucerkova, M. Nikl, Yu. Zorenko. Novel all-solid-state composite scintillators based on the epitaxial structures of LuAG garnet doped with Pr, Sc and Ce ions. *IEEE Transactions on Nuclear Science* 65 (2018) 2114 – 2119
4. **S. Witkiewicz-Lukaszek**, V. Gorbenko, T. Zorenko, K. Paprocki, O. Sidletskiy, A. Fedorov, R. Kucerkova, J. A. Mares, M. Nikl, Yu. Zorenko. Epitaxial growth of composite scintillators based on Tb₃Al₅O₁₂:Ce single crystalline films and Gd₃Al_{2.5}Ga_{2.5}O₁₂:Ce crystal substrates. *CrystEngComm* 20 (2018) 3994-4002
5. **S. Witkiewicz-Lukaszek**, V. Gorbenko, T. Zorenko, O. Sidletskiy, I. Gerasymov, A. Fedorov, A. Yoshikawa, J. A. Mares, M. Nikl, Yu. Zorenko. Development of Composite Scintillators Based on Single Crystalline Films and Crystals of Ce³⁺-Doped (Lu,Gd)₃(Al,Ga)₅O₁₂ Mixed Garnet Compounds. *Cryst. Growth Des.* 18 (2018) 1834–1842
6. **S. Witkiewicz-Lukaszek**, V. Gorbenko, T. Zorenko, K. Paprocki, O. Sidletskiy, I. Gerasymov, J.A. Mares, R. Kucerkova, M. Nikl, Yu. Zorenko. Composite scintillators based on the crystals and single crystalline films of LuAG garnet doped with Ce³⁺, Pr³⁺ and Sc³⁺ ions. *Optical Materials* 84 (2018) 593-599
7. **S. Witkiewicz-Lukaszek**, V. Gorbenko, T. Zorenko, Y. Zorenko, W. Gieszczyk, A. Mrozik, P. Bilski. Composite thermoluminescent detectors based on the Ce³⁺ doped LuAG/YAG and YAG/LuAG epitaxial structures. *Radiation Measurements* 128 (2019) 106124
8. J.A. Mares, **S. Witkiewicz-Lukaszek**, V. Gorbenko, T. Zorenko, R. Kucerkova, A. Bejtlerova, C. D'Ambrosio, J. Dlouhy, M. Nikl, Yu. Zorenko. Alpha and

gamma spectroscopy of composite scintillators based on the LuAG:Pr crystals and single crystalline films of LuAG:Ce and (Lu,Gd,Tb)AG:Ce garnets. *Optical Materials* 96 (2019) 109268

9. Witkiewicz-Lukaszek, S.; Mrozik, A.; Gorbenko, V.; Zorenko, T.; Bilski, P.; Fedorov, A.; Zorenko, Y. LPE Growth of Composite Thermoluminescent Detectors Based on the $\text{Lu}_{3-x}\text{Gd}_x\text{Al}_5\text{O}_{12}$:Ce Single Crystalline Films and YAG:Ce Crystals. *Crystals* 10 (2020) 189.
10. **S. Witkiewicz-Lukaszek**, V. Gorbenko, T. Zorenko, O. Sidletskiy, P. Arhipov, A. Fedorov, J.A. Mares, R. Kucerkova, M. Nikl, Yu. Zorenko, High-performance composite scintillators based on the single crystalline films and crystals of LuAG garnet. *CrystEngComm* (2020) opublikowany on-line 06.04.2020, <https://doi.org/10.1039/D0CE00266F>

Inne publikacje doktoranta

1. A. Kilian, P. Bilski, V. Gorbenko, T. Zorenko, **S. Witkiewicz**, K. Paprocki, Y. Zorenko. Thermoluminescent Properties of Cerium-Doped Lu_2SO_5 and Y_2SiO_5 Single Crystalline Films Scintillators Grown from PbO - B_2O_3 and Bi_2O_3 Fluxes. *Crystals* 8 (2018) 120
2. T. Zorenko, V. Gorbenko, **S. Witkiewicz-Lukaszek**, Yu. Zorenko. Luminescent properties of $(\text{La},\text{Lu},\text{Gd})_3(\text{Al},\text{Sc},\text{Ga})_5\text{O}_{12}$:Ce mixed garnets under synchrotron radiation excitation. *Journal of Luminescence* 199 (2018) 483-487
3. V. Gorbenko, T. Zorenko, **S. Witkiewicz**, K. Paprocki, A. Iskaliyeva, A.M. Kaczmarek, R. Van Deun, M.N. Khaidukov, M. Batentschuk, Yu. Zorenko. Luminescence of Ce^{3+} multicenters in Ca^{2+} - Mg^{2+} - Si^{4+} based garnet phosphors. *Journal of Luminescence* 199 (2018) 245-250
4. S. Kurosawa, A. Yoshikawa, V. Gorbenko, T. Zorenko, **S. Witkiewicz-Lukaszek**, Yu. Zorenko. Composite scintillators based on the films and crystals of $(\text{Lu},\text{Gd},\text{La})_2\text{Si}_2\text{O}_7$ pirosilicates. *IEEE Transactions on Nuclear Science* (2020) DOI: 10.1109/TNS.2020.2983657

Konferencje:

Komunikaty prezentowane osobiście

1. **S. Witkiewicz-Lukaszek**, V. Gorbenko, T. Zorenko, J.A. Mares, M. Nikl, Yu. Zorenko. Composite scintillators based on the doped LuAG crystals and films for simultaneous registration of α -particles and γ -quanta.-**komunikat**, *The 2018 Europhysical Conference on Defects in Insulating Materials EURODIM 2018, Bydgoszcz, Polska, 8-13.07.2018*
2. **S. Witkiewicz-Lukaszek**, V. Gorbenko, T. Zorenko, R. Kucerkova, J.A. Mares, M. Nikl, O. Sidletskiy, K. Bartosiewicz, S. Kurosawa, K. Kamada, A. Yoshikawa, Y. Zorenko.-New type of composite scintillators based on the single crystalline films and crystals of $\text{Gd}_3\text{Al}_{2-3}\text{Ga}_{3-2}\text{O}_{12}$:Ce garnets-**komunikat**, *8th International Symposium on Optical Materials, Wrocław, Polska, 9-14.06.2019*

Komunikaty prezentowane przez współautorów

1. V. Gorbenko, S. Witkiewicz, K. Paprocki, T. Zorenko, Yu. Zorenko, P. Arhipov, S. Tkachenko, Ia. Gerasymov, B. Grynyov, O. Sidletskiy, A. Fedorov, J. Mares, M. Nikl. Development of the novel hybrid film-crystal scintillators based on the garnet compounds. -**komunikat (współautor prezentowanego komunikatu przez Yu. Zorenko)**, *International Conference on Oxide Materials for Electronic Engineering-fabrication, properties and application, Lwów, Ukraina, 22.05-2.06. 2017*
2. Y. Zorenko, V. Gorbenko, T. Zorenko, S. Witkiewicz, O. Sidletskiy, I. Gerasymov, P. Arhipov, A. Fedorov, J. Mares, M. Nikl. Novel all-solid-state hybrid film-crystal scintillators based on the epitaxial structures of garnet compounds.-**komunikat (współautor prezentowanego komunikatu przez Yu. Zorenko)**, *SCINT 2017- 14th Int. Conference on Scintillating Materials and their Applications, Chamonix, 18-22.09.2017*
3. J.A. Mares, M. Nikl, R. Kucerkova, A. Beitlerova, V. Gorbenko, S. Witkiewicz, T. Zorenko, Yu. Zorenko. α - and γ -rays Characterization of Single Crystalline Films and Composite Scintillators.-**komunikat (współautor prezentowanego komunikatu przez J.A.Mares)**, *The 2018 Europhysical Conference on Defects in Insulating Materials EURODIM 2018, Bydgoszcz, Polska, 8-13.07.2018*
4. S. Witkiewicz-Lukaszek, V. Gorbenko, T. Zorenko, O. Sidletskiy, K. Bartosiewicz, A. Yoshikawa, J. A. Mares, M. Nikl, Y. Zorenko. Recent progress in the development of composite scintillators based on the single crystalline films of garnet compounds.-**komunikat (współautor prezentowanego komunikatu przez Yu. Zorenko)**, *10th International Conference on Luminescent Detectors and Transformers of Ionizing Radiation 9-14.09.2018, Praga, Czechy*
5. Y. Zorenko, V. Gorbenko, T. Zorenko, S. Witkiewicz-Lukaszek. LPE method as a useful tool for development of the composite luminescent materials based on the mixed garnet compounds.- **komunikat (współautor prezentowanego komunikatu przez Yu. Zorenko)**, *3rd German Polish Conference on Crystal Growth, Poznań, Polska, 17-21.03.2019*
6. S. Witkiewicz-Lukaszek, V. Gorbenko, T. Zorenko, R. Kucerkova, J.A. Mares, M. Nikl, P. Archipov, O. Sidletskiy, K. Bartosiewicz, S. Kurosawa, K. Kamada, A. Yoshikawa, Y. Zorenko. Development of composite scintillators based on the single crystals and single crystalline films of garnet compounds.- **komunikat (współautor prezentowanego komunikatu przez Yu. Zorenko)**, *8th International Symposium on Optical Materials, Wrocław, Polska, 9-14.06.2019*
7. S. Witkiewicz-Lukaszek, V. Gorbenko, T. Zorenko, Y. Zorenko, J.A. Mares, R. Kucerkova, M. Nikl, O. Sidletskiy, K. Bartosiewicz, K. Kamada, S. Kurosawa, A. Yoshikawa. Advanced three layered composite scintillators based on the epitaxial structures of garnet compounds.-**komunikat (współautor prezentowanego komunikatu przez Yu. Zorenko)**, *15th International Conference on Scintillating Materials and their Applications, Sendai, Japonia, 29.09-04.10.2019*

Postery prezentowane osobiście

1. S. Witkiewicz, V. Gorbenko, K. Paprocki, T. Zorenko, Yu. Zorenko, Ia. Gerashmov, O. Sidletskiy, A. Fedorov, J.A. Mares, M. Nikl. New hybrid scintillator based on the Lu_{1.5}Gd_{1.5}Al_{1.5}Ga_{3.5}O₁₂ single crystalline films and Gd₃Al_{2.5}2Ga_{2.5}3O₁₂ crystals for simultaneous registration of α -particles and γ -quanta. -plakat, *International Conference on Oxide Materials for Electronic Engineering-fabrication, properties and application, Lwów, Ukraina, 22.05-2.06 2017*
2. S. Witkiewicz, V. Gorbenko, T. Zorenko, J.A. Mares, A. Fedorov, Ia. Gerashmov, O. Sidletskiy, M. Nikl, Yu. Zorenko. New type of hybrid scintillator based on the Tb₃Al₅O₁₂:Ce single crystalline films and Gd₃Al_{2.5}Ga_{2.5}O₁₂:Ce crystals.-plakat, *The Phosphor Safari and The Sixth International Workshop on Advanced Spectroscopy and Optical Materials, Gdańsk, 9-14.07. 2017*
3. Yu. Zorenko, T. Zorenko, V. Gorbenko, S. Witkiewicz. Study of luminescence of Eu²⁺ and Eu³⁺ states in Ca₃Ga₂Ge₃O₁₂:Eu garnet using synchrotron radiation excitation.-plakat, *European XFEL Users' Meeting, DESY, Hamburg, 24-26.01.2017*
4. V. Gorbenko, T. Zorenko, K. Paprocki, S. Witkiewicz-Łukaszek, Yu. Zorenko. Luminescent properties of Ca₃Sc₂Si₃O₁₂:Mn and Ca₂YScMgSiO₁₂:Mn single crystalline films.-plakat, *The 2018 Europhysical Conference on Defects in Insulating Materials EURODIM 2018, Bydgoszcz, Polska, 8-13.07.2018*
5. S. Witkiewicz-Łukaszek, Y. Zorenko, V. Gorbenko, T. Zorenko, W. Gieszczyk, P. Bilski, Composite thermoluminescent detectors based on the Ce³⁺ doped LuAG/YAG and YAG/LuAG epitaxial structures.-plakat, *10th International Conference on Luminescent Detectors and Transformers of Ionizing Radiation 9-14.09.2018, Praga, Czechy*
6. Sandra Witkiewicz-Łukaszek, A. Mrozik, V. Gorbenko, T. Zorenko, P. Bilski, Y. Zorenko. LPE grown of the thermoluminescent detectors based on the Lu_{3-x}Gd_xAl₅O₁₂:Ce/YAG:Ce epitaxial structures.-plakat, *3rd German Polish Conference on Crystal Growth, Poznań, Polska, 17-21.03.2019*
7. S. Kurosawa, A. Yoshikawa, V. Gorbenko, T. Zorenko, S. Witkiewicz-Łukaszek, Yu. Zorenko. New composite scintillators based on the single crystalline films aln single crystals of (Lu, Gd, La).-plakat, *15th International Conference on Scintillating Materials and their Applications, Sendai, Japonia, 29.09-04.10.2019*

Postery prezentowane przez współautorów

1. V. Gorbenko, S. Witkiewicz, K. Paprocki, T. Zorenko, Y. Zorenko, P. Arhipov, S. Tkachenko, I. Gerashmov, B. Grynyov, I. Sidletskiy, A. Fedorov, M. Nikl. Development of the Novel Hybrid Film-Crystal Scintillators Based on the Garnet Compounds.-plakat (współautor prezentowanego plakatu przez Yu. Zorenko), *International Conference on Oxide Materials for Electronic Engineering-fabrication, properties and application, Lwów, Ukraina, 22.05-2.06 2017*
2. V. Gorbenko, T. Zorenko, K. Bartoszewicz, J. A. Mares, S. Witkiewicz, A. Iskaliyeva, J. Sadowskii, M. Nikl, Y. Zorenko. Scintillators based on the single crystalline films of (Lu,La)₃(Al,Ga)₅O₁₂:Ce mixed garnet.-plakat (współautor

prezentowanego plakatu przez V. Gorbenko), The Phosphor Safari and The Sixth International Workshop on Advanced Spectroscopy and Optical Materials, Gdańsk, 9-14.07. 2017

3. V. Gorbenko, T. Zorenko, **S. Witkiewicz**, K. Paprocki, Yu. Zorenko. Growth and luminescent properties of $\text{Ca}_3\text{Sc}_2\text{Si}_3\text{O}_{12}:\text{Pr}$ and $\text{Ca}_2\text{YScMgSiO}_{12}:\text{Pr}$ single crystalline films.-**plakat (współautor prezentowanego plakatu przez T. Zorenko)**, *The 2018 Europhysical Conference on Defects in Insulating Materials EURODIM 2018, Bydgoszcz, Polska, 8-13.07.2018*
4. W. Gieszczyk, P. Bilski, M. Kłosowski, Yu. Zorenko, T. Zorenko, K. Paprocki, **S. Witkiewicz**. Luminescent Properties of Undoped and Ce^{3+} Doped $\text{Y}_2\text{O}_3 - \text{Al}_2\text{O}_3$ Double System Crystals Prepared by Micro-Pulling Down Method.-**plakat (współautor prezentowanego plakatu przez W. Gieszczyk)**, *The 2018 Europhysical Conference on Defects in Insulating Materials EURODIM 2018, Bydgoszcz, Polska, 8-13.07.2018*
5. V. Gorbenko, Z. Galazka, T. Zorenko, K. Paprocki, **S. Witkiewicz**, Yu. Zorenko. Growth and luminescence properties of the $\beta\text{-Ga}_2\text{O}_3$ single crystalline films.-**plakat (współautor prezentowanego plakatu przez V. Gorbenko)**, *The 2018 Europhysical Conference on Defects in Insulating Materials EURODIM 2018, Bydgoszcz, Polska, 8-13.07.2018*
6. A. Mrozik, W. Gieszczyk, P. Bilski, S. Witkiewicz-Lukaszek, V. Gorbenko, Yu. Zorenko. Development of the composite thermoluminescent detectors based on the epitaxial structures of garnet and perovskite compounds.-**plakat (współautor prezentowanego plakatu przez Y. Zorenko)**, *19th International Conference on Solid State Dosimetry (SSD19), Hiroshima, Japonia, 15-20 września 2019*

Wystąpienia seminaryjne

1. **S. Witkiewicz-Łukaszek.** Hybrydowe scyntylatory na bazie warstw i kryształów granatów: krystalizacja metodą epitaksji z cieczy oraz badania ich właściwości luminescencyjnych i scyntylacyjnych. – seminarium w Instytucie Fizyki, *Uniwersytet Kazimierza Wielkiego w Bydgoszczy, 18.10.2017*
2. **S. Witkiewicz-Łukaszek.** New type of composite scintillators based on the single crystalline films and crystals $\text{Gd}_3\text{Al}_{2-3}\text{Ga}_{3-2}\text{O}_{12}:\text{Ce}$ garnets- seminarium w Instytucie Fizyki, *Uniwersytet Kazimierza Wielkiego w Bydgoszczy, 18.06.2019*

Staże

1. Instytut Fizyki, Czeska Akademia Nauk, Praga, kwiecień 2017

Warsztaty naukowe

1. Instytut Fizyki Jądrowej im. Henryka Niewodniczańskiego PAN, *XFELs for beginners, 19.04.2018*

Nagrody i wyróżnienia

1. październik 2018-czerwiec 2019- stypendium dla najlepszych doktorantów

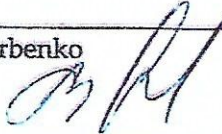
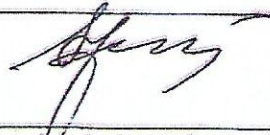
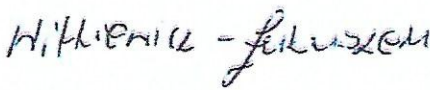
Oświadczenie autorów w powstaniu publikacji, dotyczących rozprawy doktorskiej
mgr Sandry Witkiewicz - Łukaszek pt. Kompozytowe scyntylatory na bazie warstw i kryształów granatów: krystalizacja metodą epitaksji z fazy ciekłej oraz badania ich właściwości luminescencyjnych i scyntylacyjnych

C1.1 Y. Zorenko, P. Douissard, T. Martin, F. Riva, V. Gorbenko, T. Zorenko, K. Paprocki, A. Iskalieva, S. Witkiewicz, A. Fedorov, P. Bilski, A. Twardak. Scintillating screens based on the LPE grown $Tb_3Al_5O_{12}:Ce$ single crystalline films. *Optical Materials* 65 (2017) 73-81

Autorzy	Udział
Sandra Witkiewicz - Łukaszek <i>Witkiewicz-Lukaszek</i>	-analiza całości materiału eksperymentalnego; -przygotowanie materiałów (rysunki, tabele) do publikacji; -uczestnictwo w spisaniu części manuskryptu, dotyczącej właściwości optycznych warstw oraz korekt manuskryptu po uwagach recenzentów
Yuriy Zorenko <i>S. Z.</i>	-konsepcja pracy; -redakcja i korekty tekstu publikacji
Vitalii Gorbenko <i>B. M.</i>	-przeprowadzenie procesu wzrostu warstw metodą LPE; -redakcja części manuskryptu, dotyczącej wzrostu warstw
Tetiana Zorenko <i>T. Z.</i>	-wykonanie pomiarów absorpcji oraz wydajności i zaników scyntylacyjnych warstw przy wzbudzeniu α -cząstkkami źródła ^{239}Pu
Paweł Bilski <i>P. B.</i>	-pomiar krzywych jarzenia warstw przy wzbudzeniu cząstkkami α ; -redakcja części manuskryptu dotyczącej pomiarów termoluminescencji

C1.2 V. Gorbenko, T. Zorenko, S., Witkiewicz, K. Paprocki, O. Sidletskiy, A. Fedorov, P. Bilski, A. Twardak, Y. Zorenko. LPE growth of single crystalline film scintillators based on Ce^{3+} doped $Tb_{3-x}Gd_xAl_5-yGa_2O_{12}$ mixed garnets. *Crystals* 7 (2017) 262. (zgodnie z udziałem deklarowanym w publikacji)

Autorzy	Udział
Sandra Witkiewicz - Łukaszek <i>Witkiewicz-Lukaszek</i>	-analiza wyników badań właściwości strukturalnych i optycznych warstw $Tb_{3-x}Gd_xAl_5-yGa_2O_{12}:Ce$ na podłożach GAGG; -uczestnictwo i przygotowaniu materiałów do publikacji (rysunki, tabele) oraz w napisaniu części manuskryptu dotyczącej właściwości optycznych warstw, a także korekty manuskryptu po uwagach recenzentów
Vitalii Gorbenko <i>B. M.</i>	-przeprowadzenie procesu wzrostu warstw metodą LPE; -redakcja części manuskryptu dotyczącej wzrostu warstw
Tetiana Zorenko <i>T. Z.</i>	-wykonanie pomiarów wydajności i zaników scyntylacyjnych warstw przy wzbudzeniu α -cząstkkami źródła ^{239}Pu

Paweł Bilski 	-pomiar krzywych jarzenia warstw; -redakcji części pracy dotyczącej pomiarów termoluminescencji
Yuriy Zorenko 	-koncepcja pracy; -redakcja i korekty całego tekstu głównie części „Introduction”, części III oraz „Conclusion”
C2.1 S. Witkiewicz-Lukaszek, V. Gorbenko, T. Zorenko, K. Paprocki, O. Sidletskiy, I. Gerasymov, J.A. Mares, R. Kucerkova, M. Nikl, Yu. Zorenko. Novel all-solid-state composite scintillators based on the epitaxial structures of LuAG garnet doped with Pr, Sc and Ce ions. <i>IEEE Transactions on Nuclear Science</i> 65 (2018) 2114 – 2119.	
Autorzy	Udział
Sandra Witkiewicz-Łukaszek 	-udział w powstaniu koncepcji pracy; - pomiary widm absorbcji warstw i kompozytowych scyntylatorów; -opracowanie wyników badań absorbcji, katodoluminescencji i kinetyki zaniku scyntylacji oraz przygotowanie odpowiednich rysunków i tabeli do publikacji; -opracowanie metody opisu różnic w krzywych zaniku scyntylacji kompozytowych scyntylatorów przy wzbudzeniu cząstками α i kwantami γ , wyrażonych jako stosunek t_α/t_γ lub t_γ/t_α ; -uczestnictwo w napisaniu manuskryptu pracy, oraz przeprowadzenie korekt manuskryptu po uwagach recenzentów (autor korespondencyjny)
Vitalii Gorbenko 	-przeprowadzenie procesu wzrostu kompozytowych scyntylatorów metoda LPE; -redakcji części manuskryptu dotyczącej wzrostu warstw
Tetiana Zorenko 	-wykonanie pomiarów wydajności i zaników scyntylacyjnych warstw przy wzbudzeniu α - cząstками źródła ^{239}Pu
Jiri A. Mares	-wykonanie pomiarów zaników scyntylacyjnych kompozytowych scyntylatorów przy wzbudzeniu α cząstками źródła ^{241}Am i γ kwantami źródła ^{137}Cs
Yuriy Zorenko 	-udział w powstaniu koncepcji pracy; -analiza całości materiału eksperymentalnego; -redakcja i korekty całego tekstu pracy
C2.2 S. Witkiewicz-Lukaszek, V. Gorbenko, T. Zorenko, K. Paprocki, O. Sidletskiy, I. Gerasymov, J.A. Mares, R. Kucerkova, M. Nikl, Yu. Zorenko. Composite scintillators based on the crystals and single crystalline films of LuAG garnet doped with Ce^{3+} , Pr^{3+} and Sc^{3+} ions. <i>Optical Materials</i> 84 (2018) 593-599.	
Autorzy	Udział
Sandra Witkiewicz - Łukaszek 	-udział w powstaniu koncepcji pracy; -opracowanie wyników badań absorbcji, katodoluminescencji, kinetyki zaniku scyntylacyjnego, widm amplitudowych scyntylacji oraz zależności wydajności i rozdzielczości energetycznej scyntylacji od czasu rejestracji sygnału scyntylacyjnego;

✓
2

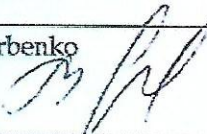
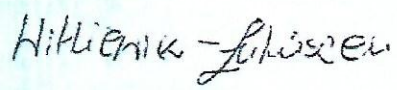
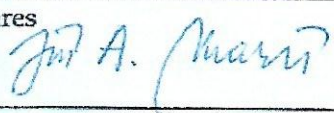
Paweł Biłski	-pomiar krzywych jarzenia warstw; -redakcji części pracy dotyczącej pomiarów termoluminescencji
Yuriy Zorenko	-koncepcja pracy; -redakcja i korekty całego tekstu głównie części „Introduction”, części III oraz „Conclusion”

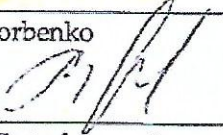
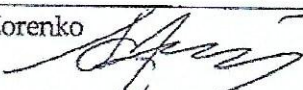
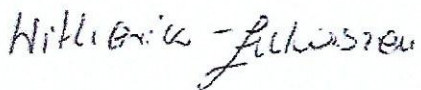
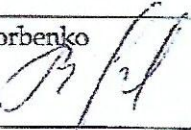
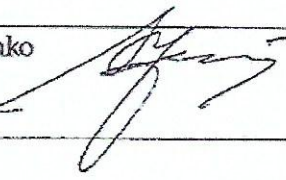
C2.1 S. Witkiewicz-Lukaszek, V. Gorbenko, T. Zorenko, K. Paprocki, O. Sidletskiy, I. Gerasymov, J.A. Mares, R. Kucerkova, M. Nikl, Yu. Zorenko. Novel all-solid-state composite scintillators based on the epitaxial structures of LuAG garnet doped with Pr, Sc and Ce ions. *IEEE Transactions on Nuclear Science* 65 (2018) 2114 – 2119.

Autorzy	Udział
Sandra Witkiewicz-Łukaszek <i>Witkiewicz - Łukaszek</i>	-udział w powstaniu koncepcji pracy; - pomiary widm absorbcji warstw i kompozytowych scyntylatorów; -przeprowadzenie wyników badań absorbcji, katodoluminescencji i kinetyki zaniku scyntylacji oraz przygotowanie odpowiednich rysunków i tabeli do publikacji; -opracowanie metody opisu różnic w krzywych zaniku scyntylacji kompozytowych scyntylatorów przy wzbudzeniu cząstками α i kwantami γ , wyrażonych jako stosunek t_{α}/t_{γ} lub t_{γ}/t_{α} ; -uczestnictwo w napisaniu manuskryptu pracy, oraz przeprowadzenie korekt manuskryptu po uwagach recenzentów (autor korespondencyjny)
Vitalii Gorbenko <i>B. R.</i>	-przeprowadzenie procesu wzrostu kompozytowych scyntylatorów metoda LPE; -redakcji części manuskryptu dotyczącej wzrostu warstw
Tetiana Zorenko <i>T. Zorenko</i>	-wykonanie pomiarów wydajności i zaników scyntylacyjnych warstw przy wzbudzeniu α -cząstками źródła ^{239}Pu
Jiri A. Mares <i>J. A. Mares</i>	-wykonanie pomiarów zaników scyntylacyjnych kompozytowych scyntylatorów przy wzbudzeniu α cząstками źródła ^{241}Am i γ kwantami źródła ^{137}Cs
Yuriy Zorenko <i>Y. Zorenko</i>	-udział w powstaniu koncepcji pracy; -analiza całości materiału eksperymentalnego; -redakcja i korekty całego tekstu pracy

C2.2 S. Witkiewicz-Lukaszek, V. Gorbenko, T. Zorenko, K. Paprocki, O. Sidletskiy, I. Gerasymov, J.A. Mares, R. Kucerkova, M. Nikl, Yu. Zorenko. Composite scintillators based on the crystals and single crystalline films of LuAG garnet doped with Ce^{3+} , Pr^{3+} and Sc^{3+} ions. *Optical Materials* 84 (2018) 593-599.

Autorzy	Udział
Sandra Witkiewicz - Łukaszek <i>Witkiewicz - Łukaszek</i>	-udział w powstaniu koncepcji pracy; -opracowanie wyników badań absorbcji, katodoluminescencji, kinetyki zaniku scyntylacyjnego, widm amplitudowych scyntylacji oraz zależności wydajności i rozdzielczości energetycznej scyntylacji od czasu rejestracji sygnału scyntylacyjnego;

	<ul style="list-style-type: none"> -wykonanie zdjęć próbek przy użyciu mikroskopu elektronowego; -opracowanie wyników badań różnic w krzywych zaniku scyntylacji od warstwowej i krystalicznej części kompozytowych scyntylatorów przy wzbudzeniu cząstkami α i kwantami γ przez stosunki t_a/t_γ lub t_γ/t_a; -uczestnictwo w napisaniu manuskryptu pracy, a także przeprowadzenie korekt po uwagach recenzentów (autor korespondencyjny)
Vitalii Gorbenko 	<ul style="list-style-type: none"> -przeprowadzenie procesu wzrostu kompozytowych scyntylatorów metoda LPE; -redakcji części manuskryptu dotyczącej wzrostu warstw
Tetiana Zorenko 	<ul style="list-style-type: none"> -wykonanie pomiarów absorpcji warstw; -wykonanie pomiarów wydajności i zaników scyntylacyjnych warstw przy wzbudzeniu α- cząstkami źródła ^{239}Pu
Jiri A. Mares 	<ul style="list-style-type: none"> -wykonanie pomiarów widm amplitudowych scyntylacji oraz analiza zależności wydajności i rozdzielczości energetycznej scyntylacji od czasu rejestracji sygnału scyntylacyjnego; -wykonanie pomiarów zaników scyntylacyjnych kompozytowych scyntylatorów przy wzbudzeniu α cząstkami źródła ^{241}Am i kwantami γ źródła ^{137}Cs
Yuriy Zorenko 	<ul style="list-style-type: none"> -udział w powstaniu koncepcji pracy; -analiza całości materiału eksperymentalnego; -redakcja i korekty całego tekstu pracy
C2.3 J.A. Mares, S. Witkiewicz-Lukaszek, V. Gorbenko, T. Zorenko, R. Kucerkova, A. Beitlerova, C. D'Ambrosio, J. Dlouhy, M. Nikl, Yu. Zorenko. Alpha and gamma spectroscopy of composite scintillators based on the LuAG:Pr crystals and single crystalline films of LuAG:Ce and (Lu,Gd,Tb)AG:Ce garnets. <i>Optical Materials</i> 96 (2019) 109268	
Autorzy	Udział
Sandra Witkiewicz - Łukaszek 	<ul style="list-style-type: none"> -udział w powstaniu koncepcji pracy; -analiza krzywych zaniku scyntylacyjnego pochodzących od różnych części scyntylatora kompozytowego; -ustalenie możliwości skutecznej modyfikacji składu warstwy przy opracowaniu kompozytowych scyntylatorów typu (Lu,Tb)AG:Ce/LuAG:Pr; -wprowadzenie parametru Δ opisującego różnice krzywych zaniku scyntylacji kompozytu przy wzbudzeniu cząstkami α i kwantami γ na różnych poziomach intensywności zaniku luminescencji; -uczestnictwo w pisaniu publikacji w części dotyczącej zaników scyntylacyjnych oraz korekty manuskryptu po uwagach recenzentów
Jiri A. Mares 	<ul style="list-style-type: none"> - napisanie i redakcja tekstu manuskryptu; -wykonanie pomiarów widm amplitudowych scyntylacji oraz analiza zależności wydajności i rozdzielczości

	<p>energetycznej scyntylacji od czasu rejestracji sygnału scyntylacyjnego;</p> <p>-wykonanie pomiarów zaników scyntylacyjnych kompozytowych scyntylatorów przy wzbudzeniu α-cząstkami ze źródła ^{241}Am i γ kwantami ze źródła ^{137}Cs</p>
Vitalii Gorbenko 	<p>-przeprowadzenie procesu wzrostu kompozytowych scyntylatorów metoda LPE;</p> <p>-redakcji części manuskryptu dotyczącej wzrostu warstw</p>
Tetiana Zorenko 	<p>- wykonanie pomiarów wydajności i zaników scyntylacyjnych warstw przy wzbudzeniu α-cząstkami źródła ^{239}Pu</p>
Yuriy Zorenko 	<p>-udział w powstaniu koncepcji pracy;</p> <p>-analiza całości materiału eksperymentalnego;</p> <p>- redakcja i korekty części tekstu pracy</p>
<p>C2.4 S. Witkiewicz-Lukaszek, V. Gorbenko, T. Zorenko, O. Sidletskiy, P. Arhipov, A. Fedorov, J.A. Mares, R. Kucerkova, M. Nikl, Yu. Zorenko, High-performance composite scintillators based on the single crystalline films and crystals of LuAG garnet, <i>CrystEngComm</i> (2020) opublikowany on-line 06.04.2020, https://doi.org/10.1039/D0CE00266J.</p>	
Autorzy	Udział
Sandra Witkiewicz - Łukaszek 	<p>-udział w powstaniu koncepcji pracy;</p> <p>prezentacja materiału pracy na konferencji EUDOM 2018;</p> <p>-analiza właściwości strukturalnych i optycznych otrzymanych warstw i kompozytowych scyntylatorów;</p> <p>-analityczne opracowanie widm amplitudowych i krzywych zaniku scyntylacyjnego kompozytowych scyntylatorów przy wzbudzeniu cząstkami α oraz kwantami γ;</p> <p>-badanie wpływu grubości warstw na właściwości kompozytowych scyntylatorów;</p> <p>-uczestnictwo w pisaniu publikacji, a także przeprowadzenie korekt manuskryptu po uwagach recenzentów (autor korespondencyjny)</p>
Vitalii Gorbenko 	<p>-przeprowadzenie procesu wzrostu kompozytowych scyntylatorów metoda LPE;</p> <p>-redakcji części manuskryptu dotyczącej wzrostu warstw</p>
Tetiana Zorenko 	<p>-wykonanie pomiarów absorpcji warstw,</p> <p>-wykonanie pomiarów wydajności i zaników scyntylacyjnych warstw przy wzbudzeniu α-cząstkami źródła ^{239}Pu</p>
Jiri A. Mares 	<p>-wykonanie pomiarów widm amplitudowych scyntylacji oraz analiza zależności wydajności i rozdzielczości energetycznej scyntylacji od czasu rejestracji sygnału scyntylacyjnego;</p> <p>-wykonanie pomiarów zaników scyntylacyjnych kompozytowych scyntylatorów przy wzbudzeniu α-cząstkami ze źródła ^{241}Am i γ kwantami ze źródła ^{137}Cs</p>
Yuriy Zorenko 	<p>-udział w powstaniu koncepcji pracy;</p> <p>-analiza całości materiału eksperymentalnego;</p> <p>-redakcja i korekty całego tekstu pracy</p>

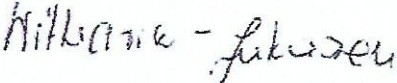
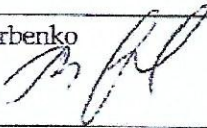
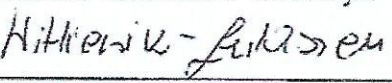
C3.2 S. Witkiewicz-Lukaszek, V. Gorbenko, T. Zorenko, O. Sidletskiy, I. Gerasimov, A. Fedorov, A. Yoshikawa, J. A. Mares, M. Nikl, Yu. Zorenko. Development of Composite Scintillators Based on Single Crystalline Films and Crystals of Ce³⁺-Doped (Lu,Gd)₃(Al,Ga)₅O₁₂ Mixed Garnet Compounds. *Cryst. Growth Des.* 18 (2018) 1834–1842

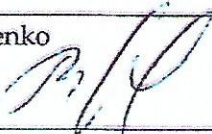
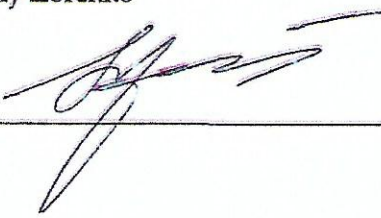
Autorzy	Udział
Sandra Witkiewicz - Łukaszek <i>Witkiewicz - Lukaszek</i>	- udział w powstaniu koncepcji pracy; - wykonanie pomiarów absorpcji warstw oraz kompozytowych scyntylatorów; - przygotowanie materiałów (rysunki, tabele) do publikacji; - uczestnictwo w pisaniu części manuskryptu, dotyczącej właściwości optycznych warstw oraz korekt manuskryptu po uwagach recenzentów
Vitalii Gorbenko <i>V. Gorbenko</i>	- przeprowadzenie procesu wzrostu kompozytowych scyntylatorów metoda LPE; - redakcji części manuskryptu dotyczącej wzrostu warstw
Tetiana Zorenko <i>T. Zorenko</i>	- wykonanie pomiarów wydajności i zaników scyntylacyjnych warstw przy wzbudzeniu α- cząstkami źródła ²³⁹ Pu
Jiri A. Mares <i>J. A. Mares</i>	- wykonanie pomiarów widm amplitudowych scyntylacji oraz analiza zależności wydajności i rozdzielczości energetycznej scyntylacji od czasu rejestracji sygnału scyntylacyjnego; - wykonanie pomiarów zaników scyntylacyjnych kompozytowych scyntylatorów przy wzbudzeniu α cząstkami źródła ²⁴¹ Am i γ kwantami źródła ¹³⁷ Cs
Yuriy Zorenko <i>Y. Zorenko</i>	udział w powstaniu koncepcji pracy; - analiza całości materiału eksperymentalnego; - redakcja i korekty całego tekstu pracy

C3.1. S. Witkiewicz-Lukaszek, V. Gorbenko, T. Zorenko, K. Paprocki, O. Sidletskiy, A. Fedorov, R. Kucerkova, J. A. Mares, M. Nikl, Yu. Zorenko. Epitaxial growth of composite scintillators based on Tb₃Al₅O₁₂:Ce single crystalline films and Gd₃Al_{2.5}Ga_{2.5}O₁₂:Ce crystal substrates. *CrystEngComm* 20 (2018) 3994–4002

Autorzy	Udział
Sandra Witkiewicz - Łukaszek <i>Witkiewicz - Lukaszek</i>	- udział w powstaniu koncepcji pracy; - prezentacja materiału pracy na konferencji IWASOM 2018; - opracowanie wyników badań absorpcji, katodoluminescencji, kinetyki zaniku scyntylacji, widm amplitudowych scyntylacji oraz zależności wydajności i rozdzielczości energetycznej scyntylacji od czasu rejestracji sygnału scyntylacyjnego; - uczestnictwo w pisaniu publikacji, a także przeprowadzenie korekt manuskryptu po uwagach recenzentów (autor korespondencyjny)
V. Gorbenko <i>V. Gorbenko</i>	- przeprowadzenie procesu wzrostu kompozytowych scyntylatorów metoda LPE; - redakcji części manuskryptu dotyczącej wzrostu warstw
Tetiana Zorenko	- wykonanie pomiarów absorpcji warstw;

	<ul style="list-style-type: none"> - wykonanie pomiarów wydajności i zaników scyntylacyjnych warstw przy wzbudzeniu α- cząstkami źródła ^{239}Pu
Jiri A. Mares	<ul style="list-style-type: none"> -wykonanie pomiarów widm amplitudowych scyntylacji oraz analiza zależności wydajności i rozdzielcości energetycznej scyntylacji od czasu rejestracji sygnału scyntylacyjnego; -wykonanie pomiarów zaników scyntylacyjnych kompozytowych scyntylatorów przy wzbudzeniu α cząstkami ze źródła ^{241}Am i γ kwantami ze źródła ^{137}Cs
Yuriy Zorenko	<ul style="list-style-type: none"> -udział w powstaniu koncepcji pracy; -analiza całości materiału eksperymentalnego; -redakcja i korekty całego tekstu pracy
<p>C4.1 S. Witkiewicz-Lukaszek, V. Gorbenko, T. Zorenko, Y. Zorenko, W. Gieszczyk, A. Mrozik, P. Bilski. Composite thermoluminescent detectors based on the Ce³⁺ doped LuAG/YAG and YAG/LuAG epitaxial structures. <i>Radiation Measurements</i> 128 (2019) 106124</p>	
Autorzy	Udział
Sandra Witkiewicz - Łukaszek <i>Hilma Łukaszek</i>	<ul style="list-style-type: none"> -udział w powstaniu koncepcji pracy; -prezentacja materiału pracy na konferencji LUMDETR 2018; -opracowanie wyników badań absorbcji, katodoluminescencji, oraz krzywych jarzenia warstw i kompozytowych struktur epitaksjalnych przy wzbudzeniu cząstkami α i β; -uczestnictwo w pisaniu publikacji oraz przeprowadzenie korekt manuskryptu po uwagach recenzentów (autor korespondencyjny)
Vitalii Gorbenko <i>P. Gorbenko</i>	<ul style="list-style-type: none"> -przeprowadzenie procesu wzrostu kompozytowych materiałów termoluminescencyjnych metoda LPE; -redakcja części manuskryptu dotyczącej wzrostu warstw
Paweł Bilski <i>B. Bilski</i>	<ul style="list-style-type: none"> -pomiar krzywych jarzenia widm warstw i kompozytowych struktur epitaksjalnych przy wzbudzeniu cząstkami α i β; -redakcja części manuskryptu dotyczącej pomiarów termoluminescencji
Tetiana Zorenko <i>T. Zorenko</i>	<ul style="list-style-type: none"> -pomiar widm absorbcji warstw i kompozytowych struktur epitaksjalnych
Yuriy Zorenko <i>Y. Zorenko</i>	<ul style="list-style-type: none"> -udział w powstaniu koncepcji pracy; -analiza całości materiału doświadczalnego; -redakcja i korekty całego tekstu pracy
<p>C4.2 S. Witkiewicz-Lukaszek, A. Mrozik, V. Gorbenko, T. Zorenko, P. Bilski, Yu. Zorenko, LPE growth of composite thermoluminescent detectors based on the Lu_{3-x}Gd_xAl₅O₁₂:Ce single crystalline films and YAG:Ce crystals, <i>Crystals</i>, 2020, 10(3), 189 (zgodnie z udziałem deklarowanym w publikacji)</p>	
Autorzy	Udział
Sandra Witkiewicz - Łukaszek <i>Hilma Łukaszek</i>	<ul style="list-style-type: none"> -prezentacja materiału pracy na konferencji PGSCC 2019; -opracowanie wyników badań absorbcji, katodoluminescencji, oraz krzywych jarzenia warstw i

	<ul style="list-style-type: none"> - wykonanie pomiarów wydajności i zaników scyntylacyjnych warstw przy wzbudzeniu α-cząstkami źródła ^{239}Pu
Jiri A. Mares 	<ul style="list-style-type: none"> -wykonanie pomiarów widm amplitudowych scyntylacji oraz analiza zależności wydajności i rozdzielczości energetycznej scyntylacji od czasu rejestracji sygnału scyntylacyjnego; -wykonanie pomiarów zaników scyntylacyjnych kompozytowych scyntylatorów przy wzbudzeniu α cząstkami ze źródła ^{241}Am i γ kwantami ze źródła ^{137}Cs
Yuriy Zorenko 	<ul style="list-style-type: none"> -udział w powstaniu koncepcji pracy; -analiza całości materiału eksperymentalnego; -redakcja i korekty całego tekstu pracy
C4.1 S. Witkiewicz-Lukaszek, V. Gorbenko, T. Zorenko, Y. Zorenko, W. Gieszczyk, A. Mrozik, P. Bilski. Composite thermoluminescent detectors based on the Ce ³⁺ doped LuAG/YAG and YAG/LuAG epitaxial structures. <i>Radiation Measurements</i> 128 (2019) 106124	
Autorzy	Udział
Sandra Witkiewicz - Łukaszek 	<ul style="list-style-type: none"> -udział w powstaniu koncepcji pracy; -prezentacja materiału pracy na konferencji LUMDETR 2018; -opracowanie wyników badań absorbacji, katodoluminescencji, oraz krzywych jarzenia warstw i kompozytowych struktur epitaksjalnych przy wzbudzeniu cząstkami α i β; -uczestnictwo w pisaniu publikacji oraz przeprowadzenie korekt manuskryptu po uwagach recenzentów (autor korespondencyjny)
Vitalii Gorbenko 	<ul style="list-style-type: none"> -przeprowadzenie procesu wzrostu kompozytowych materiałów termoluminescencyjnych metoda LPE; -redakcja części manuskryptu dotyczącej wzrostu warstw
Paweł Bilski	<ul style="list-style-type: none"> -pomiar krzywych jarzenia widm warstw i kompozytowych struktur epitaksjalnych przy wzbudzeniu cząstkami α i β; -redakcja części manuskryptu dotyczącej pomiarów termoluminescencji
Tetiana Zorenko 	<ul style="list-style-type: none"> -pomiar widm absorbacji warstw i kompozytowych struktur epitaksjalnych
Yuriy Zorenko 	<ul style="list-style-type: none"> -udział w powstaniu koncepcji pracy; -analiza całości materiału doświadczalnego; -redakcja i korekty całego tekstu pracy
C4.2 S. Witkiewicz-Lukaszek, A. Mrozik, V. Gorbenko, T. Zorenko, P. Bilski, Yu. Zorenko, LPE growth of composite thermoluminescent detectors based on the Lu _{3-x} Gd _x Al ₅ O ₁₂ :Ce single crystalline films and YAG:Ce crystals, <i>Crystals</i> , 2020, 10(3), 189 (zgodnie z udziałem deklarowanym w publikacji)	
Autorzy	Udział
Sandra Witkiewicz - Łukaszek 	<ul style="list-style-type: none"> -prezentacja materiału pracy na konferencji PGSCC 2019; -opracowanie wyników badań absorbacji, katodoluminescencji, oraz krzywych jarzenia warstw i

	<p>kompozytowych struktur epitaksjalnych przy wzbudzeniu cząstkami α i β;</p> <ul style="list-style-type: none"> - napisanie tekstu publikacji oraz przeprowadzenie korekt manuskryptu po uwagach recenzentów (autor korespondencyjny)
Vitalii Gorbenko 	<ul style="list-style-type: none"> - przeprowadzenie procesu wzrostu kompozytowych materiałów termoluminescentnych metoda LPE; - redakcji części manuskryptu dotyczącej wzrostu warstw
Paweł Bilski 	<ul style="list-style-type: none"> - pomiar krzywych jarzenia widm warstw i kompozytowych struktur epitaksjalnych przy wzbudzeniu cząstkami α i β; - redakcja części manuskryptu dotyczącej pomiarów termoluminescencji
Tetiana Zorenko 	<ul style="list-style-type: none"> - pomiar widm absorbcji warstw i kompozytowych struktur epitaksjalnych
Yuriy Zorenko 	<ul style="list-style-type: none"> - udział w powstaniu koncepcji pracy; - analiza całości materiału doświadczalnego; - redakcja i korekty tekstu manuskryptu, a głównie spisanie części „Introduction” oraz „Conclusion”

Prague, 6th May 2020

CO-AUTHORSHIP DECLARATION

concerning PhD dissertation of Sandra Witkiewicz-Łukaszek, MSc.

I hereby declare my co-authorship in the following articles:

C2.1 S. Witkiewicz-Lukaszek, V. Gorbenko, T. Zorenko, K. Paprocki, O. Sidletskiy, I. Gerasymov, J.A. Mares, R. Kucerkova, M. Nikl, Yu. Zorenko. Novel all-solid-state composite scintillators based on the epitaxial structures of LuAG garnet doped with Pr, Sc and Ce ions. *IEEE Transactions on Nuclear Science* 65 (2018) 2114 – 2119

C2.2 S. Witkiewicz-Lukaszek, V. Gorbenko, T. Zorenko, K. Paprocki, O. Sidletskiy, I. Gerasymov, J.A. Mares, R. Kucerkova, M. Nikl, Yu. Zorenko. Composite scintillators based on the crystals and single crystalline films of LuAG garnet doped with Ce³⁺, Pr³⁺ and Sc³⁺ ions. *Optical Materials* 84 (2018) 593-599

C2.3 J.A. Mares, S. Witkiewicz-Lukaszek, V. Gorbenko, T. Zorenko, R. Kucerkova, A. Beitlerova, C. D'Ambrosio, J. Dlouhy, M. Nikl, Yu. Zorenko. Alpha and gamma spectroscopy of composite scintillators based on the LuAG:Pr crystals and single crystalline films of LuAG:Ce and (Lu,Gd,Tb)AG:Ce garnets. *Optical Materials* 96 (2019) 109268

C2.4 S. Witkiewicz-Lukaszek, V. Gorbenko, T. Zorenko, O. Sidletskiy, P. Arhipov, A. Fedorov, J.A. Mares, R. Kucerkova, M. Nikl, Yu. Zorenko, High-performance composite scintillators based on the single crystalline films and crystals of LuAG garnet, CrystEngComm, *CrystEngComm* (2020) published online on 06.04.2020, <https://doi.org/10.1039/D0CE00266F>

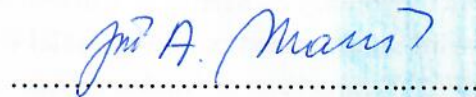
C3.1. S. Witkiewicz-Lukaszek, V. Gorbenko, T. Zorenko, K. Paprocki, O. Sidletskiy, A. Fedorov, R. Kucerkova, J. A. Mares, M. Nikl, Yu. Zorenko. Epitaxial growth of composite scintillators based on Tb₃Al₅O₁₂:Ce single crystalline films and Gd₃Al_{2.5}Ga_{2.5}O₁₂:Ce crystal substrates. *CrystEngComm* 20 (2018) 3994-4002

C3.2 S. Witkiewicz-Lukaszek, V. Gorbenko, T. Zorenko, O. Sidletskiy, I. Gerasymov, A. Fedorov, A. Yoshikawa, J. A. Mares, M. Nikl, Yu. Zorenko. Development of Composite Scintillators Based on Single Crystalline Films and Crystals of Ce³⁺-Doped (Lu,Gd)₃(Al,Ga)₅O₁₂ Mixed Garnet Compounds. *Cryst. Growth Des.* 18 (2018) 1834–1842

My contribution to these articles is the measurements of the scintillation decay response of composite scintillators under excitation by α particles from ^{241}Am and γ quanta from ^{137}Cs radioisotopes in C2.1, C2.2, C2.3, C2.4, C3.1, C3.2 publications. The measurements of pulse height spectra and estimation of the scintillation efficiency and energy resolution dependence on the shaping time of scintillation signal registration in C2.2, C2.3, C2.4, C3.1, C3.2 publications. Apart that, my contribution to C2.3 publication is related to the writing and reviewing of the manuscript as corresponding author.

I estimated my contribution of around 15% and 30% in C2.1, C2.2, C2.3, C2.4, C3.1, C3.2, and C2.3 publications, respectively. Moreover, regarding the contribution of the other co-authors, I confirm the dominant contribution of PhD student Sandra Witkiewicz-Łukaszek in the preparation of these publications as a whole.

Yours sincerely,



Jiri A. Mares

Senior scientist

Institute of Physics, Academy of Sciences of the Czech Republic, Cukrovarnicka 10
Prague 6, Czech Republic



Tel. : (+48 12) 662 8414
Fax: (+48 12) 662 8066
E-mail: pawel.bilski@ifj.edu.pl

INSTYTUT FIZYKI JĄDROWEJ
im. Henryka Niewodniczańskiego
POLSKIEJ AKADEMII NAUK
ul. Radzikowskiego 152, 31-342 Kraków
Zakład Fizyki Radiacyjnej i Dozymetrii

Kraków,

Oświadczenie współautora

Oświadczam, że w ramach współpracy naukowej opublikowałem z Panią
mgr Sandrą Witkiewicz-Łukaszek następujące prace:

C1.1 Y. Zorenko, P. Douissard, T. Martin, F. Riva, V. Gorbenko, T. Zorenko, K. Paprocki, A. Iskalieva, S. Witkiewicz, A. Fedorov, P. Bilski, A. Twardak. Scintillating screens based on the LPE grown $Tb_3Al_5O_{12}:Ce$ single crystalline films. *Optical Materials* 65 (2017) 73-81

C1.2 V. Gorebenko, T. Zorenko, S., Witkiewicz, K. Paprocki, O. Sidletskiy, A. Fedorov, P. Bilski, A. Twardak, Y. Zorenko. LPE growth of single crystalline film scintillators based on Ce^{3+} doped $Tb_3-xGd_xAl_5-yGa_5O_{12}$ mixed garnets. *Crystals* 7 (2017) 262.

C4.1 S. Witkiewicz-Lukaszek, V. Gorbenko, T. Zorenko, Y. Zorenko, W. Gieszczyk, A. Mrozik, P. Bilski. Composite thermoluminescent detectors based on the Ce^{3+} doped LuAG/YAG and YAG/LuAG epitaxial structures. *Radiation Measurements* 128 (2019) 106124

C4.2 S. Witkiewicz-Lukaszek, A. Mrozik, V. Gorbenko, T. Zorenko, P. Bilski, Yu. Zorenko, LPE growth of composite thermoluminescent detectors based on the $Lu_{3-x}Gd_xAl_5O_{12}:Ce$ single crystalline films and YAG:Ce crystals, *Crystals*, 2020, 10(3), 189.

W których mój wkład polegał na pomiarze krzywych jarzenia i widm termoluminescencji oraz pomocy przy redakcji części pracy, dotyczącej pomiarów termoluminescencji. Swój udział w pracach określам na 12-15% tym samym oświadczając, dominującą rolę Doktorantki w procesie powstania tych prac oraz przygotowania odpowiednich manuskryptów.

Z poważaniem

Paw. Bilski



UNIWERSYTET KAZIMIERZA WIELKIEGO W BYDGOSZCZY
INSTYTUT FIZYKI

ul. Powstańców Wielkopolskich 2, 85-090 Bydgoszcz, tel. (52) 321 50 74 w.59
strona: www.fizyka.ukw.edu.pl e-mail: fizyka@ukw.edu.pl



Bydgoszcz, 30.04.2020

Oświadczenie współautora

Oświadczam, że w ramach współpracy naukowej opublikowałam z Panią
mgr Sandrą Witkiewicz-Łukaszek następujące prace:

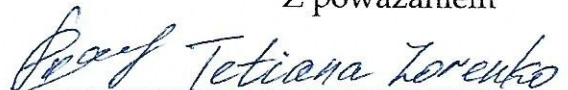
- C1.1 Y. Zorenko, P. Douissard, T. Martin, F. Riva, V. Gorbenko, T. Zorenko, K. Paprocki, A. Iskalieva, S. Witkiewicz, A. Fedorov, P. Bilski, A. Twardak. Scintillating screens based on the LPE grown $Tb_3Al_5O_{12}:Ce$ single crystalline films. *Optical Materials* 65 (2017) 73-81
- C1.2. V. Gorbenko, T. Zorenko, S. Witkiewicz, K. Paprocki, O. Sidletskiy, A. Fedorov, P. Bilski, A. Twardak, Y. Zorenko. LPE growth of single crystalline film scintillators based on Ce^{3+} doped $Tb_{3-x}Gd_xAl_{5-y}Ga_yO_{12}$ mixed garnets. *Crystals* 7 (2017) 262.
- C2.1 S. Witkiewicz-Lukaszek, V. Gorbenko, T. Zorenko, K. Paprocki, O. Sidletskiy, I. Gerasymov, J.A. Mares, R. Kucerkova, M. Nikl, Yu. Zorenko. Novel all-solid-state composite scintillators based on the epitaxial structures of LuAG garnet doped with Pr, Sc and Ce ions. *IEEE Transactions on Nuclear Science* 65 (2018) 2114 – 2119
- C2.2 S. Witkiewicz-Lukaszek, V. Gorbenko, T. Zorenko, K. Paprocki, O. Sidletskiy, I. Gerasymov, J.A. Mares, R. Kucerkova, M. Nikl, Yu. Zorenko. Composite scintillators based on the crystals and single crystalline films of LuAG garnet doped with Ce^{3+} , Pr^{3+} and Sc^{3+} ions. *Optical Materials* 84 (2018) 593-599
- C2.3 J.A. Mares, S. Witkiewicz-Lukaszek, V. Gorbenko, T. Zorenko, R. Kucerkova, A. Bejtlerova, C. D'Ambrosio, J. Dlouhy, M. Nikl, Yu. Zorenko. Alpha and gamma spectroscopy of composite scintillators based on the LuAG:Pr crystals and single crystalline films of LuAG:Ce and (Lu,Gd,Tb)AG:Ce garnets. *Optical Materials* 96 (2019) 109268
- C2.4 S. Witkiewicz-Lukaszek, V. Gorbenko, T. Zorenko, O. Sidletskiy, P. Arhipov, A. Fedorov, J.A. Mares, R. Kucerkova, M. Nikl, Yu. Zorenko, High-performance composite scintillators based on the single crystalline films and crystals of LuAG garnet, CrystEngComm, *CrystEngComm* (2020) opublikowany on-line 06.04.2020, <https://doi.org/10.1039/D0CE00266F>
- C3.1 S. Witkiewicz-Lukaszek, V. Gorbenko, T. Zorenko, K. Paprocki, O. Sidletskiy, A. Fedorov, R. Kucerkova, J. A. Mares, M. Nikl, Yu. Zorenko. Epitaxial growth of composite scintillators based on $Tb_3Al_5O_{12}:Ce$ single crystalline films and $Gd_3Al_{2.5}Ga_{2.5}O_{12}:Ce$ crystal substrates. *CrystEngComm* 20 (2018) 3994-4002
- C3.2 S. Witkiewicz-Lukaszek, V. Gorbenko, T. Zorenko, O. Sidletskiy, I. Gerasymov, A. Fedorov, A. Yoshikawa, J. A. Mares, M. Nikl, Yu. Zorenko. Development of Composite Scintillators Based on Single Crystalline Films and Crystals of Ce^{3+} -Doped $(Lu,Gd)_3(Al,Ga)_5O_{12}$ Mixed Garnet Compounds. *Cryst. Growth Des.* 18 (2018) 1834–1842

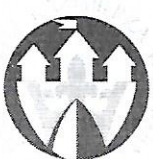
C4.1 S. Witkiewicz-Lukaszek, V. Gorbenko, T. Zorenko, Y. Zorenko, W. Gieszczyk, A. Mrozik, P. Bilski. Composite thermoluminescent detectors based on the Ce³⁺ doped LuAG/YAG and YAG/LuAG epitaxial structures. *Radiation Measurements* 128 (2019) 106124

C4.2 S. Witkiewicz-Lukaszek, A. Mrozik, V. Gorbenko, T. Zorenko, P. Bilski, Yu. Zorenko, LPE growth of composite thermoluminescent detectors based on the Lu_{3-x}Gd_xAl₅O₁₂:Ce single crystalline films and YAG:Ce crystals, *Crystals*, 2020, 10(3), 189.

We wszystkich w/w publikacjach jestem współautorem, którego rola polegała na wykonaniu pomiarów absorpcji w publikacjach C1.1, C2.2, C2.4, C3.1, C3.2, C4.1, C4.2 oraz wykonaniu pomiarów wydajności i zaników scyntylacyjnych warstw przy wzbudzeniu α- częstotliwość źródła ²³⁹Pu w pracach C1.2, C2.1, C2.2, C2.3, C2.4, C3.1. Swój wkład w powstaniu tych publikacji oceniam na 5-6 %. Oceniając także wkład innych autorów, oświadczam dominującą rolę Pani mgr Sandry Witkiewicz w powstaniu manuskryptów tych prac oraz ich publikacji.

Z poważaniem

Tetiana Zorenko



Bydgoszcz, 30.04.2020

Oświadczenie współautora

Oświadczam, że w ramach współpracy naukowej opublikowałem z Panią mgr Sandrą Witkiewicz-Łukaszek następujące prace:

- C1.1 Y. Zorenko, P. Douissard, T. Martin, F. Riva, V. Gorbenko, T. Zorenko, K. Paprocki, A. Iskalieva, S. Witkiewicz, A. Fedorov, P. Bilski, A. Twardak. Scintillating screens based on the LPE grown $Tb_3Al_5O_{12}:Ce$ single crystalline films. *Optical Materials* 65 (2017) 73-81
- C1.2. V. Gorbenko, T. Zorenko, S. Witkiewicz, K. Paprocki, O. Sidletskiy, A. Fedorov, P. Bilski, A. Twardak, Y. Zorenko. LPE growth of single crystalline film scintillators based on Ce^{3+} doped $Tb_{3-x}Gd_xAl_{5-y}Ga_yO_{12}$ mixed garnets. *Crystals* 7 (2017) 262.
- C2.1 S. Witkiewicz-Lukaszek, V. Gorbenko, T. Zorenko, K. Paprocki, O. Sidletskiy, I. Gerasymov, J.A. Mares, R. Kucerkova, M. Nikl, Yu. Zorenko. Novel all-solid-state composite scintillators based on the epitaxial structures of LuAG garnet doped with Pr, Sc and Ce ions. *IEEE Transactions on Nuclear Science* 65 (2018) 2114 – 2119
- C2.2 S. Witkiewicz-Lukaszek, V. Gorbenko, T. Zorenko, K. Paprocki, O. Sidletskiy, I. Gerasymov, J.A. Mares, R. Kucerkova, M. Nikl, Yu. Zorenko. Composite scintillators based on the crystals and single crystalline films of LuAG garnet doped with Ce^{3+} , Pr^{3+} and Sc^{3+} ions. *Optical Materials* 84 (2018) 593-599
- C2.3 J.A. Mares, S. Witkiewicz-Lukaszek, V. Gorbenko, T. Zorenko, R. Kucerkova, A. Beitlerova, C. D'Ambrosio, J. Dlouhy, M. Nikl, Yu. Zorenko. Alpha and gamma spectroscopy of composite scintillators based on the LuAG:Pr crystals and single crystalline films of LuAG:Ce and (Lu,Gd,Tb)AG:Ce garnets. *Optical Materials* 96 (2019) 109268
- C2.4 S. Witkiewicz-Lukaszek, V. Gorbenko, T. Zorenko, O. Sidletskiy, P. Arhipov, A. Fedorov, J.A. Mares, R. Kucerkova, M. Nikl, Yu. Zorenko, High-performance composite scintillators based on the single crystalline films and crystals of LuAG garnet, *CrystEngComm*, *CrystEngComm* (2020) opublikowany on-line 06.04.2020, <https://doi.org/10.1039/D0CE00266F>
- C3.1 S. Witkiewicz-Lukaszek, V. Gorbenko, T. Zorenko, K. Paprocki, O. Sidletskiy, A. Fedorov, R. Kucerkova, J. A. Mares, M. Nikl, Yu. Zorenko. Epitaxial growth of composite scintillators based on $Tb_3Al_5O_{12}:Ce$ single crystalline films and $Gd_3Al_{2.5}Ga_{2.5}O_{12}:Ce$ crystal substrates. *CrystEngComm* 20 (2018) 3994-4002
- C3.2 S. Witkiewicz-Lukaszek, V. Gorbenko, T. Zorenko, O. Sidletskiy, I. Gerasymov, A. Fedorov, A. Yoshikawa, J. A. Mares, M. Nikl, Yu. Zorenko. Development of Composite Scintillators Based on Single Crystalline Films and Crystals of Ce^{3+} -Doped $(Lu,Gd)_3(Al,Ga)_5O_{12}$ Mixed Garnet Compounds. *Cryst. Growth Des.* 18 (2018) 1834–1842

C4.1 S. Witkiewicz-Lukaszek, V. Gorbenko, T. Zorenko, Y. Zorenko, W. Gieszczyk, A. Mrozik, P. Bilski. Composite thermoluminescent detectors based on the Ce³⁺ doped LuAG/YAG and YAG/LuAG epitaxial structures. *Radiation Measurements* 128 (2019) 106124

C4.2 S. Witkiewicz-Lukaszek, A. Mrozik, V. Gorbenko, T. Zorenko, P. Bilski, Yu. Zorenko, LPE growth of composite thermoluminescent detectors based on the Lu_{3-x}Gd_xAl₅O₁₂:Ce single crystalline films and YAG:Ce crystals, *Crystals*, 2020, 10(3), 189.

We wszystkich w.w. publikacjach, które stanowią cykl powiązanych ze sobą prac jestem współautorem. Mój udział w pracach C1.1, C2.1, C2.2, C2.3, C2.4, C3.1, C3.2, C4.1 oraz C.4.2 polegał na krystalizacji badanych warstw oraz kompozytowych scyntylatorów metodą epitaksji z fazy ciekłej. Dodatkowo mój wkład polegał na pomocy przy redakcji części manuskryptów, dotyczącej wzrostu badanych materiałów. Swój udział w tych pracach określam na 15-20 %, tym samym oświadczając dominującą rolę Doktorantki w procesie powstania tych prac oraz przygotowania odpowiednich manuskryptów.

W prace C1.2 jestem pierwszym autorem i autorem korespondencyjnym i swój wkład w powstanie tej pracy oceniam na 40 %.

Z poważaniem

Bał. Vitalij Gorbenko



UNIWERSYTET KAZIMIERZA WIELKIEGO W BYDGOSZCZY
INSTYTUT FIZYKI

ul. Powstańców Wielkopolskich 2, 85-090 Bydgoszcz, tel. (52) 321 50 74 w.59
strona: www.fizyka.ukw.edu.pl e-mail: fizyka@ukw.edu.pl



Bydgoszcz, 31.04.2020

Oświadczenie współautora

Oświadczam, że w ramach współpracy naukowej opublikowałem z Panią mgr Sandrą Witkiewicz-Łukaszek następujące prace:

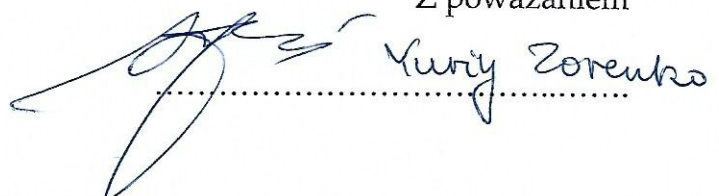
- C1.1 Y. Zorenko, P. Douissard, T. Martin, F. Riva, V. Gorbenko, T. Zorenko, K. Paprocki, A. Iskalieva, S. Witkiewicz, A. Fedorov, P. Bilski, A. Twardak. Scintillating screens based on the LPE grown $Tb_3Al_5O_{12}:Ce$ single crystalline films. *Optical Materials* 65 (2017) 73-81
- C1.2. V. Gorbenko, T. Zorenko, S. Witkiewicz, K. Paprocki, O. Sidletskiy, A. Fedorov, P. Bilski, A. Twardak, Y. Zorenko. LPE growth of single crystalline film scintillators based on Ce^{3+} doped $Tb_{3-x}Gd_xAl_{5-y}Ga_yO_{12}$ mixed garnets. *Crystals* 7 (2017) 262.
- C2.1 S. Witkiewicz-Lukaszek, V. Gorbenko, T. Zorenko, K. Paprocki, O. Sidletskiy, I. Gerasymov, J.A. Mares, R. Kucerkova, M. Nikl, Yu. Zorenko. Novel all-solid-state composite scintillators based on the epitaxial structures of LuAG garnet doped with Pr, Sc and Ce ions. *IEEE Transactions on Nuclear Science* 65 (2018) 2114 – 2119
- C2.2 S. Witkiewicz-Lukaszek, V. Gorbenko, T. Zorenko, K. Paprocki, O. Sidletskiy, I. Gerasymov, J.A. Mares, R. Kucerkova, M. Nikl, Yu. Zorenko. Composite scintillators based on the crystals and single crystalline films of LuAG garnet doped with Ce^{3+} , Pr^{3+} and Sc^{3+} ions. *Optical Materials* 84 (2018) 593-599
- C2.3 J.A. Mares, S. Witkiewicz-Lukaszek, V. Gorbenko, T. Zorenko, R. Kucerkova, A. Bejtlerova, C. D'Ambrosio, J. Dlouhy, M. Nikl, Yu. Zorenko. Alpha and gamma spectroscopy of composite scintillators based on the LuAG:Pr crystals and single crystalline films of LuAG:Ce and (Lu,Gd,Tb)AG:Ce garnets. *Optical Materials* 96 (2019) 109268
- C2.4 S. Witkiewicz-Lukaszek, V. Gorbenko, T. Zorenko, O. Sidletskiy, P. Arhipov, A. Fedorov, J.A. Mares, R. Kucerkova, M. Nikl, Yu. Zorenko, High-performance composite scintillators based on the single crystalline films and crystals of LuAG garnet, *CrystEngComm*, *CrystEngComm* (2020) opublikowany on-line 06.04.2020, <https://doi.org/10.1039/D0CE00266F>
- C3.1 S. Witkiewicz-Lukaszek, V. Gorbenko, T. Zorenko, K. Paprocki, O. Sidletskiy, A. Fedorov, R. Kucerkova, J. A. Mares, M. Nikl, Yu. Zorenko. Epitaxial growth of composite scintillators based on $Tb_3Al_5O_{12}:Ce$ single crystalline films and $Gd_3Al_{2.5}Ga_{2.5}O_{12}:Ce$ crystal substrates. *CrystEngComm* 20 (2018) 3994-4002
- C3.2 S. Witkiewicz-Lukaszek, V. Gorbenko, T. Zorenko, O. Sidletskiy, I. Gerasymov, A. Fedorov, A. Yoshikawa, J. A. Mares, M. Nikl, Yu. Zorenko. Development of Composite Scintillators Based on Single Crystalline Films and Crystals of Ce^{3+} -Doped $(Lu,Gd)_3(Al,Ga)_5O_{12}$ Mixed Garnet Compounds. *Cryst. Growth Des.* 18 (2018) 1834–1842

C4.1 S. Witkiewicz-Lukaszek, V. Gorbenko, T. Zorenko, Y. Zorenko, W. Gieszczyk, A. Mrozik, P. Bilski. Composite thermoluminescent detectors based on the Ce³⁺ doped LuAG/YAG and YAG/LuAG epitaxial structures. *Radiation Measurements* 128 (2019) 106124

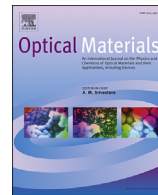
C4.2 S. Witkiewicz-Lukaszek, A. Mrozik, V. Gorbenko, T. Zorenko, P. Bilski, Yu. Zorenko, LPE growth of composite thermoluminescent detectors based on the Lu_{3-x}Gd_xAl₅O₁₂:Ce single crystalline films and YAG:Ce crystals, *Crystals*, 2020, 10(3), 189.

We wszystkich wymienionych publikacjach jestem współautorem, którego rola polegała na dyskusjach z doktorantką o koncepcji powstania tych prac oraz pomocy doktorantce przy analizie całości wyników eksperymentalnych. Dodatkowo sprawowałem opiekę naukową nad stworzonymi manuskryptami oraz wprowadziłem niezbędne korekty redakcyjne. W publikacjach C1.1, C1.2, C3.1, C3.2, jestem jedynym autorem korespondencyjnym, co oznacza, że po dyskusji z doktorantką oraz innymi współautorami byłem odpowiedzialny za ostateczną formę prac. Natomiast w pracach C2.1, C2.2 i 2.3 oraz C4.2 i C4.2 Doktorantka także była autorem korespondencyjnym. Swój udział w tych pracach określam na 20-25%, tym samym oświadczając dominującą rolę Doktorantki w całym procesie powstania tych prac oraz przygotowania odpowiednich manuskryptów.

Z poważaniem



Yuriy Zorenko



Scintillating screens based on the LPE grown $\text{Tb}_3\text{Al}_5\text{O}_{12}:\text{Ce}$ single crystalline films

Yuriy Zorenko ^{a,*}, Paul-Antoine Douissard ^{b,**}, Thierry Martin ^b, Federica Riva ^{b,c}, Vitaliy Gorbenko ^{a,d}, Tetiana Zorenko ^a, Kazimierz Paprocki ^a, Aizhan Iskalieva ^a, Sandra Witkiewicz ^a, Alexander Fedorov ^e, Paweł Bilski ^f, Anna Twardak ^f

^a Institute of Physics of Kazimierz Wielki University in Bydgoszcz, Bydgoszcz, Poland

^b European Synchrotron Radiation Facility (ESRF), Grenoble, France

^c Institute Lumière Matière, UMR5306 CNRS, Claude Bernard University Lyon 1, France

^d Electronics Department of Ivan Franko National University in Lviv, Lviv, Ukraine

^e SSI Institute for Single Crystals, National Academy of Sciences of Ukraine, Kharkiv, Ukraine

^f Institute of Nuclear Physics, Polish Academy of Sciences, Krakow, Poland

ARTICLE INFO

Article history:

Received 16 July 2016

Received in revised form

24 September 2016

Accepted 25 September 2016

Available online 30 September 2016

Keywords:

Liquid phase epitaxy

Single crystalline films

Scintillating screens

$\text{Tb}_3\text{Al}_5\text{O}_{12}$ garnet

Ce^{3+} dopant

ABSTRACT

We report in this work the creation of new heavy and efficient $\text{Tb}_3\text{Al}_5\text{O}_{12}:\text{Ce}$ (TbAG:Ce) single crystalline film (SCF) scintillators, grown by LPE method from $\text{PbO}-\text{B}_2\text{O}_3$ based flux onto $\text{Y}_3\text{Al}_5\text{O}_{12}$ (YAG) and $\text{Gd}_3\text{Ga}_2.5\text{Al}_{2.5}\text{O}_{12}$ (GAGG) substrates, for different optoelectronic applications. The luminescent and scintillation properties of the TbAG:Ce SCF screens, grown onto different types of substrates, are studied and compared with the properties of the $\text{Lu}_3\text{Al}_5\text{O}_{12}:\text{Ce}$ (LuAG:Ce) and YAG:Ce SCF counterparts. TbAG:Ce SCFs show very high scintillation light yield (LY) under α -particles excitation, which overcomes by 30% the LY of high-quality LuAG:Ce SCF samples. In comparison with YAG:Ce and LuAG:Ce SCFs, TbAG:Ce SCF screens show also significantly lower afterglow (up to 10^{-4} level at X-ray burst duration of 0.1 s), which is comparable with the afterglow level of the best samples of LSO:Ce, Tb SCFs typically being used now for microimaging. Together with a high light output of X-ray excited luminescence, such extremely low afterglow of TbAG:Ce SCF is a very good reason for future development of scintillating screens based on the mentioned garnet. We also introduce the possibility to create new types of "film-substrate" hybrid scintillators using the LPE method for simultaneous registration of different components of ionizing radiation and microimaging based on the TbAG:Ce SCF and GAGG:Ce substrates.

© 2016 Elsevier B.V. All rights reserved.

1. Introduction

Synchrotron radiation sources with energy in X-ray range make it possible to visualize X-ray images with micron-submicron spatial resolution for application in microtomography and non-destructive testing in biology, archeology and materials science. X-ray detector with spatial resolution in the micron range using a screen in the form of thin ($5 \mu\text{m}$) $\text{Y}_3\text{Al}_5\text{O}_{12}:\text{Ce}$ (YAG:Ce) garnet single crystalline films (SCF), and deposited by the liquid phase epitaxy (LPE) on YAG substrates, was first designed at the ESRF (Grenoble, France) [1,2]. Detector spatial resolution in the *micron range* was achieved using

the synchrotron radiation with energy in the 5–20 eV range [1,2].

Meanwhile, the further increase of X-ray detectors spatial resolution to submicron range can only be achieved by reducing the SCF thickness. It also requires scintillation screens with high X-rays absorption coefficient $\mu \sim \rho Z_{\text{eff}}^4$ (where ρ is density and Z_{eff} is effective atomic number of scintillator) and a good overlap of the SCF emission spectrum with the sensitivity range of typical CCD sensors [3].

In the past, two novel concepts of detectors for X-ray microtomography were proposed [4–7].

The first concept is based on the creation of hybrid multi-layer scintillators with separate pathways for registration of the optical signal coming from each scintillating layers and their final combination (Fig. 1). Using the hybrid film scintillators could improve the detector system Detective Quantum Efficiency (DQE) [4] and provide information on the incoming X-ray radiation energy [5,6].

* Corresponding author.

** Corresponding author.

E-mail address: zorenko@ukw.edu.pl (Y. Zorenko).

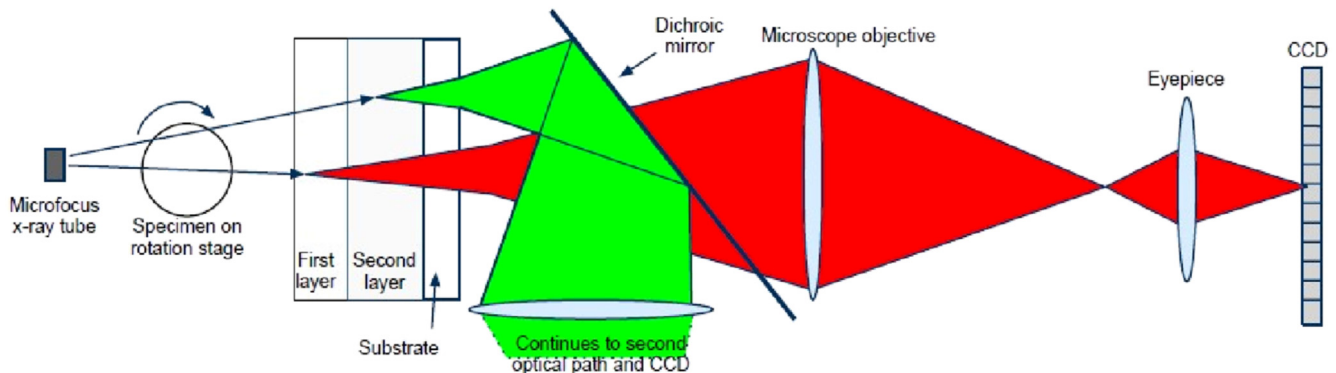


Fig. 1. Scheme of hybrid detector for X-ray micro-imaging containing two LPE grown film scintillators grown onto the same substrates [4].

The second concept is connected with the engineering of „X-ray absorption K-edge” multilayer-film scintillators, using the solid solution of oxide compounds containing for example Lu, Gd or Tb ions [7,8] (Fig. 2). In such a way, the absorption ability of the multilayer scintillator can be significantly improved in the 20–65 keV range, due to the significant broadening of the X-ray absorption K-edge in such multicomponent materials [7,8]. However such novel concept requires the development of different efficient and heavy SCF scintillator materials, which can be deposited onto the same luminescent or non-luminescent substrates.

Among the known garnet compounds, Lu₃Al₅O₁₂:Ce (LuAG:Ce) garnet ($\rho Z_{\text{eff}}^4 = 90 \cdot 10^6 \text{ g/cm}^3$), is a dense and efficient X-ray scintillator [3]. In our previous papers [9–11] we demonstrated the possibility of producing LuAG:Ce SCF grown by the LPE method onto YAG substrates.

For better matching of the CCD sensor spectral sensitivity, the optimization of SCF emission is performed in the green or red spectral region [7,11]. For this reason, we continued to investigate the crystallization of scintillating screens based on multicomponent rare-earth garnets [10,12–14]. In this work we concentrated on the study of Ce doped Tb₃Al₅O₁₂ (TbAG) garnets, grown by LPE method onto YAG and Gd₃Al_{2.5}Ga_{2.5}O₁₂ (GAGG) substrates.

Compared to YAG:Ce and LuAG:Ce, the Ce³⁺ ion emission spectrum in TbAG:Ce can be significantly shifted to the red range [15,16]. For this reason, and due to the large density and effective atomic number of TbAG ($\rho Z_{\text{eff}}^4 = 90 \cdot 10^6 \text{ g/cm}^3$) hosts, growth of

TbAG:Ce SCF can be very perspective for the development of SCF screens used in the visualization of X-ray images [10]. We present in this paper new results on TbAG:Ce films grown by LPE and compare their properties with those of LuAG:Ce and YAG:Ce SCF counterparts.

2. Growth of TbAG:Ce SCFs

Three sets of Ce-doped TbAG:Ce SCFs (denoted A, G and T sets) were grown using the LPE method onto Y₃Al₅O₁₂ (YAG) and Gd₃Al_{2.5}Ga_{2.5}O₁₂ (GAGG) substrates with different orientations from typical melt-solution (MS) based on the PbO:B₂O₃ (12:1 mole/mole) flux and the crystal-forming R₂O₃ and Al₂O₃ oxides of 4N-5N purity in a total concentration of 2.5–5 mole% with respect to the total content of the MS (Table 1). The first set of undoped TbAG and Ce³⁺ doped TbAG SCFs (A set) was grown in the Laboratory of Optoelectronic Material, University of Lviv, Ukraine from the 4 N row materials onto YAG substrates with orientation close to (211) and lattice constant of 12.011 Å [10]. The second set of TbAG:Ce SCFs (G set) was grown in the LPE Laboratory at the ESRF in Grenoble, France, using 5 N raw materials onto YAG substrates with (111) orientation. The third set of TbAG:Ce SCFs (T set) was grown in the Institute of Physics UKW in Bydgoszcz, Poland using 5 N row materials onto YAG substrates with (110) orientation (T1 set) and Gd₃Al_{2.5}Ga_{2.5}O₁₂ (GAGG) substrates with (100) orientation (T2 set) with a lattice constant of 12.233 Å.

In all growth cycles, the growth temperature T_s was in the 950–1025 °C range. The growth rate was in the range

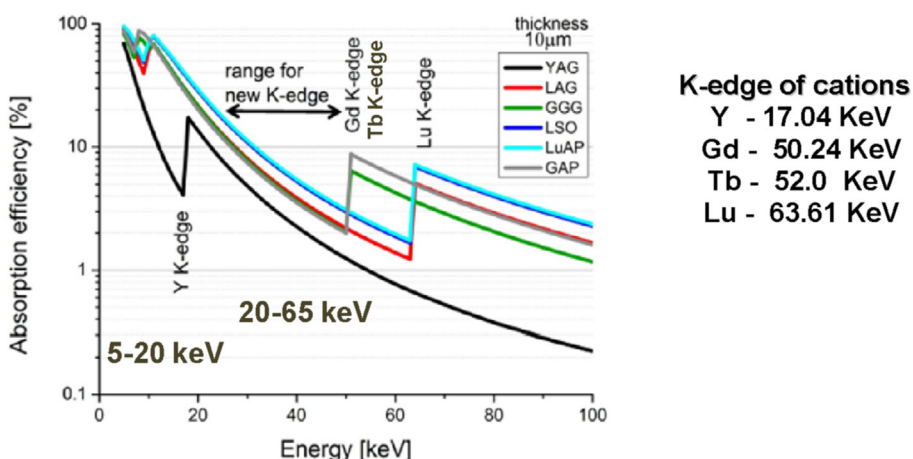


Fig. 2. Absorption ability of scintillation screens in the 20–65 keV range using the Gd, Tb and Lu ions.

Table 1

Growth conditions (type of flux and substrate; misfit $\mathbf{m} = \frac{\mathbf{a}_{\text{SCF}} - \mathbf{a}_{\text{sub}}}{\mathbf{a}_{\text{SCF}}} * 100\%$ between lattice constant of SCF and substrate), maximum of emission spectra λ_{max} , scintillation decay time $t_{1/e}/t_{1/10}$ and LY of the best TbAG:Ce SCF samples under excitation by α -particles from a Pu²³⁹ source (measured with a shaping time of 12 μs) in comparison with standard YAG:Ce SCF (386 phels/MeV) [17] and LuAG:Ce SCF, reference Gd₃Al_{2.5}Ga_{2.5}O₁₂:Ce SCF and Gd₃Al₂Ga₃O₁₂:Ce bulk crystals.

Content of garnet	Substrate	\mathbf{m} , %	λ_{max} , nm	Scintillation decay time, $t_{1/e}/t_{1/10}$, ns	LY, %
Y ₃ Al ₅ O ₁₂ :Ce SCF	YAG	—	535	57.3/132	100
Lu ₃ Al ₅ O ₁₂ :Ce SCF	YAG	-0.78	509	52.8/142	205
Tb ₃ Al ₅ O ₁₂ SCF A set	YAG	+0.52	543		
Tb ₃ Al ₅ O ₁₂ :Ce SCF A set	YAG	+0.53	558	299/1725	123
Tb ₃ Al ₅ O ₁₂ :Ce SCF G set	YAG	+0.55	552	242/1645	253–264
Tb ₃ Al ₅ O ₁₂ :Ce SCF T1 set	YAG	+0.56	560	233/1710	200–203
Tb ₃ Al ₅ O ₁₂ :Ce SCF T2 set	GAGG	-1.29	560	306/1795	190–195
Gd ₃ Al ₂ Ga ₃ O ₁₂ :Ce SC	—	—	549	275/657	318
Gd ₃ Al _{2.5} Ga _{2.5} O ₁₂ :Ce SC	—	—	547	425/1036	381

$f_s = 0.35\text{--}1.6 \mu\text{m/min}$ and the velocity of substrate rotation $\omega = 80\text{--}100 \text{ rev/min}$. The SCF thickness was in the $1.5\text{--}35 \mu\text{m}$ range.

The optimal CeO₂ oxide concentration in all three growth cycles was determined experimentally in the range 8–10.5 mole % with respect to the total content of garnet-forming components, in order to obtain the maximal light yield (LY) of SCFs under excitation by Pu²³⁹ (5.15 MeV) α -particles. The SCFs composition was determined using a JEOL JSM-820 electronic microscope, comprising an EDX microanalyzer and equipped with IXRF 500 and LN2 Eumex detectors. From the content microanalysis of the SCF samples, we found that the segregation coefficient of Ce³⁺ ions in TbAG host was 0.004–0.005 and 0.0085–0.01 in the case of YAG and GAGG substrates, respectively.

For the growth of TbAG:Ce SCF scintillators we did not use additional doping to reduce the lattice mismatch of TbAG and YAG or GAGG lattices (Table 1). Nevertheless, the stable growth of TbAG:Ce SCF was observed in all growth cycles and the three series of TbAG:Ce SCF samples. TbAG:Ce SCFs were successfully obtained onto YAG substrates with (211), (111) and (110) orientations and GAGG substrates with (100) orientation for SCF/substrate misfit \mathbf{m} in the range $-1.29\% < \mathbf{m} < +0.56\%$ (Table 1).

The structural and luminescent properties of different TbAG:Ce SCF samples, grown onto YAG and GAGG substrates, were compared with LuAG:Ce and YAG:Ce SCF counterparts, grown onto YAG substrates with (111) orientation from PbO:B₂O₃ flux.

The secondary electron images cross-section of LuAG:Ce and TbAG:Ce A SCFs with a thickness of 25 μm and 7.5 μm respectively, both grown on the YAG substrates, and TbAG:Ce T SCFs with a thickness of 35 μm , grown onto GAGG substrate, are shown in Fig. 3a and b and c, respectively. Generally, in the case of TbAG SCF growth, the formation of a transition layer (TL) with a thickness 1.5–2.5 μm between TbAG:Ce SCFs and undoped YAG and GAGG

substrates was observed (Fig. 3b and c). But in the case of LuAG:Ce SCF growth onto YAG substrates, the dimension of the TL is significantly smaller and does not overcome 200 nm (Fig. 3a).

The possible explanation of the observed differences in the dimension of TL layers in the case of LuAG and TbAG SCF crystallization needs more detailed investigations. From the measurement of the TL content, we found that the content of this layer in the case of TbAG growth onto YAG substrates presents a mixed composition between TbAG and YAG or GAGG garnets. Therefore, the difference between the lattice constants of TbAG and YAG or GAGG hosts can be steeply eliminated in this TL. After equalizing the lattice constant of SCF and substrate, the stable growth of the main volume of TbAG based SCFs is observed (Fig. 3b and c).

The XRD measurements (spectrometer DRON 4, CuK α X-ray source) were used for characterization of the structural quality of SCFs with different cation compositions (Fig. 4). The misfit $\mathbf{m} = \frac{\mathbf{a}_{\text{SCF}} - \mathbf{a}_{\text{sub}}}{\mathbf{a}_{\text{SCF}}} * 100\%$ between the LuAG and TbAG film lattices and YAG or GAGG substrate lattices being equal to -0.78%, +0.53% and -1.32%, respectively, was determined from the respective XRD patterns (Fig. 3).

Due to the possibility to grow high-optical quality TbAG SCFs both onto YAG and GAGG substrates without any additional doping (Table 1), we conclude that the limiting misfit for crystallization of R₃Al₅O₁₂ (R = rare earth ions and Y) SCF garnets onto substrates with garnet structure can be extended in comparison with [10], and determined as $-1.61 \text{ \AA} \leq \Delta a \leq +0.34 \text{ \AA}$ ($-1.32\% \leq m \leq +0.56\%$).

3. Optical and luminescent properties of TbAG:Ce SCFs

For characterization of the optical properties of Ce³⁺ doped TbAG:Ce SCFs, the absorption spectra, cathodoluminescence (CL) spectra, LY and scintillation decay kinetics measurements, as well as the thermostimulated luminescence (TSL) glow curves under

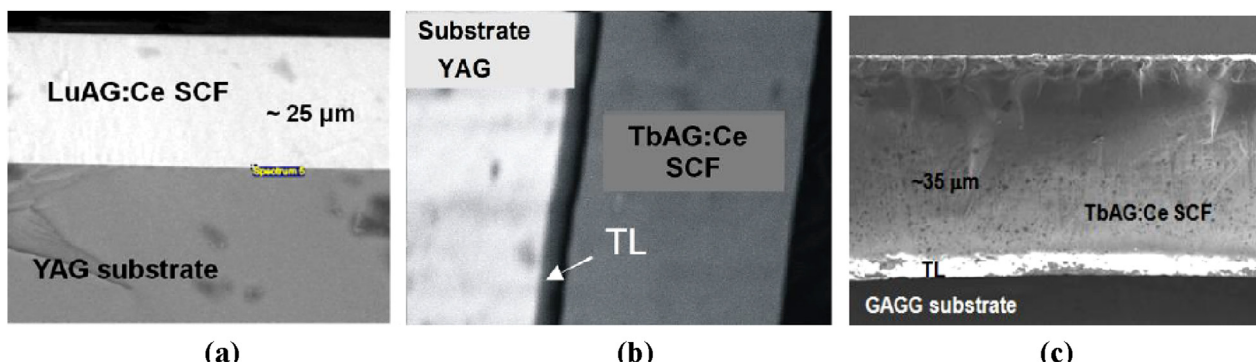


Fig. 3. Secondary electron images of the cross-section of LuAG:Ce (a) and TbAG:Ce SCFs (b) with a thickness of 25 and 7 μm , respectively, both grown on YAG substrates, and TbAG:Ce T2 SCFs with a thickness of 35 μm , grown onto GAGG substrate.

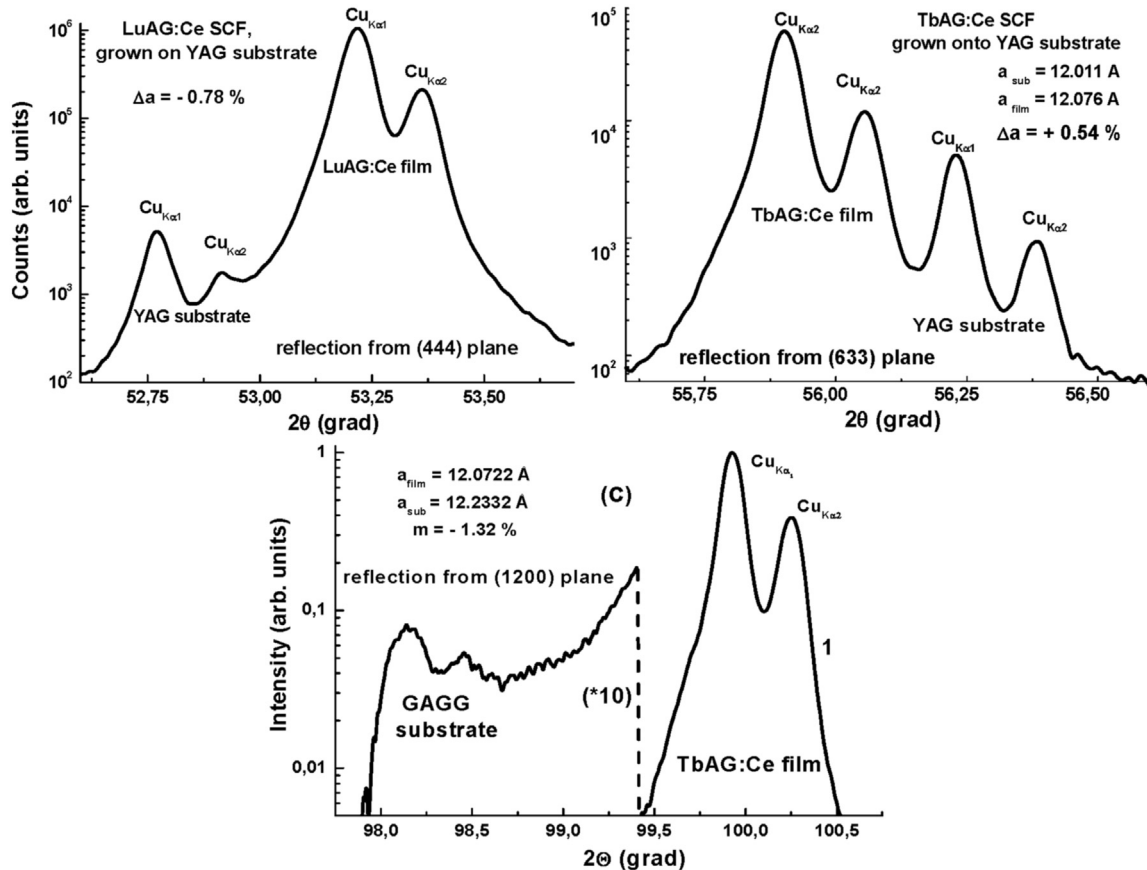


Fig. 4. XRD patterns of LuAG:Ce (a) and TbAG:Ce (c, d) SCFs, grown onto YAG substrates (a, b) and GAGG substrate (c) with (111), (211) and (100) orientations, respectively.

excitation by α -particles were measured and compared with their YAG:Ce and LuAG:Ce SCF counterparts.

The absorption spectra were measured using a Specord M40 spectrophotometer in the 200–750 nm range. The CL spectra were measured at room temperature (RT) using an electron microscope SEM JEOL JSM-820, additionally equipped with a Ocean Electronics spectrometer and a TE-cooled CCD detector working in the 200–925 nm range. The scintillation LY (with a shaping time of 12 μs) and decay kinetics measurements were performed using the setup based on a Hamamatsu H6521 PMP, multichannel analyzer and a digital TDS3052 oscilloscope under excitation by α -particles of Pu²³⁹ (5.15 MeV) source. The TSL measurements after α -particle excitation by an Am²⁴¹ source were performed in the 300–800 K temperature range using a commercial Risoe DA-20 TL/OSL reader (Denmark).

3.1. Absorption spectra

The absorption spectra of Ce-doped TbAG:Ce SCFs, grown onto YAG and GAGG substrates, in comparison with the LuAG:Ce and YAG:Ce SCFs are shown in Fig. 5. Two arrows in Fig. 5 in the 340–350 nm and 450–460 nm spectral ranges indicate the position of the absorption bands caused by the allowed $4f(2^2F_{5/2}) \rightarrow 5d^1$ transitions of the Ce³⁺ ion with the E¹ and E² energies, respectively [10,12]. The low-intensive sharp peaks in the 270–285 nm and 326 nm ranges, in the absorption spectra of TbAG:Ce SCF corresponds to the $4f^8 \rightarrow 4f^7 5d^1$ spin-allowed (sa) and spin-forbidden (sf) transitions of Tb³⁺ ions, respectively [10,12]. The 4f-5d (sf)-absorption band of Tb³⁺ ions peaked at 327 nm to a great extent is distorted by the presence in this spectral region of the 4f-5d-

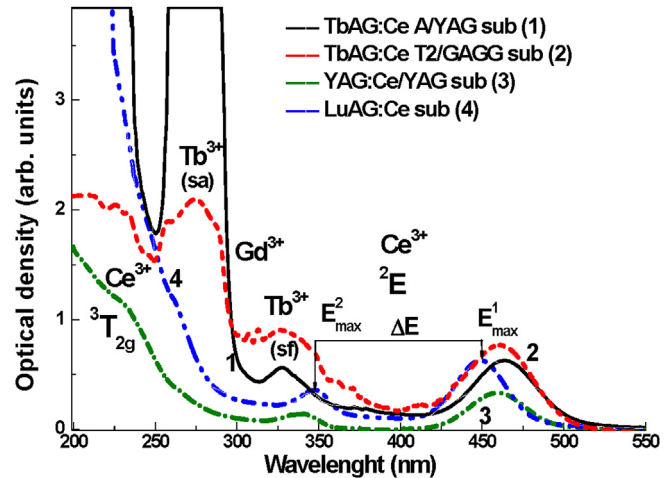


Fig. 5. Absorption spectra of Ce-doped TbAG:Ce SCFs, grown onto YAG (1) and GAGG substrates (2) in comparison with YAG:Ce (3) and LuAG:Ce (4) SCF counterparts, grown onto YAG substrates.

absorption band of Ce³⁺ ions peaked at 336 nm. The spectral closeness of these bands indicates the possibility of efficient excitation energy transfer from the host (Tb³⁺ cations) to the activator (Ce³⁺ ions) in TbAG:Ce SCF [10,12,15,16]. The sharp bands in the range of 275 and 313 nm in the absorption spectra of TbAG:Ce SCF, grown onto GAGG substrates, correspond to the absorption of Gd³⁺ impurity in the substrate (the $^6P_{7/2-3/2} \rightarrow ^8S_{7/2}$ and $^6J_{7/2} \rightarrow ^8S_{7/2}$ transitions, respectively).

Increase of the crystal field strength in the dodecahedral positions of the garnet host in a series of Ce-doped SCF with different garnet compositions is accompanied by shifting the $4f^7 \rightarrow 5d^1$ Ce^{3+} absorption bands in the 340–350 nm and 450–460 nm ranges (Fig. 5). Generally, the magnitude of the crystal field strength is proportional to the difference $\Delta E = E^1 - E^2$ between the maxima of the mentioned Ce^{3+} absorption bands (Table 2). The crystal field strength increases by 20–22% in TbAG garnets in comparison with LuAG garnets (Table 2).

3.2. CL spectra

Fig. 6 shows the CL spectra under e-beam excitation of different TbAG:Ce SCFs (curve 1–3), grown onto YAG (1, 2) and GAGG (3) substrates, in comparison with LuAG:Ce (curve 4) and YAG:Ce (curve 5) SCF counterparts. An increase in the magnitude of the crystal field strength of garnets in the series of Ce-doped SCF of mentioned garnet compounds is accompanied by the strong shift of the emission spectra peak position in the long-wavelength range from 506 nm in LuAG:Ce to 535 nm in YAG:Ce and 552–661 nm in TbAG:Ce SCFs. This also results in a change of the emission color from green for LuAG:Ce SCF to yellow for YAG:Ce SCF and deep orange for TbAG:Ce SCFs. The observed differences in the positions of the Ce^{3+} emission band in the A, B and T series of TbAG:Ce SCF samples (Fig. 6) can be caused by some deviation in the Ce^{3+} concentration in the mentioned samples due to slightly different conditions of LPE growth of these samples onto YAG and GAGG substrates with different orientations.

From Fig. 6 it also appears that the CL spectra for all SCFs under e-beam excitation are well fitted to the range of spectral sensitivity of a back-side illuminated CCD camera which is typically used for X-ray microimaging with SCF screens (curve 6). A good agreement of the SCF emission with CCD sensitivity range is observed for TbAG:Ce SCFs (curves 1–3).

3.3. LY measurements under α -particles and X ray excitations

The RL photoelectron LY of TbAG:Ce SCFs is presented in Table 1 and compared to LuAG:Ce and YAG:Ce standard SCF samples. It is measured with a shaping time of 12 μs under excitation by α -particles from a ^{239}Pu (5.15 MeV) source.

For TbAG:Ce SCFs coming from set A, we have recorded a satisfying LY, which was equal to 123% in comparison with that of the standard YAG:Ce SCF with a photoelectron LY of 386 Phels/MeV (Table 1). At the same time, the LY of TbAG:Ce A SCFs from this set is significantly smaller (in 1.66 time) than the LY of the best samples of LuAG:Ce SCF analogues (Table 1) [11].

Further increase of the LY in the mentioned SCF can be achieved by using initial raw powders of highest (5 N) purity and by optimizing the relation between the Ce^{3+} ions and Pb^{2+} trace impurity concentrations in SCF. Indeed, the LY of TbAG:Ce SCF samples, grown from the charge prepared with raw materials of 5 N purity onto YAG substrates (G and T1 sets), is very high and significantly

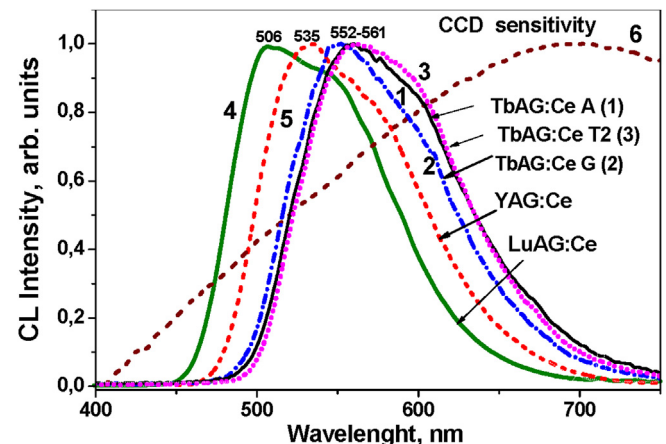


Fig. 6. CL spectra of Ce-doped TbAG:Ce A (1), TbAG:Ce G (2), TbAG:Ce T2 (3), LuAG:Ce (4) and YAG:Ce (5) SCFs under e-beam excitation in comparison with the spectral sensitivity of a typical back-side illuminated CCD camera (6).

(by 1.9–2.64 times) overcomes the LY of YAG:Ce reference SCF (Table 1). The best LY is achieved for TbAG:Ce SCF samples from the G serie (Table 2). Namely, the LY of the best samples from this set overcome by 23–29% the LY of high-quality LuAG:Ce SCFs produced in this laboratory [11]. Without any doubt, this LY is one of the highest ever obtained garnet SCF scintillators grown by the LPE from traditional $\text{PbO}-\text{B}_2\text{O}_3$ based flux [11,14].

It is important to note that the LY of TbAG:Ce SCF scintillators of G and T series is comparable with the LY of high-quality $\text{Gd}_3\text{Al}_{2.5-2}\text{Ga}_{2.5-3}\text{O}_{12}:\text{Ce}$ bulk SC analogues. This fact also enables producing with the help of the LPE method the new type of hybrid scintillators based on the epitaxial structures of garnet compounds. Such type hybrid scintillators can contain film and substrate scintillators with the optimized contents and high LY, taking into account also the requirement that the decay times of the signals coming from the film and substrate components of the hybrid scintillator can differ by at least 2 times [18]. Such a demand is fully realized in the case of TbAG:Ce SCF/ $\text{Gd}_3\text{Al}_{2.5}\text{Ga}_{2.5}\text{O}_{12}:\text{Ce}$ SC hybrid scintillators grown by the LPE method (Fig. 7). These scintillators can be proposed for different types of application, first of all, for registration of the components of mixed ionizing flux [18] and multi-layer screens for visualization of X-ray image as well [7].

Under 8 keV X-ray irradiation, the light output of the TbAG:Ce SCFs was also compared to a reference 500 μm thick YAG:Ce, 11 μm LuAG:Ce SCF and 6 μm thick LSO:Tb, Ce SCF, see Table 3.

Similarly to the LY under α -particles excitation, the maximum light output of 98%* under X-ray excitation was found in the 13.2 μm thick TbAG:Ce G SCFs. The light output decreased to 48% for TbAG A sample prepared with low purity raw material onto (110) oriented YAG substrates (Table 3). Anyway, it is worth to note that the light output of the X ray excited luminescence of TbAG:Ce SCFs is large and comparable with the best samples of LuAG:Ce and

Table 2

Difference between the positions of E^1 and E^2 absorption bands maxima connected with the $4f^7 \rightarrow 5d^1$ transitions of Ce^{3+} ions in $\text{R}_3\text{Al}_5\text{O}_{12}:\text{Ce}$ SCFs ($\text{R} = \text{Tb}, \text{Y}, \text{Lu}$), which is proportional to the crystal field strength of garnet compounds, position of Ce^{3+} photoluminescence (PL) band and decay time of Ce^{3+} emission under excitation in the Ce^{3+} absorption band at 440 nm.

Garnets type	E_1 , nm	E_2 , nm	$\Delta E = E^1 - E^2$, eV	Maxima of Ce^{3+} PL emission, nm	Decay time of PL, ns
TbAG:Ce T2	336	464.5	0.9 0.99	585	37; 1355
TbAG:Ce A	339	461.5	0.97	577	33; 814
TbAG:Ce G	339.5	460.5	0.96	570	35; 385
YAG:Ce	341	460	0.9 0.91	535	68
LuAG:Ce	348	449	0.8 0.81	506	52

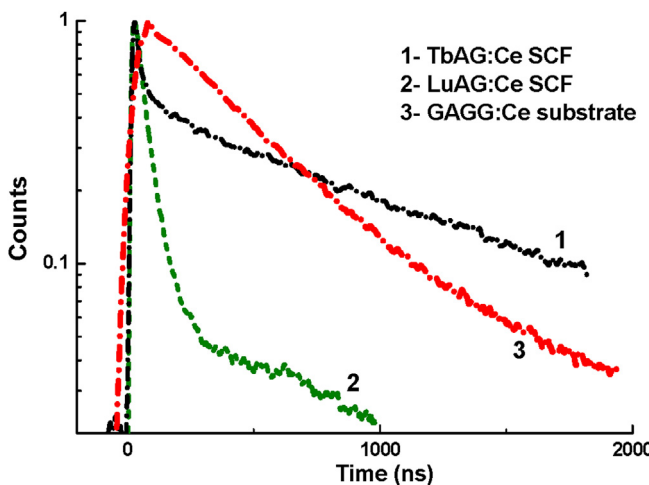


Fig. 7. Scintillation decay kinetics of $\text{Tb}_3\text{Al}_5\text{O}_{12}:\text{Ce}$ T2 (1), LuAG:Ce (2) SCFs and GAGG:Ce substrate (3) under α -particles excitation of ^{239}Pu source.

Table 3

Relative LY of the series of TbAG:Ce SCFs under X-ray excitation, measured with microscope optics and CCD camera. Results are corrected by X-ray absorption efficiency (film thickness and scintillator content) and compared to reference YAG:Ce SC.

Samples	$h, \mu\text{m}$	LY, %
YAG:Ce SC	500	100
LuAG:Ce SCF	11	77
LSO:Ce, Tb SCF	6	127
TbAG:Ce SCF A	7	48
TbAG:Ce SCF G	13.2	98 ^a

^a The light output of TbAG:Ce SCF G sample can be enhanced by a factor 1.5–2 due to more rough surface than in the case of TbAG:Ce A sample.

LSO:Ce, Tb SCF counterpart. This can be a good reason for the future development of scintillating screen based on the mentioned SCFs.

3.4. Scintillation decay kinetics of TbAG:Ce SCFs under α -particles excitation

The scintillation decay kinetics of $\text{Tb}_3\text{Al}_5\text{O}_{12}:\text{Ce}$ SCFs under α -particles excitation from a ^{239}Pu source is shown in Fig. 7, in comparison with LuAG:Ce SCF and GAGG:Ce substrate. As one can see from this figure, TbAG:Ce SCF scintillators demonstrate a substantially slower non-exponential decay kinetics as compared to their LuAG:Ce SCF counterpart (curve 1 and 2, respectively). Such slower and complicated decay kinetics of the Ce^{3+} luminescence is typical for Tb^{3+} based garnet hosts, where the energy transfer via the sublattice of Tb^{3+} cations is significant [15,16] in comparison with LuAG:Ce SCFs, where the direct energy transfer from the host to Ce^{3+} ions dominates [11]. The conditions of the $\text{Tb}^{3+} \rightarrow \text{Ce}^{3+}$ energy transfer in TbAG garnet host is considered in more details in Section 4, see also [13].

Scintillation decay times $t_{1/e}$ and $t_{1/10}$ of the best samples from different TbAG:Ce SCF series were measured under excitation by α -particles of Pu^{239} sources and shown in Table 1 in comparison with standard YAG:Ce and LuAG:Ce SCF counterparts, $\text{Gd}_3\text{Al}_2.5\text{Ga}_2.5\text{O}_{12}:\text{Ce}$ and $\text{Gd}_3\text{Al}_2\text{Ga}_3\text{O}_{12}:\text{Ce}$ reference bulk crystals. Generally, the decay kinetics of TbAG:Ce SCFs can be presented by the superposition of two decay components with the decay in the hundreds and thousands ns range (Fig. 7 and Table 1). As one can see from Table 1, the decay times $t_{1/e}$ and $t_{1/10}$ for the TbAG:Ce SCF samples notably depends on the conditions of SCF growth, namely,

the concentrations of Ce^{3+} and Pb^{2+} related dopants as a function of the SCF growth temperature, type of substrates, etc. Namely, the largest values of $t_{1/e}$ and $t_{1/10}$ decay times (306 and 1795 ns, respectively) are observed in TbAG:Ce SCF grown onto GAGG substrate whereas in the case of TbAG:Ce SCFs grown onto YAG substrates the scintillation decay kinetics is slightly faster (Table 1).

3.5. TSL properties of TbAG:Ce SCFs and their afterglow

The results from TSL investigations of different α -particles irradiated TbAG:Ce SCFs above RT range are shown in Fig. 8 (curves 1, 2) in comparison with LuAG:Ce SCFs (curve 3). The TSL mechanism in these SCFs is connected with the electrons liberated from traps and their subsequent recombination with the holes localized around Ce^{3+} ions [11,14].

In TbAG:Ce SCFs, a strong shift of the main TSL peak position (415–430 K) is observed (Fig. 6, curves 1, 2) in comparison with LuAG:Ce SCFs with a main TSL peak at 590 K (curve 3) [see also 11, 14]. Additionally a significant decrease of the TSL signal for TbAG:Ce SCFs in the 500–650 K high-temperature range is observed in comparison with LuAG:Ce SCF sample (Fig. 8). This result is in good correlation with the significant increase of the LY in TbAG:Ce SCFs from G and T series in comparison with LuAG:Ce SCF counterpart (Table 1).

The nature of these traps in the garnet SCFs has not been determined yet. Most probably, due to the expected low concentration of antisite defects and oxygen vacancies in the SCF samples, grown at relatively low (~1000 °C) temperatures in oxygen containing (air) atmosphere, the traps can be related mainly to the presence of Pb^{2+} (from flux) and Pt^{4+} (from crucible) contamination in these SCF samples [8,11]. As a consequence, various locally non-compensated lattice defects can be created in SCFs, for instance oxygen or cation vacancies around the mentioned impurities, which may result in the formation of trap levels in the forbidden band gap, the appearance of a slow component in the decay kinetics of the Ce^{3+} luminescence and in a decrease of the scintillation efficiency of SCF scintillators.

The results of TSL measurements are also well correlated with the afterglow measurements performed on TbAG:Ce SCF, in comparison with LuAG:Ce SCF and standard YAG:Ce crystal (Fig. 9). We found that the afterglow level of TbAG:Ce SCF is very low and significantly better than that in YAG:Ce SC standard sample and LuAG:Ce SCF counterpart. It is worth to note here that TbAG:Ce shows a very low afterglow level comparable with high quality

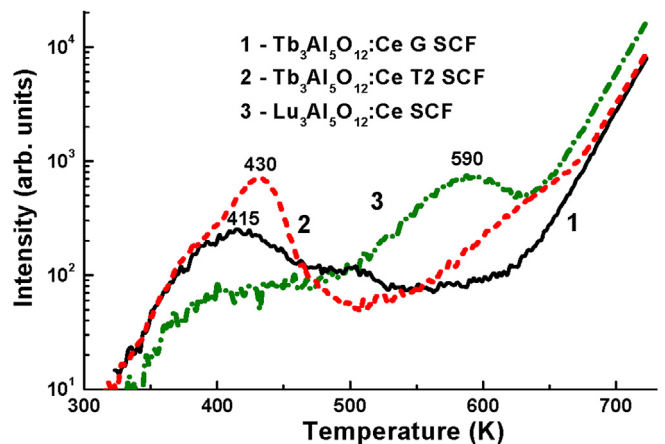


Fig. 8. TSL (in the log scale) of different TbAG:Ce (1, 2) SCFs in comparison with LuAG:Ce SCF (3) after the irradiation by α -particles of ^{241}Am sources, registered in the range of Ce^{3+} emission.

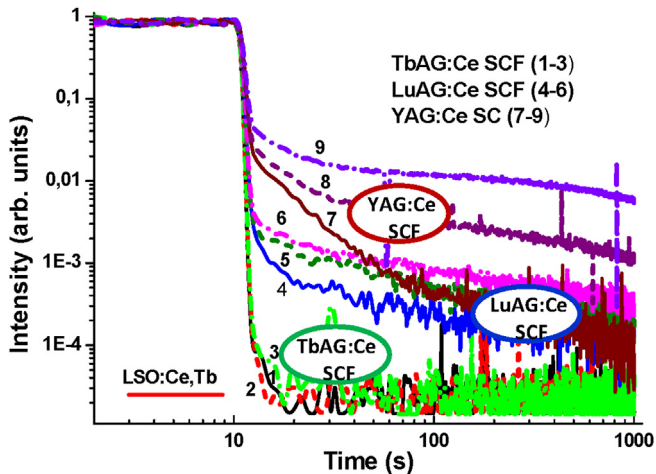


Fig. 9. Afterglow under 8 keV X-rays (CuK_α) of TbAG:Ce G SCFs (1–3) in comparison with LuAG:Ce SCF counterpart (4–6) and YAG:Ce standard SC sample (7–9) with a X-ray burst duration of 0.1 s (1, 4, 7), 1.0 s (2, 5, 8) and 10 s (3, 6, 9), respectively.

LSO:Ce, Tb SCFs (Fig. 9), see also [19]. Together with a high light output under X-ray excited luminescence, this can also be a good reason for pushing the development of scintillating screen based on the mentioned SCFs.

4. Photoluminescence study and energy transfer in TbAG:Ce SCF

The PL spectra of the TbAG and different Ce^{3+} doped TbAG:Ce

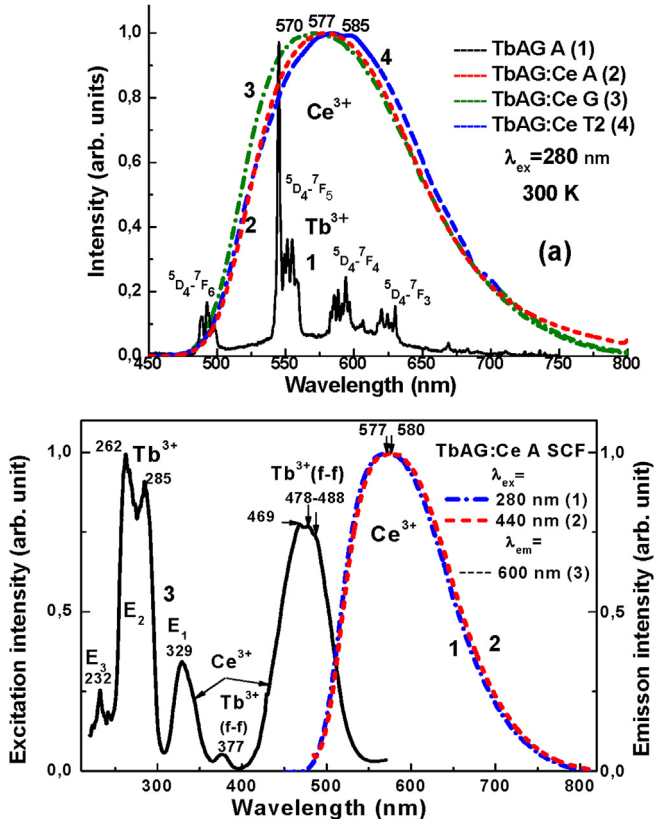


Fig. 10. (a) PL spectra of TbAG SCF and different TbAG:Ce SCFs (A, G, T2 series) under excitation in the Tb^{3+} absorption band at 280 nm. (b) – PL spectra under excitation in the Tb^{3+} absorption band at 280 nm (1) and Ce^{3+} absorption band at 440 nm (2) and PL excitation spectra (3) of Ce^{3+} luminescence at 600 nm in TbAG:Ce A SCFs. $T = 300 \text{ K}$.

SCFs, grown onto YAG substrate, at 300 K under excitation in the absorption bands of Tb^{3+} cations are shown in Fig. 10a. The PL spectra of TbAG:Ce A SCF at 300 K under excitation in the absorption bands of Tb^{3+} cations and Ce^{3+} ions and excitation spectra of the Ce^{3+} luminescence in TbAG host are shown in Fig. 10b.

From the emission and excitation spectra of TbAG:Ce A SCF, presented in Fig. 10, we can confirm in this work that the effective energy transfer from Tb^{3+} cations to Ce^{3+} ions is realized in TbAG host both under high-energy e-beam excitation (Fig. 5) and excitation in the Tb^{3+} related absorption bands. The emission spectra of undoped TbAG SCFs under excitation in the Tb^{3+} related absorption band at 280 nm show sharp low-intensity bands peaked at 490, 543 and 590 nm corresponding to the $5\text{D}_4 \rightarrow 7\text{F}_j$ ($j = 6-4$) transitions of Tb^{3+} cations (Fig. 10a, curve 1). At the same time, under the same excitation, the PL spectra of all TbAG:Ce SCFs samples consist only of the dominant Ce^{3+} emission band, which corresponds to the $5\text{d}^1 \rightarrow 4\text{f}$ ($2\text{F}_{5/2,7/2}$) radiative transitions of Ce^{3+} ions. Therefore, a effective energy transfer between the Tb^{3+} cations and Ce^{3+} ions exists in TbAG:Ce SCFs. Depending on the LPE growth conditions, influencing the Ce^{3+} concentrations in the SCFs, the position of the Ce^{3+} emission band is slightly shifted to the 570–580 nm range (Fig. 10a, curve 1–3).

The PL spectra of TbAG:Ce A SCFs under excitation in the in the E_2 absorption band of Tb^{3+} ions at 280 nm (Fig. 10b, curve 1) and Ce^{3+} ions at 440 nm (Fig. 10b, curve 2) consist only of the wide band peaked in the 570–585 nm range. It is worth noting that the emission spectrum of Ce^{3+} ions, under excitation in E_2 absorption band of Tb^{3+} ions at 280 nm (curve 1), is probably slightly modified by the TbAG host luminescence (Fig. 10a, curve 1). Namely, the maximum of the spectrum is slightly shifted from 577 nm to 580 nm in comparison to the emission spectra under excitation in the Ce^{3+} absorption band at 440 nm (curve 3), due to presence of the low-intensity bands corresponding to the transitions of Tb^{3+} cations (Fig. 10a, curve 1).

The excitation spectrum of the Ce^{3+} emission monitored at 600 nm in the TbAG:Ce SCFs (at 300 K) is shown in Fig. 10b, curve 3. In this spectrum, the bands in the 220–330 nm range correspond to the $4\text{f}^8 \rightarrow 4\text{f}^7 5\text{d}^1$ transitions of the Tb^{3+} ions with the main maxima peaked at 232 nm (E_3), 262 and 285 nm (E_2 band) and 329 nm (E_1 band). In the 330–550 nm range the excitation spectrum of the Ce^{3+} luminescence in TbAG:Ce SCF consists of the band peaked at 377 nm, caused by the $7\text{F}_6 \rightarrow 5\text{D}_3$ transitions of Tb^{3+} cations; another group of excitation bands in the 480 nm range, corresponding to the $7\text{F}_6 \rightarrow 5\text{D}_4$ transitions, which are overlapped with the respective Ce^{3+} -related excitation band (Fig. 10b, curve 3). This also confirms the existence of the very efficient energy transfer between the TbAG host and the Ce^{3+} ions; namely, the Ce^{3+} luminescence can be effectively excited not only from the d-f bands but also from the f-f bands of the Tb^{3+} cations. The excitation bands of the Ce^{3+} luminescence in TbAG:Ce SCFs peaked at 469 nm and at 334 nm are related to the $4\text{f}(2\text{F}_{5/2,7/2}) \rightarrow 5\text{d}^1$ transitions of Ce^{3+} ions; the long-wavelength band being strongly overlapped with the E_1 band of Tb^{3+} cations.

For investigation of the energy transfer processes between Tb^{3+} and Ce^{3+} ions, we also studied the luminescence decay kinetics in TbAG and different TbAG:Ce SCFs under excitation in the absorption bands of Tb^{3+} cations (at 260 nm) and Ce^{3+} ions (at 440 nm) (Fig. 11a and b, respectively).

The comparison of the decay kinetics from the Tb^{3+} luminescence host in TbAG and TbAG:Ce SCFs at 300 K is shown in Fig. 11a, curves 1 and 2, respectively. Under excitation at a wavelength of 262 nm (in the E_2 band vicinity of the Tb^{3+} cation), the decay kinetics of the Tb^{3+} luminescence in TbAG SCFs monitored at a wavelength of 543 nm ($2\text{F}_6 \rightarrow 5\text{D}_4$ transitions) at 300 K (Fig. 11a, curve 1), can be modeled by the sum of exponential functions

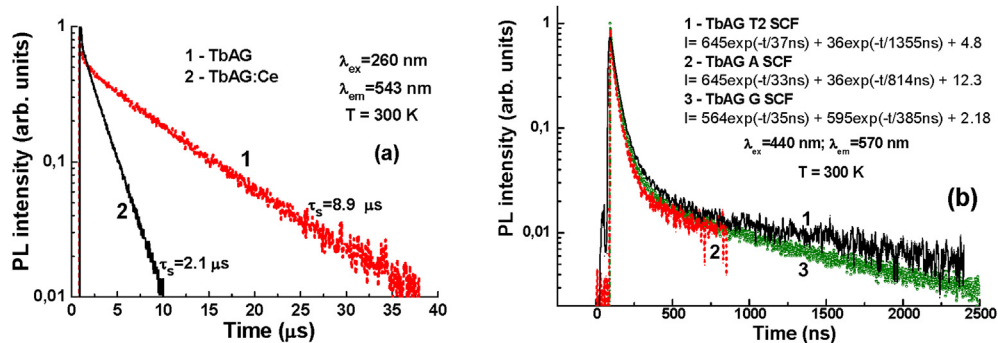


Fig. 11. Luminescence decay kinetics of Tb^{3+} cations in TbAG SCF (a1) and TbAG:Ce SCF (a2) at 543 nm under excitation at a wavelength of 262 nm in the f-d Tb^{3+} absorption band (a) and luminescence decay kinetics of Ce^{3+} ions in the different TbAG:Ce SCFs (b) under excitation in the Ce^{3+} absorption band at 440 nm (b).

$I(t) = \sum A_i \exp(-t/\tau_i) + \text{background}$. It allows one to separate two components of the luminescence of Tb^{3+} cations in TbAG: a low intensity and fast decay component with a decay time $\tau_f = 0.2 \mu\text{s}$ and a main slow component with a decay time $\tau_s = 8.9 \mu\text{s}$. The two-component decay kinetics of the Tb^{3+} luminescence in TbAG host indicates the significant influence of the transitions from $^5\text{D}_3$ level on the radiative transitions from $^5\text{D}_4$ level of Tb^{3+} cations. Comparison of the obtained values of τ_f and τ_s for TbAG at 300 K with the analogous values $\tau_f = 0.39 \text{ ms}$ and $\tau_s = 3.9 \text{ ms}$ corresponding to the radiative transitions from $^5\text{D}_3$ and $^5\text{D}_4$ levels in YAG:Tb [20] points to the substantial reduction of the decay time from these levels in the TbAG host due to the concentration quenching of the Tb^{3+} cations luminescence.

The doping of TbAG SCFs by Ce^{3+} ions leads to a strong acceleration of the decay curve of the host TbAG luminescence and a decrease of the main components lifetime from $8.9 \mu\text{s}$ in TbAG to $2.1 \mu\text{s}$ in TbAG:Ce SCFs. Such a decrease of τ_s values enable us to estimate the kind of energy transfer which is realized in the TbAG:Ce scintillators. Specifically, a decrease of the decay time of the TbAG host luminescence in the case of Ce^{3+} doping can be caused by the Förster effective resonance energy transfer between Tb^{3+} cations to Ce^{3+} ions through nonradiative dipole–dipole coupling, which results in the lifetime reduction of Tb^{3+} ion excited levels.

The Ce^{3+} luminescence decay kinetics in the different TbAG:Ce SCFs at 300 K under excitation in the E_1 f-d absorption band of these ions at 404 nm is presented in Fig. 11b. As one can see from Fig. 9b, curves 1–3, the decay kinetics of the Ce^{3+} luminescence in TbAG:Ce host under excitation in Ce^{3+} absorption band at 440 nm cannot be fitted with a single exponential decay. Along with the fast components with a decay time of 32–37 ns caused by the radiative transitions of Ce^{3+} ions, the slow parts of the decay curves with a lifetime in the 0.355–1355 ns range are also observed, which are probably due to the energy transfer process between Ce^{3+} and Tb^{3+} ions, most probably from both $^4\text{D}_3$ and $^5\text{D}_4$ radiative levels [9,12,13]. It is worth to note that along with all the studied TbAG:Ce SCF samples, the fastest decay kinetics is observed in the TbAG:Ce G SCF (Fig. 11b, curve 3). This also corresponds to the fastest scintillation decay kinetics and the highest LY in all grown SCFs series.

5. Conclusion

We report in this work the development of new heavy and efficient $\text{Tb}_3\text{Al}_5\text{O}_{12}:\text{Ce}$ (TbAG:Ce) single crystalline film (SCF) scintillators, grown by the LPE method from PbO based flux, for different optoelectronic applications, first of all for microimaging techniques and detectors for registration of low-energy particles and quanta.

We demonstrated for the first time the possibility to grow without lattice compensation TbAG:Ce SCFs by the LPE method both onto YAG and $\text{Gd}_3\text{Al}_2\text{Ga}_2\text{O}_{12}$ (GAGG) substrates with lattice constants of 12.01 and 12.232 Å, respectively. The crystallization mechanism of these SCFs involves the formation of transition layers between the SCF and substrate for reducing their lattice mismatch. Due to the TbAG SCF crystallization onto YAG and GAGG substrates with the mentioned lattice parameters, the boundary conditions for film-substrate misfit concerning the LPE growth of those rare-earth garnets SCFs must be reconsidered with respect to the data presented in Ref. [10] and a new wider condition $-1.29\% < m < +0.56\%$ can be considered (Table 1).

The luminescent and scintillation properties of the TbAG:Ce SCFs, grown onto YAG and GAGG substrates from PbO based flux, are studied and compared with the properties of the $\text{Lu}_3\text{Al}_5\text{O}_{12}:\text{Ce}$ and YAG:Ce SCF counterparts. We confirmed the presence of a very effective energy transfer from TbAG host to Ce^{3+} ions using the photoluminescence emission and excitation spectra and photoluminescence decay kinetics of Tb^{3+} cations and Ce^{3+} activators.

Apart from the excellent structural quality, the SCFs of TbAG:Ce garnet, grown both onto YAG and GAGG substrates, possess a very high scintillation LY under α -particles excitation, which exceeds by up to 30% the LY of the best LuAG:Ce SCFs samples, obtained from PbO based flux. *Without any doubt, this LY is one of the highest ever obtained with garnet SCF scintillators grown by the LPE method from traditional PbO-B₂O₃ based flux [11,14].*

TbAG:Ce SCF screens show also extremely low afterglow (up to 10^{-4} level at X-ray burst duration of 0.1 s), which is comparable with the afterglow level of the best LSO:Ce, Tb SCF samples being used nowadays for microimaging. Together with a high light output of the X-ray excited luminescence, such a low afterglow level is a very good reason for future development of scintillating screens based on the mentioned garnet.

Taking into account that the $\text{Tb}_3\text{Al}_5\text{O}_{12}:\text{Ce}$ SCFs can be grown also onto GAGG substrates, these SCFs and the high-quality $\text{Gd}_3\text{Al}_2\text{Ga}_3\text{O}_{12}:\text{Ce}$ crystals can be used for creation of new types of “film-substrate” hybrid scintillators using the LPE method (see Fig. 1), for simultaneous registration of different ionization radiations and microimaging as well.

Acknowledgments

The work was performed in the framework of Polish NCN No 2012/07/B/ST5/02376 and NANOLUX2014 No 286 projects and partly also supported by the Ministry of Education and Science of Ukraine in the framework of FK 64/44 and SF-20 F projects.

References

- [1] A. Koch, C. Raven, P. Spanne, A.J. Snigirev, Opt. Soc. Am. A 15 (1998) 1940.
- [2] A. Koch, F. Peyrin, P. Heurtier, B. Chambaz, B. Ferrand, W. Ludwig, M. Couchaud, Proc SPIE 3659, 1999, p. 170.
- [3] T. Martin, A. Koch, J. Synchrotron Rad. 13 (2006) 180.
- [4] T. Martin, P.-A. Douissard, Z. Seeley, N. Cherepy, S. Payne, E. Mathieu, J. Schuladen, IEEE Transaction Nucl. Sci. 59 (2013) 2269–2274.
- [5] D.S. Rigie, P.J. La Rivière, in: Nuclear Science Symposium and Medical Imaging Conference (NSS/MIC), IEEE Transaction on Nuclear Science, 2011, pp. 4009–4012.
- [6] D. Modgil, D.S. Rigie, Y. Wang, X. Xiao, P.A. Vargas, P.J. La Rivière, Phys. Med. Biol. 60 (2015) 8025–8045.
- [7] F. Riva, T. Martin, P.-A. Douissard, C. Dujardin, Towards a New Generation of Thin Scintillating Films to Fit the Synchrotron Needs, 2014. <http://www-success.kharkov.ua/news/4ws/riva.pdf>.
- [8] F. Riva, P.-A. Douissard, T. Martin, Yu Zorenko, C. Dujardin, CrystEngComm 18 (2016) 608.
- [9] Yu Zorenko, V. Gorbenko, I. Konstankevych, B. Grinev, M. Globus, Nucl. Instrum. Methods Phys. Res. A486 (2002) 309.
- [10] Yu Zorenko, V. Gorbenko, Radiat. Meas. 42 (2007) 907.
- [11] P.-A. Douissard, T. Martin, F. Riva, Yu Zorenko, T. Zorenko, A. Fedorov, P. Bilski, A. Twardak, IEEE Trans. Nucl. Sci. 55 (4) (2016), <http://dx.doi.org/10.1109/TNS.2015.2514>.
- [12] Y. Zorenko, T. Voznyak, V. Vistovsky, T. Zorenko, S. Nedilko, M. Batentschuk, A. Osvet, A. Winnacker, G. Zimmerer, V. Kolobanov, D. Spassky, Radiat. Meas. 42 (2007) 648–651.
- [13] Yu Zorenko, V. Gorbenko, V. Savchyn, T. Zorenko, A. Fedorov, H. Wrzesiński, Ya Vasylkiv, Radiat. Meas. 56 (2013) 150–154.
- [14] Yu Zorenko, YuV. Gorbenko, T. Zorenko, O. Sidletskiy, A. Fedorov, P. Bilski, A. Twardak, Phys. Status Solidi RRL 9 (2015) 489.
- [15] F. Kummer, F. Zwischka, A. Ellens, A. Debray, G. Waitl, Int. Patent App. No: WO 01/08452, 2001.
- [16] M. Batentschuk, A. Osvet, G. Schierning, A. Klier, J. Schneider, A. Winnacker, Radiat. Meas. 38 (2004) 539–543.
- [17] J.A. Mares, A. Bejtlerova, M. Nikl, N. Solovieva, K. Nitsch, M. Kucera, M. Kubova, V. Gorbenko, Yu Zorenko, Radiat. Meas. 42 (2007) 533.
- [18] YuV. Zorenko, S.S. Novosad, M.V. Pashkovskii, A.B. Lyskovich, V.G. Savitskii, M.M. Batenchuk, P.S. Malyutinov, N.I. Patsagan, I.V. Nazar, V.I. Gorbenko, J. Appl. Spectrosc. 52 (1990) 645.
- [19] P.-A. Douissard, A. Cecilia, T. Martin, V. Chevalier, M. Couchaud, T. Baumbach, K. Dupré, M. Kühbacher, A. Rack, J. Synchrotron Rad. 17 (2010) 571.
- [20] J.Y. Choe, D. Ravichandran, S.M. Blomquist, K.W. Kirchner, E.W. Fortsythe, D.C. Morton, J. Luminescence 93 (2001) 119.

Article

LPE Growth of Single Crystalline Film Scintillators Based on Ce³⁺ Doped Tb_{3-x}Gd_xAl_{5-y}Ga_yO₁₂ Mixed Garnets

Vitalii Gorbenko ^{1,*}, Tetiana Zorenko ¹, Sandra Witkiewicz ¹, Kazimierz Paprocki ¹, Oleg Sidletskiy ², Alexander Fedorov ³, Paweł Bilski ⁴ , Anna Twardak ⁴ and Yuriy Zorenko ^{1,*} 

¹ Institute of Physics, Kazimierz Wielki University in Bydgoszcz, 85090 Bydgoszcz, Poland; tzorenko@ukw.edu.pl (T.Z.); s-witkiewicz@wp.pl (S.W.); paprocki@ukw.edu.pl (K.P.)

² Institute for Scintillation Materials, National Academy of Sciences of Ukraine, 61001 Kharkiv, Ukraine; osidletskiy@yahoo.com

³ SSI Institute for Single Crystals, National Academy of Sciences of Ukraine, 61178 Kharkiv, Ukraine; fedorov@xray.isc.kharkov.com

⁴ Institute of Nuclear Physics, Polish Academy of Sciences, 31342 Krakow, Poland; pawel.bilski@ifj.edu.pl (P.B.); anna.twardak@gmail.com (A.T.)

* Correspondence: gorbenko@ukw.edu.pl (V.G.); zorenko@ukw.edu.pl (Y.Z.)

Received: 24 July 2017; Accepted: 25 August 2017; Published: 30 August 2017

Abstract: The growth of single crystalline films (SCFs) with excellent scintillation properties based on the Tb_{1.5}Gd_{1.5}Al_{5-y}Ga_yO₁₂:Ce mixed garnet at y = 2–3.85 by Liquid Phase Epitaxy (LPE) method onto Gd₃Al_{2.5}Ga_{2.5}O₁₂ (GAGG) substrates from BaO based flux is reported in this work. We have found that the best scintillation properties are shown by Tb_{1.5}Gd_{1.5}Al₃Ga₂O₁₂:Ce SCFs. These SCFs possess the highest light yield (LY) ever obtained in our group for LPE grown garnet SCF scintillators exceeding by at least 10% the LY of previously reported Lu_{1.5}Gd_{1.5}Al_{2.75}Ga_{2.25}O₁₂:Ce and Gd₃Al_{2-2.75}Ga_{3-2.25}O₁₂:Ce SCF scintillators, grown from BaO based flux. Under α-particles excitation, the Tb_{1.5}Gd_{1.5}Al₃Ga₂O₁₂:Ce SCF show LY comparable with that of high-quality Gd₃Al_{2.5}Ga_{2.5}O₁₂:Ce single crystal (SC) scintillator with the LY above 10,000 photons/MeV but faster (at least by 2 times) scintillation decay times t_{1/e} and t_{1/20} of 230 and 730 ns, respectively. The LY of Tb_{1.5}Gd_{1.5}Al_{2.5}Ga_{2.5}O₁₂:Ce SCFs, grown from PbO flux, is comparable with the LY of their counterparts grown from BaO flux, but these SCFs possess slightly slower scintillation response with decay times t_{1/e} and t_{1/20} of 330 and 990 ns, respectively. Taking into account that the SCFs of the Tb_{1.5}Gd_{1.5}Al_{3-2.25}Ga_{2-2.75}O₁₂:Ce garnet can also be grown onto Ce³⁺ doped GAGG substrates, the LPE method can also be used for the creation of the hybrid film-substrate scintillators for simultaneous registration of the different components of ionization fluxes.

Keywords: liquid phase epitaxy; single crystalline films; scintillators; mixed garnets; Tb³⁺ cations

1. Introduction

The development of detectors for 2D/3D microimaging using X-ray sources and synchrotron radiation demands the creation of thin (from a few microns thick up to 20 microns) single crystalline film (SCF) scintillating screens with an extremely high ability for X-ray absorption and a micron-submicron spatial resolution [1–4]. More recently, for this purpose, the visible emitting scintillating screens based on the SCF of Ce doped Y₃Al₅O₁₂ (YAG) and Lu₃Al₅O₁₂ (LuAG) garnets grown by the Liquid Phase Epitaxy (LPE) method have been used and the spatial resolution of the detector in the micron range has been achieved using synchrotron radiation with energy in the 8–20 keV range [1,2]. After that, the SCFs of Eu³⁺, Tb³⁺ doped Gd₃Al₅O₁₂ (GGG) and Sc³⁺ doped LuAG garnets [3,4], Tb³⁺ and double Tb³⁺, Ce³⁺ doped Lu₂SiO₅ (LSO) orthosilicates [5–14], Ce³⁺, Tb³⁺ and

Eu^{3+} doped LuAlO_3 (LuAP) and $(\text{Gd},\text{Lu})\text{AlO}_3$ (GLAP) perovskites [15–19] and recently Ce^{3+} doped $\text{Tb}_3\text{Al}_5\text{O}_{12}$ (TbAG) garnets [20,21], have also been successfully developed in the last decade for microimaging detectors using the LPE method.

The fabrication of screens with higher spatial resolution of X-ray images in the submicron range demands the creation of new scintillating film screens with extremely high absorption ability for X-rays—which is proportional to ϱZ_{eff}^4 , where ϱ is the density and Z_{eff} is the effective atomic number of scintillators [2,3]—as well as the development of novel concepts for microimaging.

During the last years, two novel concepts for the creation of a detector for microtomography have been proposed [15,19,21]. The first concept is related to the engineering of K-edge of X-ray absorption multilayer-film scintillators using the solid solution of oxide compounds containing the Lu, Gd and Tb ions [15,19,21]. Indeed, the absorption ability of the film scintillator can be significantly improved in the 20–65 keV range due to the significant broadening of the K-edge of X-ray absorption in such mixed materials [15,19,21]. The second concept is based on using the complex multilayer-film scintillator with a separate pathway for registration of the optical signal from each layer and final overlapping of the images coming from the different parts of the complex scintillator [15,21]. By using such multilayer-film scintillators one can significantly improve the contrast and resolution of images even in the submicron range. Two such novel concepts also demand the fabrication of different sets of heavy and efficient SCF scintillators which can be deposited onto the same substrates.

The Ce^{3+} doped $\text{Lu}_{3-x}\text{Gd}_x\text{Al}_{5-y}\text{Ga}_y\text{O}_{12}$ and $\text{Gd}_3\text{Al}_{5-y}\text{Ga}_y\text{O}_{12}$ mixed garnets are related to the efficient and heavy scintillators with very high (up to 50,000 photons/MeV) light yield (LY) under γ quanta excitation [22–25]. For this reason, these compounds are also used for the fabrication of the scintillation screens with high absorption ability for X-rays [26–33]. With the aim of increasing the energy transfer efficiency from the host of mixed garnets to the Ce^{3+} ions, the $\text{Tb}_3\text{Al}_5\text{O}_{12}$, $\text{Lu}_{3-x}\text{Tb}_x\text{Al}_5\text{O}_{12}$ and $\text{Gd}_{3-x}\text{Tb}_x\text{Al}_5\text{O}_{12}$ SCFs were also crystallized by the LPE method and their luminescent and scintillation properties were investigated [20,21,34,35]. The Ga co-doped analogues of these garnets can also be considered as very interesting matrixes for this purpose and their luminescent and scintillation properties were briefly reported by us as well [36]. At the same time, the possibility of the creation of the efficient SCF scintillators on the basis of the mentioned Tb containing garnets by the LPE method still needs the following technological and experimental evidence. First of all, estimation of the real potential of different garnet compositions for producing the scintillation screens strongly requires the LPE crystallization of these compounds in the SCF form from the different types of fluxes due to very large influence of flux related dopants on their scintillation characteristics [31,33,37,38] as well as the crystal analogs of these garnets using MPD [39] or Czochralski methods.

In this paper, we present the new results of the research on the creation of the advanced SCF scintillation screens based on Ce doped $\text{Tb}_{1.5}\text{Gd}_{1.5}\text{Al}_{5-y}\text{Ga}_y\text{O}_{12}$ mixed garnets at $y = 2\text{--}3.85$, grown by the LPE method from the novel lead free BaO based flux (later called $\text{Tb}_{1.5}\text{Gd}_{1.5}\text{Al}_{5-y}\text{Ga}_y\text{O}_{12}:\text{Ce}$ (BaO) SCFs) and compare their properties with those of $\text{Tb}_{3-x}\text{Gd}_x\text{Al}_{5-y}\text{Ga}_y\text{O}_{12}$ SCFs at $x = 0\text{--}2.1$ and $y = 0\text{--}2.75$, grown from the traditional PbO based flux [21,37] (later called $\text{Tb}_{3-x}\text{Gd}_x\text{Al}_{5-y}\text{Ga}_y\text{O}_{12}:\text{Ce}$ (PbO) SCFs).

For engineering the scintillator composition we apply the combination of Ce^{3+} 5d-level positioning [20] and band-gap engineering [40] in the Ce doped $\text{Tb}_{3-x}\text{Gd}_x\text{Al}_{5-y}\text{Ga}_y\text{O}_{12}$ mixed garnet using the substitution by Gd^{3+} cations of the dodecahedral sites of $\text{Tb}_3\text{Al}_5\text{O}_{12}$ garnet lattice with the concentration $x = 1.5$ and the substitution by Ga^{3+} ions of the Al^{3+} cations in both the tetrahedral and octahedral positions of the garnet host at concentration $y = 2\text{--}3.85$. Additionally, we can expect an increase in the energy transfer efficiency from the host of the $\text{Tb}_{3-x}\text{Gd}_x\text{Al}_{5-y}\text{Ga}_y\text{O}_{12}$ garnet to the Ce^{3+} ions using the sublattices of Tb^{3+} and Gd^{3+} cations.

2. Growth of $\text{Tb}_{3-x}\text{Gd}_x\text{Al}_{5-y}\text{Ga}_y\text{O}_{12}:\text{Ce}$ Single Crystalline Films

The SCFs of $\text{Tb}_{3-x}\text{Gd}_x\text{Al}_{5-y}\text{Ga}_y\text{O}_{12}:\text{Ce}$ garnets were grown by the LPE method onto $\text{Gd}_3\text{Al}_{2.5}\text{Ga}_{2.5}\text{O}_{12}$ (GAGG) substrates with a relatively high lattice constant of 12.228 Å in comparison with

the traditional $\text{Y}_3\text{Al}_5\text{O}_{12}$ (YAG) substrates with a lattice constant of 12.003 Å from supercooled melt solutions using both $\text{BaO}\text{-B}_2\text{O}_3\text{-BaF}_2$ and $\text{PbO}\text{-B}_2\text{O}_3$ fluxes. Firstly, the sets of optical quality perfect SCF samples—with x values in the 0–2.1 range, y values changing in the 0–2.85 range and thickness in the 16–38 μm range—were crystallized onto GAGG substrates with a square of $1 \times 1 \text{ cm}^2$ with the (100) orientation (Figure 1, left) using the conventional PbO flux for more detail determination of the optimal ranges of Gd and Ga concentrations x and y , respectively, in comparison with work [36]. After that, other sets of optically good quality $\text{Tb}_{1.5}\text{Gd}_{1.5}\text{Al}_{5-y}\text{Ga}_y\text{O}_{12}\text{:Ce}$ SCF samples—with y values changing in the 2–3.8 range and thickness in the 10.5–22 μm range—were also successfully crystallized onto GAGG substrates from novel lead-free BaO based flux (see Figure 1, middle and right figures, and Table 1). The components of this flux have significantly smaller influence on their scintillation properties than in the case of PbO flux grown SCF scintillators [31,33,37,38]. At the same time, the high viscosity of this BaO based flux leads to formation of different structural macro-defects and strongly decreases the uniformity of SCF surface [31,33,37]. Such unwanted effects are also observed in the case of growing the $\text{Tb}_{1.5}\text{Gd}_{1.5}\text{Al}_{5-y}\text{Ga}_y\text{O}_{12}\text{:Ce}$ SCFs from BaO based flux. For this reason, *using the PbO-B₂O₃ solvent—due to its low viscosity and good kinematic properties—is preferable for producing high quality SCF scintillators* for ensuring the best structural and surface quality of screens for high-resolution X-ray imaging [6,7,18,19].



Figure 1. Images of undoped $\text{Gd}_3\text{Al}_{2.5}\text{Ga}_{2.5}\text{O}_{12}$ (GAGG) substrate (**left**), $\text{Tb}_3\text{Al}_{2.5}\text{Ga}_{2.5}\text{O}_{12}\text{:Ce}$ (PbO) (**middle**) and $\text{Tb}_{1.5}\text{Gd}_{1.5}\text{Al}_3\text{Ga}_2\text{O}_{12}\text{:Ce}$ (BaO) (**right**) SCF scintillators, grown by the LPE method onto GAGG substrates.

Table 1. Growth conditions, luminescent and scintillation properties of $\text{Tb}_{3-x}\text{Gd}_x\text{Al}_{5-y}\text{Ga}_y\text{O}_{12}\text{:Ce}$ SCFs. M—SCF/substrate misfit, λ_{\max} —maximum of CL spectra, $t_{1/e}$ and $t_{1/20}$ scintillation decay times to 1/e and 1/20 levels, respectively; LY—photoelectron light yield under α -particle excitation by ^{239}Pu (5.15 MeV) source with respect to the standard YAG:Ce SCF with a photoelectron LY of 360 phels/MeV (light yield of 2650 photons/MeV) [38] and reference $\text{Gd}_3\text{Al}_{2.5}\text{Ga}_{2.5}\text{O}_{12}\text{:Ce}$ bulk crystals with a photoelectron LY of 1300–1370 phels/MeV (light yield of about 10,100 photons/MeV).

Content of SCF Samples	Flux	Substrate	m, %	λ_{\max} , nm	$t_{1/e}/t_{1/20}$, ns	LY, %	Reference
YAG:Ce	PbO	YAG	-	535	67.3	100	[21,31]
LuAG:Ce	PbO	YAG	-0.82	509	52.8	205	[21,31]
Tb_{1.5}Gd_{1.5}Al₃Ga₂O₁₂:Ce	BaO	GAGG	-1.30	553	228/728	380	
Tb _{1.5} Gd _{1.5} Al _{2.5} Ga _{2.5} O ₁₂ :Ce	BaO	GAGG	-0.79	543	201/893	270	
Tb _{1.5} Gd _{1.5} Al _{1.5} Ga _{3.5} O ₁₂ :Ce	BaO	GAGG	+0.05	543	183/728	160	
Tb _{1.5} Gd _{1.5} Al _{1.15} Ga _{3.85} O ₁₂ :Ce	BaO	GAGG	+0.5	543	103/868	50	
Tb ₃ Al ₅ O ₁₂ :Ce	PbO	GAGG	-1.29	560	306/1795	195	[21]
Tb ₃ Al ₃ Ga ₂ O ₁₂ :Ce	PbO	GAGG	-0.49	543	435/1340	200	[36]
Tb₃Al_{2.5}Ga_{2.5}O₁₂:Ce	PbO	GAGG	-0.37	543	456/1368	235	[36]
Tb ₂ GdAl _{2.5} Ga _{2.5} O ₁₂ :Ce	PbO	GAGG	-0.20	543	291/883	254	[36]
Tb_{1.5}Gd_{1.5}Al_{2.5}Ga_{2.5}O₁₂:Ce	PbO	GAGG	-0.12	543	333/990	380	[36]
TbGd ₂ Al _{2.5} Ga _{2.5} O ₁₂ :Ce	PbO	GAGG	-0.04	543	299/88	160	[36]
Gd₃Al_{2.5}Ga_{2.5}O₁₂:Ce SC	-	-	-	547	441/1536	381	[21,31]
Gd ₃ Al ₂ Ga ₃ O ₁₂ :Ce SC	-	-	-	549	240/876	365	[21,31]

The concentration of CeO₂ activating oxide was 10 and 5 mole% with respect to the garnet-forming components in the cases of SCF growth using PbO and BaO based fluxes, respectively.

The composition of SCF samples was determined using a JEOL JSM-820 electronic microscope, equipped by an EDX microanalyzer with IXRF 500 and LN2 Eumex detectors. From the microanalysis of the content of the SCF samples we have also found that the segregation coefficient of Ga^{3+} ions in $\text{Tb}_3\text{Al}_{5-y}\text{Ga}_y\text{O}_{12}:\text{Ce}$ and $\text{Tb}_{3-x}\text{Gd}_x\text{Al}_{5-y}\text{Ga}_y\text{O}_{12}:\text{Ce}$ SCFs, grown from PbO based flux, was equal to 0.59–0.65 and 0.735–0.82, respectively (Table 2). The segregation coefficient of Gd^{3+} ions in $\text{Tb}_{3-x}\text{Gd}_x\text{Al}_{5-y}\text{Ga}_y\text{O}_{12}:\text{Ce}$ (PbO) SCFs was equal to 0.95–1.05. The segregation coefficient of Ce^{3+} ions was equal to about 0.004–0.005 and 0.0095–0.02 in $\text{Tb}_3\text{Al}_{5-y}\text{Ga}_y\text{O}_{12}:\text{Ce}$ SCF and $\text{Tb}_{3-x}\text{Gd}_x\text{Al}_{5-y}\text{Ga}_y\text{O}_{12}:\text{Ce}$ SCFs, in the case of using PbO based flux for their growth (Table 2).

We have also found that the segregation coefficients of Ga^{3+} and Ce^{3+} ions in $\text{Tb}_{3-x}\text{Gd}_x\text{Al}_{5-y}\text{Ga}_y\text{O}_{12}:\text{Ce}$ SCFs in the case of using BaO based flux were significantly larger. Specifically, the segregation coefficient of Ga^{3+} ions in these SCFs, grown from BaO based flux, was equal to 1.0–1.1 and was notably larger than the respective values in the SCFs grown from PbO based flux (Table 2). The segregation coefficient of Ce^{3+} ions in the $\text{Tb}_{3-x}\text{Gd}_x\text{Al}_{5-y}\text{Ga}_y\text{O}_{12}:\text{Ce}$ SCFs was also significantly larger in the case of using BaO based flux and was equal to 0.012–0.14 in comparison with the 0.004–0.005 value in $\text{Tb}_3\text{Al}_{5-y}\text{Ga}_y\text{O}_{12}:\text{Ce}$ and 0.0095–0.02 in $\text{Tb}_{3-x}\text{Gd}_x\text{Al}_{5-y}\text{Ga}_y\text{O}_{12}:\text{Ce}$ SCF counterparts grown from PbO based flux (Table 2). At the same time, the segregation coefficient of Gd^{3+} ions, being equal to 1.0–1.1 in the case of $\text{Tb}_{3-x}\text{Gd}_x\text{Al}_{5-y}\text{Ga}_y\text{O}_{12}:\text{Ce}$ SCFs, grown from BaO based flux, was only slightly larger than that in the case of using PbO based flux (Table 2).

The XRD measurements (spectrometer DRON 4, $\text{CuK}\alpha$ X-ray source) were used for characterization of the structural quality of $\text{Tb}_{1.5}\text{Gd}_{1.5}\text{Al}_{5-y}\text{Ga}_y\text{O}_{12}:\text{Ce}$ SCFs, grown from BaO based flux (Figure 2). From the respective XRD patterns of these SCFs at y value in the 2–3.85 range (Figure 2), we can also estimate the lattice constants of the different garnet compositions and the misfit between the lattice constants of SCFs and GAGG substrate $\Delta a = (a_{\text{SCF}} - a_{\text{sub}})/a_{\text{sub}} \times 100\%$ (Table 1). Namely, the lattice constant of $\text{Tb}_{1.5}\text{Gd}_{1.5}\text{Al}_{5-y}\text{Ga}_y\text{O}_{12}:\text{Ce}$ (BaO) SCFs at $y = 2$ –3.85 changed from 12.069 Å for $\text{Tb}_{1.5}\text{Gd}_{1.5}\text{Al}_3\text{Ga}_2\text{O}_{12}:\text{Ce}$ SCFs to 12.2913 Å for $\text{Tb}_{1.5}\text{Gd}_{1.5}\text{Al}_{1.2}\text{Ga}_{3.8}\text{O}_{12}:\text{Ce}$ SCFs (Figure 2) and the value of misfit m changed from −1.3% to +0.52% for these SCF samples (Table 1).

Table 2. Segregation coefficients of different ions in $\text{Tb}_{3-x}\text{Gd}_x\text{Al}_{5-y}\text{Ga}_y\text{O}_{12}:\text{Ce}$ SCFs grown onto GAGG substrates.

Garnet Content	Type of Flux	Segregation Coefficient		
		Gd^{3+}	Ga^{3+}	Ce^{3+}
$\text{Tb}_3\text{Al}_{5-2.9}\text{Ga}_{0-2.1}\text{O}_{12}:\text{Ce}$	PbO		0.59–0.65	0.004–0.005
$\text{Tb}_{2-0.9}\text{Gd}_{1-2.1}\text{Al}_{2.25-2.4}\text{Ga}_{2.75-2.6}\text{O}_{12}:\text{Ce}$	PbO	1.0–1.1	0.735–0.82	0.0095–0.02
$\text{Tb}_{1.5}\text{Gd}_{1.5}\text{Al}_{3-1.15}\text{Ga}_{2-3.85}\text{O}_{12}:\text{Ce}$	BaO	1.0–1.05	1.0–1.1	0.012–0.14

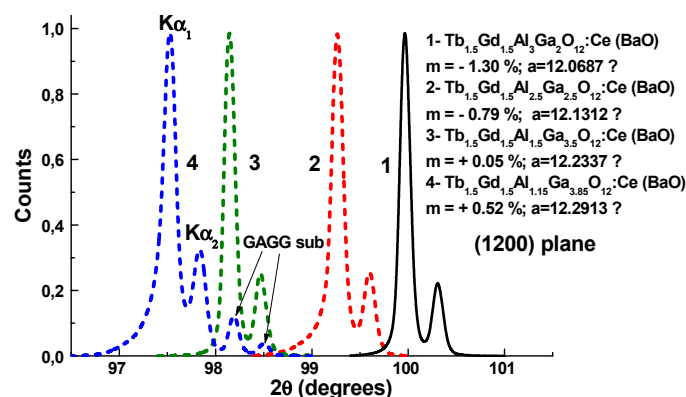


Figure 2. XRD patterns of (1200) planes of $\text{Tb}_{1.5}\text{Gd}_{1.5}\text{Al}_{5-y}\text{Ga}_y\text{O}_{12}:\text{Ce}$ (BaO) SCFs at $y = 2$ (1); 2.5 (2); 3.5 (3) and 3.85 (4). The film/substrate lattice misfit m lies in the $-1.3\% < m < +0.5\%$ range.

The measurements of rocking curves in the ω and $2\theta-\omega$ scanning modes were applied for characterization of the structural quality of $Tb_{1.5}Gd_{1.5}Al_{5-y}Ga_yO_{12}:Ce$ (BaO) SCFs at different Ga content y in the 2.0–3.85 range (Figure 3a,b, respectively). As can be seen from these figures, the quality of the SCFs, which is proportional to FWHM of rocking curves, significantly increases at lower SCF-substrate misfit values m in $Tb_{1.5}Gd_{1.5}Al_{5-y}Ga_yO_{12}:Ce$ (BaO) SCFs. Namely, the smallest FWHM values of 0.0182 and 0.0121 degrees are observed for $Tb_{1.5}Gd_{1.5}Al_{1.5}Ga_{3.5}O_{12}:Ce$ (BaO) SCFs (Figure 3a,b, respectively) grown onto GAGG substrates with the lowest SCF/substrate misfit value $m = +0.05\%$ (Table 1).

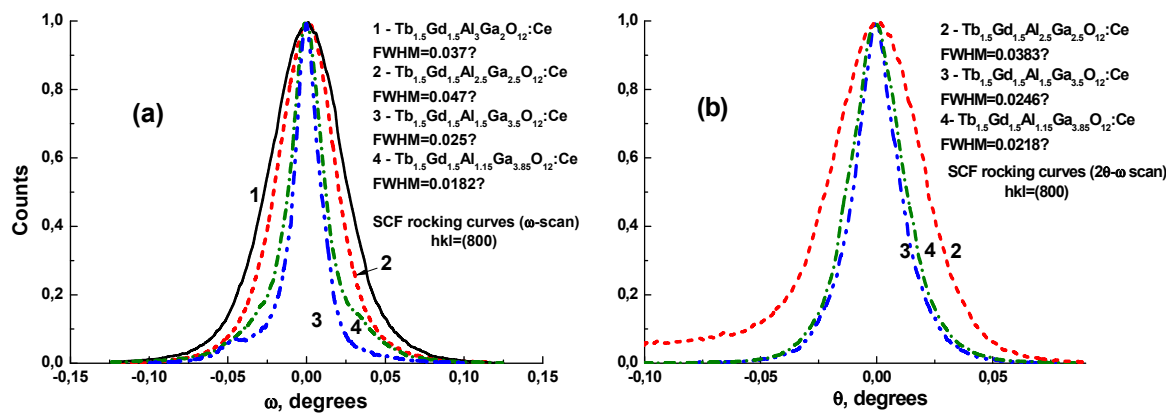


Figure 3. Rocking curves of $Tb_{1.5}Gd_{1.5}Al_{5-y}Ga_yO_{12}:Ce$ (BaO) SCFs grown onto GGAG substrates at different y values: $y = 2$ (1); 2.5 (2); 3.5 (3) and 3.85 (4) recorded in ω (a) and $2\theta-\omega$ (b) scanning modes.

3. Luminescent and Scintillation Properties of $Tb_{3-x}Gd_xAl_{5-y}Ga_yO_{12}:Ce$ Single Crystalline Films

For characterization of the optical properties of Ce^{3+} doped $Tb_{3-x}Gd_xAl_{5-y}Ga_yO_{12}:Ce$ SCFs, the cathodoluminescence (CL) spectra, LY and scintillation decay kinetics measurements as well as the thermostimulated luminescence (TSL) glow curves under excitation by α -particles were performed.

The CL spectra were measured at the room temperature (RT) using an electron microscope SEM JEOL JSM-820, additionally equipped with a spectrometer Stellar Net with TE-cooled CCD detector working in the 200–1200 nm range. The scintillation LY with a shaping time of 14 μs and decay kinetics measurements were performed using the setup based on a Hamamatsu H6521 PMT, multichannel analyzer and digital TDS3052 oscilloscope under excitation by α -particles of Pu^{239} (5.15 MeV) source. The energy resolution (ER) of SCF scintillators is calculated as a ratio of the FWHM of the full energy peak to the peak's centroid position: $E = \text{FWHM}/\text{centroid} [\%]$. The TSL measurements were performed in the 300–800 K temperature range using a commercial Risoe DA-20 TL/OSL reader (Denmark) after α -particle excitation by the Am^{241} source which is built into the DA-20 reader. The TL glow curves were registered from 50 °C to 450 °C at the rate of 5 °C·s⁻¹. The measurements were conducted with a Shott BG 39 green filter, with transmission from 350 to 700 nm. This filter is well adapted for the registration of Ce^{3+} luminescence in the SCF samples under study. Meanwhile, the spectrally resolved TSL spectra of $Tb_{3-x}Gd_xAl_{5-y}Ga_yO_{12}$ SCF with different Gd^{3+} and Tb^{3+} content (not present in the paper) show only Ce^{3+} luminescence in the green-yellow ranges and absence of the emission of Tb^{3+} or Gd^{3+} cations.

3.1. Cathodoluminescence Spectra

The RT CL spectra of $Tb_3Al_{5-y}Ga_yO_{12}:Ce$ and $Tb_{3-x}Gd_xAl_{5-y}Ga_yO_{12}:Ce$ SCFs, grown from PbO based flux, with close y values in the 2–2.5 range and different x values in the 0–2 range, are shown in Figure 4a,b, respectively, in comparison with the spectrum of TbAG:Ce SCF (Figure 4a, curve 1). The RT CL spectra of $Tb_{1.5}Gd_{1.5}Al_{5-y}Ga_yO_{12}:Ce$ SCFs, grown from BaO based flux, with different y

values in the 2–3.85 range, are presented in Figure 4c, curves 1–4 in comparison with the CL spectra of standard $\text{Gd}_3\text{Al}_{2.5}\text{Ga}_{2.5}\text{O}_{12}:\text{Ce}$ bulk SC (Figure 4b, curve 5).

The CL spectra of all the SCFs under study show only the dominant luminescence of Ce^{3+} or Tb^{3+} ions in the visible range without any bands in the UV range related to the luminescence of antisite defects [41–44], which typically are observed in the bulk crystal analogues of these garnets [45,46].

The results, presented in Figure 4a–c, indicate that the complicated $\text{Gd}^{3+} \rightarrow \text{Tb}^{3+} \rightarrow \text{Ce}^{3+} \rightarrow \text{Tb}^{3+}$ cascade energy transfer is observed in the $\text{Tb}_{3-x}\text{Gd}_x\text{Al}_{5-y}\text{Ga}_y\text{O}_{12}:\text{Ce}$ mixed garnet, with large content of Gd^{3+} and Ga^{3+} cations due to overlapping of the Gd^{3+} and Tb^{3+} emission bands and the absorption bands of Tb^{3+} and Ce^{3+} ions [47–51]. Namely, the change of the positions of Ce^{3+} and Tb^{3+} 4f-5d absorption and emission bands at different concentrations of Tb^{3+} , Gd^{3+} and Ga^{3+} cations leads to a strong variation of the efficiency of $\text{Gd}^{3+} \rightarrow \text{Tb}^{3+} \rightarrow \text{Ce}^{3+} \rightarrow \text{Tb}^{3+}$ energy transfer processes in $\text{Tb}_{3-x}\text{Gd}_x\text{Al}_{5-y}\text{Ga}_y\text{O}_{12}:\text{Ce}$ SCFs and results in the respective changes of their CL spectra (Figure 4a–c).

The estimation of the optimal content of Gd^{3+} and Ga^{3+} cations in $\text{Tb}_{3-x}\text{Gd}_x\text{Al}_{5-y}\text{Ga}_y\text{O}_{12}:\text{Ce}$ SCFs in the $x = 1–1.5$ and $y = 2–3$ ranges was firstly performed in [36]. We will explain such a choice in this work in more detail based on the results of their CL spectra (Figure 4a,b). Alloying of Ga^{3+} ions in $\text{Tb}_3\text{Al}_5\text{O}_{12}:\text{Ce}$ (PbO) SCF in the concentration range above $x = 2$ leads to a decrease of the garnet band gap value [34] and increasing the centroid shift of O-Ga bonding in comparison with O-Al bonding. That results in the subsequent blue shift of the Ce^{3+} emission spectra in $\text{Tb}_3\text{Al}_{5-y}\text{Ga}_y\text{O}_{12}:\text{Ce}$ (PbO) SCFs (Figure 4a, curves 2 and 3) and $\text{Tb}_{1.5}\text{Gd}_{1.5}\text{Al}_{5-y}\text{Ga}_y\text{O}_{12}:\text{Ce}$ (BaO) SCFs (Figure 4c, curves 1–4). It is most important here that increasing the level of Ga^{3+} alloying in these SCFs above $y = 2–2.5$ also leads to a strong decrease of the Ce^{3+} emission contribution to the total spectrum of the CL luminescence of these SCF samples (Figure 4a,c).

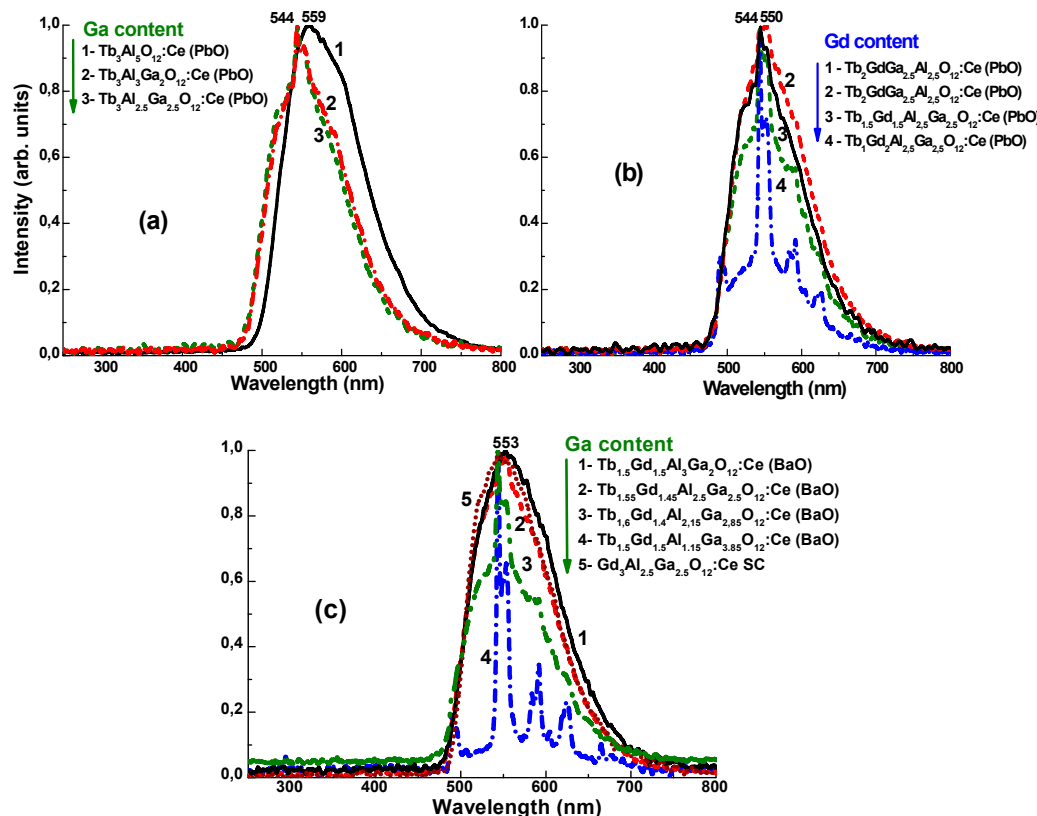


Figure 4. Normalized CL spectra at 300 K of $\text{Tb}_3\text{Al}_{5-y}\text{Ga}_y\text{O}_{12}:\text{Ce}$ (PbO) (a), $\text{Tb}_{3-x}\text{Gd}_x\text{Al}_{5-y}\text{Ga}_y\text{O}_{12}:\text{Ce}$ (PbO) (b) and $\text{Tb}_{3-x}\text{Gd}_x\text{Al}_{5-y}\text{Ga}_y\text{O}_{12}:\text{Ce}$ (BaO) (c) SCFs with different x and y values (see legend of the figure) in comparison with CL spectra of $\text{Tb}_3\text{Al}_5\text{O}_{12}:\text{Ce}$ (PbO) SCF (1a) and $\text{Gd}_3\text{Al}_{2.5}\text{Ga}_{2.5}\text{O}_{12}:\text{Ce}$ bulk SC (5b).

Alloying of Gd^{3+} ions in $\text{Tb}_3\text{Al}_{5-y}\text{Ga}_y\text{O}_{12}:\text{Ce}$ (PbO) SCFs in the concentration range $x = 0\text{--}1.5$ has an opposite effect than the Ga^{3+} alloying and leads to the notable red shift of their CL spectra. The Gd^{3+} alloying in concentrations up to $x = 1$ increases the Ce^{3+} luminescence contribution (Figure 4b, curves 2) in comparison with the CL spectra of Gd free SCF samples (Figure 4a, curve 1). Meanwhile, the Gd^{3+} alloying in the concentration range above $x = 1.0$ in $\text{Tb}_{3-x}\text{Gd}_x\text{Al}_{5-y}\text{Ga}_y\text{O}_{12}:\text{Ce}$ (PbO) SCFs also results in the notable decrease of the Ce^{3+} emission contribution to the total spectrum of the SCF luminescence and respective increase of the Tb^{3+} luminescence contribution (Figure 4a, curves 3–5). This can be caused by variation of the efficiency of $\text{Gd}^{3+}\rightarrow\text{Tb}^{3+}$ and $\text{Tb}^{3+}\rightarrow\text{Ce}^{3+}$ energy transfer processes in $\text{Tb}_{3-x}\text{Gd}_x\text{Al}_{5-y}\text{Ga}_y\text{O}_{12}:\text{Ce}$ SCFs due to the change of the respective positions of Ce^{3+} and Tb^{3+} absorption and emission bands at different concentration of Tb^{3+} and Gd^{3+} cations.

Based on the results presented in Figure 4a,b, we can confirm here that the optimal values of the Gd^{3+} and Ga^{3+} concentrations in $\text{Tb}_{3-x}\text{Gd}_x\text{Al}_{5-y}\text{Ga}_y\text{O}_{12}:\text{Ce}$ SCFs are $x = 1\text{--}1.5$ and $y = 2\text{--}2.5$ ranges, respectively. At these concentrations the respective CL spectra of $\text{Tb}_{1.5}\text{Gd}_{1.5}\text{Al}_{3-2.5}\text{Ga}_{2-2.5}\text{O}_{12}:\text{Ce}$ (PbO) and (BaO) SCFs show the dominant Ce^{3+} emission band with relatively small contribution of the Tb^{3+} luminescence (Figure 4b, curves 2 and 3 and Figure 4c, curves 1 and 2).

3.2. Scintillation Decay Kinetics

The scintillation decay kinetics of $\text{Tb}_{3-x}\text{Gd}_x\text{Al}_{5-y}\text{Ga}_y\text{O}_{12}:\text{Ce}$ and $\text{Tb}_{1.5}\text{Gd}_{1.5}\text{Al}_{5-y}\text{Ga}_y\text{O}_{12}:\text{Ce}$ SCFs, grown both from PbO (a) and BaO (b) fluxes with different x and y values in the 0–2 and 2–2.5 ranges, respectively, are shown correspondingly in Figure 5a,b. Generally, the $\text{Tb}_{3-x}\text{Gd}_x\text{Al}_{5-y}\text{Ga}_y\text{O}_{12}:\text{Ce}$ SCF scintillators demonstrate the notably slower non-exponential kinetics similarly to their YAG:Ce and LuAG:Ce SCF counterparts [21,36]. Such slower decay kinetics of the Ce^{3+} luminescence is typical for Tb^{3+} and Gd^{3+} based SCF scintillators, where the cascade energy transfer via both sublattices of Gd^{3+} and Tb^{3+} cations is more complicated [36] in comparison with their YAG:Ce and LuAG:Ce SCF analogues, where the direct energy transfer from the garnet host to Ce^{3+} ions dominates [21].

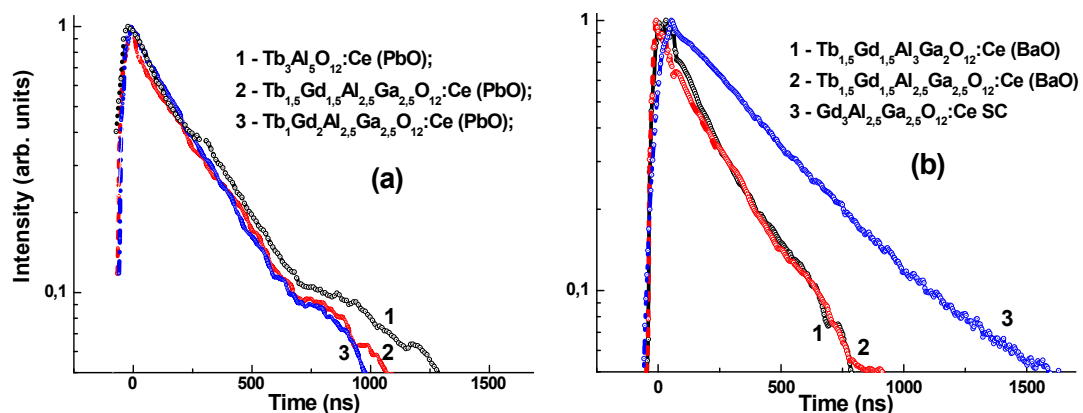


Figure 5. (a) The normalized scintillation decay kinetics of $\text{Tb}_{3-x}\text{Gd}_x\text{Al}_{2.5}\text{Ga}_{2.5}\text{O}_{12}:\text{Ce}$ (PbO) SCFs (curves 2, 3) with different Gd and Ga contents in comparison with the decay kinetics of the $\text{Tb}_3\text{Al}_5\text{O}_{12}:\text{Ce}$ (PbO) SCF counterpart (curve 1); (b) the normalized scintillation decay kinetics of $\text{Tb}_{1.5}\text{Gd}_{1.5}\text{Al}_{5-y}\text{Ga}_y\text{O}_{12}:\text{Ce}$ (BaO) SCFs (curves 1, 2) with different Ga content in comparison with the decay kinetics of $\text{Gd}_3\text{Al}_{2.5}\text{Ga}_{2.5}\text{O}_{12}:\text{Ce}$ bulk SC (curve 3).

The influence of Ga^{3+} and Gd^{3+} alloying on the scintillation decay of $\text{Tb}_{3-x}\text{Gd}_x\text{Al}_{5-y}\text{Ga}_y\text{O}_{12}:\text{Ce}$ (PbO) SCFs was firstly considered in [36]. We will explain the choice of optimal Gd^{3+} and Ga^{3+} concentrations in these SCFs in more detail based on the results of their scintillation decay kinetics (Figure 5a). The Ga^{3+} alloying with the concentration up to $y = 2.5$ in $\text{Tb}_3\text{Al}_{5-y}\text{Ga}_y\text{O}_{12}:\text{Ce}$ (PbO) SCFs leads to a significant slowdown of the decay kinetics of the Ce^{3+} emission in comparison with the TbAG:Ce SCF due to the lowering of the bottom of the conductive band and the arising electron

transitions from the excited levels of Ce^{3+} to the conductive band. This results in the strong elongation of the scintillation decay of $\text{Tb}_3\text{Al}_{5-y}\text{Ga}_y\text{O}_{12}:\text{Ce}$ (PbO) SCFs (not present in Figure 5a). Contrary to the influence of Ga^{3+} cations, the Gd^{3+} alloying in the concentration range $x = 1.5\text{--}2$ strongly accelerates the scintillation decay of $\text{Tb}_{3-x}\text{Gd}_x\text{Al}_{2.5}\text{Ga}_{2.5}\text{O}_{12}:\text{Ce}$ (PbO) SCFs (Figure 5a, curves 2 and 3). It is also important to note here that the scintillation decay times $t_{1/e}$ and $t_{1/20}$ in $\text{Tb}_{3-x}\text{Gd}_x\text{Al}_{5-y}\text{Ga}_y\text{O}_{12}$ (PbO) SCFs at high Gd and Ga concentrations ($x = 1.5\text{--}2$; $y = 2.5$) (Figure 5a, curves 2 and 3) are close or even faster with respect to the corresponding values for $\text{Tb}_3\text{Al}_5\text{O}_{12}:\text{Ce}$ SCF (see also Table 1).

The $\text{Tb}_{1.5}\text{Gd}_{1.5}\text{Al}_{5-y}\text{Ga}_y\text{O}_{12}:\text{Ce}$ SCF scintillators, grown from the BaO based flux (Figure 5b), demonstrate significantly more exponential kinetics than that in their SCF counterparts, grown from the PbO based flux (Figure 5a). Such a difference can be caused by eliminating the delay of energy transfer from the garnet hosts to Ce^{3+} ions caused by the defect centers related to the Pb^{2+} ions in $\text{Tb}_{3-x}\text{Gd}_x\text{Al}_{5-y}\text{Ga}_y\text{O}_{12}:\text{Ce}$ (PbO) SCF scintillators. The concentration of these defect centers is significantly smaller in their analogues, prepared from the BaO based flux due to the very low contamination with Ba^{2+} ions.

It is necessary also to note here that the scintillation decay of $\text{Tb}_{1.5}\text{Gd}_{1.5}\text{Al}_{3-2.5}\text{Ga}_{2-2.5}\text{O}_{12}:\text{Ce}$ (BaO) SCFs (Figure 5b, curves 1 and 2) is also notably faster than that in $\text{Gd}_3\text{Al}_{2.5}\text{Ga}_{2.5}\text{O}_{12}:\text{Ce}$ SC counterparts (Figure 5b, curve 3) which can also be used as a substrate for producing SCF scintillators. In such a way these SCFs and the high-quality $\text{Gd}_3\text{Al}_{2.5}\text{Ga}_{2.5}\text{O}_{12}:\text{Ce}$ SCs can also be used for the creation of advanced hybrid film-substrate scintillators using the LPE method for simultaneous registration of the different components of ionization fluxes [52]. In such scintillators, the separation of the signal coming from the film and crystal parts of the hybrid scintillator can be performed using the differences in their scintillation decay kinetics (Figure 5b, curves 1 and 3, respectively).

3.3. TSL Properties

The results of the TSL investigations after irradiation by alpha particles of $\text{Tb}_{3-x}\text{Gd}_x\text{Al}_{5-y}\text{Ga}_y\text{O}_{12}:\text{Ce}$ SCFs with different x and y values, grown from both PbO (a) and BaO (b) based fluxes, in the above RT range are shown in Figure 6. The TSL in these SCFs arises at the thermal liberation of electrons from traps and their recombination with the holes localized around Ce^{3+} ions [21,28,33,42,43]. Taking into account the low temperature of SCF preparation in oxygen containing atmosphere (air), the formation of these traps can be caused mainly by the presence of Pb^{2+} and Ba^{2+} (from flux) and Pt^{4+} (from crucible) contaminations in SCF samples. This leads to the creation of different locally non-compensated lattice defects, such as the oxygen or cation vacancies, around the mentioned impurities, which act as trapping centers [21,31,36,53,54].

In $\text{Tb}_3\text{Al}_5\text{O}_{12}:\text{Ce}$ (PbO) SCFs, the position of the main TSL peak is located at 440 K (Figure 6a, curve 1). Ga^{3+} alloying of $\text{Tb}_3\text{Al}_{5-y}\text{Ga}_y\text{O}_{12}:\text{Ce}$ SCFs in the concentration range up to $y = 2$ leads to the shift of the TSL peaks to 407 K and substantially decreases the TSL signal in the 350–600 K range (Figure 6a, curve 2) (see also [31,36]). Gd^{3+} alloying additionally shifts the TSL peak to 390 K and slightly decreases the TSL signal of $\text{Tb}_{1.5}\text{Gd}_{1.5}\text{Al}_{3-2.5}\text{Ga}_{2-2.5}\text{O}_{12}:\text{Ce}$ (PbO) SCFs in the 450–650 K high-temperature range in comparison with Gd free SCF samples (Figure 6a, curve 3). These results are in good correlation with the significant increase of the LY in $\text{Tb}_{1.5}\text{Gd}_{1.5}\text{Al}_{3-2.5}\text{Ga}_{2-2.5}\text{O}_{12}:\text{Ce}$ (PbO) SCFs (Table 1), most probably due to elimination of the participation of high-temperature trap-related centers in the scintillation processes in the SCF samples with the mentioned optimal content.

Using the lead free BaO based flux for the growth of $\text{Tb}_{3-x}\text{Gd}_x\text{Al}_{5-y}\text{Ga}_y\text{O}_{12}:\text{Ce}$ SCFs leads also to the low intensity of the TSL peaks in the above RT range in SCF scintillators (Figure 6b). Namely, the TSL intensity of $\text{Tb}_{1.5}\text{Gd}_{1.5}\text{Al}_{3-2.5}\text{Ga}_{2-2.5}\text{O}_{12}:\text{Ce}$ (BaO) SCFs in the 450–600 K range is also negligible (Figure 6b). This result is in good correlation with the high LY in $\text{Tb}_{1.5}\text{Gd}_{1.5}\text{Al}_{3-2.5}\text{Ga}_{2-2.5}\text{O}_{12}:\text{Ce}$ (BaO) SCFs (Table 1), due to the low Ba^{2+} contamination and related with them p-trapping centers as well as to the additional elimination of the trap-related phenomena in the scintillation processes in these SCFs by Ga^{3+} and Gd^{3+} alloying.

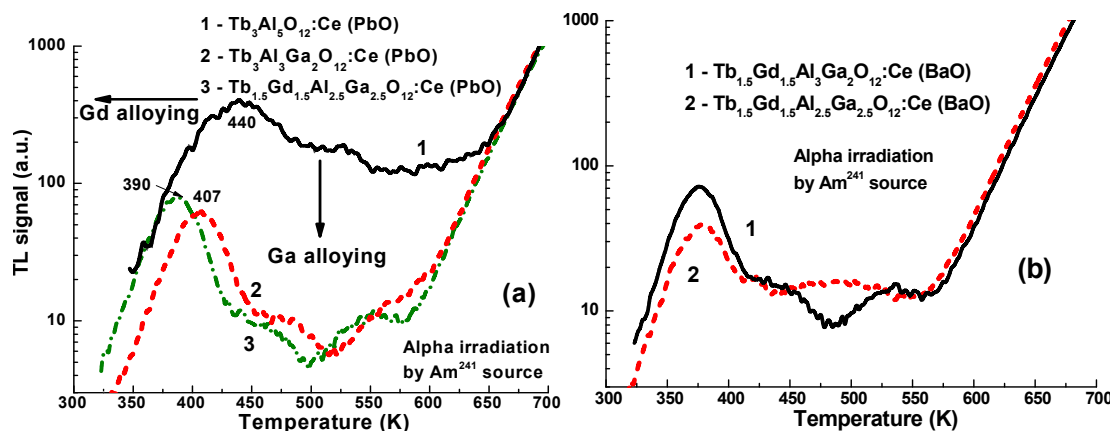


Figure 6. TSL (in the log scale) of $\text{Tb}_{3-x}\text{Gd}_x\text{Al}_{5-y}\text{Ga}_y\text{O}_{12}:\text{Ce}$ (PbO) (a) with a different content of Gd^{3+} and Ga^{3+} cations (see legend of the figure) and $\text{Tb}_{1.5}\text{Gd}_{1.5}\text{Al}_{3.25}\text{Ga}_{2.25}\text{O}_{12}:\text{Ce}$ (BaO) (b) SCFs after irradiation by Am^{241} α -particles and registration of the Ce^{3+} luminescence.

Thus, the Ga^{3+} alloying in the concentration range $y = 2\text{--}2.5$ positively affects not only the scintillation properties of melt-grown mixed garnet crystals with a large concentration of antisite defects and oxygen vacancies [22–24] but antisite free SCF counterparts as well [31–33] due to burying the trap levels by the bottom of the conductive band in the Ga-containing garnets. The additional positive effect on the elimination of the trap centers in scintillation phenomena, which is observed in $\text{Tb}_{3-x}\text{Gd}_x\text{Al}_{5-y}\text{Ga}_y\text{O}_{12}:\text{Ce}$ SCF samples, is most probably caused by burying the deeper trap levels by high-energy states of Tb^{3+} and Gd^{3+} cations in such Tb,Gd-rich garnets [36].

3.4. Photoelectron Light Yield Measurements

The scintillation LY of $\text{Tb}_{3-x}\text{Gd}_x\text{Al}_{5-y}\text{Ga}_y\text{O}_{12}:\text{Ce}$ SCFs, grown from PbO and BaO based fluxes at different content of Gd^{3+} and Ga^{3+} cations, measured with a shaping time of 14 μs under excitation by α -particles of Pu^{239} (5.15 MeV) source, is shown in Table 1 and Figure 7.

In principle, the simultaneous influence of Gd^{3+} and Ga^{3+} doping of TbAG:Ce SCFs can also result in a strong increase in the LY of $\text{Tb}_{3-x}\text{Gd}_x\text{Al}_{5-y}\text{Ga}_y\text{O}_{12}:\text{Ce}$ SCF scintillators at $x = 0\text{--}1.5$ and $y = 2\text{--}3$ [21,36]. Thus, the determination of the optimal content and ratio between the Gd^{3+} and Ga^{3+} cations in the TbAG:Ce garnet host is the most important task for the optimization of the properties of $\text{Tb}_{3-x}\text{Gd}_x\text{Al}_{5-y}\text{Ga}_y\text{O}_{12}:\text{Ce}$ SCF scintillators in the case of growth from both PbO and especially lead free BaO based flux.

We have observed that Ga^{3+} doping in the concentration range $y = 2\text{--}2.5$ leads to the increase of the LY of $\text{Tb}_3\text{Al}_{5-y}\text{Ga}_y\text{O}_{12}:\text{Ce}$ (PbO) SCF scintillators. Indeed, with the Ga^{3+} doping at the concentration $y = 2.5$, the LY of these scintillators notably (up to 20%) overcomes the LY of the $\text{Tb}_3\text{Al}_5\text{O}_{12}:\text{Ce}$ SCF sample (Table 1). This is caused mainly by the elimination of trap-related phenomena in $\text{Tb}_3\text{Al}_{5-y}\text{Ga}_y\text{O}_{12}:\text{Ce}$ SCF scintillators due to the decrease of the $\text{Tb}_3\text{Al}_5\text{O}_{12}$ band gap in the case of Ga alloying in the mentioned concentration range (see Part 3.3 for details).

In addition to the positive trend caused by the doping with Ga^{3+} ions, the significant increase of the LY is observed in $\text{Tb}_{3-x}\text{Gd}_x\text{Al}_{5-y}\text{Ga}_y\text{O}_{12}:\text{Ce}$ (PbO) SCFs due to Gd^{3+} doping at the concentration $x = 1\text{--}1.5$ (Table 1). This effect can be caused by the deepest localization of the Ce^{3+} emitting levels inside the band gap and better separation of them with respect to the levels of conductive band. Namely, the $\text{Tb}_{1.5}\text{Gd}_{1.5}\text{Al}_{2.5}\text{Ga}_{2.5}\text{O}_{12}:\text{Ce}$ (PbO) SCF possess excellent scintillation properties (Table 1 and Figure 7). The photoelectron LY of this SCF sample significantly overcomes the LY of the best samples of LuAG:Ce SCF [53], Lu_{1.5}Gd_{1.5}Al_{2.75}Ga_{2.25}O₁₂:Ce SCF [31] and $\text{Tb}_3\text{Al}_5\text{O}_{12}:\text{Ce}$ SCF [21], grown from PbO based flux, up to 1.85, 2.62 and 1.95 times, respectively (see Table 1). This LY is

the highest one ever obtained in our group for the garnet SCF scintillators grown by the LPE from traditional PbO-B₂O₃ based flux [21,31,36,38,53].

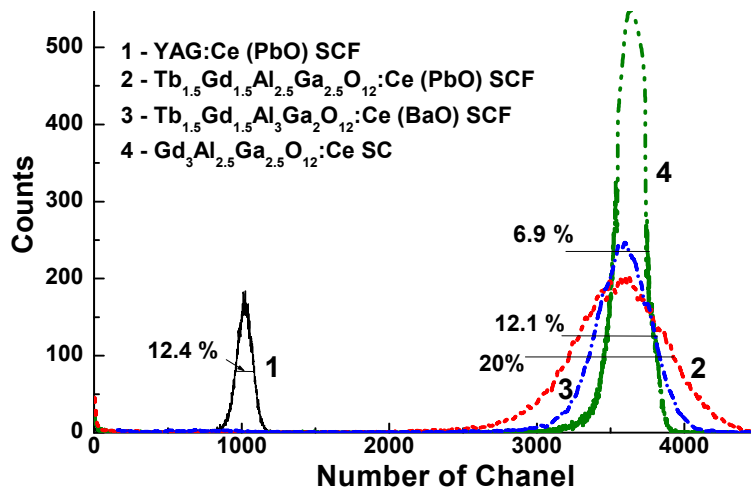


Figure 7. Pulse height spectra of Tb_{1.5}Gd_{1.5}Al_{2.5}Ga_{2.5}O₁₂:Ce (PbO) (2) (LY = 1368 phels/MeV (380%); E = 20%) and Tb_{1.5}Gd_{1.5}Al₃Ga₂O₁₂:Ce (BaO) (3) (LY = 1370 phels/MeV (380%); E = 12.1%) in comparison with YAG:Ce SCFs (1) (LY = 360 phels/MeV (100%), E = 12.4%) and Gd₃Al_{2.5}Ga_{2.5}O₁₂:Ce SC (4) (LY = 1375 phels/MeV (381%); E = 6.9%) excited by α -particles of ²³⁹Pu (5.15 MeV) source and registered with a shaping time of 14 μ s.

The elimination of Pb²⁺ contamination by using the lead-free BaO based flux in principle can result in the improvement of the LY and energy resolution of Tb_{3-x}Gd_xAl_{5-y}Ga_yO₁₂:Ce SCF scintillators (Table 1 and Figure 7). Indeed, the Tb_{1.5}Gd_{1.5}Al₃Ga₂O₁₂:Ce (BaO) SCF sample also possess excellent scintillation properties. Probably due to the elimination of the quenching and trap related phenomena caused by lead ions, the best LY and energy resolution in these SCF is observed at lower Ga concentration y = 2 in the Tb_{1.5}Gd_{1.5}Al₃Ga₂O₁₂:Ce (BaO) SCF sample than in the case of using the PbO based flux (Table 1). The LY of these SCFs also notably (up to 10%) exceeds the LY of the best Lu_{3-x}Gd_xAl_{5-y}Ga_yO₁₂:Ce (BaO) and Gd₃Al_{5-y}Ga_yO₁₂:Ce (BaO) SCF scintillators [31] (Table 1). *Without doubt, this is the highest LY for garnet SCF scintillators, grown by the LPE method from BaO based flux in our group* [31]. Hoverer, the increase of the LY of Tb_{3-x}Gd_xAl_{5-y}Ga_yO₁₂:Ce SCFs due to the elimination of negative influence of Pb²⁺ flux related dopants is relatively small and is not so significant as in the case of producing Lu_{1-x}Gd_xAl_{5-y}Ga_yO₁₂:Ce and Gd₃Al_{5-y}Ga_yO₁₂:Ce SCFs scintillators from PbO and BaO based fluxes [31]. This can be caused by a more favourable situation in terms of the energy transfer phenomena via the sublattice of Tb³⁺ cations to Ce³⁺ ions in the case of Tb_{3-x}Gd_xAl_{5-y}Ga_yO₁₂:Ce (PbO) SCFs which enables the production of these scintillators with high LY and excellent structural quality from the traditional PbO based flux.

Thus, the main reason for such an increase of the LY of Tb_{3-x}Gd_xAl_{5-y}Ga_yO₁₂:Ce SCFs is the optimized cation content with respect to the crystal field strength and energy transfer efficiency to Ce³⁺ ions directly from the mixed garnet host and via the sublattice of Tb³⁺ and Gd³⁺ cations. Most probably, the relative position of Ce³⁺ levels with respect to the levels of Tb³⁺ and Gd³⁺ cations is optimal in Tb_{1.4-1.5}Gd_{1.6-1.5}Al_{3-2.5}Ga_{2-2.5}O₁₂:Ce garnet hosts from the point of view of efficiency of the complicated Gd³⁺ \rightarrow Tb³⁺ \rightarrow Ce³⁺ \rightarrow Tb³⁺ energy transfer in these matrixes. The details of such a transfer are presented in the separate papers [34,35,49–51].

It is also important to note that the LY of Tb_{1.5}Gd_{1.5}Al_{2.5}Ga_{2.5}O₁₂:Ce (PbO) and Tb_{1.5}Gd_{1.5}Al₃Ga₂O₁₂:Ce (BaO) SCFs is comparable with that in the high-quality Gd₃Al_{2.5-2}Ga_{2.5-3}O₁₂:Ce SC samples (Table 1 and Figure 7). This also enables producing the hybrid film-substrate detectors using the LPE method with high LY both in film and substrate scintillators with optimized contents, taking into

account the requirement for the decay times of the signals coming from the film and substrate components of the hybrid scintillator differs by a factor of at least two [52]. Such a demand is fully realized in the case of $\text{Tb}_{1.5}\text{Gd}_{1.5}\text{Al}_3\text{Ga}_2\text{O}_{12}:\text{Ce}$ (BaO) SCF/ $\text{Gd}_3\text{Al}_{2.5}\text{Ga}_{2.5}\text{O}_{12}:\text{Ce}$ SC hybrid scintillators (Figure 4b). These scintillators can be proposed for different types of application, especially for registration of the components of mixed ionizing flux [52] and multi-layer screens for visualization of X-ray images [21].

4. Conclusions

In this work, we report the creation of advanced single crystalline film (SCF) screens with excellent scintillation properties based on the $\text{Tb}_{1.5}\text{Gd}_{1.5}\text{Al}_{3-2.5}\text{Ga}_{2-2.5}\text{O}_{12}:\text{Ce}$ mixed garnet compounds grown by the LPE method from both novel lead free BaO and traditional PbO based fluxes onto $\text{Gd}_3\text{Al}_{2.5}\text{Ga}_{2.5}\text{O}_{12}$ (GAGG) substrates.

The optimization of Gd^{3+} and Ga^{3+} content in the $\text{Tb}_{3-x}\text{Gd}_x\text{Al}_{5-y}\text{Ga}_y\text{O}_{12}:\text{Ce}$ garnet at $x = 1.5$ and $y = 2-2.5$ results in the strong improvement of the energy transfer efficiency from the Tb^{3+} - Gd^{3+} based matrix to Ce^{3+} ions due to the modification of the band gap value and Ce^{3+} energy structure, as well as the elimination of the TSL peaks above room temperature. Namely, the $\text{Tb}_{1.5}\text{Gd}_{1.5}\text{Al}_3\text{Ga}_2\text{O}_{12}:\text{Ce}$ SCFs grown from BaO based flux under α -particle excitation possess the highest LY values among all the LPE grown garnet SCF scintillators obtained in our group, which exceeds by at least 10% the LY of the best samples of the recently developed $\text{Lu}_{1.5}\text{Gd}_{1.5}\text{Al}_{2.75}\text{Ga}_{2.25}\text{O}_{12}:\text{Ce}$ and $\text{Gd}_3\text{Al}_{2.75}\text{Ga}_{2.25}\text{O}_{12}:\text{Ce}$ SCF scintillators grown from BaO based flux [31]. The photoelectron LY of these SCF scintillators under excitation by ^{239}Pu (5.15 MeV) source is comparable with that in high-quality $\text{Gd}_3\text{Al}_{2.5-3}\text{Ga}_{2.5-3}\text{O}_{12}:\text{Ce}$ reference bulk crystal analogue with a photoelectron LY of 1370 phels/MeV (light yield of about 10,000 photons/MeV). $\text{Tb}_{1.5}\text{Gd}_{1.5}\text{Al}_3\text{Ga}_2\text{O}_{12}:\text{Ce}$ SCFs also have a relatively fast scintillation response in the hundred ns range under α -particle excitation with decay times $t_{1/e}$ and $t_{1/20}$ of 230 and 730 ns, respectively. Meanwhile, the structural uniformity and optical quality of these SCF scintillators are strongly influenced by the high-viscosity of BaO based melt.

The SCFs of $\text{Tb}_{1.5}\text{Gd}_{1.5}\text{Al}_{2.5}\text{Ga}_{2.5}\text{O}_{12}:\text{Ce}$ garnets, grown from PbO based flux onto GAGG substrates, possess very high structural quality and excellent scintillation properties. Under α -particle excitation, the LY of $\text{Tb}_{1.5}\text{Gd}_{1.5}\text{Al}_{2.5}\text{Ga}_{2.5}\text{O}_{12}:\text{Ce}$ (PbO) SCFs is comparable with that of their analogues grown from BaO flux and these SCFs possess only slightly slower scintillation response with decay times $t_{1/e}$ and $t_{1/20}$ of 330 and 990 ns, respectively. It is important to note that the negative quenching influence of the Pb^{2+} flux related dopants is not so significant during manufacturing the $\text{Tb}_{1.5}\text{Gd}_{1.5}\text{Al}_{2.5}\text{Ga}_{2.5}\text{O}_{12}:\text{Ce}$ SCF scintillators as in the case of $\text{Lu}_{1-x}\text{Gd}_x\text{Al}_{5-y}\text{Ga}_y\text{O}_{12}:\text{Ce}$ and $\text{Gd}_3\text{Al}_{5-y}\text{Ga}_y\text{O}_{12}:\text{Ce}$ SCFs analogues grown from PbO based fluxes [31]. This enables the production of $\text{Tb}_{3-x}\text{Gd}_x\text{Al}_{5-y}\text{Ga}_y\text{O}_{12}:\text{Ce}$ SCF scintillators with high LY and excellent structural quality from the traditional PbO based flux. Most probably, this positive trend is observed only in the Tb containing scintillators, where very complicated but efficient energy transfer from Tb^{3+} and Gd^{3+} cation sub-lattices to Ce^{3+} ions can be realized in comparison with Lu- and Gd-containing scintillators where such transfer is absent.

We have also found that the scintillation decay of $\text{Tb}_{1.5}\text{Gd}_{1.5}\text{Al}_{2.5}\text{Ga}_{2.5}\text{O}_{12}:\text{Ce}$ (PbO) and especially $\text{Tb}_{1.5}\text{Gd}_{1.5}\text{Al}_3\text{Ga}_2\text{O}_{12}:\text{Ce}$ (BaO) SCFs in the 0–2 μs range is notably faster (at least by 2 times) than that in $\text{Gd}_3\text{Al}_{2.5}\text{Ga}_{2.5}\text{O}_{12}:\text{Ce}$ SC counterparts which can also be used as a substrate for producing SCF scintillators. In such a way these SCFs and the high-quality $\text{Gd}_3\text{Al}_{2.5}\text{Ga}_{2.5}\text{O}_{12}:\text{Ce}$ crystals can be used for the creation of hybrid film-substrate scintillators using the LPE method for simultaneous registration of the different components of ionization fluxes. In such types of hybrid scintillators, the separation of the signal coming from the film and crystal parts can be performed using the differences in the scintillation decay kinetics.

Acknowledgments: The work was performed in the framework of NCN No 2016/21/B/ST8/03200 and NCBR NANOLUX2014 No 286 projects and also partly supported by the Ministry of Education and Science of Ukraine in the framework of SF-20 F projects.

Author Contributions: Vitalii Gorbenko performed the SCF growth experiments and wrote growth part of paper, Tetiana Zorenko performed the scintillation LY and decay kinetic measurements, Kazimierz Paprocki performed the CL spectra measurements; Alexander Fedorov performed the XRD investigations and analysis of SCF structural quality, Oleg Sidletskiy performed the GAGG substrates preparation; Sandra Witkiewicz collected and analyzed the SCF optical properties; Paweł Bilski and Anna Twardak performed the TSL measurements of the SCF samples and Yuriy Zorenko analyzed experimental materials and wrote the Introduction, Third part and Conclusion of the paper.

Conflicts of Interest: The authors declare no conflict of interest.

References

1. Koch, A.; Raven, C.; Spanne, P.; Snigirev, A. X-ray imaging with submicrometer resolution employing transparent luminescent screens. *J. Opt. Soc. Am. A* **1998**, *15*, 1940–1951. [[CrossRef](#)]
2. Koch, A.; Peyrin, F.; Heurtier, P.; Ferrand, B.; Chambaz, B.; Ludwig, W.; Couchaud, M. X-ray camera for computed microtomography of biological samples with micrometer resolution using $\text{Lu}_3\text{Al}_5\text{O}_{12}$ and $\text{Y}_3\text{Al}_5\text{O}_{12}$ scintillators. *Proc. SPIE* **1999**, *3659*, 170–179.
3. Martin, T.; Koch, A. Recent developments in X-ray imaging with micrometer spatial resolution. *J. Synchrotron Radiat.* **2006**, *13*, 180–194. [[CrossRef](#)] [[PubMed](#)]
4. Zorenko, Y.; Gorbenko, V.; Voznyak, T.; Martin, T.; Douissard, P.-A.; Mares, J.A.; Nikl, M. LuAG:Pr, LuAG:La, and LuAP:Ce thin film scintillators for visualisation of X-ray images. *Int. Soc. Opt. Photonics* **2009**, *7310*, 731007.
5. Martin, T.; Douissard, P.-A.; Couchaud, M.; Cecilia, A.; Baumbach, T.; Dupré, K.; Rack, A. LSO-based single crystal film scintillator for synchrotron-based hard X-ray micro-imaging. *IEEE Trans. Nucl. Sci.* **2009**, *56*, 1412–1418. [[CrossRef](#)]
6. Douissard, P.-A.; Cecilia, A.; Rochet, X.; Chapel, X.; Martin, T.; Van De Kamp, T.; Helfen, L.; Baumbach, T.; Luquot, L.; Xiao, X.; et al. A versatile indirect detector design for hard X-ray microimaging. *J. Instrum.* **2012**, *7*, P09016. [[CrossRef](#)]
7. Douissard, P.-A.; Cecilia, A.; Martin, T.; Chevalier, V.; Couchaud, M.; Baumbach, T.; Dupré, K.; Kühbacher, M.; Rack, A. A novel epitaxially grown LSO-based thin-film scintillator for micro-imaging using hard synchrotron radiation. *J. Synchrotron Radiat.* **2010**, *17*, 571–583. [[CrossRef](#)] [[PubMed](#)]
8. Cecilia, A.; Rack, A.; Douissard, P.-A.; Martin, T.; dos Santos Rolo, T.; Vagovič, P.; Hamann, E.; van de Kamp, T.; Riedel, A.; Fiederle, M.; et al. LPE grown LSO:Tb scintillator films for high-resolution X-ray imaging applications at synchrotron light sources. *Nucl. Instrum. Meth. A* **2011**, *648*, S321–S323. [[CrossRef](#)]
9. Zorenko, Y.; Nikl, M.; Gorbenko, V.; Savchyn, V.; Voznyak, T.; Kucerkova, R.; Sidletskiy, O.; Grynyov, B.; Fedorov, A. Growth and luminescent properties of Lu_2SiO_5 and $\text{Lu}_2\text{SiO}_5:\text{Ce}$ single crystalline films. *Opt. Mater.* **2011**, *33*, 846–852. [[CrossRef](#)]
10. Zorenko, Y.; Gorbenko, V.; Savchyn, V.; Voznyak, T.; Grinyov, B.; Sidletskiy, O.; Kurtsev, D.; Fedorov, A.; Baumer, V.; Nikl, M.; et al. Growth and luminescent properties of $\text{Lu}_2\text{SiO}_5:\text{Ce}$ and $(\text{Lu}_{1-x}\text{Gd}_x)_2\text{SiO}_5:\text{Ce}$ single crystalline films. *J. Cryst. Growth* **2011**, *337*, 72–80. [[CrossRef](#)]
11. Zorenko, Y.; Gorbenko, V.; Savchyn, V.; Voznyak, T.; Gorbenko, V.V.; Nikl, M.; Mares, J.A.; Sidletskiy, O.; Grynyov, B.; Fedorov, A.; et al. Scintillation and luminescent properties of undoped and Ce^{3+} doped Y_2SiO_5 and Lu_2SiO_5 single crystalline films grown by LPE method. *Opt. Mater.* **2012**, *34*, 1969–1974. [[CrossRef](#)]
12. Zorenko, Y.; Gorbenko, V.; Savchyn, V.; Zorenko, T.; Grinyov, B.; Sidletskiy, O.; Fedorov, A.; Mares, J.A.; Nikl, M.; Kucera, M. $\text{Lu}_2\text{SiO}_5:\text{Ce}$ and $\text{Y}_2\text{SiO}_5:\text{Ce}$ single crystals and single crystalline film scintillators: Comparison of the luminescent and scintillation properties. *Radiat. Meas.* **2013**, *56*, 84–89. [[CrossRef](#)]
13. Twardak, A.; Bilski, B.; Zorenko, Y.; Zorenko, T.; Gorbenko, V.; Mandowska, E.; Mandowski, A.; Sidletskiy, O.; Mares, J. Thermoluminescent properties of undoped and Ce-Doped lutetium orthosilicate and yttrium orthosilicate single crystals and single crystalline films scintillators. *IEEE Trans. Nucl. Sci.* **2014**, *61*, 276–281. [[CrossRef](#)]
14. Zorenko, Y.; Gorbenko, V.; Savchyn, V.; Zorenko, T.; Grinyov, B.; Sidletskiy, O.; Fedorov, A. Growth and luminescent properties of Ce and Ce-Tb doped $(\text{Y}, \text{Lu}, \text{Gd})_2\text{SiO}_5:\text{Ce}$ single crystalline films. *J. Cryst. Growth* **2014**, *401*, 577–583. [[CrossRef](#)]
15. Riva, F. Towards a New Generation of Thin Scintillating Films to Fit the Synchrotron Needs. Available online: <http://www.success.kharkov.ua/news/4ws/riva.pdf> (accessed on 27 August 2017).

16. Zorenko, Y.; Gorbenko, V.; Nikl, M.; Mares, J.A.; Martin, T.; Douissard, P.-A. Development of novel UV emitting single crystalline film scintillators. *IEEE Trans. Nucl. Sci.* **2010**, *57*, 1335–1342. [[CrossRef](#)]
17. Zorenko, Y.; Gorbenko, V.; Savchyn, V.; Voznyak, T.; Sidletskiy, O.; Grinyov, B.; Nikl, M.; Mares, J.A.; Martin, T.; Douissard, P.-A. Single crystalline film scintillators based on the orthosilicate, perovskite and garnet compounds. *IEEE Trans. Nucl. Sci.* **2012**, *59*, 2260–2268. [[CrossRef](#)]
18. Douissard, P.-A.; Martin, T.; Riva, F.; Mathieu, E.; Zorenko, Y.; Savchyn, V.; Zorenko, T.; Fedorov, A. Scintillating screens for micro-imaging based on the Ce-Tb doped LuAP single crystal films. *IEEE Trans. Nucl. Sci.* **2014**, *61*, 433–438. [[CrossRef](#)]
19. Riva, F.; Douissard, P.-A.; Martin, T.; Carlá, F.; Zorenko, Y.; Dujardin, C. Epitaxial growth of gadolinium and lutetium-based aluminum perovskite thin films for X-ray micro-imaging applications. *CrystEngComm* **2016**, *18*, 608–615. [[CrossRef](#)]
20. Zorenko, Y.; Gorbenko, V. Growth peculiarities of the $R_3Al_5O_{12}$ ($R = Lu, Yb, Tb, Eu-Y$) single crystalline film phosphors by liquid phase epitaxy. *Radiat. Meas.* **2007**, *42*, 907–910. [[CrossRef](#)]
21. Zorenko, Y.; Douissard, P.-A.; Martin, T.; Riva, F.; Gorbenko, V.; Zorenko, T.; Paprocki, K.; Iskaliyeva, A.; Witkiewicz, S.; Fedorov, A. Scintillating screens based on the LPE grown $Tb_3Al_5O_{12}:Ce$ single crystalline films. *Opt. Mater.* **2017**, *65*, 73–81. [[CrossRef](#)]
22. Kamada, K.; Endo, T.; Tsutumi, K.; Yanagida, T.; Fujimoto, Y.; Fukabori, A.; Yoshikawa, A.; Pejchal, J.; Nikl, M. Composition engineering in cerium-doped $(Lu, Gd)_3(Ga, Al)_5O_{12}$ single-crystal scintillators. *Cryst. Growth Des.* **2011**, *11*, 4484–4490. [[CrossRef](#)]
23. Kamada, K.; Kurosawa, S.; Prusa, P.; Nikl, M.; Kochurikhin, V.V.; Endo, T.; Tsutumi, K.; Sato, H.; Yokota, Y.; Sugiyama, K.; et al. Cz grown 2-in. size $Ce:Gd_3(Al, Ga)_5O_{12}$ single crystal; relationship between Al, Ga site occupancy and scintillation properties. *Opt. Mater.* **2014**, *36*, 1942–1945. [[CrossRef](#)]
24. Kamada, K.; Nikl, M.; Kurosawa, S.; Beitlerova, A.; Nagura, A.; Shoji, Y.; Pejchal, J.; Ohashi, Y.; Yokota, Y.; Yoshikawa, A. Alkali earth co-doping effects on luminescence and scintillation properties of Ce doped $Gd_3Al_2Ga_3O_{12}$ scintillator. *Opt. Mater.* **2015**, *41*, 63–66. [[CrossRef](#)]
25. Wang, C.; Wu, Y.; Ding, D.; Li, H.; Chen, X.; Shi, J.; Ren, G. Optical and scintillation properties of Ce-doped $(Gd_2Y_1)Ga_{2.7}Al_{2.3}O_{12}$ single crystal grown by Czochralski method. *Nucl. Instrum. Meth. A* **2016**, *820*, 8–13. [[CrossRef](#)]
26. Zorenko, Y.; Gorbenko, V.; Savchyn, V.; Zorenko, T.; Fedorov, A.; Wrzesiński, H.; Vasylkiv, Y. Multi-component Ce doped $(Gd, Y, La, Lu)_3(AlGaSc)_5O_{12}$ garnets—A new story in the development of scintillating single crystalline film screens. *Radiat. Meas.* **2013**, *56*, 150–154. [[CrossRef](#)]
27. Zorenko, Y.; Gorbenko, V.; Savchyn, V.; Zorenko, T.; Fedorov, A.; Sidletskiy, O. Novel scintillating screens based on the single crystalline films of Ce doped multi-component $(Gd, Y, Lu)_3(Al, Sc)_5O_{12}$ garnets. *IEEE Trans. Nucl. Sci.* **2014**, *61*, 439–442. [[CrossRef](#)]
28. Zorenko, Y.; Gorbenko, V.; Savchyn, V.; Zorenko, T.; Fedorov, A.; Sidletskiy, O. Development of scintillating screens based on the single crystalline films of Ce doped $(Gd, Y)_3(Al, Ga, Sc)_5O_{12}$ multi-component garnets. *J. Cryst. Growth* **2014**, *401*, 532–536. [[CrossRef](#)]
29. Zorenko, Y.; Gorbenko, V.; Vasylkiv, J.; Zelenyj, A.; Fedorov, A.; Kucerkova, R.; Mares, J.A.; Nikl, M.; Bilski, P.; Twardak, A. Growth and luminescent properties of scintillators based on the single crystalline films of $Lu_{3-x}Gd_xAl_5O_{12}:Ce$ garnet. *Mater. Res. Bull.* **2015**, *64*, 355–363. [[CrossRef](#)]
30. Zorenko, Y.; Gorbenko, V.; Vasylkiv, J.; Strzyżewski, T.; Fedorov, A.; Kucerkova, R.; Mares, J.A.; Nikl, M.; Bilski, P.; Twardak, A. Growth and luminescent properties of scintillators based on the single crystalline films of $(Lu, Gd)_3(Al, Ga)_5O_{12}:Ce$ garnets. *J. Lumin.* **2016**, *169*, 828–837. [[CrossRef](#)]
31. Zorenko, Y.; Gorbenko, V.; Zorenko, T.; Sidletskiy, O.; Fedorov, A.; Bilski, P.; Twardak, A. High-perfomance Ce-doped multicomponent garnet single crystalline film scintillators. *Phys. Status Solidi-R.* **2015**, *9*, 489–493. [[CrossRef](#)]
32. Prusa, P.; Kucera, M.; Mares, J.A.; Hanus, M.; Beitlerova, A.; Onderisinova, Z.; Nikl, M. Scintillation properties of the Ce-doped multicomponent garnet epitaxial films. *Opt. Mater.* **2013**, *35*, 2444–2448. [[CrossRef](#)]
33. Prusa, P.; Kucera, M.; Mares, J.A.; Onderisinova, Z.; Hanus, M.; Babin, V.; Beitlerova, A.; Nikl, M. Composition tailoring in Ce-doped multicomponent garnet epitaxial film scintillators. *Cryst. Growth Des.* **2015**, *15*, 3715–3723. [[CrossRef](#)]

34. Bartosiewicz, K.; Babin, V.; Nikl, M.; Mares, J.A.; Zorenko, Y.; Gorbenko, V. Luminescence and energy transfer processes in $(\text{Lu}, \text{Tb})_3\text{Al}_5\text{O}_{12}$ single crystalline films doped with Ce^{3+} . *J. Lumin.* **2016**, *173*, 141–148. [[CrossRef](#)]
35. Bartosiewicz, K.; Babin, V.; Mares, J.A.; Bejtlerova, A.; Zorenko, Y.; Iskaliyeva, A.; Gorbenko, V.; Bryknar, Z.; Nikl, M. Luminescence and energy transfer processes in Ce^{3+} activated $(\text{Gd}, \text{Tb})_3\text{Al}_5\text{O}_{12}$ single crystalline films. *J. Lumin.* **2017**, *188*, 60–66. [[CrossRef](#)]
36. Zorenko, Y.; Gorbenko, V.; Zorenko, T.; Paprocki, K.; Bilski, P.; Twardak, A.; Voznyak, T.; Sidletskiy, O.; Gerasimov, Y.; Grynnov, B.; et al. Composition engineering of single crystalline films based on the multicomponent garnet compounds. *Opt. Mater.* **2016**, *61*, 3–10. [[CrossRef](#)]
37. Zorenko, Y.; Nikl, M.; Mares, J.A.; Gorbenko, V.; Savchyn, V.; Voznyak, T.; Kucera, M.; Bejtlerova, A.; Kucerkova, R.; Fedorov, A. The luminescent and scintillation properties of YAlO_3 and $\text{YAlO}_3:\text{Ce}$ single crystalline films grown by liquid phase epitaxy from BaO-based flux. *Phys. Status Solidi A* **2009**, *206*, 2586–2592. [[CrossRef](#)]
38. Mares, J.A.; Bejtlerova, A.; Nikl, M.; Solovieva, N.; Nitsch, K.; Kucera, M.; Kubova, M.; Gorbenko, V.; Zorenko, Y. Scintillation and optical properties of YAG:Ce films grown by liquid phase epitaxy. *Radiat. Meas.* **2007**, *42*, 533–536. [[CrossRef](#)]
39. Chani, V.I.; Yoshikawa, A.; Machida, H.; Fukuda, T. $(\text{Tb}, \text{Yb})_3\text{Al}_5\text{O}_{12}$ garnet: Crystal-chemistry and fiber growth by micro-pulling-down technique. *Mat. Sci. Eng. B* **2000**, *75*, 53–60. [[CrossRef](#)]
40. Fasoli, M.; Vedda, A.; Nikl, M.; Jiang, C.; Uberuaga, B.; Andersson, D.; McClellan, K.; Stanek, C.R. Band-gap engineering for removing shallow traps in rare-earth $\text{Lu}_3\text{Al}_5\text{O}_{12}$ garnet scintillators using Ga^{3+} doping. *Phys. Rev. B* **2011**, *84*, 081102. [[CrossRef](#)]
41. Geller, S.; Espinosa, G.P.; Fullmer, L.D.; Crandall, P.B. Thermal expansion of some garnets. *Mater. Res. Bull.* **1972**, *7*, 1219–1224. [[CrossRef](#)]
42. Ashurov, M.K.; Voronko, Y.; Osiko, V.V.; Sobol, A.A.; Timoshechkin, M.I. Spectroscopic study of stoichiometry deviation in crystals with garnet structure. *Phys. Status Solidi A* **1977**, *42*, 101–110. [[CrossRef](#)]
43. Lupei, V.; Lupei, A.; Tiseanu, C.; Georgescu, S.; Stoicescu, C.; Nanau, P.M. High-resolution optical spectroscopy of YAG:Nd: A test for structural and distribution models. *Phys. Rev. B* **1995**, *51*, 8–17. [[CrossRef](#)]
44. Kuklja, M.M. Defects in yttrium aluminium perovskite and garnet crystals: Atomistic study. *J. Phys. Condens. Mater.* **2000**, *12*, 2953–2967. [[CrossRef](#)]
45. Zorenko, Y.; Voloshinovskii, A.; Savchyn, V.; Voznyak, T.; Nikl, M.; Nejezchleb, K.; Mikhailin, V.; Kolobanov, V.; Spassky, D. Exciton and antisite defect-related luminescence in $\text{Lu}_3\text{Al}_5\text{O}_{12}$ and $\text{Y}_3\text{Al}_5\text{O}_{12}$ garnets. *Phys. Status Solidi B* **2007**, *244*, 2180–2189. [[CrossRef](#)]
46. Zorenko, Y.; Voloshynovskii, A.; Vistovsky, V.; Grinberg, M.; Kornyllo, A.; Łukasiewicz, T.; Świrkowicz, M. Antisite defect-related luminescence in $(\text{LaLu})_3\text{Lu}_2\text{Ga}_3\text{O}_{12}$ garnet single crystals. *Phys. Status Solidi B* **2007**, *244*, 3271–3278. [[CrossRef](#)]
47. Kummer, F.; Zwaschka, F.; Ellens, A.; Debray, A.; Waitl, G. Luminous Substance for a Light Source and Light Source Associated Therewith. U.S. Patent WO/2001/008452, 1 February 2001.
48. Batentschuk, M.; Osvet, A.; Schiering, G.; Klier, A.; Schneider, J.; Winnacker, A. Simultaneous excitation of Ce^{3+} and Eu^{3+} ions in $\text{Tb}_3\text{Al}_5\text{O}_{12}$. *Radiat. Meas.* **2004**, *38*, 539–543. [[CrossRef](#)]
49. Turos-Matysiak, R.; Gryk, W.; Grinberg, M.; Lin, Y.S.; Liu, R.S. $\text{Tb}^{3+} \rightarrow \text{Ce}^{3+}$ energy transfer in $\text{Y}_{3-x-y}\text{Tb}_y\text{Gd}_x\text{Al}_5\text{O}_{12}$ ($x = 0.65$, $y = 0.575$) doped with Ce^{3+} . *Radiat. Meas.* **2007**, *42*, 755–758. [[CrossRef](#)]
50. Zorenko, Y.; Voznyak, T.; Vistovsky, V.; Zorenko, T.; Nedliko, S.; Batentschuk, M.; Osvet, A.; Winnacker, A.; Zimmerer, G.; Kolobanov, V.; et al. Energy transfer to Ce^{3+} ions in $\text{Tb}_3\text{Al}_5\text{O}_{12}:\text{Ce}$ single crystalline films. *Radiat. Meas.* **2007**, *42*, 648–651. [[CrossRef](#)]
51. Zorenko, Y.; Gorbenko, V.; Voznyak, T.; Zorenko, T.; Kuklinski, B.; Turos-Matysiak, R.; Grinberg, M. Luminescence properties of phosphors based on $\text{Tb}_3\text{Al}_5\text{O}_{12}$ (TbAG) terbium-aluminum garnet. *Opt. Spectrosc.* **2009**, *106*, 365–374. [[CrossRef](#)]
52. Zorenko, Y.V.; Novosad, S.S.; Pashkovskii, M.V.; Lyskovich, A.B.; Savitskii, V.G.; Batenchuk, M.M.; Malyutenkova, P.S.; Patsagan, N.I.; Nazar, I.V.; Gorbenko, V.I. Epitaxial structures of garnets as scintillation detectors of ionizing radiation. *J. Appl. Spectrosc.* **1990**, *52*, 645–649. [[CrossRef](#)]

53. Douissard, P.-A.; Martin, T.; Riva, F.; Zorenko, Y.; Zorenko, T.; Paprocki, K.; Bilski, P.; Twardak, A. Epitaxial growth of LuAG:Ce and LuAG:Ce, Pr films and their scintillation properties. *IEEE Trans. Nucl. Sci.* **2016**, *63*, 1726–1732. [[CrossRef](#)]
54. Nikl, M.; Mihokova, E.; Pejchal, J.; Vedda, A.; Zorenko, Y.; Nejezchleb, K. The antisite LuAl defect-related trap in Lu₃Al₅O₁₂:Ce single crystal. *Phys. Status Solidi B* **2005**, *242*, R119–R121. [[CrossRef](#)]



© 2017 by the authors. Licensee MDPI, Basel, Switzerland. This article is an open access article distributed under the terms and conditions of the Creative Commons Attribution (CC BY) license (<http://creativecommons.org/licenses/by/4.0/>).

Novel all-solid-state composite scintillators based on the epitaxial structures of LuAG garnet doped with Pr, Sc and Ce ions

S. Witkiewicz-Lukaszek*, V. Gorbenko, T. Zorenko, K. Paprocki, O. Sidletsksiy, I. Gerasymov,
J.A. Mares, R. Kucerkova, M. Nikl, Yu. Zorenko*

Abstract— This work presents our achievement in the development of new types of advanced composite scintillators based on the single crystalline films (SCFs) of $\text{Lu}_3\text{Al}_5\text{O}_{12}$ (LuAG) garnet, doped with Pr^{3+} and Sc^{3+} ions, and substrate from single crystals (SCs) of Ce^{3+} doped LuAG using the technology of liquid phase epitaxy (LPE). We show the possibility of the simultaneous registration of α -particles and γ -quanta by means of separation of the decay kinetics of SCF and crystal parts of such composite scintillators. Namely, the significant differences in the scintillation decay kinetics of LuAG:Pr SCF / LuAG:Ce SC and LuAG:Sc SCF / LuAG:Ce SC composite scintillators under excitation by α -particles of ^{241}Am (5.5 MeV) source and γ -quanta of ^{137}Cs (662 keV) source are observed. Thus, such types of composite scintillators can be successfully applied for separation of the signals coming from their film and crystal parts at the registration of the mixed radiation fluxes of α -particles and γ -quanta.

Index Terms— α -particles and γ -quanta, composite scintillator, liquid phase epitaxy, LuAG, films and crystals, Ce^{3+} , Pr^{3+} and Sc^{3+} dopants

I. INTRODUCTION

THE technology of the liquid phase epitaxy (LPE) offers today the possibility of developing the luminescent materials based on the single crystalline films (SCFs) of different oxide compounds [1-3]. The fields of application of such SCFs now include cathodoluminescent screens [4, 5], laser media [6, 7], scintillators for registration of α - and β -particles and low-energy ionizing radiation [1, 8, 9] and scintillating screens for microtomography detectors using X-ray sources and synchrotron radiation [10, 11].

The LPE method opens also the possibility of creating the advanced types of composite scintillators of “phoswich-type” (phosphor sandwich) for registration of the different components of ionizing radiation, for instance, for analysis of

Sandra Witkiewicz-Lukaszek is with the Institute of Physics, Kazimierz Wielki University in Bydgoszcz, Powstańców Wielkopolskich str., 2, 85090 Bydgoszcz, Poland and from Faculty of Technical Physics, Poznan University of Technology, Piotrowo 3, 60-965 Poznan, Poland (e-mail: s-witkiewicz@wp.pl).

Vitalii Gorbenko, Tetiana Zorenko and Yuriy Zorenko are with the Institute of Physics, Kazimierz Wielki University in Bydgoszcz, Powstańców Wielkopolskich str., 2, 85090 Bydgoszcz, Poland and from Electronic Department Ivan Franko National University in Lviv, Ukraine (e-mail: gorbenko@ukw.edu.pl, tzorenko@ukw.edu.pl, zorenko@ukw.edu.pl).

Oleg Sidletsksiy and Iaroslav Gerasymov are with the Institute for Scintillation Materials (ISM), National Academy of Sciences of Ukraine, av. Nauki 60, 61001 Kharkiv, Ukraine (e-mail: osidletsksiy@yahoo.com, yarosgerasimov@gmail.com).

Jiri A. Mares and Martin Nikl are with the Institute of Physics, AS Czech Republic, Cukrovnicka str., 10, 16253 Prague, Czech Republic (e-mail: amares@fzu.cz, nikl@fzu.cz)

the content of mixed fluxes of particles and photons with various penetrating depths [1, 12-14]. Such composite scintillators (CS) present the all-solid-state crystalline systems, including one or two SCFs intended for registration of low penetrating α - and β -particles, and a bulk single crystal (SC) substrate for registration of the highly penetrating radiation (X or γ rays).

The advantages of these types of composite scintillators in comparison with the well-known analogues based on the splice of different scintillation crystals [15] are as follows. Such types of composite scintillators present the epitaxial structure with a sharp interface between the composing scintillators with quite close refractive indices. This permits to substantially eliminate the light losses at the interface of scintillators, enhancing the selectivity of registration of the different components of mixed ionizing radiations. The LPE method for composite scintillator production permits also to obtain the thickness of film scintillators close to the penetration depth of registered particles. Namely, the thickness of film scintillators, which is necessary for the complete absorption of α -particles of ^{239}Pu and ^{241}Am sources, typically is equal to 8-10 μm [1].

The different types of composite scintillators have been recently considered by some of us in [1, 12-14]. The first types of composite scintillators were created on the basis on the LPE grown epitaxial structures of $\text{Y}_3\text{Al}_5\text{O}_{12}$ garnet (YAG) [1]. Namely, one-layered composite scintillators based on the YAG:Ce SCF and YAG:Nd SC substrate (YAG:Ce SCF/YAG:Nd SC) and YAG:Ce SCF and YAG:Sc SC substrate (YAG:Ce SCF/YAG:Sc SC) as well as triply-layered composite scintillator based on the YAG:Ce SCF, YAG:Nd SCF and YAG:Sc SC substrate (YAG:Ce SCF/YAG:Nd SCF/YAG:Sc SC) were grown by the LPE method and later examined under simultaneous excitation by α particles and γ quanta [1]. The separation of the scintillation signals coming from SCF and SC parts of composite scintillator was performed using the discrimination of their scintillation decay kinetics.

It should be noted that due to the low density $\rho=6.7 \text{ g/cm}^3$ and effective atomic number $Z_{\text{eff}}=29$, the scintillators based on the YAG SCs may be used only for registration of low-energy ionizing radiation [1, 12]. Therefore, there is a demand to fabricate composite scintillator for registration of the mixed fluxes of particles and high-energy quanta with using other garnet compounds, which are characterized by high values of ρ and Z_{eff} [12, 13].

Among possible candidates of such oxide compounds, the $\text{Lu}_3\text{Al}_5\text{O}_{12}$ garnet (LuAG) first of all attracts our attention [9,

10]. LuAG host has significantly higher density $\rho = 6.7 \text{ g/cm}^3$ and effective atomic number $Z_{\text{eff}}=61$ in comparison with YAG. LuAG:Ce, LuAG:Pr and LuAG:Sc are the well-known scintillators for radiation monitoring and computer tomography [3, 16]. Therefore, the LuAG is a very promising material for creation of SCF scintillators and composite scintillator on their base as well. As activators, which can effectively emit in LuAG hosts with different wavelengths and fast enough decay kinetics of scintillations, the Pr^{3+} , Sc^{3+} and Ce^{3+} ions can be considered (Table 1) [9, 16-24]. Therefore, the different combinations of novel composite scintillators based on the epitaxial structures of LuAG garnet compounds, doped with mentioned ions, can be created using the LPE method.

In this work, we present for the first time the results of the research directed on creation of the novel types of composite scintillator based on the Ce^{3+} and Pr^{3+} doped LuAG SCFs and LuAG:Ce SC substrates grown by the LPE method.

TABLE I
LUMINESCENT PROPERTIES OF COMPOUNDS BASED ON LUAG GARNET

Type of garnet	Position of main emission band, nm	Decay time (1/e) of main component of luminescence, ns	Reference
$\text{Lu}_3\text{Al}_5\text{O}_{12}:\text{Ce}$	515	49.5-58	16, 17
$\text{Lu}_3\text{Al}_5\text{O}_{12}:\text{Pr}$	310	19-28	16-18
$\text{Lu}_3\text{Al}_5\text{O}_{12}:\text{Sc}$	280	245-610	19-24

II. GROWTH OF COMPOSITE SCINTILLATORS BASED ON LUAG:PR AND LUAG:SC SCFs AND LUAG:CE SCs

Two types of composite scintillators based on LuAG:Pr SCF and LuAG:Sc SCF were grown by LPE method onto LuAG:Ce substrates from super-cooled melt solutions using $\text{PbO-B}_2\text{O}_3$ flux. For comparison, the sets of LuAG:Sc and LuAG:Pr SCF samples were also grown from the same melt onto YAG substrates. The growth conditions of the SCF and composite scintillators, selected for the investigation of the content and structural properties as well as for the study of their absorption, cathodoluminescence and scintillation properties, were summarized in Table 2.

TABLE II
GROWTH CONDITIONS OF LUAG:PR SCF/LUAG:CE SC AND LUAG:SC SCF/LUAG:CE SC COMPOSITE SCINTILLATORS IN COMPARISON WITH LUAG:PR AND LUAG:SC SCFs, GROWN ONTO YAG SUBSTRATES

Type of SCF	Substrate	$h, \mu\text{m}$	T, °C	f, $\mu\text{m}/\text{min}$	LY, %
$\text{Y}_3\text{Al}_5\text{O}_{12}:\text{Ce}$	$\text{Y}_3\text{Al}_5\text{O}_{12}$	54			100
$\text{Lu}_3\text{Al}_5\text{O}_{12}:\text{Pr}$	$\text{Y}_3\text{Al}_5\text{O}_{12}$	19	975	0.19	100
$\text{Lu}_3\text{Al}_5\text{O}_{12}:\text{Pr}$	$\text{Lu}_3\text{Al}_5\text{O}_{12}:\text{Ce}$	9.5	980	0.16	96
$\text{Lu}_3\text{Al}_5\text{O}_{12}:\text{Sc}$	$\text{Y}_3\text{Al}_5\text{O}_{12}$	8	985	0.13	52
$\text{Lu}_3\text{Al}_5\text{O}_{12}:\text{Sc}$	$\text{Lu}_3\text{Al}_5\text{O}_{12}:\text{Ce}$	10	980	0.14	54

h - SCF thickness, f - velocity of SCF growth; T - SCF growth temperature. LY - light yield of scintillation under excitation by α -particles of ^{239}Pu sources and registration of scintillation with a shaping time of 12 μs in comparison with standard YAG:Ce SCF scintillator with a photoelectron LY of 360 phels/MeV (a LY of 2600 ph/MeV).

III EXPERIMENTAL TECHNIQUE

For characterization of the luminescent and scintillation properties of the composite scintillators based on the Pr^{3+} and Sc^{3+} doped LuAG SCFs and LuAG:Ce substrates, the absorption spectra, cathodoluminescence (CL) spectra, LY and scintillation decay kinetics measurements under excitation by α -particles and γ -quanta were applied. The absorption

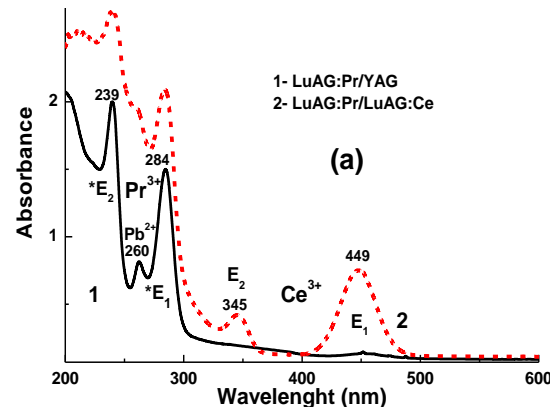
spectra were measured using a Jasco 760 UV-Vis spectrometer in the 200-1100 nm range. The CL spectra were measured using an electron microscope SEM JEOL JSM-820, additionally equipped with a spectrometer Stellar Net and TE-cooled CCD detector working in the 200-925 nm range. The scintillation LY (pulse height spectra measured with a shaping time of 12 μs) was firstly measured after each SCF growth circle using the setup based on a Hamamatsu H6521 photomultipliers (PMP), multi-channel analyzer and digital Tektronix TDS3052 oscilloscope under excitation by α -particles of ^{239}Pu (5.15 MeV) source (Table 2). The spectra were compared with standard YAG:Ce SCF sample with a photoelectron yield of 360 phels/MeV and LY of 2650 photons/MeV [25, 26] and also with the reference LuAG:Ce substrates, produced in the ISM, Kharkiv, Ukraine. All measurements were performed at the room temperature (RT).

Scintillation response investigations of the selected composite scintillators (see Table 3) were performed using the set-up consisting of a hybrid PMT (HPMT DEP PP0475B), measuring electronics and PC control. Pulse height spectra and scintillation decay kinetics were measured under excitation by α -particles with of ^{241}Am (energy 5.4857 MeV) radioisotope and with γ -rays of ^{137}Cs (energy 661.66 keV) radioisotope. The time resolution of our set-up was below 10 ns. It is important to note here that the α -particles of ^{239}Pu and ^{241}Am sources allow exciting only the epitaxial layers of SCF samples (not their substrates) because the penetration depths of α -particles in the studied samples are approximately 12-15 μm .

III. ABSORPTION, CATHODOLUMINESCENCE AND SCINTILLATION PROPERTIES OF COMPOSITE SCINTILLATORS BASED ON THE LUAG:PR AND LUAG:SC SCFs AND LUAG:CE SUBSTRATES

A. Absorption spectra

The absorption spectra in the 200-600 nm range of the two composite scintillators of LuAG:Pr SCF/LuAG:Ce SC and LuAG:Sc SCF/ LuAG:Ce SC types in comparison with the absorption spectra of LuAG:Pr and LuAG:Sc SCFs, grown onto YAG substrates, are shown in Fig.1a and 1b, respectively. The absorption bands E_1 at 446-449 nm and E_2 at 344-345 nm in the spectra of LuAG:Pr SCF/LuAG:Ce SC and LuAG:Sc SCF/LuAG:Ce SC composite scintillators (Fig.1a and 1b, respectively) are related to the 4f-5d (^2E) transitions of Ce^{3+} ions in LuAG:Ce SC substrate. Other Ce^{3+} absorption bands E_3 in these scintillators are located below 230 nm and related to the 4f-5d (T_{2g}) transitions. The bands $*E_1$ and $*E_2$



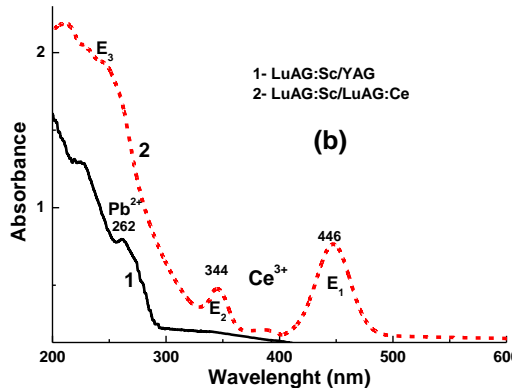


Fig.1 RT absorption spectra of composite scintillators based on the LuAG:Pr (2a) and LuAG:Sc (2b) SCFs, grown onto LuAG:Ce substrates, in comparison with absorption spectra of LuAG:Pr (1a) and LuAG:Sc (1b) SCFs, grown onto YAG substrate.

peaked at 284 nm and 239 nm correspond to the $4f(^3H_4) \rightarrow 5d^{1,2}$ transitions of Pr³⁺ ions (Fig.1a). In both figures, the bands peaked at 260 and 262 nm related to the $^1S_0 \rightarrow ^3P_1$ transitions of Pb²⁺ flux impurity in the SCF samples.

B. Cathodoluminescence spectra

The normalized CL spectra of two types of LuAG:Pr SCF/ LuAG:Ce SC and LuAG:Sc SCF/LuAG:Ce SC composite scintillators in comparison with the CL spectra of LuAG:Pr and LuAG:Sc SCFs and LuAG:Ce SC substrates are shown in Figures 2a and 2b, respectively. The luminescence bands in the visible range peaked at 512 nm in the CL spectra of LuAG:Ce SC (Fig.2a and 2b, curves 1) are related to the $5d^1-4f$ transitions of Ce³⁺ ions while the emission bands in the UV range are caused by the Lu_{Al} antisite-defect related emission centers [27, 2]. The dominant luminescence bands in the UV range peaked at 312 and 380 nm and the low-intensive sharp emission band in the visible range in the CL spectra of LuAG:Pr SCFs (Fig.2a, curve 2) are related to the $5d^1-4f$ and $4f-4f$ radiative luminescence transitions of Pr³⁺ ions. Meanwhile, apart from the Pr³⁺ related emission bands in the UV and visible ranges, the Ce³⁺ emission band peaked at 512 nm prevails in the CL spectra of LuAG:Pr SCF / LuAG:Ce SC composite scintillator (Fig.2a, curve 3). This means that the LuAG:Pr SCF component of composite scintillator excites the luminescence of Ce³⁺ ions in the LuAG:Ce substrate due to the reabsorption of the UV part of emission of LuAG:Pr SCFs by the absorption band of Ce³⁺ ions in LuAG:Ce SC peaked around 344 nm (Fig.1a) [17]. The dominant luminescence bands in the UV range peaked at 312 and 380 nm and the low-intensive sharp emission band in the visible range in the CL spectra of LuAG:Pr SCF (Fig.2a, curve 2) are related to the $5d^1-4f$ and $4f-4f$ radiative luminescence transitions of Pr³⁺ ions. Meanwhile, apart from the Pr³⁺ related emission bands in the UV and visible ranges, the Ce³⁺ emission band peaked at 512 nm prevails in the CL spectra of LuAG:Pr SCF / LuAG:Ce SC composite scintillator (Fig.2a, curve 3). This means that the LuAG:Pr SCF component of composite scintillator excites the luminescence of Ce³⁺ ions in the LuAG:Ce substrate due to the reabsorption of the UV part of emission of LuAG:Pr SCFs by the absorption band of Ce³⁺ ions in LuAG:Ce SCs peaked around 344 nm (Fig.1a) [17].

The dominant luminescence bands in the UV range peaked at 280 nm in the CL spectra of LuAG:Sc SCFs (Fig.2b, curve

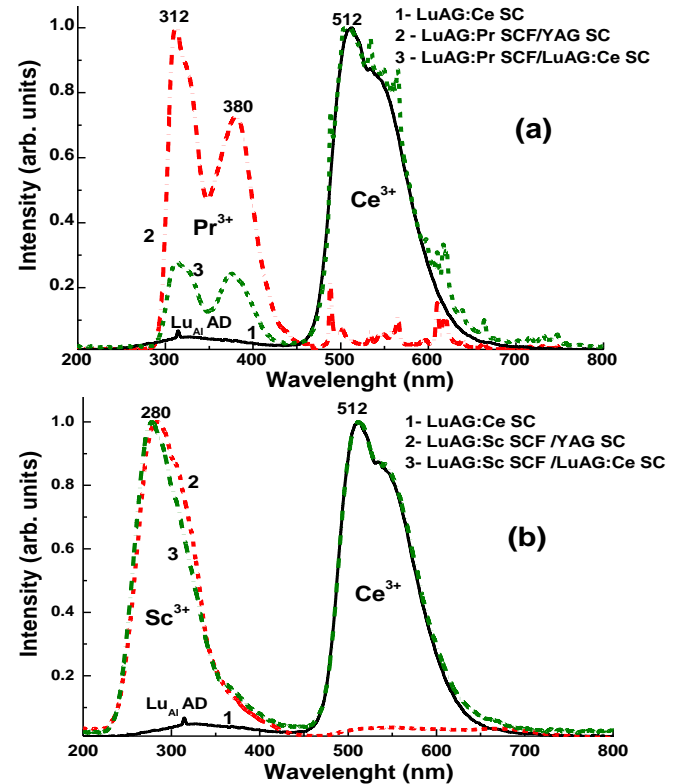


Fig.2 Normalized CL spectra of LuAG:Pr SCF/LuAG:Ce SC (3a) and LuAG:Sc SCF/ LuAG:Ce SC (3b) composite scintillators in comparison with LuAG:Ce SC substrate (1a, 1b) and LuAG:Pr (2a) or LuAG:Sc (2b) SCFs, grown onto YAG substrates.

2) are caused by the luminescence of Sc_{Al} isoelectronic impurity [21-24]. At the same time, in the CL spectra of LuAG:Sc SCF/LuAG:Ce SC composite scintillator, besides of the Sc³⁺ related emission bands in the UV range, the Ce³⁺ emission band in the visible range peaked at 512 nm is also observed and these emission bands are comparable in the intensity (Fig.2b, curve 3). Similarly to the previous type of composite scintillators, the emission of LuAG:Sc SCF component excites the luminescence of Ce³⁺ ions in the LuAG:Ce substrate due to the reabsorption of the UV emission band of LuAG:Sc SCF by the absorption band of Ce³⁺ ions in LuAG:Ce SC peaked around 344 nm (Fig.1b, curve 2).

Generally, such observation of the excitation of Ce³⁺ luminescence in LuAG:Ce substrate by the emission of LuAG:Pr and LuAG:Sc SCFs can make the serious problem in the principal functionality of LuAG:Pr SCF/LuAG:Ce and LuAG:Sc SCF/LuAG:Ce SC composite scintillators. Meanwhile, the analysis of the scintillation decay kinetics shows that such unwanted behaviors of composite scintillators are not so significant in the case of separation of different signals coming from their SCF and SC parts under registration of α -particles and γ -ray excitation (see curves 1 and 2, respectively).

C. Scintillation decay kinetics

Fig.3 presents the scintillation decay curves of LuAG:Pr SCF/LuAG:Ce SC (a) and LuAG:Sc SCF/LuAG:Ce SC(b) composite scintillators and LuAG:Ce substrate (c), measured under both α -particles and γ -ray excitation (see curves 1 and 2, respectively).

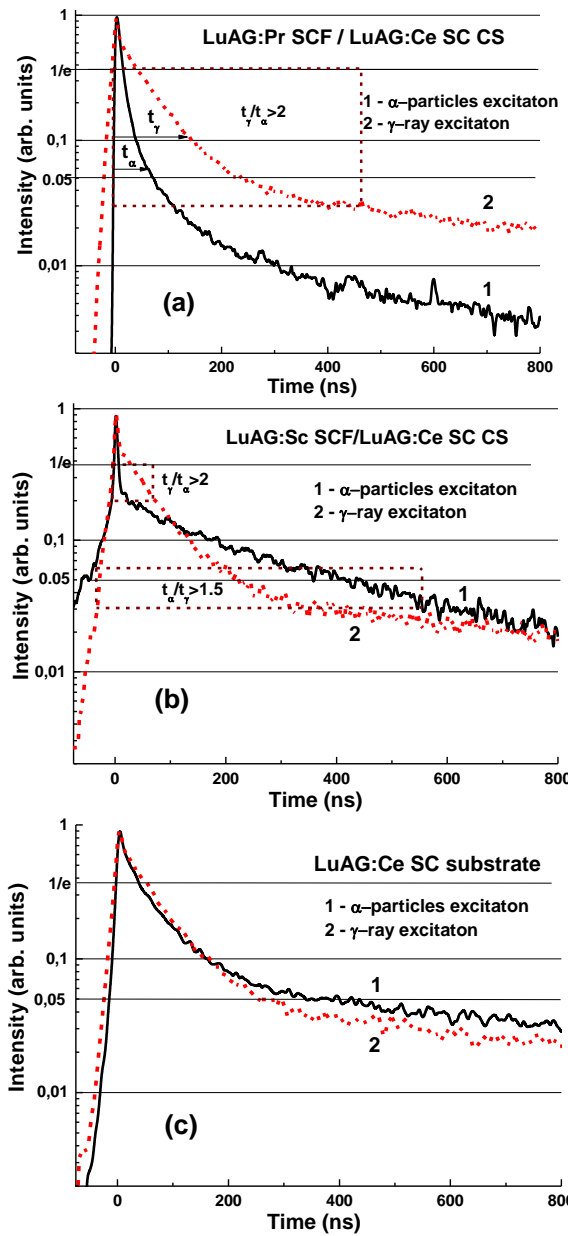


Fig. 3. Scintillation decay of LuAG:Pr SCF/LuAG:Ce SC (a) and LuAG:Sc SCF/LuAG:Ce SC (b) composite scintillators in comparison with LuAG:Ce SC (c) substrate under α -particles and γ -ray excitation by ^{241}Am and ^{137}Cs sources. The optimal time ranges for the scintillation registration using such types of composite scintillators are indicated, when the t_α/t_γ or t_γ/t_α ratio reach the values above 1.5-2.0.

Generally for registration of the difference in the scintillation decay kinetics of the bulk and film components of composite scintillator, it is very important to analyze firstly the decay curves under α -particles and γ -ray excitation of substrates, prepared from bulk crystals of garnet compounds, in a broad range of decay intensity. Firstly we have performed such analysis for LuAG:Ce substrate with a thickness of 1 mm for the scintillation intensity decay to 1/e, 0.1 and 0.05 levels (Fig. 3c and Table 3). As one can see from Fig. 3c, the decay curves of LuAG:Ce SC substrate under α -particles and γ -ray excitation are very close in the initial stage of decay up to 150 ns. In a wider time interval (above 150 ns) the decay curves of LuAG:Ce SC substrate under γ -ray excitation are notably faster than those in the case of α -particles excitation. Most probably,

TABLE III

TIME t_α AND t_γ VALUES OF SCINTILLATION INTENSITY DECAY TO 1/e, 0.1 AND 0.05 LEVELS OF LUAG:PR/LUAG:CE AND LUAG:SC/LUAG:CE COMPOSITE SCINTILLATORS AND REFERENCE LUAG:CE SC SUBSTRATE UNDER α -PARTICLES AND γ -QUANTA EXCITATION OF ^{241}Am (5.4857 MEV) AND ^{137}Cs (661.66 KEV) SOURCES, RESPECTIVELY.

Intensity of decay to level	Time, ns					
	LuAG:Ce crystal		LuAG:Pr/LuAG:Ce		LuAG:Sc/LuAG:Ce	
Excitation source	α	γ	α	γ	α	γ
1/e	37	53	15	41	7	30
0.1	161	166	39	143	188	136
0.05	336	250	71	238	412	213

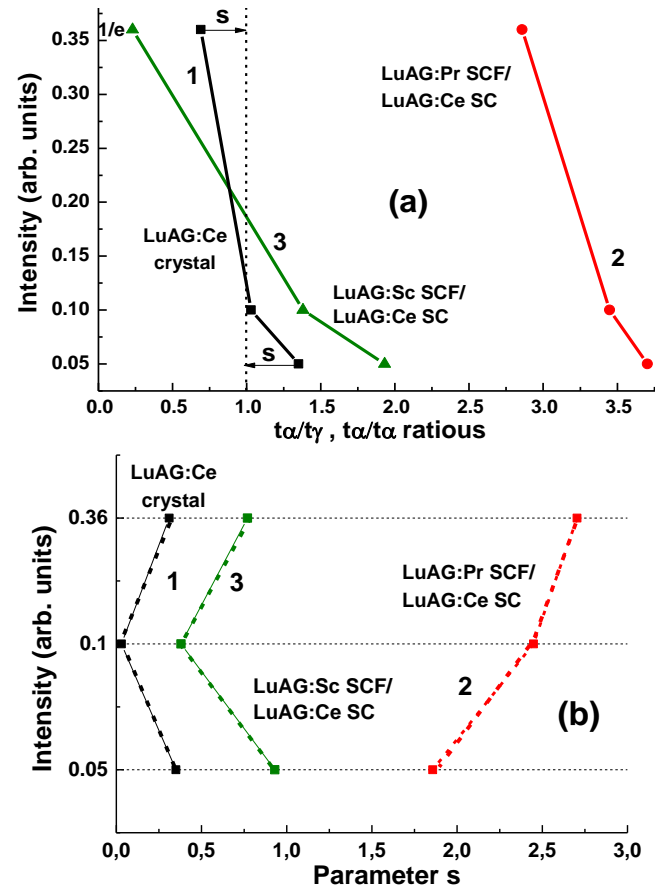


Fig.4. Plots of t_α/t_γ , t_γ/t_α ratios (a) of the scintillation decay times under α - and γ -excitation and parameters s (b) vs. the intensity of scintillation decay to 1/e, 0.1 and 0.05 levels for LuAG:Pr SCF/LuAG:Ce SC (2) and LuAG:Sc SCF/LuAG:Ce SC (3) composite scintillators and reference LuAG:Ce SC substrate (1).

this is a fundamental behavior of scintillation materials and can be connected with the peculiarities of interaction of α -particles and γ -quanta with the scintillator material [26].

We can expect that the rate of separation of the scintillation signal at the registration of α -particles and γ -rays can be significantly improved in the composite epitaxial structures based on the films and crystals of different oxide compounds in comparison with crystal-scintillators. Indeed, for LuAG:Pr SCF/LuAG:Ce SC structure the scintillating signal coming from the SCF and SC components of composite scintillator can be separated in the whole time interval from 0 to 700 ns (Fig.3a). Another situation is observed in the case of LuAG:Sc SCF/LuAG:Ce SC structure (Fig.3b). The separation of the signal

coming from SCF and SC substrate parts of this composite scintillator can be obtained in the two relatively narrow time intervals: 0-100 ns and 150-800 ns where the scintillation response under α -particles excitation is faster than that under γ -rays excitation and vice versa, respectively.

The above mentioned conclusions are confirmed also by comparison of the differences in the decay times at 1/e, 0.1 and 0.05 levels for the decay curves under α -particles and γ -quanta excitation (so called $t_\alpha t_\gamma$, or $t_\gamma t_\alpha$ ratios) in LuAG:Pr SCF/LuAG:Ce SC and LuAG:Sc SCF/LuAG:Ce SC composite scintillators and the reference LuAG:Ce crystal (Fig.4). As one can see from this figure, t_γ/t_α ratio is notably higher (2.86-3.71) in LuAG:Pr SCF/LuAG:Ce SC composite scintillator, than that in LuAG:Ce crystal (see Fig. 4a). The differences in the t_α/t_γ ratio do not significantly change for LuAG:Pr SCF/LuAG:Ce SC composite scintillator, at different registration levels and can be presented in Fig.4a as the vertical line with small slope (curves 2). This means that separation of scintillation from the SCF and SC components of such composite scintillator can be obtained with the maximal possible rate at all suitable decay levels in the 0-700 ns time interval due to faster by 3-4 times scintillation response under α -particles excitation in comparison with the response under γ -rays excitation (Table 3).

In LuAG:Sc SCF/LuAG:Ce SC composite scintillators, the $t_\alpha t_\gamma$ or $t_\gamma t_\alpha$ ratios are also significantly higher at 1/e and 0.01 levels than those in LuAG:Ce crystal. Meanwhile, the differences in the t_α/t_γ ratio significantly change for such type of composite scintillator at different registration levels and can be presented in Fig.4a as the vertical line with large slope (curves 3). This means that the separation of scintillation from the SCF and SC components of such composite scintillator can be obtained with maximal rate only in the two narrow time intervals: 0-100 ns and 150-500 ns where the scintillation response under α -particles excitation is by 4 times faster and 2 times slower, respectively, than that corresponding to the case of γ -rays excitation (Table 3).

For better comparison of the different types of composite scintillators, the parameter $s = t_\alpha/t_\gamma - 1$ or $s = t_\gamma/t_\alpha - 1$ has been introduced for the consideration. This parameter is proportional to the rate of the decay curves separation under α -particles and γ -ray excitations at chosen decay time levels. The dependence of s values at the different scintillation decay levels is shown in Fig.4b. The best situation for composite scintillators functionality takes place when the high and uniform s value is observed in the whole decay time levels. In comparison with the LuAG:Ce crystal (Fig.4b, curve 1), the largest s values and the monotonic trend of s values change at different decay time levels are observed for LuAG:Pr SCF/LuAG:Ce SC composite scintillator (Fig.4b, curve 2). On the contrary, LuAG:Sc SCF/LuAG:Ce SC composite scintillator possesses the significantly smaller s values and there is no definite trend of the s value changes at different decay time levels (Fig.4b, curve 3).

V. CONCLUSION

Two new types of advanced composite scintillators based on the LuAG:Pr and LuAG:Sc single crystalline films (SCF) with thickness in the 10-12 μm range and LuAG:Ce substrates

with a thickness of 1 mm were produced by the LPE method from melt solutions using PbO-B₂O₃ flux.

For characterization of the luminescent and scintillation properties of SCF and bulk crystal parts of composite scintillators, the absorption spectra, CL spectra and scintillation decay kinetics under α -particles excitation by ²⁴¹Am (5.5 MeV) source and γ -ray excitation by ¹³⁷Cs (0.662 MeV) source were applied.

Under γ -ray and α -particles excitations, the notable differences in the scintillation decay kinetics of LuAG:Pr SCF / LuAG:Ce SC and LuAG:Sc SCF/LuAG:Ce SC composite scintillators are observed. Such differences can be characterized by t_α/t_γ or t_γ/t_α decay time ratios, which for the mentioned composite scintillators occur within the 2.86-3.71 and 1.93-3.44 ranges, respectively, at scintillation decay intensity within two decades from the 1/e level down to 0.05 levels.

At the same time, the LuAG:Pr SCF/LuAG:Ce SC composite scintillator possesses significant advantage with respect to LuAG:Sc SCF/LuAG:Ce SC counterpart due to the fact that scintillating signal coming from the SCF and SC components of the first type composite scintillator can be separated with large t_α/t_γ decay time ratio in the whole time interval from 0 to 700 ns. Thus, the mentioned types of composite scintillator can be successfully applied for separation of the signals coming from their film and bulk parts at the registration of the mixed radiation fluxes containing α -particles and γ -photons.

Meanwhile, the epitaxial structures LuAG:Sc SCF/LuAG:Ce SC also show good enough scintillation properties. For this reason, we hope that after optimization of the concentration of dopants and scintillation parameters of SCF and substrate scintillators this combination of LuAG based compounds can be also concurrent with other combinations for creation of composite scintillators for simultaneous registration of α -particles and γ -quanta.

ACKNOWLEDGMENT

The work was performed in the framework of Polish NCN 2016/21/B/ST8/03200 project and Czech Science Foundation 16-15569S project.

REFERENCES

1. Yu. Zorenko, S.S. Novosad, M.V. Pashkovskii, A.B. Lyskovich, V.G. Savitskii, M.M. Batenchuk, P.S. Malyutchenko, N. I. Patsagan, I. V. Nazar, V.I. Gorbenko, "Epitaxial structures of garnets as scintillation detectors of ionizing radiation," *Journal of Applied Spectroscopy*, vol. no. 52, pp. 645-649, 1990.
2. B. Ferrand, B. Chambaz, M. Couchaud, "Liquid phase epitaxy: A versatile technique for the development of miniature optical components in single crystal dielectric media," *Optical Materials*, vol. 11, pp. 101-114, 1999.
3. "Nanocomposite, Ceramic, and Thin Film Scintillators," Ed. By M. Nikl, Pan Stanford Publ. Singapore 2017. ISBN 978-981-4745-22-2, pp. 2016. - 350.
4. J. M. Robertson, M. V. Van Tol, "Cathodoluminescent garnet layers," *Thin Solid Films*, vol. 114, pp. 221-240, 1984.
5. Z. D. Hrytskiv, Y. Zorenko, V. Gorbenko, A.D. Pedan, V. I. Shkliarskyi, "Single crystalline film screens for cathode-ray tubes: New life of television scanning optical microscopy," *Radiation Measurements*, vol. 42, pp. 933-936, 2007.

6. E. Molva, "Microchip lasers and their applications in optical Microsystems," *Optical Materials*, vol. 11, pp. 289-299, 1999.
7. M. Klimczak, M. Malinowski, J. Sarnecki, R. J. Piramidowicz, "Luminescence properties in the visible of Dy:YAG/YAG planar waveguides," *Luminescence*, vol. 129, pp. 1869-1873, 2009.
8. Yu. Zorenko, M. Batenchuk, V. Gorbenko, M. Pashkovsky, "Single crystalline oxide films of the Al₂O₃-Y₂O₃-R₂O₃ system as optical sensors of various types of ionizing radiations: significant advantages over volume analogues," *Optical Inorganic Dielectric Materials and Devices*, A. Krumins, D. K. Millers, A. Sternberg, J. Spigulis, Proc. SPIE. 1997, 2967, pp. 101-104.
9. Yu. Zorenko, V. Gorbenko, I. Konstankevych, B. Grinev, M. Globus, "Scintillation properties of Lu₃Al₅O₁₂:Ce single-crystalline films," *Nuclear Instrument and Methods for Physical Research A*, vol. 486, pp. 309-314, 2002.
10. A. Koch, C. Raven, P. Spanne, A. Snigirev, "X-ray imaging with submicrometer resolution employing transparent luminescent screens" *J. Opt. Soc. Am.*, A15, 1940-1951, 1998.
11. T. Martin, A. Koch, "Recent development in X-ray imaging with micrometer spatial resolution" *Journal of Synchrotron Radiation*, vol. 13, pp. 180-194, 2006.
12. Y. Zorenko, V. Gorbenko, I. Konstankevych, M. Pashkovsky, M. Globus, B. Grinyov, V. Tarasov, P. Dorenbos, C.W.E. Van Eijk, E. Van Loef, "Scintillators on the base of single crystalline films of Al₂O₃-Y₂O₃ system oxides," *Proceedings of the 5th Intern. Conference on Inorganic Scintillators and Their Applications*, V. Mikhailin, Moscow State University, pp. 476-481, 2000.
13. M. Globus, B. Grinyov, M. Ratner, V. Tarasov, V. Lyubinskiy, Yu. Zorenko, I. Konstankevych, "New Type of Scintillation Detectors for Biological, Medical, and Radiation Monitoring Applications," *IEEE Nuclear Science Symposium and Medical Imaging Conference*, no. 1, pp. 352-356, 2002.
14. Yu. Zorenko, V. Gorbenko, T. Voznyak, I. Konstankevych, V. Savchyn, M. Batentschuk, A. Winnacker, Ch. J. Brabec, "Scintillators Based on CdWO₄ and CdWO₄:Bi Single Crystalline Films," *IEEE Transaction on Nuclear Science*, vol. 59 (5 PART 2), art. no. 6236274, pp. 2281-2285, 2012.
15. S. Gobiein, "Phoswich Detectors for High Energy Backgrounds", Dec. 29, 2017. [Online]. Available: <http://www.detectors.saint-gobain.com>.
16. M. Nikl, A. Yoshikawa, K. Kamada, K. Nejezchleb, C.R. Stanek, J.A. Mares, K. Blazek, M. Nikl, "Development of LuAG-based scintillator crystals - A review," *Crystal Growth and Characterization of Materials*, vol. 59, pp. 47-72, 2013.
17. J.M. Ogieglo, A. Zych, T. Justel, A. Meijerink, C.R. Ronda, Luminescence and energy transfer in Lu₃Al₅O₁₂ scintillators co-doped with Ce³⁺ and Pr³⁺. *Optical Materials*. vol. 35, pp. 322-331, 2013.
18. Yu. Zorenko, V. Gorbenko, T. Voznyak, T. Martin, P.-A. Douissard, J.A. Mares, M. Nikl, "LuAG:Pr, LuAG:La, and LuAP:Ce thin film scintillators for visualization of x-ray images". Proc. SPIE, vol. 7310, 731007(8pp), 2009.
19. M. Nikl, J. Tous, J. A. Mares, P. Prusa, E. Mihokova, K. Blazek, A. Vedda, Yu. Zorenko, V. Gorbenko, V. Babin, "Lu₃Al₅O₁₂-based materials for high 2D-resolution scintillation detectors" Proc. SPIE. vol. 7310, P. 731008(10 pp), 2009.
20. V. Gorbenko, A. Krasnikov, M. Nikl, S. Zazubovich, Yu. Zorenko, „Luminescence characteristics of LuAG:Pr and YAG:Pr single crystalline films". *Optical materials*, vol. 31, pp. 1805-1807, 2009.
21. N.N. Ryskin, P. Dorenbos, C.W.E. van Eijk, S. Kh. Batygov. "Scintillation properties of Lu₃Al_{5-x}Sc_xO₁₂", *J. Phys.: Condens. Matter*, vol.6. pp.10423, 1994.
22. Yu. V. Zorenko, "Luminescence of La³⁺ and Sc³⁺ Isoelectronic Impurities in Lu₃Al₅O₁₂ Single Crystalline Films", *Optics and Spectroscopy*, vol. 100, № 4, pp. 572-580, 2004.
23. Yu. Zorenko, V. Gorbenko, A. Voloshinovskii, G. Stryganyuk, S. Nedliko, V. Degoda, O. Chykova, "Luminescence of Sc-related centers in single crystalline films of Lu₃Al₅O₁₂ garnet", *Phys. stat. sol. (c)*, vol.2, №1, pp. 105-108, 2005.
24. Yu. Zorenko, V. Gorbenko, T. Voznyak, V. Savchyn, S. Nizhankovskiy, A. Dan'ko, V. Puzikov, V. Laguta, J.A. Mares, M. Nikl, K. Nejezchleb, M. Batentschuk, A. Winnacker, "Luminescent and scintillation properties of Lu₃Al₅O₁₂:Sc single crystal and single crystalline films", *Optical Materials*, vol. 34, pp. 2080-2085, 2012.
25. Yu. Zorenko, V. Gorbenko, T. Zorenko, O. Sidletskiy, A. Fedorov, P. Bilski and A. Twardak, "High-performance Ce-doped multicomponent garnet single crystalline film scintillators", *Physica Status Solidi RRL*, vol.9, pp.489-493, 2015.
26. S. Witkiewicz-Lukaszek, V. Gorbenko, T. Zorenko, O. Sidletskiy, I. Gerasymov, A. Fedorov, A. Yoshikawa, J.A. Mares, M. Nikl, Yu. Zorenko, "Development of composite scintillators based on the single crystalline films and crystals of Ce³⁺ doped (Lu,Gd)₃(Al,Ga)₅O₁₂ mixed garnet compounds," *Crystal Growth@Dec.* 2017, DOI: 10.1021/acs.cgd.7b01695.
27. Y. Zorenko, A. Voloshinovskii, L. Konstankevych, V. Kolobanov, V. Mikhailin, D. Spassky, "Luminescence of excitons and antisite defects in the phosphors based on garnet compounds," *Radiation Measurements*, vol.38, pp. 677-680, 2004.
28. Yu. Zorenko, "Luminescence of isoelectronic impurities and anti-site defects in garnets," *Phys. Stat. Sol. (c)*, vol. 2, pp. 375-379, 2005.



Composite scintillators based on the crystals and single crystalline films of LuAG garnet doped with Ce³⁺, Pr³⁺ and Sc³⁺ ions

S. Witkiewicz-Lukaszek^{a,e,*}, V. Gorbenko^{a,b}, T. Zorenko^{a,b}, K. Paprocki^a, O. Sidletska^c, I. Gerasymov^c, J.A. Mares^d, R. Kucerkova^d, M. Nikl^d, Yu Zorenko^{a,b,*}

^a Institute of Physics, Kazimierz Wielki University in Bydgoszcz, Powstańców Wielkopolskich Str., 2, 85090, Bydgoszcz, Poland

^b Electronic Department, Ivan Franko National University in Lviv, Dragomanova Str., 5, 79005, Lviv, Ukraine

^c Institute for Scintillation Materials, National Academy of Sciences of Ukraine, Av. Nauki 60, 61001, Kharkiv, Ukraine

^d Institute of Physics, Academy of Sciences of Czech Republic, Cukrovarnicka Str., 10, 16200, Prague, Czech Republic

^e Faculty of Technical Physics, Poznan University of Technology, Piotrowo Str., 3, 60-965, Poznan, Poland



ARTICLE INFO

Keywords:

α -particles and γ -quanta
Composite scintillator
Liquid phase epitaxy
LuAG
Films and crystals
 Ce^{3+} , Pr^{3+} and Sc^{3+} dopants

ABSTRACT

This work is devoted to the development of new types of advanced composite scintillators based on the single crystalline films (SCFs) of $\text{Lu}_3\text{Al}_5\text{O}_{12}$ (LuAG) garnet, doped with Pr^{3+} and Sc^{3+} ions, and substrate from single crystals (SCs) of Ce^{3+} doped LuAG using the technology of liquid phase epitaxy (LPE). We show the possibility of the simultaneous registration of α -particles and γ -quanta by means of separation of the decay kinetics of SCF and crystal parts of such composite scintillators. Namely, the significant differences in the pulse height spectra and the scintillation decay kinetics of LuAG:Pr SCF/LuAG:Ce SC and LuAG:Sc SC/LuAG:Ce SC composite scintillators under excitation by α -particles of ^{241}Am (5.5 MeV) source and γ -quanta of ^{137}Cs (662 keV) source are observed. For these reasons, such types of composite scintillators can be applied for separation of the signals coming from their film and crystal parts at the registration of the mixed radiation fluxes of α -particles and γ -quanta.

1. Introduction

The technology of the liquid phase epitaxy (LPE) offers today the possibility of developing the luminescent materials based on the single crystalline films (SCFs) of different oxide compounds [1–3]. The fields of application of such SCFs nowadays include laser media [4,5], cathodoluminescent screens [6,7], scintillators for registration of α - and β -particles and low-energy ionizing radiation [1,8,9] and scintillating screens for microtomography detectors using X-ray sources and synchrotron radiation [10,11].

The LPE method opens also the possibility of creating the advanced types of composite scintillators of “phoswich-type” (phosphor sandwich) for registration of the different components of ionizing radiation, for instance, for analysis of the content of mixed fluxes of particles and photons with various penetrating depths [1,12–14]. Such composite scintillators (CS) present the epitaxial structure (Fig. 1), including one or two SCFs, which enables registration of the low penetrating α - and β -particles, and a bulk single crystal (SC) substrate for registration of the highly penetrating radiation (X or γ rays).

There are many advantages of these types of composite scintillators

in comparison with the analogues based on the splice of different scintillation crystals [15]. Such types of composite scintillators present the all-solid state structure with a sharp interface between the composing scintillators with quite close refractive indices (Fig. 1). This permits to substantially eliminate the light losses at the interface of scintillators, enhancing the selectivity of registration of the different components of mixed ionizing radiations. The LPE method for composite scintillator manufacturing permits also to obtain the thickness of film scintillators close to the penetration depth of registered particles. Specifically, the thickness of film scintillators, which is necessary for the complete absorption of α -particles of ^{239}Pu and ^{241}Am sources, typically is equal to 10–12 μm (Fig. 1) [1].

The different types of composite scintillators have been recently considered by some of us in Refs. [1,12–14]. The first type of composite scintillators was created on the basis on the LPE grown epitaxial structures of $\text{Y}_3\text{Al}_5\text{O}_{12}$ garnet (YAG) [1]. Firstly one-layered composite scintillators based on the YAG:Ce SCF and YAG:Nd SC substrate (YAG:Ce SCF/YAG:Nd SC) and YAG:Ce SCF and YAG:Sc SC substrate (YAG:Ce SCF/YAG:Sc SC) as well as triply-layered composite scintillator based on the YAG:Ce SCF, YAG:Nd SCF and YAG:Sc SC substrate

* Corresponding authors. Institute of Physics, Kazimierz Wielki University in Bydgoszcz, Powstańców Wielkopolskich Str., 2, 85090, Bydgoszcz, Poland.

E-mail addresses: s-witkiewicz@wp.pl (S. Witkiewicz-Lukaszek), zorenko@ukw.edu.pl (Y. Zorenko).

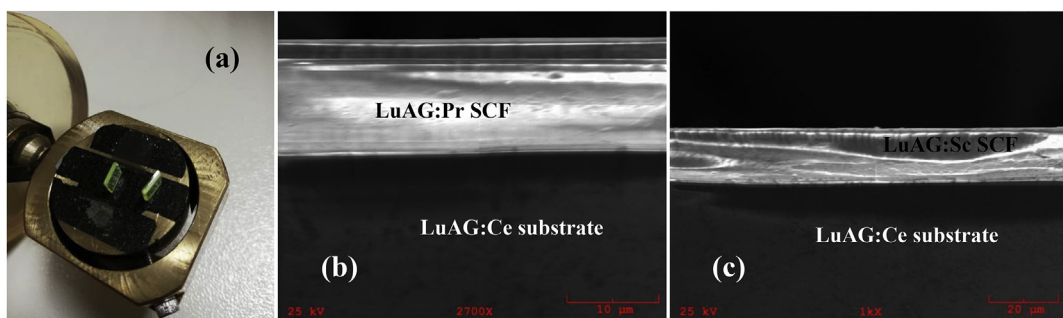


Fig. 1. (A) - view of composite scintillators on the top of the electronic microscope holder, (b, c) – the SCF/substrate cleavages of LuAG:Pr SCF/LuAG:Ce (b) and LuAG:Sc SCF/LuAG:Ce SC (c) epitaxial structures at the magnification of 2700 × (b) and 1000 × (c), respectively.

(YAG:Ce SCF/YAG:Nd SCF/YAG:Sc SC) were grown by the LPE method and examined under simultaneous excitation by α -particles and γ -quanta [1]. The separation of the scintillation signals coming from SCF and SC parts of composite scintillator was performed using the discrimination of their scintillation decay kinetics.

It should be noted that due to the low density $\rho = 4.56 \text{ g/cm}^3$ and effective atomic number $Z_{\text{eff}} = 29$, the scintillators based on the YAG SC may be used only for registration of low-energy ionizing radiation [1,12]. Therefore, there is a demand to fabricate composite scintillator for registration of the mixed fluxes of particles and high-energy quanta using other garnet compounds, which are characterized by high values of ρ and Z_{eff} [12,13].

From all the possible candidates of such oxide compounds, the $\text{Lu}_3\text{Al}_5\text{O}_{12}$ garnet (LuAG) first of all attracts our attention [9,10]. LuAG host has significantly higher density $\rho = 6.71 \text{ g/cm}^3$ and effective atomic number $Z_{\text{eff}} = 61$ in comparison with YAG. LuAG:Ce, LuAG:Pr and LuAG:Sc are the well-known scintillators for radiation monitoring and computer tomography [3,16]. Therefore, the LuAG is very promising material for creation of SCF scintillators and composite scintillators on their base as well. As activators, which can effectively emit in LuAG host with different wavelengths and fast enough decay kinetics of scintillations, the Pr^{3+} , Sc^{3+} and Ce^{3+} ions can be considered (Table 1) [9,16–24]. Namely, the position of emission band of LuAG:Ce, LuAG:Pr and LuAG:Sc compounds under high-energy excitation is located at 515, 310 and 280 nm, respectively, and the corresponding decay times of main component of the luminescence of Ce^{3+} , Pr^{3+} and Sc^{3+} dopants in LuAG host are equal to 49.5–58 ns, 1–28 ns and 245–610 ns, respectively [16–24]. Therefore, the different combinations of novel composite scintillators based on the epitaxial structures of LuAG garnet compounds, doped with the mentioned ions, can be created using the LPE method.

In this work, we present the new results of the research directed on creation of the novel types of composite scintillator based on the Ce^{3+} and Pr^{3+} doped LuAG SCFs and LuAG:Ce substrates grown by the

LPE method.

2. Growth of composite scintillators based on LuAG:Pr and LuAG:Sc SCFs and LuAG:Ce SCs

Two types of composite scintillators based on LuAG:Pr and LuAG:Sc SCFs were grown by the LPE method onto LuAG:Ce substrates from super-cooled melt solutions using $\text{PbO-B}_2\text{O}_3$ flux (Fig. 1). For comparison, the sets of LuAG:Sc and LuAG:Pr SCF samples were also grown from the same melt onto YAG substrates. The growth conditions of the SCFs and composite scintillators, selected for investigation of the content and structural properties as well as for the study of their absorption, cathodoluminescence and scintillation properties, were summarized in Table 1.

3. Experimental technique

For characterization of the luminescent and scintillation properties of the composite scintillators based on the Pr^{3+} and Sc^{3+} doped LuAG SCFs and LuAG:Ce substrates, the absorption spectra, cathodoluminescence (CL) spectra, LY, energy resolution and scintillation decay kinetics measurements under excitation by α -particles and γ -quanta were applied. The absorption spectra were measured using a Jasco 760 UV-Vis spectrometer in the 200–1100 nm range. The CL spectra were measured using an electron microscope SEM JEOL JSM-820 ($U = 30 \text{ kV}$, $I = 0.1 \mu\text{A}$), additionally equipped with a spectrometer Stellar Net and TE-cooled CCD detector working in the 200–925 nm range. The scintillation LY (pulse height spectra measured with a shaping time of $12 \mu\text{s}$) was firstly measured after each SCF growth circle using the setup based on a Hamamatsu H6521 photomultipliers (PMP), multi-channel analyzer and digital Tektronix TDS3052 oscilloscope under excitation by α -particles of Pu^{239} (5.15 MeV) source (Table 2). The spectra were compared with the standard YAG:Ce SCF sample with a photoelectron yield of 360 phels/MeV and a LY of 2650 photons/MeV [25,26] and also with the reference LuAG:Ce substrates, produced in the ISM, Kharkiv, Ukraine. All measurements were performed at the

Table 1

Growth conditions of LuAG:Pr SCF/LuAG:Ce SC and LuAG:Sc SCF/LuAG:Ce SC composite scintillators in comparison with LuAG:Pr and LuAG:Sc SCFs, grown onto YAG substrates. h - SCF thickness, f - velocity of SCF growth; T - SCF growth temperature. LY- light yield of scintillation under excitation by α -particles of Pu^{239} sources and registration of scintillation with a shaping time of $12 \mu\text{s}$ in comparison with standard YAG:Ce SCF scintillator with a photo-electron LY of 360 phels/MeV (a LY of 2600 ph/MeV).

Type of SCF and SC	Substrate	$h, \mu\text{m}$	$T, ^\circ\text{C}$	$f, \mu\text{m/min}$	LY, %
$\text{Y}_3\text{Al}_5\text{O}_{12}\text{:Ce}$	$\text{Y}_3\text{Al}_5\text{O}_{12}$	54			100
$\text{Lu}_3\text{Al}_5\text{O}_{12}\text{:Pr}$	$\text{Y}_3\text{Al}_5\text{O}_{12}$	19	975	0.19	100
$\text{Lu}_3\text{Al}_5\text{O}_{12}\text{:Pr}$	$\text{Lu}_3\text{Al}_5\text{O}_{12}\text{:Ce}$	12.3	980	0.21	96
$\text{Lu}_3\text{Al}_5\text{O}_{12}\text{:Sc}$	$\text{Y}_3\text{Al}_5\text{O}_{12}$	10.2	985	0.165	52
$\text{Lu}_3\text{Al}_5\text{O}_{12}\text{:Sc}$	$\text{Lu}_3\text{Al}_5\text{O}_{12}\text{:Ce}$	15	980	0.21	54
LuAG:Ce SC		500			130

Table 2

Time t_{e} and t_{γ} values of scintillation intensity decay to $1/e$, 0.1 and 0.05 levels of LuAG:Pr SCF/LuAG:Ce SC and LuAG:Sc SCF/LuAG:Ce SC composite scintillators and reference LuAG:Ce SC substrate under α -particles and γ -quanta excitation of Pu^{239} (5.15 MeV) and Cs^{137} (661.66 keV) sources, respectively.

Intensity of decay to level	Time, ns					
	LuAG:Ce crystal		LuAG:Pr/LuAG:Ce		LuAG:Sc/LuAG:Ce	
Excitation source	α	γ	α	γ	α	γ
	1/e	37	53	15	41	102
	0.1	161	166	39	143	454
	0.05	336	250	71	238	920
						416

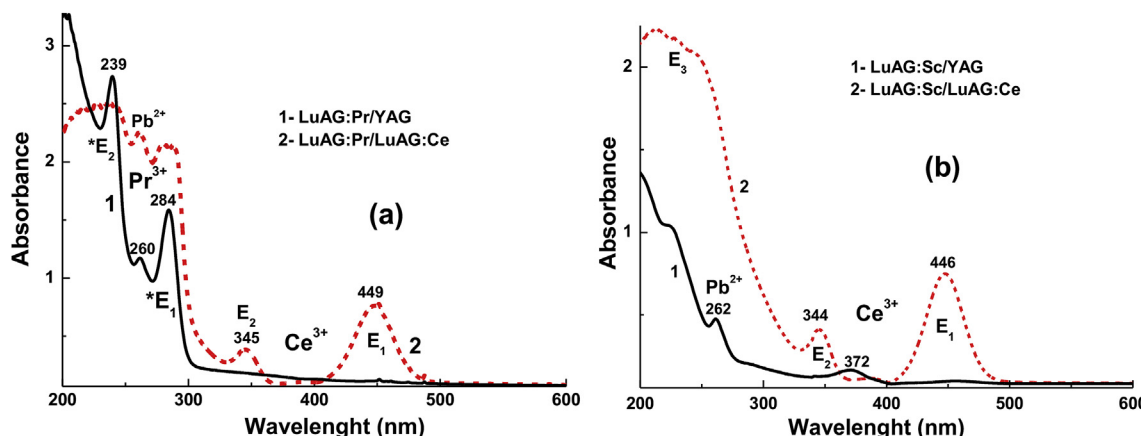


Fig. 2. RT absorption spectra of composite scintillators based on the LuAG:Pr SCFs (a, curve 2) and LuAG:Sc SCFs (b, curve 2), grown onto LuAG:Ce substrates, in comparison with absorption spectra of LuAG:Pr SCFs (a, curve 1) and LuAG:Sc SCFs (b, curve 1), grown onto YAG substrates.

room temperature (RT).

Scintillation response investigations of the selected composite scintillators (see Table 2) were performed using the set-up consisting of a hybrid PMT (HPMT DEP PP0475B), measuring electronics and PC control. Pulse height spectra were measured under excitation by α -particles with ^{241}Am (an energy of 5.4857 MeV) radioisotope and with γ -rays of ^{137}Cs (an energy of 661.66 keV) radioisotope. It is important to note here that the α -particles of ^{239}Pu and ^{241}Am sources allow exciting only the epitaxial layers of SCF samples (not their substrates) because the penetration depths of α -particles in the studied samples are approximately 12–15 μm .

4. Absorption and cathodoluminescence properties of LuAG:Pr and LuAG:Sc SCFs and LuAG:Ce substrates

The absorption spectra of the two composite scintillators of LuAG:Pr SCF/LuAG:Ce SCs and LuAG:Sc SCF/LuAG:Ce SCs in comparison with the absorption spectra of LuAG:Pr and LuAG:Sc SCFs, grown onto YAG substrates, are shown in Fig. 2, a and b, respectively. The absorption bands E₁ at 446–449 nm and E₂ at 344–345 nm in the spectra of LuAG:Pr SCF/LuAG:Ce SC and LuAG:Sc SCF/LuAG:Ce SC composite scintillators (Fig. 2, a and b, respectively) are related to the 4f-5d (^2E) transitions of Ce³⁺ ions in LuAG:Ce SC substrate. Other Ce³⁺ absorption bands E₃ in these scintillators are located below 230 nm and related to the 4f-5d (T_{2g}) transitions. The bands *E₁ and *E₂ peaked at 239 nm and 284 nm correspond to the 4f ($^3\text{H}_4$) \rightarrow 5d^{1,2} transitions of Pr³⁺ ions (Fig. 1a). The bands peaked at 260 and 262 nm in Fig. 1a and b are related to the $^1\text{S}_0\rightarrow^3\text{P}_1$ transitions of Pb²⁺ flux impurity in the SCF samples. Meanwhile, the observed band at 372 nm in the absorption spectra of LuAG:Sc/YAG epitaxial structure can be related to the absorption of Pb²⁺ based dimer centers or/and absorption of F⁺ centers in the YAG substrate.

The normalized CL spectra of LuAG:Pr SCF/LuAG:Ce SC and LuAG:Sc SCF/LuAG:Ce SC composite scintillators in comparison with the CL spectra of LuAG:Pr and LuAG:Sc SCFs and LuAG:Ce SC substrates are shown in Fig. 3, a and b, respectively. The luminescence bands in the visible range peaked at 512 nm in the CL spectra of LuAG:Ce SCs (Fig. 3, a and b, curves 1) are related to the 5 d¹-4f transitions of Ce³⁺ ions while the emission bands in the UV range are caused by the Lu_{Al} antisite-defect related emission centers [27,28]. The dominant luminescence bands in the UV range peaked at 312 and 380 nm and the low-intensive sharp emission band in the visible range in the CL spectra of LuAG:Pr SCFs (Fig. 3 a, curve 2) are related to the 5 d¹-4f and 4f-4f radiative luminescence transitions of Pr³⁺ ions. Meanwhile, apart from the Pr³⁺ related emission bands in the UV and visible ranges, the Ce³⁺ emission band peaked at 512 nm is prevailing in the CL spectra of

LuAG:Pr SCF/LuAG:Ce SC composite scintillator (Fig. 3 a, curve 3). This means that the LuAG:Pr SCF component of composite scintillator excites the luminescence of Ce³⁺ ions in the LuAG:Ce substrate due to the reabsorption of the UV part of emission of LuAG:Pr SCFs by the absorption band of Ce³⁺ ions in LuAG:Ce SC peaked around 344 nm (Fig. 2 a) [17]. The dominant luminescence bands in the UV range peaked at 312 and 380 nm and the low-intensive sharp emission band in the visible range in the CL spectra of LuAG:Pr SCFs (Fig. 3 a, curve 2) are related to the 5 d¹-4f and 4f-4f radiative transitions of Pr³⁺ ions. Meanwhile, apart from the Pr³⁺ related emission bands in the UV and visible ranges, the Ce³⁺ emission band peaked at 512 nm prevails in the CL spectra of LuAG:Pr SCF/LuAG:Ce composite scintillator (Fig. 3 a, curve 3). This means that the LuAG:Pr SCF component of composite scintillator excites the luminescence of Ce³⁺ ions in the LuAG:Ce substrate due to the reabsorption of the UV part of emission of LuAG:Pr SCF by the absorption band of Ce³⁺ ions in LuAG:Ce SC peaked around 344 nm (Fig. 2 a) [17].

The dominant luminescence bands in the UV range peaked at 280 nm in the CL spectra of LuAG:Sc SCFs (Fig. 3 b, curve 2) are caused by the luminescence of Sc_{Al} isoelectronic impurity [21–24]. At the same time, in the CL spectra of LuAG:Sc SCF/LuAG:Ce SC composite scintillator, besides of the Sc³⁺ related emission bands in the UV range, the Ce³⁺ emission band in the visible range peaked at 512 nm is also observed and these emission bands are comparable in the intensity (Fig. 3 b, curve 3). Similarly to the previous type of composite scintillators, the emission of LuAG:Sc SCF component excites the luminescence of Ce³⁺ ions in the LuAG:Ce substrate due to the reabsorption of the UV emission band of LuAG:Sc SCFs by the absorption band of Ce³⁺ ions in LuAG:Ce SCs peaked around 344 nm (Fig. 2 b, curve 2).

Such observation of the excitation of the Ce³⁺ luminescence in LuAG:Ce substrate by the emission of LuAG:Pr and LuAG:Sc SCFs can make the large problem for the principal functionality of LuAG:Pr SCF/LuAG:Ce and LuAG:Sc SCF/LuAG:Ce SC composite scintillators. Meanwhile, the analysis of the scintillation decay kinetics shows that such unwanted behavior of composite scintillators is not so significant in the case of separation of different signals coming from their SCF and SC parts under registration of α -particles and γ -rays, respectively.

5. Scintillation properties of composite scintillators based on Pr³⁺ and Sc³⁺ doped SCFs and LuAG:Ce substrates

5.1. Pulse height spectra

The pulse height spectra of the main γ - or α -ray lines of ^{137}Cs and ^{241}Am sources registered by LuAG:Pr SCF/LuAG:Ce SC and LuAG:Sc SCF/LuAG:Ce SC composite scintillators are presented in Fig. 4a and b,

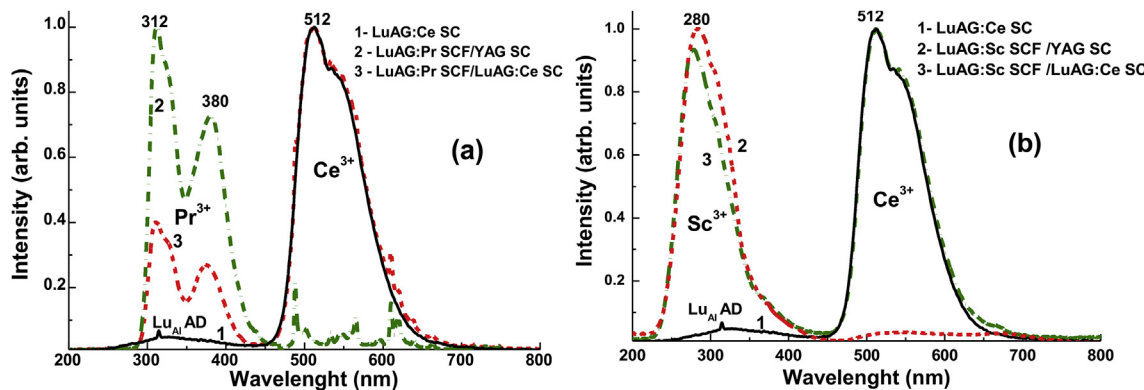


Fig. 3. Normalized CL spectra of LuAG:Pr SCF/LuAG:Ce SCs (a, curve 3) and LuAG:Sc SCF/LuAG:Ce SC (b, curve 3) composite scintillators in comparison with LuAG:Ce SC substrate (a and b, curves 1) and LuAG:Pr (a, curve 2) or LuAG:Sc (b, curve 2) SCFs, grown onto YAG substrates.

respectively. The main peaks in Fig. 4a correspond to the total energy absorption of α -rays with an energy of 5.4857 MeV. The peaks in the left part of the spectrum correspond to the absorption of the low-energy emission line of ^{241}Am with an energy of 59.6467 keV. It is worth to note that the positions of the main photopeaks, observed in Fig. 4a, are substantially different for LuAG:Pr and LuAG:Sc SCF components for both composite scintillators and for LuAG:Ce substrate. This means that α -particles excite only SCF parts of composite scintillators. Fig. 4a shows also that the LY value of LuAG:Pr and LuAG:Sc SCF samples under excitation by α -particles is smaller by 1.3 and 2.3 times, respectively, in comparison with the LY value for LuAG:Ce substrate. These results on the LY of composite scintillators under α -particles excitation by ^{241}Am source are consistent with the results obtained at these samples presented in Table 1 under excitation by ^{239}Pu source. Such lower LY of SCF samples is caused mainly by the negative influence of Pb flux related impurity on the scintillation properties of SCFs of different oxide compounds, grown from PbO based flux [3,24].

Under γ -quanta excitation of LuAG:Pr/LuAG:Ce and LuAG:Sc/LuAG:Ce composite scintillators by ^{137}Cs source, the main peaks were observed in the pulse high spectra, corresponding to the total absorption of γ radiation with an energy of 661.66 keV (Fig. 4b). The additional peak is observed at lower energy at 32.006 keV, corresponding to the low-energy energy line of ^{137}Cs source. It is characteristic that the main photopeaks, observed in Fig. 4b, have similar positions for both LuAG:Pr/LuAG:Ce and LuAG:Sc/LuAG:Ce composite scintillators and LuAG:Ce substrate and this means that γ -rays excite mainly the substrate.

Fig. 5a presents the LY of LuAG:Pr/LuAG:Ce and LuAG:Sc/LuAG:Ce composite scintillators and LuAG:Ce substrate evaluated in the photons per MeV (ph/MeV) and measured with the different shaping times in

the 0.5–10 μs range under α -particles and γ -rays excitation. Namely, for LuAG:Ce substrates and LuAG:Pr/LuAG:Ce and LuAG:Sc/LuAG:Ce composite scintillators, excited by α -particles of ^{241}Am source with an energy of 5.4857 MeV, the LY increases from values of 1584, 963 and 461 ph/MeV to 3255, 1253 and 620 ph/MeV for the shaping times from 0.5 to 10 μs , respectively. On the contrary, we have observed very similar LY values under the 661.66 keV γ -ray excitation for LuAG:Pr SCF/LuAG:Ce SC and LuAG:Sc SCF/LuAG:Ce SC composite scintillators and LuAG:Ce substrate. Specifically, the LY values in these scintillators change from 12570 to 15420 ph/MeV to 22215–26810 ph/MeV when the shaping times increase in the 0.5–10 μs interval.

The energy resolution of LuAG:Pr SCF/LuAG:Ce SC and LuAG:Sc SCF/LuAG:Ce SC composite scintillators and LuAG:Ce substrate measured at the 0.5–10 μs shaping time under excitation by α -particles and γ -quanta is shown in Fig. 5b. As can be seen from Fig. 5b, the energy resolution of LuAG:Pr SCF/LuAG:Ce SC and LuAG:Sc SCF/LuAG:Ce SC composite scintillators under α -particles excitation by ^{241}Am (5.4857 MeV) source (e.g., LuAG:Pr and LuAG:Sc SCFs) lies in the 28.7–20.3% and 16.6–12.3% ranges, respectively, and is notably worse as compared to the energy resolution of LuAG:Ce substrate lying in the 13.2–11.4% range. This is caused mainly by the significantly lower LY of SCF samples as compared to the LY of SC substrate (Fig. 4a). Under γ -ray excitation at 662 keV of ^{137}Cs source we have observed rather close values of the energy resolution of LuAG:Pr SCF/LuAG:Ce SC and LuAG:Sc SCF/LuAG:Ce SC composite scintillators in the 15.2–9.2% and 14.2–10.3% ranges, respectively, and LuAG:Ce substrate lying in the 13.4–10.3% range (Fig. 5b).

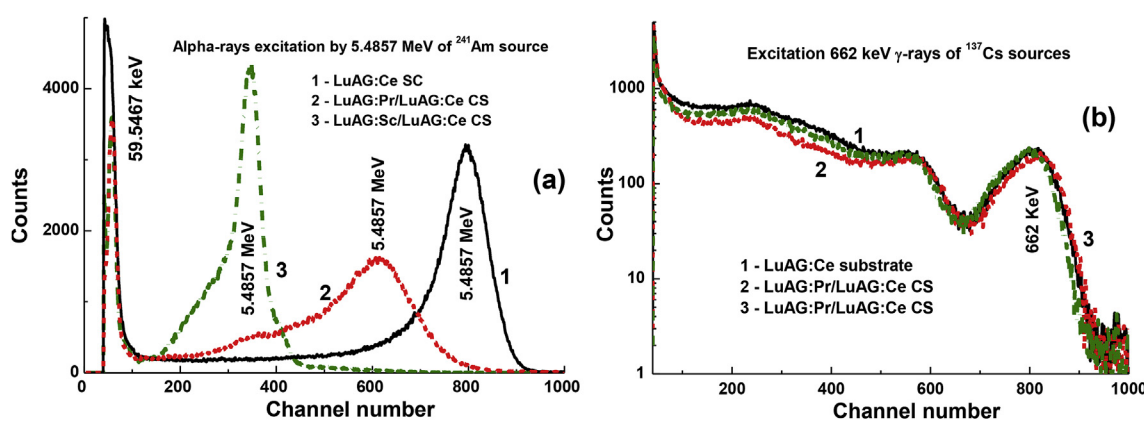


Fig. 4. Pulse height spectra of LuAG:Ce substrate (1), LuAG:Pr/LuAG:Ce (2) and LuAG:Sc/LuAG:Ce (3) composite scintillators measured under α -particles excitation with an energy of 5.4857 MeV of ^{241}Am source (a) and under γ -ray excitation of ^{137}Cs source with an energy of 661.66 keV (b).

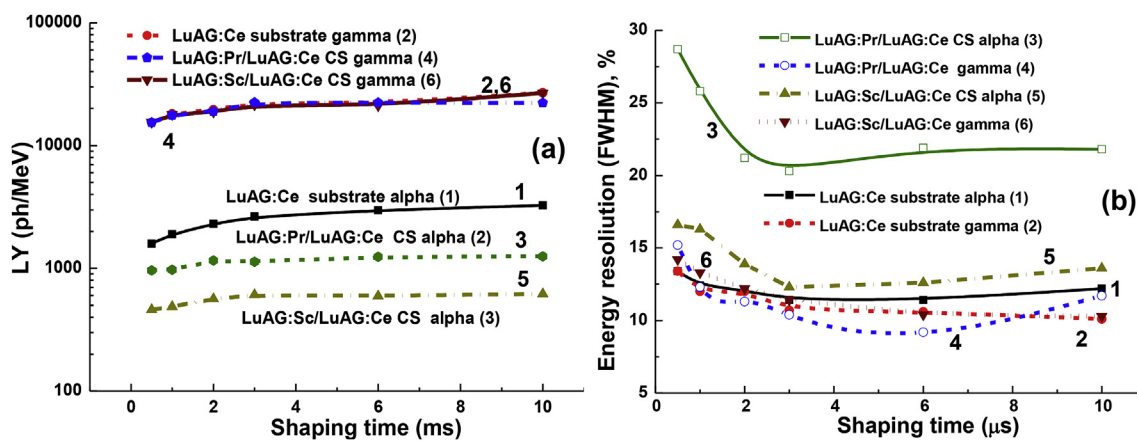


Fig. 5. Dependence of LY values (a) and energy resolution (b) versus shaping time T of LuAG:Pr/LuAG:Ce (3, 4) and LuAG:Sc/LuAG:Ce (5, 6) composite scintillators and LuAG:Ce substrates (1, 4) measured under α -particles excitation by ^{241}Am source with an energy of 5.4857 MeV (1, 3, 5) and γ -ray excitations excitation by ^{137}Cs source with an energy of 661.66 keV (2, 4, 6). $T = 0.5, 1, 2, 3, 6$ and $10 \mu\text{s}$.

5.2. Scintillation decay kinetics

Fig. 6 presents the scintillation decay curves of LuAG:Pr SCF/ LuAG:Ce SC (a) and LuAG:Sc SCF/LuAG:Ce SC(b) composite scintillators and LuAG:Ce substrates (c), measured under both α -particles and γ -ray excitation (see curves 1 and 2, respectively) (see Fig. 7).

Generally for registration of the difference in the scintillation decay kinetics of the bulk and film components of composite scintillator, it is

very important to analyze firstly the decay curves under α -particles and γ -ray excitation of substrates, prepared from bulk crystals of garnet compounds, in a broad range of decay intensity. Firstly we perform such analysis for LuAG:Ce substrate with a thickness of 1 mm for the scintillation intensity decay to $1/e$, 0.1 and 0.05 levels (Fig. 6c and Table 2). As one can see from Fig. 6c, the decay curves of LuAG:Ce SC substrate under α -particles and γ -ray excitation are very close in the initial stage of decay up to 150 ns. In a wider time interval (above

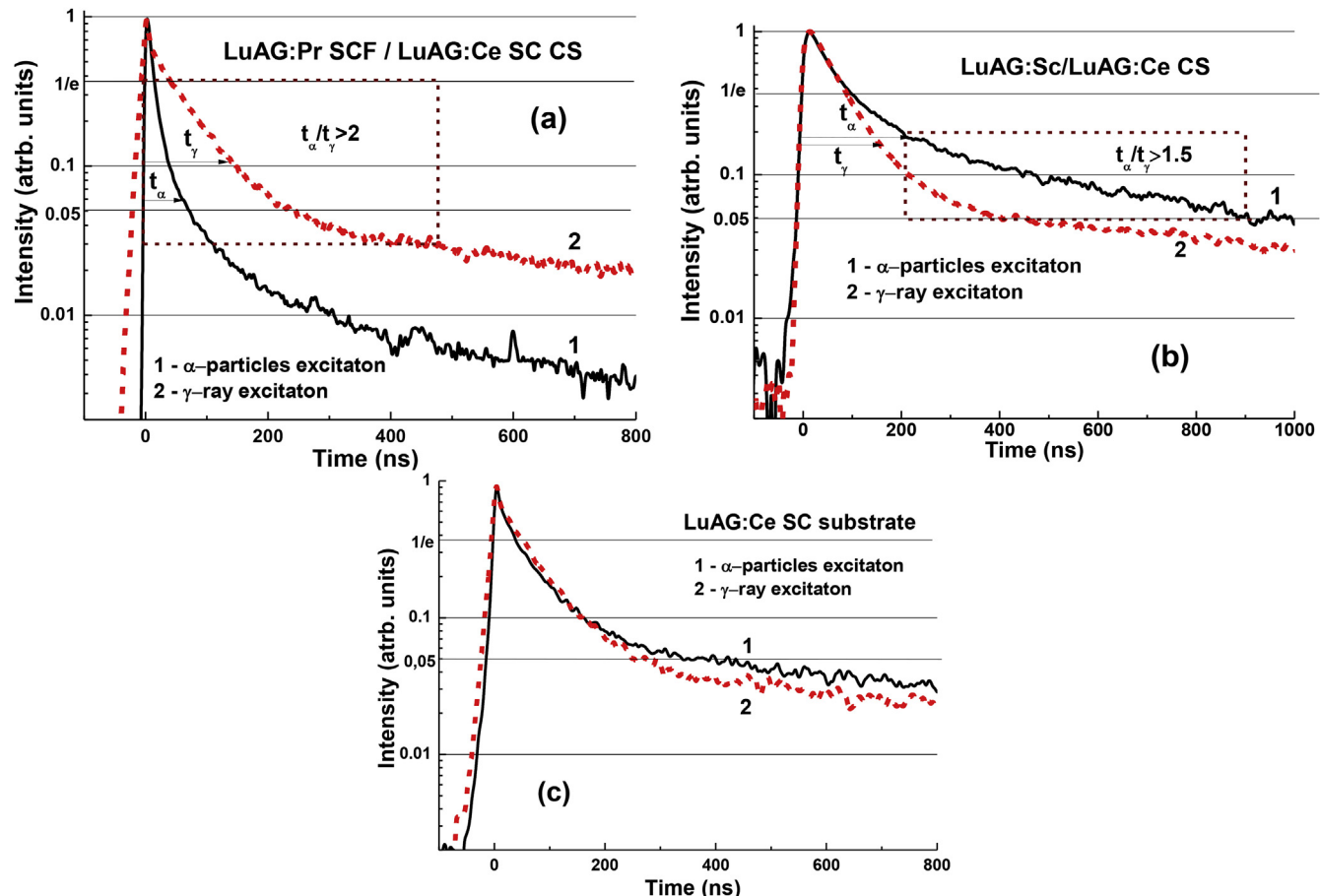


Fig. 6. Scintillation decay of LuAG:Pr SCF/LuAG:Ce SC (a) and LuAG:Sc SCF/LuAG:Ce SC (b) CSs in comparison with LuAG:Ce SCs (c) substrate under α -particles and γ -ray excitation by ^{241}Am and ^{137}Cs sources. The optimal time ranges for the scintillation registration using such type CSs are indicated, when the t_α/t_γ ratio reaches the values above 2.0 (a) and above 2.0 and 1.5 (b).

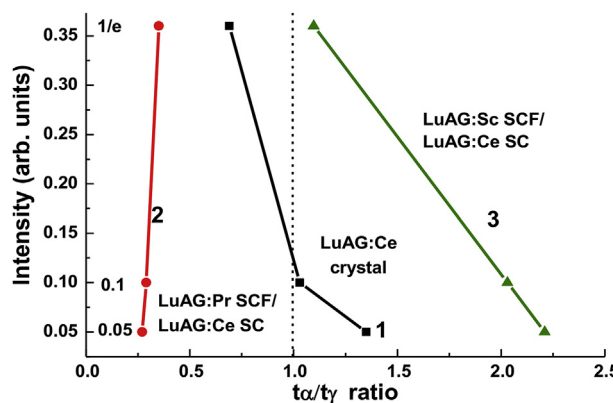


Fig. 7. Plots of t_α/t_γ ratio of the decay times under α - and γ -excitation on the intensity of scintillation decay to $1/e$, 0.1 and 0.05 levels for LuAG:Pr SCF/LuAG:Ce SC (2) and LuAG:Sc SCF/LuAG:Ce SC (3) composite scintillators and reference LuAG:Ce SC substrate (1).

150 ns) the decay curves of LuAG:Ce SC substrate under γ -ray excitation are notably faster than those in the case of α -particles excitation. Most probably, this is a fundamental behavior of scintillation materials and can be connected with the peculiarities of interaction of α -particles and γ -quanta with the scintillator material [26].

We can expect that the rate of separation of the scintillation signal at the registration of α -particles and γ -rays can be significantly improved in the composite epitaxial structures based on the films and crystals of different oxide compounds in comparison with crystal-scintillators. Indeed, for LUAG:Pr SCF/LuAG:Ce SC structure the scintillating signal coming from the SCF and SC components of composite scintillator can be separated in the whole time interval from 0 to 700 ns (Fig. 6a). Close situation is observed in the case of LuAG:Sc SCF/LuAG:Ce SC structure (Fig. 6b). The separation of the signal coming from SCF and SC substrate parts of this composite scintillator can be obtained also in the whole time interval, especially in the 200–900 ns range where the scintillation response under α -particles excitation is significantly slower than that under γ -ray excitation.

The above mentioned conclusions are confirmed also by comparison of the differences in the decay times at $1/e$, 0.1 and 0.05 levels for the decay curves under α -particles and γ -quanta excitation (so called t_α/t_γ ratio) in LuAG:Pr SCF/LuAG:Ce SC and LuAG:Sc SCF/LuAG:Ce SC composite scintillators and the reference LuAG:Ce crystal (Fig. 7). As one can see from this figure, the t_α/t_γ ratio is notably higher (0.27–0.35) in LuAG:Pr SCF/LuAG:Ce SC composite scintillator than that in LuAG:Ce crystal. The differences in the t_α/t_γ ratio do not significantly change for LuAG:Pr SCF/LuAG:Ce SC composite scintillator, at different registration levels and can be presented in Fig. 7 as the vertical line with small slope (curves 2). This means that separation of scintillation from the SCF and SC components of such composite scintillator can be obtained with the maximal possible rate at all suitable decay levels in the 0–700 ns time interval due to the faster by 3–4 times scintillation response under α -particles excitation in comparison with the response under γ -ray excitation (Table 2).

In LuAG:Sc SCF/LuAG:Ce SC composite scintillators, the t_α/t_γ ratio is also significantly higher at $1/e$ and 0.01 levels than that in LuAG:Ce crystal. Meanwhile, the differences in the t_α/t_γ ratio significantly change for such type of composite scintillator at different registration levels and can be presented in Fig. 6 as the vertical line with large slope (curves 3). This means that the optimal separation of scintillation from the SCF and SC components of such composite scintillator can be obtained with maximal rate in the time intervals 200–900 ns where the scintillation response under α -particles excitation is by 1.5–2.2 time slower than that corresponding to the case of γ -rays excitation (Table 2).

6. Conclusion

Two new types of advanced composite scintillators based on the LuAG:Pr and LuAG:Sc single crystalline films (SCF) with the thickness from 10 to 15 μm and LuAG:Ce substrates with a thickness of 1 mm were produced by the LPE method from melt solutions using $\text{PbO-B}_2\text{O}_3$ flux.

For the characterization of the luminescent and scintillation properties of LuAG:Pr and LuAG:Sc SCF and bulk crystal parts of composite scintillators, the absorption spectra, CL spectra and scintillation decay kinetics under α -particles excitation by ^{241}Am (5.5 MeV) source and γ -ray excitation by ^{137}Cs (0.662 MeV) source were applied.

Under γ -ray and α -particle excitations, the notable differences in the scintillation decay kinetics of LuAG:Pr SCF/LuAG:Ce SC and LuAG:Sc SCF/LuAG:Ce SC composite scintillators are observed. Such differences can be characterized by the t_α/t_γ decay time ratio, which for the mentioned composite scintillators occurs within the 0.27–0.35 and 1.1–2.2 ranges, respectively, at scintillation decay intensity within two decades from the $1/e$ level down to 0.05 level.

The LuAG:Pr SCF/LuAG:Ce SC composite scintillator possesses some advantage with respect to LuAG:Sc SCF/LuAG:Ce SC counterpart due to the fact that scintillating signal coming from the SCF and SC components of the first type composite scintillator can be separated with the largest t_α/t_γ decay time ratio in the whole time interval from 0 to 700 ns. Meanwhile, in LuAG:Sc SCF/LuAG:Ce SC composite scintillator the signal coming from the SCF and SC components also can be simply separated with the large t_α/t_γ decay time ratio in the time interval from 200 to 900 ns. Thus, both types of the above mentioned composite scintillators can be successfully applied for separation of the signals coming from their film and bulk parts at the registration of the mixed radiation fluxes containing α -particles and γ -photons.

Concluding, we also hope that after optimization of the concentration of dopants and scintillation parameters of SCF and substrate scintillators the LuAG:Pr SCF/LuAG:Ce and LuAG:Sc SCF/LuAG:Ce combination can be concurrent with other combinations of garnet compounds for creation of composite scintillators for efficient simultaneous registration of α -particles and γ -quanta.

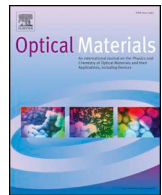
Acknowledgment

The work was performed in the framework of Polish NCN 2016/21/B/ST8/03200 project and Czech Science Foundation 16-15569S project and partly supported in the frame of Ukrainian MESY No SL 76 F project.

References

- [1] Yu Zorenko, S.S. Novosad, M.V. Pashkovskii, A.B. Lyskovich, V.G. Savitskii, M.M. Batenchuk, P.S. Malyutinov, N.I. Patsagan, I.V. Nazar, V.I. Gorbenko, J. Appl. Spectrosc. 52 (1990) 645.
- [2] B. Ferrand, B. Chambaz, M. Couchaud, Opt. Mater. 11 (1999) 101.
- [3] M. Nikl (Ed.), Nanocomposite, Ceramic, and Thin Film Scintillators, Pan Stanford Publ, Singapore, 978-981-4745-22-2, 2017.
- [4] E. Molva, Opt. Mater. 11 (1999) 289.
- [5] M. Klimczak, M. Malinowski, J. Sarnecki, R.J. Piramidowicz, J. Lumin. 129 (2009) 1869.
- [6] J.M. Robertson, M.V. Van Tol, Thin Solid Films 114 (1984) 221.
- [7] Z.D. Hrytskiv, Y. Zorenko, V. Gorbenko, A.D. Pedan, V.I. Shkliarskyi, Radiat. Meas. 42 (2007) 933.
- [8] Yu Zorenko, M. Batenchuk, V. Gorbenko, M. Pashkovsky, Proc. SPIE 2967 (1997) 101.
- [9] Yu Zorenko, V. Gorbenko, I. Konstankeyvych, B. Grinev, M. Globus, Nucl. Instrum. Meth. Phys. Res. A 486 (2002) 309–314.
- [10] A. Koch, C. Raven, P. Spanne, A. Snigirev, J. Opt. Soc. Am. A15 (1998) 1940.
- [11] T. Martin, A. Koch, J. Synchrotron Radiat. 13 (2006) 180.
- [12] Y. Zorenko, V. Gorbenko, I. Konstankeyvych, M. Pashkovsky, M. Globus, B. Grinov, V. Tarasov, P. Dorenbos, C.W.E. Van Eijk, E. Van Loef, V. Mikhailin (Ed.), Proceedings of the 5th Intern. Conference on Inorganic Scintillators and their Applications, Moscow State University, 2000.
- [13] M. Globus, B. Grinov, M. Ratner, V. Tarasov, V. Lyubinskiy, Yu Zorenko, I. Konstankeyvych, IEEE Nuclear Science Symposium and Medical Imaging

- Conference, 2002, p. 352.
- [14] Yu Zorenko, V. Gorbenko, T. Voznyak, I. Konstankevych, V. Savchyn, M. Batentschuk, A. Winnacker, Ch J. Brabec, IEEE Trans. Nucl. Sci. 59 (2012) 2281.
 - [15] S. Gobiein, Phoswich Detectors for High Energy Backgrounds, (Dec. 29, 2017) [Online]. Available: <http://www.detectors.saint-gobain.com>.
 - [16] M. Nikl, A. Yoshikawa, K. Kamada, K. Nejezchleb, C.R. Stanek, J.A. Mares, K. Blazek, M. Nikl, Cryst. Growth Charact. Mater. 59 (2013) 47.
 - [17] J.M. Ogieglo, A. Zych, T. Justel, A. Meijerink, C.R. Ronda, Opt. Mater. 35 (2013) 322.
 - [18] Yu Zorenko, V. Gorbenko, T. Voznyak, T. Martin, P.-A. Douissard, J.A. Mares, M. Nikl, Proc. SPIE 7310 (2009) 731007.
 - [19] M. Nikl, J. Tous, J.A. Mares, P. Prusa, E. Mihokova, K. Blazek, A. Vedda, Yu Zorenko, V. Gorbenko, V. Babin, Proc. SPIE 7310 (2009) 731008.
 - [20] V. Gorbenko, A. Krasnikov, M. Nikl, S. Zazubovich, Yu Zorenko, Opt. Mater. 31 (2009) 1805.
 - [21] N.N. Ryskin, P. Dorenbos, C.W.E. van Eijk, S. Kh Batygov, J. Phys. Condens. Matter 6 (1994) 10423.
 - [22] Yu V. Zorenko, Optic Spectrosc. 100 (2004) 572.
 - [23] Yu Zorenko, V. Gorbenko, A. Voloshinovskii, G. Stryganyuk, S. Nedilko, V. Degoda, O. Chykova, Phys. Stat. Sol. (c) 2 (2005) 105.
 - [24] Yu Zorenko, V. Gorbenko, T. Voznyak, V. Savchyn, S. Nizhankovskiy, A. Dan'ko, V. Puzikov, V. Laguta, J.A. Mares, M. Nikl, K. Nejezchleb, M. Batentschuk, A. Winnacker, Opt. Mater. 34 (2012) 2080.
 - [25] Yu Zorenko, V. Gorbenko, T. Zorenko, O. Sidletskiy, A. Fedorov, P. Bilski, A. Twardak, Phys. Stat. Sol. RRL 9 (2015) 489.
 - [26] S. Witkiewicz-Lukaszek, V. Gorbenko, T. Zorenko, O. Sidletskiy, I. Gerasymov, A. Fedorov, A. Yoshikawa, J.A. Mares, M. Nikl, Yu Zorenko, @Dec. 18, Cryst. Growth (2018) 1834.
 - [27] Y. Zorenko, A. Voloshinovskii, L. Konstankevych, V. Kolobanov, V. Mikhailin, D. Spassky, Radiat. Meas. 38 (2004) 677.
 - [28] Yu Zorenko, Phys. Stat. Sol. (c) 2 (2005) 375.



Alpha and gamma spectroscopy of composite scintillators based on the LuAG:Pr crystals and single crystalline films of LuAG:Ce and (Lu,Gd,Tb)AG:Ce garnets



J.A. Mares^{a,*}, S. Witkiewicz-Lukaszek^b, V. Gorbenko^b, T. Zorenko^b, R. Kucerkova^a, A. Beitlerova^a, C. D'Ambrosio^c, J. Dlouhy^a, M. Nikl^a, Yu Zorenko^b

^a Institute of Physics, Academy of Sciences of the Czech Republic, Cukrovarnicka 10, 16253, Prague 6, Czech Republic

^b Institute of Physics, Kazimierz Wielki University in Bydgoszcz, Powstancow Wielkopolskich 2, 85090, Bydgoszcz, Poland

^c CERN, EP-LHB Group, Geneva23, CH1211, Switzerland

ARTICLE INFO

Keywords:

Composite scintillators
Alpha and gamma spectroscopy
Garnets
Liquid phase epitaxy
LuAG:Pr crystals
LuAG:Ce and (Lu,Gd,Tb)AG:Ce single
crystalline films

ABSTRACT

Alpha and gamma spectroscopy (pulse height spectra and scintillation decay time profiles) were used to study scintillating properties of composite scintillators systems consisting of single crystalline films (SCF) and single crystal (SC) substrate plates. α -particles of ^{241}Am of energy 5.4857 MeV and γ -quanta of ^{137}Cs of energy 661.66 keV are used as excitation sources of SCFs or SC substrates, respectively. As SC substrates mainly LuAG:Pr single crystal plates are used and these plates are characterized by light yield (LY) between $10\text{--}21 \times 10^3$ ph/MeV, Energy Resolution (ER) $\sim 5\%$ at 661.66 keV and good proportionality. LuAG:Ce, $\text{Lu}_{2-x}\text{GdTb}_x\text{AG:Ce}$ and $\text{Lu}_{3-x}\text{Tb}_x\text{AG:Ce}$ SCFs at $x = 0.15\text{--}2.285$ were prepared by LPE method onto LuAG:Pr substrates and investigated. LY of LuAG:Ce SCF under α -particles excitation is about of 60% than that of LuAG:Pr SC substrate. The LY of $\text{Lu}_{3-x}\text{Tb}_x\text{AG:Ce}$ SCFs depend nonlinearly on Tb^{3+} concentration in the 0.15–2.285 range and changed from 60–62% to 106–109%, respectively, in comparison with LY of LuAG:Pr SC substrate. Detailed scintillation decay time profiles have shown that there are differences between the decay curves of composite scintillators under α -particles and γ -quanta excitations. Such differences are characterized using the t_α/t_γ ratio between the time of scintillation decay to $1/e$, 0.1, 0.05 and 0.02 levels under α -particles excitation (t_α) and γ -quanta excitation (t_γ). From all studied types of composite scintillators, based on the LuAG:Pr substrates, the highest value of t_α/t_γ ratio can be reached for $\text{Lu}_{3-x}\text{Tb}_x\text{AG:Ce}$ SCF/LuAG:Pr SC substrate composite scintillators at Tb content $x = 2.15\text{--}2.275$, where this ratio is equal to 4.2–6.2 at scintillation decay level of 0.1.

1. Introduction

The latest development in X- or γ -ray high resolution imaging radiography enables to reach imagining of objects of a few μm sizes [1–3]. Nowadays, the significant progress in high resolution imaging is obtained using the scintillating screens, based on single crystalline films (SCF) from various oxide compounds of garnet structure (e.g. LuAG:Ce, LuAG:Pr) prepared by liquid phase epitaxy (LPE) method [4–12]. This new progress resulted in screens having spatial resolution even in the submicron range [2,3]. For such a high resolution micro-radiography the scintillation light generated by X- or γ -rays transmitted through very thin crystalline scintillating plates is detected [2,6]. Thickness of crystalline plates is between 5 and 100 μm and these plates are glued on a single crystal (SC) substrate material. But besides crystal plates also

SCF screens were also tested in microradiography and in other applications such as scintillators for registration of α -, β - or other heavy particles, cathodoluminescence screens, and laser accessories [8–11,13,14].

Recently, a new technological approach based on the LPE method was developed for production of SCF based scintillators [3,4,15–18]. The LPE method allows growing thin SCFs with thickness from a few μm up to thick $\sim 100 \mu\text{m}$ onto bulk single crystal SC substrates of 0.5–2 mm thickness. Besides simple epitaxial structures (SCF and undoped substrate crystal) the LPE method enables to prepare also multilayer scintillating devices consisting from a few SCF layers deposited onto the same SC substrate [14,16,18]. These advanced kinds are called “composite” scintillators of phoswich type (phosphor sandwich). The multilayer SCFs or composite scintillators can be also used to resolve

* Corresponding author.

E-mail address: amares@fzu.cz (J.A. Mares).

different components of ionizing radiation beams, e.g. heavy particles and γ -quanta [14,16].

Main goal of this paper is to show how to characterize and how to measure scintillating properties of the SCFs and the single crystal substrates. For this purpose, we selected heavy, high Z_{eff} and fast LuAG crystals, doped with Ce^{3+} , Pr^{3+} and Sc^{3+} ions, as substrates for composite scintillators production. LuAG has density 6.71 g/cm³ and effective atomic number $Z_{\text{eff}} = 58.7$ [19,20]. Basic scintillating properties of SCFs or SC substrates were measured using pulse height spectra (or theirs scintillating response) [19,21–23]. Scintillating response covers the following properties as (i) N_{phels} photoelectron (in phels/MeV) and light yields (LY in ph/MeV) using chosen type of photomultiplier (PMT) but later absolute LYs of scintillators were evaluated from N_{phels} photoelectron yield, (ii) photopeak energy resolutions (ER) of used energy of ionizing radiation, (iii) non-proportionality of LY (measured only on SC substrate crystals) and (iv) scintillation intensity time profiles (decays characterized by τ lifetime values) [13,14,24–26].

From various type of composite scintillators we selected a sets of those based on the LuAG:Pr SC substrates. Namely, we have investigated several types of composite scintillators, based on the SCF of LuAG:Ce garnet, and SCFs of mixed Lu_{2-x}GdTb_xAl₅O₁₂:Ce and Lu_{3-x}Tb_xAG:Ce garnets with x value rending in the 0.15–2.285 range, grown by LPE method onto LuAG:Pr substrates. The change of cation content in the Lu₂Gd_{1-x}Tb_xAG:Ce and Lu_{3-x}Tb_xAG:Ce garnets scintillators enable the effective change of their scintillation properties suitable for creation of the composite scintillators [18,25]. For comparison, we have also studied and simulated the scintillating decay time profiles of Lu_{3-x}Tb_xAG:Ce ($x = 0.64$; 1.05 and 2.15) SCFs scintillators, grown onto undoped YAG substrates with those grown onto LuAG:Pr SC ones under α -particles and γ -ray excitations.

2. Experimental

2.1. Growth of composite scintillators

The sets of three types of composite scintillators based on LuAG:Ce, Lu_{2-x}GdTb_xAG:Ce and Lu_{3-x}Tb_xAG:Ce ($x = 0.15$ –0.3 and 1.65–2.285) SCFs and LuAG:Pr substrate (produced by Crytur Ltd., Turnov, Czech Republic) were grown by LPE method from super-cooled melt solutions using PbO–B₂O₃ flux in Institute of Physics UKW in Bydgoszcz (Table 1). The Tb concentration in the melt solution for SCF growth of the Tb containing garnets was in the $x = 0.15$ –2.0 range. Taking into account of the value of segregation coefficient of Tb³⁺ ions at LPE growth of Lu_{3-x}Tb_xAG:Ce SCFs onto LuAG substrates, been equal to 1.0 at the nominal Tb content in the $x = 0.15$ –0.3 range, and equal to 1.075 at Tb content in the $x = 1$ –2.0 range, the real terbium

concentrations in SCF samples were in the 0.15–0.3 and 1.65–2.285 ranges, respectively. The CeO₂ activator concentration in the melt solution for growth of all SCF samples was 10%, but due to very low segregation coefficient of Ce³⁺ ions at LPE growth onto LuAG substrates, the real Ce³⁺ content in SCF scintillators was in the 0.045–0.0825% range. For comparison, the sets of Lu_{3-x}Tb_xAG:Ce ($x = 0.65$, 1.05 and 2.15) SCF samples were also grown from the same melt onto YAG substrates (see [25,27] for details). It is important to note here that we do not used any additional doping for the elimination of the SCF/substrate misfit between Lu_{2-x}GdTb_xAl₅O₁₂:Ce and Lu_{3-x}Tb_xAG:Ce ($x = 1.65$ –2.285) and LuAG:Pr substrate as well between Lu_{3-x}Tb_xAG:Ce ($x = 0.65$ –2.15) SCFs and YAG substrate.

2.2. Investigation of scintillation characteristics

Three kinds of ionizing radiation could be used to excite and measure scintillating properties of the SCFs or composite scintillators and the SC substrates. These ionizing radiations are α - and β -particles and γ -quanta [22]. It is necessary to note that each of these ionizing sources interact differently with SCFs and SC substrates. Main difference between SCFs and the SC substrates is caused due to large difference between thickness of SCFs (1–80 μm) and SC substrates (0.5–2 mm). If we use γ -quanta for excitation of scintillation as 661.66 keV energy of ¹³⁷Cs radioisotope, a total attenuation coefficient of LuAG SC substrate is of about 0.095 cm²/g (see Fig. 1 and [24]) and this value allows excitation of scintillation in SC substrates but practically not of very thin SCFs. In opposite to γ -ray interaction, where mainly Compton scattering is present [20], α -particles (He²⁺ ions) interact immediately with electrons of the ions in SCF lattice and their penetration depth in LuAG garnet is about 10–12 μm [26]. Therefore, α -particles can excite only SCF layers while γ -ray quanta excite primarily the SC substrates and almost no SCF. For β -particles (high energy electrons) with average energy of 1.1 MeV their penetration depth in LuAG should be around of 0.8 mm [22]. Fig. 2 presents schema of transmission of α -particles and γ -quanta through SCF LuAG crystal and similar garnet structure crystals. From above mentioned properties of ionizing radiation we can conclude that for measurements of scintillating properties of SCFs or composite scintillators we should use (i) alpha spectroscopy - α -particles for scintillating response of SCFs and (ii) gamma spectroscopy - γ -quanta for scintillating response of the SC substrates [19,21,28,29]. Scintillation measurements of pulse height spectra using both α -particles and γ -quanta excitation sources were carried in two basic configuration:

(a) α -particle un-collimated source is placed directly on the upper sample area of measured samples (SCF/substrate, composite

Table 1

Scintillation properties of LuAG:Ce SCF/LuAG:Pr SC substrate, Lu_{1.7}Gd Tb_{0.3}AG:Ce SCF/LuAG:Pr SC and Lu_{3-x}Tb_xAG:Ce SCF/LuAG:Pr SC ($x = 0.15$, 1.65 and 2.285) composite scintillators and LuAG:Pr SC substrate measured under α -particles excitation of ²⁴¹Am (5.4857 MeV) and γ -rays quanta of ¹³⁷Cs (661.66 keV) at shaping times from 0.5 to 10 μs (*from 3 to 6 μs).

Sample SCF/Substrate	Sample thickness [μm]	LY [ph/MeV] excitation ²⁴¹ Am α -rays from 0.5 to 10 μs < Para Run-on->	LY [ph/MeV] excitation ¹³⁷ Cs γ -rays from 0.5 to 10 μs < Para Run-on->	ER (%) at 5.4857 MeV of ²⁴¹ Am α -rays from 0.5 to 10 μs	ER (%) at 661.66 keV of ¹³⁷ Cs γ -rays from 0.5 to 10 μs
LuAG:Pr SC substrate	1 mm	3057–4372	9718–12764	16.9–28.4	Photopeak 4.1–2.1
LuAG:Ce SCF/LuAG:Pr SC	27	1895–2622	9680–15414	13.7–22.7	14.1–13.4
Lu _{2.85} Tb _{0.15} AG:Ce SCF/LuAG:Pr SC	15	1721–2339	6597–11147	17.8–43.5	16.5–15.2
Lu _{1.7} GdTb _{0.3} AG:Ce SCF/LuAG:Pr	20	547–835	6129–9853	23.3–65.9	14.9–13.9
Lu _{1.35} Tb _{1.65} AG:Ce SCF/LuAG:Pr SC	38	1703–2252*	7438–7149*	21–22.5*	14.2–15.6*
Lu _{0.715} Tb _{2.285} AG:Ce SCF/LuAG:Pr SC	32	3234–4707*	7821–9107*	31.7–9.6*	18.8–12.7*

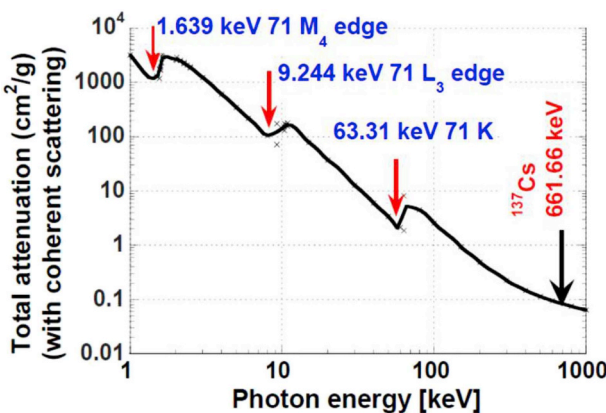


Fig. 1. Linear attenuation coefficient of LuAG crystal calculated from X-Ray and Gamma-Ray Data [24].

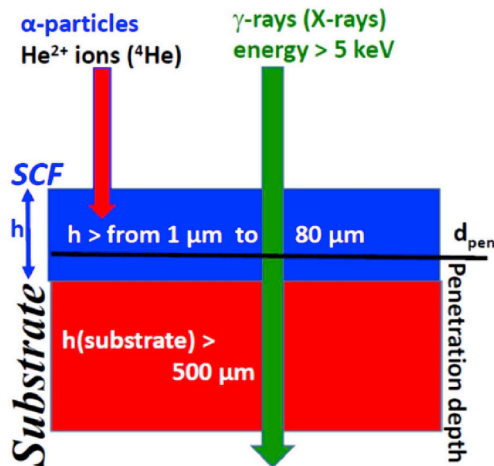


Fig. 2. Schema of transmission of α -particles and γ -quanta through SCF and the substrate (h – thicknesses of SCF are in the range 1 μm up to 100 μm , thicknesses of substrates are in the range 0.5–2 mm and d_{pen} – penetration depths of the α -particles are of about 10–12 μm for heavy (Lu,Gd) based or multi-component garnets [26]).

scintillator or even the SC substrates) and the lower sample area is in contact with the photocathode window via thin silicon oil layer used for improves light connection with the photocathode [19,21,26].

(b) At γ -quanta excitation samples are usually covered with Teflon tape with an exception of the lower sample side which is in direct contact with the photocathode window via silicone oil again. The used γ -quanta sources are un-collimated ones are placed a few mm (between 2 and 8 mm) above upper sides of the samples.

From different α -particles and γ -quanta radioactive sources we used those “stable” with relatively long half-life as (i) α -particle source ²⁴¹Am of energy 5.4857 MeV or (ii) γ -quanta source ¹³⁷Cs of energy 661.66 keV. Both these sources have half-lives \sim 450 years and \sim 30 years, respectively, and they allow reliable scintillation response measurements (N_{phels} photoelectron and absolute LY yields, energy resolution, non-proportionality and decay time profiles) [12,15–17].

Real measurements of scintillating properties of SCF/substrate, composite scintillators and the SC substrates were carried out with “special” hybrid photomultiplier (HPMT) which consists of only a front photocathode and an anode which is Si/PIN diode [19,21,22,28,29]. The whole set-up consists of that special HPMT with preamplifier (Model DEP PP0475B, the Netherlands), an ORTEC model 672 spectroscopy amplifier, an ORTEC model 972TM multichannel buffer and a

control PC. This set-up was calibrated in photoelectrons (N_{phels} photo-electron yield) using single, double and multi-photoelectron peaks [21]. Light Yield (LY) in photons/MeV was determined using (i) average quantum efficiency $\langle Q_{\text{ave}} \rangle$ and by (ii) set-up has high light collection efficiency from sample into HPMT (maximizing of reflection of generating scintillating photons into HPMT). $\langle Q_{\text{ave}} \rangle$ was calculated by integration of wavelength dependent $Q_{\text{eff}}(\lambda)$ of the used HPMT (values of $Q_{\text{eff}}(\lambda)$ were given by the manufacturer) with wavelength dependent scintillation intensity $I(\lambda)$ in the wavelength range of scintillation emission spectrum [28,29]. The set-up we used allows N_{phels} photo-electron yield measurements using shaping times from 0.5 to 10 μs [13,19]. Measurements of pulse height spectra was carried out using MAESTRO program which includes single Gaussian fits of measured photopeak bands. The energy dependent $N_{\text{phels}}(E)$ peaks and half-widths FWHM(E) were determined from the Gaussian fits and so LY(E) and Energy resolutions (ER) were from the fits calculated.

Scintillation time decay profiles were measured again using either with α -particles of ²⁴¹Am of energy 5.4857 MeV or with γ -quanta of energy 661.66 MeV of ¹³⁷Cs. Samples were put onto front photocathode window (with silicone oil between) of Hamamatsu PMT R375 and the radioactive sources are placed (i) on upper side of samples if α -particles were used or (ii) a few mm above upper side of samples if γ -quanta were used but upper sides of samples were covered by Teflon tape again [19,26]. Output signal from the used PMT is detected by an oscilloscope 500 MHz Tektronix TDS 3052S. α - particles and γ -quanta generate accidentally scintillating photons in measured samples and individual scintillating decays are recorded by the oscilloscope and finally the decays are summarized and averaged using PC.

3. Results and discussions

3.1. Characterization of scintillating properties of the SC substrates

LuAG crystals doped with Ce³⁺, Pr³⁺ and Sc³⁺ are used as SC substrates for SCFs [13,16,17]. The cathodoluminescence of LuAG crystals with these dopants are presented in Fig. 3(a) and (b). The most intense broad emission bands are peaking at \approx 515 nm (Ce³⁺), at \approx 310 nm (Pr³⁺) and at \approx 260 nm (Sc³⁺). Pulse height spectra of LuAG substrate crystals, doped with Ce³⁺, Pr³⁺ and Sc³⁺ ions, measured at 661.66 keV energy of ¹³⁷Cs radioisotope are presented in Fig. 4. Photo-peak positions of Ce³⁺, Pr³⁺ and Sc³⁺ dopants depends on (i) the main emission peak and on (ii) on the quantum efficiency curve of used HPMT (details in [19,21]). These pulse height spectra of 661.66 keV energy of ¹³⁷Cs show the main photo-peaks and additionally the escape-peaks, which are lying on low energy side of the main photo-peak. These escape peaks are observed on Pr³⁺ and Sc³⁺ dopants clearly but that on Ce³⁺-doped such observation is less considerable [15]. Besides the photo- and escape peaks, low-energy ¹³⁷Cs peaks are observed also at 32.006 keV. All these pulse height spectra were measured on 1 mm thick LuAG crystal samples from which the SC substrates were prepared.

Scintillating response N_{phels} photoelectron yields (and evaluated absolute LY values) were measured using different shaping times 0.5, 1, 2, 3, 6 and 10 μs . LY values for each shaping time are given in Fig. 5. Ce³⁺, Pr³⁺ and Sc³⁺ doped LuAG crystals can be characterized by the following scintillating properties:

- (a) LuAG:Ce can reach LY $\approx 15\text{--}28 \times 10^3$ ph/MeV in the shaping time range 0.5–10 μs , ER at 661.66 keV is $\approx 9\%$ and nonproportionality (at 1 μs shaping time) is in the range 70–100% from 10 to 1300 keV; change beginning of this row
- (b) LuAG:Pr can reach LY in the range $\approx 10\text{--}21 \times 10^3$ ph/MeV in the shaping time range 0.5–10 μs , ER at 661.66 keV is $\sim 5\%$ and nonproportionality (at 1 μs shaping time) is in the range 80–100% from 10 to 1300 keV;
- (c) LuAG:Sc can reach LY in the range $\approx 16\text{--}22 \times 10^3$ ph/MeV in the

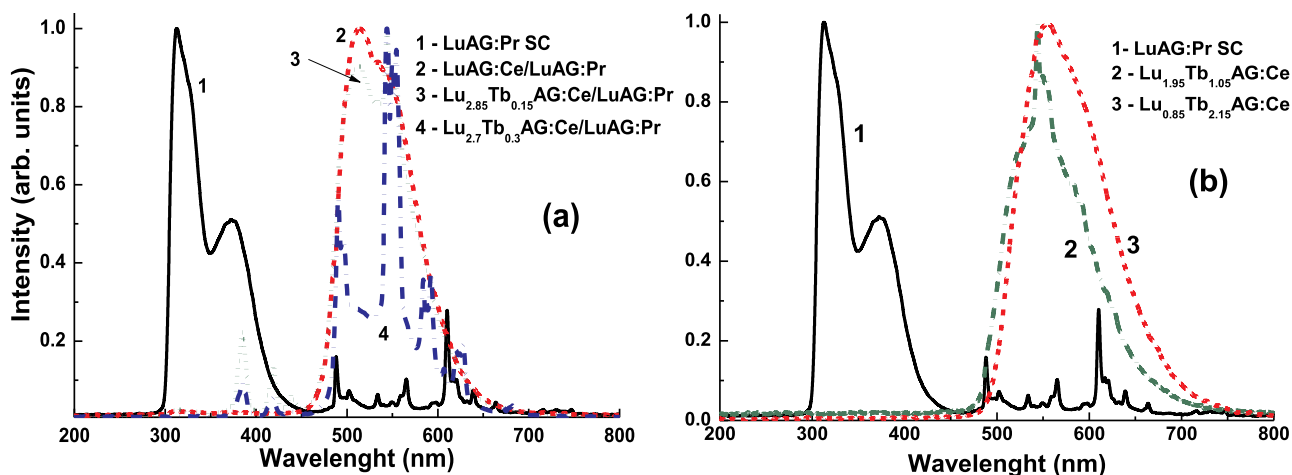


Fig. 3. Cathodoluminescence spectra of the components of composite scintillators: LuAG:Pr crystal substrate (1a and 1b), LuAG:Ce SCF (2a), Lu_{2.85}Tb_{0.15}AG:Ce SCF (3a), Lu_{2.7}Tb_{0.3}AG:Ce SCF (4a), Lu_{1.95}Tb_{1.05}AG:Ce SCF (2b) and Lu_{0.85}Tb_{2.15}AG:Ce SCF (3b).

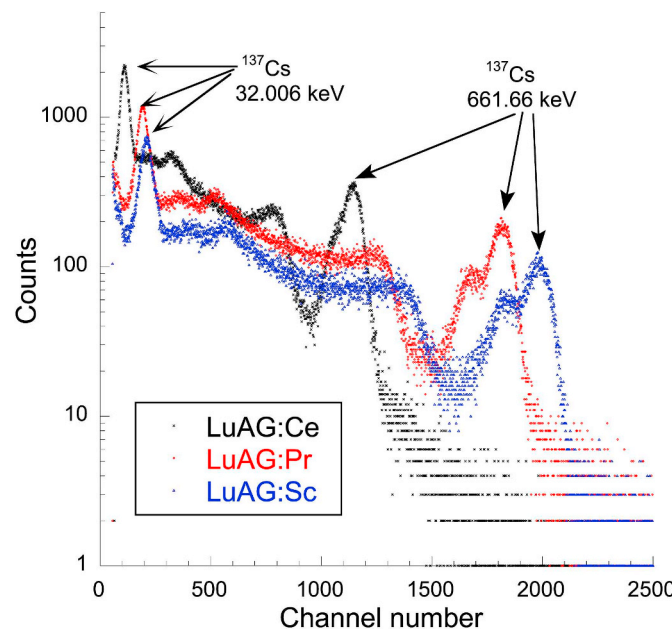


Fig. 4. Pulse height spectra of Ce³⁺, Pr³⁺ and Sc³⁺ doped LuAG crystals under excitation by the energy 661.66 keV of γ -ray radiation of ¹³⁷Cs radioisotope (measured using HPMT set-up with shaping time 10 μ s).

shaping time range 0.5–10 μ s, ER at 661.66 keV is ~5% and non-proportionality (related to LY value at 661.66 keV) was evaluated from LY energy dependence measured at various energies in the energy range 10–1300 keV (details of these measurements will be published later). Results of investigation basic scintillating parameters have shown that Ce³⁺, Pr³⁺ and Sc³⁺ doped LuAG crystals have appropriate parameters to be used as SC substrates for composite scintillators.

ER values will be discussed in the next part 3.2. and non-proportionality (related to LY value at 661.66 keV) was evaluated from LY energy dependence measured at various energies in the energy range 10–1300 keV (details of these measurements will be published later). Results of investigation basic scintillating parameters have shown that Ce³⁺, Pr³⁺ and Sc³⁺ doped LuAG crystals have appropriate parameters to be used as SC substrates for composite scintillators.

3.2. Characterization of scintillating properties of SCFs

For characterization of scintillating properties of composite scintillators of SCF/substrate type, we selected two groups of samples based on the LuAG:Pr SC substrates. Firstly, the samples of LuAG:Ce SCF/LuAG:Pr SC, Lu_{2.85}Tb_{0.15}AG:Ce SCF/LuAG:Pr SC and

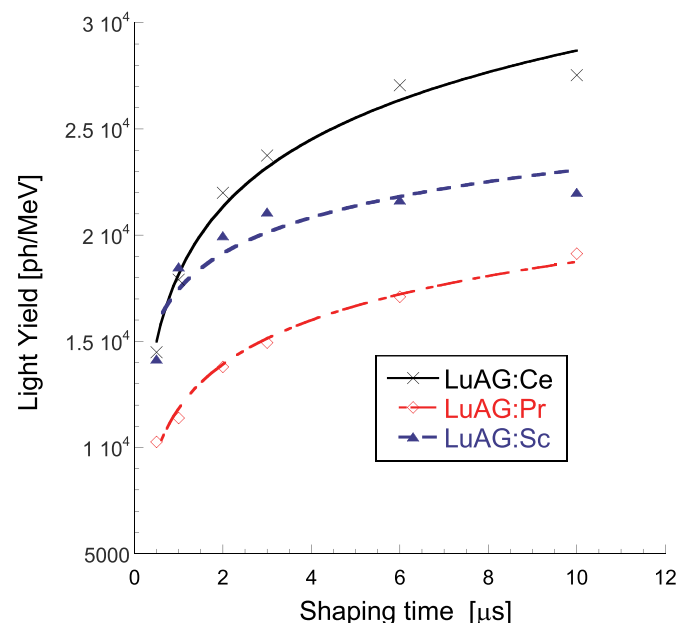


Fig. 5. LY as a function of shaping times of the substrates Ce³⁺, Pr³⁺ and Sc³⁺ doped LuAG single crystals measured using HPMT set-up (shaping times in the range 0.5–10 μ s)

Lu_{1.7}GdTb_{0.3}Al₅O₁₂:Ce SCF/LuAG:Pr SC composite scintillators and reference LuAG:Pr SC substrate were investigated in detail. Later the set of Lu_{3-x}Tb_xAl₅O₁₂:Ce SCFs/LuAG:Pr SC substrate composite scintillators were grown at x = 1.65 and 2.285 and ones properties were investigated in comparison with properties of the first group.

Pulse height spectra of the first group of composite scintillators and LuAG:Pr substrate under α -particles excitation by energy 5.4857 MeV energy of ²⁴¹Am radioisotope are presented in Fig. 6. Besides the main broad peak of total absorption of α -particles of 5.4857 MeV of ²⁴¹Am the narrow γ -quanta photopeak at energy 59.54 keV of ²⁴¹Am radioisotope is also observed.

Under α -particles excitation by ²⁴¹Am radioisotope (see Fig. 6) observed pulse height spectra of composite scintillators and LuAG:Pr substrate consist of wide bands peaking at different channel number values. Evaluated LY yields for the shaping times 0.5–1 – 2–3 – 6–10 μ s are displayed in Fig. 7 and in Table 1. The highest LY ~60% of that of LuAG:Pr SC substrate under α -particles excitation exhibits composite scintillator on the base of LuAG:Ce SCF/LuAG:Pr SC substrate.

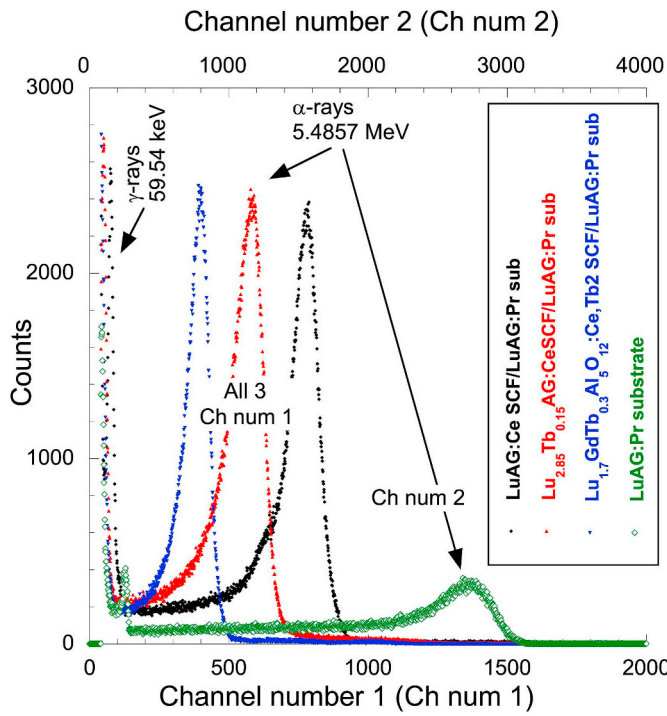


Fig. 6. Pulse height spectra of composite scintillators based on the LuAG:Ce SCF, Lu_{2.85}Tb_{0.15}AG:Ce SCF and Lu_{1.7}GdTb_{0.3}Al₅O₁₂:Ce SCF grown onto the same LuAG:Pr SC substrate, under excitation of α -particles of ^{241}Am of energy 5.4857 MeV (measured using HPMT set-up with shaping time 3 μs).

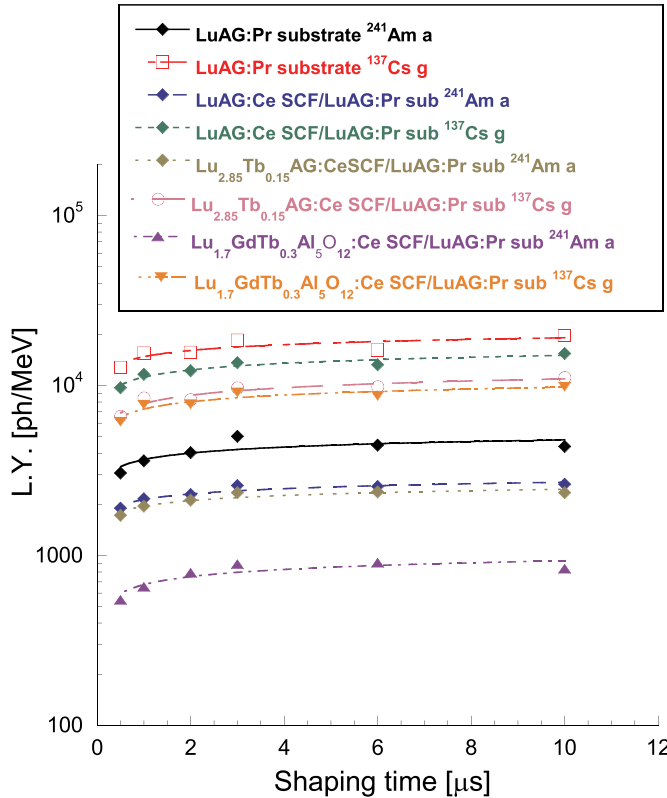


Fig. 7. LY as a function of shaping times of the composite scintillators based on the same LuAG:Pr SC substrate with the following SCFs - LuAG:Ce SCF, Lu_{2.85}Tb_{0.15}AG:Ce and Lu_{1.7}GdTb_{0.3} Al₅O₁₂:Ce under excitation either by α -particles of ^{241}Am radioisotope (5.4857 MeV) or γ -quanta of ^{137}Cs of energy 661.66 keV (measured using HPMT set-up).

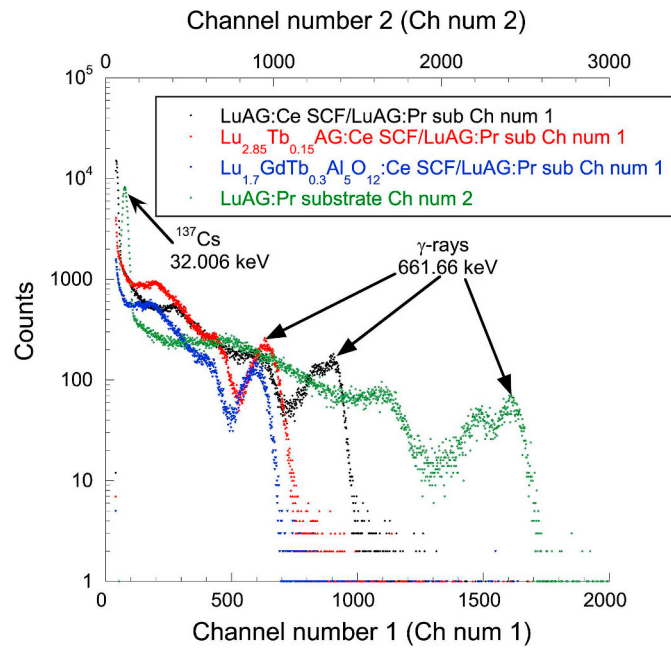


Fig. 8. Pulse height spectra of composite scintillators based on the LuAG:Ce SCF, Lu_{2.85}Tb_{0.15}AG:Ce SCF and Lu_{1.7}GdTb_{0.3}Al₅O₁₂:Ce SCF grown onto the same LuAG:Pr SC substrate under excitation of γ -quanta of ^{137}Cs of energy 661.66 keV (measured using HPMT set-up with shaping time 3 μs).

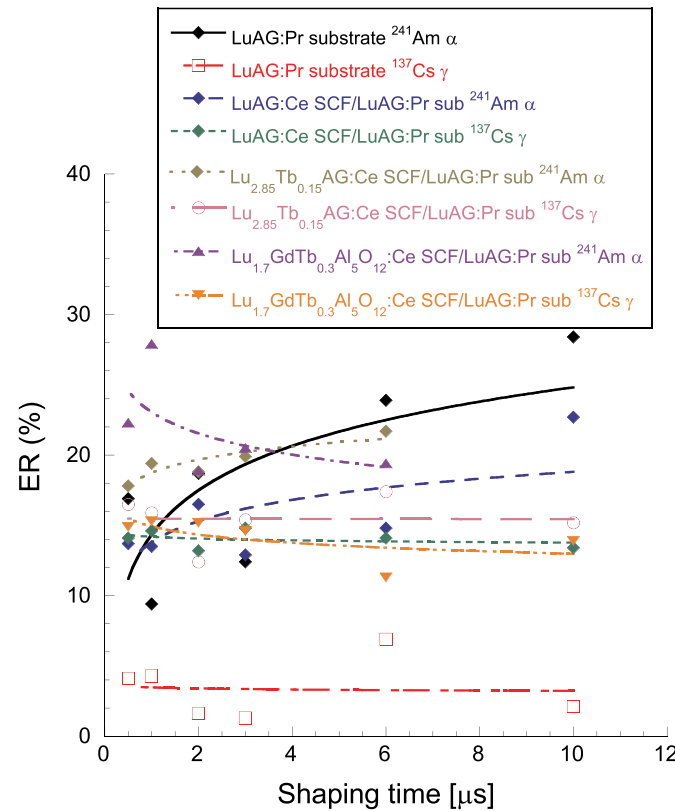


Fig. 9. ER as a function of shaping times of the composite scintillators based on the same LuAG:Pr SC substrate and the following SCFs - LuAG:Ce SCF, Lu_{2.85}Tb_{0.15}AG:Ce SCF and Lu_{1.7}GdTb_{0.3}Al₅O₁₂:Ce SCF under excitation either by α -particles of ^{241}Am radioisotope of energy 5.4857 MeV or γ -ray radiation of ^{137}Cs of energy 661.66 keV (measured using HPMT set-up).

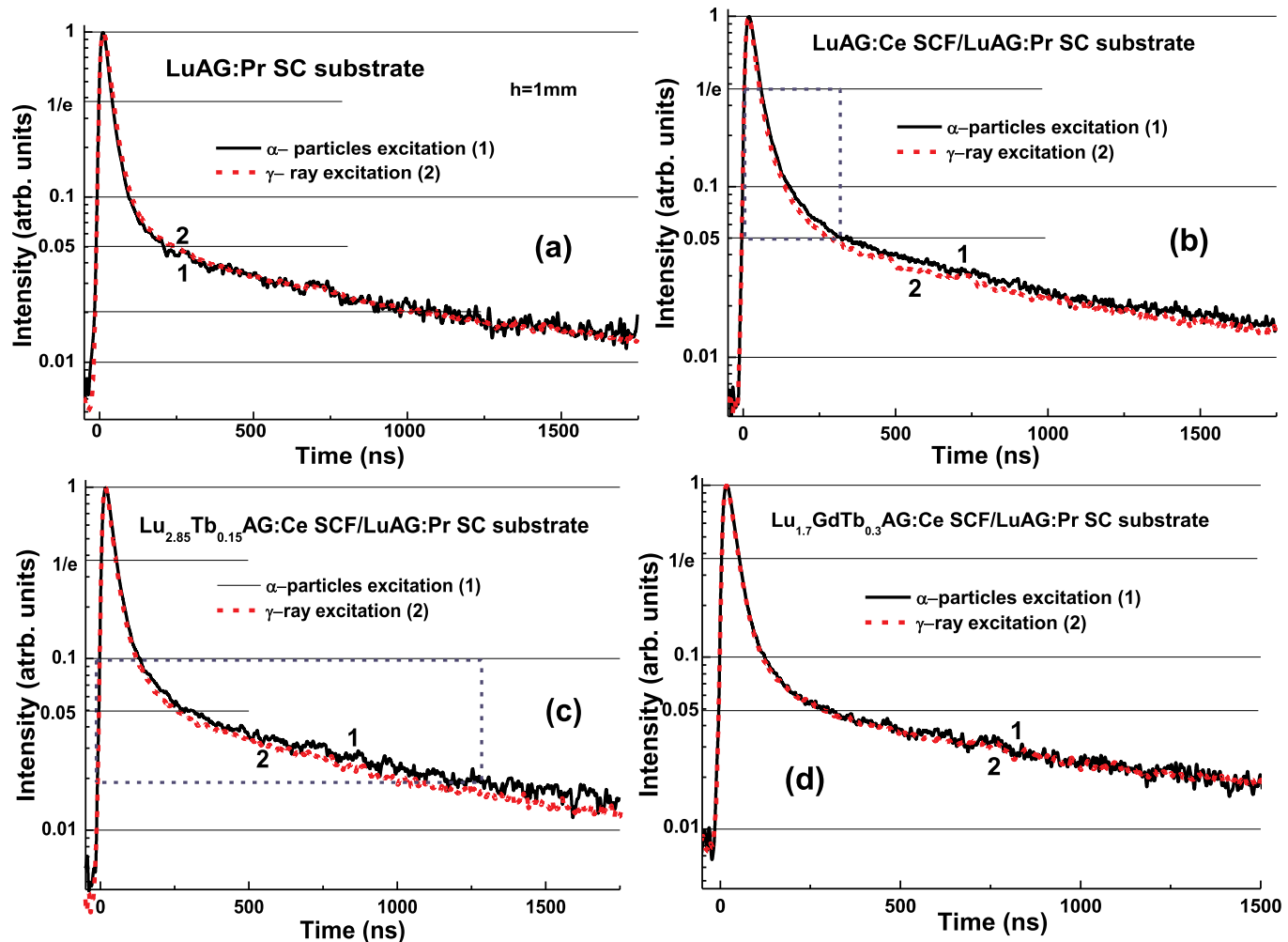


Fig. 10. Scintillation decay curves of LuAG:Pr SC substrate (a) and LuAG:Ce SCF/LuAG:Pr SC (b), Lu_{2.85}Tb_{0.15}AG:Ce SCF/LuAG:Pr SC (c) and Lu_{1.7}GdTb_{0.3}AG:Ce SCF/LuAG:Pr SC (d) composite scintillators of under α -particles (1) and γ -quanta (2) excitation by ²⁴¹Am and ¹³⁷Cs sources, respectively.

Table 2

Scintillation decay parameters of the LuAG:Pr SC substrate and LuAG:Ce SCF/LuAG:Pr SC, Lu_{1.7}GdTb_{0.3}AG:Ce SCF/LuAG:Pr SC and Lu_{3-x}TbxAG:Ce SCF/LuAG:Pr SC ($x = 0.15, 1.65$ and 2.285) composite scintillator under by α -particles of ²⁴¹Am (5.4857 MeV) source and γ -quanta by ¹³⁷Cs (661.66 keV) source (compositions see column at the left).

Sample	Excitation	τ_{fast} [ns]/(relat. amp) %	$\tau_{\text{slow}}(1)$ [ns]/(relat. amp) %	$\tau_{\text{slow}}(2)$ [ns]/(relat. amp) %
LuAG:Pr substrate	α -particles	20.5 (92.7)	108 (4.9)	996 (2.4)
LuAG:Pr substrate	γ -rays	23.1 (92.7)	121 (4.6)	937 (2.7)
LuAG:Ce SCF/LuAG:Pr SC	α -particles	26.5 (85.4)	99.3 (11.1)	965 (3.5)
LuAG:Ce SCF/LuAG:Pr SC	γ -rays	21.2 (82.4)	81.1 (14.6)	991 (3)
Lu _{2.85} Tb _{0.15} AG:Ce SCF/LuAG:Pr SC	α -particles	24.3 (88.4)	103 (8.5)	1010 (3.1)
Lu _{2.85} Tb _{0.15} AG:Ce SCF/LuAG:Pr SC	γ -rays	21.1 (85.1)	79.2 (11.9)	969 (3.0)
Lu _{1.7} GdTb _{0.3} AG:Ce SCF/LuAG:Pr SC	α -particles	23.6 (89.5)	91.7 (7.4)	1007 (3.1)
Lu _{1.7} GdTb _{0.3} AG:Ce SCF/LuAG:Pr SC	γ -rays	22.0 (90.7)	106.1 (6.6)	1022.1 (2.7)
Lu _{1.35} Tb _{1.65} AG:Ce SCF/LuAG:Pr SC	α -particles	31.0 (86.4)	454 (11.7)	6067 (1.8)
Lu _{1.35} Tb _{1.65} AG:Ce SCF/LuAG:Pr SC	γ -rays	40.7 (85.4)	273 (11.7)	3226 (2.8)
Lu _{0.715} Tb _{2.285} AG:Ce SCF/LuAG:Pr SC	α -particles	53.3 (84)	395 (12.8)	3667 (2.7)
Lu _{0.715} Tb _{2.285} AG:Ce SCF/LuAG:Pr SC	γ -rays	58.8 (89)	608 (8.4)	4252 (2.6)

Meanwhile, Tb³⁺ codoping of LuAG:Ce SCF in concentration range $x = 0.15$ – 0.3 leads to the decrease of LY of SCFs scintillators (see Figs. 6 and 7); and the Lu_{2.85}Tb_{0.15}AG:Ce SCF/LuAG:Pr SC and Lu_{1.7}GdTb_{0.3}Al₅O₁₂:Ce/LuAG:Pr SC composite scintillators exhibit less intense LY than that mentioned above (Table 1). Most interesting here is that the LY of highly Tb³⁺ doped Lu_{3-x}TbxAG:Ce ($x > 2$) is comparable and even little bit large that that in LuAG:Pr substrate (Table 1).

Pulse height spectra under γ -quanta excitation by the energy of

661.66 keV of ¹³⁷Cs radioisotope of first group of composite scintillators under study are presented in Fig. 8. Besides the ¹³⁷Cs photopeaks, the escape peaks were observed also on low energy sides of the photopeaks (see Fig. 8). Apart the photo- and escape peaks, the low-energy ¹³⁷Cs peak are observed also at 32.006 keV.

It is important to note, that we have observed different positions of ¹³⁷Cs photopeaks from the LuAG:Ce SCF/LuAG:Pr SC, Lu_{2.85}Tb_{0.15}AG:Ce SCF/LuAG:Pr and Lu_{1.7}GdTb_{0.3}Al₅O₁₂:Ce/LuAG:Pr

Table 3

Time dependence of scintillation intensity decays from the initial value at $t = 0$ to values $1/e$, 0.1, 0.05 and 0.02 level for LuAG:Pr SC substrate and LuAG:Ce/LuAG:Pr, Lu_{2.85}Tb_{0.15}AG:Ce/LuAG:Pr and Lu_{1.75}GdTb_{0.3}AG:Ce/LuAG:Pr composite scintillators.

Intensity decay level	LuAG:Pr substrate		LuAG:Ce/LuAG:Pr		Lu _{2.85} Tb _{0.15} AG:Ce/LuAG:Pr		Lu _{1.75} GdTb _{0.3} AG:Ce/LuAG:Pr	
	t_γ [ns]	t_α [ns]	t_γ [ns]	t_α [ns]	t_γ [ns]	t_α [ns]	t_γ [ns]	t_α [ns]
1/e	47.5	44.4	50.6	55.3	47.9	51.4	50	50
0.1	110.25	102.4	138.6	155.4	122.4	134.0	126.1	126.1
0.05	250.4	231.3	295.6	326.7	254.7	315.4	306.2	306.2
0.02	1090.5	1145						

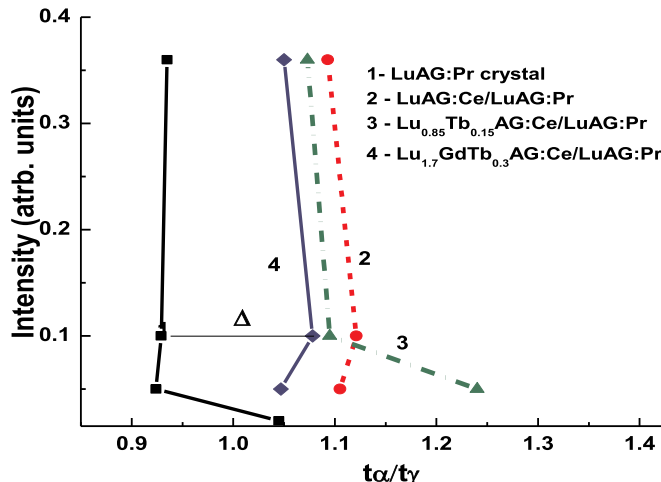


Fig. 11. A plot of t_α/t_γ ratio of the decay time under α - and γ -excitations on intensity of scintillation decay to $1/e$, 0.1 and 0.05 levels for LuAG:Pr SC substrate (1), LuAG:Ce SCF/LuAG:Pr SC (2), Lu_{2.85}Tb_{0.15}AG:Ce SCF/LuAG:Pr SC (3) and Lu_{1.7}GdTb_{0.3}AG:Ce SCF/LuAG:Pr SC (4) composite scintillators.

epitaxial structures. The largest LY is observed in LuAG:Ce SCF/LuAG:Pr SC sample, when for last epitaxial structures the LY is decreased with increasing of Tb content in 0.15–0.3 range in SCFs samples. That means that LY of SCF scintillators is notably influenced on the total scintillation LY of (Lu,Gd,Tb)AG:Ce based SCFs/LuAG:Pr SC composite scintillators under γ -quanta excitation.

In our opinion, such unwanted properties of composite scintillators under study can be related mainly to use of LuAG:Pr substrate. Recently we have investigated the scintillation properties of LuAG:Pr SCF/LuAG:Ce SC and LuAG:Sc SCF/LuAG:Ce SC composite scintillators [16]. Meanwhile, for such types of composite scintillators, the positions of main photo-peaks under γ -quanta excitation by ^{137}Cs source is quite close to the peak position in LuAG:Ce substrate [16]. Similar behaviour were observed also for Lu_{1.5}Gd_{1.5}Al₂Ga₃O₁₂:Ce SCF/GAGG:Ce and TbAG:Ce SCF/GAGG:Ce SC composite scintillators, where no influence of SCF components on the position of main photo-peak of composite scintillators is observed under γ -quanta excitation [14]. For this reason, we can conclude, that the difference in the position of photo-peaks of composite scintillators and substrate under γ -quanta excitation is observed only in the case when the emission spectra of substrates are strongly different with respect to the luminescence spectrum of SCFs (Fig. 3).

Detailed values of LYs of the first group of composite scintillators both under α -particles and γ -quanta excitation are summarized in Table 1 (or are sketched in Fig. 7). Table 1 presents also ER values under α -particles and γ -quanta excitation and these values as function of shaping times are presented in Fig. 9. Under γ -quanta excitation by 661.66 keV of ^{137}Cs the best ER has one of LuAG:Pr substrates $\sim 5\%$ while other LuAG:Ce and LuAG:Sc substrates have ER higher ~ 14 –16%. Under α -particle excitation the ER of 5.4857 MeV of ^{241}Am of the substrates and SCFs are in the range 15–25% (see Fig. 9 and Table 1).

3.3. Scintillation decay time profiles of composite scintillators

Scintillation decay time profiles of LuAG:Ce SCF/LuAG:Pr SC, Lu_{2.85}Tb_{0.15}AG:Ce/LuAG:Pr SC, Lu_{1.7}GdTb_{0.3}AG:Ce/LuAG:Pr SC, Lu_{1.35}Tb_{1.65}AG:Ce/LuAG:Pr and Lu_{0.715}Tb_{2.285}AG:Ce/LuAG:Pr composite scintillators and as well as LuAG:Pr SC substrate have been measured under α -particles (^{241}Am) and γ -quanta (^{137}Cs) excitation. Additionally we have simulated scintillation decay time profiles for Lu_{3-x}Tb_xAG:Ce SCFs at $x = 0.65$; 1.05 and 2.15, grown mainly onto YAG substrates [25,27], under α -particles excitation with decay profile of LuAG:Pr substrate under γ -quanta excitation. We have calculated either (i) scintillation decay intensities at values $1/e$, 0.1, 0.05 or 0.07 and 0.02 (this last value was calculated only for LuAG:Pr SC substrate) or (ii) fits of individual decay time curves were carried using 3-exponential approximation [12,14,25,27]. We have also calculated a ratio t_α/t_γ of scintillation time decay intensities at above given decay intensity values for α -particles or γ -quanta excitation.

Detailed results of scintillation decay time curves of composite scintillators based on LuAG:Pr SC substrate are sketched in Fig. 10 (a) – (d), parameters of 3-exponential fits are presented in Table 2 and selected decay time intensities levels t_α or t_γ are summarized in Table 3. Fig. 10(a) shows scintillation decay kinetic of LuAG:Pr SC substrate under α -particles and γ -quanta excitation. This crystal has almost the same values of the fast decay lifetimes $\tau_{\text{fast}}(\alpha) = 20.5$ ns and $\tau_{\text{fast}}(\gamma) = 23.1$ ns and their relative amplitude is the same $\sim 92.7\%$. On LuAG:Pr SC substrate we have observed slower decay components with lifetimes ~ 110 ns and 1000 ns but both have very low relative amplitude (see Table 2). Other decay time curves 10(b), 10(c) and 10(d) are decay time curves of investigated composite scintillators under α -particles and γ -quanta excitation. Here, for all three composite scintillators we have observed small differences between under α -particles and γ -quanta excited decay time curves. Detailed explanation of behaviour of decay time curves from Fig. 10 can explain a plot of selected decay time intensity values versus t_α/t_γ ratio presented in Fig. 11. These plots of t_α/t_γ and intensities of scintillation decays to $1/e$, 0.1 and 0.05 levels for LuAG:Pr SC substrate (1) as well as for LuAG:Ce SCF/LuAG:Pr SC (2), Lu_{2.85}Tb_{0.15}AG:Ce SCF/LuAG:Pr SC (3) and Lu_{1.7}GdTb_{0.3}AG:Ce SCF/LuAG:Pr SC (4) composite scintillators show differences between decay curves under α -particles or γ -quanta excitations of composite scintillators. Parameter Δ (definition see Fig. 11 (a)) shows a plot of difference between t_α/t_γ ratios for individual composite scintillators. Figs. 10 and 11 show the most important result that there is possibility of simultaneous registration of α -particles and γ -quanta by the way of separation of the scintillation decay time profiles of LuAG:Pr substrate crystals (Fig. 10(a)) and those of various composite scintillators based on the LuAG:Ce SCF/LuAG:Pr SC (Fig. 10(b)); Lu_{2.85}Tb_{0.15}AG:Ce SCF/LuAG:Pr SC (Fig. 10(c)) and Lu_{1.7}GdTb_{0.3}AG:Ce SCF/LuAG:Pr SC (Fig. 10(d)) epitaxial structures.

Finally, we also add one of the newest important results which is connected with the consideration of possibility of the creation of Lu_{3-x}Tb_xAG:Ce SCF/LuAG:Pr SC substrate composite scintillator at $x = 0.65$ –2.285 [25,27]. Fig. 12 (a) presents of simulation of the differences in scintillation decay kinetic of Lu_{3-x}Tb_xAG:Ce SCFs at $x = 0.65$; 1.05 and 2, grown onto YAG substrates, under α -particles excitation,

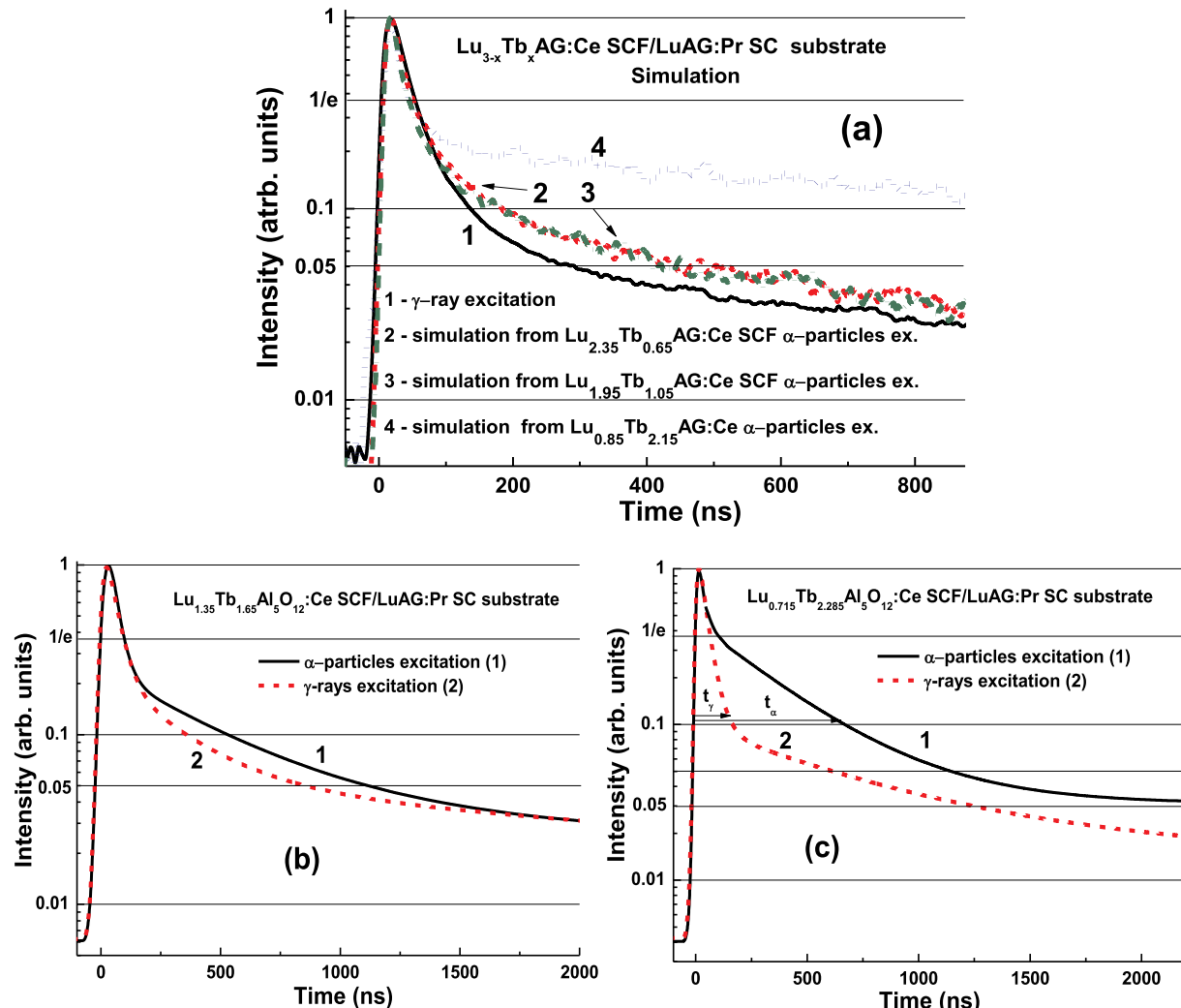


Fig. 12. (a) – simulation of the scintillation decay of $\text{Lu}_{3-x}\text{Tb}_x\text{AG:Ce}$ SCF/LuAG:Pr SC composite scintillators at Tb content $x = 0.65$ (2); 1.05 (3) and 2.15 (4) under γ -ray (1) and α -particles (2–4) excitation by ^{137}Cs and ^{241}Am sources, respectively. (b, c) - scintillation decay curves of $\text{Lu}_{3-x}\text{Tb}_x\text{AG:Ce}$ SCF/LuAG:Pr SC composite scintillators at Tb content $x = 1.65$ (b) and 2.285 (c) under α -particles (1) and γ -ray (2) excitation by mentioned above sources.

Table 4

Time dependence of scintillation intensity decays from the initial values at $t = 0$ to $1/e$, 0.1 and 0.05 levels for $\text{Lu}_{3-x}\text{Tb}_x\text{Al}_5\text{O}_{12}:\text{Ce}$ SCF/ LuAG:Pr SC composite scintillators at $x = 0.65$; 1.65, 2.15 and 2.275.

Intensity Decay level	$\text{Lu}_{0.25}\text{Tb}_{0.65}\text{Al}_5\text{O}_{12}:\text{Ce}$ / LuAG:Pr		$\text{Lu}_{1.35}\text{Tb}_{1.65}\text{Al}_5\text{O}_{12}:\text{Ce}$ / LuAG:Pr		$\text{Lu}_{0.85}\text{Tb}_{2.15}\text{Al}_5\text{O}_{12}:\text{Ce}$ / LuAG:Pr		$\text{Lu}_{0.71}\text{Tb}_{2.275}\text{Al}_5\text{O}_{12}:\text{Ce}$ / LuAG:Pr	
	t_α [ns]	t_γ [ns]	t_α [ns]	t_γ [ns]	t_α [ns]	t_γ [ns]	t_α [ns]	t_γ [ns]
1/e	51.3	54	101.3	107.2	45.4	56.8	109.5	70.3
0.1	184	141.5	540	373	863	139.2	744	178
0.07							1484.5	622.5
0.05	445	296.7	1138	863				1284

and LuAG:Pr substrate under γ -quanta excitation (parameters of scintillation decay of measured scintillators are given in Table 4). As can be seen from Fig. 12 (a) and Table 4, in the Tb^{3+} containing garnets (as lattice ions) due to an effective $\text{Tb}^{3+} \rightarrow \text{Ce}^{3+}$ energy transfer and elongation of the decay time of Ce^{3+} luminescence [18,27], the significantly large differences between t_α and t_γ scintillation decay intensities values are observed in $\text{Lu}_{3-x}\text{Tb}_x\text{AG:Ce}$ SCFs/LuAG:Pe composite scintillators when the Tb^{3+} cation concentration is above $x = 1.5$. Therefore, we were supposed here, that in the case of successful crystallization of $\text{Lu}_{3-x}\text{Tb}_x\text{AG:Ce}$ SCFs onto LuAG:Pr substrate at $x > 1.5$, the separation of the scintillation signal under α -particles and γ -quanta excitation can be

significantly higher.

The following results on LPE growth to confirm such our assumption. The crystallization of $\text{Lu}_{3-x}\text{Tb}_x\text{AG:Ce}$ SCFs onto LuAG:Sc substrates at nominal Tb content $x = 1.5$ and 2.0 at significant (above 1%) SCF/substrate lattice misfit were successfully performed in the first time. In such way the two sets of $\text{Lu}_{3-x}\text{Tb}_x\text{AG:Ce}$ SCFs/LuAG:Pr SC composite scintillators were created with real Tb content $x = 1.6$ –1.65 and 2.275–2.285 in the SCF samples, respectively. The results of the investigation of the scintillation decay kinetic of this group of composite scintillators under α -particles and γ -quanta excitation are presented in Fig. 12 (a) and (b) and Table 4. We can see from these Figures and

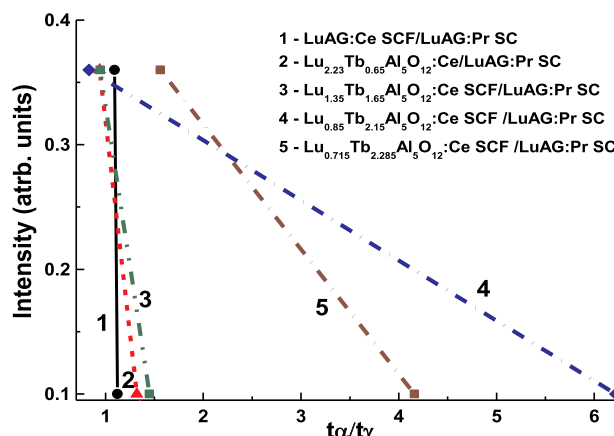


Fig. 13. A plot of t_α/t_γ ratio of the decay time under α - and γ -excitations on intensity of scintillation decay to 1/e and 0.1 levels for LuAG:Ce SCF/LuAG:Pr SC (1) and Lu_{3-x}Tb_xAG:Ce SCF/LuAG:Pr SC composite scintillators at Tb content $x = 0.65$ (2), 1.65 (3), 2.15 (4) and 2.285 (5).

Tables that the differences between t_α and t_γ scintillation decay intensities values are notable increased with increasing Tb content in Lu_{3-x}Tb_xAG:Ce SCF samples in $x = 1.6\text{--}2.285$ range. Moreover, the highest separation of decay curves is observed in case when the Tb³⁺ cation concentration is large than 2.0. In this case the respective t_α/t_γ ratio can reach the values above 4.2 in the 0.1–3 μs time range (Fig. 13 curve 5).

Taking into account the results, presented in Fig. 12 (a) for Lu_{0.85}Tb_{2.15}AG:Ce SCF/LuAG:Pr SC and in Fig. 12 (c) for Lu_{0.725}Tb_{2.275}AG:Ce SCF/LuAG:Pr SC epitaxial structures, we can claim in this paper the creation of the new effective composite scintillator for detection and resolving of α -particles or γ -quanta in ionizing radiation. These scintillators are based on the epitaxial structures of Lu_{3-x}Tb_xAG:Ce SCF with Tb content x above 2.0 and LuAG:Pr SC substrate. For this type of scintillator at Tb concentration in the 2.15–2.285 range the respective t_α/t_γ ratio can reach the values of 4.2–6.2 at scintillation decay level of 0.1.

4. Conclusions

This work presents the results of investigation of advanced composite scintillators consisting of SCF scintillators, based on the mixed garnet compounds, grown by the LPE method onto the substrate-scintillators prepared from the doped bulk LuAG crystals. Pulse height spectra under (i) α -particles excitation by ²⁴¹Am radioisotope allow obtaining scintillation response only from SCF scintillators if their thickness is higher ($> 10 \mu\text{m}$) than α -particles penetration depth. Under γ -quanta excitation by ¹³⁷Cs radioisotopes the scintillation response of composite scintillators is caused mainly by the LuAG:Pr SC substrate due to very small absorption of these quanta in the SCF scintillators.

We have investigated different SC substrates for creation of the composite scintillators using LPE growth method, producing from LuAG:Pr, LuAG:Ce and LuAG:Sc SCs. Pr³⁺, Ce³⁺ and Sc³⁺ doped LuAG SCs show suitable scintillating properties as (i) LYs $\sim 15\text{--}28 \times 10^3$, $10\text{--}21 \times 10^3$ and $1 \times 10^3 \text{ ph}/\text{MeV}$, respectively, (ii) LuAG:Pr has the best energy resolution $\sim 5\%$ at 661.66 keV and (iii) LY proportionality of these crystals is between ~ 70 and 100% in the energy range 10–1300 keV. Therefore, all these doped LuAG SC crystals can be considered as good substrates for creation of composite scintillators using LPE growth method. Namely, these type of substrates with thickness about of 1 mm enable detecting of γ -quanta of ¹³⁷Cs radiation or similar ones (e.g. ²²Na, ⁵⁴Mn or ⁶⁰Co).

LuAG:Ce, Lu_{1.7}GdTb_{0.3}AG:Ce and Lu_{3-x}Tb_xAG:Ce ($x = 0.15\text{--}2.285$) SCFs were prepared onto LuAG:Pr SC substrates. These SCFs have thicknesses above 10 μm which exceeds the penetration depths of α

particles of ²⁴¹Am in LuAG garnet [26,30]. Using this radioisotope, we characterized the scintillating properties of above mentioned SCFs and observed that in the shaping time range 0.5–10 μs (i) the LY of LuAG:Ce SCF is about of 60% in comparison with LuAG:Pr SC substrate; (ii) the LY of Lu_{3-x}Tb_xAG:Ce nonlinearly changing at change of Tb concentration in the 0.15–2.285 range from 59 to 62% for Lu_{3-x}Tb_xAG:Ce to 106–109% for Lu_{0.725}Tb_{2.285}AG:Ce; (iii) the SCF scintillators show comparable ER with one for LuAG:Pr substrate under excitation by 5.4857 MeV line of ²⁴¹Am isotope (of 13–40% and 17–28%, respectively).

Scintillating decay time profiles of both LuAG:Pr SC substrate and those of SCFs under α -particles and γ -quanta excitation show one fast component with decay time between 20.5 and 26.5 ns and two slow components with decay time between 80 and 108 ns and around 1000 ns, respectively. The differences in the scintillation decay time t_α/t_γ under α -particles or γ -quanta excitation both for SCFs and LuAG:Pr SC substrate are different for the different decay levels of composite scintillators. Namely, the t_α/t_γ ratio at 1/e and 0.05 levels is changed between 0.94–0.93 for LuAG:Ce SCF/LuAG:Pr SC and between 1.07 and 1.24 for Lu_{2.85}Tb_{0.15}AG:Ce SCF/LuAG:Pr SC and Lu_{1.7}GdTb_{0.3}AG:Ce SCF/LuAG:Pr SC.

We also grown of the Lu_{1-x}Tb_xAG:Ce SCFs at $x = 0.65\text{--}2.15$ onto undoped YAG substrates [27] and recently grown of the Lu_{1-x}Tb_xAG:Ce SCFs at $x = 1.65\text{--}2.285$ onto LuAG:Pr SC substrates and investigated their scintillation properties under α -particles excitation. For the SCFs of highly doped Tb³⁺ based mixed garnets much slower scintillation decay time profiles are observed in comparison with Lu_{2.85}Tb_{0.15}AG:Ce and Lu_{1.7}GdTb_{0.3}AG:Ce SCFs with low Tb content. Taking into account this result and possibility of LPE growth of Lu_{1-x}Tb_xAG:Ce SCFs at $x > 1.5$ not only onto YAG [27], but also onto LuAG substrates, we can claim in this work the creation of advanced Lu_{1-x}Tb_xAG:Ce SCF/LuAG:Pr SC composite scintillators. For this type of composite scintillators much higher ratio $t_\alpha/t_\gamma \sim 4.2\text{--}6.2$ is observed for Lu_{0.725}Tb_{2.285}AG:Ce SCF/LuAG:Pr SC substrate epitaxial structures. We also expected that such type of advanced composite scintillator can be effectively used to simultaneous detection of various components in the mixed fluxes of ionizing radiation, including α - or β -particles, ions and γ -quanta.

Acknowledgements

This work is performed in the framework of Polish NCN No 2018/31/B/ST8/03390 project and in the project LM2015058 of Czech Ministry of Education, Youth and Sports. The work is supported by Operational Programme Research, Development and Education financed by European Structural and Investment Funds and the Czech Ministry of Education, Youth and Sports (Project No. SOLI2D1 CZ.02.1.01/0.0/0.0/16_019/0000760).

References

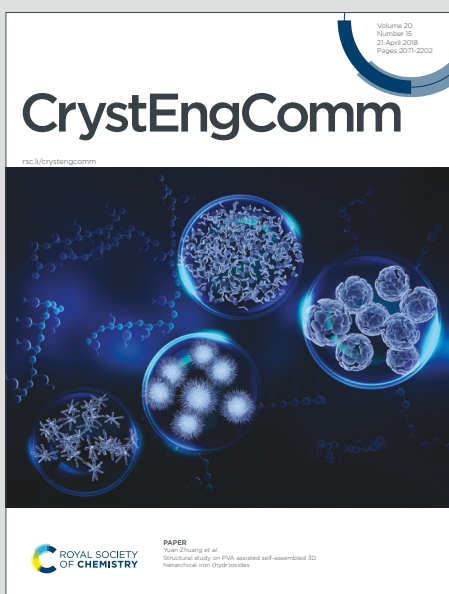
- [1] J. Tous, M. Horvath, L. Pina, K. Blazek, B. Sopko, High-resolution application of YAG:Ce and LuAG:Ce imaging detectors with CCD X-ray camera, NIM Phys Res. A 591 (2008) 264–267.
- [2] T. Martin, A. Koch, Recent development in X-ray imaging with micrometer spatial resolution, J. Synchrotron Radiat. 13 (2006) 180–194.
- [3] T. Martin, P.-A. Douissard, M. Couchaud, A. Cecilia, T. Baumbach, K. Dupré, A. Rack, LSO-based single crystal film scintillator for synchrotron-based hard X-ray microimaging, IEEE Trans. Nucl. Sci. 56 (2009) 1412–1418.
- [4] J.M. Robertson, M.V. van Tool, Cathodoluminescent garnet layers, Thin Solid Films 114 (1984) 221–240.
- [5] H.J. Levinstein, R.W. Landorf, S.L. Blank, The growth of high quality garnet thin films for supercooled melts, Appl. Phys. Lett. 19 (1971) 486–488.
- [6] P. Görnert, S. Bornmann, F. Voigt, M. Wendt, Study of the liquid phase epitaxy process of garnet layers by induced striations, Phys. Status Solidi A 41 (1977) 505–511.
- [7] P.-A. Douissard, A. Cecilia, T. Martin, V. Chevalier, M. Couchaud, T. Baumbach, K. Dupré, M. Kühbacher, A. Rack, A novel epitaxially grown LSO-based thin-film scintillator for micro-imaging using hard synchrotron radiation, J. Synchrotron Radiat. 17 (2010) 571–583.

- [8] B. Ferrand, B. Chambaz, M. Couchaud, Liquid phase epitaxy: a versatile technique for the development of miniature optical components in single crystal dielectric media, *Opt. Mater.* 11 (1999) 101–114.
- [9] N. Tolstik, S. Heinrich, A. Kahn, E. Volkova, V. Maltsev, N. Kuleshov, G. Huber, N. Leonyuk, High-temperature growth and spectroscopic characterization of Er,Yb:YAl₃(BO₃)₄ epitaxial thin layers, *Opt. Mater.* 32 (2010) 1377–1379.
- [10] W. Bolafios, M. Segura, J. Cugat, J.J. Carvajal, X. Mateos, M.C. Pujol, R. Solé, et al., Crystal growth and characterization of epitaxial layers of laser and nonlinear optical materials for thin-disk and waveguide laser applications, *Opt. Mater.* 32 (2010) 1380–1384.
- [11] Douissard Paul-Antoine, T. Martin, F. Riva, Yu Zorenko, T. Zorenko, K. Paprocki, Fedorov, P. Bilski, A. Twardak, Epitaxial growth of LuAG:Ce and LuAG:Ce,Pr films and their scintillation properties, *IEEE Trans. Nucl. Sci.* 63 (2016) 1726–1732.
- [12] Y. Zorenko, V. Gorbenko, T. Zorenko, K. Paprocki, M. Nikl, J.A. Mares, P. Bilski, A. Twardak, O. Sidletskiy, I. Gerasimov, B. Grinyov, A. Fedorov, Scintillating screens based on the single crystalline films of multicomponent garnets: new achievements and possibilities, *IEEE Trans. Nucl. Sci.* 63 (2016) 497–502.
- [13] P. Prusa, M. Nikl, J.A. Mares, M. Kucera, K. Nitsch, A. Bejtlerova, The α -particle excited scintillation response of YAG:Ce thin films grown by liquid phase epitaxy, *Phys. Status Solidi A* 206 (2009) 1494–1500.
- [14] S. Witkiewicz-Lukaszek, V. Gorbenko, T. Zorenko, O. Sidletskiy, I. Gerasimov, A. Fedorov, A. Yoshikawa, J.A. Mares, Zorenko Yu, Development of composite scintillators based on single crystalline films and crystals of Ce³⁺-doped (Lu,Gd) 3(Al,Ga)5O12 mixed garnet compounds, *Cryst. Growth Des.* 18 (2018) 1834–1842.
- [15] S. Shimadzu, M. Suzuji, Y. Koizumi, H. Ishibashi, S. Kubota, Light output and decay curve of GSO:Ce under electron, proton, alpha particle and fission fragment excitations, *NIM Phys. Res. A* 537 (2005) 57–60.
- [16] S. Witkiewicz-Lukaszek, V. Gorbenko, T. Zorenko, K. Paprocki, O. Sidletskiy, I. Gerasimov, J.A. Mares, R. Kucerkova, M. Nikl, Zorenko Yu, Composite scintillators based on the crystals and single crystalline films of LuAG garnet doped with Ce³⁺, Pr³⁺ and Sc³⁺, *Opt. Mater.* 84 (2018) 593–599.
- [17] Y. Zorenko, V. Gorbenko, T. Voznyak, V. Savchyn, S. Nizhankovskiy, A. Dan'ko, V. Puzikov, V. Laguta, J.A. Mares, M. Nikl, K. Nejezchleb, M. Batentschuk, A. Winnacker, Luminous and scintillation properties of Lu₃Al₅O₁₂:Sc single crystal and single crystalline films, *Opt. Mater.* 34 (2012) 2080–2085.
- [18] S. Witkiewicz-Lukaszek, V. Gorbenko, T. Zorenko, K. Paprocki, O. Sidletskiy, A. Fedorov, R. Kucerkova, J.A. Mares, M. Nikl, Yu Zorenko, Epitaxial growth of composite scintillators based on Tb₃Al₅O₁₂:Ce single crystalline films and Gd₃Al_{2.5}Ga_{2.5}O₁₂:Ce crystal substrates, *CrystEngComm* 20 (2018) 3994–4002.
- [19] J.A. Mares, A. Bejtlerova, P. Prusa, K. Blazek, P. Horodsky, K. Kamada, A. Yoshikawa, C. D'Ambrosio, M. Nikl, Energy resolution studies of Ce- and Pr-doped aluminum and multicomponent garnets: the escape and photopeaks, *J. Lumin.* 169 (2016) 701–705.
- [20] W. Chewpraditkul, L. Swidierski, M. Moszynski, T. Szczesniak, A. Syntfeld-Kazuch, C. Wanarak, P. Limsuwan, Scintillation properties of LuAG:Ce, YAG:Ce and LYSO:Ce crystals for gamma-ray detection, *IEEE Trans. Nucl. Sci.* 56 (2009) 3800–3805.
- [21] C. D'Ambrosio, H. Leutz, Hybrid photon detectors, *NIM Phys. Res. A* 501 (2003) 463–498.
- [22] F. Glenn, Knoll, *Radiation Detection and Measurements*, third ed., John Wiley & Sons, Inc., New York, 2000.
- [23] M. Moszynski, T. Szczesniak, M. Kapusta, M. Szawlowski, J. Iwanowska, M. Gierlik, A. Syntfeld-Kazuch, M. Swidierski, C.L. Melcher, L.A. Ericsson, J. Glodo, Characterization of scintillators by modern photomultipliers – a new source of errors, *IEEE Trans. Nucl. Sci.* 57 (2010) 1367–1374.
- [24] X-ray and gamma-ray Data, www.nist.gov/PhysRefData.
- [25] K. Bartosiewicz, V. Babin, M. Nikl, J.A. Mares, Y. Zorenko, V. Gorbenko, Luminescence and energy transfer processes in (Lu,Th)3Al₅O₁₂ single crystalline films doped with Ce³⁺, *J. Lumin.* 173 (2016) 141–148.
- [26] P. Prusa, T. Cechak, J.A. Mares, M. Nikl, A. Bejtlerova, N. Solovieva, Y.V. Zorenko, V.I. Gorbenko, J. Tous, K. Blazek, The α -particle excited scintillation response of the liquid phase epitaxy grown LuAG:Ce thin films, *Appl. Phys. Lett.* 92 (2008) 41903–1–041903–3 041903–41911–3.
- [27] K. Bartosiewicz, V. Babin, J.A. Mares, A. Bejtlerova, Y. Zorenko, A. Iskaliyeva, V. Gorbenko, Z. Brykna, M. Nikl, Luminescence and energy transfer processes in Ce³⁺ activated (Gd,Tb)₃Al₅O₁₂ single crystalline films, *J. Lumin.* 188 (2017) 60–66.
- [28] J.T.M. de Haas, P. Dorenbos, C. of Inorganic, W.E. van Eijk, Measuring the absolute light yield of scintillators, *NIM Phys. Res. A* 537 (2005) 97–100.
- [29] E. Shibamura, S. Sasaki, N.N.T. Tran, Systematic study of inorganic and organic scintillator light yields, *JPS Conf. Proc.* 11 (2016) 20004–1–020004–6 020004–20011–6.
- [30] W. Wolszczak, P. Dorenbos, Nonproportional response of scintillators to alpha particle excitation, *IEEE Trans. Nucl. Sci.* 64 (2017) 1580–1591.

CrystEngComm

Accepted Manuscript

This article can be cited before page numbers have been issued, to do this please use: S. Witkiewicz-Lukaszyk, V. Gorbenko, T. Zorenko, O. Sidletskiy, P. Arhipov, A. Fedorov, J. Mares, R. Kucerkova, M. Nikl and Y. Zorenko, *CrystEngComm*, 2020, DOI: 10.1039/D0CE00266F.



This is an Accepted Manuscript, which has been through the Royal Society of Chemistry peer review process and has been accepted for publication.

Accepted Manuscripts are published online shortly after acceptance, before technical editing, formatting and proof reading. Using this free service, authors can make their results available to the community, in citable form, before we publish the edited article. We will replace this Accepted Manuscript with the edited and formatted Advance Article as soon as it is available.

You can find more information about Accepted Manuscripts in the [Information for Authors](#).

Please note that technical editing may introduce minor changes to the text and/or graphics, which may alter content. The journal's standard [Terms & Conditions](#) and the [Ethical guidelines](#) still apply. In no event shall the Royal Society of Chemistry be held responsible for any errors or omissions in this Accepted Manuscript or any consequences arising from the use of any information it contains.

Liquid Phase Epitaxy growth of high-performance composite scintillators based on the single crystalline films and crystals of LuAG garnet

Received 00th January 20xx,
Accepted 00th January 20xx

DOI: 10.1039/x0xx00000x

www.rsc.org/

S. Witkiewicz-Lukaszek^{a*}, V. Gorbenko^a, T. Zorenko^a, O. Sidletskiy^b, P. Arhipov^b,
A. Fedorov^c, J.A. Mares^d, R. Kucerkova^d, M. Nikl^d, Yu. Zorenko^{a*}

Abstract. This work is devoted to the development of two novel types of advanced composite scintillators based on the single crystalline films (SCFs) of $\text{Lu}_3\text{Al}_5\text{O}_{12}$ garnet (LuAG), doped with Ce^{3+} and Pr^{3+} ions, and substrate from single crystals (SCs) of Sc^{3+} doped LuAG using the liquid phase epitaxy (LPE) method. We show the possibility for simultaneous registration of α -particles and γ -quanta using separation of the decay kinetics of SCF and crystal parts of such composite scintillators. Namely, the large differences in the respective scintillation decay kinetics and decay time values t_α and t_γ are observed for LuAG:Ce SCF / LuAG:Sc SC and LuAG:Pr SCF / LuAG:Sc SC composite scintillators under excitation by α -particles of ^{241}Am (5.5 MeV) source and γ -quanta of ^{137}Cs (662 keV) source. Thus, the both developed types of composite scintillators can be applied for simultaneous registration of α -particles and γ -quanta in the mixed radiation fluxes. The rate of discrimination of the scintillation signals, coming from SCF and SC parts of LuAG:Ce SCF / LuAG:Sc SC composite scintillator, expressed by t_γ/t_α ratio, is equal to 1.34-1.96 in the 0-1100 ns time interval. For LuAG:Pr SCF / LuAG:Sc SC composite scintillators, more significant differences in the scintillation decay kinetics are achieved. In this case, the t_γ/t_α ratio for these composite scintillators reaches the values 9.6-15.6 in the wide 0-2500 ns time interval. This is the best result from all the developed by us types of composite scintillators based on the epitaxial structures of garnet compounds.

1 Introduction

The scintillators are the materials that convert X-ray energy into ultraviolet (UV) or visible light, which is detected by suitable photosensitive detectors, such as photodiodes (PD) or photomultipliers (PMT). The history of scintillators started from the 19th century, when X-rays and natural radioactivity were discovered. Nowadays scintillators are applied not only for the detection of X- and γ -rays, but also for other types of ionizing radiation. Scintillators are widely used in particle detection in nuclear research, cosmic ray measurements, radiation monitoring of the environment, radiation beam control, security technique, imaging in industry, medicine and biology and other important optoelectronic applications.

Nowadays there are many technologies for producing scintillators in the different crystalline forms. For growth of the bulk single crystal (SC) scintillators, the Czochralski, Horizontal Directional Crystallization (HDC) (modification of the Bridgman-Stockbarger technique) and Edge Defined Film Fed (EDFF) methods are usually used [1, 2]. The micro-pulling-down (MPD) growth method is very popular for producing the long (up to one meter) scintillation fibers with the diameter of a few millimeters [3, 4]. The liquid phase epitaxy (LPE) method is a versatile tool for producing the single crystalline films (SCF) scintillators based on the different oxide compounds [5-7]. The fields of application of such SCF scintillators today include the registration of α - and β - particles and low-energy quanta of ionizing radiation [5, 8, 9] as well as the scintillating screens for microradiography detectors with high spatial resolution using X-ray sources and synchrotron radiation [10, 11].

The LPE method enables also the development of composite scintillators of "phoswich-type" (phosphor sandwich) for simultaneous registration of the different components of ionizing radiation. Such composite scintillators can be applied for analysis of

^a Institute of Physics, Kazimierz Wielki University in Bydgoszcz, Powstańców Wielkopolskich str., 2, 85090 Bydgoszcz, Poland; *corresponding authors e-mail: zorenko@ukw.edu.pl.

^b Institute for Single Crystals, National Academy of Sciences of Ukraine, Nauki av., 60, 61178 Kharkiv, Ukraine

^c Institute for Scintillation Materials, National Academy of Sciences of Ukraine, Nauki av., 60, 61001 Kharkiv, Ukraine.

^d Institute of Physics, Academy of Sciences of Czech Republic, Cukrovarnická str., 10, 16200 Prague, Czech Republic.

ARTICLE

the content of mixed fluxes of photons and particles with various penetrating depths [5, 12-14]. Namely, a LPE grown composite scintillator presents the epitaxial structure, consisting of the SCF scintillator for detection of the low penetrating α -particles, and a bulk SC substrate for registration of the highly penetrating X or γ rays (Fig.1 left).

There are many advantages of these types of composite scintillators in comparison with the analogues based on the splice of different scintillation crystals [15]. Such composite scintillators present the epitaxial structure with a sharp interface between the composing scintillators with close refractive indices (Fig.1). This enables to decrease the losses of light at the interface of scintillators, enhancing the selectivity of registration of the different components of mixed ionizing radiations.

The LPE method for composite scintillator manufacturing permits also to obtain the thickness of film scintillators close to the penetration depth of registered particles. Specifically, the thickness of film scintillators, which is necessary for the complete absorption of α -particles of ^{239}Pu and ^{241}Am sources, typically is equal to 12-15 μm (Fig.1) [5].

The different types of composite scintillators have been recently considered by some of us in [5, 12-14]. The first type of composite scintillators were LPE grown epitaxial structures based on the Ce^{3+} and Nd^{3+} doped SCFs and Nd^{3+} and Sc^{3+} crystals of $\text{Y}_3\text{Al}_5\text{O}_{12}$ garnet (YAG) [5, 30]. One-layered YAG:Ce SCF/ YAG:Nd SC and YAG:Ce SCF/YAG:Sc SC composite scintillators as well as doubly-layered YAG:Ce SCF/YAG:Nd SCF/ YAG:Sc SC composite scintillators were grown by the LPE method and examined under excitation by α -particles and γ -quanta [5]. The separation of the scintillation signals coming from the SCF and SC parts of composite scintillator was performed using the difference in their scintillation decay kinetics [5].

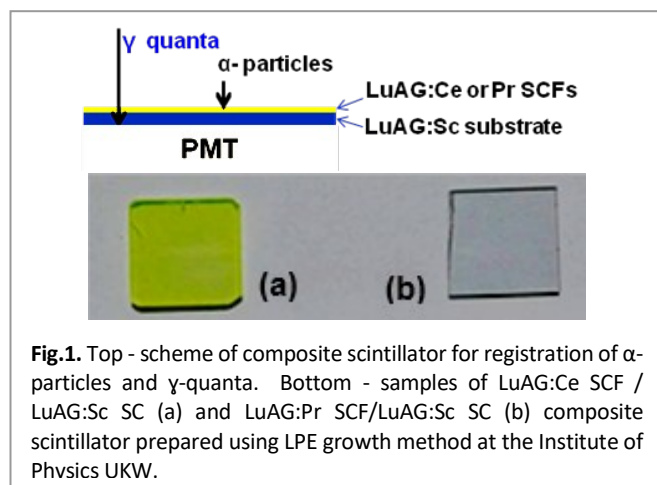


Fig.1. Top - scheme of composite scintillator for registration of α -particles and γ -quanta. Bottom - samples of LuAG:Ce SCF / LuAG:Sc SC (a) and LuAG:Pr SCF/LuAG:Sc SC (b) composite scintillator prepared using LPE growth method at the Institute of Physics UKW.

For evaluation of the suitable materials for a composition scintillator in terms of ability for detection of the mixed ionizing radiations it is important to use appropriate parameters of materials. Of most importance for that is the density (ρ), the effective atomic number (Z_{eff}) and the amount of light absorbed per thickness of the material (absorption coefficient $\mu = \rho Z^4$) in comparison with YAG. Meanwhile, due to the quite low values of density $\rho=4.56 \text{ g/cm}^3$, effective atomic number $Z_{\text{eff}}=29$ and absorption coefficient $\mu=3.8*10^6 \text{ g/cm}^3$, the scintillators based on the YAG SC substrates may be used only for registration of low-energy ionizing radiation [5, 12]. Therefore, there is a demand to fabricate composite scintillator for registration of the mixed fluxes of particles and high-energy quanta using other garnet compounds, which are characterized by high values of ρ and Z_{eff} [12, 13].

From all the possible candidates of heavy materials for creation of composite scintillators, the $\text{Lu}_3\text{Al}_5\text{O}_{12}$ garnet (LuAG) first of all attracts our attention [9, 10]. LuAG host has significantly higher density $\rho=6.73 \text{ g/cm}^3$, effective atomic number $Z_{\text{eff}}=58.9$ and absorption coefficient $\mu=81*10^6 \text{ g/cm}^3$ in comparison with YAG. LuAG:Ce, LuAG:Pr and LuAG:Sc bulk SCs are the well-known scintillators for radiation monitoring and computer tomography [7, 16]. Therefore, the LuAG is a very promising material for creation of SCF scintillators and composite scintillators on its base as well. As activators, which can effectively emit in LuAG host with different wavelengths and decay kinetics of scintillations, the Pr^{3+} , Sc^{3+} and Ce^{3+} ions can be considered [9, 16-25, 34]. Namely, the position of emission bands of LuAG:Ce, LuAG:Pr and LuAG:Sc compounds under high-energy excitation is located at 515 nm, 310 nm and 275-330 nm, respectively, and the corresponding decay times of the main component of the luminescence of Ce^{3+} , Pr^{3+} and Sc^{3+} dopants in LuAG host are equal to 50-58 ns, 19-28 ns and 245-610 ns, respectively, depending on the concentration of dopants [16-25]. Therefore, the different combinations of novel composite scintillators based on the epitaxial structures of LuAG garnet compounds, doped with the mentioned ions, can be created using the LPE method.

In our previous works, we considered the scintillation properties of the two types composite scintillators, based on the Ce^{3+} and Sc^{3+} doped LuAG SCFs, grown using the LPE method onto LuAG:Ce substrates [26, 27]. The results of our investigation show that the LuAG:Pr SCF/ LuAG:Ce SC and LuAG:Sc SC/LuAG:Ce SC epitaxial structures are promising ones for detection of α -particles and γ -rays by means of the registration scintillation signals (pulse height spectra and decay kinetics) coming correspondingly from the SCF and SC parts of composite scintillators. Meanwhile, we also search for other

combination of LuAG based garnet compounds where the discrimination of the scintillation decay kinetics or other properties of SCF and SC parts of composite scintillator can be large in the wide time interval under excitation by α -particles and γ -quanta.

This work is the next important stage of searching for new types of composite scintillators for registration of the different components of mixed ionizing radiation, including α -particles and γ -rays. In our paper, we present the results of development of two novel composite scintillators, based on the LuAG:Sc SC substrates and Ce³⁺ and Pr³⁺ doped LuAG SCFs, prepared using the LPE method.

2 Growth of composite detectors

For creation of the composite scintillators, the LuAG:Sc substrates with (100) orientation with the 1*1 cm² size and the 1 mm thickness were used. The LuAG:Sc substrates were prepared from the respective crystal with a Sc concentration of 0.5 at. %, grown using the Czochralski (Cz) method in ISMA, Ukraine.

Two types of the composite scintillators, based on the LuAG:Ce SCF and LuAG:Sc SC substrate, and LuAG:Pr SCF and LuAG:Sc SC substrate, were crystallized using the LPE growth method from over-cooling melt solutions using PbO-B₂O₃ flux in IP UKW, Poland. Fig.1 (at the top) shows the samples of LuAG:Ce SCF / LuAG:Sc SC and LuAG:Pr SCF/LuAG:Sc SC composite scintillators. For comparison with the properties of composite scintillators, the LuAG:Ce and LuAG:Pr SCFs were crystallized also onto undoped YAG substrates at the same growth conditions. The SCFs were completely transparent and possess mirror-like surface (see Fig.1, bottom part of the figure). The concentration of Ce³⁺ and Pr³⁺ dopants in the LuAG:Ce and LuAG:Pr SCFs under study, determined using a microanalyzer EDS at SEM JEOL JSM-820 microscope, were in the 0.17-0.23 % and 0.2-0.25 % ranges, respectively.

The growth conditions of the composite scintillators and respective LuAG:Ce and LuAG:Pr SCF samples, selected for

investigation of the content and structural properties, as well as for studying their absorption, cathodoluminescence and scintillation properties were summarized in Table 1.

The structural quality of LuAG:Ce and LuAG:Pr SCF parts of composite scintillators was confirmed using the X ray diffraction (XRD) method using modified DRON-3 spectrometer.

The Fig.2 shows the XRD patterns of (12 0 0) planes for both SCFs in comparison with LuAG:Sc substrate. The full width at half maximum (FWHM) of XRD peaks and lattice constants of the garnet samples under study were determined from respective patterns. As can be seen from this figure, the structural quality of LuAG:Ce and LuAG:Pr SCF samples, proportional to FWHM of the respective XRD peaks (0.12 and 0.14 degrees, respectively), is very close to that of LuAG:Sc substrate (0.14 degree). The LuAG:Ce and LuAG:Pr SCFs possess quite smaller lattice constants of 11.9103 Å and 11.9121 Å, respectively, in comparison with those for LuAG:Sc substrate (11.9157 Å) due to the absence of Lu_{Al} antisite defects in the films and difference in the concentration of the respective dopants.

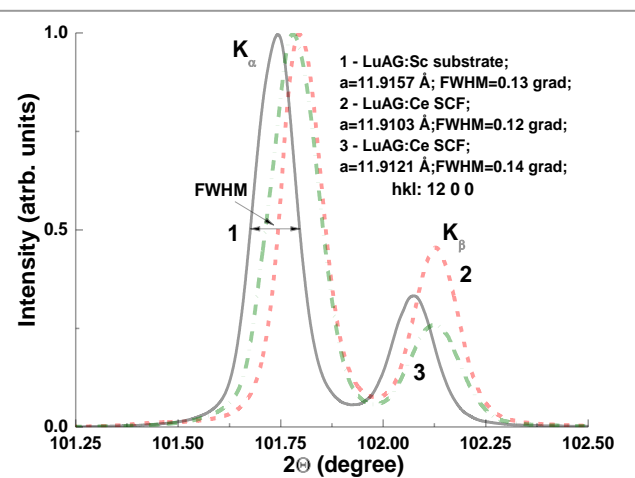


Fig.2. Normalized XRD patterns of (12 0 0) planes of LuAG:Ce (1), LuAG:Pr (2) SCFs in comparison with LuAG:Sc substrate (3).

Table 1. Growth conditions of LuAG:Sc SC, LuAG:Ce and LuAG:Pr SCFs and LuAG:Ce SCF / LuAG:Sc SC and LuAG:Pr SCF / LuAG:Sc SC composite scintillators as well as their LY under excitation by α -particles of ²³⁹Pu (5.15 MeV) radioisotope, measured with a shaping time of 12 μ s, in comparison with YAG:Ce SCF standard sample with a photoelectron LY of 360 phels/MeV (a LY of 2650 photon/MeV). h - SCF thickness, f - velocity of SCF growth; T - SCF growth temperature. The thickness h of the films was measured using the weight method and calculated as $h = M_{SCF/sub} - m_{sub} / \rho * S$, where M is the mass of SCF and substrate; m - mass of substrate; ρ - density of material; S - surface of substrate.

SCF number	Type of SCF/SC	Substrate type	h, μ m	T, °C	f, μ m/min	LY, %
	LuAG:Sc SC	-	1000	-	-	173
a0	LuAG:Ce SCF	YAG	10	980	0.2	114
b0	LuAG:Pr SCF	YAG	19	975	0.19	100
a1	LuAG:Ce SCF	LuAG:Sc	30	976	0.375	106
a2	LuAG:Ce SCF	LuAG:Sc	21	985	0.2	126
b1	LuAG:Pr SCF	LuAG:Sc	29	965	0.32	59
b2	LuAG:Pr SCF	LuAG:Sc	12	965	0.27	54

3 Experimental technique

For characterization of the properties of LuAG:Ce SCF/LuAG:Sc SC and LuAG:Pr SCF/ LuAG:Sc SC composite scintillators, LuAG:Sc substrates, as well as the LuAG:Ce and LuAG:Pr SCFs, the absorption spectra, cathodoluminescence (CL) spectra, scintillation LY, energy resolution and scintillation decay kinetics measurements under excitation by α -particles and γ -quanta were used.

The absorption spectra were measured using a Jasco 760 UV-Vis spectrometer in the 200-1100 nm range. The CL spectra were measured using an electron microscope SEM JEOL JSM-820 ($U=30$ kV, $I=0.1$ μ A), additionally equipped with a spectrometer Stellar Net and TE-cooled CCD detector working in the 200-925 nm range. The scintillation LY (pulse height spectra measured with a shaping time of 12 μ s) was firstly measured in IP UKW after each SCF growth circle using the setup based on a Hamamatsu H6521 photomultipliers (PMP), multi-channel analyzer and digital Tektronix TDS3052 oscilloscope under excitation by α -particles of Pu^{239} (5.15 MeV) source (Table 1). The spectra were compared with the standard YAG:Ce SCF sample with a photoelectron yield of 360 phels/MeV and a LY of 2650 photons/MeV [25] and also with the reference LuAG:Sc substrate. All the measurements were performed at the room temperature (RT).

Scintillation response investigations of the selected composite scintillators (see Table 1) were performed at FZU in Prague using the set-up consisting of a hybrid PMT (HPMT DEP PP0475B with pre-amplifier), measuring electronics (Ortec 672 Spectroscopy Amplifier and 927 ASPEC MCA) and PC control. The pulse height spectra were measured under excitation by α -particles of ^{241}Am (an energy of 5.4857 MeV) radioisotope and by γ -rays of ^{137}Cs (an energy of 661.66 keV) radioisotope. It is important to note here that the α -particles of ^{239}Pu and ^{241}Am sources allow exciting only the epitaxial layers of SCF samples (not their substrates) because the penetration depth of α -particles in the studied samples is approximately 12-15 μ m.

4 Absorption, luminescent and scintillation properties of composite scintillators based on the LuAG:Ce, LuAG:Pr SCFs and LuAG:Sc substrates

4.1 Absorption spectra

The absorption spectra of the LuAG:Ce SCF/LuAG:Sc SC and LuAG:Pr SCF/LuAG:Sc SC composite scintillators are presented in Fig.3 in comparison with the absorption spectra of the LuAG:Ce and LuAG:Pr SCFs, grown onto YAG substrates. The E_2 and E_1 bands, peaked at 346 and 447 nm in Fig.3a, correspond to the 4f-5d^{1,2} transitions of Ce³⁺ ions in LuAG:Ce SCF samples. Similarly, the E_2 and

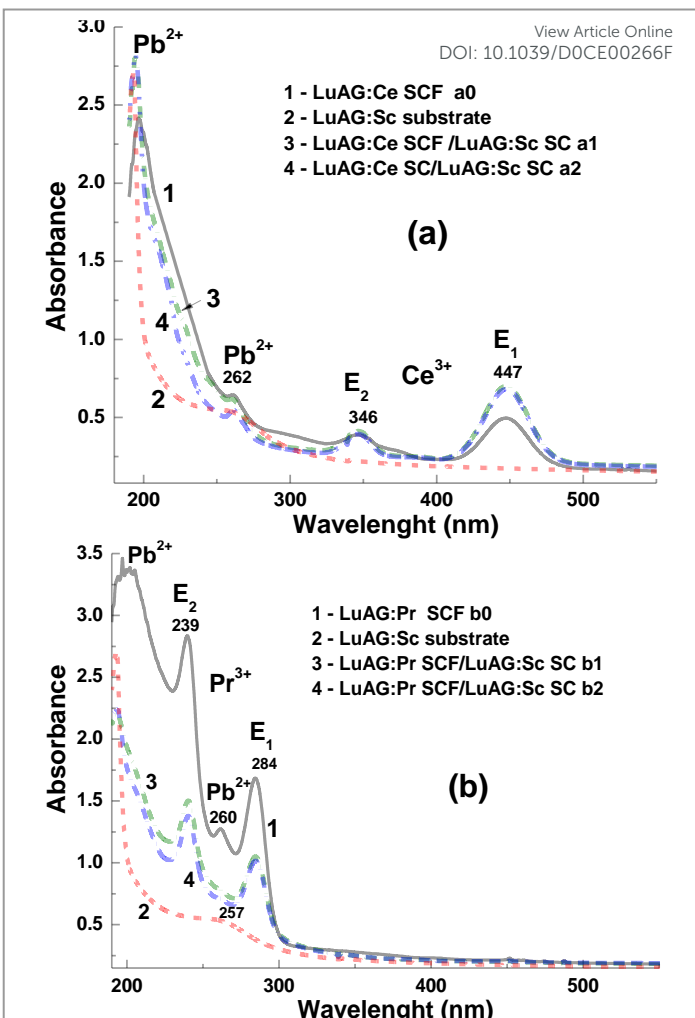


Fig.3. Absorption spectra of two samples of LuAG:Ce SCF/LuAG:Sc SC (a, curves 3, 4) composite scintillators and LuAG:Pr SCF/LuAG:Sc SC (b, curves 3, 4) composite scintillators in comparison with the absorption spectra of LuAG:Ce (a, curve 1) and LuAG:Pr (b, curve 1) SCFs, grown onto YAG substrates, and LuAG:Sc substrates (a and b, curves 2).

E_1 bands, peaked at 239 and 284 nm in Fig.3b, correspond to the 4f-5d^{1,2} transitions of Pr³⁺ ions in LuAG:Pr SCFs. In the both figures, the absorption bands, peaked at 260-262 nm and below 200 nm, are related correspondingly to the $^1S_0 \rightarrow ^3P_1$ and $^1S_0 \rightarrow ^3P_1$ transitions of Pb²⁺ flux related impurity in the SCF samples.

It is worth to note also that the absorption spectra of LuAG:Sc substrate possess the wide low-intensive band peaked around 257 nm. These bands are not related to the intrinsic transitions of Sc³⁺ ions and most probably are caused by the very common O²⁻→Fe³⁺ transitions of Fe³⁺ trace impurities [28, 29] in the raw materials for producing the LuAG:Pr SCs.

4.2 Cathodoluminescence spectra

The normalized CL spectra of LuAG:Sc SC substrates are shown as curves 1 in Fig.4a and 4b. The most intensive peaks at 307 nm in

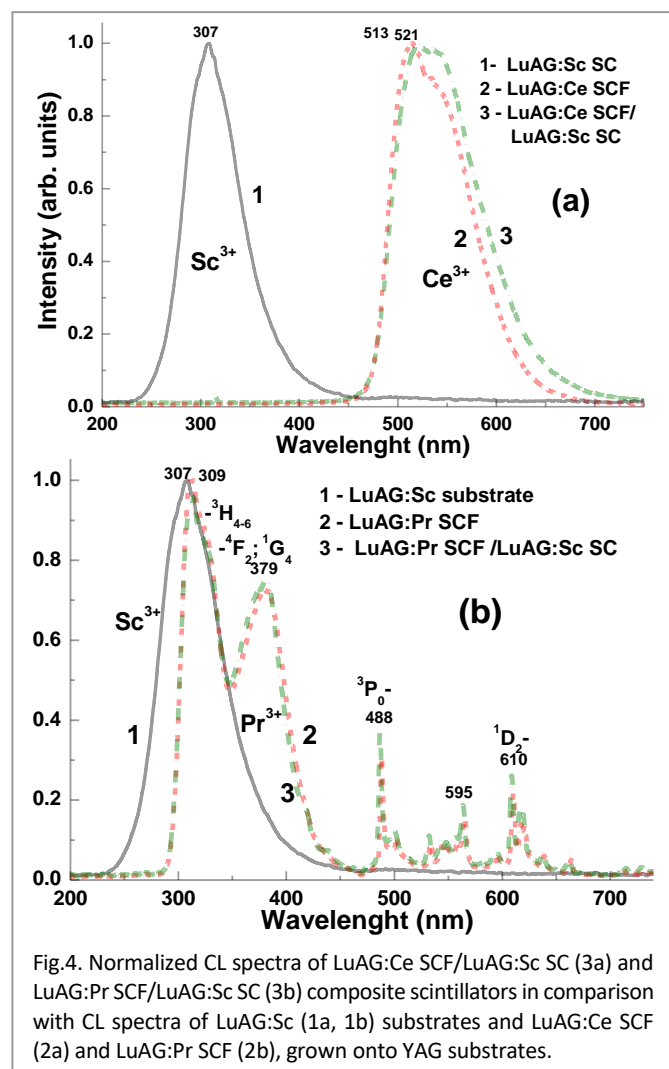


Fig.4. Normalized CL spectra of LuAG:Ce SCF/LuAG:Sc SC (3a) and LuAG:Pr SCF/LuAG:Sc SC (3b) composite scintillators in comparison with CL spectra of LuAG:Sc (1a, 1b) substrates and LuAG:Ce SCF (2a) and LuAG:Pr SCF (2b), grown onto YAG substrates.

LuAG:Sc SCs correspond to the luminescence of excitons bound with the Sc³⁺ isoelectronic impurities in both Al³⁺ octahedral sites and Lu³⁺ dodecahedral sites of the garnet lattice [21-24].

The visible luminescence bands peaked in the 513-521 nm range in the CL spectra of LuAG:Ce SCFs and LuAG:Ce SCF/LuAG:Sc SCs (Fig.4a, curves 3 and 4) are related to the 5d¹-4f(²F_{5/2,7/2}) transitions of Ce³⁺ ions in the mentioned SCF samples. The intensive UV emission bands, peaked at 309 and 379 nm, in the CL spectra of LuAG:Pr SCF and LuAG:Pr SCF/LuAG:Sc SC composite scintillator (Fig.4b, curves 2 and 3) are related to the 5d¹-4f(³H₄₋₆, ³H₅, ⁴F₂, ¹G₄) transitions of Pr³⁺ ions in SCF samples. The sharp emission bands in the visible range of LuAG:Pr SCF samples correspond to the 4f-4f transitions from the ³P₀- and ¹D₂-radiative levels to the ³H_J levels of Pr³⁺ ions (Fig.4b).

4.3. α - and γ -ray spectroscopy of LuAG:Ce SCF/LuAG:Sc SC and LuAG:Pr SCF/ LuAG:Sc SC composite scintillators

4.3.1. Pulse height spectra. The pulse height spectra of the main α - and γ -ray lines of ²⁴¹Am and ¹³⁷Cs sources, registered by two

samples of LuAG:Ce SCF/LuAG:Sc SC composite scintillators and two samples of LuAG:Pr SCF/LuAG:Sc SC composite scintillators, are presented in Figs.5 and 6, respectively. The main peaks in Fig.5a and 6a correspond to the total energy absorption of α -rays with an energy of 5.4857 MeV. The peaks in the left part of the spectrum correspond to the absorption of the low-energy γ -ray of ²⁴¹Am (59.6467 keV). It is worth to note that positions or/and shape of the main photopeaks, observed in Fig.5a and 6a, are different for LuAG:Ce and LuAG:Pr SCF components for the both types of composite scintillators and for LuAG:Sc substrates. This means that α -particles excite only SCF parts of composite scintillators. Fig.5a and 6a show also that the LY value of LuAG:Ce and LuAG:Ce SCFs under excitation by α -particles of ²⁴¹Am source is lower by 1.7-2 and 3.35-4.25 times, respectively, in comparison with the LY value for LuAG:Sc substrates. These results on the LY of composite scintillators under α -particle

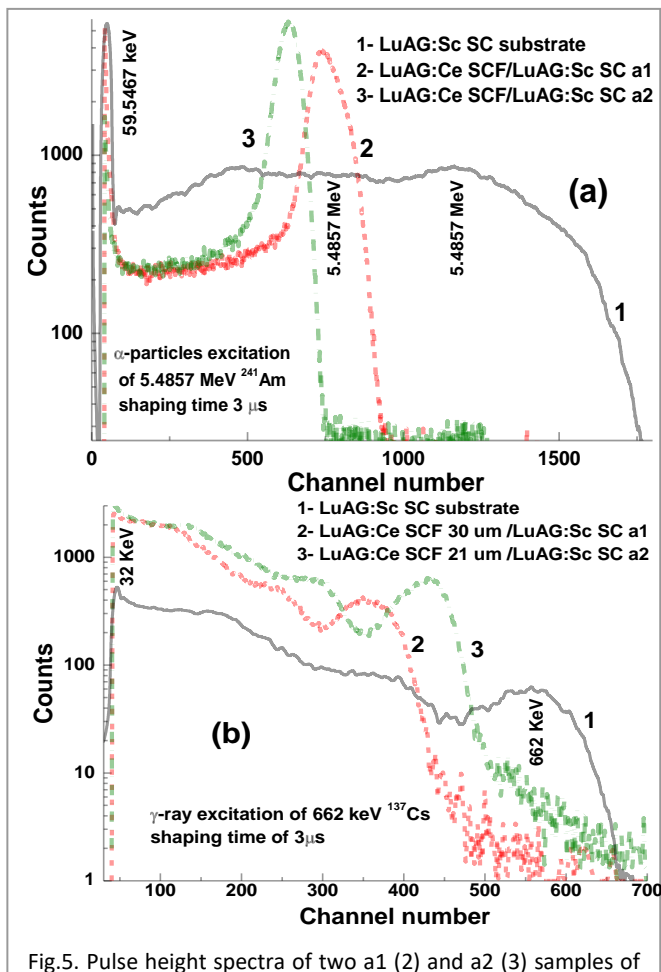


Fig.5. Pulse height spectra of two a1 (2) and a2 (3) samples of LuAG:Ce SCF/LuAG:Sc SC composite scintillators and LuAG:Sc substrate (1) measured using α -particle excitation with an energy of 5.4857 MeV of ²⁴¹Am source (a) and using γ -ray excitation of ¹³⁷Cs source with an energy of 661.66 keV (b).

ARTICLE

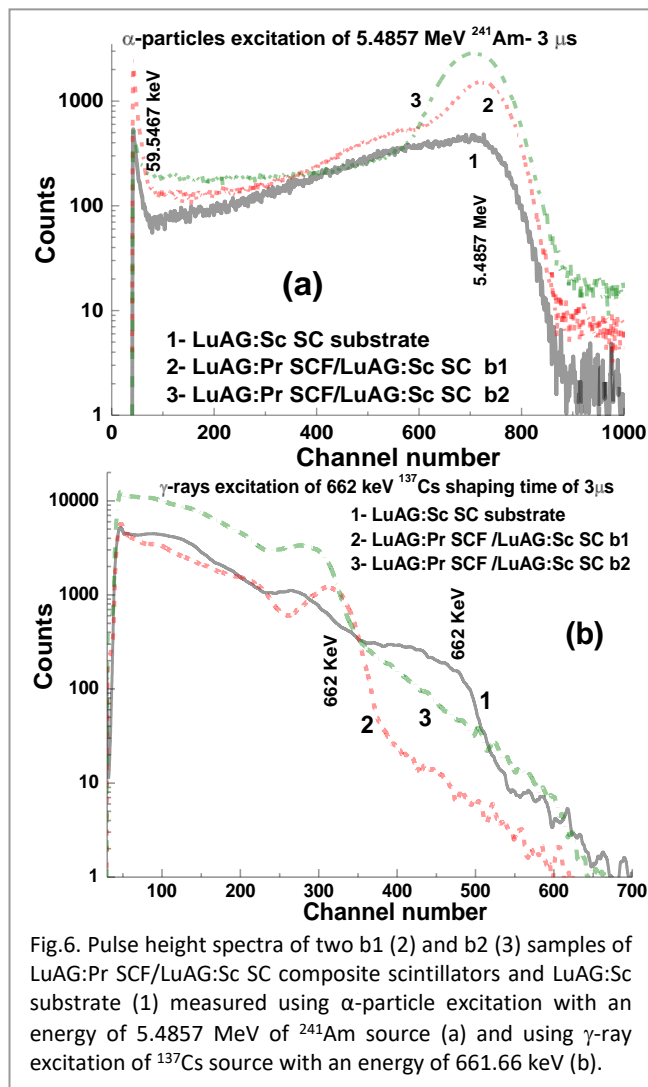


Fig. 6. Pulse height spectra of two b1 (2) and b2 (3) samples of LuAG:Pr SCF/LuAG:Sc SC composite scintillators and LuAG:Sc substrate (1) measured using α -particle excitation with an energy of 5.4857 MeV of ^{241}Am source (a) and using γ -ray excitation of ^{137}Cs source with an energy of 661.66 keV (b).

excitation by ^{241}Am source are consistent with the results obtained for these samples presented in Table 1 under excitation by ^{239}Pu source. The different LY of two SCF samples in the series of LuAG:Ce and LuAG:Pr SCF scintillators in Fig. 5a and 6a are caused mainly by the different influence of Pb^{2+} flux related impurity on the scintillation properties of these SCFs, grown from PbO based flux at different temperatures (Table 1) (see also [8, 24]).

Under γ -ray excitation of LuAG:Ce SCF/LuAG:Sc SC and LuAG:Pr SCF/LuAG:Ce SC composite scintillators by ^{137}Cs source, the main peaks were observed in the pulse height spectra, corresponding to the total absorption of γ radiation with an energy of 661.66 keV (Fig. 5b and 6b). The additional peak is observed at lower energy at 32.006 keV, corresponding to the low-energy energy line of ^{137}Cs source.

It is worth to note, that the main photopeaks, observed in Fig. 5b and 6b, have different positions for both LuAG:Ce SCF/LuAG:Sc and LuAG:Pr SCF/LuAG:Sc SC composite scintillators and LuAG:Sc substrates. This means that γ -quanta excite not only the substrate

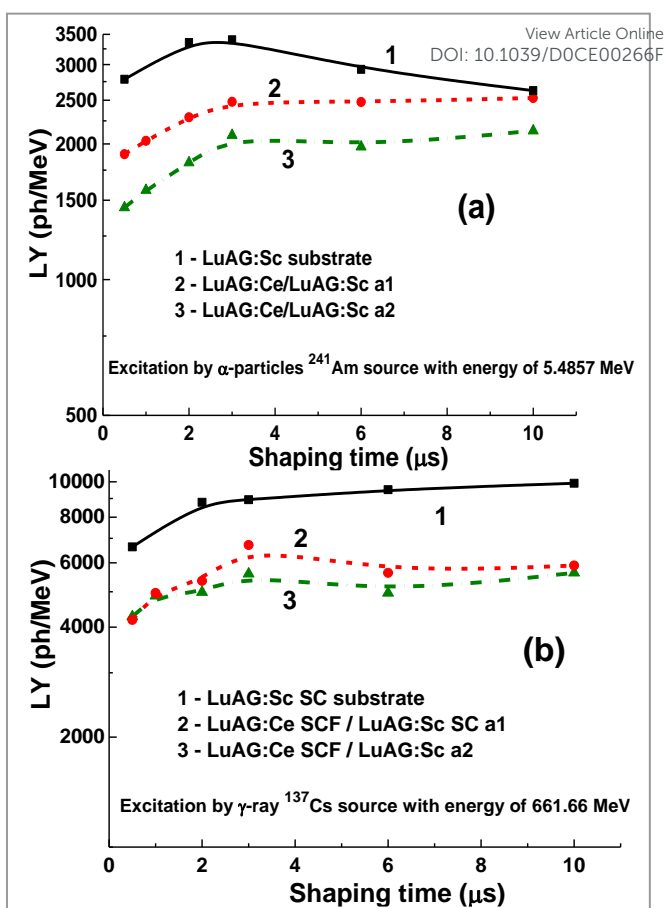


Fig. 7. Dependence of LY values of a1 (2) and a2 (3) samples of LuAG:Ce SCF/LuAG:Sc SC composite scintillators and LuAG:Sc substrate (1), measured under α -particle excitation by ^{241}Am source with an energy of 5.4857 MeV (a) and γ -ray excitation by ^{137}Cs source with an energy of 661.66 keV (b).

but SCF scintillators as well and the LY of SCF scintillators notably influences the total scintillation LY of LuAG:Ce SCF/LuAG:Sc SC and LuAG:Pr SCF/LuAG:Sc SC composite scintillators under γ -ray excitation. For this reason, the position of main photopeaks, corresponding to the absorption of 661.66 keV line of ^{137}Cs source by composite scintillators, depends on the LY and thickness of SCF parts of composite scintillators.

Such unwanted properties of the composite scintillators under study contradict with the results of our previous investigations [27, 28, 32, 33] and can be related mainly to the use of UV emitting LuAG:Sc substrate. Recently we have investigated of the pulse height spectra of LuAG:Pr SCF/LuAG:Ce and LuAG:Sc SCF/LuAG:Ce SC composite scintillators and LuAG:Ce substrate [27, 28], where similar positions of the main photopeaks for composite scintillators and substrate are observed. Similar behavior we have also observed for $\text{Lu}_{1.5}\text{Gd}_{1.5}\text{Al}_2\text{Ga}_3\text{O}_{12}:\text{Ce}$ SCF/GAGG:Ce and TbAG:Ce SCF/GAGG:Ce SC composite scintillators, where inappreciable influence of SCF components on position of the main photopeak of composite

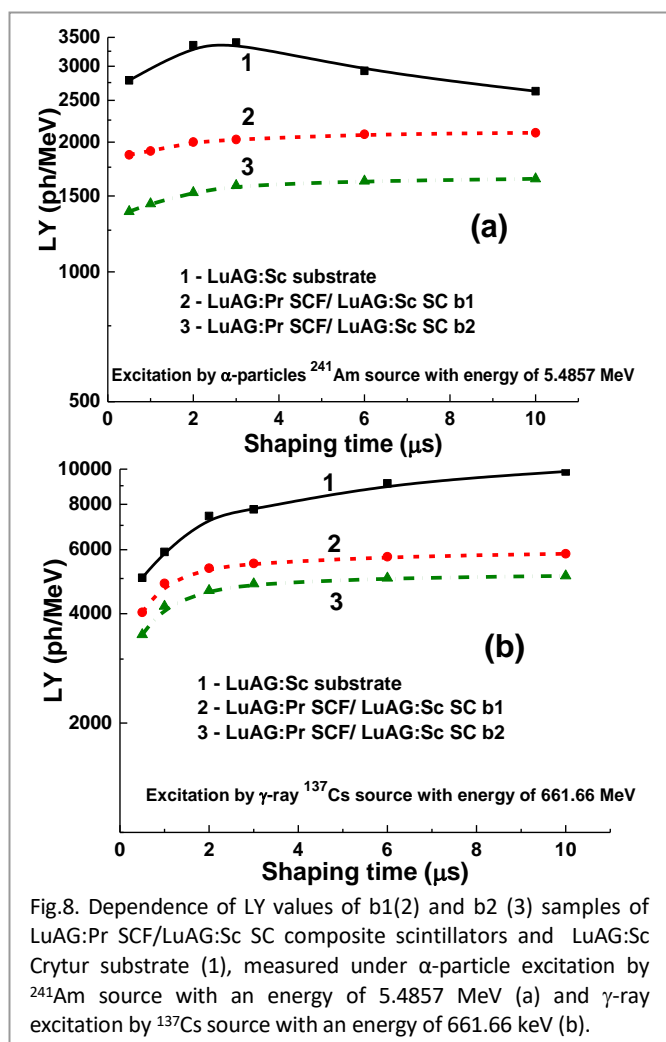


Fig.8. Dependence of LY values of b1(2) and b2 (3) samples of LuAG:Pr SCF/LuAG:Sc SC composite scintillators and LuAG:Sc Crytur substrate (1), measured under α -particle excitation by ^{241}Am source with an energy of 5.4857 MeV (a) and γ -ray excitation by ^{137}Cs source with an energy of 661.66 keV (b).

scintillators is observed under γ -quantum excitation [32, 33]. For this reason, we can conclude that the difference in the position of photopeaks of composite scintillators and substrate under γ -quantum excitation can be observed in the case when the emission spectra of LuAG based substrates (e. g., LuAG:Sc and LuAG:Pr) are

located in the UV range and differ from the luminescence spectrum of SCF scintillators (Fig.4).
View Article Online
DOI: 10.1039/DCE00266F

4.3.2 LY. Figs.7 and 8 show the LY of two samples of LuAG:Ce SCF/LuAG:Sc SC and LuAG:Pr/LuAG:Sc composite scintillators in comparison to LuAG:Sc substrate, evaluated in the photons per MeV (ph/MeV) and measured within the 0.5-10 μs shaping time interval under α -particle excitation by ^{241}Am source with an energy of 5.4857 MeV (a) and γ -ray excitation by ^{137}Cs source with an energy of 661.66 keV (b). The LY $_{\alpha}$ and LY $_{\gamma}$ values and LY $_{\alpha}$ /LY $_{\gamma}$ ratios of the scintillators under study, measured with “fast” and “slow” shaping times of 0.5 and 10 μs , under α -particle and γ -quantum excitations, respectively, are shown Table 2.

We have found that the Ce $^{3+}$ doped SCFs and LuAG:Sc substrate possess quite similar dependence of LY on shaping time (Fig.7a). Under α -particle excitation, the maximal LY values, being equal to 3405 and 2480 ph/MeV, are observed at a shaping time of 3 μs for LuAG:Sc substrate and LuAG:Ce SCF/LuAG:Sc SC a2 composite scintillator, respectively (Fig.7a). Under γ -ray excitation the respective maximal LY values for these scintillators are equal to 9910 and 6710 ph/MeV, respectively (Fig.7b). Therefore, we can correctly estimate the LY $_{\alpha}$ /LY $_{\gamma}$ value for LuAG:Sc SC scintillators, which is equal to 0.34 for a shaping time of 3 μs .

Under α -particle excitation, maximal LY values of 3404 ph/MeV is observed for LuAG:Sc substrate at a shaping time of 3 μs when for LuAG:Pr SCF/LuAG:Sc SC b2 sample a maximal LY value of 2102 ph/MeV is observed at a shaping time of 10 μs (Fig.8a). Under γ -ray excitation, the maximal LY values for these scintillators, being equal to 9851 and 5451 ph/MeV, respectively, are observed at a shaping time of 10 μs (Fig.8b). Finally, we have found that the LY $_{\alpha}$ /LY $_{\gamma}$ value for LuAG:Sc SC scintillator, changing in the 0.4-0.27 range within the 0.5-10 μs shaping time interval (Table 2).

Table 2. LY (in ph/MeV) of LuAG:Sc substrate and a1, a2 samples of LuAG:Ce SCF/LuAG:Sc and b1, b2 samples of LuAG:Pr SCF/LuAG:Sc SC composite scintillators, measured in two shaping time of 0.5 and 10 μs .

LY, ph/MeV	LuAG:Sc substrate	LuAG:Ce SCF / LuAG:Sc SC a1	LuAG:Ce SCF / LuAG:Sc SC a2	LuAG:Pr SCF / LuAG:Sc SC b1	LuAG:Pr SCF / LuAG:Sc SC b2
LY $_{\alpha}$ for shaping time of 0.5 μs	2783	1898	1445	1380	1869
LY $_{\alpha}$ for shaping time of 10 μs	2625	2528	2139	1644	2102
LY $_{\gamma}$ for shaping time of 0.5 μs	6634	4187	4276	3504	4034
LY $_{\gamma}$ for shaping time of 10 μs	9851	5900	5633	5084	5451
LY $_{\alpha}$ /LY $_{\gamma}$ for shaping time of 0.5 μs	0.40	0.45	0.34	0.39	0.46
LY $_{\alpha}$ /LY $_{\gamma}$ for shaping time of 10 μs	0.27	0.43	0.37	0.32	0.36

ARTICLE

4.3.3. Energy resolution. The dependences of the energy resolution of composite scintillators and their substrates, measured at the 0.5-10 μ s shaping time under excitation by α -particles and γ -quanta, are presented in Fig.9 and Fig.10. As can be seen from Fig.9a, the LuAG:Ce SCF parts of a1 and a2 composite scintillators at the α -particles excitation show quite good resolution in the 10.6-12.8 % and 13.6-17.4 % ranges, respectively, with small deviation from average values in the mentioned ranges. The energy resolution of LuAG:Pr SCF parts of b1 and b2 composite scintillators in the 22.1-24.0 % and 30.7-34.7 % ranges, respectively, is significantly smaller in comparison with that of LuAG:Ce SCFs mainly due to lower LY of the first ones (Fig.10a). The energy resolution of LuAG:Sc SC substrates for the registration of α -particles depends on the shaping time and shows deviation with the shaping time in the 24.6-29.4 % range (Fig.9a and 10a, curves 1). Meanwhile, under registration of γ -quanta, the energy resolution of

these substrates is much better and lies in the 7.8-12.3 % range (Fig.9b and 10b, curves 1).

View Article Online
DOI: 10.1039/DCE00266F

4.4. Scintillation decay kinetics.

For registration of the difference in the scintillation decay kinetics of the bulk and film components of composite scintillator, it is very important to analyze firstly the decay curves under α -particle and γ -ray excitations of substrates, prepared from bulk crystals of garnet compounds, in a broad range of decay intensity. Fig.11 presents the scintillation decay kinetics of LuAG:Sc substrate, under α -particles and γ -ray excitations. As we can see from this figure, the LuAG:Sc substrate shows notably different scintillation decay kinetics under α -particles and γ -quanta excitation due to the differences in the interaction of particles and quanta with the materials of scintillator of the same content. Such a difference between the scintillation decay profiles in the case of α -particle and γ -quanta

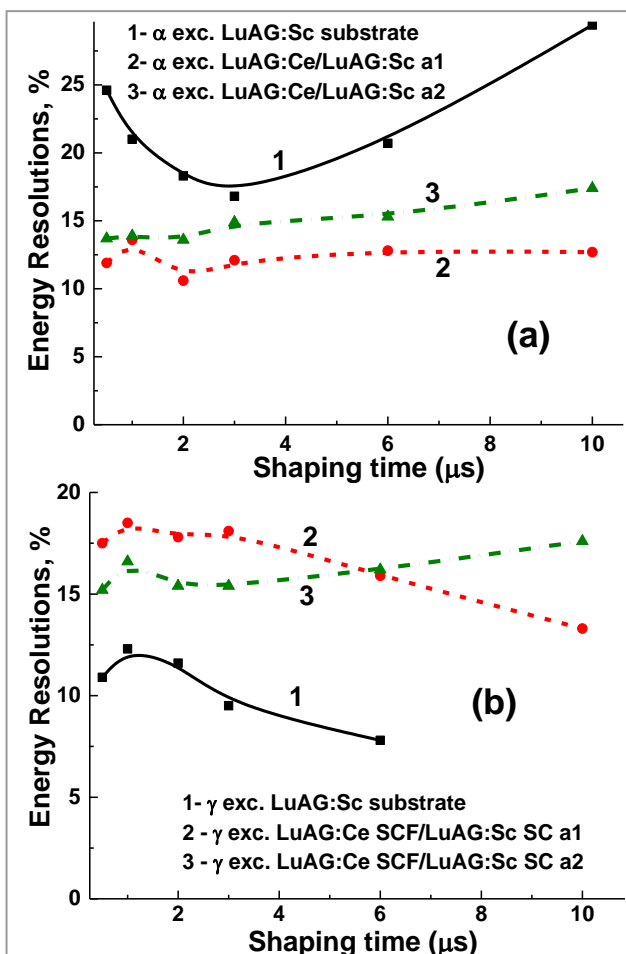


Fig.9. Energy resolution versus shaping time of two a1 (2) and a2 (3) samples of LuAG:Ce SCF/ LuAG:Sc SC CS and LuAG:Sc substrate, measured with shaping time in the 0.5-10 μ s interval under α -particle excitation by ^{241}Am source with an energy of 5.4857 MeV (a) and γ -ray excitation by ^{137}Cs source with an

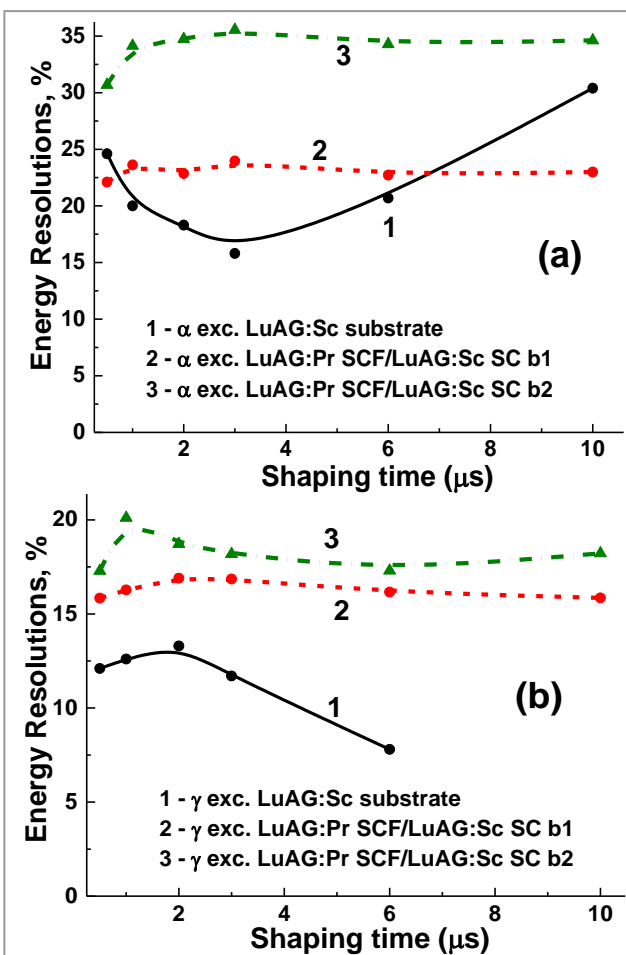


Fig.10. Energy resolution versus shaping time of two b1 (2) and b2 (3) samples of LuAG:Pr SCF/LuAG:Sc SC CS and LuAG:Sc substrate, measured with shaping time in the 0.5-10 μ s interval under α -particles excitation by ^{241}Am source with an energy of 5.4857 MeV (a) and γ -ray excitation by ^{137}Cs source with an energy of 661.66 keV (b).

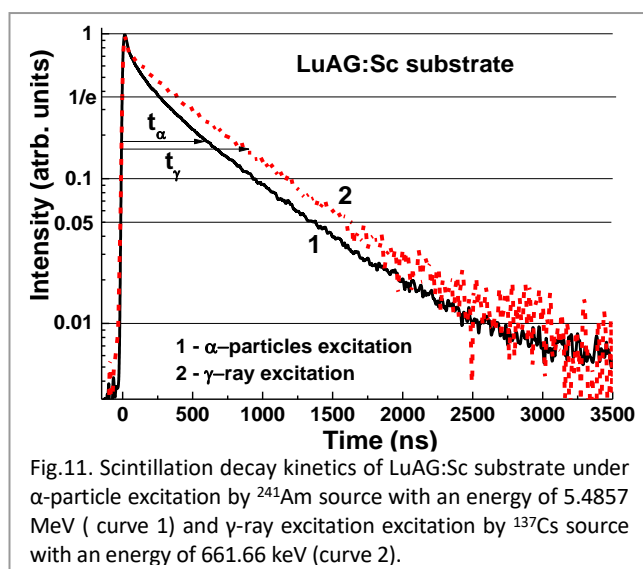


Fig.11. Scintillation decay kinetics of LuAG:Sc substrate under α -particle excitation by ^{241}Am source with an energy of 5.4857 MeV (curve 1) and γ -ray excitation by ^{137}Cs source with an energy of 661.66 keV (curve 2).

excitation LuAG:Sc substrate (Fig.11), can be presented using the so-called t_α and t_γ values as well as the t_γ/t_α or t_α/t_γ ratios of intensity decay to $1/e$, 0.1 and 0.05 levels (Table 3).

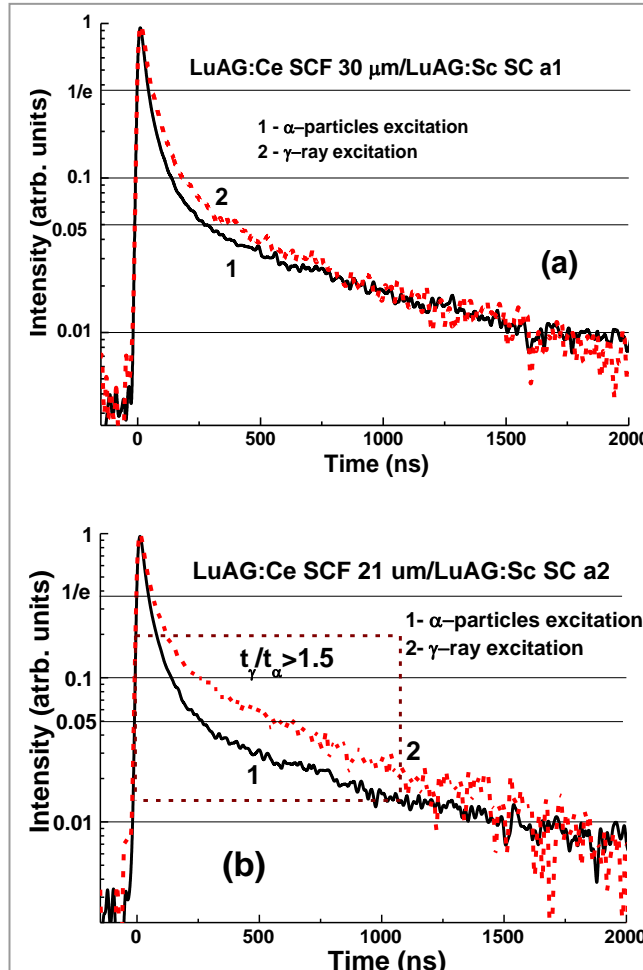


Fig.12. Scintillation decay kinetics of LuAG:Ce SCF/LuAG:Sc SC a1 (a) and LuAG:Ce SCF/ LuAG:Sc SC a2 (b) composite scintillators with a SCF thickness of 30 and 21 μm , respectively, under α -particle excitation by ^{241}Am source with an energy of 5.4857 MeV (1) and γ -ray excitation by ^{137}Cs source (2).

Table 3. Time dependence of intensity of scintillation decay from the initial value at $t = 0$ to $1/e$, 0.1, and 0.05 levels for LuAG:Sc substrate.

Intensity	LuAG:Sc substrate		
	t_α , ns	t_γ , ns	t_α/t_γ ratio
1/e	264	396	1.5
0.1	946	1231	1.30
0.05	1394	1814	1.30

We can expect that the rate of separation of the scintillation signal at the registration of α -particles and γ -rays can be significantly improved in the composite epitaxial structures based on the films and crystals of different garnet compounds in comparison with crystal-substrate scintillators. Indeed, for two LuAG:Ce SCF/LuAG:SC SC epitaxial structures, the scintillating signal coming from the SCF and SC components of composite scintillator can be separated in the time interval from 0 to 1000 ns (Fig.12), especially for a2 sample with a SCF thickness of 21 μm (Fig.12b). Meanwhile, much better situation is observed in the case of LuAG:Pr SCF/LuAG:Sc SC structures (Fig.13). The separation of the signal coming from SCF and SC substrate parts of

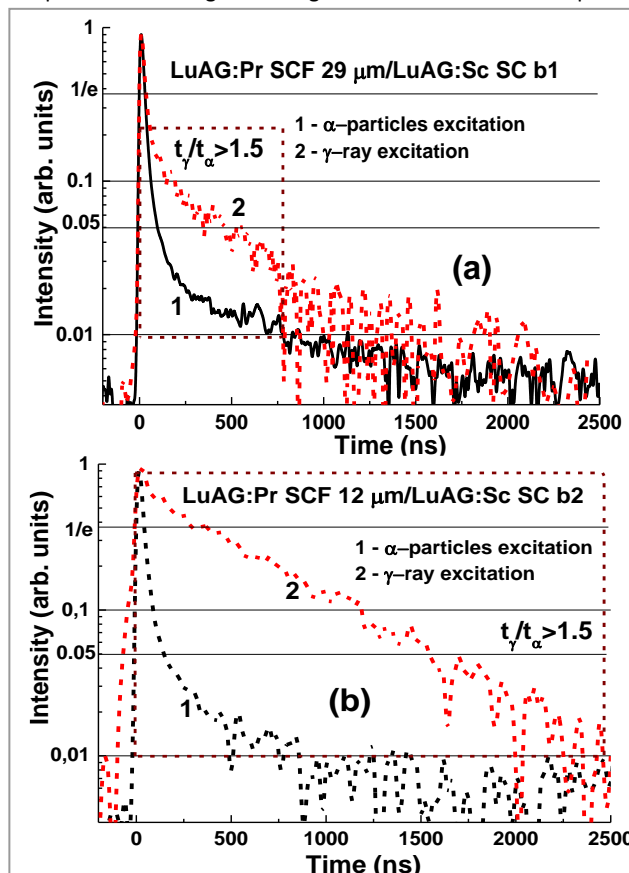


Fig.13. Scintillation decay kinetics of LuAG:Pr SCF/LuAG:Sc SC b1 (a) and LuAG:Ce SCF/ LuAG:Sc SC b2 (b) composite scintillators with a SCF thickness of 29 and 12 μm , respectively, under α -particle excitation by ^{241}Am source with an energy of 5.4857 MeV (1) and γ -ray excitation by ^{137}Cs source with an energy of 661.66 keV (2).

View Article Online

Table 4. Time dependence of intensity of scintillation decay from the initial value at $t = 0$ to $1/e$, 0.1 and 0.05 level for LuAG:Ce SCF/LuAG:Sc66F SC a1 and a2 composite scintillator samples under α -particle excitation by ^{241}Am source and γ -ray excitation by ^{137}Cs source.

Intensity	LuAG:Ce SCF/LuAG:Sc SC a1			LuAG:Ce SCF/LuAG:Sc SC a2		
	t_α , ns	t_γ , ns	t_γ/t_α ratio	t_α , ns	t_γ , ns	t_γ/t_α ratio
1/e	43.6	57.8	1.32	46.9	63.3	1.34
0.1	148.5	192.1	1.29	150.3	267.8	1.8
0.05	270.8	382.6	1.41	266	713.8	2.68
0.01	1941.4	2187	1.13	1741.4	3430.3	1.96

this composite scintillator can be obtained in the much wider time interval, especially for b2 sample with a SCF thickness of 12 μm (Fig.13b), where the scintillation response under γ -ray excitation in the 100-1000 ns time range is significantly slower than that under α -particle excitation.

The above mentioned conclusions are confirmed also by comparison of the differences in the decay times at $1/e$, 0.1, 0.05 and 0.01 levels for the decay curves under α -particle and γ -quantum excitations (so called t_γ/t_α ratio) in LuAG:Ce SCF/LuAG:Sc SC and LuAG:Pr SCF/LuAG:Sc SC composite scintillators and the reference LuAG:Sc crystal substrate (Fig.14).

As one can see from this figure, the t_γ/t_α ratio is notably higher (1.32-1.96) in LuAG:Ce SCF/ LuAG:Sc SC composite scintillators (Fig.14a, curve 2) than that in LuAG:Sc SC substrate (Fig.14a, curve 1), between the 0.2 and 0.01 intensity levels. Thus, the differences in the t_γ/t_α ratio significantly change for LuAG:Ce SCF/LuAG:Sc SC composite scintillator at different registration levels and can be presented in Fig.14a as the inclined curves with large slope (curves 2 and 3). This means that separation of scintillations from the SCF and SC components of such composite scintillator can be obtained with the maximal possible rate in some intervals between the 0.2 and 0.01 intensity levels in the 0-1000 ns time interval (dashed rectangle in Fig.12b). In such rectangle the faster by 1.34-1.96 times scintillation response under α -particle excitation is observed in comparison with the response under γ -ray excitation (Table 4).

In LuAG:Pr SCF/ LuAG:Sc SC composite scintillators, the t_γ/t_α ratio for $1/e$ to 0.01 levels is significantly higher than that in LuAG:Sc

substrate, especially for b2 sample (Fig.14b). The differences in the t_γ/t_α ratio significantly change for such type of composite scintillator at different registration levels and can be presented in Fig.14b as the two inclined lines with large slopes (curves 4). As can be seen from Fig.13b, and Fig.14b, the optimal separation of scintillation from the SCF and SC components of such composite scintillator with maximal rate can be obtained in the wide area from $1/e$ to 0.01 levels in time intervals of 0-2500 ns (Fig.13b) where the scintillation response under γ -ray excitation is by 1.5-4.5 time slower than that corresponding to the case of α -particle excitation (Table 5).

5 Discussion

A crucial parameter for analysis of the differences between the decay curves of the composite scintillator under α -particle and γ -quantum excitations is t_α/t_γ or t_γ/t_α ratios, which need to be "as large as possible in the wide time interval" for the chosen components of SCF and substrate scintillators [5]. Generally, the scintillation signal from two scintillators can be easily separated if t_α/t_γ or t_γ/t_α ratio is above 1.5 [15]. Such a demand is fully satisfied for the both type of composite scintillators under study (Fig.14a, curve 3 and 14b, curves 4, 5).

Meanwhile, for the best b2 sample of LuAG:Pr SCF/LuAG:Sc SC composite scintillator, the t_γ/t_α values above 1.5 are observed in much wider range of scintillation intensity decay from 0.2 to 0.01 levels (Fig.14b, curve 4, 5) than those in the case of the best a2 sample of LuAG:Ce SCF/LuAG:Sc SC composite scintillator, where the t_γ/t_α values above 1.5 are observed in the narrow interval of intensity decay between 0.2 and 0.01 levels (Fig.12b and Fig.14a, curve 3). The reasons

Table 5. Time dependence of scintillation intensity decay from the initial value at $t = 0$ to $1/e$, 0.1, and 0.05 levels for LuAG:Pr SCF/LuAG:Sc SC b1 and b2 composite scintillator samples under α -particle excitation by ^{241}Am source and γ -ray excitation by ^{137}Cs source.

Intensity	LuAG:Pr/LuAG:Sc b1			LuAG:Pr/LuAG:Sc b2		
	t_α , ns	t_γ , ns	t_γ/t_α ratio	t_α , ns	t_γ , ns	t_γ/t_α ratio
1/e	23.4	36.9	1.35	42.7	408.8	9.6
0.1	65.2	309.8	4.75	93.5	1377.2	14.7
0.05	95.6	897.8	9.39	134	2087	15.6

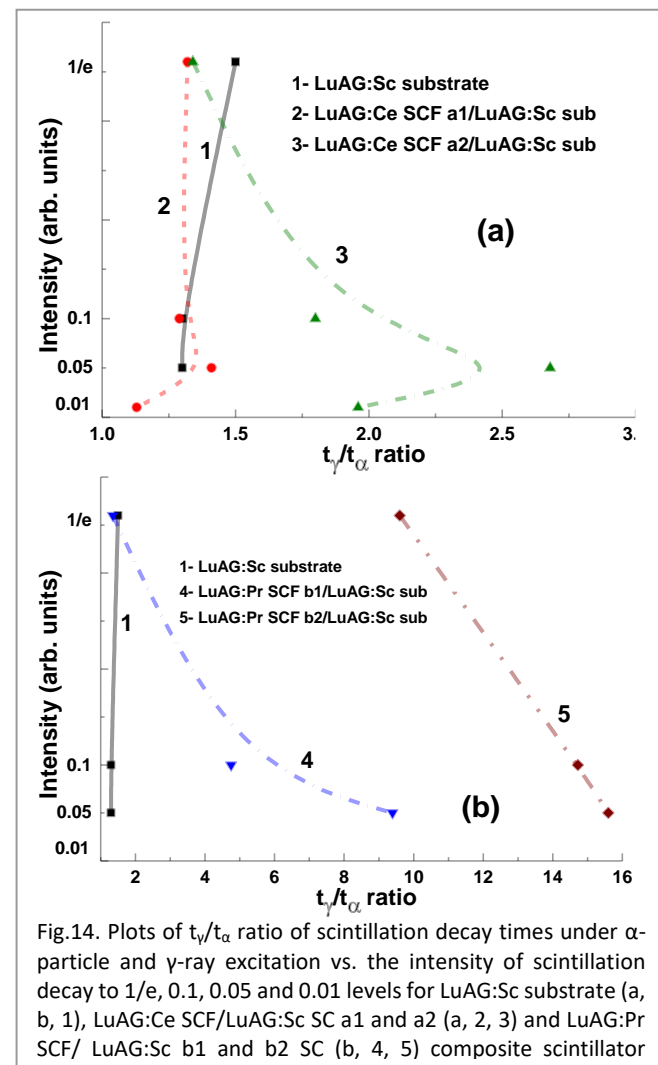


Fig.14. Plots of t_γ/t_α ratio of scintillation decay times under α -particle and γ -ray excitation vs. the intensity of scintillation decay to $1/e$, 0.1, 0.05 and 0.01 levels for LuAG:Sc substrate (a, b, 1), LuAG:Ce SCF/LuAG:Sc SC a1 and a2 (a, 2, 3) and LuAG:Pr SCF/ LuAG:Sc b1 and b2 SC (b, 4, 5) composite scintillator

for the mentioned differences in the separation of the scintillation signals under α -particle and especially γ -ray excitations can be addressed to the different types of activators and thicknesses of SCF parts of the both types of composite scintillators (see Fig.15). Generally, under γ -ray excitation of composite scintillators, the γ -quanta are always absorbed partly by SCF scintillators. The rate of absorbed γ -quanta strongly depends on the SCF thickness (Fig.15). For this reason, the initial parts of the decay curves of composite scintillators under γ -ray excitation follow to the decay kinetics of SCF parts (Fig.15). Namely, the initial parts of the decay kinetics are faster for LuAG:Pr SCF/LuAG:Sc composite scintillator (Fig.15b, curve 3) in comparison with LuAG:Ce SCF/LuAG:Sc SC counterpart (Fig.15a, curves 2 and 3) due to the faster decay kinetics of the Pr^{3+} luminescence than that in the case of Ce^{3+} dopant [20, 25]. The shape of scintillation decay of composite scintillators under γ -quantum excitation will depend also on the ratio between the scintillation LY of their SCF and substrate parts and the ratio between thicknesses of SCF and substrate. Indeed, if the thickness of the films is optimal (10-

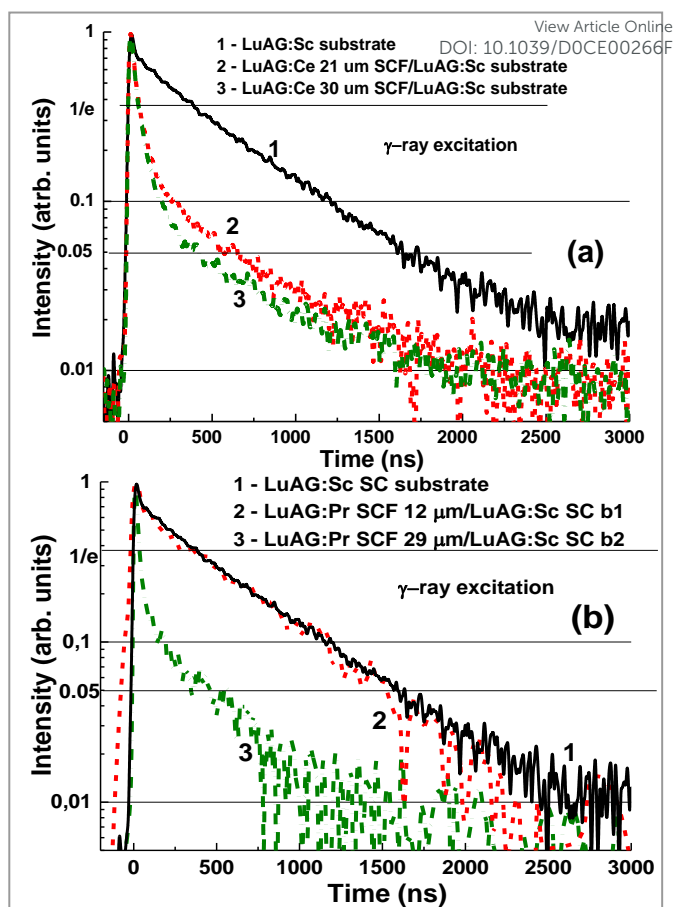


Fig.15. Scintillation decay kinetics of LuAG:Sc substrate (curve 1a and 1b), LuAG:Ce SCF/LuAG:Sc SC a1 and a2 (curve 2a) and composite scintillators with a SCF thickness of 30 and 21 μm , respectively, and LuAG:Pr SCF/LuAG:Sc SC b1 (curve b2) and b2 (curve b3) composite scintillators under γ -ray excitation by ^{137}Cs source with an energy of 661.66 keV.

12 μm), the influence of SCF on scintillation signal coming from LuAG:Sc substrate is small (Fig.15b, curves 1 and 2). However, when the thickness of LuAG:Ce or LuAG:Pr SCFs is relatively large (20-30 μm), such influence is significant yet (Fig.15a, curves 2,3 and Fig.15b, curve 3). Therefore, the choice of the respective thickness of SCF and substrate parts of composite scintillators is crucial for the optimization of their properties.

Generally, it is optimal that the thickness of composite scintillators is equal or slightly larger than the passway (or penetration depth) of particles in the materials. For LuAG host, such SCF thickness lies in the 10-12 μm range. In this case the unwanted absorption of γ -quanta by SCF scintillators will be minimal as well (Fig.13b, curve 2). Meanwhile, due to necessity of the absorption of γ -quanta with the energy in the range from tens to hundred KeV, the thickness of LuAG:Sc substrate needs to be “as thick as possible” in the conditions of LPE growth of composite scintillators. However, taking into account the problems with stable mounting of heavy and

ARTICLE

thick substrate in Pt holder for LPE growth, the most optimal range for the LuAG:Sc substrate thickness lies between 1 and 2 mm.

Meanwhile, taking into account the good results for the case of using LuAG:Sc substrates with a thickness of 1mm for producing the LuAG:Ce SCF/LuAG:Sc SC composite scintillators, we estimate also the difference in scintillation decay kinetics of LuAG:Pr SCF/LuAG:Sc SC composite scintillators under α -particle and γ -quantum excitation based on the data presented in Fig.13b. The result of such estimation for LuAG:Pr SCF 12 μm /LuAG:Sc 1mm composite scintillator is very encouraging (Fig.13b and Table 6). Namely, the scintillation decay profiles (Fig.13b) and the plot of t_{γ}/t_{α} ratio vs. the intensity of scintillation decay (Fig.14b, curve 5) show nice conditions for discrimination of the scintillation signals under α -particle and γ -quantum excitation. Namely, the t_{γ}/t_{α} ratio changes from 9.6 to 15.6 in the whole range of intensity decay up to 0.05 level. It is worth to mention here that the LuAG:Pr SCF/LuAG:Sc SC composite shows the best scintillation performance from all the developed by us types of composite scintillators based on the LPE grown epitaxial structures of garnet compounds [26, 27, 31, 33].

Conclusion

Two new types of advanced composite scintillators, based on the LuAG:Ce and LuAG:Pr single crystalline films (SCFs) with the thickness from 12 to 30 μm , and LuAG:Sc substrate with a thickness of 1 mm, prepared from the respective single crystal (SC) with a Sc concentration of 0.5 %, were produced by the LPE method from melt solutions using PbO-B₂O₃ flux.

Under excitation using α -particles by ²⁴¹Am (5.5 MeV) source and γ -quanta of ¹³⁷Cs (0.662 MeV) source, the notable differences in the scintillation decay kinetics of LuAG:Ce SCF/LuAG:Sc SC and LuAG:Pr SCF/LuAG:Sc SC composite scintillators are observed. Such differences can be characterized by the t_{γ}/t_{α} scintillation intensity decay time ratio, which for the mentioned types of composite scintillators occurs within the 1.32-1.96 and 1.35-15.6 ranges, respectively, at the decay intensity within two decades from the 1/e level down to 0.05 level. Thus, both types of the mentioned above composite scintillators in principle can be applied for separation of the signals coming from their film and bulk parts at registration of the mixed radiation fluxes containing α -particles and γ -rays.

In LuAG:Ce SCF/ LuAG:Sc SC composite scintillator the signal coming from the SCF and SC components can be separated with the large enough t_{α}/t_{γ} decay time ratio (>1.5) in the quite narrow range

of scintillation intensity decay from the 0.1 level down to 0.01 level in the time interval from 0 to 1.75 μs . Meanwhile, the LuAG:Pr SCF/LuAG:Sc SC composite scintillator possesses some advantages with respect to LuAG:Ce SCF/LuAG:Sc SC counterpart due to the fact that scintillating signal coming from the SCF and SC components of this type composite scintillator can be separated with the large t_{γ}/t_{α} decay time ratio in the mentioned ranges of scintillation intensity decay and time intervals.

Furthermore, after optimization of the LuAG:Pr SCF thickness in the 12-15 μm range and the thickness of LuAG:Sc substrate above 1 mm, the best scintillation figure of merit of LuAG:Pr SCF/ LuAG:Sc SC composite scintillators can be achieved. Namely, the scintillating signals from LuAG:Pr 12 μm SCF/LuAG:Sc 1 mm SC composite scintillator sample under α -particle and γ -ray excitation can be separated with the extremely large t_{γ}/t_{α} decay time ratio in the 1.35-15.6 interval in the whole range of scintillation intensity decay from the 1/e level down to 0.01 level and the wide time interval from 0 to 2.5 μs . For today, this is the best result for all of the developed composite scintillators on the base of the epitaxial structures of garnet compounds.

Acknowledgment

The work was performed in the framework of Polish NCN 2018/31/B/ST8/03390 project and Czech Science Foundation 16-15569S project.

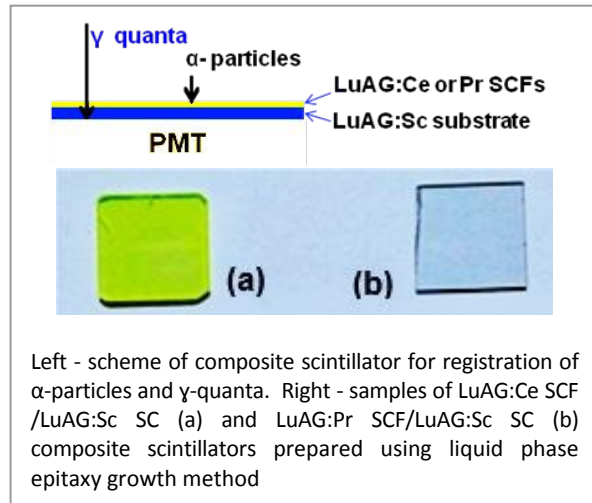
References

1. M. Globus, Boris Grinyov, Jon Kying Kim. Inorganic scintillators for modern and traditional applications, Institute for Single Crystals, Kharkiv, 2015.
2. M. Nikl, A. Yoshikawa, *Advanced Optical Materials*, 2015, 3, 463-481.
3. A. Yoshikawa, V. Chani, *MRS Bulleting, Recent Advances in Bulk Crystal Growth*, 2009, 34, 266-270.
4. V. Kononets, K. Lebbou, O. Sidletskiy, Yu. Zorenko, M. Lucchini, K. Pauwels, E. Auffray, *Springer Proceeding in Physics*, 2018, 200, 114-128.
5. Yu. Zorenko, S. Novosad, M. Pashkovskii, A. Lyskovich, V. Savitskii, M. Batenchuk, P. Malyutenkov, N. Patsagan, I. Nazar, V. Gorbenko, *Journal of Applied Spectroscopy* 1990, 52, 645-649.

- 6.B. Ferrand, B. Chambaz, M. Couchaud, *Optical Materials* 1999, 11, 101-114.
- 7.Nanocomposite, Ceramic, and Thin Film Scintillators, Ed. By M. Nikl, Pan Stanford Publ. Singapore, 2017. ISBN 978-981-4745-22-2.
- 8.Yu. Zorenko, M. Batenchuk, V. Gorbenko, M. Pashkovsky, *Proc. SPIE*, 1997, 2967, 101-104.
- 9.Yu. Zorenko, V. Gorbenko, I. Konstankevych, B. Grinev, M. Globus, *Nuclear Instrument and Methods for Physical Research A* 2002, 486, 309-314.
10. A. Koch, C. Raven, P. Spanne, A. Snigirev, *J. Opt. Soc. Am.* 1998, A15, 1940-1951.
11. T. Martin, A. Koch, *Journal of Synchrotron Radiation*, 2006, 13, 180-194.
12. Yu. Zorenko, V. Gorbenko, I. Konstankevych, M. Pashkovsky, M. Globus, B. Grinyov, V. Tarasov, P. Dorenbos, C.W.E. Van Eijk, E. Van Loef, *Proceedings of the 5th Intern. Conference on Inorganic Scintillators and Their Applications*, Moscow, 2000, 476-481.
13. M. Globus, B. Grinyov, M. Ratner, V. Tarasov, V. Lyubinskiy, Yu. Zorenko, I. Konstankevych, *IEEE Nuclear Science Symposium and Medical Imaging Conference*, 2002, 1, 352-356.
14. Yu. Zorenko, V. Gorbenko, T. Voznyak, I. Konstankevych, V. Savchyn, M. Batentschuk, A. Winnacker, Ch. J. Brabec, *IEEE Transaction on Nuclear Science*, 2012, 59, 2281-2285.
15. Phoswich Detectors for High Energy Backgrounds (Saint Gobain), Feb. 19, 2020. Available at <http://www.detectors.saint-gobain.com>.
16. M. Nikl, A. Yoshikawa, K. Kamada, K. Nejezchleb, C.R. Stanek, J.A. Mares, K. Blazek, *Progress in Crystal Growth and Characterization of Materials*, 2013, 59, 47-72.
17. J.M. Ogięto, A. Zych, T. Justel, A. Meijerink, C.R. Ronda, *Optical Materials* 2013, 35, 322-331.
18. Yu. Zorenko, V. Gorbenko, T. Voznyak, T. Martin, P.-A. Douissard, J.A. Mares, M. Nikl, *Proc. SPIE*, 2009, 7310, 731007.
19. M. Nikl, J. Tous, J. A. Mares, P. Prusa, E. Mihokova, K. Blazek, A. Vedda, Yu. Zorenko, V. Gorbenko, V. Babin, *Proc. SPIE*, 2009, 7310, 731008.
20. V. Gorbenko, A. Krasnikov, M. Nikl, S. Zazubovich, Yu. Zorenko, *Optical Materials*, 2009, 31, 1805-1807.
21. N.N. Ryskin, P. Dorenbos, C.W.E. van Eijk, S. Kh. Batygov, *J. Phys.: Condens. Matter.* 1994, 6, 10423-10434.
22. Yu. V. Zorenko, *Optics and Spectroscopy*, 2006, 100, 572-580.
23. Yu. Zorenko, V. Gorbenko, A. Voloshinovskii, G. Stryganyuk, S. Nedilko, V. Degoda, O. Chykova, *Phys. stat. sol. (c)*, 2005, 2, 105-108. DOI: 10.1002/PSSC.200500266F
24. Yu. Zorenko, V. Gorbenko, T. Voznyak, V. Savchyn, S. Nizhankovskiy, A. Dan'ko, V. Puzikov, V. Laguta, J.A. Mares, M. Nikl, K. Nejezchleb, M. Batentschuk, A. Winnacker, *Optical Materials*, 2012, 34, 2080-2085.
25. Yu. Zorenko, V. Gorbenko, T. Zorenko, O. Sidletskiy, A. Fedorov, P. Bilski, A. Twardak, *Physica Status Solidi RRL*, 2015, 9, 489-493.
26. S. Witkiewicz-Lukaszek, V. Gorbenko, T. Zorenko, K. Paprocki, O. Sidletskiy, I. Gerasymov, J.A. Mares, R. Kucerkova, M. Nikl, Yu. Zorenko, *IEEE Transaction on Nuclear Science*, 2018, 65, 2114-2119.
27. S. Witkiewicz-Lukaszek, V. Gorbenko, T. Zorenko, K. Paprocki, O. Sidletskiy, I. Gerasymov, J.A. Mares, R. Kucerkova, M. Nikl, Yu. Zorenko, *Optical Materials*, 2018, 84, 593-599.
28. Yu. Zorenko, M. Batentschuk, V. Gorbenko, M. Pashkovsky, I. Konstankevych, *Journal of Applied Spectroscopy*, 1999, 66, 819-823.
29. T. Zorenko, Yu. Zorenko, B. Pavlyk, R. Turchak, V. Gorbenko, I. Konstankevych, V. Savchyn and T. Voznyak, *Radiation Measurements*, 2007, 42, 557-560.
30. T. Zorenko, V. Gorbenko, A. Petrosyan, W. Gieszczyk, P. Bilski, Yu. Zorenko, *Optical Materials*, 2018, 86, 376-381.
31. Yu. Zorenko, T. Zorenko, T. Voznyak, A. Mandowski, Xia Qi, M. Batentschuk, J. Fridrich, *IOP Conf. Ser. Mater. Sci. Eng.*, 2010, 15, 2060.
32. S. Witkiewicz-Lukaszek, V. Gorbenko, T. Zorenko, O. Sidletskiy, I. Gerasymov, A. Fedorov, A. Yoshikawa, J.A. Mares, M. Nikl, Yu. Zorenko, *Crystal Growth@Dec.* 2018, 18, 1834-142.
33. S. Witkiewicz-Lukaszek, V. Gorbenko, T. Zorenko, K. Paprocki, O. Sidletskiy, A. Fedorov, J.A. Mares, R. Kucerkova, M. Nikl, Yu. Zorenko, *CrystEngComm*, 2018, 20, 3994-4002.
34. J.A. Mares, S. Witkiewicz-Lukaszek, V. Gorbenko, T. Zorenko, R. Kucerkova, A. Beitlerova, C. D'Ambrosio, J. Doluhy, M. Nikl, Yu. Zorenko, *Optical Materials*, 2019, 109268.

TOC figure

[View Article Online](#)
DOI: 10.1039/D0CE00266F



Development of Composite Scintillators Based on Single Crystalline Films and Crystals of Ce³⁺-Doped (Lu,Gd)₃(Al,Ga)₅O₁₂ Mixed Garnet Compounds

S. Witkiewicz-Lukaszek,^{†,#} V. Gorbenko,[†] T. Zorenko,[†] O. Sidletskiy,[‡] I. Gerasymov,[‡] A. Fedorov,[§] A. Yoshikawa,^{||} J. A. Mares,[⊥] M. Nikl,[⊥] and Yu. Zorenko^{*,†,ID}

[†]Institute of Physics, Kazimierz Wielki University in Bydgoszcz, Powstańców Wielkopolskich str., 2, 85090 Bydgoszcz, Poland

[‡]Institute for Scintillation Materials, National Academy of Sciences of Ukraine, av. Nauky, 60, 61001 Kharkiv, Ukraine

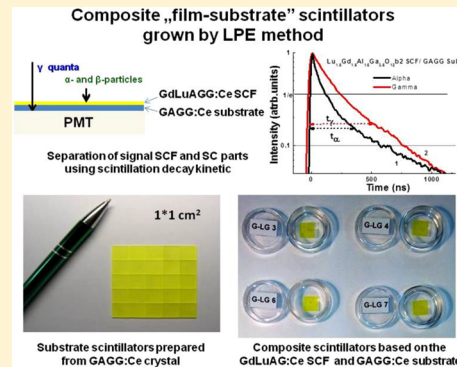
[§]SSI Institute for Single Crystals, National Academy of Sciences of Ukraine, av. Nauky, 60, 61178 Kharkiv, Ukraine

^{||}Institute for Materials Research, Tohoku University, 2-1-1 Katahira, Aoba-ku, Sendai 980-8577, Japan

[⊥]Institute of Physics, Academy of Science of Czech Republic, Cukrovarnicka str., 10, 16253 Prague, Czech Republic

[#]Faculty of Technical Physics, Poznań University of Technology, Piotrowo Street 3, 60-965 Poznań, Poland

ABSTRACT: The possibility of growth by the liquid phase epitaxy method of a new type of advanced composite scintillator based on Ce³⁺-doped single crystalline films (SCFs) of Lu_{1.5}Gd_{1.5}Al_{1.5}Ga_{3.5}O₁₂ garnet and substrates from single crystals (SCs) of Gd₃Al_{2.5}Ga_{2.5}O₁₂:Ce garnet is evidenced for the first time in this work. We show the possibility of the simultaneous registration of α -particles and γ -quanta by way of separation of the scintillation pulse height spectra and decay kinetics of SCF and crystal parts of such a composite scintillator. Namely, the significant differences in the scintillation decay kinetics of Lu_{1.5}Gd_{1.5}Al_{1.5}Ga_{3.5}O₁₂:Ce SCF/Gd₃Al_{2.5}Ga_{2.5}O₁₂:Ce SC composite scintillator under excitation by α -particles of a ²⁴¹Am (5.5 MeV) source and γ -quanta of ¹³⁷Cs (662 keV) source are observed. The respective t_{α}/t_{γ} decay times ratio in the 0–500 ns range reach up to 0.5 for this type of composite scintillator; e.g., the SCF scintillators is two times faster than the substrate scintillator. For this reason, such a type of composite scintillator can be successfully applied for the separation of the signals coming from its film and crystal parts at the registration of the mixed radiation fluxes of α -particles and γ -quanta.



1. INTRODUCTION

The technology of liquid phase epitaxy (LPE) offers now the possibility of developing luminescent materials based on the single crystalline film (SCF) of different oxide compounds.^{1–3} The fields of application of such SCFs now include cathodoluminescent screens,^{4,5} laser media,^{6,7} scintillators for registration of α - and β -particles and low-energy quanta,^{1,8,9} and scintillating screens for microtomography detectors using X-ray sources and synchrotron radiation.^{10,11}

The LPE method also opens the possibility of creating advanced types of composite scintillators (CSs) of “phoswich-type” (phosphor sandwich) for registration of the different components of ionizing radiation, for instance, for analysis of the content of mixed fluxes of particles and quanta with various penetrating depths.^{1,12–14} Such CSs present the all-solid-state crystalline systems, including one or two SCFs intended for registration of low penetrating α - and β -particles, and a bulk single crystal (SC) substrate, serving to register high penetrating radiation (X- or γ -rays).

The advantages of these types of CSs in comparison with their well-known analogues based on alkali-halide crystals¹⁵ are as follows. Such CSs are an “all-solid-state” single crystalline

system with a sharp interface between the composing scintillators with close refractive indices and a uniform distribution of the activated dopant in the volume of SCF and SC scintillators. This permits substantially eliminating the light losses at the interface of scintillators, enhancing the selectivity of registration of the different components of mixed ionizing radiations. The LPE method for CS production is an advanced method that permits accomplishing the control of different parameters of the obtained material. In particular, the thickness of film scintillators for registered particles can be obtained close to the penetration depth which is necessary for the complete absorption of α -particles (typically 10–15 μ m).¹

The possible types of CSs have been recently considered by some of us in refs 1, 12–14. The first type of CSs was created on the basis on the LPE grown epitaxial structures of Y₃Al₅O₁₂ garnet (YAG).¹ Namely, the doubly layered CSs based on the YAG:Ce SCF and YAG:Nd SC substrate were grown by the LPE method and later examined under simultaneous excitation

Received: December 5, 2017

Revised: January 6, 2018

Published: January 29, 2018

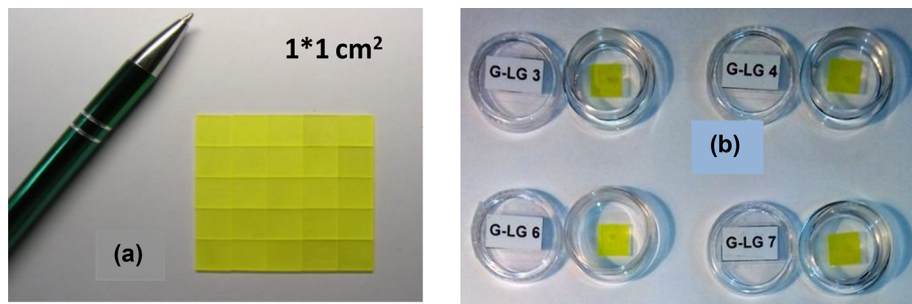


Figure 1. Substrate scintillators prepared from GAGG:Ce crystals (a) and composite scintillators of G-LG type based on the GAGG:Ce substrates and LGAGG:Ce SCFs (b).

by α -particles and γ -quanta.¹ The separation of the scintillation signals coming from SCF and SC parts of CS was performed using the discrimination of their scintillation decay kinetics. For this type of CS, a photomultiplier (PMT) for scintillation registration can be conveniently chosen with maximum sensitivity in the blue-yellow range, where the coincidence of the emission maxima of the composing scintillators is observed. This type of CS possesses high decay lifetime resolution of the SC and SCF components, which differ by almost 2 orders of magnitude in comparison with its well-known analogue based on the splice of NaI:Tl SC/CsI:Tl SC scintillators where the decay lifetime of the scintillations from the components of CS is of the same order of magnitude.¹⁵ Meanwhile, the disadvantages of such type of CSs are low light yield (LY) of the YAG:Nd SC (12% in comparison with LY of NaI:Tl SC under γ -ray ²⁴¹Am (59.5 keV) excitation) and the presence in them of unwanted intrinsic emission in the UV spectral range, caused by the luminescence of Y_{Al} antisite defect related centers.¹⁶

The second type of CS based on the YAG:Ce SCF and YAG:Sc SC substrates was also proposed in refs 1 and 12 and tested for selective registration of mixed radiation of particles and quanta. Apart from the difference in the scintillation decay kinetics, the separation of the partial components of the mixed fluxes in this type of CS may also be performed by registration of the differences in the emission spectra of the SCF and SC parts of the CS scintillator, peaked correspondingly at 530 and 280 nm.^{1,12,17} The advantage of this composition in comparison with the above examined type of CS is considerably higher LY of the YAG:Sc SC (about of 25% in comparison with LY of NaI:Tl SC under γ -ray ²⁴¹Am excitation).^{1,17} Meanwhile, the disadvantage of such type of CSs is the noticeable temperature quenching of the YAG:Sc luminescence in the room temperature (RT) range.¹⁷

The advanced triply layered CSs based on the combination of YAG:Ce and YAG:Nd SCFs, sequentially growing by the LPE method onto YAG:Sc SC substrates, were proposed also in refs 1 and 12 for the registration of the α - and β -particles on the background of X-ray or soft γ -quanta. The registration of the signals from the different parts of CS is performed by determination of the differences in the decay kinetics of the scintillations with typical lifetimes $t_{1/e}$ of 70 ns for YAG:Ce SCF, 3.0 μ s for YAG:Nd SCF and 0.9 μ s for YAG:Sc SC.¹ It should be noted that due to the low density $\rho = 4.5 \text{ g/cm}^3$ and effective atomic number $Z_{eff} = 29$, the YAG:Nd and YAG:Sc SCs may be used only for registration of low-energy ionizing radiation.^{1,12} Therefore, it is promising to fabricate CSs for registration of the mixed fluxes of particles and high-energy

quanta with using single crystalline oxide compounds, which are characterized by high values of ρ and Z_{eff} .^{12,13}

Among possible candidates of such oxide compounds, the cadmium tungstate CdWO₄ (CWO) first attracts our attention.¹⁴ AWO₄ (A = Cd, Ca, Zn) tungstates have high densities $\rho = 6.1\text{--}7.4 \text{ g/cm}^3$ and effective atomic numbers $Z_{eff} = 61\text{--}66$. CdWO₄, CaWO₄, and ZnWO₄ SCs are the well-known scintillators for radiation monitoring and computer tomography.^{18,19} Therefore, the tungstates are very promising materials for creation of SCF scintillators as well. As activators, which can effectively emit in AWO₄ (A = Cd, Ca, Zn) hosts, Bi³⁺ and Pb²⁺ ions can be first tested.^{14,20} Namely, the two types of CSs based on CWO:Bi SCF onto CWO:SC substrates and CWO:Bi SCF onto CWO:Bi SC substrates were grown by the LPE method and successfully examined for the registration of α -particles and X-rays.¹⁴ The separation of the scintillation signals was performed using the differences in the decay kinetics of CWO:Bi SCF and CWO:SC parts with a lifetime $t_{1/e}$ of 12.9 and 8.0 μ s, respectively.¹⁴ The disadvantages of such types of CSs are the long scintillation decay, the relatively low ratio of time discrimination of scintillations coming from the SCF and SC parts, as well as the significant temperature quenching of the CWO:SC luminescence in the RT range.^{18,20}

The novel approach for development of scintillation materials including the composition engineering of the cation content and band gap engineering of heavy garnet compounds^{21,22} also opens a wide possibility for development of advanced types of CSs based on the mentioned garnets. The bulk SCs of the Gd₃Al_{5-x}Ga_xO₁₂ garnets at $x = 2\text{--}3$ are now on the top list of scintillators with very high (up to 50 000 photons/MeV) light yield (LY) under excitation by γ quanta of ¹³⁷Cs (662 keV) source.²¹ The solid solution of Lu_{3-x}Gd_xAl_{5-y}Ga_yO₁₂ mixed garnets at $x = 1\text{--}3$; $y = 2\text{--}3$ are also very promising materials for creation of the SCF scintillation screens with high absorption ability for X-rays and very high efficiency for the registration of α -particles.²³⁻²⁶ The best scintillation properties of Lu_{3-x}Gd_xAl_{5-y}Ga_yO₁₂ mixed garnets are achieved at nominal content in the melt solution of Gd and Ga $x = 1.5$ and $y = 3.5$, respectively.^{23,24} With the aim of increasing the energy transfer efficiency from the host of mixed garnets to the Ce³⁺ ions, the Lu_{3-x}Tb_xAl₅O₁₂ and Gd_{3-x}Tb_xAl₅O₁₂ SCFs were also crystallized by the LPE method, and their luminescent and scintillation properties were reported as well.^{27,28} The Ga codoped analogues of these garnets can be also considered as very interesting matrixes for this purpose.^{28,29} At the same time, the possibility of growth by the LPE method of the new types of advanced CSs based on the SCF and SC of the mentioned above garnets needs the technological and experimental evidence. For this reason, in our

Table 1. Growth Conditions of LGAGG:Ce SCFs and CSs as well as Their LY under Excitation by the α -Particles of ^{239}Pu (5.15 MeV) Radioisotope, Measured with Shaping Time 12 μs in Comparison with YAG:Ce SCF Standard Sample with Photoelectron LY of 360 phels/MeV (a LY of 2650 photon/MeV), $\text{Gd}_3\text{Ga}_{2.5}\text{Al}_{2.5}\text{O}_{12}:\text{Ce}$ Substrate and Reference $\text{Gd}_3\text{Ga}_3\text{Al}_3\text{O}_{12}:\text{Ce}$ Crystals from ISM, Kharkiv (KH), and Tohoku, University, Japan (JPN)^a

no SCF and SC	nominal content of SCFs in melt solution	substrate type and their size, cm^2	real content of SCFs	$h, \mu\text{m}$	$T, ^\circ\text{C}$	$f, \mu\text{m}/\text{min}$	LY, %
YAG:Ce 42–6	$\text{Y}_3\text{Al}_5\text{O}_{12}:\text{Ce}$	YAG; 1 × 1	$\text{Y}_3\text{Al}_5\text{O}_{12}:\text{Ce}$	54			1.0
LGAGG:Ce a3	$\text{Lu}_{1.5}\text{Gd}_{1.5}\text{Al}_{1.5}\text{Ga}_{3.5}\text{O}_{12}:\text{Ce}$	GAGG:Ce; 0.5 × 0.5	$\text{Lu}_{1.85}\text{Gd}_{1.14}\text{Ce}_{0.006}$ $\text{Pb}_{0.001}\text{Al}_{2.77}\text{Ga}_{2.23}\text{O}_{12}$	12.5	1020	0.21	1.05
LGAGG:Ce a4	$\text{Lu}_{1.5}\text{Gd}_{1.5}\text{Al}_{1.5}\text{Ga}_{3.5}\text{O}_{12}:\text{Ce}$	GAGG:Ce; 0.5 × 0.5	$\text{Lu}_{1.66}\text{Gd}_{1.33}\text{Ce}_{0.008}$ $\text{Pb}_{0.003}\text{Al}_{2.81}\text{Ga}_{2.19}\text{O}_{12}$	16	1010	0.27	0.96
LGAGG:Ce a6	$\text{Lu}_{1.5}\text{Gd}_{1.5}\text{Al}_{1.5}\text{Ga}_{3.5}\text{O}_{12}:\text{Ce}$	GAGG:Ce; 0.5 × 0.5	$\text{Lu}_{1.52}\text{Gd}_{1.47}\text{Ce}_{0.0065}$ $\text{Pb}_{0.001}\text{Al}_{2.815}\text{Ga}_{2.175}\text{O}_{12}$	15	1007	0.30	1.45
LGAGG:Ce b2	$\text{Lu}_{1.5}\text{Gd}_{1.5}\text{Al}_{1.5}\text{Ga}_{3.5}\text{O}_{12}:\text{Ce}$	GAGG:Ce; 1 × 1	$\text{Lu}_{1.415}\text{Gd}_{1.52}\text{Ce}_{0.055}$ $\text{Pb}_{0.01}\text{Al}_{2.38}\text{Ga}_{2.44}\text{O}_{12}$	30	995	0.66	1.0
LGAGG:Ce b5	$\text{Lu}_{1.5}\text{Gd}_{1.5}\text{Al}_{1.5}\text{Ga}_{3.5}\text{O}_{12}:\text{Ce}$	GAGG:Ce; 1 × 1	$\text{Lu}_{1.62}\text{Gd}_{1.37}\text{Ce}_{0.005}$ $\text{Pb}_{0.001}\text{Al}_{2.7}\text{Ga}_{2.3}\text{O}_{12}$	18	1000	0.35	0.75
GAGG:Ce KH	$\text{Gd}_3\text{Al}_{2.5}\text{Ga}_{2.5}\text{O}_{12}:\text{Ce}$	—; 1 × 1			900		340
GAGG:Ce JPN	$\text{Gd}_3\text{Al}_2\text{Ga}_3\text{O}_{12}:\text{Ce}$	—; 1 × 1			1000		331

^a h - SCF thickness; f - velocity of SCF growth; T - SCF growth temperature.

work we present for the first time the results of research directed on the creation of the advanced CSs based on the SCF of Ce^{3+} -doped $\text{Lu}_{1.5}\text{Gd}_{1.5}\text{Al}_{1.5}\text{Ga}_{3.5}\text{O}_{12}$ mixed garnets and substrates from SC of $\text{Gd}_3\text{Al}_{2-3}\text{Ga}_{3-2}\text{O}_{12}:\text{Ce}$ garnets by the LPE method.

2. GROWTH OF COMPOSITE SCINTILLATORS BASED ON $\text{Lu}_{1.5}\text{Gd}_{1.5}\text{Al}_{1.5}\text{Ga}_{3.5}\text{O}_{12}:\text{Ce}$ SCF AND $\text{Gd}_3\text{Al}_{2.5}\text{Ga}_{2.5}\text{O}_{12}:\text{Ce}$ CRYSTALS

The two sets (a and b series) of CSs of G-LG type based on the SCFs with nominal content $\text{Lu}_{1.5}\text{Gd}_{1.5}\text{Al}_{1.5}\text{Ga}_{3.5}\text{O}_{12}:\text{Ce}$ (LGAGG:Ce) were grown by the vertically deepening LPE method onto $\text{Gd}_3\text{Al}_{2.5}\text{Ga}_{2.5}\text{O}_{12}:\text{Ce}$ (GAGG:Ce) substrates with a lattice constant of 12.228 Å from supercooling melt solutions using $\text{PbO-B}_2\text{O}_3$ flux (Figure 1). For comparison, the sets of LGAGG:Ce SCF samples were also grown onto undoped GAGG substrates. The growth conditions of the SCF and composite scintillators (of the SCF and the substrate) were investigated, and the content and structural properties as well their absorption, cathodoluminescence, and scintillation properties are presented in Table 1 in detail.

The real composition of SCF scintillators was determined using a JEOL JSM-820 electronic microscope, equipped by an EDX microanalyzer with IXRF 500 and LN2 Eumex detectors. Composition from the EDX microanalyzer was compared with the content $\text{Lu}_{1.5}\text{Gd}_{1.5}\text{Al}_{1.5}\text{Ga}_{3.5}\text{O}_{12}:\text{Ce}$ in the melt solution 1. As can be seen from Table 1, the content of Lu and Gd cations in SCFs is strongly affected by the temperature and velocity of their growth. Generally, at higher growth temperatures, the large content of Lu cations up to $x = 1.62-1.85$ is observed in LGAGG:Ce a3, a4, and b5 SCF samples in comparison with the calculated value $x = 1.5$ in the melt solution, whereas at lower growth temperatures the concentration of Gd cations in SCFs is quite close to the calculated value, namely, $x = 1.52$ for b2 sample (Table 1 and Figure 2, curves 1, 2 and 3, 4, respectively). Meanwhile, the content of Ga cations in SCFs, grown onto GAGG substrates, less affects the growth temperature in the range of higher temperatures (Figure 2, curve 5) but is notably increased at lower growth temperatures (Figure 2, curve 6). It is also worth to note here that the segregation coefficient of Ga ions in SCF grown from the melt

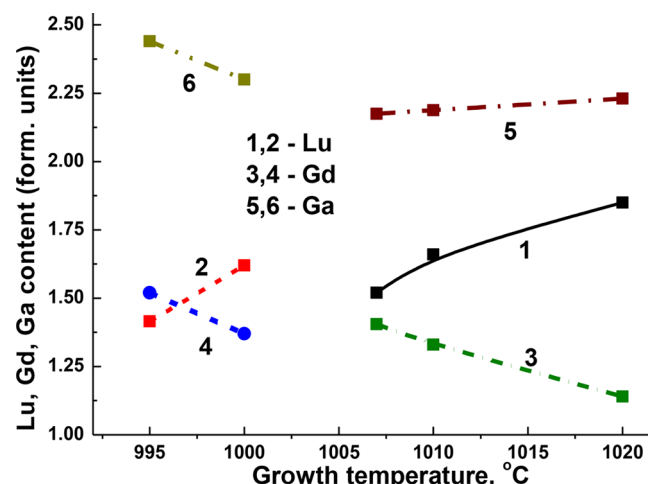


Figure 2. Dependence of Lu (1, 2) and Gd (3, 4) content in SCFs with nominal content $\text{Lu}_{1.5}\text{Gd}_{1.5}\text{Al}_{1.5}\text{Ga}_{3.5}\text{O}_{12}$, grown onto GAGG (1, 3) and GAGG:Ce (2, 4) substrates.

solution with the nominal content $\text{Lu}_{1.5}\text{Gd}_{1.5}\text{Al}_{1.5}\text{Ga}_{3.5}\text{O}_{12}:\text{Ce}$ onto GAGG and GAGG:Ce substrates is slightly larger than that reported in ref 24 and equal to 0.64–0.70 for growth temperatures in the 1020–995 °C range.

The concentration of Ce activator and Pb flux related dopant typically increases with decreasing the growth temperature and vice versa. Meanwhile, for reaching the highest scintillation LY the most important is the value of $K = \text{Ce}/\text{Pb}$ ion ratio in SCFs, and this ratio is the largest ($K = 6.5$) in a6 sample, whose LY is significantly higher than that in other samples under study with $K = \text{Ce}/\text{Pb}$ ratio in the 2.7–5 range. For b5 SCF sample the Ce and Gd concentrations are too small ($x = 0.005$ and 1.35) that cannot allow reaching a high LY of scintillation even at a relatively high Ce/Pb ratio $K = 5$ (see Table 1).

The X-ray diffraction (XRD) measurements (spectrometer DRON 4, $\text{CuK}\alpha$ X-ray source) were used for characterization of the structural quality of $\text{Lu}_{1.5}\text{Gd}_{1.5}\text{Al}_{1.5}\text{Ga}_{3.5}\text{O}_{12}:\text{Ce}$ SCFs, grown onto $\text{Gd}_3\text{Al}_{2.5}\text{Ga}_{2.5}\text{O}_{12}:\text{Ce}$ SC substrates with the lattice constant 12.228 Å (Figure 3). From the respective XRD patterns of these SCFs, we can also calculate the lattice

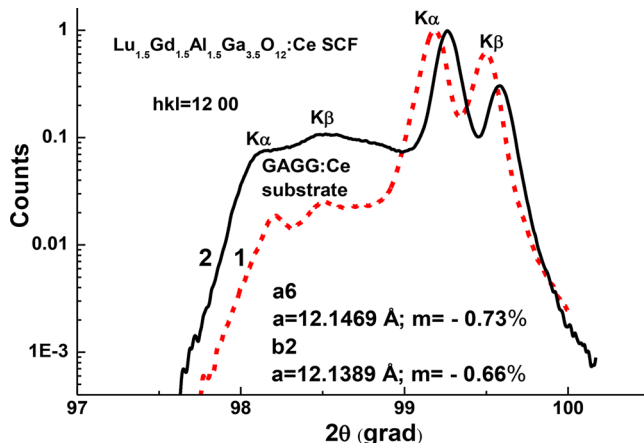


Figure 3. XRD patterns of (1200) planes of $\text{Lu}_{1.5}\text{Gd}_{1.5}\text{Al}_{1.5}\text{Ga}_{3.5}\text{O}_{12}:\text{Ce}$ SCF a6 and b2 samples grown onto $\text{Gd}_3\text{Al}_{2.5}\text{Ga}_{2.5}\text{O}_{12}:\text{Ce}$ substrates with a lattice constant of 12.228 \AA . The SCF/substrate lattice misfit m lies in the $-(0.66-0.77)\%$ range.

constants of the respective garnet compositions and estimate the misfit between the lattice constants of SCFs and GAGG substrate $\Delta a = (a_{\text{SCF}} - a_{\text{sub}})/a_{\text{sub}} \times 100\%$ (Figure 3). Namely, the lattice constant of $\text{Lu}_{1.5}\text{Gd}_{1.5}\text{Al}_{1.5}\text{Ga}_{3.5}\text{O}_{12}:\text{Ce}$ a6 and b2 SCF samples due to the deviation of the cation content was changed from 12.1389 \AA in a6 sample to 12.1469 \AA in b2 sample and the value of misfit m changed from -0.73% to -0.66% for these SCF samples (Figure 3).

3. LUMINESCENT AND SCINTILLATION PROPERTIES OF CSS BASED ON THE LGAGG:CE SCFs AND GAGG:CE SUBSTRATES

For characterization of the luminescent and scintillation properties of the CSs based on the Ce^{3+} -doped LGAGG:Ce SCFs and GAGG:Ce substrates, the absorption spectra, cathodoluminescence (CL) spectra, LY and scintillation decay kinetics measurements under excitation by α -particles and γ -quanta were applied. The CL spectra were measured at the room temperature (RT) using an electron microscope SEM JEOL JSM-820, additionally equipped with a spectrometer Stellar Net and TE-cooled CCD detector working in the 200–925 nm range. The scintillation LY (pulse height spectra measured with a shaping time of $12 \mu\text{s}$) was first measured after

each SCF growth circle using the setup based on a Hamamatsu H6521 photomultipliers (PMP), multichannel analyzer, and digital Tektronix TDS3052 oscilloscope under excitation by α -particles of Pu^{239} (5.15 MeV) radioscope. The spectra were compared with a standard YAG:Ce SCF sample with a photoelectron yield of 360 phels/MeV and LY of 2650 photons/MeV^{24,30} and also with reference $\text{Gd}_3\text{Ga}_{2.5}\text{Al}_{2.5}\text{O}_{12}:\text{Ce}$ substrates, produced either in the ISM, Kharkiv, Ukraine (GAGG:Ce KH), or high-quality $\text{Gd}_3\text{Ga}_3\text{Al}_2\text{O}_{12}:\text{Ce}$ crystals, produced in Tohoku University, Japan (GAGG:Ce JPN).

Scintillation response investigations of the selected CSs (see Table 1) were performed using a setup consisting of a hybrid PMT (HPMT DEP PP0475B), measuring electronics and PC control. Pulse height spectra were measured under excitation by α -particles with ^{241}Am (energy 5.4857 MeV) radioisotope and with γ -rays of ^{137}Cs (energy 661.66 keV) radioisotope. It is important to note here that the α -particles of ^{239}Pu and ^{241}Am sources allow exciting only the epitaxial layers of SCF samples (not their substrates) because the penetration depths of α -particles in the studied samples are approximately $12-15 \mu\text{m}$.

3.1. Absorption Spectra. The absorption spectra of the two samples of LGAGG:Ce SCFs, grown onto undoped GAGG substrates and of the GAGG:Ce SC substrate, are presented in Figure 4a. The sharp bands peaked at 275 and 313 nm in the spectra both of SCFs and substrate are caused by the $^8\text{S}_{1/2} \rightarrow ^6\text{I}_{3/2-7/2}$ transitions of Gd^{3+} ions. The first absorption band of Gd^{3+} ions strongly overlapped with the absorption bands peaked in the 260–265 nm range, which are caused by the intrinsic $^1\text{S}_0 \rightarrow ^3\text{P}_1$ transitions of Pb^{2+} flux related impurity.^{30,31}

The absorption bands in the 340–347 nm and 450–465 nm ranges (labeled as E_2 and E_1 bands, respectively) of LGAGG:Ce SCF samples and GAGG:Ce substrate are related to the 4f-5d(^2E) transitions of Ce^{3+} ions. Other Ce^{3+} absorption bands in these scintillators are located below 230 nm and related to the 4f-5d(T_{2g}) transitions.¹⁵ Due to the different temperatures of SCF growth and the respective deviation of the SCF content (Table 1), we observe notable changes in the absorption spectra of different SCFs with nominally the same content in the melt (Figure 4a, curves 2 and 3).

The difference in the positions of E_1 and E_2 bands $\Delta E_{\text{Abs}} = E_1 - E_2$ is proportional to the crystal field strength (CFS) in the dodecahedral positions of the garnet lattice, where the Ce^{3+}

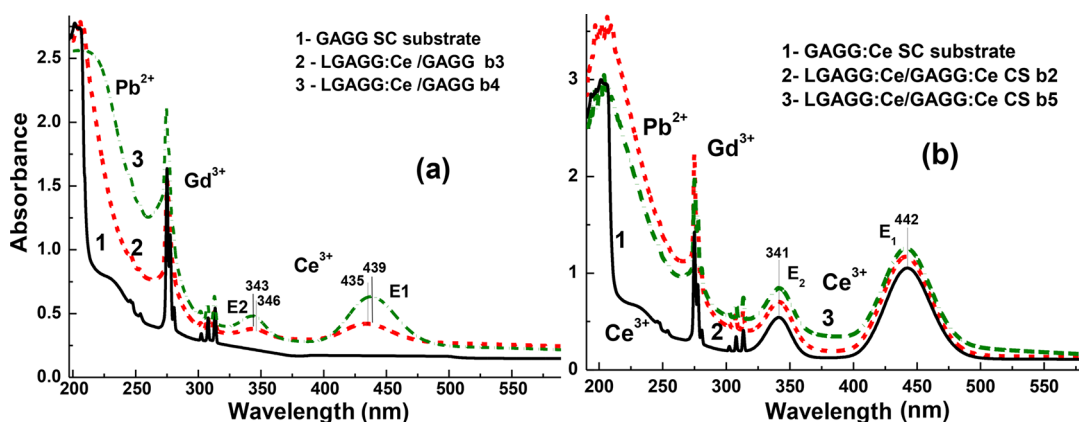


Figure 4. (a) RT absorption spectra of LGAGG:Ce b3 and b4 SCFs, grown onto undoped GAGG substrates in comparison with absorption spectra of GAGG substrate (3); (b) absorption spectra of b2 (1) and b5 (2) samples of LGAGG:Ce/GAGG:Ce CSs in comparison with absorption spectra of GAGG:Ce substrate (3).

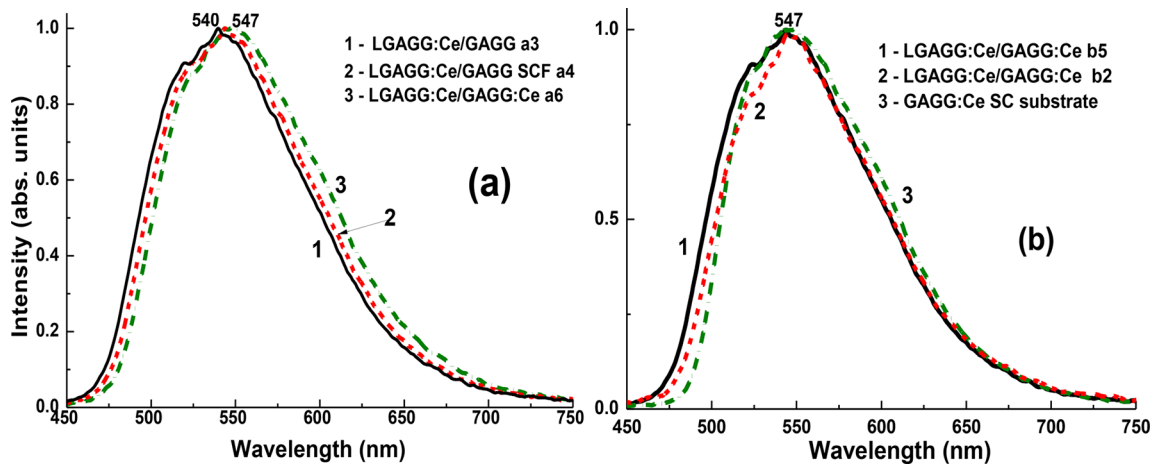


Figure 5. Normalized CL spectra at RT of a3 (1a), a4 (2a), and a6 (3a) samples of LGAGG:Ce/GAGG SCFs (a) and b5 (1b) and b2 (2b) samples of LGAGG:Ce/GAGG:Ce CSs in comparison with GAGG:Ce substrate (3).

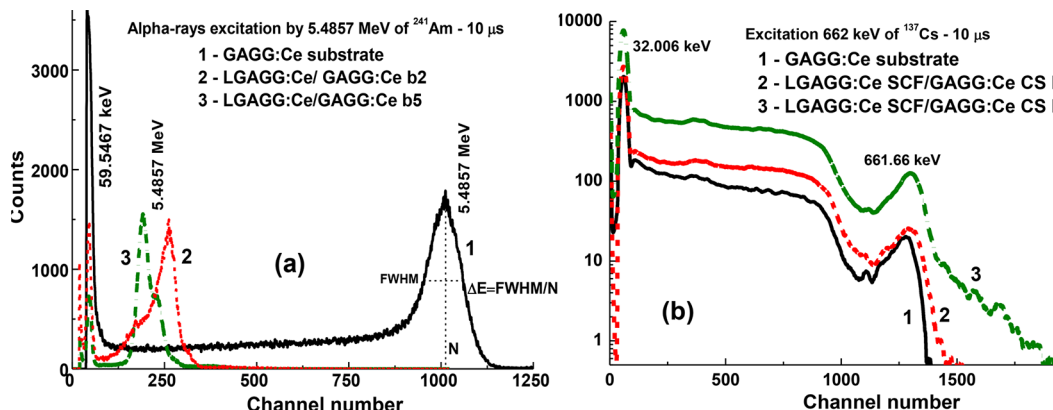


Figure 6. Pulse height spectra of b2 (1) and b5 (2) samples of LGAGG:Ce/GAGG:Ce CSs and GAGG:Ce substrate (3) measured using α -particle excitation with an energy of 5.4857 MeV of ^{241}Am source (a) and using γ -ray excitation of ^{137}Cs source with an energy of 661.66 keV (b).

ions are localized, and is very sensitive for CFS changing. Namely, we have observed the shift of positions of E_1 and E_2 Ce^{3+} absorption bands and change of the respective ΔE_{Abs} values from 0.732 to 0.789 eV in a3 and a4 SCF samples, respectively (Figure 4a, curves 2 and 3). On the basis of the ΔE_{Abs} values for these SCF samples, we have also found about a 4.8–11.7% decrease of CFS in $\text{Lu}_{1.5}\text{Gd}_{1.5}\text{Ga}_{1.5}\text{Al}_{3.5}\text{O}_{12}:\text{Ce}$ garnet in comparison with $\text{Gd}_3\text{Ga}_{2.5}\text{Al}_{2.5}\text{O}_{12}:\text{Ce}$ garnets ($\Delta E_{\text{Abs}} = 0.829$ eV, curve 3b).^{4,17}

The absorption spectra of CSs based on the epitaxial structures containing of GAGG:Ce substrate with a thickness of 1 mm and LGAGG:Ce SCFs with different thickness represent the mixture of the absorption spectra of their SCF and SC components (Figure 4b). The differences in the absorption spectra shown in Figure 3b are mainly related to the UV part of spectra and caused by the different contribution of the absorption of Pb^{2+} and Ce^{3+} ions in the SCFs under study.

3.2. Cathodoluminescence Spectra. The normalized CL spectra of three LGAGG:Ce SCFs a3, a4, a6 samples and two LGAGG:Ce SCFs in a6 and b2 CS samples and GAGG:Ce substrate are shown in Figure 5, panels a and b, respectively. The dominant wide luminescence bands, consisting of two bands peaking in the 520–527 nm and 540–547 nm ranges in the spectra of all the mentioned SCFs and substrate, correspond to the $5d^1 \rightarrow 4f$ ($^2\text{F}_{5/2,7/2}$) transitions of Ce^{3+} ions in the mentioned garnet hosts. The positions of these

bands are slightly red-shifted, and their fwhm increase sharply in a3, a4, and a6 LGAGG:Ce SCFs due to the increase of Gd content in the SCF samples grown at lower temperatures and to the increase of respective CFS in the dodecahedral position of the garnet host (Figure 5a).

The CL spectra of LGAGG:Ce SCFs in b2 CS sample (curve 2) and GAGG:Ce substrate (curve 3) with a larger Gd concentration also show the small red shift in comparison with the CL spectra of LGAGG:Ce SCF in b5 CS sample with smaller Gd content (Figure 5b, curve 1). Meanwhile, the CL spectra of all SCFs and substrates under study are rather spectrally close, and that is very suitable for registration of scintillation by one PMT with sensitivity in the 450–750 nm range with a maximum at 540–545 nm.

3.3. α - and γ -rays Spectroscopy of LGAGG:Ce/GAGG:Ce Composite Scintillators. For investigation of the scintillation properties of LGAGG:Ce/GAGG:Ce CSs under α -particle and γ -ray excitation, b2 and b5 samples with dimension $1 \times 1 \text{ cm}^2$ were selected (Table 1).

3.3.1. LY and Energy Resolution. Pulse height spectra of the main γ -ray or α -particle lines of ^{241}Am and ^{137}Cs registered by b2 and b5 samples of LGAGG:Ce/GAGG:Ce CS are presented in Figure 6, panels a and b, respectively. The main peak in Figure 6a corresponds to the total energy absorption of α -particles of ^{241}Am with an energy of 5.4857 MeV. The peak in the left part of the spectrum corresponds to the absorption of

low-energy emission line of ^{241}Am with energy of 59.6467 keV. It is worth to note that the positions of the main photopeaks, observed in Figure 6a, are substantially different for b2 and b5 samples of LGAGG:Ce/GAGG:Ce CS and for GAGG:Ce SC substrate. This means that α -particles excite only SCFs parts of CSs. Figure 6a shows also that the LY of LGAGG:Ce SCFs b2 and b5 samples under excitation by α -particles is smaller respectively by 3.8 and 5.3 times in comparison with the LY of the GAGG:Ce substrate. These results on the LY of b2 and b5 SCF samples under α -particles excitation by the ^{241}Am source are coherent with the results on these samples presented in Table 1 under excitation by the ^{239}Pu source. Such lower LY of SCF samples is caused by the negative influence of Pb flux related impurity on the scintillation properties of SCFs of many oxide compounds grown from PbO based flux.^{24,30}

Under γ -quanta excitation of b2 and b5 CS samples by ^{137}Cs source, the main peaks were observed in pulse high spectra, corresponding to the total absorption of γ -radiation with energy of 661.66 keV (Figure 6b). An additional peak is observed at lower energy at 32.006 keV, corresponding to low-energy energy line of ^{137}Cs source. It is characteristic that the positions of the main photopeaks, observed in Figure 6b, have roughly the same positions both for LGAGG:Ce SCFs and GAGG:Ce substrate and that means that γ -rays excite mainly the substrate and almost the SCF epitaxial layers.

Figure 7 presents the LY of LGAGG:Ce b2 and b5 CS samples and GAGG:Ce substrate evaluated in photons ph/

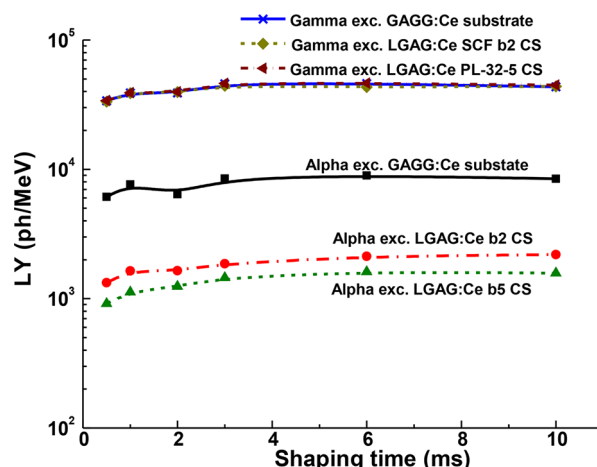


Figure 7. LY values versus shaping time of LGAGG:Ce/GAGG:Ce b2 and b5 and GAGG:Ce substrate measured under α -particles excitation by ^{241}Am source with an energy of 5.4857 MeV and γ -ray excitations by ^{137}Cs source with an energy of 661.66 keV.

MeV and measured with different shaping times in the 0.5–10 μs range under α -particle and γ -ray excitation. Namely, for b2 and b5 CS samples, excited by α -particles of ^{241}Am source with an energy of 5.4857 MeV, the LY increasing from value of 1300 to 2100 ph/MeV and from 914 to 1567 ph/MeV for shaping times from 0.5 to 10 μs , respectively. On the contrary, we have observed very similar LY values under γ -ray of 661.66 keV for both LGAGG:Ce SCFs (b2 and b5 CS samples) and for GAGG:Ce substrate. Specifically, the LY values are changed from 30 000 to 47 000 ph/MeV when the shaping times increase in the 0.5–10 μs interval.

From the data presented in Figure 7, we have also calculated the ratio between the LY of $\text{Gd}_3\text{Ga}_{2.5}\text{Al}_{2.5}\text{O}_{12}:\text{Ce}$ SC under α - and γ -excitations. Namely, for the shaping time of 10 μs this

ratio is equal to $\text{LY}_\alpha/\text{LY}_\gamma = 0.194$. This means that the LY of the $\text{Gd}_3\text{Ga}_{2.5}\text{Al}_{2.5}\text{O}_{12}:\text{Ce}$ garnet under particles excitation can be also 5-fold lower than the values obtained under excitation by γ -radiation. The energy resolution of LGAGG:Ce/GAGG:Ce b2 and b5 CS samples and GAGG:Ce substrate measured with the 0.5–10 μs shaping time under excitation by α -particles and γ -quanta is shown in Figure 8. As can be seen from Figure 8,

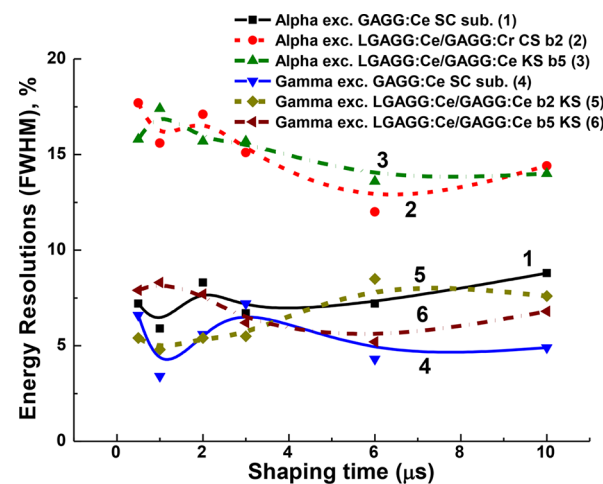


Figure 8. Energy resolutions versus shaping time of LGAGG:Ce/GAGG:Ce b2 and b5 CSs (2, 3, 5, 6) and GAGG:Ce substrate (1, 4) measured under α -particles excitation by ^{241}Am source with an energy of 5.4857 MeV (1–3) and γ -ray excitations excitation by ^{137}Cs source with an energy of 661.66 keV (4–6).

the energy resolution of LGAGG:Ce/GAGG:Ce CS samples under α -particles excitation by ^{241}Am (5.4857 MeV) source (e.g., LGAGG:Ce SCFs) lies in the 16–11% range and is significantly worse as compared to the energy resolution of GAGG:Ce substrate lying in the 6–8% range. This is caused mainly by the significantly lower LY of SCF samples as compared with the LY of SC substrate (Figure 7).

3.3.2. Scintillation Decay Kinetics. Figure 9 presents scintillation decay curves of LGAGG:Ce/GAGG:Ce CSs b2 and b5 samples (parts a, b), $\text{Gd}_3\text{Ga}_{2.5}\text{Al}_{2.5}\text{O}_{12}:\text{Ce}$ KH substrate (part c) and the reference $\text{Gd}_3\text{Ga}_3\text{Al}_2\text{O}_{12}:\text{Ce}$ JPN SC (part d) measured both under α -particles and γ -ray excitations; see curves 1 and 2, respectively. The deconvolution of the decay curves was performed by the 3-exponential approximation $I = A_i \exp(-t/\tau_i) + \text{const}$, and the respective decay lifetimes of the components of such approximation are presented in Table 2. The decay curve of $\text{Gd}_3\text{Ga}_{2.5}\text{Al}_{2.5}\text{O}_{12}:\text{Ce}$ KH substrate and $\text{Gd}_3\text{Ga}_{2.5}\text{Al}_{2.5}\text{O}_{12}:\text{Ce}$ SC JPN under α -particle or γ -ray excitation shows only two slow decay time components with a respective lifetime of 355 and 1065 ns and 155 and 555 ns. The decay kinetics of b2 and b5 samples of LGAGG:Ce/GAGG:Ce CSs, besides the slow decay components, consists of the fast decay components with lifetimes of 46–53 ns and 94–109 ns under α -particle or γ -ray excitation, respectively (see Table 1). Two slow decay values are also observed in the SCF samples under α -particles or γ -rays excitation: $\tau_{\text{slow}}(1)$ component with the lifetime between 296 and 430 ns and $\tau_{\text{slow}}(2)$ component with the lifetime between 1390–1915 ns (Table 2).

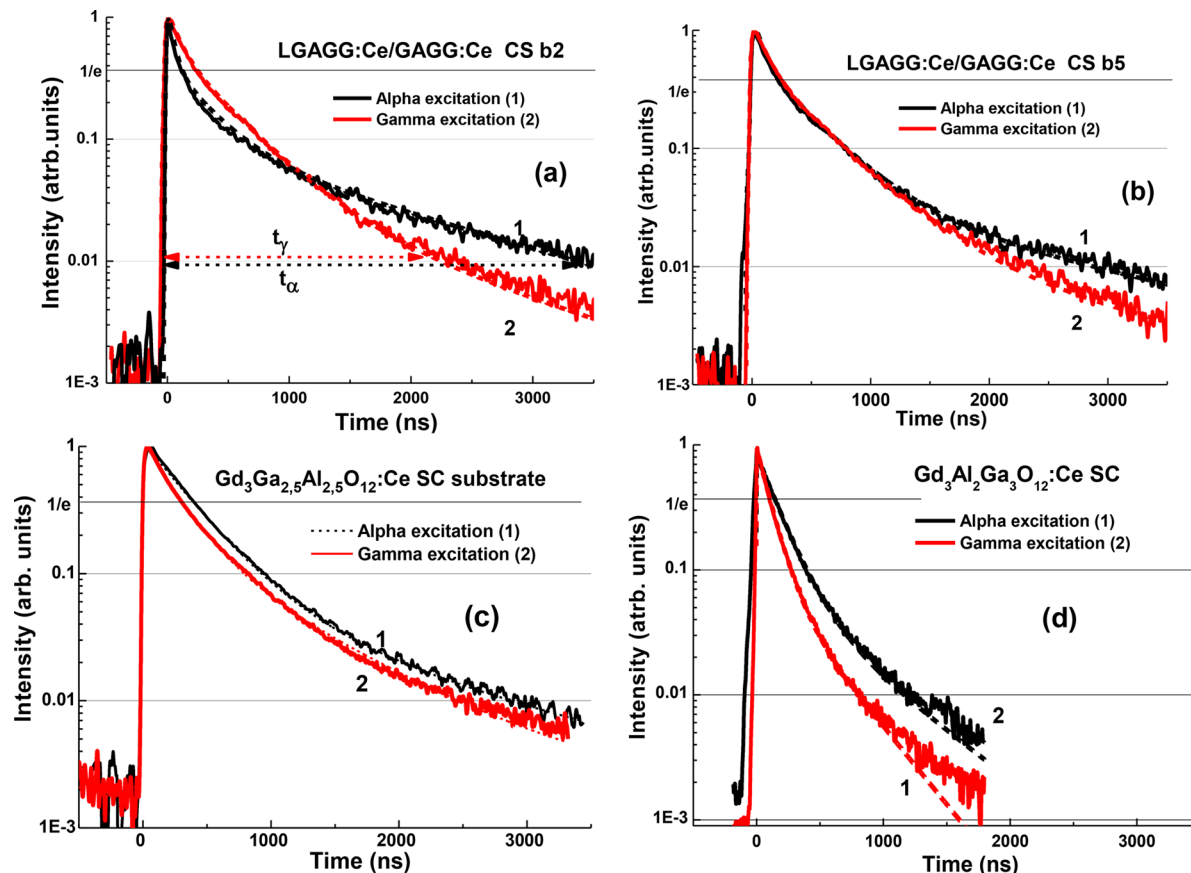


Figure 9. Scintillation decay of b2 (a) and b5 (b) samples of LGAGG:Ce/GAGG:Ce CSs, Gd₃Ga_{2.5}Al_{2.5}O₁₂:Ce KH substrate (c) and reference Gd₃Al₂Ga₃O₁₂:Ce JPN SC (d) under α -particles (1) and γ -ray (2) excitation by ²⁴¹Am and ¹³⁷Cs sources, respectively.

Table 2. Scintillation Decay Times of the GAGG:Ce KH Substrate, Reference Gd₃Al₂Ga₃O₁₂:Ce JPN SC and b2 and b5 SCF Samples of LGAGG:Ce/GAGG:Ce CSs under Excitation by α -Particles of ²⁴¹Am (5.4857 MeV) Source and γ -rays Excitations by ¹³⁷Cs (661.66 keV) Source

sample	excitation	τ_{fast} ns	$\tau_{\text{slow}}(1)$ ns	$\tau_{\text{slow}}(2)$ ns
Gd ₃ Al _{2.5} Ga _{2.5} O ₁₂ :Ce KH substrate	α -particles		355	1065
Gd ₃ Al _{2.5} Ga _{2.5} O ₁₂ :Ce KH substrate	γ -rays		281	939
Gd ₃ Al ₂ Ga ₃ O ₁₂ :Ce JPN SC	α -particles		159	555
Gd ₃ Al ₂ Ga ₃ O ₁₂ :Ce JPN SC	γ -rays		99	349
LGAGG:Ce/GAGG:Ce CS b2	α -particles	45	297	1515
LGAGG:Ce/GAGG:Ce CS b2	γ -rays	94	398	1391
LGAGG:Ce/GAGG:Ce CS b5	α -particles	56	381	1916
LGAGG:Ce/GAGG:Ce CS b5	γ -rays	109	431	1885

4. DISCUSSION

Generally for registration of the difference in the scintillation decay kinetics of the bulk and film components of composite scintillators, it is very important to analyze the decay curves under α -particles and γ -quanta excitations of crystal substrates, prepared from bulk crystal of garnet compounds, in the whole range of intensity decay. We first perform such analysis for Gd₃Al_{2.5}Ga_{2.5}O₁₂:Ce substrate and reference Gd₃Al₂Ga₃O₁₂:Ce SC with the same thickness of 1 mm for the scintillation intensity decay to 1/e, 0.1, and 0.01 levels (Table 3 and Figure 9, panels c and d, respectively). As can see from Figure 9c,d, the decay curves of both SCs under α -particles and γ -quanta excitation are systematically very close or even faster than in the case of α -particles excitation. Most probably, this is a fundamental behavior of scintillation materials and can be connected with the peculiarities of the interaction of the α -particles and γ -quanta with the material of scintillator. This conclusion is confirmed also by comparison of the differences

Table 3. Time Values t_α and t_γ of Scintillation Intensity Decay to 1/e, 0.1, and 0.01 Levels of LGAGG:Ce/GAGG:Ce b2 and b5 CSs, GAGG:Ce KH Substrate and Reference Gd₃Al₂O₁₂:Ce JPN SC under α -Particles and γ -Quanta Excitations by of ²⁴¹Am (5.4857 MeV) and ¹³⁷Cs (661.66 keV) Sources, Respectively

intensity decay level	Gd ₃ Ga _{2.5} Al _{2.5} O ₁₂ :Ce substrate		Gd ₃ Al ₂ O ₁₂ :Ce SC JPN		LGAGG:Ce/GAGG:Ce CS b2		LGAGG:Ce/GAGG:Ce CS b5	
	t_γ ns	t_α ns	t_γ ns	t_α ns	t_γ ns	t_α ns	t_γ ns	t_α ns
1/e	3010	3898	102	145	246	122	264	236
0.1	790	926	269	398	784	632	781	797
0.01	2467	2876	808	1160	2250	3350	2170	2882

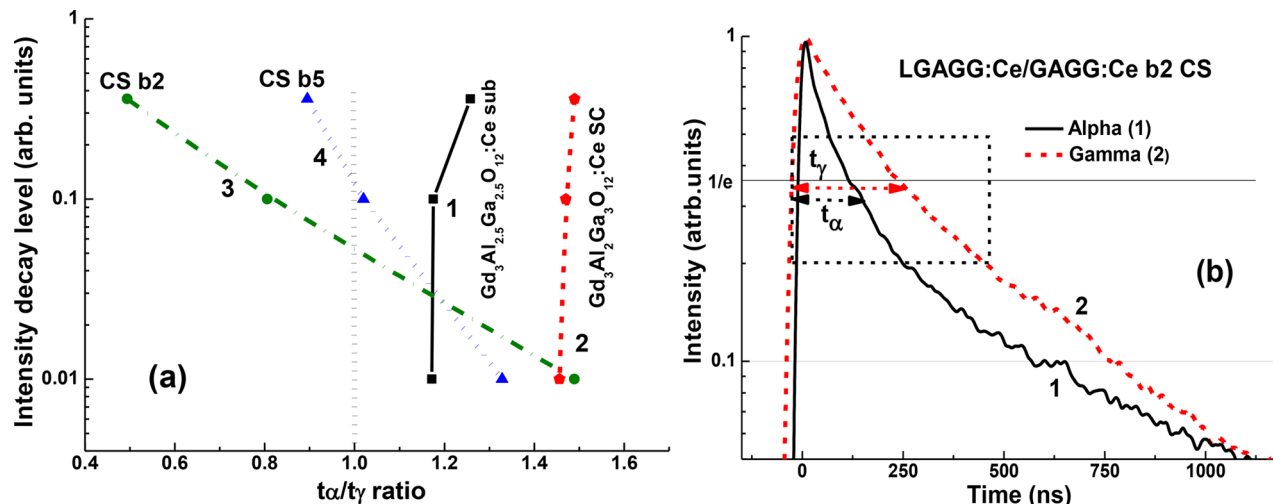


Figure 10. (a) Plot of t_α/t_γ ratio on intensity of scintillation decay to $1/e$, 0.1, and 0.01 levels for Gd₃Al_{2.5}Ga_{2.5}O₁₂:Ce SC KH substrate (1), reference Gd₃Al₂O₁₂:Ce JPN SC (2) and b2 (3) and b5 (4) samples of LGAGG:Ce/GAGG:Ce CSs under α -particles and γ -quanta excitations, respectively. (b) The optimal time range for the scintillation registration LGAGG:Ce/GAGG:Ce b2 CS, when the t_α/t_γ ratio reaches the value above 1.5.

in the decay times at $1/e$, 0.1, and 0.01 level for decay curves under α -particles and γ -quanta excitations (so-called t_α/t_γ ratio) in Gd₃Al_{2.5}Ga_{2.5}O₁₂:Ce KH substrate and Gd₃Al₂Ga₃O₁₂:Ce JPN SCs (Figure 10). As can see from this figure, t_α/t_γ ratio is notably higher in SC sample with large Ga content. Meanwhile, the differences in the t_α/t_γ ratio are not significantly changed for Gd₃Al_{2.5}Ga_{2.5}O₁₂:Ce KH substrate and Gd₃Al₂Ga₃O₁₂:Ce JPN SCs at different registration levels and can be presented in Figure 10 as the vertical line with small slope (curves 1 and 2, respectively).

We can expect the t_α/t_γ ratio, e.g., the rate of separation of the scintillation signal at the registration of the α -particles and γ -quanta, can be significantly improved in the composite epitaxial structures based on the films and crystals of different oxide compounds in comparison with crystal scintillators. Figure 10a shows values of the t_α/t_γ ratio for scintillation decay kinetics for b2 and b5 samples of LGAGG:Ce/GAGG:Ce CSs to $1/e$, 0.1, and 0.01 levels (curves 1 and 2, respectively). Table 3 presents also the respective decay time values to the mentioned levels for both samples of CS under α -particles γ -quanta excitations. The results presented in Figure 10a and Tables 3 show that for both CS samples under study, the best separation of scintillation decay curves under α - and γ -excitation is observed at the $1/e$ level. Most clearly the separation of the decay curves, related to the excitation of CSs by α -particles and γ -quanta, is observed for b2 sample at $1/e$ and 0.01 levels of intensity decay (Figure 10a and Table 3), and the respective t_α/t_γ ratio is equal to 0.495 and 1.49. Thus, the decay times of the film and bulk parts of b2 sample of LGAGG:Ce/GAGG:Ce CSs at the $1/e$ level differ by two times under registration of α -particles and γ -quanta, respectively, and such t_α/t_γ ratio is completely enough for discrimination of the signal coming from different parts of this type of CS (Figure 10b). Finally, the optimal conditions for scintillation registration using this type of CS can be chosen between 0.5 and 0.2 levels of intensity decay in the 0–500 ns time range, where t_α/t_γ reach up to the value above 1.5 (dashed rectangle in Figure 10b).

CONCLUSIONS

A new type of advanced composite scintillators (CSs) based on the single crystalline films (SCFs) of mixed garnet with Lu_{1.5}Gd_{1.5}Al_{1.5}Ga_{3.5}O₁₂:Ce (LGAGG:Ce) nominal content and thickness in the 12.5–30 μm range and Gd₃Al_{2.5}Ga_{2.5}O₁₂:Ce (GAGG:Ce) single crystal substrates with a thickness of 1 mm was produced by the LPE method from melt solutions using PbO-B₂O₃ flux at the SCF/substrate lattice misfit lies in the –(0.66–0.77) % range.

For the characterization of the luminescent and scintillation properties of SCF and bulk crystal parts of composite scintillators, the absorption spectra, CL spectra, LY and scintillation decay kinetics under α -particles excitation by ²³⁹Pu (5.15 MeV) and ²⁴¹Am (5.5 MeV) sources and γ -quanta excitation by ¹³⁷Cs (0.662 MeV) source were applied. Under γ -quanta excitation by ¹³⁷Cs source and α -particles excitations by ²⁴¹Am source, the scintillation LY of Gd₃Al_{2.5}Ga_{2.5}O₁₂:Ce crystal is equal to $\text{LY}_\gamma = 46\,000 \text{ ph}/\text{MeV}$ and $\text{LY}_\alpha = 8950 \text{ ph}/\text{MeV}$, respectively, at registration of scintillation with a shaping time of 6 μs ; e.g., the $\text{LY}_\alpha/\text{LY}_\gamma$ ratio for this scintillator is equal to 0.195. We have also found that the LY of SCF scintillators under α -particles excitation of ²³⁹Pu and ²⁴¹Am sources is less by 4 times than the LY of GAGG:Ce substrate due to the strong negative influence of Pb²⁺ flux related impurity on LY of Ce³⁺-doped SCF scintillators.

Under γ -quanta excitation by ¹³⁷Cs source and α -particles excitations by ²⁴¹Am source, the notable difference in the scintillation decay kinetics of Gd₃Al_{2.5}Ga_{2.5}O₁₂:Ce and Gd₃Al_{2.5}Ga_{2.5}O₁₂:Ce crystals is observed. Such difference can be characterized by the t_α/t_γ decay time ratio, which for the mentioned crystals lies in the 1.26–1.75 and 1.46–1.49 ranges, respectively, at scintillation intensity decay in two decades from 1.0 up to 0.01 levels. This means that the scintillation decay kinetics of Gd₃Al_{2.5}Ga_{2.5}O₁₂:Ce and Gd₃Al_{2.5}Ga_{2.5}O₁₂:Ce crystals under α -particles excitations is systematically faster than in the case of γ -quanta excitation, and such phenomenon is a fundamental property of the scintillation materials.

We have also found significant differences in the scintillation decay kinetics of LGAGG:Ce/GAGG:Ce composite scintillators under excitation by γ -quanta of ¹³⁷Cs source and α -

particles excitations by ^{241}Am source. The respective t_α/t_γ decay time of the intensity decay to the 1/e level under excitation by α -particles of ^{241}Am source and γ -quanta of ^{137}Cs source reaches up to 0.495; e.g., the SCF scintillators is two times faster than substrate–scintillators ratio in the 0–500 ns range. Therefore, such type of composite scintillators can be successfully applied for separation of the signals coming from their film and bulk parts of CS at the registration of the mixed radiation fluxes containing α -particles and γ -quanta.

AUTHOR INFORMATION

Corresponding Author

*E-mail: zorenko@ukw.edu.pl.

ORCID

Yu. Zorenko: 0000-0001-6641-3172

Notes

The authors declare no competing financial interest.

ACKNOWLEDGMENTS

The work was performed in the framework of Polish NCN 2016/21/B/ST8/03200 project and Czech Science Foundation 16-15569S project.

REFERENCES

- (1) Zorenko, Yu. V.; Novosad, S. S.; Pashkovskii, M. V.; Lyskovich, A. B.; Savitskii, V. G.; Batenchuk, M. M.; Malyutenkova, P. S.; Patsagan, N. I.; Nazar, I. V.; Gorbenko, V. I. *J. Appl. Spectrosc.* **1990**, *52*, 645–649.
- (2) Ferrand, B.; Chambaz, B.; Couchaud, M. *Opt. Mater.* **1999**, *11*, 101–114.
- (3) Nikl, M. *Nanocomposite, Ceramic, and Thin Film Scintillators*; Pan Stanford, 2016; p 350.
- (4) Robertson, J. M.; Van Tol, M. V. *Thin Solid Films* **1984**, *114*, 221–240.
- (5) Hrytskiv, Z. D.; Zorenko, Y.; Gorbenko, V.; Pedan, A. D.; Shkliarsky, V. I. *Radiat. Meas.* **2007**, *42*, 933–936.
- (6) Molva, E. *Opt. Mater.* **1999**, *11*, 289–299.
- (7) Klimczak, M.; Malinowski, M.; Sarnecki, J.; Piramidowicz, R. J. *Lumin.* **2009**, *129*, 1869–1873.
- (8) Zorenko, Yu.; Batenchuk, M.; Gorbenco, V.; Pashkovsky, M. *Proc. SPIE* **1996**, *2967*, 101–104.
- (9) Zorenko, Yu.; Gorbenko, V.; Konstankevych, I.; Grinev, B.; Globus, M. *Nucl. Instrum. Methods Phys. Res., Sect. A* **2002**, *486*, 309–314.
- (10) Koch, A.; Raven, C.; Spanne, P.; Snigirev, A. *J. Opt. Soc. Am. A* **1998**, *15*, 1940–1951.
- (11) Martin, T.; Koch, A. *J. Synchrotron Radiat.* **2006**, *13*, 180–194.
- (12) Zorenko, Y.; Gorbenko, V.; Konstankevych, I.; Pashkovsky, M.; Globus, M.; Grinyov, B.; Tarasov, V.; Dorenbos, P.; Van Eijk, C. W. E.; Van Loef, E. In *Proceedings of the 5th International Conference on Inorganic Scintillators and Their Applications*, 2000; pp 476–481.
- (13) Globus, M.; Grinyov, B.; Ratner, M.; Tarasov, V.; Lyubinskiy, V.; Zorenko, Yu.; Konstankevych, I. *IEEE Nuclear Science Symposium and Medical Imaging Conference* **2002**, *1*, 352–356.
- (14) Zorenko, Yu.; Gorbenko, V.; Voznyak, T.; Konstankevych, I.; Savchyn, V.; Batentschuk, M.; Winnacker, A.; Brabec, Ch. *J. IEEE Trans. Nucl. Sci.* **2012**, *59*, 2281–2285.
- (15) Phoswich Detectors for High Energy Backgrounds (Saint Gobain). <http://www.detectors.saint-gobain.com>.
- (16) Zorenko, Y.; Voloshinovskii, A.; Konstankevych, I.; Kolobanov, V.; Mikhailin, V.; Spassky, D. *Radiat. Meas.* **2004**, *38*, 677–680.
- (17) Valbis, Ya. A.; Volzhenskaja, L. G.; Dubov, Yu. G.; Zorenko, Yu. V.; Nazar, I. V.; Patszagan, N. I. *Opt. Spectrosc.* **1987**, *63*, 1058–1063.
- (18) Limarenko, L. N.; Zorenko, Yu. V.; Batenchuk, M. M.; Moroz, Z. T.; Pashkovskii, M. V.; Konstankevich, I. V. *J. Appl. Spectrosc.* **2000**, *67*, 287–294.
- (19) Borodenko, Yu.; Gryniow, B.; Martynov, V.; Piveň, L.; Solski, I.; Zorenko, Yu.; Moroz, Z.; Pashkovskii, M. *Surface* **2002**, *6*, 6–9.
- (20) Zorenko, Yu. *V. J. Appl. Spectrosc.* **1998**, *65*, 218–223.
- (21) Kamada, K.; Endo, T.; Tsutumi, K.; Pejchal, J.; Nikl, M.; Yanagida, T.; Fujimoto, A.; Fukabori, A.; Yoshikawa, A. *Cryst. Growth Des.* **2011**, *11*, 4484.
- (22) Fasoli, M.; Vedda, A.; Nikl, M.; Jiang, C.; Uberuaga, B.; Andersson, D.; McClellan, K.; Stanek, C. *Phys. Rev. B: Condens. Matter Mater. Phys.* **2011**, *84*, 081102.
- (23) Zorenko, Yu.; Gorbenko, V.; Vasylkiv, Ja.; Strzyżewski, T.; Fedorov, A.; Kucerkova, R.; Mares, J. A.; Nikl, M.; Bilski, P.; Twardak, A. *J. Lumin.* **2016**, *169*, 828–837.
- (24) Prusa, P.; Kucera, M.; Mares, J. A.; Hanus, M.; Bejtlerova, A.; Onderisnova, Z.; Nikl, M. *Opt. Mater.* **2013**, *35*, 2444.
- (25) Prusa, P.; Kucera, M.; Mares, J. A.; Onderisnova, Z.; Hanus, M.; Babin, V.; Bejtlerova, A.; Nikl, M. *Cryst. Growth Des.* **2015**, *15*, 3715.
- (26) Bartosiewicz, K.; Babin, V.; Mares, J. A.; Bejtlerova, A.; Zorenko, Yu.; Iskaliyeva, A.; Gorbenko, V.; Bryknar, Z.; Nikl, M. *J. Lumin.* **2017**, *188*, 60–66.
- (27) Zorenko, Y.; Gorbenko, V.; Zorenko, T.; Paprocki, K.; Nikl, M.; Mares, J. A.; Bilski, P.; Twardak, A.; Sidletskiy, O.; Gerasimov, I.; Grinyov, B.; Fedorov, A. *IEEE Trans. Nucl. Sci.* **2016**, *63* (2), 497–502.
- (28) Zorenko, Y.; Gorbenko, V.; Zorenko, T.; Paprocki, K.; Bilski, P.; Twardak, A.; Voznyak, T.; Sidletskiy, O.; Gerasimov, I.; Grinyov, B.; Fedorov, A. *Opt. Mater.* **2016**, *61*, 3–10.
- (29) Gorbenko, V.; Zorenko, T.; Witkiewicz, S.; Paprocki, K.; Sidletskiy, O.; Fedorov, A.; Bilski, P.; Twardak, A.; Zorenko, Y. *Crystals* **2017**, *7* (15), 262.
- (30) Glass, H. L.; Elliot, M. F. *J. Cryst. Growth* **1974**, *27*, 253–260.
- (31) Zorenko, Y.; Gorbenko, V.; Voznyak, T.; Zorenko, T. *Phys. Status Solidi B* **2008**, *245*, 1618–1622.



Cite this: *CrystEngComm*, 2018, **20**,
3994

Epitaxial growth of composite scintillators based on $\text{Tb}_3\text{Al}_5\text{O}_{12}:\text{Ce}$ single crystalline films and $\text{Gd}_3\text{Al}_{2.5}\text{Ga}_{2.5}\text{O}_{12}:\text{Ce}$ crystal substrates

S. Witkiewicz-Lukaszek,^a V. Gorbenko,^a T. Zorenko,^a K. Paprocki,^a O. Sidletskiy,^b A. Fedorov,^c R. Kucerkova,^d J. A. Mares,^d M. Nikl^d and Yu. Zorenko ^{*a}

This work presents our latest achievements in the development of advanced composite scintillators for simultaneous registration of α -particles and γ -quanta in mixed ionizing fluxes based on single crystalline films (SCFs) of $\text{Tb}_3\text{Al}_5\text{O}_{12}:\text{Ce}$ (TbAG:Ce) garnet and $\text{Gd}_3\text{Al}_{2.5}\text{Ga}_{2.5}\text{O}_{12}:\text{Ce}$ (GAGG:Ce) single crystal (SC) substrates using the liquid phase epitaxy (LPE) growth method from a melt-solution based on a $\text{PbO}-\text{B}_2\text{O}_3$ flux. The separation of the signals from the SCF and SC components of such composite scintillators can be realized by means of registration of the difference in the scintillation decay times of SCF and substrate scintillators and can be achieved at a large $K = t(\text{SCF})/t(\text{SC})$ ratio, which is usually above 2. The TbAG:Ce SCFs exhibit relatively fast scintillation response under α -particle excitation with decay times of $t_{1/e} = 344-380$ ns and $t_{1/100} = 3130-3770$ ns. Meanwhile, the scintillation response of TbAG:Ce SCFs under α -particle excitation is significantly slower in the 500–4000 ns range than that of the GAGG:Ce crystals with decay times of $t_{1/e} = 270-280$ ns and $t_{1/20} = 1280-1300$ ns. We have found that for TbAG:Ce/GAGG:Ce composite scintillators, the optimal K ratio changes from 2.0 to 3.0 at the registration of scintillations with shaping times of 700–4000 ns. For this reason, TbAG:Ce/GAGG:Ce composite scintillators possess the best scintillation properties among all known LPE grown analogues for simultaneous registration of α -particles and γ -quanta in mixed fluxes.

Received 5th April 2018,
Accepted 30th May 2018

DOI: 10.1039/c8ce00536b

rsc.li/crystengcomm

1 Introduction

The technology of liquid phase epitaxy (LPE) offers today the possibility of developing luminescent materials based on single crystalline films (SCFs) of different oxide compounds^{1–3} for applications such as cathodoluminescent screens,^{4,5} laser media,^{6,7} scintillators for registration of α - and β -particles and low-energy X- or γ -ray quanta^{1,8,9} and scintillating screens for microtomography detectors using X-ray sources and synchrotron radiation.^{10,11}

The LPE method opens also the possibility of creating advanced composite scintillators (CSs) of “phoswich-type” (phosphor sandwich) for the registration of different components of ionizing radiation, namely, for analysis of the content of mixed fluxes of particles and quanta with various pen-

etration depths.^{1,12–14} Such composite scintillators present epitaxial crystalline structures, including one or two SCFs intended for registration of low penetrating α - and β -particles, and bulk single crystal (SC) substrates for registration of high penetrating radiation (X- or γ -rays) (Fig. 1a).

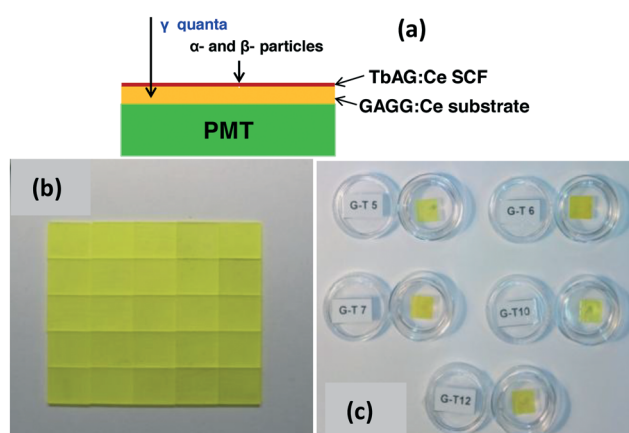


Fig. 1 (a) Principal scheme of a composite scintillator; (b) and (c) substrate scintillators prepared from GAGG:Ce crystals (b) and composite scintillators of GT type based on the GAGG:Ce substrates and TbAG:Ce SCFs (c).

^a Institute of Physics, Kazimierz Wielki University in Bydgoszcz, Powstańców Wielkopolskich str., 2, 85090 Bydgoszcz, Poland. E-mail: zorenko@ukw.edu.pl

^b Institute for Scintillation Materials, National Academy of Sciences of Ukraine, av. Nauki 60, 61001 Kharkiv, Ukraine

^c SSI Institute for Single Crystals, National Academy of Sciences of Ukraine, av. Nauki 60, 61178 Kharkiv, Ukraine

^d Institute of Physics, Academy of Sciences of Czech Republic, Cukrovarnicka str., 10, 16200 Prague, Czech Republic

^e Faculty of Technical Physics, Poznan University of Technology, Piotrowo str., 3, 60965 Poznan, Poland

The advantages of these types of composite scintillators in comparison with the well-known analogues based on the splice of different scintillation crystals are considered in a previous work.¹⁵ Such types of composite scintillators present epitaxial single crystalline structures with a sharp interface between the composite scintillators with quite close refractive indices. This allows substantial elimination of the light losses at the interface of scintillators, to enhance the selectivity of registration of the different components of mixed ionizing radiation. The LPE method for composite scintillator production permits also obtaining of the thickness of film scintillators quite close to the penetration depth of registered particles. Namely, the thickness of film scintillators, which is necessary for the complete absorption of α -particles of ^{239}Pu and ^{241}Am radioisotopes, is typically equal to 12–15 μm .¹

Different types of composite scintillators have been recently considered by some of us.^{1,12–14} The first type of composite scintillator was created based on LPE grown epitaxial structures of $\text{Y}_3\text{Al}_5\text{O}_{12}$ garnet (YAG).¹ Namely, double-layered composite scintillators based on YAG:Ce SCF/YAG:Nd SC and YAG:Ce SCF/YAG:Sc SC structures as well as triple-layered composite scintillators based on a YAG:Ce SCF/YAG:Nd SCF/YAG:Sc SC structure were grown by the LPE method and later examined under simultaneous excitation by α - or β -particles and γ -quanta.¹ The separation of the scintillation signals coming from the SCF and SC parts of the composite scintillators was performed using the discrimination of their scintillation decay kinetics.

It should be noted that due to their low density $\rho = 4.5 \text{ g cm}^{-3}$ and effective atomic number $Z_{\text{eff}} = 29$, the scintillators based on YAG SCs may be used only for registration of low-energy ionizing radiation.^{1,12} Therefore, it is promising to fabricate composite scintillators for registration of the mixed fluxes of α - or β - particles and high-energy γ -quanta using other garnet compounds, which are characterized by high values of ρ and Z_{eff} .^{12,13}

Among the possible candidates for such oxide compounds, the $\text{Lu}_3\text{Al}_5\text{O}_{12}$ garnet (LuAG) first of all has attracted our attention.^{9,10} The LuAG host has a significantly high density of $\rho = 6.7 \text{ g cm}^{-3}$ and effective atomic number of $Z_{\text{eff}} = 61$ in comparison with YAG. LuAG:Ce, LuAG:Pr and LuAG:Sc are the well-known scintillators for radiation monitoring and computer tomography.^{3,16} Therefore, LuAG garnet is a very promising material for creation of SCF scintillators as well as the composite scintillators on the base of this compound. As activators, which allow effective emission in LuAG hosts with different decay kinetics, Ce^{3+} , Pr^{3+} and Sc^{3+} ions can be firstly considered.^{9,17–20}

The novel approach for development of scintillation materials including composition engineering of the cation content and band gap engineering of heavy garnet compounds^{21,22} also opens a wide possibility for development of advanced types of composite scintillators based on the mentioned garnets. The bulk SCs of the $\text{Gd}_3\text{Al}_{5-x}\text{Ga}_x\text{O}_{12}$ garnet with $x = 2–3$ are now on the top list of scintillators with a very high light yield (LY) up to 50 000 photons per MeV under excitation by γ quanta of a ^{137}Cs (662 keV) source.²¹ Solid solutions of

$\text{Lu}_{3-x}\text{Gd}_x\text{Al}_{5-y}\text{Ga}_y\text{O}_{12}$ mixed garnets at $x = 1–3$ and $y = 2–3$ are also very promising materials for creation of SCF scintillation screens with high X-ray absorption ability and very high efficiency for the registration of α -particles.^{23–26} With the aim of increasing the energy transfer efficiency from the mixed garnet host to the Ce^{3+} ions, $\text{Lu}_{3-x}\text{Tb}_x\text{Al}_5\text{O}_{12}$ and $\text{Tb}_3\text{Al}_5\text{O}_{12}$ SCFs were also crystallized by the LPE method and their luminescence and scintillation properties were reported as well.^{27–29}

At the same time, the possibility of growth by the LPE method of the new types of advanced composite scintillators based on the SCFs and SCs of all the above mentioned garnets needs technological and experimental evidence. For this reason, in our work we present for the first time the results of the research directed on creation using the LPE method of composite scintillators based on SCFs of Ce^{3+} doped $\text{Tb}_3\text{Al}_5\text{O}_{12}$ garnet (TbAG:Ce) (Fig. 1c) and substrates from SCs of $\text{Gd}_3\text{Al}_{2.5}\text{Ga}_{2.5}\text{O}_{12}:\text{Ce}$ (GAGG:Ce) garnet (Fig. 1b).

2 LPE growth of TbAG:Ce/GAGG:Ce composite scintillators

A set of composite scintillators based on TbAG:Ce SCFs were grown by the LPE method onto GAGG:Ce substrates from super-cooling melt solutions using a $\text{PbO}-\text{B}_2\text{O}_3$ flux (Fig. 1b and c). For comparison, TbAG:Ce SCF samples T1 and T2 were also grown onto undoped YAG and GAGG substrates, respectively (see ref. 28 for details). The growth conditions for the SCF and composite scintillators, selected for investigation of their content and structural properties as well as for studying their absorption, cathodoluminescence and scintillation properties, are summarized in Table 1.

The XRD measurements (DRON 4 spectrometer, Cu K_{α} X-ray source) were used for characterization of the structural quality of TbAG:Ce SCFs, grown onto YAG and GAGG:Ce SC substrates with a lattice constant of 12.0064 and 12.2332 Å, respectively (Fig. 2). From the respective XRD patterns of these SCFs (Fig. 2a and b) we can also calculate the lattice constants of the respective garnet between the lattice constants of TbAG:Ce SCFs and the GAGG:Ce substrate $\Delta a = (a_{\text{SCF}} - a_{\text{sub}})/a_{\text{sub}} \times 100\%$. Namely, the lattice constants of TbAG:Ce T1 and GT7 SCFs, grown onto YAG and GAGG:Ce substrates, are equal to 12.0730 Å and 12.0722 Å, and the value of misfit m is equal to +0.55% and -1.32% for these SCF samples, respectively (Fig. 2a and b and Table 1).

3 Luminescence and scintillation properties of TbAG:Ce SCF/GAGG:Ce SC composite scintillators

For characterization of the luminescence and scintillation properties of the composite scintillators based on the Ce^{3+} doped TbAG SCFs and GAGG substrates, absorption spectra, cathodoluminescence (CL) spectra, LY and scintillation decay kinetics measurements under excitation by α -particles and γ -quanta were applied. The absorption spectra were measured

Table 1 Growth conditions for TbAG:Ce/GAGG:Ce composite scintillators and their LY under excitation by a ^{239}Pu source (5.15 MeV) and registration with a shaping time of 12 μs and the reference GAGG:Ce substrate. m – SCF/substrate misfit, h – SCF thickness, f – velocity of SCF growth; T – SCF growth temperature

SCF number	Nominal content of SCFs in melt-solution	Substrate	m , %	h , μm	T , $^{\circ}\text{C}$	f , $\mu\text{m min}^{-1}$	LY, %
42-6	$\text{Y}_3\text{Al}_5\text{O}_{12}$:Ce	YAG	n. m.	54			100
T1	$\text{Tb}_3\text{Al}_5\text{O}_{12}$:Ce	YAG	+0.55	20	990	0.66	200–205
T2	$\text{Tb}_3\text{Al}_5\text{O}_{12}$:Ce	GAGG	-1.29	16	1005	0.36	190–195
GT6	$\text{Tb}_3\text{Al}_5\text{O}_{12}$:Ce/GAGG:Ce	GAGG:Ce	n. m.	50	995	1.0	175
GT7	$\text{Tb}_3\text{Al}_5\text{O}_{12}$:Ce/GAGG:Ce	GAGG:Ce	-1.32	16	990	0.25	197
Substrate	$\text{Gd}_3\text{Al}_{2.5}\text{Ga}_{2.5}\text{O}_{12}$:Ce SC				900		340

using a Jasco 760 UV-vis spectrometer in the 200–1100 nm range. The CL spectra were measured at room temperature (RT) using an electron microscope SEM JEOL JSM-820, additionally equipped with a Stellar Net spectrometer and TE-cooled CCD detector working in the 200–925 nm range. The scintillation LY (pulse height spectra measured with a shaping time of 12 μs) was firstly measured after each SCF growth cycle using a setup based on a Hamamatsu H6521 photomultiplier tube (PMT), multichannel analyzer and digital Tektronix TDS3052 oscilloscope under excitation by α -particles of a ^{239}Pu (5.15 MeV) source. The spectra were compared with those of the standard YAG:Ce SCF sample with a photoelectron (phel) light yield of 360 phels per MeV and a LY of 2650 photons per MeV^{30,31} and also with those of the reference $\text{Gd}_3\text{Ga}_{2.5}\text{Al}_{2.5}\text{O}_{12}$:Ce (GAGG:Ce) substrate, produced in the ISM, Kharkiv, Ukraine. All measurements were performed at room temperature (RT).

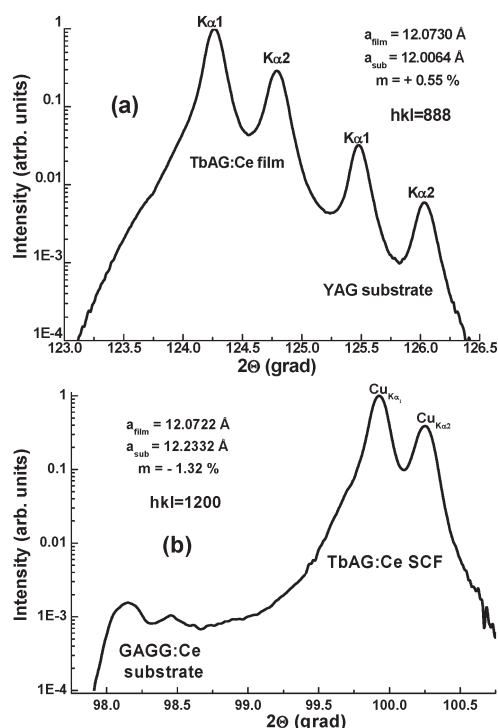


Fig. 2 XRD patterns of the (111) and (1200) planes of TbAG:Ce SCFs, grown onto YAG (a) and GAGG:Ce (b) substrates with (111) (a) and (100) (d) orientations.

Scintillation response investigations of the selected composite scintillators (see Table 1) were performed using a set-up consisting of a hybrid PMT (HPMT DEP PP0475B), measuring electronics and PC control. Pulse height spectra were measured under excitation by α -particles of a ^{241}Am (energy 5.4857 MeV) radioisotope and γ -rays of a ^{137}Cs (energy 661.66 keV) radioisotope. It is important to note here that the α -particles of ^{239}Pu and ^{241}Am sources allow exciting only the epitaxial layers of the SCF samples (not their substrates) because the penetration depth of the α -particles in the studied samples is approximately 12–15 μm .

3.1 Absorption spectra

The absorption spectra of two TbAG:Ce/GAGG:Ce composite scintillators are presented in Fig. 3 in comparison with the absorption spectra of two TbAG:Ce SCFs, grown onto YAG and GAGG substrates, as well as the absorption spectra of the GAGG:Ce substrate.

The sharp bands peaking around 275 and 313 nm in the spectra of both TbAG:Ce/GAGG:Ce composite scintillators, TbAG:Ce SCFs, grown onto the GAGG substrate, and the GAGG:Ce substrate are caused by the $^8\text{S}_{7/2} \rightarrow {}^6\text{I}_{3/2-7/2}$ and ${}^8\text{S}_{7/2} \rightarrow {}^6\text{P}_{3/2-7/2}$ transitions of Gd^{3+} ions, respectively. The 275 nm absorption band of Gd^{3+} ions strongly overlaps with the absorption bands peaking in the 260–265 nm range, which

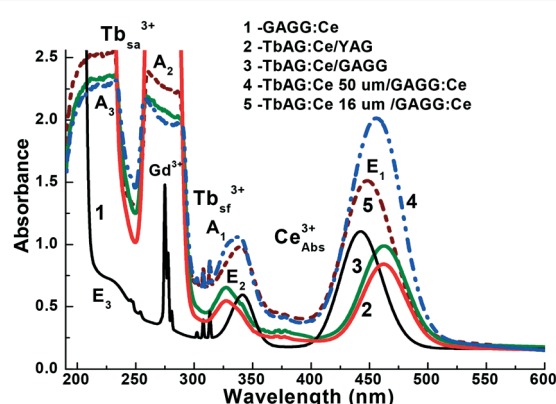


Fig. 3 RT absorption spectra of two TbAG:Ce/GAGG:Ce CS samples GT6 (4) and GT7 (5) in comparison with absorption spectra of two TbAG:Ce SCFs, grown onto YAG (2) and GAGG (3) substrates and absorption spectra of the GAGG:Ce substrate (1).

are caused by the $^1S_0 \rightarrow ^3P_1$ transitions of Pb^{2+} flux related impurity.^{32,33}

The intensive broad bands in the 326 nm (A_1) and 200–300 nm (A_2, A_3) ranges, in the absorption spectra of TbAG:Ce SCFs, correspond to the $4f^8 \rightarrow 4f^75d^1$ spin-forbidden (sf) (A_1) and spin-allowed (sa) (A_2, A_3) transitions of Tb^{3+} ions, respectively.^{34–37} The $4f\text{--}5d$ (sf)-absorption band (A_1) of Tb^{3+} ions peaking at 327 nm to a great extent is distorted by the presence of the $4f\text{--}5d$ -absorption band (E_2) of Ce^{3+} ions peaking at 336 nm in this spectral region.

The absorption bands in the 340–347 nm (E_2) and 450–465 nm (E_1) ranges of the TbAG:Ce/YAG SCFs, TbAG:Ce/GAGG SCFs, TbAG:Ce/GAGG:Ce composite scintillators and GAGG:Ce substrate are related to the $4f\text{--}5d$ (E_2) transitions of Ce^{3+} ions. Other Ce^{3+} absorption bands in these scintillators are located below 230 nm (E_3) and related to the $4f\text{--}5d$ (T_{2g}) transitions. Due to the different temperatures of SCF growth and the respective deviation of the Ce^{3+} and Pb^{2+} content in the SCFs under study (Table 1), we observe notable changes in the absorption spectra of TbAG:Ce SCFs with nominally the same content in the melt, grown onto YAG and GAGG substrates (Fig. 3, curves 2 and 3).

The difference in the positions of E_1 and E_2 bands $\Delta E_{Abs} = E_1 - E_2$ is proportional to the crystal field strength (CFS) in the dodecahedral positions of the garnet lattice, where the Ce^{3+} ions are localized, and is very sensitive to the change in CFS. Namely, we have observed the shift of positions of E_1 and E_2 Ce^{3+} absorption bands and the change of the respective ΔE_{Abs} values from 0.95–0.975 eV in both TbAG:Ce SCF samples (Fig. 3, curves 2 and 3) in comparison with the GAGG:Ce substrate where the ΔE_{Abs} value is equal to 0.827 eV (Fig. 3, curve 1). Based on the ΔE_{Abs} values for these SCF and substrate samples, we have also found an about 15–18% increase of CFS in the $Tb_3Al_5O_{12}$:Ce garnet in comparison with the $Gd_3Ga_{2.5}Al_{2.5}O_{12}$:Ce garnet.

The absorption spectra of the composite scintillators based on the epitaxial structures containing the GAGG:Ce substrate with a thickness of 1 mm and TbAG:Ce SCFs with different thicknesses represent the mixture of the absorption spectra of their SCF and SC components (Fig. 3, curves 1–5). The differences in the absorption spectra in Fig. 3 between TbAG:Ce SCFs and TbAG:Ce/GAGG:Ce composite scintillators in the range of the E_2 and E_1 Ce^{3+} absorption bands are related to the contribution of the GAGG:Ce substrate, which slightly decrease in the case of a large TbAG:Ce SCF thickness (Fig. 3, curves 4 and 5, respectively).

3.2 Cathodoluminescence spectra

The normalized CL spectra of the TbAG:Ce SCFs, TbAG:Ce/GAGG:Ce composite scintillators and GAGG:Ce substrate are shown in Fig. 4. The dominant doublet luminescence bands peaking at 550–560 nm in the spectra of the SCFs, composite scintillators and substrate correspond to the $5d^1 \rightarrow 4f$ ($^2F_{5/2,7/2}$) transitions of Ce^{3+} ions in the TbAG and GAGG garnet hosts. Due to the same nominal content, the

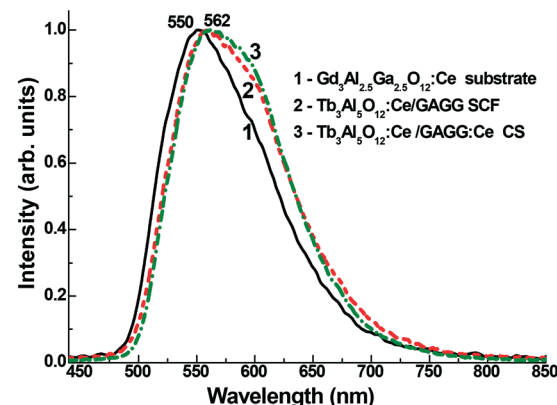


Fig. 4 CL spectra of the $Gd_3Al_{2.5}Ga_{2.5}O_{12}$:Ce SC substrate (1), TbAG:Ce/GAGG T2 SCFs (2) and TbAG:Ce/GAGG:Ce GT7 composite scintillators (3).

CL spectra of TbAG:Ce SCFs and TbAG:Ce/GAGG:Ce composite scintillators are very close (Fig. 4, curves 2 and 3). The different positions of the maxima of the Ce^{3+} emission bands at 550 and 562 nm in the CL spectra of TbAG:Ce SCFs and the GAGG:Ce substrate, respectively, are caused by the different CFS and Stokes shift, which is equal to 0.53 and 0.474 eV, respectively, in the respective garnet hosts.

3.3 α -Particle and γ -ray spectroscopy of TbAG:Ce/GAGG:Ce composite scintillators

For investigation of the scintillation properties of TbAG:Ce/GAGG:Ce composite scintillators under α -particle and γ -ray excitation, samples GT6 and GT7 with dimensions of $1 \times 1 \text{ cm}^2$ were selected (Table 1).

3.3.1 Pulse height spectra. The pulse height spectra of the main γ - or α -ray lines of ^{137}Cs and ^{241}Am sources registered by the TbAG:Ce/GAGG:Ce CSs and GAGG:Ce substrate are presented in Fig. 5a and b, respectively. The main peaks in Fig. 5a correspond to the total energy absorption of α -rays with an energy of 5.4857 MeV. The peaks in the left part of the spectrum correspond to the absorption of the low-energy emission line of ^{241}Am with an energy of 59.6467 keV. It is worth noting that the positions of the main photo-peaks, observed in Fig. 5a, are substantially different for samples GT6 and GT7 of TbAG:Ce/GAGG:Ce composite scintillators and for the GAGG:Ce SC substrate. This means that α -particles excite only the SCF parts of the composite scintillators. Fig. 5a shows also that the LY value of TbAG:Ce SCFs in samples GT6 and GT7 under excitation by α -particles is 1.42 and 1.48 times smaller, respectively, in comparison with the LY value of the GAGG:Ce substrate. These results on the LY of GT6 and GT7 composite scintillators under α -particle excitation by the ^{241}Am source are consistent with the results obtained with these samples presented in Table 1 under excitation by the ^{239}Pu source. Such a lower LY of SCF samples is caused by the lower energy emission spectrum of TbAG:Ce SCFs in comparison with the spectrum of the GAGG:Ce substrate (Fig. 4) and a negative influence of Pb flux related

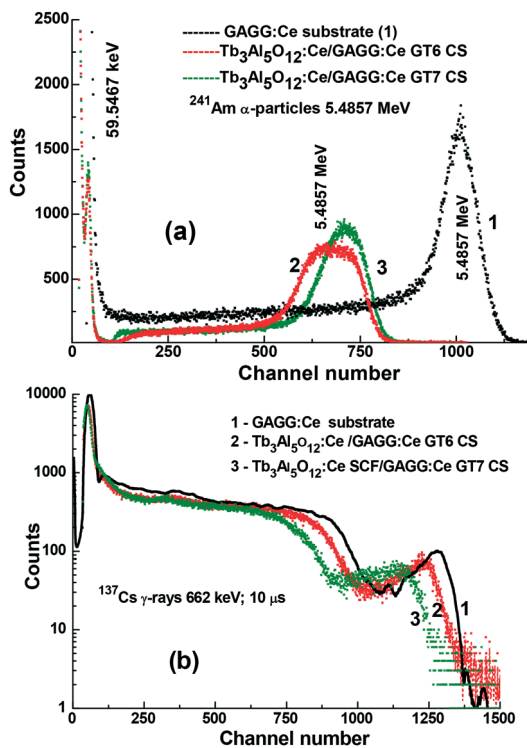


Fig. 5 Pulse height spectra of the TbAG:Ce/GAGG:Ce GT6 (2) and GT7 (3) composite scintillators and GAGG:Ce substrate (1) measured under α -particle excitation by the ^{241}Am source with an energy of 5.4857 MeV (a) and under γ -ray excitation by the ^{137}Cs source with an energy of 661.66 keV (b).

impurity on the scintillation properties of SCFs of different oxide compounds, grown from the PbO based flux.^{24,30}

Under γ quanta excitation of TbAG:Ce/GAGG:Ce GT6 and GT7 composite scintillators by the ^{137}Cs source, the main peaks were observed in the pulse height spectra, corresponding to the total absorption of γ radiation with an energy of 661.66 keV (Fig. 5b). An additional peak is observed at a lower energy of 32.006 keV, corresponding to the low-energy line of the ^{137}Cs source. It is characteristic that the positions of the main photo-peaks, observed in Fig. 5b, have similar positions for both TbAG:Ce/GAGG:Ce composite scintillators and the GAGG:Ce substrate and this means that γ -rays excite mainly the substrate.

Fig. 6a presents the LY of the TbAG:Ce GT6 and GT7 composite scintillators and GAGG:Ce substrate evaluated in terms of photons per MeV (ph per MeV) and measured with different shaping times in the 0.5–10 μs range under α -particle and γ -ray excitation. Fig. 6b shows relative change of the LY of the TbAG:Ce GT6 and GT7 composite scintillators and GAGG:Ce substrate, measured with shaping times in the 1–10 μs time range, with respect to the LY of these samples, measured at the shortest shaping time of 0.5 μs . Namely, for GT6 and GT7 composite scintillators, excited by α -particles of the ^{241}Am source with an energy of 5.4857 MeV, the LY increases from values of 2210–2280 ph per MeV (100%) to 3880–4250 ph per MeV (170–192%) for shaping times from 0.5 to 10 μs , respectively. In contrast, we have ob-

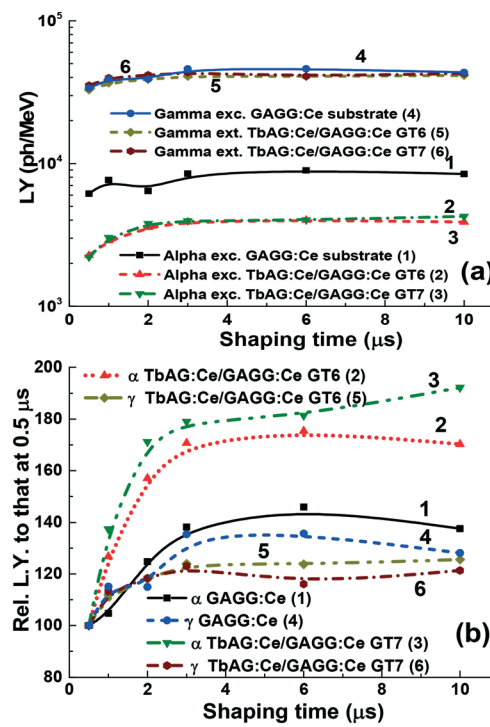


Fig. 6 Dependence of LY values (a) and values of relative $\{\text{LY}(T \mu\text{s})/\text{LY}(0.5 \mu\text{s})\} \times 100\%$ ratio (b) versus shaping time T of TbAG:Ce/GAGG:Ce GT6 (2, 5) and GT7 (3, 6) composite scintillators and the GAGG:Ce substrate (1, 4) measured under α -particle excitation by the ^{241}Am source with an energy of 5.4857 MeV (1–3) and γ -ray excitation by the ^{137}Cs source with an energy of 661.66 keV (4–6). $T = 0.5, 1, 2, 3, 6$ and 10 μs .

served very similar LY values under γ -ray excitation (661.66 keV) for both TbAG:Ce SCFs (GT6 and GT7 composite scintillators) and the GAGG:Ce substrate. Specifically, the LY values in these scintillators change from 32 880 ph per MeV (100%) to 43 430 ph per MeV (125.5%) when the shaping times increase in the 0.5–10 μs interval.

The energy resolution of the TbAG:Ce/GAGG:Ce GT6 and GT7 composite scintillators and GAGG:Ce substrate measured at the 0.5–10 μs shaping time under excitation by α -particles and γ -quanta is shown in Fig. 7. As can be seen from Fig. 7, the energy resolution of TbAG:Ce/GAGG:Ce GT6 and GT7 composite scintillators under α -particle excitation by the ^{241}Am (5.4857 MeV) source (e.g., TbAG:Ce SCFs) lies in the 31.8–16.6 and 17.7–14.4% ranges, respectively, and is significantly worse as compared to the energy resolution of the GAGG:Ce substrate lying in the 7.2–8.8% range. This is caused mainly by the significantly lower LY of SCF samples as compared to the LY of the SC substrate (Fig. 7). Under γ -ray excitation at 662 keV of ^{137}Cs we have observed rather close values of the energy resolution of TbAG:Ce/GAGG:Ce GT6 and GT7 composite scintillators in the 10.8–8.2% and 9.6–8.8% ranges, respectively, and the GAGG:Ce substrate lying in the 6.6–4.3% range (Fig. 7).

3.3.2 Scintillation decay kinetics. Fig. 8 presents the scintillation decay curves of TbAG:Ce/GAGG:Ce GT6 and GT7

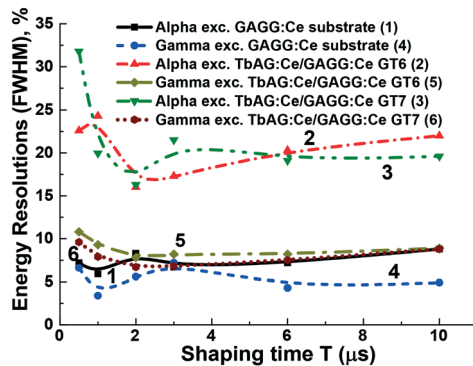


Fig. 7 Energy resolutions versus shaping time of the TbAG:Ce/GAGG:Ce GT6 (2, 5) and GT7 (3, 6) composite scintillators and GAGG:Ce substrate (1, 2) measured under α -particle excitation by the ^{241}Am source with an energy of 5.4857 MeV (1–3) and γ -ray excitation by the ^{137}Cs source with an energy of 661.66 keV (4–6).

composite scintillators (parts a and b) in comparison with the reference GAGG:Ce substrate (part c) measured under both α -particle and γ -ray excitation, see curves 1 and 2, respectively.

The deconvolution of the decay curves was performed using the 3-exponential approximation $I = A_i \exp(-t/\tau_i) + \text{const}$ and the respective decay lifetimes of the components of such approximation are presented in Table 2. The decay curves of the GAGG:Ce substrate show only two slow decay components with lifetimes of 355 and 1060 ns under α -particles excitation and 281 and 940 ns under γ -rays excitation (see Table 2).

4. Discussion

Generally for registration of the difference in the scintillation decay kinetics of the bulk substrate and thin film components of composite scintillators, it is very important to analyze the decay curves under α -particle and γ -quantum excitation of the crystal substrates, prepared from bulk crystals of garnet compounds, in the whole range of decay intensity. We perform such an analysis for the $\text{Gd}_{3}\text{Al}_{2.5}\text{Ga}_{2.5}\text{O}_{12}:\text{Ce}$ substrate with a thickness of 1 mm for a decrease of scintillation decay intensity to $1/e$, 0.1, 0.05 and 0.01 levels (Table 2 and Fig. 8c). As can be seen from Fig. 8c, the decay curve of the GAGG:Ce SC under γ -quanta excitation is faster than that in the case of α -particle excitation. In our opinion, such behavior of scintillation materials can be connected with the peculiarities of the interaction of the α -particles and γ -quanta with the material of the scintillator. This conclusion is confirmed also by comparison of the differences in the decay times at $1/e$, 0.1, 0.05 and 0.01 levels for the decay curves under α -particle and γ -quantum excitation (the so called t_α/t_γ ratio) in the GAGG:Ce substrate (Fig. 9, curve 1). The differences in the t_α/t_γ ratio are not significantly changed for the GAGG:Ce SC substrate at different registration levels and can be presented in Fig. 9 as the vertical line with a small slope (curve 1). Meanwhile, the t_α/t_γ ratio, i.e. the rate of separation

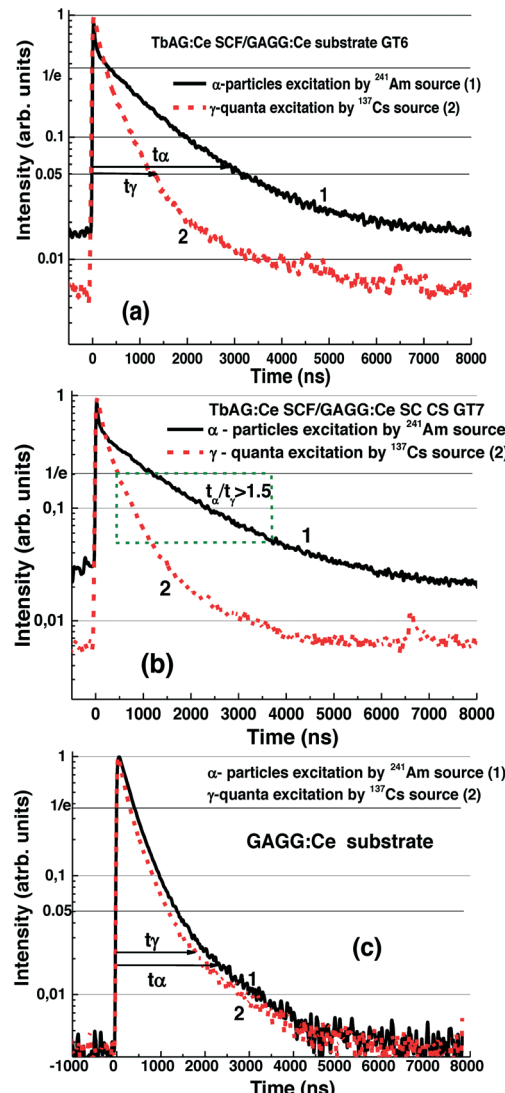


Fig. 8 Scintillation decay of $\text{Tb}_3\text{Al}_5\text{O}_{12}:\text{Ce}/\text{GAGG}:\text{Ce}$ GT6 (a) and GT7 (b) composite scintillators in comparison with the $\text{Gd}_3\text{Ga}_{2.5}\text{Al}_{2.5}\text{O}_{12}:\text{Ce}$ SC substrate (c) under α -particle (1) and γ -ray (2) excitation by ^{241}Am and ^{137}Cs sources, respectively.

of the scintillation signal at the registration of the α -particles and γ -quanta, can be significantly improved in the composite epitaxial structures based on the SCFs and crystals of different oxide compounds in comparison with crystal scintillators.

Fig. 9 shows the values of the t_α/t_γ ratio for the scintillation decay kinetics for samples GT6 and GT7 of TbAG:Ce/GAGG:Ce composite scintillators to $1/e$, 0.1 and 0.01 levels (curves 2 and 3, respectively). Table 3 presents also the respective decay time values to the mentioned levels for both samples of composite scintillators under α -particle and γ -quanta excitation. As can be seen in Fig. 8a and b, the separation of the decay curves, related to the excitation of composite scintillators by α -particles and γ -quanta, is observed both for samples GT6 and GT7 at all levels of intensity decay (see also Table 3). The results presented in Fig. 9 and Table 3

Table 2 Scintillation decay times of the $\text{Tb}_3\text{Al}_5\text{O}_{12}:\text{Ce}/\text{GAGG}:\text{Ce}$ GT6 and GT7 composite scintillators and the reference GAGG:Ce substrate under excitation by α -particles of the ^{241}Am (5.4857 MeV) source and γ -ray excitation by the ^{137}Cs (661.66 keV) source

Sample	Excitation	τ_{fast} , ns	$\tau_{\text{slow}}(1)$, ns	$\tau_{\text{slow}}(2)$, ns
$\text{Gd}_3\text{Al}_{2.5}\text{Ga}_{2.5}\text{O}_{12}:\text{Ce}$ substrate	α -particles	—	355	1060
$\text{Gd}_3\text{Al}_{2.5}\text{Ga}_{2.5}\text{O}_{12}:\text{Ce}$ substrate	γ -rays	—	281	940
$\text{Tb}_3\text{Al}_5\text{O}_{12}:\text{Ce}/\text{GAGG}:\text{Ce}$ GT6	α -particles	28.9	351	1290
$\text{Tb}_3\text{Al}_5\text{O}_{12}:\text{Ce}/\text{GAGG}:\text{Ce}$ GT6	γ -rays	112	434	1890
$\text{Tb}_3\text{Al}_5\text{O}_{12}:\text{Ce}/\text{GAGG}:\text{Ce}$ GT7	α -particles	19.8	297	1480
$\text{Tb}_3\text{Al}_5\text{O}_{12}:\text{Ce}/\text{GAGG}:\text{Ce}$ GT7	γ -rays	102	374	1260

show that for both composite scintillators under study, the best separation of scintillation decay curves under α and γ excitation is observed at low levels of registration of scintillation responses. Namely, the respective t_α/t_γ ratio at the 1/10 level is equal to 2.0 and 3.0, respectively. Thus, the decay times of the film and bulk parts of sample GT7 of TbAG:Ce/GAGG:Ce composite scintillators at the 1/10 level differ three fold under registration of α -particles and γ -quanta, respectively, and such a t_α/t_γ ratio is completely enough for discrimination of the signal coming from different parts of this type of composite scintillator (Fig. 8b). Finally, taking into account the necessity of the compromised decision between the intensity of scintillation response and the value of the t_α/t_γ ratio, the optimum conditions for scintillation registration using this type of composite scintillator can be chosen

between 1/e and 0.05 levels of intensity decay in the 500–4000 ns time range, where t_α/t_γ reaches values of above 1.5 (the dashed rectangle in Fig. 8b).

Thus, we have shown the possibility of simultaneous registration of α -particles and γ -quanta by means of separation of the scintillation decay kinetics of the SCF and crystal parts of the composite scintillators. The significant differences in the scintillation decay kinetics of TbAG:Ce/GAGG:Ce composite scintillators under excitation by α -particles of the ^{241}Am (5.5 MeV) source and γ -quanta of the ^{137}Cs (662 keV) source are observed in Fig. 8a and b as well as in Fig. 9. We have proved that this type of composite scintillator can be successfully applied for the separation of the signals coming from the film and bulk parts at the registration of α particles and γ quanta in mixed radiation fluxes.

Conclusions

A set of novel advanced composite scintillators (CSs) based on single crystalline films (SCFs) of $\text{Tb}_3\text{Al}_5\text{O}_{12}:\text{Ce}$ (TbAG:Ce) garnet and $\text{Gd}_3\text{Al}_{2.5}\text{Ga}_{2.5}\text{O}_{12}:\text{Ce}$ (GAGG:Ce) single crystal (SC) substrates with a thickness of 16–50 μm were produced by the LPE method from a melt solution using a $\text{PbO}-\text{B}_2\text{O}_3$ flux with a SCF/substrate lattice misfit equal to -1.32% .

For characterization of the luminescence and scintillation properties of the SCF and bulk crystal parts of the composite scintillators, the absorption spectra, CL spectra, LY and scintillation decay kinetics measurements under α -particle excitation by ^{239}Pu (5.15 MeV) and ^{241}Am (5.5 MeV) sources and γ -quanta excitation by a ^{137}Cs (0.662 MeV) source were applied. The light yield (LY) of TbAG:Ce SCFs under α -particle excitation by the ^{239}Pu source (5.15 MeV) is 1.75–1.97 times larger than the LY of the reference YAG:Ce SCFs but it is 1.42–1.49 times smaller than that of the GAGG:Ce substrate. The TbAG:Ce SCFs exhibit also relatively fast scintillation response with decay times of $t_{1/e} = 345$ –380 ns and $t_{1/20} = 3140$ –3770 ns. Meanwhile, the scintillation response of TbAG:Ce SCFs under α -particle excitation is significantly slower in the 400–4000 ns range than that of the GAGG:Ce SCs with scintillation decay times of $t_{1/e} = 405$ ns and $t_{1/20} = 1380$ ns.

We have also found significant differences in the scintillation decay kinetics of TbAG:Ce/GAGG:Ce composite scintillators under excitation by γ -quanta of the ^{137}Cs source and α -particle excitation of the ^{241}Am source. The respective t_α/t_γ

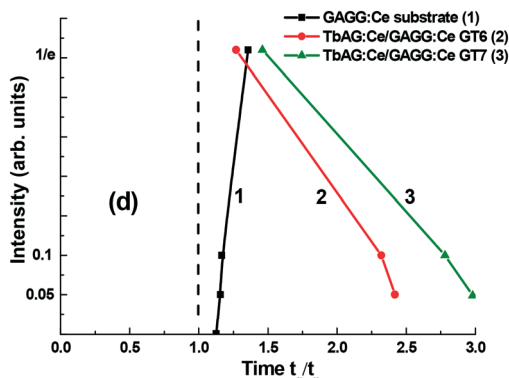


Fig. 9 Plot of the α/γ ratio of the decay time under α and γ excitation versus the intensity of scintillation decay to 1/e, 0.1, 0.05 and 0.01 levels for the two TbAG:Ce/GAGG:Ce composite scintillators (2, 3) and the GAGG:Ce SC substrate (1).

Table 3 Time dependence of scintillation intensity decay from the initial value at $t = 0$ to 1/e, 0.1, and 0.01 levels in the TbAG:Ce/GAGG:Ce GT6 and GT7 composite scintillators and the reference GAGG:Ce substrate

Intensity decay level	GAGG:Ce substrate		TbAG:Ce/GAGG:Ce GT6		TbAG:Ce SCF/GAGG:Ce GT7	
	t_γ , ns	t_α , ns	t_γ , ns	t_α , ns	t_γ , ns	t_α , ns
1/e	300	405	270	345	260	380
0.1	850	990	850	1980	840	2330
0.05	1190	1380	1300	3140	1260	3770
0.001	2780	3130	3520		3280	

decay time of the intensity decay to the 0.05 level under excitation by α -particles of the ^{241}Am source and γ -quanta of the ^{137}Cs source reaches up to 2–3, *i.e.*, the SCF scintillators are two–three times slower than the substrate scintillator in the 400–4000 ns range. For this reason the epitaxial structures based on the TbAG:Ce SCFs, grown onto the GAGG:Ce SC substrate, can be used as composite scintillators for simultaneous registration of the components of mixed ionizing fluxes, specifically α -particles and γ -quanta, respectively.

Separation of the signals from the SCF and SC components of composite scintillators can be realized by means of registration of the difference in the scintillation decay kinetics of SCF and substrate scintillators and can be surely achieved at large (>2) ratios of $t_{1/e}$ or $t_{1/20}$ (SCF)/ $t_{1/e}$ or $t_{1/20}$ (substrate). Indeed, for the composite scintillators based on TbAG:Ce SCFs, grown onto the GAGG:Ce substrate, the optimal t_α/t_γ decay time ratio changes from 2.0 to 3.0 at the registration of scintillations with changing the shaping time from 500 to 4000 ns which is completely enough for discrimination of signals coming from different parts of a composite scintillator of this type. For this reason, the TbAG:Ce SCF/GAGG:Ce composite scintillators possess at present the best scintillation properties among all known analogues, grown by the LPE method.

Conflicts of interest

There are no conflicts to declare.

Acknowledgements

This work was performed in the framework of the Polish National Scientific Center (NCN) 2016/21/B/ST8/03200 project, the Czech Science Foundation 16-15569S project and the CERN-CZ project LM2015058 Research Infrastructure for Experiments at CERN, Ministry of Education, Youth and Sports of the Czech Republic.

References

- 1 Yu. Zorenko, S. S. Novosad, M. V. Pashkovskii, A. B. Lyskovich, V. G. Savitskii, M. M. Batenchuk, P. S. Malyutnenkov, N. I. Patsagan, I. V. Nazar and V. I. Gorbenko, *J. Appl. Spectrosc.*, 1990, **52**, 645–649.
- 2 B. Ferrand, B. Chambaz and M. Couchaud, *Opt. Mater.*, 1999, **11**, 101–114.
- 3 M. Nikl, *Nanocomposite, Ceramic, and Thin Film Scintillators*, Pan Stanford, 2016, p. 350.
- 4 J. M. Robertson and M. V. Van Tol, *Thin Solid Films*, 1984, **114**, 221–240.
- 5 Z. D. Hrytskiv, Y. Zorenko, V. Gorbenko, A. D. Pedan and V. I. Shkliarsyi, *Radiat. Meas.*, 2007, **42**, 933–936.
- 6 E. Molva, *Opt. Mater.*, 1999, **11**, 289–299.
- 7 M. Klimczak, M. Malinowski, J. Sarnecki and R. J. Piramidowicz, *Luminescence*, 2009, **129**, 1869–1873.
- 8 Yu. Zorenko, M. Batenchuk, V. Gorbenko and M. Pashkovsky, *Proc. SPIE*, 1997, **2967**, 101.
- 9 Yu. Zorenko, V. Gorbenko, I. Konstankevych, B. Grinev and M. Globus, *Nucl. Instrum. Methods Phys. Res.*, 2002, **486**, 309–314.
- 10 A. Koch, C. Raven, P. Spanne and A. J. Snigirev, *J. Opt. Soc. Am.*, 1998, **15**, 1940–1951.
- 11 T. Martin and A. Koch, *J. Synchrotron Radiat.*, 2006, **13**, 180–194.
- 12 Y. Zorenko, V. Gorbenko, I. Konstankevych, M. Pashkovsky, M. Globus, B. Grinyov, V. Tarasov, P. Dorenbos, C. W. E. Van Eijk and E. Van Loef, *5th Intern. Conference on Inorganic Scintillators and Their Applications*, 2000, pp. 476–481.
- 13 M. Globus, B. Grinyov, M. Ratner, V. Tarasov, V. Lyubinskiy, Yu. Zorenko and I. Konstankevych, *IEEE Nucl. Sci. Symp. Med. Imaging Conf. Rec.*, 2002, **1**, 352–356.
- 14 Y. Zorenko, V. Gorbenko, V. Savchyn, T. Voznyak, M. Batentschuk, A. Winnacker, Q. Xia and C. Brabec, *Mater. Res. Soc. Symp. Proc.*, 2012, **1341**, 119–124.
- 15 <https://www.crystals.saint-gobain.com/sites/imdf.crystals.com/files/documents/sgc-scintillation-materials-and-assemblies.pdf>.
- 16 Y. Zorenko, A. Voloshinovskii, I. Konstankevych, V. Kolobanov, V. Mikhailin and D. Spassky, *Radiat. Meas.*, 2004, **38**, 677–680.
- 17 Ya. A. Valbis, L. G. Volzhenskaja, Yu. G. Dubov, Yu. Zorenko, I. V. Nazar and N. I. Patsagan, *Opt. Spectrosc.*, 1987, **63**, 1058–1063.
- 18 L. N. Limarenko, Yu. V. Zorenko, M. M. Batenchuk, Z. T. Moroz, M. V. Pashkovskii and I. V. Konstankevich, *J. Appl. Spectrosc.*, 2000, **67**, 211–216.
- 19 Yu. Borodenko, B. Gryniov, V. Martynov, L. Piven, I. Solski, Yu. Zorenko, Z. Moroz and M. Pashkovskii, *J. Surf. Invest.: X-Ray, Synchrotron Neutron Tech.*, 2002, **6**, 6–9.
- 20 Yu. V. Zorenko, *J. Appl. Spectrosc.*, 1998, **65**, 211–215.
- 21 K. Kamada, T. Endo, K. Tsutumi, J. Pejchal, M. Nikl, K. Tsutumi, A. Fujimoto, A. Fukabori and A. Yoshikava, *Cryst. Growth Des.*, 2011, **11**, 4484–4490.
- 22 M. Fasoli, A. Vedda, M. Nikl, C. Jiang, B. Uberuaga, D. Andersson, K. McClellan and C. Stanek, *Phys. Rev. B: Condens. Matter Mater. Phys.*, 2011, **84**, 081102(R).
- 23 Yu. Zorenko, V. Gorbenko, Ja. Vasylkiv, T. Strzyżewski, A. Fedorov, R. Kucerkova, J. A. Mares, M. Nikl, P. Bilski and A. Twardak, *J. Lumin.*, 2016, **169**, 828–837.
- 24 P. Prusa, M. Kucera, J. A. Mares, M. Hanus, A. Bejtlerova, Z. Onderisinova and M. Nikl, *Opt. Mater.*, 2013, **35**, 2444–2448.
- 25 P. Prusa, M. Kucera, J. A. Mares, Z. Onderisinova, M. Hanus, V. Babin, A. Bejtlerova and M. Nikl, *Cryst. Growth Des.*, 2015, **15**, 3715–3723.
- 26 K. Bartosiewicz, V. Babin, J. A. Mares, A. Bejtlerova, Yu. Zorenko, A. Iskaliyeva, V. Gorbenko, Z. Bryknar and M. Nikl, *J. Lumin.*, 2017, **88**, 60–66.
- 27 Y. Zorenko, V. Gorbenko, T. Zorenko, K. Paprocki, M. Nikl, J. A. Mares, P. Bilski, A. Twardak, O. Sidletskiy, I. Gerasymov, B. Grinyov and A. Fedorov, *IEEE Trans. Nucl. Sci.*, 2016, **63**, 496–502.
- 28 Y. Zorenko, V. Gorbenko, T. Zorenko, K. Paprocki, M. Nikl, J. A. Mares, P. Bilski, A. Twardak, T. Voznyak, O. Sidletskiy,

- I. Gerasymov, B. Grinyov and A. Fedorov, *Opt. Mater.*, 2016, **61**, 3–10.
- 29 Yu. Zorenko, P.-A. Douissard, T. Martin, F. Riva, V. Gorbenko, T. Zorenko, K. Paprocki, A. Iskalieva, S. Witkiewicz, A. Fedorov, P. Bilski and A. Twardak, *Opt. Mater.*, 2017, **65**, 73–81.
- 30 V. Gorbenko, T. Zorenko, S. Witkiewicz, K. Paprocki, O. Sidletskiy, A. Fedorov, P. Bilski, A. Twardak and Yu. Zorenko, *Crystals*, 2017, **7**(15), 262.
- 31 S. Witkiewicz-Lukaszek, V. Gorbenko, T. Zorenko, O. Sidletskiy, I. Gerasymov, A. Fedorov, A. Yoshikawa, J. A. Mares, M. Nikl and Yu. Zorenko, *Cryst. Growth Des.*, 2018, **18**, 1834–1842.
- 32 H. L. Glass and M. F. Elliot, *J. Cryst. Growth*, 1974, **27**, 253–260.
- 33 Y. Zorenko, V. Gorbenko, T. Voznyak and T. Zorenko, *Phys. Status Solidi B*, 2008, **245**, 1618–1622.
- 34 Y. Zorenko and V. Gorbenko, *Radiat. Meas.*, 2007, **42**, 907–910.
- 35 Y. Zorenko, T. Voznyak, V. Vistovsky, T. Zorenko, S. Nedliko, M. Batentschuk, A. Osvet, A. Winnacker, G. Zimmerer, V. Kolobanov and D. Spassky, *Radiat. Meas.*, 2007, **42**, 648–651.
- 36 F. Kummer, F. Zwischka, A. Ellens, A. Debray and G. Waitl, *Int. Patent App.* No: WO 01/08452, 2001.
- 37 M. Batentschuk, A. Osvet, G. Schierning, A. Klier, J. Schneider and A. Winnacker, *Radiat. Meas.*, 2004, **38**, 539–543.



Composite thermoluminescent detectors based on the Ce³⁺ doped LuAG/YAG and YAG/LuAG epitaxial structures

S. Witkiewicz-Lukaszek^{a,c,*}, V. Gorbenko^a, T. Zorenko^a, Yu Zorenko^{a,**}, W. Gieszczyk^b, A. Mrozik^b, P. Bilski^b

^a Institute of Physics, Kazimierz Wielki University in Bydgoszcz, Powstańców Wielkopolskich Str., 2, 85090, Bydgoszcz, Poland

^b The Henryk Niewodniczański Institute of Nuclear Physics, Polish Academy of Sciences (IFJ PAN), 152 Radzikowskiego Str., 31-342, Kraków, Poland

^c Poznań University of Technology, Piotrowo 3, 60965 Poznań, Poland



ARTICLE INFO

Keywords:
YAG and LuAG garnets
Ce³⁺ dopant
Crystals
Films
Liquid phase epitaxy
Scintillators

ABSTRACT

This work presents the first results on creation of composite thermoluminescent (TL) detectors based on the film-crystal epitaxial structures of garnet compounds for the simultaneous registration of the mixed ionization fluxes containing α- and β-particles. Two types of TL detectors containing combinations of the single crystalline films (SCFs) and single crystal (SC) substrates of Ce³⁺ doped Y₃Al₅O₁₂ (YAG) and Lu₃Al₅O₁₂ (LuAG) garnets, were considered. The LuAG:Ce SCF/YAG:Ce SC and YAG:Ce SCF/LuAG:Ce SC epitaxial structures were grown by the liquid phase epitaxy (LPE) method from (overcooled) supercooled? melt-solution based on the PbO–B₂O₃ flux and their thermoluminescent properties were examined under excitation by α- and β-particles of ²⁴²Am and ⁹⁰Sr – ⁹⁰Y sources. The registration of α- and β-particles was performed using differences between TL glow curves of SCFs and substrates. The first results on separation of TL signals from SCF and SC components for LuAG:Ce SCF/YAG:Ce SC and YAG:Ce SCF/LuAG:Ce SC epitaxial structures under α- and β-excitation are encouraging. This enables consideration of these epitaxial structures as prototypes at the next steps of producing the composite TL detectors based on different oxide materials using the LPE growth method.

1. Introduction

The composite scintillators and detectors for the simultaneous registration of the different components of mixed ionization fluxes and microimaging are now a new hot topic of the luminescent materials engineering. Such engineering is based on both the novel decisions in creating the bulk and film scintillators (Nikl and Yoshikawa, 2015, Nikl, ed., 2017) and the technologies of their production such as the Czochralski method (Nikl et al., 2014) and the liquid phase epitaxy (LPE) growth technique (Zorenko et al., 1990, 2003; Ferrand et al., 1999). The possibility of the simultaneous registration of α-particles and γ-quanta by means of separation of the scintillation decay kinetics of the film and crystal parts of composite scintillators, based on the epitaxial structures of different garnet compounds, has been recently demonstrated in several our works (Zorenko et al., 1990; Globus et al., 2002; Witkiewicz-Lukaszek et al., 2018a,b,c,d). (see Table 1)

Meanwhile, the mentioned composite scintillation detectors are difficult to be used in some cases, namely, for registration of the quanta and particles with continuously changed energies by means of

separation of the scintillation decay kinetics, for instance, at the registration of β-particles. The application of composite scintillators presupposes the active mode of *in situ* registration of incoming ionization fluxes. Using such a mode of registration is not always possible, especially in the case of low doses of radiation and the long-time radiation exposition. The scintillation technique possesses also other limitations to analysis of the liquid and gas radioactive materials or high-doses sources.

The above mentioned problems demand consideration of other approaches for producing the composite detectors of ionization radiation.

Now we start considering the new possibility for simultaneous registration of the different components of mixed ionization fluxes, using differences between the thermostimulated luminescence (TSL) glow curves, coming from the film and substrate parts of a composite detector (Fig. 1a). This our work presents the first attempt in creation of the composite TSL detectors in the form of the epitaxial structures based on SCs and SCFs of garnet compounds. For this purpose, we consider in this work the combinations of the well-known optical materials - the Ce³⁺ doped Lu₃Al₅O₁₂ (LuAG) and Y₃Al₅O₁₂ (YAG) garnets (Fig. 1a).

* Corresponding author. Institute of Physics, Kazimierz Wielki University in Bydgoszcz, Powstańców Wielkopolskich Str., 2, 85090, Bydgoszcz, Poland.

** Corresponding author.

E-mail addresses: s-witkiewicz@wp.pl (S. Witkiewicz-Lukaszek), zorenko@ukw.edu.pl (Y. Zorenko).

Table 1

Positions of the main TSL peaks in YAG:Ce and LuAG:Ce SCs and SCFs as well as in YAG substrate after irradiation by α - and β -particles.* - most intensive TSL peaks.

SC and SCF content	α - particles	β -particles
YAG:Ce SC	110, 165, 230, 305, 410	110, 165, 230, 305, 410
YAG:Ce SCF	80, 180, 220	
YAG substrate		120, 185, 300
LuAG:Ce SC	120, 210, 295, 345, 430, 475	120, 210, 295, 345, 430, 475
LuAG:Ce SCF	140, 305	
YAG substrate		80, 165, 205, 315
LuAG:Ce SCF/YAG:Ce SC	135, 225, 325*	105, 215*, 310, 400
YAG:Ce SCF/LuAG:Ce SC	80, 180*, 220	125, 220, 300, 345*, 430, 470

2. Growth of composite detectors and experimental technique

The LuAG:Ce and YAG:Ce substrates with a thickness of 0.5 and 1 mm were prepared from the respective SCs of these garnets grown by the Czochralski method. The LuAG:Ce SCF/YAG:Ce SC and YAG:Ce SCF/LuAG:Ce SC epitaxial structures with SCF thickness in the 15–30 μm range onto both sides of substrates were grown using the LPE method from the melt-solution based on the $\text{PbO-B}_2\text{O}_3$ flux onto the mentioned YAG:Ce and LuAG:Ce substrates (Fig. 2). The LuAG:Ce and YAG:Ce SCFs, with SCF thickness in the above mentioned range, grown onto undoped YAG substrates with the 0.5 mm thickness, were also selected with the aim of comparison with the properties of composite detectors and LuAG:Ce and YAG:Ce SC substrates. The CeO_2 activator concentration in the melt solution was 10 mol %. Meanwhile, due to very low segregation coefficient at LPE growth of YAG:Ce and LuAG:Ce SCFs, the Ce^{3+} concentration in SCF samples, detected by EMA analysis, was significantly lower and quite comparable with the Ce^{3+} content in SC counterparts of these garnets in the 0.23–0.45 at. % range.

The structural quality of LuAG:Ce SCF/YAG:Ce SC and YAG:Ce SCF/LuAG:Ce SC composite detectors was characterized by X-ray diffraction (Fig. 1). As can be seen from the XRD patterns of the mentioned epitaxial structures (Fig. 3), both LuAG:Ce and YAG:Ce SCFs can be crystallized onto YAG and LuAG substrates at relatively high misfit values $m = (a_{\text{SCF}} - a_{\text{sub}})/a_{\text{sub}} * 100\%$ between the lattice constants of SCF a_{SCF} and substrate a_{sub} , being equal to -0.82% and $+0.75\%$, respectively. This result is quite coherent with the data presented recently (Zorenko and Goebenko, 2007c). Meanwhile, the possibility of crystallization of YAG SCFs onto LuAG substrates by the LPE method is not-trivial fact and for the first time is confirmed in this work.

The absorption spectra of the samples under study were measured using a Jasco 760 UV-Vis spectrometer in the 200–1100 nm range. The CL spectra were measured at the room temperature (RT) using an electron microscope SEM JEOL JSM-820, additionally equipped with a spectrometer Stellar Net and TE-cooled CCD detector working in the 200–925 nm range. The e-beam excitation source is located at the 90-degree angle to the sample surface (perpendicular excitation), and the luminescence is collected by lens at the 45-degree angle to the sample surface. For TL measurement we used an automatic Risø TL/OSL-DA20 reader under α -particles (49.976 Gy) excitation by ^{241}Am source and β -particles (0.97 Gy) excitation by $^{90}\text{Sr}/^{90}\text{Y}$ source of the samples under study (Fig. 1b). The TSL growth curves were recorded using the green filter which well separated the Ce^{3+} luminescence in the compounds under study.

3. Experimental results

3.1. Absorption spectra

The absorption spectra of LuAG:Ce SCF/YAG:Ce SC and YAG:Ce

SCF/LuAG:Ce SC composite detectors in comparison with the spectra of YAG:Ce and LuAG:Ce SC substrates are shown in Fig. 4. The spectra of the mentioned LPE grown epitaxial structures (Fig. 4, curve 3 and 4, respectively) present the superposition of the absorption spectra of YAG:Ce and LuAG:Ce SC substrates (Fig. 4, curves 1 and 2) and LuAG:Ce and YAG:Ce SCFs, respectively. For this reason, the maxima of the absorption bands of composite detectors are shifted with respect to the absorption maxima of the respective substrates (Fig. 4).

The absorption bands peaked in the 448–458 nm and at 340–346.5 nm ranges in the spectra of composite detectors and SC samples are related to the $4f^2(^2F_{5/2}) \rightarrow 5d^{1,2}(^2E)$ transitions of Ce^{3+} ions (E_1 and E_2 bands, respectively). The absorption bands peaked in the 220–225 nm range are related to the $4f^2(^2F_{5/2}) \rightarrow 5d^{1,2}(T_{2g})$ transitions of Ce^{3+} ions (E_3 band). Meanwhile, the bands peaked around 260 nm correspond to the absorption of Pb^{2+} flux related impurity in LuAG:Ce and YAG:Ce SCFs.

The positions of E_1 and E_2 absorption bands are shifted due to the change in the crystal field strength (CFS) in the dodecahedral positions of YAG and LuAG hosts, where the Ce^{3+} ions are localized. The difference ΔE in the positions of E_1 and E_2 absorption bands is proportional to the CFS. Namely, the ΔE values are equal to 0.936 eV and 0.81 eV, for YAG:Ce and LuAG:Ce SCs, respectively; e.g., the CFS in the dodecahedral sites of YAG is by 15.5% larger than that in LuAG.

3.2. Cathodoluminescence spectra (CL)

The normalized CL spectra of the film parts of YAG:Ce SCF/LuAG:Ce SC and LuAG:Ce SCF/YAG:Ce SC composite detectors in the comparison with the CL spectra of YAG:Ce and LuAG:Ce SC substrates are shown in Fig. 5. The observed wide luminescence bands in the visible range, peaked at 521 and 509 nm for YAG:Ce and LuAG:Ce SCFs, as well as at 535 and 521 nm for their SC counterparts are related to the $5d^1-4f(^2F_{5/2,7/2})$ transitions of Ce^{3+} ions in the YAG and LuAG hosts (Zorenko, et al., 2007a). The observed shift in the positions of the Ce^{3+} emission bands in YAG:Ce and LuAG:Ce SCF and SC counterparts is due to the change in the CFS in the dodecahedral sites of YAG and LuAG hosts and some deviation in the Ce^{3+} concentration in SCF and SC samples.

3.3. Thermoluminescence spectra

The TL glow curves of SCs of YAG:Ce and LuAG:Ce garnets under excitation by α - and β -particles of ^{241}Am and $^{90}\text{Sr} + ^{90}\text{Y}$ sources, are shown Fig. 6a and c, respectively. The respective TL glow curves for YAG:Ce and LuAG:Ce SCF counterparts, grown onto undoped YAG substrates, are presented in Fig. 6c and d, respectively. It is important to note here that under α -particle excitation the TSL glow curves correspond exclusively to SCFs due to larger values of their thickness (above 15 μm) in comparison with the calculated passway for α -particles with an energy of 5 MeV in these materials in the 10–12 μm range. Meanwhile, the penetrations depths of β -particles of $^{90}\text{Sr} + ^{90}\text{Y}$ source with a typical energy of 546.0 KeV and 2279.5 KeV, respectively, are significantly larger in the LuAG and YAG hosts and equal to 0.8 of 1.3 mm, respectively, for an average energy of 1.1 MeV. Therefore, in the case of YAG:Ce SCF/YAG SC and LuAG:Ce/YAG SC epitaxial structures, the energy of α -particles of ^{241}Am source is completely stopped by SCFs when the energy of β -ray from $^{90}\text{Sr} + ^{90}\text{Y}$ source is absorbed mainly in the undoped YAG SC substrate.

Due to the fact that Ce^{3+} ions are typical hole trapping centers (Dorenbos, 2003), all the TSL peaks, observed in Fig. 6a; 6b, curve 1; 6c and 6d, curve 1, correspond to the *electron trapping centers*. As can be seen from Fig. 6a and c, SCs of YAG:Ce and LuAG:Ce garnets show similar TSL properties under excitation by α - and β -particles but the integral intensity of the TSL peaks is strongly determined by the absorbed dose of radiation (curves 1 and 2, respectively). Meanwhile, the SCFs of these garnets show noticeable differences in the positions of the TSL peaks with respect to their SC counterparts due to the significant

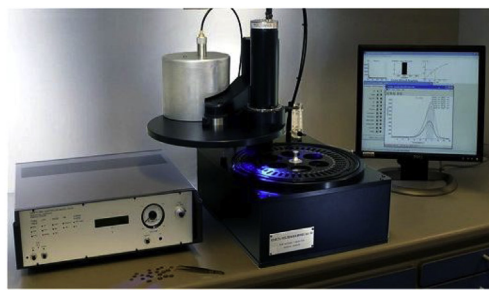
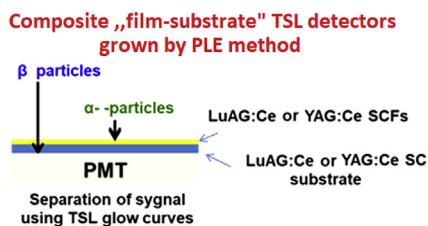


Fig. 1. (a) - principal scheme of composite TSL detector. (b) - Risø TL/OSL-DA-20 reader at INP PAN in Krakow.

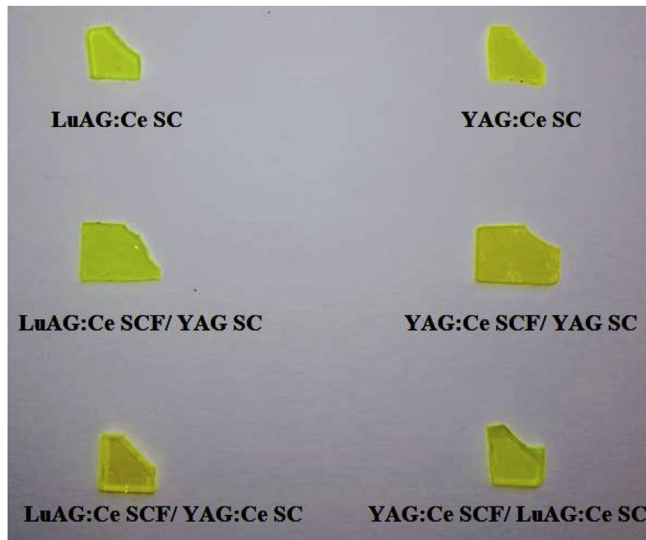


Fig. 2. YAG:Ce and LuAG:Ce SC substrates (at the top), LuAG:Ce and YAG:Ce SCFs (in the middle) as well as composite TL detector samples based on the LuAG:Ce and YAG:Ce SCs and SCFs, grown by the LPE method onto YAG:Ce (bottom, left part) and YAG:Ce (bottom, right part) SC substrates. The specific shape of the samples is related to removal of triangular fragment with the $3.75 \times 3.75 \times 5.25$ mm dimensions. These fragments were used to measure TL in Risø TL/OSL-DA-20 reader.

difference in the methods of their preparation. Namely, the YAG:Ce and LuAG:Ce SCs, grown from the melt at 1930–2050 °C range, possess large concentration of the Y_{Al} and Lu_{Al} antisite defects and oxygen vacancies, which play the role of electron trapping centers (Zorenko et al., 2007b). On the contrary, due to absence of the Y_{Al} and Lu_{Al} antisite defects and

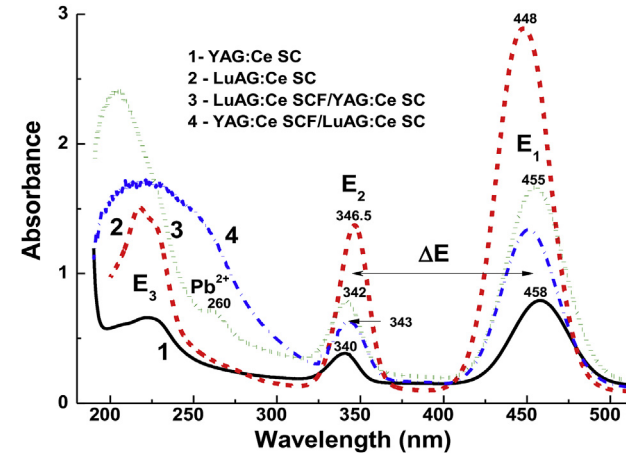


Fig. 4. Absorption spectra of LuAG:Ce SCF/YAG:Ce SC (3) and YAG:Ce SCF/LuAG:Ce SC (4) composite detectors (3) in comparison with spectra of YAG:Ce (1) and LuAG:Ce (2) SC substrates.

very low concentration of the charged oxygen vacancies as emission and trapping centers in YAG:Ce and LuAG:Ce SCFs, grown from the melt-solution at low (950–1000 °C) temperatures (Zorenko et al., 2007b), the TSL glow curves in these films (Fig. 5b and d, curves 1) possess significantly more simple structure than that in their SC counterparts.

Most probably, in the case of undoped YAG substrates the role of emission centers in the green range can play the trace impurity of Ce^{3+} , Tb^{3+} or Nd^{3+} ions. In the frame of this assumption, all the mentioned TSL peaks also can correspond to the electronic trapping centers.

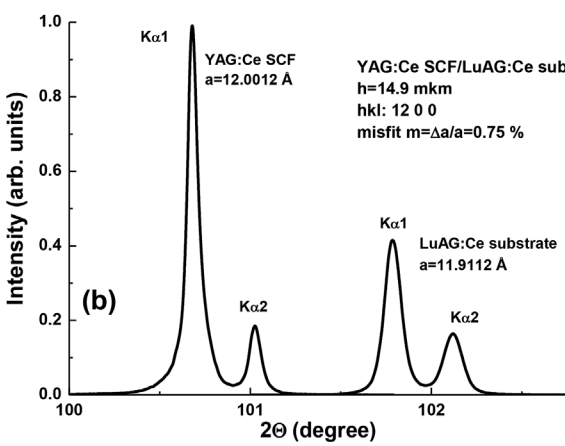
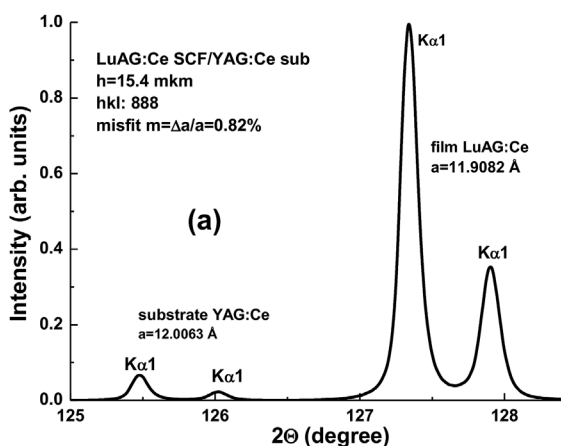


Fig. 3. XRD patterns of LuAG:Ce SCF/YAG:Ce SC (a) and YAG:Ce SCF/LuAG:Ce SC (b) composite detectors. The respective SCF/substrate misfit m is equal to - 0.82% (a) and 0.75% (b), respectively.

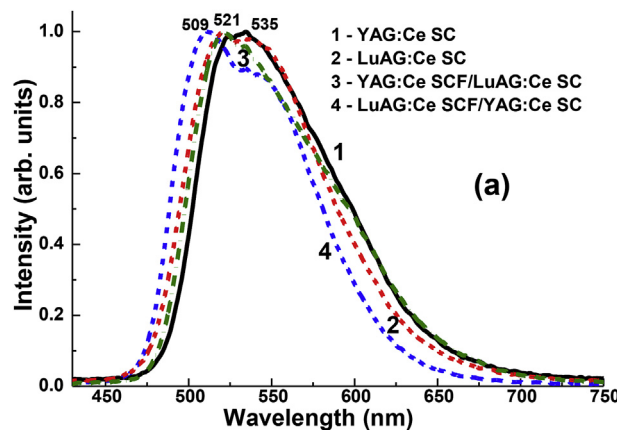


Fig. 5. Normalized CL spectra of film parts of YAG:Ce SCF/YAG:Ce SC (3) and LuAG:Ce SCF/YAG:Ce SC (4) composite detectors in comparison with CL spectra of YAG:Ce (1) and LuAG:Ce SCs (2).

3.4. TSL properties of composite detectors

The observed differences in the positions of the main TSL peaks in the SC and SCF of YAG:Ce and LuAG:Ce garnet compounds (Fig. 6) open the possibility for creation of the pilot sets of composite TSL detectors based on the LuAG:Ce SCF/YAG:Ce SC and YAG:Ce SCF/LuAG:Ce SC epitaxial structures, grown by the LPE method.

The TL glow curves of LuAG:Ce SCF/YAG:Ce SC and YAG:Ce SCF/LuAG:Ce SC epitaxial structures after irradiation by α - and β -particles show noticeable differences (Fig. 7). Namely, for LuAG:Ce SCF/YAG:Ce SC structure, the main peaks are observed at 325 °C and 215 °C after irradiation α - and β -particles, respectively, when for the YAG:Ce SCF/LuAG:Ce SC structures the corresponding peaks are located at 180 °C and 345 °C, respectively. As it is mentioned above, α -particles of ^{241}Am (5.5 MeV) source with a typical passway in the LuAG and YAG hosts of 10–12 μm are fully stopped in SCF parts of a composite detector with a thickness of several tens microns, when β -particles of $^{90}\text{Sr} + ^{90}\text{Y}$ source

with an average energy of 1.1 MeV can penetrate in the whole 1.3 mm thick YAG and 0.8 mm LuAG SC substrates. Therefore, the TSL signals from SCF and SC parts the both composite detectors under study correspond mainly to the registration of α -particles and β -particles, respectively. In our opinion, the most suitable ranges for registration of differences in the TSL glow curves for LuAG:Ce SCF/YAG:Ce SC and YAG:Ce SCF/LuAG:Ce SC composite detectors lies between 150 and 400 °C and 100–400 °C, where the largest difference (at least by one order of magnitude) between the respective TSL peaks is observed for SCF and SC parts of composite detectors (Fig. 7).

4. Conclusions

With the aim of creation of composite thermoluminescent (TL) detectors based on the single crystalline films (SCFs) and single crystals (SCs) of garnet compounds for the simultaneous registration of the mixed ionization fluxes, containing α - and β -particles, the LuAG:Ce SCF/YAG:Ce SC and YAG:Ce SCF/LuAG:Ce SC epitaxial structures with SCF thickness in the 15–30 μm range and a SC substrate thickness of 1 mm were grown by the liquid phase epitaxy (LPE) method. The thermoluminescent properties of the mentioned epitaxial structures were examined under excitation by α - and β -particles of ^{242}Am and $^{90}\text{Sr} - ^{90}\text{Y}$ sources, respectively. The registration of α - and β -particles by the SCF and SC components of composite detectors was performed using differences between the TL glow curves of SCF and substrate.

The first results on separation of the TL signals from SCF and SC components for the LuAG:Ce SCF/YAG:Ce SC and YAG:Ce SCF/LuAG:Ce SC epitaxial structures after α - and β -excitation are encouraging. We have observed the significant differences in the positions (up to 80°) and intensity (more than by one order of magnitude) of the main TSL peaks of the glow curves of SCF and SC components of these epitaxial structures after α - and β -particle irradiation. For this reason, we expect that the mentioned combinations of the garnet compounds in these epitaxial structures can be considered as prototypes in the future development of a new generation of composite TL detectors based on the different oxide compounds using the LPE growth method.

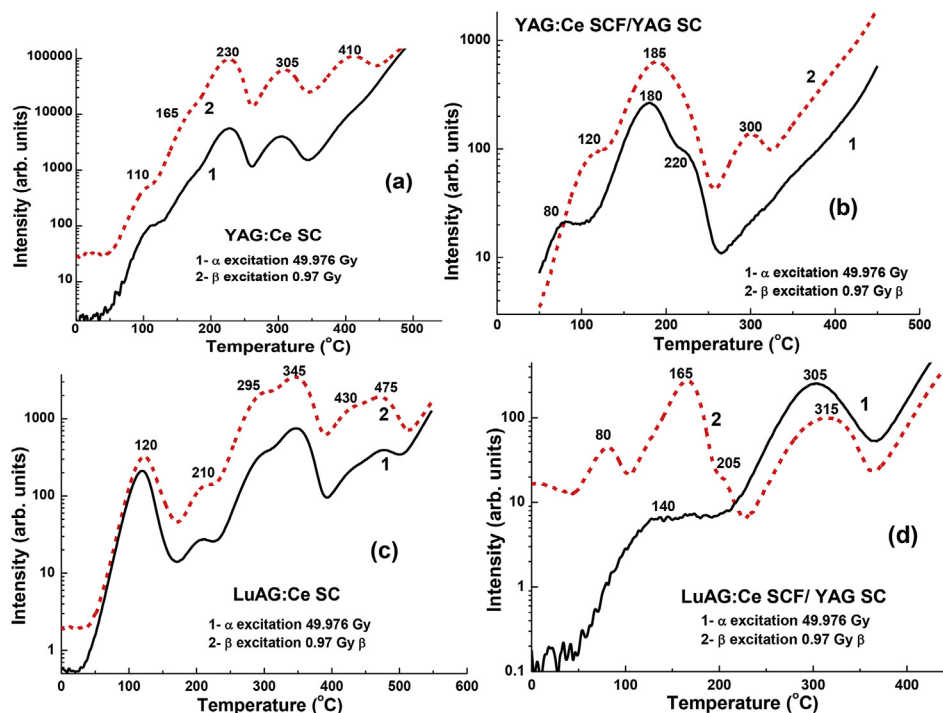


Fig. 6. Glow curves of YAG:Ce SCs (a), YAG:Ce SCFs (b), LuAG:Ce SCs (c) and LuAG:Ce (d) SCFs after irradiation by α - (1) and β - (2) particles, respectively. YAG:Ce and LuAG:Ce SCFs were grown onto YAG substrates.

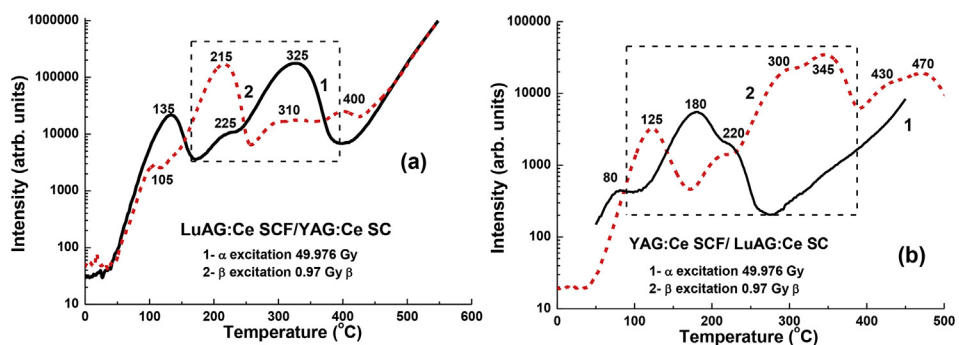


Fig. 7. TSL glow curves of LuAG:Ce SCF/YAG:Ce SC (a) and YAG:Ce SCF/LuAG:Ce SC (b) epitaxial structures after irradiation by α - (1) and β - (2) particles, respectively. The dashed rectangle indicates the most suitable range for registration differences in the TSL glow curves for SCF and SC parts of composite detectors.

Acknowledgements

The work was supported by National Scientific Center of Poland project No 2018/31/B/ST8/03390.

References

- Dorenbos, P., 2003. Relation between Eu^{2+} and Ce^{3+} f \leftrightarrow d-transition energies in inorganic compounds. *J. Phys. Condens. Matter* 15, 8417–8434.
- Ferrand, B., Chambaz, B., Couchaud, M., 1999. Liquid phase epitaxy: a versatile technique for the development of miniature optical components in single crystal dielectric media. *Opt. Mater.* 11, 101–114.
- Globus, M., Grinyov, B., Ratner, M., Tarasov, V., Lyubinskiy, V., Zorenko, Yu., Konstankevych, I., 2002. New type of scintillation phoswich detectors for biological, medical and radiation monitoring applications. *IEEE Nucl. Sci. Symp. Med. Imag. Conf.* 1, 352–356.
- Nikl, M. (Ed.), 2017. Nanocomposite, Ceramic, and Thin Film Scintillators. Pan Stanford, New York9789814745239..
- Nikl, M., Yoshikawa, A., 2015. Recent R&D trends in inorganic single-crystal scintillator materials for radiation detection. *Adv. Opt. Mater.* 3, 463–481.
- Nikl, M., Kamada, K., Babin, V., Pejchal, J., Pilarova, K., Mihokova, E., Bejtlerova, A., Bartosiewicz, K., Kurosawa, S., Yoshikawa, A., 2014. Defect engineering in Ce-doped aluminum garnet single crystal scintillators. *Cryst. Growth Des.* 14, 4827–4833.
- Witkiewicz-Lukaszek, S., Gorbenko, V., Zorenko, T., Sidletskiy, O., Gerasimov, I., Fedorov, A., Mares, J.A., Kucerkova, R., Nikl, M., Zorenko, Yu., 2018a. *Cryst. Growth Des.* 18, 1834–1842.
- Witkiewicz-Lukaszek, S., Gorbenko, V., Zorenko, T., Paprocki, K., Sidletskiy, O., Gerasimov, I., Mares, J.A., Kucerkova, R., Nikl, M., Zorenko, Yu., 2018b. Novel all-solid-state composite scintillators based on the epitaxial structures of LuAG garnet doped with Pr, Sc and Ce ions. *IEEE TNS* 65, 2114–2119.
- Witkiewicz-Lukaszek, S., Gorbenko, V., Zorenko, T., Paprocki, K., Sidletskiy, O., Gerasimov, I., Mares, J.A., Kucerkova, R., Nikl, M., Zorenko, Yu., 2018c. Composite scintillators based on the crystals and single crystalline films of LuAG garnet doped with Ce^{3+} , Pr^{3+} and Sc^{3+} ions. *Opt. Mater.* 84, 593–599.
- Witkiewicz-Lukaszek, S., Gorbenko, V., Zorenko, T., Paprocki, K., Sidletskiy, O., Fedorov, A., Mares, J.A., Kucerkova, R., Nikl, M., Zorenko, Yu., 2018d. Epitaxial growth of composite scintillator based on the $\text{Tb}_3\text{Al}_5\text{O}_{12}$:Ce single crystalline film and $\text{Gd}_3\text{Al}_{2.5}\text{Ga}_{2.5}\text{O}_{12}$:Ce crystal substrates. *CrystEngComm* 20, 3994–4002.
- Zorenko, Yu., Gorbenko, V., 2007c. Growth peculiarities of the $\text{R}_3\text{Al}_5\text{O}_{12}$ (R = Lu, Yb, Tb, Eu-Y) single crystalline film phosphors by Liquid Phase Epitaxy. *Radiat. Meas.* 42, 907–910.
- Zorenko, Yu., Novosad, S., Pashkovskii, M., Lyskovich, A., Savitskii, V., Batenchuk, M., Nazar, I., Gorbenko, V., 1990. Epitaxial structures of garnets as scintillation detectors of ionizing radiation. *J. Appl. Spectrosc.* 52, 645–649.
- Zorenko, Yu., Konstankevych, I., Globus, M., Grinyov, B., Lyubinskij, V., 2003. New scintillation detectors based on oxide single crystal films for biological microtomography. *Nucl. Instrum. Methods Phys. Res.* 486, 93–96.
- Zorenko, Yu., Voloshinovskii, A., Savchyn, V., Vozniak, T., Nikl, M., Nejezchleb, K., Mikhailin, V., Kolobanov, V., Spassky, D., 2007a. Exciton and antisite defect-related luminescence in $\text{Lu}_3\text{Al}_5\text{O}_{12}$ and $\text{Y}_3\text{Al}_5\text{O}_{12}$ garnets. *Phys. Status Solidi* 244, 2180–2189.
- Zorenko, Yu., Gorbenko, V., Mihokova, E., Nikl, M., Nejezchleb, K., Vedda, A., Kolobanov, V., Spassky, D., 2007b. Single crystalline film scintillators based on Ce- and Pr-doped aluminium garnets. *Radiat. Meas.* 42, 521–527.

Article

LPE Growth of Composite Thermoluminescent Detectors Based on the $\text{Lu}_{3-x}\text{Gd}_x\text{Al}_5\text{O}_{12}:\text{Ce}$ Single Crystalline Films and YAG:Ce Crystals

Sandra Witkiewicz-Lukaszek ^{1,*}, Anna Mrozik ², Vitalii Gorbenko ¹, Tetiana Zorenko ¹, Paweł Bilski ² , A. Fedorov ³ and Yuriy Zorenko ^{1,*} 

¹ Institute of Physics, Kazimierz Wielki University in Bydgoszcz, 85090 Bydgoszcz, Poland; gorbenko@ukw.edu.pl (V.G.); tetiana.zorenko@ukw.edu.pl (T.Z.)

² Institute of Nuclear Physics, Polish Academy of Sciences, 31342 Krakow, Poland; anna.mrozik@ifj.edu.pl (A.M.); pawel.bilski@ifj.edu.pl (P.B.)

³ SSI Institute for Single Crystals, National Academy of Sciences of Ukraine, 61178 Kharkiv, Ukraine; fedorov@xyz.ua

* Correspondence: s-witkiewicz@wp.pl (S.W.-L.); zorenko@ukw.edu.pl (Y.Z.); Tel.: +48-693330878 (Y.Z.)

Received: 4 February 2020; Accepted: 6 March 2020; Published: 10 March 2020



Abstract: This work is dedicated to the development of new types of composite thermoluminescent (TL) detectors for simultaneous registration of the different components of ionization radiation based on the single crystalline films (SCFs) of Ce^{3+} -doped $\text{Lu}_{3-x}\text{Gd}_x\text{Al}_5\text{O}_{12}:\text{Ce}$ ($x = 0\text{--}1.5$) garnet and $\text{Y}_3\text{Al}_5\text{O}_{12}:\text{Ce}$ (YAG:Ce) substrates using the liquid phase epitaxy (LPE) growth method. For this purpose, the TL properties of the mentioned epitaxial structures were examined in Risø TL/OSL-DA-20 reader under excitation by α - and β -particles from ^{242}Am and ^{90}Sr - ^{90}Y sources. We have shown that the cation engineering of SCF content can result in more significant separation of the TL glow curves of SCFs and substrates under α - and β -particle excitations in comparison with the prototype of such composite detectors based on the $\text{Lu}_3\text{Al}_5\text{O}_{12}:\text{Ce}$ (LuAG:Ce)/YAG:Ce epitaxial structure. Specifically, the difference between the TL glow curves of $\text{Lu}_{1.5}\text{Gd}_{1.5}\text{Al}_5\text{O}_{12}:\text{Ce}$ SCFs and YAG:Ce substrates increases up to 120 K in comparison with a respective value of 80 degrees in the prototype based on the LuAG:Ce/YAG:Ce epitaxial structure. Therefore, the LPE-grown epitaxial structures containing $\text{Lu}_{1.5}\text{Gd}_{1.5}\text{Al}_5\text{O}_{12}:\text{Ce}$ SCFs and Ce^{3+} -doped YAG:Ce substrate can be successfully applied for simultaneous registration of α - and β -particles in mixed fluxes of ionization radiation.

Keywords: liquid phase epitaxy; single crystalline films; mixed garnets; thermoluminescence; TL detector cations

1. Introduction

The advancement of composite scintillators (CSs) and thermoluminescent (TL) detectors for the registration of the components of mixed ionization fluxes is now an actual subject of luminescent materials engineering. The basis for such novel engineering are the latest decisions in creating bulk single crystal (SC) and single crystalline film (SCF) scintillators [1,2] as well as the technologies of their production using the Czochralski method [3,4] and the liquid phase epitaxy (LPE) growth technique, respectively [5–11]. Namely, in our previous work, we have shown the possibility of simultaneous registration of α -particles and γ -quanta using the separation of the scintillation decay kinetics of the film (SCF) and crystal (SC) parts of composite scintillators, based on the epitaxial structures of different garnet compounds [12–16].

The application of composite scintillators presupposes the active *in situ* mode of the registration of incoming ionization fluxes. Meanwhile, such a mode of registration is not always possible to use

in the case of low doses of radiation and a long-time exposition of radiation. Namely, particles and quanta with different energies cannot be registered using the separation between scintillation decay kinetics curves. There are also restrictions in application of the above-mentioned materials regarding the analysis of liquid and gaseous radioactive materials or the registration of high-dose sources.

The problems described above stimulated us to developing new approaches in the production of composite ionizing radiation detectors. One solution is to develop TL detectors for the simultaneous registration of different components of mixed ionization fluxes using the differences in the thermoluminescence (TL) glow curves. Particularly, such differences can be described by $\Delta T = T_F - T_S$ parameter, e.g., the difference between the position of the main TL peaks, recording from the film (T_F) and substrate (T_S) parts of the composite detector (Figure 1a).

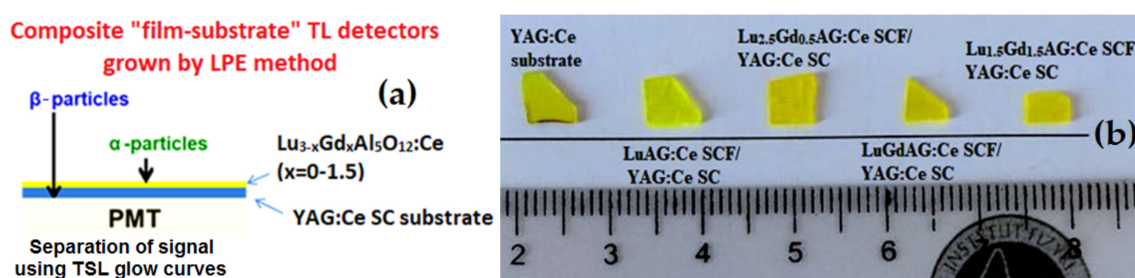


Figure 1. (a) principal scheme of the composite thermoluminescent (TL) detector, based on the $\text{Lu}_{3-x}\text{Gd}_x\text{Al}_5\text{O}_{12}:\text{Ce}$ (YAG:Ce) single crystal (SC) epitaxial structure with single crystalline film (SCF) and SC thickness in the 12–15 μm and 0.9–1.0 mm ranges, respectively, and photomultiplier (PMT); (b) the set of TL detectors based on the liquid phase epitaxy (LPE)-grown epitaxial structures containing $\text{Lu}_{3-x}\text{Gd}_x\text{Al}_5\text{O}_{12}:\text{Ce}$ SCFs at $x = 0$ –1.5 and YAG:Ce substrates. The irregular shapes of the samples result from cutting the fragment of these samples with a 3.75 mm \times 3.5 mm \times 5.25 mm size for TL measurements using a Risø TL/OSL-DA-20 reader.

The possibility of the creation of such types of composite TL detectors for the simultaneous registration of α - and β -particle excitation was shown firstly by us in [17]. This work is a continuation of the research in this direction and dedicated to the development of new types of composite TL detectors for the simultaneous registration of the different components of mixed ionization fluxes based on the SCFs of Ce^{3+} -doped $\text{Lu}_{3-x}\text{Gd}_x\text{Al}_5\text{O}_{12}:\text{Ce}$ ($x = 0$ –1.5) garnet and $\text{Y}_3\text{Al}_5\text{O}_{12}:\text{Ce}$ (YAG:Ce) SC substrates using the LPE growth method.

Recently, the SCFs of $\text{Lu}_{3-x}\text{Gd}_x\text{Al}_5\text{O}_{12}:\text{Ce}$ garnet with the Gd content, x , from 0 up to 2.5 has been successfully crystallized by the LPE method onto undoped YAG substrates from the melt-solutions based on $\text{PbO-B}_2\text{O}_3$ flux, and their optical properties have been investigated as well [12]. In the present work, we used the LPE-grown epitaxial structures, containing $\text{Lu}_{3-x}\text{Gd}_x\text{Al}_5\text{O}_{12}:\text{Ce}$ SCFs with different Gd concentrations in the $x = 0$ –1.5 range, and Ce^{3+} -doped YAG:Ce substrates for the simultaneous registration of α - and β -particles in the mixed ionization fluxes. For this purpose, the TL properties of the epitaxial structures were examined under excitation by α - and β -particles from ^{242}Am and ^{90}Sr – ^{90}Y sources, respectively. We expected that the cation engineering of SCF content would result in more significant separation of the TL glow curves of SCFs and substrates in comparison with the prototype of such composite detectors based on the LuAG:Ce SCF/YAG:Ce SC epitaxial structure [17].

2. Growth of Composite Detectors

Four sets of composite detectors, based on the epitaxial structures containing $\text{Lu}_{3-x}\text{Gd}_x\text{Al}_5\text{O}_{12}:\text{Ce}$ SCFs with Gd content $x = 0$, 0.5, 1, and 1.5 and YAG:Ce substrates with the (110) orientation and a thickness of 0.5 mm, were crystallized using the LPE method from the melt-solution based on $\text{PbO-B}_2\text{O}_3$ flux (Figure 1). The conditions of the growth of these structures are presented in Table 1.

Table 1. Conditions of the LPE growth of $\text{Lu}_{3-x}\text{Gd}_x\text{Al}_5\text{O}_{12}:\text{Ce}$ SCFs at $x = 0\text{--}1.5$ onto YAG:Ce substrates. H—SCF thickness; f and T—velocity and temperature of the SCFs growth; \mathbf{a} —SCF lattice constants, m—SCF/substrate misfit, LY—relative photoelectron light yield (LY) of SCFs under α -particle excitation in comparison with the LY of YAG:Ce SCF standard samples with a LY of 2.65 ph/KeV.

Nominal Content of SCFs in Melt-Solution	Substrate	m, %	h, μm	T, $^{\circ}\text{C}$	f, $\mu\text{m}/\text{min}$	LY, %
YAG:Ce SC	YAG					128
LuAG:Ce SCF	YAG:Ce	0.83	37	973	0.43	98
$\text{Lu}_{2.5}\text{Gd}_{0.5}\text{AG}:\text{Ce}$ SCF	YAG:Ce	0.49	51	970	0.73	63
$\text{Lu}_2\text{GdAG}:\text{Ce}$ SCF	YAG:Ce		16	970	0.53	54
$\text{Lu}_{1.5}\text{Gd}_{1.5}\text{AG}:\text{Ce}$ SCF	YAG:Ce	0.04	20	975	0.4	45

Due to the fact that the segregation coefficient of Gd^{3+} ions in the LPE growth of LuAG-based SCF onto YAG substrates is equal to 0.95–1.05 [18], the content of SCFs was close to a nominal content of garnets in the melt-solution. The concentration of Ce^{3+} ions in SCFs and YAG:Ce substrates was in the 0.25–0.5 at % range.

XRD measurements were used for the characterization of the structural quality of $\text{Lu}_{3-x}\text{Gd}_x\text{Al}_5\text{O}_{12}:\text{Ce}$ SCF samples with different Gd content and determination of the SCF lattice constants and SCF/substrate misfit m (Figure 2).

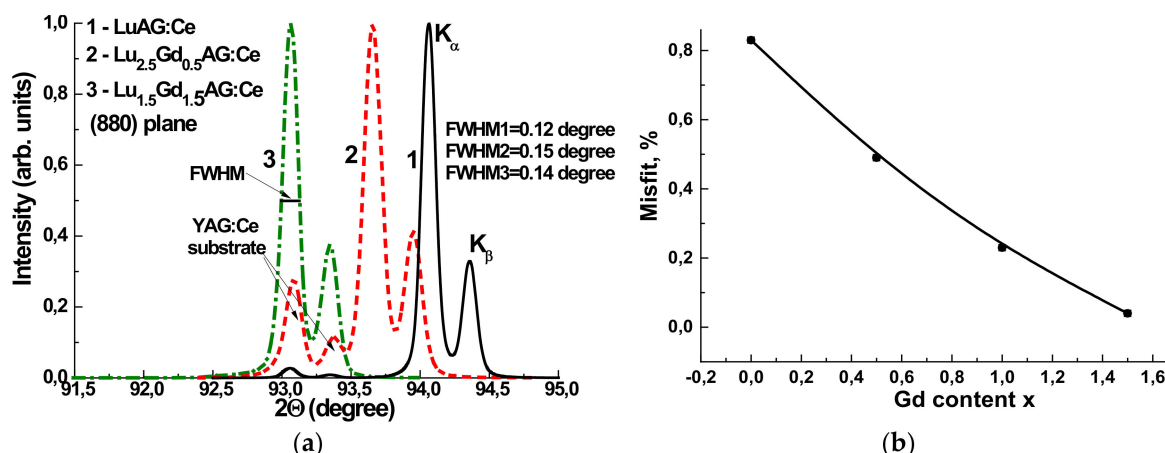


Figure 2. (a) XRD patterns of (880) planes of $\text{Lu}_{3-x}\text{Gd}_x\text{Al}_5\text{O}_{12}:\text{Ce}$ SCFs at $x = 0, 0.5$, and 1.5 , grown onto YAG:Ce substrates; (b) the dependence of the misfit between the lattice constants of $\text{Lu}_{3-x}\text{Gd}_x\text{Al}_5\text{O}_{12}:\text{Ce}$ SCF and YAG substrate on Gd content x .

From the respective XRD patterns of the $\text{Lu}_{3-x}\text{Gd}_x\text{Al}_5\text{O}_{12}:\text{Ce}$ SCFs at x value ranging from 0 to 1.5 we also calculated the lattice constant of the different garnet compositions and estimated the misfit between the lattice constants of SCF and YAG substrate $\Delta\mathbf{a} = (\mathbf{a}_{\text{SCF}} - \mathbf{a}_{\text{sub}}/\mathbf{a}_{\text{sub}}) \times 100\%$ (Table 1). We found that the lattice constant of $\text{Lu}_{3-x}\text{Gd}_x\text{Al}_5\text{O}_{12}:\text{Ce}$ SCF and the misfit value m steeply depends on the Gd content in accordance with Vegard's law. Namely, the lattice constant changed from 11.902 Å for LuAG SCFs to 11.998 Å for $\text{Lu}_{1.5}\text{Gd}_{1.5}\text{Al}_5\text{O}_{12}:\text{Ce}$ SCFs. The value of misfit m varies from −0.83% for LuAG SCF to 0.04% for $\text{Lu}_{1.5}\text{Gd}_{1.5}\text{Al}_5\text{O}_{12}:\text{Ce}$ SCF (Figure 1b), i.e., the last sample was grown practically without SCF/substrate misfit.

The full width at half maximum (FWHM) of the XRD peaks of the garnet samples under study was also determined from the respective patterns. As can be seen from this figure, the structural quality of $\text{Lu}_{2.5}\text{Gd}_{0.5}\text{AG}:\text{Ce}$ and $\text{Lu}_{1.5}\text{Gd}_{1.5}\text{AG}:\text{Ce}$ SCF samples, proportional to the FWHM of the respective XRD peaks (0.15 and 0.14 degree, respectively), is very close to that of LuAG:Ce SC (0.12 degree).

3. Experimental Technique

For the characterization of the luminescent properties of the $\text{Lu}_{3-x}\text{Gd}_x\text{Al}_5\text{O}_{12}:\text{Ce}$ SCF/YAG:Ce SC structures, we used absorption spectra, cathodoluminescence (CL), and thermoluminescent (TL) spectra. The absorption spectra were measured using a Jasco 760 UV-Vis spectrometer (Jasco Int. Co. Ltd., Tokyo, Japan) in the 200–1100 nm range. The CL spectra were measured at room temperature (RT) using a SEM JEOL JSM-820 electron microscope (JEOL, Tokyo, Japan) additionally equipped with a spectrometer Stellar Net with a TE-cooled Charge Coupled Device (CCD) detector working in the 200–925 nm range (StellarNet Inc, Tampa, FL, USA).

The TL glow curves were measured under the excitation by α - and β -particles from ^{241}Am and ^{90}Sr + ^{90}Y sources. For measuring the TL in a Risø TL/OSL-DA-20 reader (Risø DTU, Roskilde, Denmark) we used the triangular fragment of samples with $3.75 \text{ mm} \times 3.75 \text{ mm} \times 5.25 \text{ mm}$ dimensions.

It is worth to note here that the mechanism of TL in the SCF samples under study was connected with the electron liberation from deeper electron traps and their subsequent recombination with the holes localized around Ce^{3+} ions [17,18]. Therefore, for the registration of the TL glow curves, a “green” Schott BG 39 filter was used. The transmittance range of this filter, extending from 350 to 700 nm, was well matched with the emission range of the Ce^{3+} luminescence in the SCF samples.

4. Optical Properties of $\text{Lu}_{3-x}\text{Gd}_x\text{Al}_5\text{O}_{12}:\text{Ce}$ SCFs/YAG:Ce Epitaxial Structures

4.1. Absorption Spectra

The absorption spectra of $\text{Lu}_{3-x}\text{Gd}_x\text{Al}_5\text{O}_{12}:\text{Ce}$ SCF/YAG:Ce SC epitaxial structures in comparison with the absorption spectrum of the YAG:Ce substrate are shown in Figure 3. It is worth noting that the absorption spectra of the epitaxial structures represent the mixes of the spectra of the YAG:Ce substrate and the respective SCF sample with a total thickness in the 32–100 μm range (see Table 1).

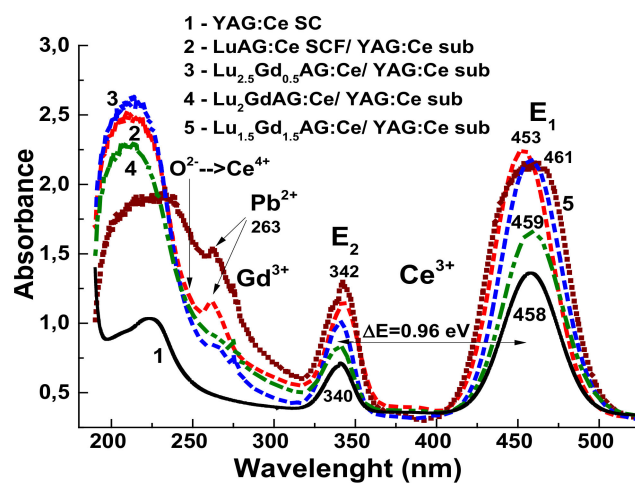


Figure 3. Absorption spectra of LuAG:Ce SCF/YAG:Ce SC, $\text{Lu}_{2.5}\text{Gd}_{0.5}\text{AG:Ce}$ SCF/YAG:Ce, LuGdAG:Ce SCF/YAG:Ce SC, and $\text{Lu}_{1.5}\text{Gd}_{1.5}\text{AG:Ce}$ SCF/YAG:Ce composite detectors in comparison with YAG:Ce substrate.

The absorption bands peaked within 453–461 nm and at the 340–342 nm range in the spectra of all the composite detector samples and YAG:Ce substrates were related to the $4f(^2\text{F}_{5/2}) \rightarrow 5d^{1,2}(^2\text{E})$ transitions of Ce^{3+} ions E_1 and E_2 bands, respectively. The ΔE values, proportional to the crystal field strength on the dodecahedral position of the garnet lattice [18,19], were equal approximately to 1 eV for these samples.

The bands that peaked around 263 nm correspond to the absorption of Pb^{2+} flux-related impurity in $\text{Lu}_{3-x}\text{Gd}_x\text{Al}_5\text{O}_{12}:\text{Ce}$ SCFs and caused by the $^1\text{S}_0 \rightarrow ^3\text{P}_1$ transitions of these ions [18]. The intensity of this band increased with raising the Gd content in SCFs. Such behavior was connected with

increasing the lattice constant of the garnet and respective dimension of the dodecahedral sites for the localization of the Pb^{2+} ions with large ionic radii (1.29 Å) in comparison with Lu^{3+} (0.997 Å) and Gd^{3+} (1.078 Å) cations. Meanwhile, the concentration of this impurity even in the highly Gd-doped SCFs was still below the detection limit (100 ppm) of a SEM JEOL JSM-820 electron microscope used for the microanalyses of the samples' content and only the intensity of Pb^{2+} -related absorption bands (Figure 3) could be used for the estimation of the concentration of these ions.

The large Pb^{2+} ion content in Gd-doped samples could also be contributed to the decrease of the scintillation LY of these SCFs (see Table 1). A negative influence of Pb^{2+} on the LY of SCF scintillators was recently observed for many types of SCF scintillators [6,9,18]. Such influence can also be connected with the possible creation of $\text{Pb}^{2+}\text{-Ce}^{4+}$ pairs with local charge and local compensation at relatively large concentration of lead ions in SCF samples. Indeed, the absorption spectrum of $\text{Lu}_{1.5}\text{Gd}_{1.5}\text{Al}_5\text{O}_{12}\text{:Ce}$ SCF (Figure 2, curve 5) shows the presence of an additional broad band peak at approximately 255 nm. Most probably, this band was related to the $\text{O}^{2+}\rightarrow\text{Ce}^{4+}$ charge transfer transitions (CTT). The confirmation of this conclusion was a close position of these bands in the mentioned SCF sample to the similar $\text{O}^{2+}\rightarrow\text{Ce}^{4+}$ CTT band in Ca^{2+} - and Mg^{2+} -doped LuAG:Ce SCs [20,21].

4.2. Cathodoluminescence Spectra

The normalized CL spectra of $\text{Lu}_{3-x}\text{Gd}_x\text{Al}_5\text{O}_{12}\text{:Ce}$ SCFs at $x = 0, 0.5$, and 1.5 in comparison with the CL spectrum of YAG:Ce substrate are shown in Figure 4. The maximum of Ce^{3+} emission bands was shifted (see Figure 4b) to the red range with increasing Gd content in the SCF samples due to increasing crystal field strength in the dodecahedral position of the garnet lattice, see also [18,19].

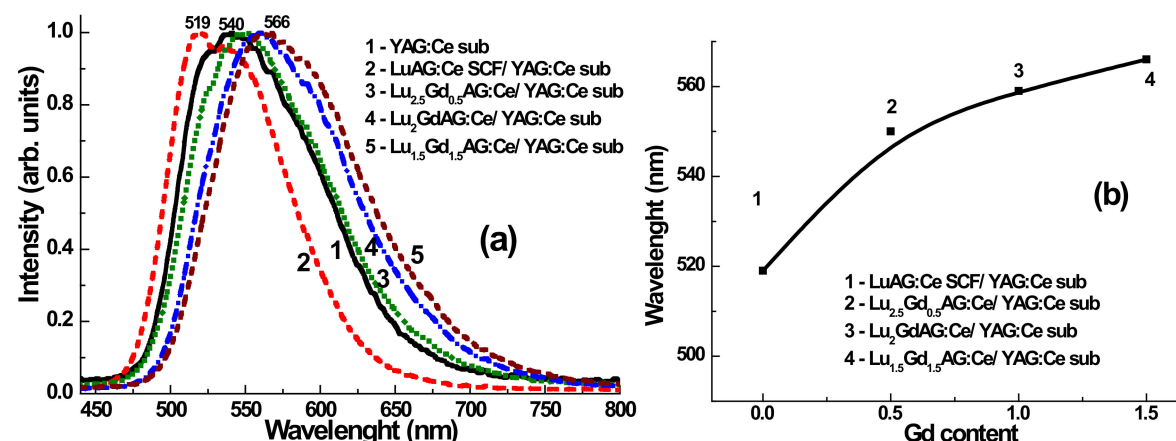


Figure 4. CL spectra (a) of LuAG:Ce, $\text{Lu}_{2.5}\text{Gd}_{0.5}\text{AG:Ce}$, LuGdAG:Ce, $\text{Lu}_{1.5}\text{Gd}_{1.5}\text{AG:Ce}$ SCFs in comparison with YAG:Ce substrate and (b) shift of emission band.

4.3. Thermoluminescence Spectra

The first attempt to create a composite TL detector based on the LuAG:Ce SCF/YAG:Ce epitaxial structures was described in our previous work [17]. The observed difference (about 80 degrees) between the position of the main TSL peaks of the SC and SCF parts of the composite detector under α - and β -particle excitation enabled the simultaneous registration of these particles in the mixed ionization fluxes. Meanwhile, the optimization of the TSL properties of such a type of composite detector is also possible and was considered in this work.

In the first stage, we analyzed the thermoluminescent curves for substrate. Figure 5 shows the similar TSL properties under excitation by α - and β -particles, but the integral intensity of the TSL peaks is strongly determined by the absorbed dose of radiation (curves 1 and 2, respectively). The TSL glow curves of $\text{Lu}_{3-x}\text{Gd}_x\text{Al}_5\text{O}_{12}\text{:Ce}$ SCFs/YAG:Ce SC epitaxial structures with different Gd content x under excitation by α - and β -particles from ^{241}Am and $^{90}\text{Sr} + ^{90}\text{Y}$ sources, respectively, are shown in Figure 6.

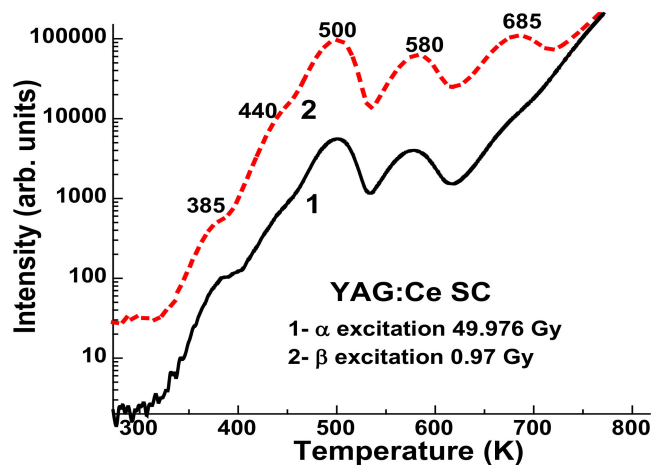


Figure 5. Glow curves of YAG:Ce SC after irradiation by α - (1) and β - (2) particles, respectively.

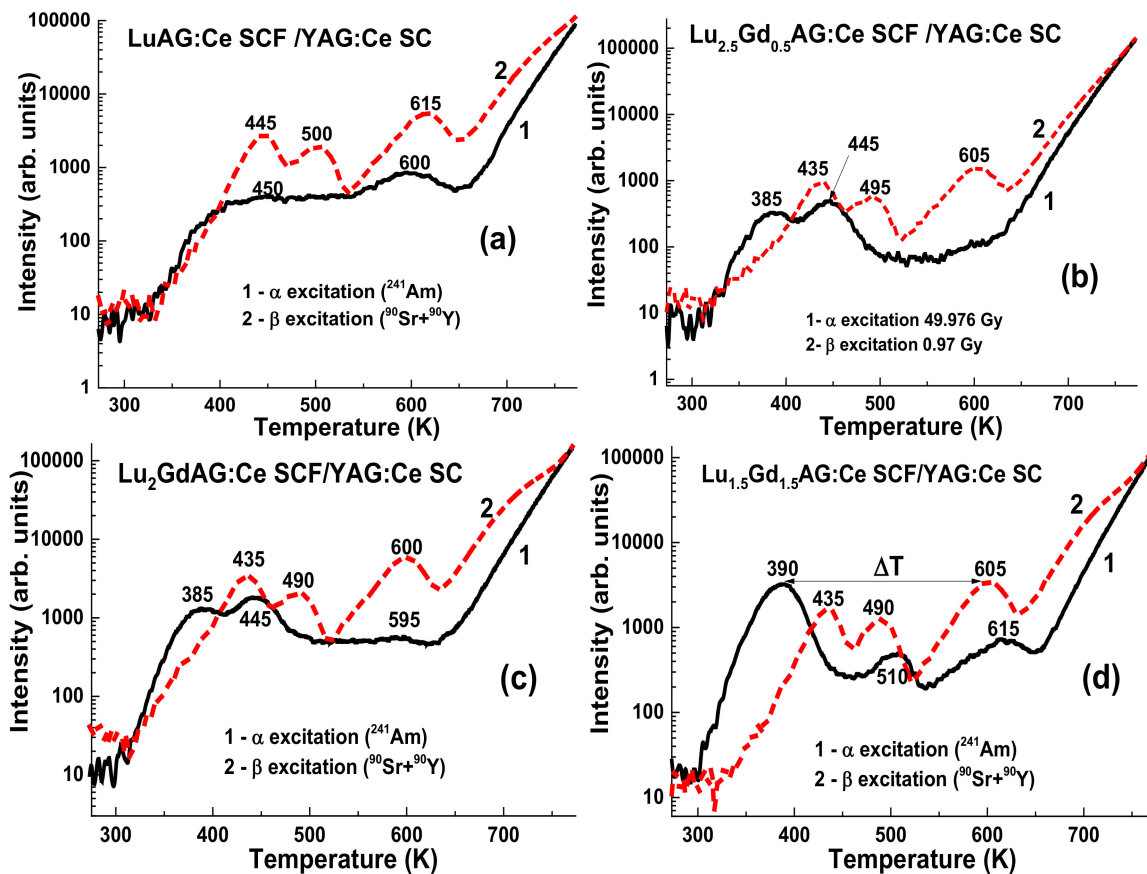


Figure 6. TL glow curves of LuAG:Ce SCF/YAG:Ce SC (a), $\text{Lu}_{2.5}\text{Gd}_{0.5}\text{AG:Ce SCF/YAG:Ce SC}$ (b), $\text{Lu}_2\text{GdAG:Ce SCF/YAG:Ce SC}$ (c), and $\text{Lu}_{1.5}\text{Gd}_{1.5}\text{AG:Ce SCF/YAG:Ce SC}$ (d) composite detectors after irradiation by α - (1) and β - (2) particles, respectively.

As mentioned above, the α -particles from an ^{241}Am (5.5 MeV) source with a typical passway in the LuAG of $12\text{--}15 \mu\text{m}$ were fully stopped in the SCF parts of a composite detector with a thickness of several tens of microns, when β -particles from a $^{90}\text{Sr} + ^{90}\text{Y}$ source with an average energy of 1.1 MeV could penetrate in the whole substrates. Therefore, due to the high thickness of the SCF samples in the $16\text{--}51 \mu\text{m}$ range (Table 1), the TSL glow curves under α -particle excitation correspond exclusively to SCFs.

As can be seen from Figure 6a, after α -particle irradiation, the main peak of the LuAG:Ce SCF/YAG:Ce SC structure was observed at 600 K. This result is consistent with the results of our previous work [17]. In accordance with the results of the work in [18], increasing the Gd content in the $\text{Lu}_{3-x}\text{Gd}_x\text{Al}_5\text{O}_{12}:\text{Ce}$ SCFs led to the shift of position of the main TSL peaks to the low temperature range, to 390 K in the $\text{Lu}_{1.5}\text{Gd}_{1.5}\text{Al}_5\text{O}_{12}:\text{Ce}$ SCF sample (Table 2 and Figure 6d). Meanwhile, the position of the main TL peaks in the $\text{Lu}_{3-x}\text{Gd}_x\text{Al}_5\text{O}_{12}:\text{Ce}$ SCF/YAG:Ce SC structure after β -particle irradiation did not change notably (Table 1) due to the fact that the β -particles were mainly absorbed by the YAG:Ce substrate. Therefore, the difference ΔT between the main TL peaks of SCF and substrate parts of a composite detector, corresponding to the registration of α - and β -particles, increased steeply with an increasing Gd content x in the $\text{Lu}_{3-x}\text{Gd}_x\text{Al}_5\text{O}_{12}:\text{Ce}$ SCFs. Namely, ΔT value is equal of 215 degrees for $\text{Lu}_{1.5}\text{Gd}_{1.5}\text{Al}_5\text{O}_{12}:\text{Ce}$ SCFs (Figures 6d and 7, curve 2).

Table 2. Position of the main TL peaks in $\text{Lu}_{3-x}\text{Gd}_x\text{Al}_5\text{O}_{12}:\text{Ce}$ SCF/YAG:Ce SC composite structures after irradiation by α - and β -particles. * the main TL peaks.

SC and SCF Content	α -Particles (^{241}Am)	β -Particles ($^{90}\text{Sr} + ^{90}\text{Y}$)
LuAG:Ce SCF/YAG:Ce SC	450, 600 *	445, 500, 615 *
$\text{Lu}_{2.5}\text{Gd}_{0.5}\text{AG}:\text{Ce}$ SCF/YAG:Ce SC	385, 445 *	435, 495, 605 *
$\text{Lu}_2\text{GdAG}:\text{Ce}$ SCF/YAG:Ce SC	385, 445 *, 593	435, 490, 600 *
$\text{Lu}_{1.5}\text{Gd}_{1.5}\text{AG}:\text{Ce}$ SCF/YAG:Ce SC	390 *, 510, 615	435, 490, 605 *

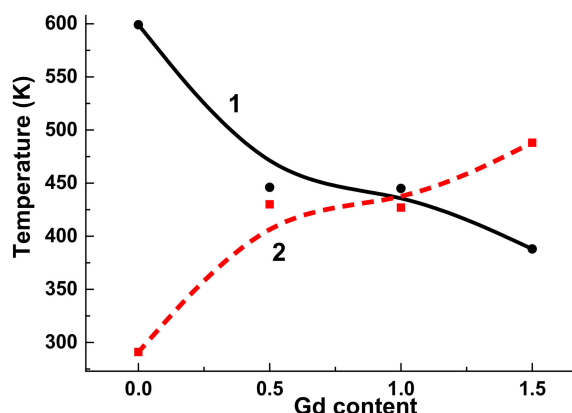


Figure 7. Dependence of position of the main TL peaks in $\text{Lu}_{3-x}\text{Gd}_x\text{Al}_5\text{O}_{12}:\text{Ce}$ SCF/YAG:Ce SC epitaxial structures under α -particle (^{241}Am) excitation (1) and the difference between the main TSL peaks of SCFs and SC parts of $\text{Lu}_{3-x}\text{Gd}_x\text{Al}_5\text{O}_{12}:\text{Ce}$ SCF/YAG:Ce SC composite detectors under α -particle (^{241}Am) and β -particle ($^{90}\text{Sr} + ^{90}\text{Y}$) excitation (2).

It is important to note that due to the large feeding in the case of the TL peak positions in the low temperature range, of the most optimal was the location of the TL peaks of $\text{Lu}_{3-x}\text{Gd}_x\text{Al}_5\text{O}_{12}:\text{Ce}$ SCFs in the range above 150 K. For this reason, the creation of a composite detector based on the $\text{Lu}_2\text{GdAl}_5\text{O}_{12}:\text{Ce}$ SCF/YAG:Ce SC epitaxial structure was the optimal option. For such a type of composite detector the ΔT value is equal to 155 degrees, which is completely enough for the simultaneous registration of TL signals coming from the SCF and SC parts of a composite detector in the case of the registration of α - and β -particles, respectively.

5. Conclusions

The creation of novel types of composite TL detectors based on the $\text{Lu}_{3-x}\text{Gd}_x\text{Al}_5\text{O}_{12}:\text{Ce}$ SCF/YAG:Ce SC epitaxial structures for simultaneous registration of the mixed ionization fluxes, containing α - and β -particles, is reported in this work. The detectors, consisting of $\text{Lu}_{3-x}\text{Gd}_x\text{Al}_5\text{O}_{12}:\text{Ce}$ SCFs with Gd content in the $x = 0\text{--}1.5$ range, were fabricated using the liquid phase epitaxy (LPE) growth method onto YAG:Ce substrates. The registration of α - and β -particles by the SCF and SC

components of composite detectors was performed using the differences between TL glow curves of these components of composite detectors.

The results of testing of $\text{Lu}_{3-x}\text{Gd}_x\text{Al}_5\text{O}_{12}:\text{Ce}$ SCF/YAG:Ce SC epitaxial structures are encouraging. In the $\text{Lu}_{3-x}\text{Gd}_x\text{Al}_5\text{O}_{12}:\text{Ce}$ SCF/YAG:Ce SC detector, the difference between the positions of the main TL peaks of the glow curves of the SCF and SC components after α - and β -particle irradiation, ΔT , increases steeply from 15 to 215 degrees with an increasing Gd content in the 0–1.5 range. Therefore, such a ΔT value is significantly larger than the 80 degrees obtained recently for an LuAG:Ce SCF/YAG:Ce SC epitaxial structure. Meanwhile, due to feeding influence, the optimal garnet combination for the creation of a composite detector is the $\text{Lu}_2\text{GdAl}_5\text{O}_{12}:\text{Ce}$ SCF/YAG:Ce SC epitaxial structure with the ΔT value above 150 degrees.

The obtained results confirm the assumption that the cation engineering of SCF content enables the significant improvement of the TL properties of composite detectors. Namely, the application of such an approach leads to an increase in the difference between the TL glow curves of $\text{Lu}_{2-1.5}\text{Gd}_{1-1.5}\text{Al}_5\text{O}_{12}:\text{Ce}$ SCFs and YAG:Ce substrates up to 150–215 degrees in comparison with a respective value of 80 degrees for the prototype of a composite detector based on LuAG:Ce/YAG:Ce epitaxial structures [17].

Author Contributions: S.W.-L. collected and analyzed the SCF structural and optical properties and participated in writing and preparation of the paper; V.G. performed SCF growth experiments and wrote the growth part of the paper; A.F. measured the XRD patterns of the SCF samples; T.Z. performed and analyzed the absorption and cathodoluminescence measurements; P.B. and A.M. performed the TSL measurements of the SCF samples; and Y.Z. analyzed all of the experimental materials and wrote the introduction, third part, and conclusion of the paper. All authors have read and agreed to the published version of the manuscript.

Funding: This research received no external funding.

Acknowledgments: The work was supported by the Miniatura NCN 2018/02/X/ST8/02686 and Polish NCN 2018/31/Z/ST8/00007 projects.

Conflicts of Interest: The authors declare no conflict of interest.

References

1. Nikl, M. *Nanocomposite, Ceramic, and Thin Film Scintillators*; Jenny Stanford Publishing: New York, NY, USA, 2017.
2. Nikl, M.; Yoshikawa, A. Recent R&D Trends in Inorganic Single-Crystal Scintillator Materials for Radiation detection. *Adv. Opt. Mater.* **2015**, *3*, 463–481. [[CrossRef](#)]
3. Nikl, M.; Kamada, K.; Babin, V.; Pejchal, J.; Pilarova, K.; Mihokova, E.; Beitlerova, A.; Bartosiewicz, K.; Kurosawa, S.; Yoshikawa, A. Defect engineering in Ce-doped aluminum garnet single crystal scintillators. *Cryst. Growth Des.* **2014**, *14*, 4827–4833. [[CrossRef](#)]
4. Dujardin, C.; Auffray, E.; Bourret-Courchesne, E.; Dorenbos, P.; Lecoq, P.; Nikl, M.; Vasil'ev, A.N.; Yoshikawa, A.; Zhu, R.-Y. Needs, trends, and advances in inorganic scintillators. *IEEE Trans. Nucl. Sci.* **2018**, *65*, 1977–1997. [[CrossRef](#)]
5. Robertson, J.M.; Van Tol, M.W. Cathodoluminescent garnet layers. *Thin Solid Film.* **1984**, *114*, 221–240. [[CrossRef](#)]
6. Zorenko, Y.V.; Novosad, S.S.; Pashkovskii, M.V.; Lyskovich, A.B.; Savitskii, V.G.; Batenchuk, M.M.; Malyutenkova, P.S.; Patsagan, N.I.; Nazar, I.V.; Gorbenko, V.I. Epitaxial structures of garnets as scintillation detectors of ionizing radiation. *J. Appl. Spectrosc.* **1990**, *52*, 645–649. [[CrossRef](#)]
7. Ferrand, B.; Chambaz, B.; Couchaud, M. Liquid phase epitaxy: A versatile technique for the development of miniature optical components in single crystal dielectric media. *Opt. Mater.* **1991**, *11*, 101–114. [[CrossRef](#)]
8. Molva, E. Microchip lasers and their applications in optical microsystems. *Opt. Mater.* **1999**, *11*, 289–299. [[CrossRef](#)]
9. Zorenko, Y.; Konstankevych, I.; Globus, M.; Grynyov, B.; Lyubinskij, V. New scintillation detectors based on oxide single crystal films for biological microtomography. *Nucl. Instrum. Methods Phys. Res. A* **2003**, *486*, 93–96. [[CrossRef](#)]
10. Klimczak, M.; Malinowski, M.; Sarnecki, J.; Piramidowicz, R.J. Luminescence properties in the visible of Dy:YAG/YAG planar waveguides. *J. Lumin.* **2009**, *129*, 1869–1873. [[CrossRef](#)]

11. Martin, T.; Koch, A. Recent developments in X-ray imaging with micrometer spatial resolution. *J. Synchrotron Radiat.* **2006**, *13*, 180–194. [[CrossRef](#)] [[PubMed](#)]
12. Witkiewicz-Lukaszek, S.; Gorbenko, V.; Zorenko, T.; Sidletskiy, O.; Gerasymov, I.; Fedorov, A.; Yoshikawa, A.; Mares, J.A.; Nikl, M.; Zorenko, Y. Development of composite scintillators based on single crystalline films and crystals of Ce³⁺-doped (Lu,Gd)₃(Al,Ga)₅O₁₂ mixed garnet compounds. *Cryst. Growth Des.* **2018**, *18*, 1834–1842. [[CrossRef](#)]
13. Witkiewicz-Lukaszek, S.; Gorbenko, V.; Zorenko, T.; Paprocki, K.; Sidletskiy, O.; Fedorov, A.; Mares, J.A.; Kucerkova, R.; Nikl, M.; Zorenko, Y. Epitaxial growth of composite scintillators based on Tb₃Al₅O₁₂:Ce single crystalline films and Gd₃Al_{2.5}Ga_{2.5}O₁₂:Ce crystal substrates. *CrystEngComm* **2018**, *20*, 3994–4002. [[CrossRef](#)]
14. Witkiewicz-Lukaszek, S.; Gorbenko, V.; Zorenko, T.; Paprocki, K.; Sidletskiy, O.; Gerasymov, I.; Mares, J.A.; Kucerkova, R.; Nikl, M.; Zorenko, Y. Novel all-solid-state composite scintillators based on the epitaxial structures of LuAG garnet doped with Pr, Sc, and Ce Ions. *IEEE Trans. Nucl. Sci.* **2018**, *65*, 2114–2119. [[CrossRef](#)]
15. Witkiewicz-Lukaszek, S.; Gorbenko, V.; Zorenko, T.; Paprocki, K.; Sidletskiy, O.; Gerasymov, I.; Mares, J.A.; Kucerkova, R.; Nikl, M.; Zorenko, Y. Composite scintillators based on the crystals and single crystalline films of LuAG garnet doped with Ce³⁺, Pr³⁺ and Sc³⁺ ions. *Opt. Mater.* **2018**, *84*, 593–599. [[CrossRef](#)]
16. Mares, A.; Witkiewicz-Lukaszek, S.; Gorbenko, V.; Zorenko, T.; Kucerkova, R.; Beitlerova, A.; D'Ambrosio, C.; Dlouhy, J.; Nikl, M.; Zorenko, Y. Alpha and gamma spectroscopy of composite scintillators based on the LuAG:Pr crystals and single crystalline films of LuAG:Ce and (Lu,Gd,Tb)AG: Ce garnets. *Opt. Mater.* **2019**, *96*, 109268. [[CrossRef](#)]
17. Witkiewicz-Lukaszek, S.; Gorbenko, V.; Zorenko, T.; Zorenko, Y.; Gieszczyk, W.; Mrozik, A.; Bilski, P. Composite thermoluminescent detectors based on the Ce³⁺ doped LuAG/YAG and YAG/LuAG epitaxial structures. *Radiat. Meas.* **2019**, *128*, 106–124. [[CrossRef](#)]
18. Zorenko, Y.; Gorbenko, V.; Vasylkiv, J.; Zelenyj, A.; Fedorov, A.; Kucerkova, R.; Mares, J.A.; Nikl, M.; Bilski, P.; Twardak, A. Growth and luminescent properties of scintillators based on the single crystalline films of Lu_{3-x}Gd_xAl₅O₁₂: Ce garnet. *Mater. Res. Bull.* **2015**, *64*, 355–363. [[CrossRef](#)]
19. Wu, J.L.; Gundiah, G.; Cheetham, A.K. Structure–property correlations in Ce-doped garnet phosphors for use in solid state lighting. *Chem. Phys. Lett.* **2007**, *441*, 250. [[CrossRef](#)]
20. Tyagi, M.; Meng, F.; Koschan, M.; Donnald, S.B.; Rothfuss, H.; Melcher, C.L. Effect of codoping on scintillation and optical properties of a Ce-doped Gd₃Ga₃Al₂O₁₂ scintillator. *J. Phys. D Appl. Phys.* **2013**, *46*, 475302. [[CrossRef](#)]
21. Wu, Y.; Meng, F.; Li, Q.; Koschan, M.; Melcher, C.L. Role of Ce⁴⁺ in the scintillation mechanism of codoped Gd₃Ga₃Al₂O₁₂Ce. *Phys. Rev. Appl.* **2014**, *2*, 044009. [[CrossRef](#)]



© 2020 by the authors. Licensee MDPI, Basel, Switzerland. This article is an open access article distributed under the terms and conditions of the Creative Commons Attribution (CC BY) license (<http://creativecommons.org/licenses/by/4.0/>).